INFORMATION TO USERS

This manuscript has been reproduced from the microfilm master. UMI films the text directly from the original or copy submitted. Thus, some thesis and dissertation copies are in typewriter face, while others may be from any type of computer printer.

The quality of this reproduction is dependent upon the quality of the copy submitted. Broken or indistinct print, colored or poor quality illustrations and photographs, print bleedthrough, substandard margins, and improper alignment can adversely affect reproduction.

In the unlikely event that the author did not send UMI a complete manuscript and there are missing pages, these will be noted. Also, if unauthorized copyright material had to be removed, a note will indicate the deletion.

Oversize materials (e.g., maps, drawings, charts) are reproduced by sectioning the original, beginning at the upper left-hand corner and continuing from left to right in equal sections with small overlaps.

Photographs included in the original manuscript have been reproduced xerographically in this copy. Higher quality 6" x 9" black and white photographic prints are available for any photographs or illustrations appearing in this copy for an additional charge. Contact UMI directly to order.

UMI®

University of Alberta

Fluorescent Derivatization of Arginine- and Carbonyl-Containing Analytes for Analysis by Capillary Electrophoresis with Laser-Induced Fluorescence Detection

By

Heather Cain

A thesis submitted to the Faculty of Graduate Studies and Research in partial fulfillment of the requirements for the degree of Master of Science

Department of Chemistry

Edmonton, Alberta
Fall 2000

Canada

University of Alberta

Library Release Form

Name of Author: Heather Cain

Title of Thesis: Fluorescent Derivatization of Arginine- and Carbonyl-Containing Analytes for Analysis by Capillary Electrophoresis with Laser-Induced Fluorescence Detection

Degree: Master of Science

Year this Degree Granted: 2000

71 Ewart Crescent S.E.
Medicine Hat, Alberta
T1B 2W3

July 21, 2000

Abstract

Microcystin-LR was shown to be successfully derivatized via an arginine-labelling reaction with the fluorescent tags 5-TAMRA-SE and 5-BMF through analysis by MALDI-MS, ESI-MS and CZE-LIF. A microcystin-LR fluorescent flow displacement immunoassay was constructed and the resulting calibration curve had a correlation coefficient of +0.9922 with a limit of detection of 10^{-10} M.

A carbonyl-labelling reaction was developed and found to be most efficient, through analysis by ESI-MS and CZE-LIF, when performed in the absence of 18-Crown-6 and/or TED and when two molar equivalents of 5-BMF were reacted. The reactant limitation was 10^{-8} moles and the reaction time optimizations were not conclusive.

The optimized carbonyl-labelling reaction was then applied to a series of FFAs. MECK-LIF analysis showed product peaks for every acid in the series with migration times of 6.3 – 9.8 minutes with LODs ranging from 0.1 – 2.2 nM. ESI-MS analysis confirmed that each carbonyl-labelling reaction performed was successful.

University of Alberta

Faculty of Graduate Studies and Research

The undersigned certify that they have read, and recommend to the Faculty of Graduate Studies and Research for acceptance, a thesis en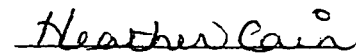titled **Fluorescent Derivatization of Arginine- and Carbonyl-Containing Analytes for Analysis by Capillary Electrophoresis with Laser-Induced Fluorescence Detection** submitted by **Heather Cain** in partial fulfillment of the requirements for the degree of **Master of Science.**

Dr. N. J. Dovichi
(Supervisor)

Dr. F. F. Cantwell
(Committee Chair & Examiner)

Dr. X. C. Le
(Committee member)

July 4, 2000

Acknowledgements

First and foremost, I would like to thank my parents, David and Joyce Cain, for all their love and support throughout my educational career. Their constant encouragement and friendship were what sustained me through the strenuous times. I would like express my gratitude to Hossein Ahmadzadeh for all of his support and guidance throughout my work. My appreciation also goes to Dawn Richards for providing me with the Grignard-poly-AAP-coated capillary and more importantly for being generous enough to take time out of her busy work schedule to revise my thesis. I would also like to acknowledge Dr. A. Morales for performing the ESI-MS analysis on my samples and for always being there for help. Last but not least, I would like to thank Dr. N. J. Dovichi (who has been my most inspirational professor to date), Dr. X. C. Le, NSERC operating and everyone in the Northern Lights Laser Lab for providing me with a graduate experience that I will always cherish.

Table of Contents

List of Tables

List of Figures

List of Abbreviations and Symbols

Acetonitrile	ACN
Alanine	Ala
Alpha	α
N-(4-Aminobutyl)-N-ethylisoluminol	ABEI
N-(4-Aminobutyl)-N-methylisoluminol	ABMI
3-Amino-9-methoxy-10-phenyl-2,6,8-trimethyldeca-4(E)6(E)-dienoic acid	Adda
p-Aminophenol	AP
p-(9-Anthroyloxy)phenacyl bromide	PBr
9-Anthryldiazomethane	ADAM
Antibody	Ab
Antigen	Ag
Apparent velocity	v_{app}
Applied voltage	V
Arginine	Arg, R
Argon ion	Ar^+
Atomic mass units	amu
Background standard deviation or noise	σ
Baseline width of a peak	W
Beta	β
Bimolecular nucleophilic substitution	S_N2
α-Bromo-2'-acetonaphthone	BAN

3-Bromoacetyl-7-methoxycoumarin	BrAMC
3-Bromoacetyl-6,7-methylenedioxycoumarin	BrAMDC
4-Bromomethyl-7-acetoxycoumarin	BrMAC
3-Bromomethyl-6,7-dimethoxy-1-methyl-2(1H)-quinoxalinone	BrDMEQ
5-(Bromomethyl)fluorescein	5-BMF
4-Bromomethyl-7-methoxycoumarin	BrMMC
3-Bromomethyl-6,7-methylenedioxy-1-methyl-2(1H)-quinoxalinone	BrMMEQ
2-Bromo-2'-nitroacetophenone	NPA
p-Bromophenacyl bromide	BPB
Calcium chloride	$CaCl_2$
Capillary electrophoresis	CE
Capillary zone electrophoresis	CZE
Carbon-nitrogen bond	C-N
5-Carboxytetramethylrhodamine, succinimidyl ester	5-TAMRA-SE
Centimetre (10^{-2} m)	cm
Charge of ion	q
Column length	L
Concentration	C
Concentration limit of detection	LOD_c
Correlation coefficient	r
Critical micelle concentration	CMC
Current of electrolyte	I
Cyclodextrin(s)	CD(s)

Cyclodextrin-modified CZE	CD-CZE
Cyclodextrin-modified MEKC	CD-MEKC
Degrees	°
Degrees Celsius	°C
Density of water or buffer	ρ
Diameter of capillary	D
1,4-Diazabicyclo[2.2.2]octane	TED
Dielectric constant	ε
Diffusion constant	D_I
2,5-Dihydroxybenzoic acid	DHB
6,7-Dimethoxy-1-methyl-2(1H)-quinoxalinone-3-propionylcarboxylic acid hydrazide	DMEQ-Hz
5-(Dimethylamino)naphthalene-1-sulfonhydrazide	DNS-Hz
5-(Dimethylamino)-1-naphthalenesulfonyl-semipiperazide	DNS-PZ
N,N-Dimethylformamide	DMF
4-(N,N-Dimethylminosulfonyl)-7-(5-aminopentylamino)-2,1,3-benzoxadiazole	DBD-CD
(+)- and (-)-4-(N,N-Dimethylminosulfonyl)-7-(3-aminopyrrolidin-1-yl)-2,1,3-benzoxadiazole	DBD-APy
4-(N,N-Dimethylminosulfonyl)-7-(1-piperazinyl)-2,1,3-benzoxadiazole	DBD-PZ
2,4-Dimethoxyaniline	DMA
3,5-Dinitrobenzoyl chloride	DNBC

2,4-Dinitrophenylhydrazine	DNPH
3,5-Dinitrophenyl isocyanate	DNPI
Distance from the injector to the detector	l
Duration of injection	t_{inj}
Electric field	E
Electroosmotic flow	EOF
Electroosmotic flow velocity	v_{eo}
Electrophoretic migration velocity	v_{ep}
Electrophoretic mobility	μ_{ep}
Electrospray ionization	ESI
Emission intensity detected vertically	I_{vv}
Emission intensity detected horizontally	I_{vh}
Enzyme-linked immunosorbent assay	ELISA
Erythro-β-methylaspartic acid	MeASP
Fluorescence anisotropy	r
Fraction of allowable peak broadening	θ
Free fatty acids	FFAs
Full-width at half-maximum	FWHM, $W_{1/2}$
Gamma	γ
Gas chromatography	GC
Glutamic acid	Glu
Grams	g
Gravitational constant	g

Heat generated per unit volume	Q
Height of elevated capillary	Δh
Helium-Neon	He-Ne
High performance liquid chromatography	HPLC
Hour	h
2-(4-Hydrazinocarbonylphenyl)-4,5-diphenylimidazole	HCPI
Hydrogen	H
Hydroxamic acid	HA
Hydroxide	OH
Indirect UV detection	IUVD
50 % Inhibition concentration	IC_{50}
Injection voltage	V_{inj}
Inner diameter	d, I.D.
Input/Output board	I/O
Ionic strength of the electrolyte	C
Ionized silanol groups	SiO^-
Kilovolts	kV
Labelled product	M*
Laser-induced fluorescence	LIF
Laser-induced fluorescence polarization	LIFP
Length	L
Length of sample plug	L_{inj}
Leucine	Leu, L

Limit of detection	LOD
Liquid chromatography	LC
Litre	L
Mass injected	m_{inj}
Mass limit of detection	LOD_m
Mass spectrometry	MS
Mass-to-charge ratio	m/z
Matrix assisted laser desorption ionization	MALDI
Mercaptopropyltrimethoxysilane	MTS
Methanol	MeOH
N-methyldehydroalanine	Mdha
Metre	m
Micellar electrokinetic chromatography	MEKC
Microgram (10^{-6} g)	μg
Microlitre (10^{-6} L)	μL
Micrometre (10^{-6} m)	μm
Migration time	t_m
Migration time of micellar phase	t_{mc}
Migration time of neutral species	t_{eo}, t_o
Milligram (10^{-3} g)	mg
Millilitre (10^{-3} L)	mL
Millimetre (10^{-3} m)	mm
Millimolar (10^{-3} M)	mM

Milliwatts	mW
Minute	min
Molar	M
Molar absorptivity	ε
Molar conductance of the solution	λ
Moles	mol
Moles injected	m_{inj}
Monodansyl cadaverine	MDC
Nanolitre (10^{-9} L)	nL
Nanometre (10^{-9} m)	nm
Nanomolar (10^{-9} M)	nM
2-(2,3-Naphthalimino)ethyl trifluoromethanesulfonate	NE-Otf
p-Nitrobenzyloxyamine hydrochloride	PNBA
p-Nitrophenacyl bromide	NPB
2-Nitrophenylhydrazine	NPH
Nonaqueous CE	NACE
Number of injections	n
Number of theoretical plates	N
Numerical aperture	NA
Outer diameter	O.D.
Peak variance caused by analyte-wall interactions	σ_{wall}^2
Peak variance due to initial zone width	σ_{inj}^2
Peak variance due to Joule heating	σ_{Joule}^2

Peak variance due to mass diffusion	σ_{diff}^2
Penicillin-G	PEN-G
Phenacylbromide	PB
(-)-Phenylethylamine	S(-)-PEA
p-Phenylphenacyl bromide	PPB
Photomultiplier tube	PMT
Picogram (10^{-12} g)	pg
Picomolar (10^{-12} M)	pM
Poly-acryloylaminopropanol	Poly-AAP
Poly(4-nitrobenzyl *p*-styrenesulfonate)	PS-NB
Poly[(2-phthalimino)ethyl *p*-styrenesulfonate]	PS-PE
Potassium	K
Potassium carbonate	K_2CO_3
Potassium hydroxide	KOH
Potassium sulfate	K_2SO_4
Pounds per square inch	PSI
Pressure drop	ΔP
Protein phosphatase inhibition assay	PPIA
Pyridinium dichromate	PDC
Quantum yield	ϕ
Radius	r
Resistance of the electrolyte	R
Resolution	R

Reversed-phase	RP
Ribonucleic acid	RNA
Seconds	s
Signal peak height	h
Sodium	Na
Sodium dodecyl sulfate	SDS
Sodium hydride	NaH
Sodium hydroxide	NaOH
Sodium phosphate dibasic	Na_2HPO_4
Sodium phosphate monobasic	NaH_2PO_4
Standard deviation	σ
Stationary liquid phase	SLP
N-Succinimidyl-4-maleimidobutyrate	GMBS
Time-of-flight	TOF
Total peak variance	σ_{tot}^2
Total velocity	v_{Total}
Triethylenediamine	TED
Ultraviolet	UV
Ultraviolet-visible region	UV-Vis
Unlabelled product	M
Variance	σ^2
Velocity of an anion	v_{-Ion}
Velocity of a cation	v_{+Ion}

Viscosity of buffer	η
Volts	V
Volume injected	V_{inj}
Volume of the capillary	V_{cap}
Zeta potential	ζw

Chapter 1

Introduction

1.1 Introduction

The term "electrophoresis" was coined by Michaelis[1] in 1909. In 1937 Tiselius[2] provided the first demonstration of the potential use of electrophoretic analysis. However this approach was limited by the incomplete separations of proteins, the large sample volume required, the necessity of low electrical fields for separation due to Joule heating and the length of time required to perform the procedure. These disadvantages are still present in conventional slab gel electrophoresis.

In 1953, Edstrom[3] discovered that the use of small-diameter silk fibres in electrophoresis allowed for improved detection of RNA contained within a single cell. In 1967 Hjertén[4] described work on free zone electrophoresis using 3-mm diameter glass tubes and a dual wavelength UV transmission detector. He recognized the value of glass capillaries in effectively minimizing thermal effects but could not use capillaries due to lack of a useful detector. It was not until 1979 that the first report of capillary free zone electrophoresis was presented by Everaerts and co-workers[5,6] in which separations were performed using 200-μm diameter Teflon™ capillaries. In 1981 and 1983 Jorgenson and Lukacs[7,8] published a set of papers that spawned an explosion of interest in capillary electrophoresis (CE).

The first application of fluorescence detection in CE was reported by Jorgenson and Lukacs[7] in 1981 who utilized a special fluorescence detector. Later in 1985, Zare's group[9] reported the premiere use of lasers for fluorescence detection in capillary electrophoresis. Laser-induced fluorescence (LIF) detection utilizing a sheath flow cuvette was developed in 1988 by Cheng and Dovichi.[10] Several different detection techniques, including electrochemical[11-14], fluorescence[15,16], laser-induced

2

fluorescence[9,10,17-24], and UV absorbance detection[25-31], have been used with CE. LIF

detection in CE exhibits the best performance characteristics compared to other detection

modes in terms of sensitivity, limits of detection, and linearity of signal. High-sensitivity

detection limits for CE-LIF range from 1000 molecules to one molecule of fluorescent

dye.[10,32-36]

1.2 Theory[37-39]

1.2.1 Basic concepts

CE is a remarkably simple separation technique. The basic instrumentation

consists of four main parts (Figure 1.1). A capillary is required for the separation, a high

voltage power supply is utilized to drive the separation, a detector is required to

determine the presence and amount of analyte, and a Plexi-glass safety interlock-

equipped enclosure is used to protect the operator from the high voltage. To perform a

capillary zone electrophoretic separation, the capillary is filled with an appropriate

separation buffer at the desired pH and sample is introduced at the inlet. Both ends of the

capillary and the platinum wire electrode are placed into buffer reservoirs and up to

30,000 V is applied to the system. The ionic species in the sample plug migrate with

electrophoretic mobilities (direction and velocity) determined by their charge and mass,

and eventually pass a detector where information is collected and stored by a data

collection system.

In the early 1980s, Jorgenson and Lukacs[7] discussed the theory and basis for

electrophoretic separation in capillaries. The mechanism of separation in electrophoresis

3

Figure 1.1: General schematic of a CE instrument.

Net Flow

Data Collection

High Voltage Power Supply

Capillary

Light Source

Optics

Detector

Inlet Buffer / Sample Injection

Plexi-glass Safety Interlocked box

Outlet Buffer
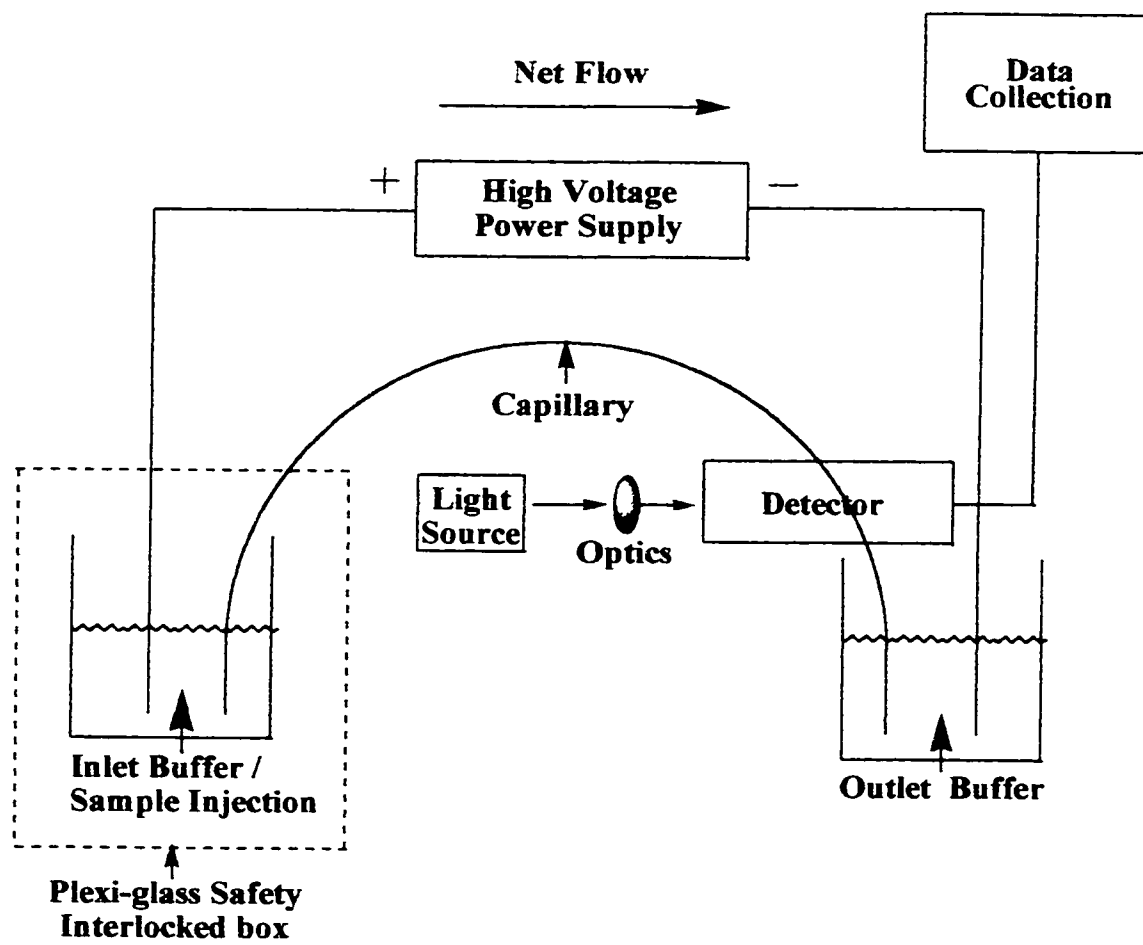
is based on the movement of ions in an applied electric field. The electrophoretic migration velocity, v_{ep}, of an ion in an electric field is given by

$$v_{ep} = V\mu_{ep}/L \qquad (1\text{-}1)$$

where v_{ep} is the velocity in m/s, V is the applied voltage in volts, μ_{ep} is the electrophoretic mobility of the singly charged ion ($m^2s^{-1}V^{-1}$), and L is the column length in meters. The time, t_m, for an analyte to move a distance l is given by

$$t_m = l/v_{ep} = lL/V\mu_{ep} = L^2/V\mu_{ep} \qquad (1\text{-}2)$$

where l is the distance from the injector to the detector (termed the effective length of the capillary). If the detector is at the end of the capillary, l = L. The detector is assumed to be at the end of the capillary (l = L) for the remaining equations. From Equations 1-1 and 1-2 one can see that differences in μ_{ep} lead to separation, the velocity increases linearly with potential and for an end-column detector, time is proportional to column length squared. Electrophoretic mobility can be experimentally determined from the migration time and separation voltage by

$$\mu_{ep} = L^2/t_mV. \qquad (1\text{-}3)$$

The Debye-Hückel-Henry theory may be used to approximate the electrophoretic mobility, μ_{ep}, of a charged species

5

$$\mu_{ep} = q/6\pi\eta r \qquad\qquad\qquad (1\text{-}4)$$

where η is the viscosity of the buffer, q is the charge of the particle and r is the Stokes' radius of the particle. The mass of the particle may be related to the Stokes' radius by M $= (4/3)\pi r^3 V$, where V is the partial specific volume of the solute. From Equation 1-4 it is seen that the velocity of a molecule depends on its charge-to-size ratio.

The velocity of an analyte in CE will also depend upon the rate of electroosmotic flow (EOF). EOF was first identified in the late 1800's when Helmholtz[40] conducted experiments involving the application of an electric field to a horizontal glass tube containing an aqueous salt solution. He found that the silica imparted a layer of negative charge to the inner surface of the tube which, under an applied electric field, led to the movement of fluid toward the outlet end or cathode. As shown by the expanded region of the inner wall of a capillary in Figure 1.2, the ionized silanol groups (SiO⁻) of the capillary wall attract cationic species from the buffer. Silanols are weakly acidic, and ionize at pH values above approximately 3. The buffer pH will determine the fraction of the silanol groups that will be ionized. The magnitude of EOF increases directly with pH until all the silanols are fully ionized. Hydrated cations in solution associate with ionized SiO⁻ groups to form an electrical double layer. The electric field in the electrical double layer is termed the zeta potential (ζ_w). The ionic layer that is formed has a positive charge density that decreases exponentially as the distance from the wall increases. The electrical double layer consists of a static inner Stern layer close to the surface and a mobile outer layer, termed the Helmholtz plane. Upon application of the field, hydrated cations in the outer layer move toward the cathode, creating a net flow of the bulk liquid

6

Figure 1.2: An illustration of the electrical double layer formed in bare silica capillaries. The negative and positive charges at the capillary wall represent the ionized silanol groups and electrolyte ions, respectively.
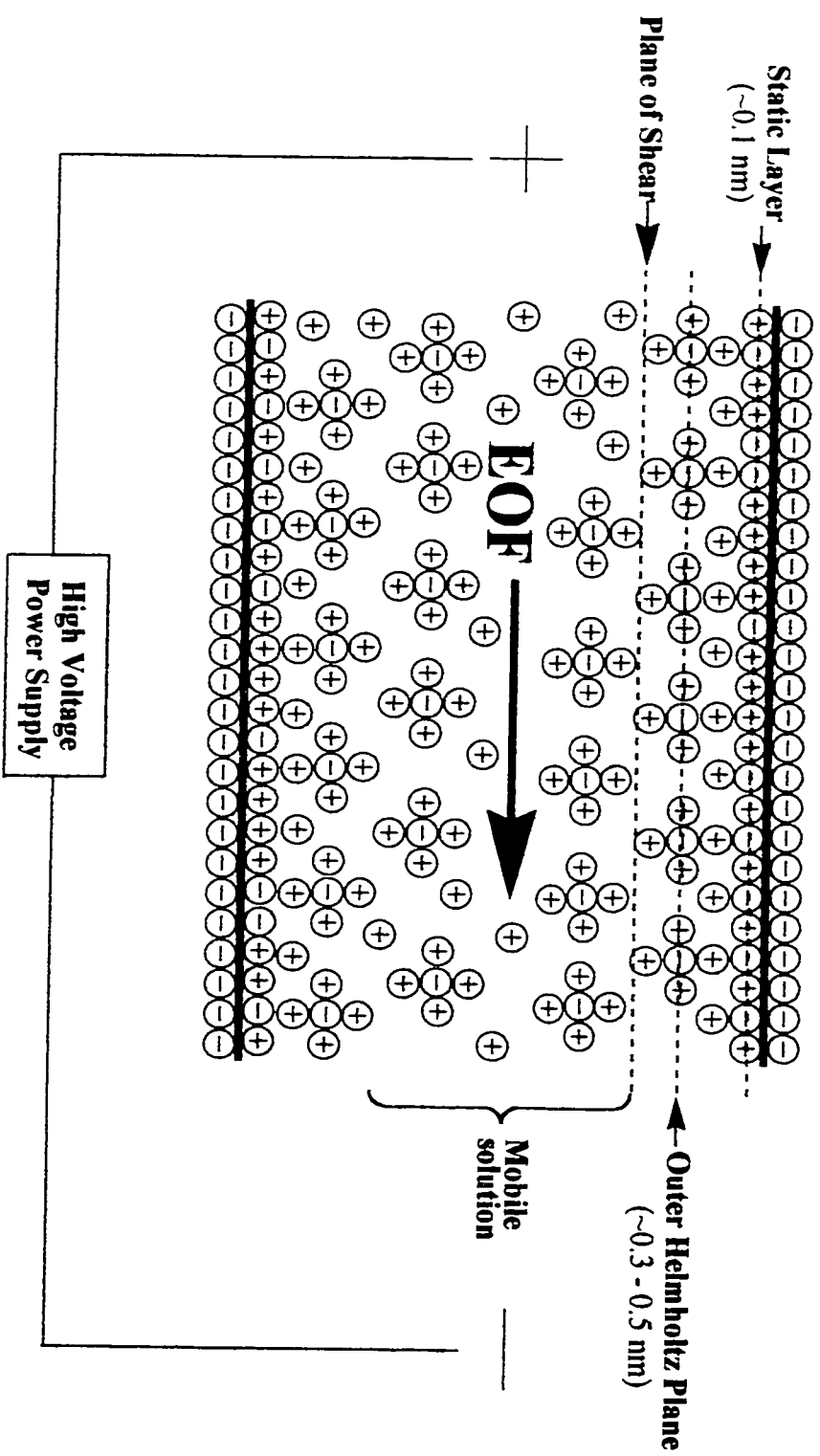
in the capillary in the same direction (Figure 1.2). The rate of movement is dependent

upon the field strength and the charge density of the capillary wall. The capillary wall is

also a source of frictional retardation of flow. The balance between electroosmosis and

friction creates a flat or plug flow profile, except for a few nanometers near the capillary

wall. A comparison of the velocity profiles of pressure driven parabolic flow and voltage

driven electroosmotic flow can be found in Figure 1.3. The flat flow profile

characteristic of CE eliminates one source of band broadening, mass transfer.

The velocity of electroosmotic flow, v_{eo}, like the velocity of electrophoretic flow,

is proportional to the applied voltage

$$v_{eo} = V\mu_{eo}/L \qquad (1\text{-}5)$$

where μ_{eo} is the electroosmotic mobility which is given by

$$\mu_{eo} = \varepsilon\xi_w/\eta \qquad (1\text{-}6)$$

where ε is the dielectric constant of the solvent (dimensionless), ξ_w is the zeta potential of

the capillary wall and η is the viscosity of the solvent (kg m^{-1} s^{-1}). Electroosmotic

mobility can be determined experimentally by injecting a neutral species and measuring

the time, t_{eo}, at which it is detected

$$\mu_{eo} = L^2/t_{eo}V. \qquad (1\text{-}7)$$

Figure 1.3: Velocity profiles in pressure driven parabolic flow or laminar flow

(A) and voltage driven electroosmotic flow (B).

A)

(+)   (-)
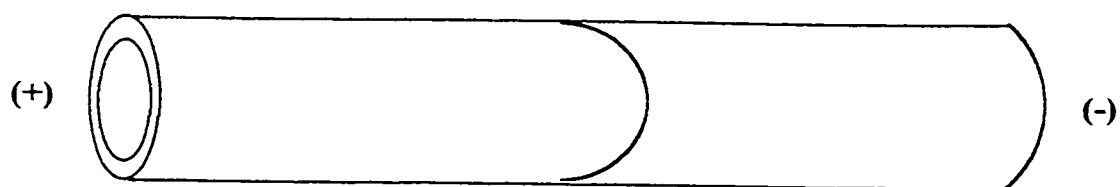
B)

(+)   (-)
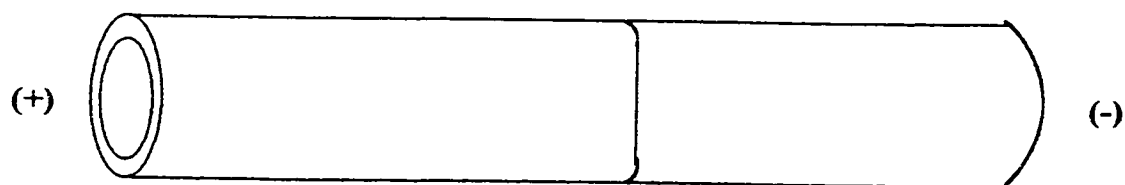
The apparent velocity, v_{app}, of a singly charged ion in an electric field will therefore be a combination of its electrophoretic (v_{ep}) and electroosmotic (v_{eo}) velocities

$$v_{app} = v_{ep} + v_{eo} = (\mu_{ep} + \mu_{eo}) (V/L). \qquad (1-8)$$

An illustration of total velocity can be found in Figure 1.4.

1.2.2 Shape of the analyte zone and sources of band broadening

The characteristics of a Gaussian profile describe the peak maximum and the peak width of peaks in CE. The peak maximum is dependent on the initial concentration of solute. The peak width depends on the length of time from initial conditions (i.e., application of sample into the system) and the diffusion constant, D_i. The width of the peak can be given in terms of standard deviation (σ), full-width at half-maximum (FWHM = $W_{\frac{1}{2}}$ = 1.7σ), or its baseline width ($W = 4\sigma$). The baseline width of a peak is measured by drawing tangents to the peak at the inflection points and measuring the peak width at the baseline. The width of a Gaussian curve is termed the standard deviation, σ, which is given by

$$\sigma = (2D_i t_m)^{\frac{1}{2}} \qquad (1-9)$$

and the square of the standard deviation, σ^2, is called variance,

$$\sigma^2 = 2D_i t_m. \qquad (1-10)$$

10

Figure 1.4: An illustration of total velocity for an analyte which is the vector sum of

the electrophoretic velocity of sample (v) and the velocity imparted by

electroosmotic flow (v_{eo}).
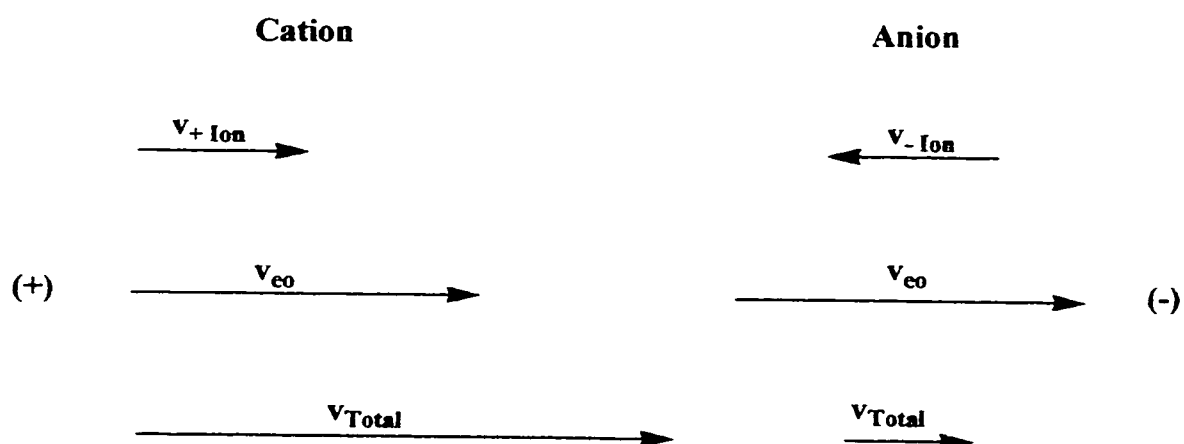
Remembering that

$$t_m = L/v_{app} = L^2/(\mu_{ep} + \mu_{eo})V \qquad (1\text{-}11)$$

we may substitute into Equation 1-10, to obtain

$$\sigma^2 = \sigma_{diff}^2 = 2D_iL^2/(\mu_{ep} + \mu_{eo})V. \qquad (1\text{-}12)$$

This peak variance, σ_{diff}^2, is due to mass diffusion. Other factors which contribute to the observed electropherogram as band broadening, the practical result of variance, include not only mass diffusion, but also initial zone width (σ_{inj}^2), Joule heating (σ_{Joule}^2) and adsorption of analytes to the capillary wall (σ_{wall}^2). The variance of the multiple dispersive phenomena on the analyte may be summed as

$$\sigma_{tot}^2 = \sigma_{diff}^2 + \sigma_{Joule}^2 + \sigma_{inj}^2 + \sigma_{wall}^2. \qquad (1\text{-}13)$$

1.2.3 Variance due to Joule heating

When an electric field is applied to a capillary containing an electrolyte, Joule heat is generated uniformly across the circumference of the tube. The heat generated per unit volume, Q, in a capillary of radius, r, is

$$Q = VI/\pi Lr^2 = V^2/\pi Lr^2R = \lambda CV^2/\pi L^2 = \lambda CE^2/\pi \qquad (1\text{-}14)$$

where I is the current of the electrolyte, R is the resistance of the electrolyte, λ is the

molar conductance of the solution, C is the ionic strength of the electrolyte, and E is the

electric field (V/L). Since heat can only be removed near the capillary wall, a

temperature gradient exists across the radius of the tube. A temperature gradient creates

a mobility gradient across the tube radius which contributes to band broadening. A

reduction of Joule heat production can be achieved by increasing the cross-sectional area

of the capillary or by reducing the capillary current. The latter is preferred, since

increasing the diameter of the capillary results in a reduction of the surface-to-volume

ratio, which thus leads to less efficient heat dissipation. The choices to reduce the

capillary current lie in carrying out the separation at a lower voltage or reducing the ionic

strength of the separation buffer.

The greater the surface-to-volume ratio of a capillary the more efficiently Joule

heat is dissipated. The smaller the diameter of a capillary the larger its surface-to-volume

ratio becomes. This is why the small internal diameters of fused silica capillaries have

been the key to high-resolution CE. The inside diameter of fused silica capillaries varies

from 5 to 200 μm and the outside diameter varies from 100 to 400 μm. The optimal

capillary inner diameter is 50 to 75μm. Capillaries with smaller inner diameters are

subject to plugging, and the high surface-to-volume ratio increases the risk of analyte

adsorption.

1.2.4 Variance due to initial zone width

Introduction, or as it is sometimes referred, "injection" or "loading", of sample into the capillary can be accomplished hydrostatically by siphoning or electrokinetically by applying a voltage. With hydrostatic injection the sample is introduced by immersing the inlet end of the capillary into a vial containing the sample and either pressurizing the inlet vial or applying a vacuum to the outlet end of the capillary. Sample introduction by gravity relies on the siphoning of sample into the capillary by elevating the injection (inlet) end of the capillary relative to the outlet end. With electrokinetic loading, the injection (inlet) end of the capillary is immersed in the sample and a high voltage is applied across the capillary.

An electrokinetic injection is performed by applying a low voltage (1 – 10 kV) for a duration of time determined by capillary length and inner diameter. For an electro-kinetic injection, the volume injected, V_{inj}, is given by

$$V_{inj} = V_{cap}(t_{inj}/t_m)(V_{inj}/V) \qquad (1\text{-}15)$$

where V_{cap} is the volume of the capillary, t_{inj} is the duration of the injection, and V_{inj} is the voltage used for injection. Equation 1-15 assumes that the conductivity of the sample is the same as that of the separation buffer. The moles injected, m_{inj}, for an electrokinetic injection is given by

$$m_{inj} = CV_{inj} \qquad (1\text{-}16)$$

where C is the concentration of the sample being injected.

The sample volume entering the capillary by hydrostatic injection is calculated by determining the rate of sample loading from the Poiseuille Equation

$$\text{Flow rate (nL/s)} = \Delta PD^4\pi/128\eta L \qquad\qquad (1\text{-}17)$$

where ΔP is the pressure drop, and D is the diameter of the capillary. For gravity based injections, the pressure drop is determined as follows

$$\Delta P = pg\Delta h \qquad\qquad (1\text{-}18)$$

where p is the density of water or buffer, g is the gravitational constant (980 cm/s^2) and Δh is the height of the elevated capillary. The injection volume produced in a hydrostatic injection is given by

$$V_{inj} = pg\pi r^4 \Delta ht_{inj}/8\eta L \qquad\qquad (1\text{-}19)$$

where r is the capillary radius.

In CE only a minute amount of sample is loaded into the capillary to avoid excess band broadening. The volume of a capillary, V_{column}, is given by the volume of a cylinder of length, L, and inner diameter, d,

$$V_{column} = \pi d^2 L/4. \qquad\qquad (1\text{-}20)$$

15

The maximum allowable injection volume to avoid noticeable peak broadening may be estimated as[41]

$$V_{inject} = \theta V_{column}/N^{\frac{1}{2}} \qquad (1\text{-}21)$$

where θ is the fraction of allowable peak broadening, and N is the number of theoretical plates for the separation which will be defined later in this chapter. Sternberg[42] derived the commonly used equation describing variance due to sample introduction

$$\sigma_{inj}^2 = L_{inj}^2/12 \qquad (1\text{-}22)$$

where L_{inj} is the length of the sample introduction plug. This formula assumes that the sample is introduced as a rectangular plug, which is a close approximation for CE. The sample introduction plug should not exceed 1 – 5 % of the total capillary length otherwise band broadening will occur.

1.2.5 Variance caused by analyte-wall interactions

The interaction of analyte and capillary wall, or components within the sample solution are numerous, complex and sample-specific. The best approach to understanding the band broadening due to adsorption is the approach of McManigall and Swedberg.[43] Approaches to minimizing or eliminating protein adsorption include the use

of buffer additives and dynamic or covalently coupled capillary coatings like poly-acryloylaminopropanol (poly-AAP).[44]

1.2.6 Resolution, efficiency and other useful formulas

The efficiency of separation can be represented as a number of theoretical plates (N), identical in definition to that used in chromatography. The number of theoretical plates is given by

$$N = 16(L/W)^2 \qquad (1\text{-}23)$$

where W is the baseline width of a peak. If Equation 1-12 is substituted into Equation 1-23 we get

$$N = L^2/\sigma_{diff}^2 = (\mu_{ep} + \mu_{eo})V/2D_i. \qquad (1\text{-}24)$$

Equation 1-24 predicts that efficiency is only diffusion-limited and increases directly with applied voltage. Equation 1-24 also suggests that the use of higher field strengths will lead to high efficiency but this will be at the expense of increased Joule heat. Efficiency in CE is much higher than in HPLC because there is no requirement for mass transfer between phases and because the flow profile in EOF-driven systems is flat (approximating plug flow) in contrast to the laminar-flow profiles characteristic of pressure-driven flow in chromatography columns (Figure 1.3).

The resolution, R, for two peaks with similar widths is defined as[45]

$$R = (2)(t_{m2} - t_{m1})/(w_2 + w_1) \qquad (1\text{-}25)$$

where t_1 and t_2 are the migration times of two peaks and w_1 and w_2 are their respective peak widths at the baseline. Resolution in CE can also be defined as

$$R = (\tfrac{1}{4})[\Delta\mu_{ep}N^{\frac{1}{2}}/(\mu_{ep} + \mu_{eo})]. \qquad (1\text{-}26)$$

Equation 1-26 implies that resolution will be greatest when μ_{ep} and μ_{eo} are of similar magnitude but have opposite sign; however resolution will be at the expense of analysis time. The mass limit of detection in moles, LOD_m, is given by

$$LOD_m = 3\sigma\,(m_{inj}/h) \qquad (1\text{-}27)$$

where σ is the background standard deviation or noise, h is the signal peak height and m_{inj} was defined in Equation 1-16. The concentration limit of detection, LOD_c, is given by

$$LOD_c = 3\sigma\,(C/h) \qquad (1\text{-}28)$$

where C is the concentration of the sample injected.

1.3 Instrument design

1.3.1 CE-LIF

The CE-LIF detection system used in this work has been described in detail elsewhere[17] of which a schematic diagram can be found in Figure 1.5. The inlet or injection end of a polyimide coated capillary (Polymicro Technologies, Phoenix, AZ, USA) is immersed into the sample or running buffer along with a platinum wire electrode which is connected to a high voltage power supply (CZE1000R, Spellman, Plainview, NY, USA). The polyimide coating on the outlet or detection end of the capillary is removed through the use of a gentle flame while continuously flushing the capillary with run buffer. The uncoated detection end of the capillary is then placed inside a 250-µm square flow chamber constructed from optical quality quartz (NSG Precision Cells, Farmingdale, NY, USA). This flow chamber is termed the sheath flow cuvette and is used to provide hydrodynamic focusing of the capillary flow and to reduce light scattering of the laser beam. The sheath flow cuvette is held in a grounded stainless steel holder. Analyte exiting the capillary is ensheathed by a flowing buffer stream and is forced to pass through the centre of the cuvette. Migrating species are excited by a 543.5 nm beam from a 0.8-mW Helium-Neon (He-Ne) laser (Melles Griot, Nepean, ON, Canada) or a 488 nm beam from a 15-mW argon ion (Ar$^+$) laser (Model 2211-15SL, Uniphase, San Jose, CA,USA) focused ~30 µm from the tip of the capillary's outlet or detection end by a 6.3 x 0.20 NA microscope objective (Melles Griot, Nepean, ON, Canada). Fluorescence is collected at right angles by a 60 x 0.70 NA microscope objective (Model 60x-LWD, Universe Kogaku (America), Oyster Bay, NY, USA) and passed through a bandpass filter, either 590DF35 or 518DF25 (Omega Optical,

19

Figure 1.5: The schematic diagram of the CE-LIF instrument.

Data collection

PMT

Pinhole

Bandpass filter

Ar$^+$ Laser (488nm)

Outlet buffer

Sheath flow cuvette

Focusing objective

Mirror

Capillary

Inlet buffer / Sample injection

Auxiliary microscope

Sheath flow buffer

Plexi-glass Safety Interlocked box
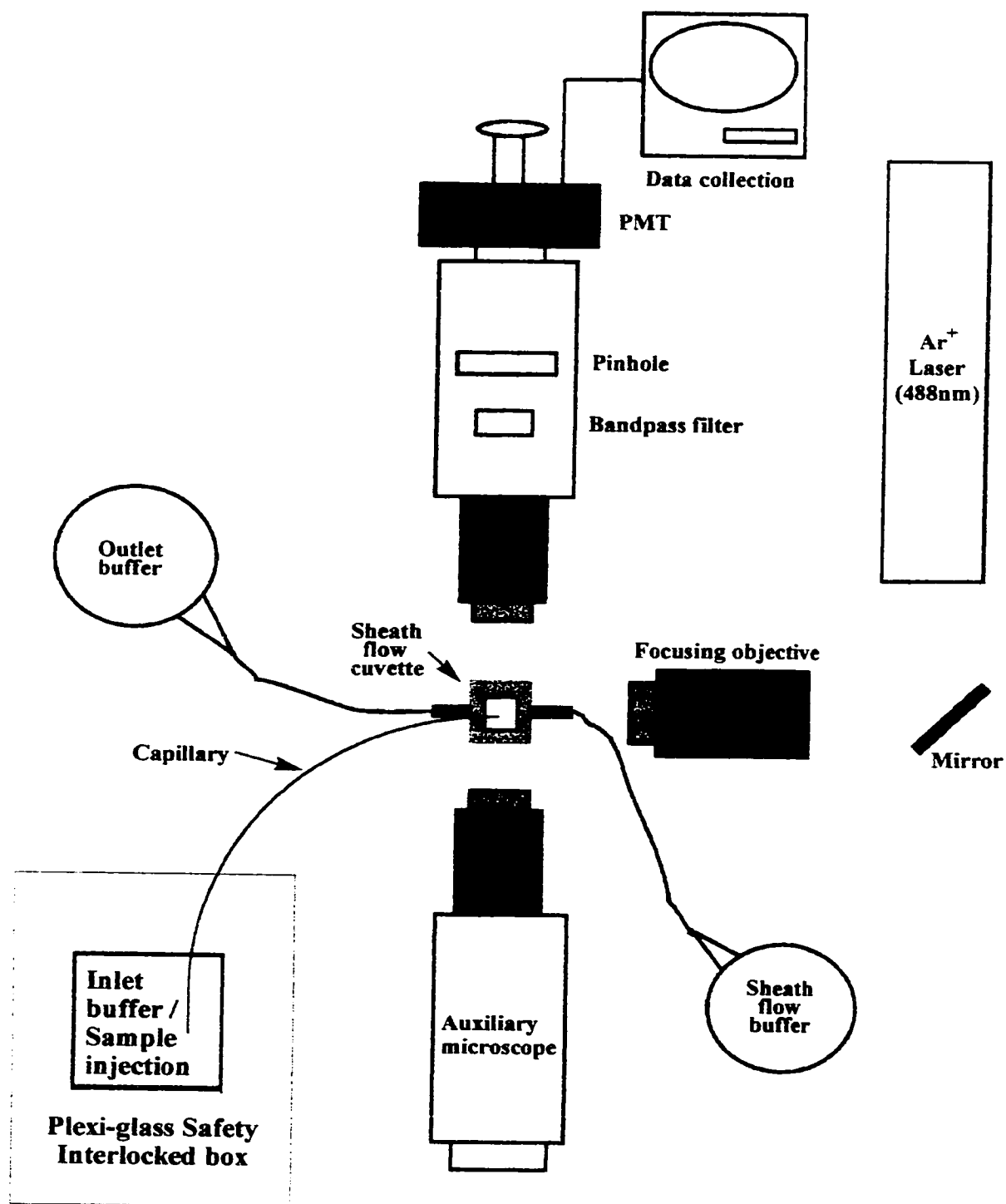
Brattleboro, VT, USA), and a 200 μm radius pinhole. The bandpass filters are used to block Raman scatter and the pinhole is used to restrict the field of view of the detector. Fluorescence is then detected by a R1477 photomultiplier tube (PMT) obtained from Hamamatsu (Bridgewater, Middlesex, N J, USA). The analogue PMT signal is collected at 10 Hz and digitized by a Macintosh IIsi via a NB-MIO-16XH-18 I/O board (National Instruments, Austin, TX, USA). The same input/output (I/O) board is used to control the power supply for CE. A LabVIEW (National Instruments, Austin, TX, USA) program was utilized to control the injection time and voltage, the running voltage, and data collection.

1.4 CE techniques

1.4.1 Capillary zone electrophoresis (CZE)

Jorgenson and Lukacs[7] discussed the theory and basis for capillary zone electrophoresis (CZE), the most commonly used CE format, in the early 1980s. CZE is the most popular format for analytical electrophoresis because it allows more reliable quantitation due to individual components in a complex matrix being physically separated from all other components. Various research groups have used CZE to analyze ionic species for this reason[46-58]. To perform a CZE separation, both ends of the capillary are immersed in electrolyte-filled reservoirs containing electrodes connected to a high voltage power supply. The capillary is filled with the same electrolyte solution as the reservoirs. Next, a sample plug is injected at the inlet end of the capillary and up to 30,000 V is applied to the system for separation. The ionic species in the sample plug migrate along the length of the capillary according to their electrophoretic mobilities

21

(direction and velocity) which are determined by their mass-to-charge ratio as described in Section 1.2.1 and illustrated in Figure 1.6. Thus, each sample produces a discrete sample zone (hence, the term CZE) similar to a chromatographic separation. A positive applied field will result in cations migrating out first, followed by neutrals and anions respectively. Varying the pH of the electrolyte used for separation can alter the electrophoretic mobility of a charged ion and the capillary current. As ionic species migrate through the outlet end of the capillary a detector observes them and an electronic signal is sent to a data acquisition/analysis system.

1.4.2 Cyclodextrin-modified CE separations

CE was first utilized for enantiomeric separations by Gassman in 1985.[9,59] Cyclodextrins (CDs) have been extensively used as buffer additives in the enantiomeric separation of analytes using CE because of their demonstrated success and ease of handling.[60-87] CDs are neutral, cyclic oligosaccharides containing 6, 7, or 8 glucose units (alpha, beta or gamma, respectively). The structural formula of cyclodextrins can be found in Figure 1.7. The most commonly used cyclodextrin in CE is the β-CD which has a cavity diameter of 0.78 nm. Since CDs are neutral, they do not influence the conductivity of the CE buffer systems. The shape of a CD is funnel-like with an outside surface and rim of secondary hydroxyl groups which create a hydrophilic shell and an internal cavity which contains no hydroxyl groups and thus, exhibits a hydrophobic character. The hydrophilic shell of CDs makes most of these compounds highly soluble in aqueous solution. The hydrophobic nature of CDs allows them to form inclusion complexes with aromatic and alkyl groups plus hydrophobic compounds. The chiral

22

Figure 1.6: Mobility of charged and uncharged molecules in an applied field.
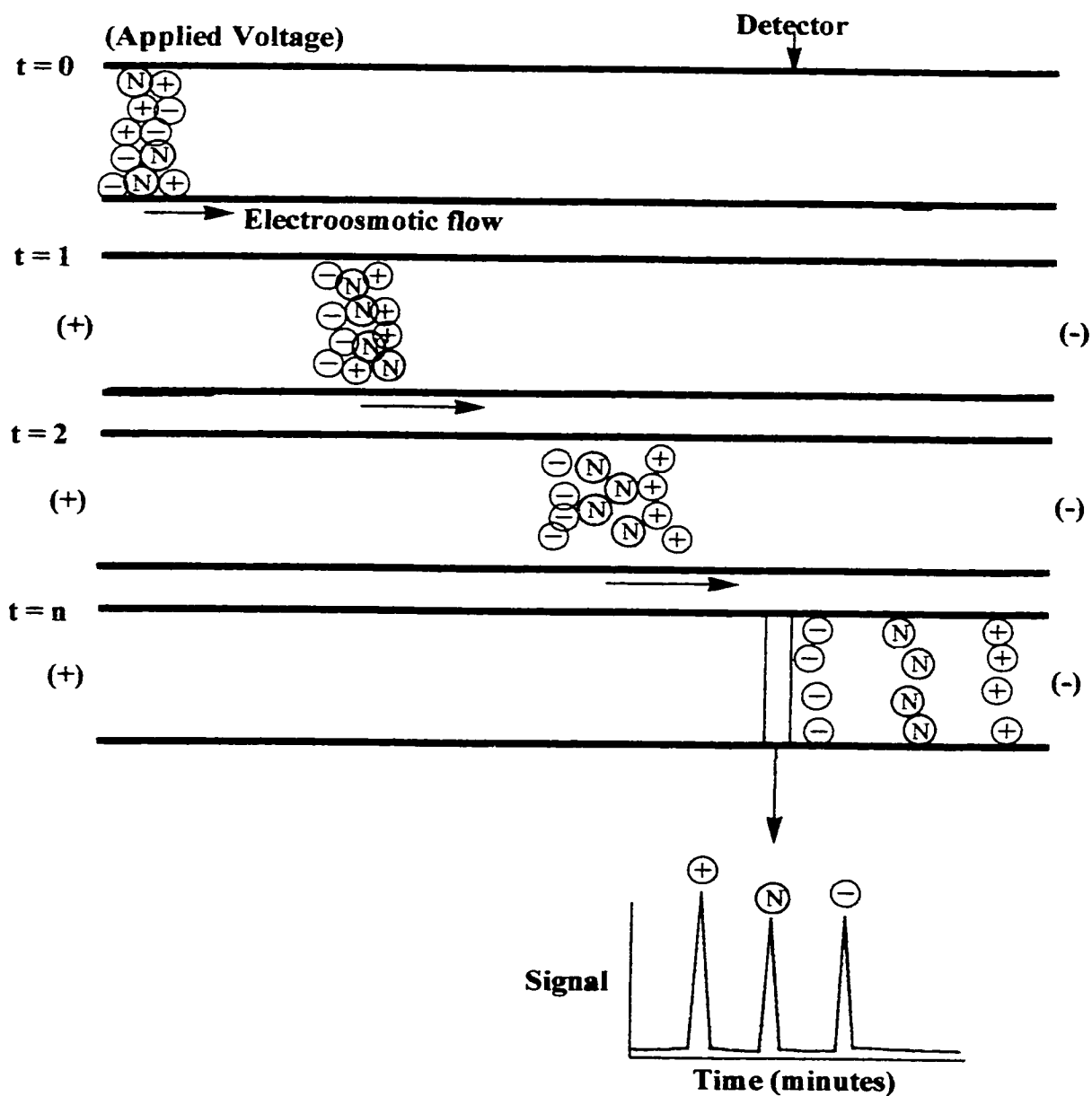
Figure 1.7: Structural formula of cyclodextrins, where n = 1, 2, or 3 for α, β, or γ-cyclodextrins, respectively, and R_1, R_2, and R_3 = H or CH_3 for native forms or their methyl ester derivatives.
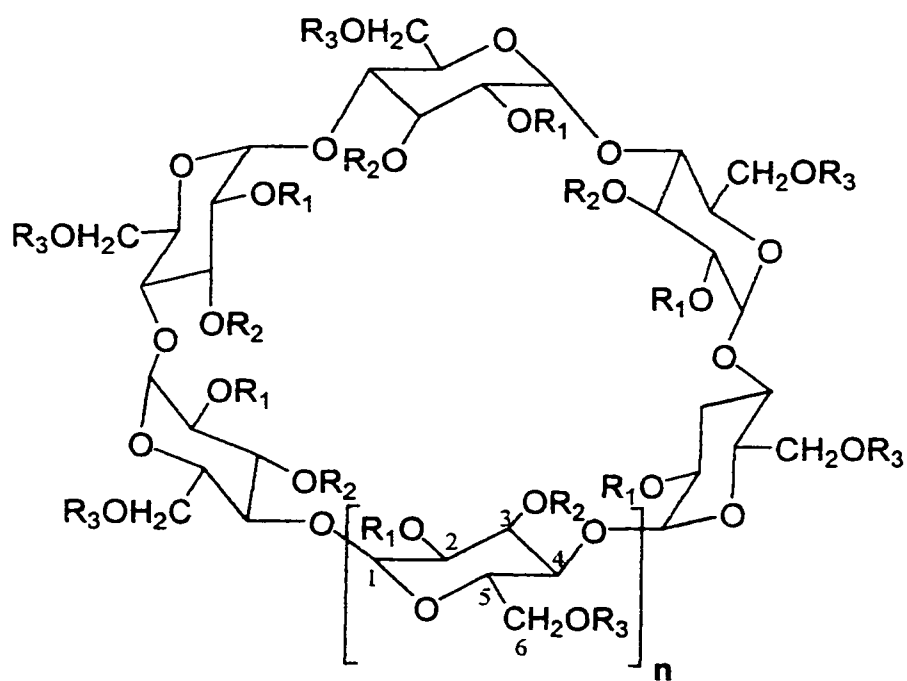
recognition in CDs comes from the asymmetric carbons of the glucose units with their hydroxyl groups present on the outside surface. Derivatization of the hydroxyl groups of CDs leads to changes in both selectivity and solubility. The complex stability between a CD and its guest molecule is governed by factors like hydrophobic interactions, solvation effects and hydrogen bonds. Substantial differences in the complex formation constant are found even for structurally similar compounds like enantiomers. For this reason, CDs are successfully employed for the separation of enantiomers.[60-87] Many excellent reviews[88-93] and books have been published on the use of cyclodextrins in CE.[37,39,94-97]

1.4.3 Micellar electrokinetic chromatography (MEKC)

MEKC is an adaptation of CE which was initially conceived by Terabe et al. in 1984 for the electrokinetic analysis of neutral compounds but is also effective for the separation of ionic compounds that have similar electrophoretic mobilities.[98,99] This technique utilizes a background electrolyte containing a surfactant at a concentration above its critical micelle concentration (CMC), called the micellar pseudostationary phase, with which solutes can interact. The CMC is defined as the concentration at which individual surfactant molecules begin to form molecular aggregates. The CMC of a surfactant can be determined by plotting conductivity versus concentration (Figure 1.8A). This plot indicates the CMC by a change in slope. Separation in MEKC is obtained due to differences in electrophoretic mobilities, as in CZE, as well as differences in partitioning. Depending on the nature of the surfactant, partitioning can be based on hydrophobicity, ionic attraction, and hydrogen bonding.

The most widely used MEKC system employs sodium dodecyl sulfate (SDS) as

Figure 1.8: A. Determination of CMC by plotting the conductivity versus

[surfactant], which will show a break at the CMC. B. Structure of

sodium dodecyl sulfate (SDS). C. SDS micelle.

A.

B.

Hydrophobic Tail Group   Hydrophilic Head Group

C.

The microenvironment
in the micelle has
properties of a nonpolar
solvent.

The head groups on
the exterior of the
micelle are charged
groups, most
commonly sulfate
(shown) and/or
tetraalkylammonium.
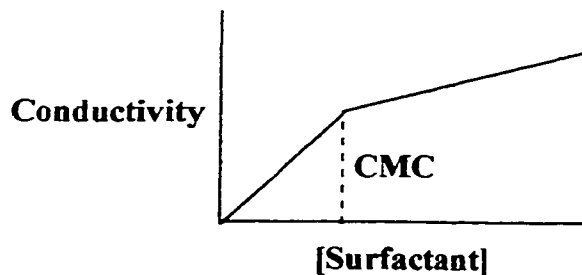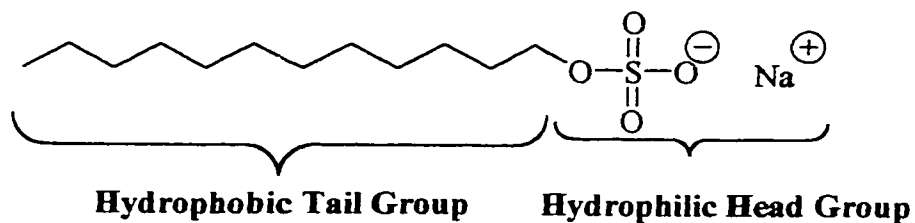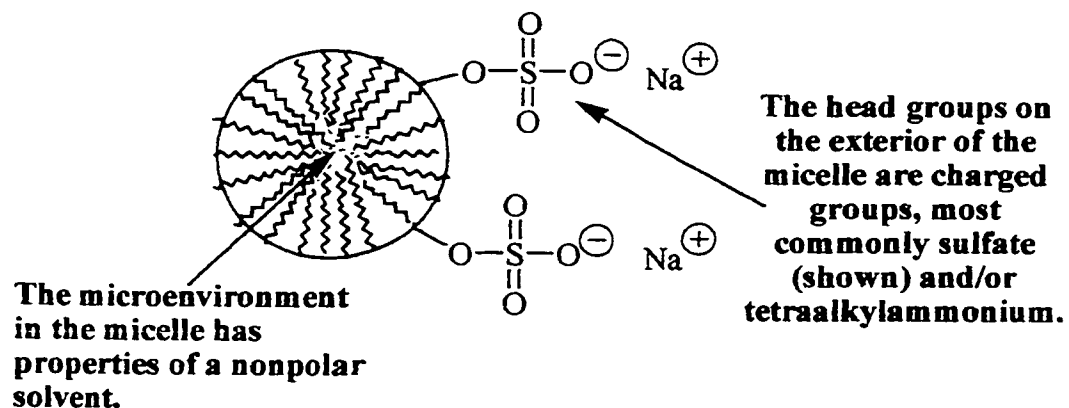
the surfactant. SDS is comprised of a hydrophobic tail and a negatively charged, hydrophobic head as shown in Figure 1.8B. As the concentration of SDS is increased to its CMC (~ 8 mM) individual surfactant molecules begin to interact with each other. The hydrophobic tails line up and exclude water, while the charged head groups orient toward the surface of the aggregates. The resulting micelles are hydrophobic on the surface but hydrophobic in the interior as shown in Figure 1.8C. Depending on concentration organic solvents will reduce the CMC or not allow micelles to form at all. The aggregation number, which is the average number of surfactant monomers per micelle, for SDS in water is approximately 62.

A schematic of MEKC can be found in Figure 1.9. In MEKC, surfactant is added to the background electrolyte at concentrations in excess of its CMC. Once the micelles are generated analytes will partition between the aqueous and the micellar phase depending on their hydrophobic character. Generally, the electroosmotic mobility is greater than the electrophoretic mobility of the micelles and thus, they move slowly toward the outlet end or cathode. Since micelles have an electrophoretic mobility a migration window is created. For neutral analytes, this migration window is defined by the electroosmotic flow or the time it takes an unretained neutral solute to traverse the column, t_0, and the micelle migration time, t_{mc}. A hydrophilic, neutral analyte with no affinity for the micellar phase will migrate at t_0 while one that spends all of its time with the micellar phase will migrate at t_{mc}. Neutral analytes which partition between the two phases depending on their hydrophobicity will migrate at an intermediate time. Charged species will display more complex interactions since they have the potential for electrophoretic migration and electroosmotic interaction with the micelles in addition to

27

Figure 1.9: Schematic of MEKC. The negative and positive charges at the capillary wall represent the ionized silanol groups and electrolyte ions, respectively. The single arrows represent mobility vectors, whereas double arrows represent a potential partitioning equilibrium for each of the solute charge types shown.

28
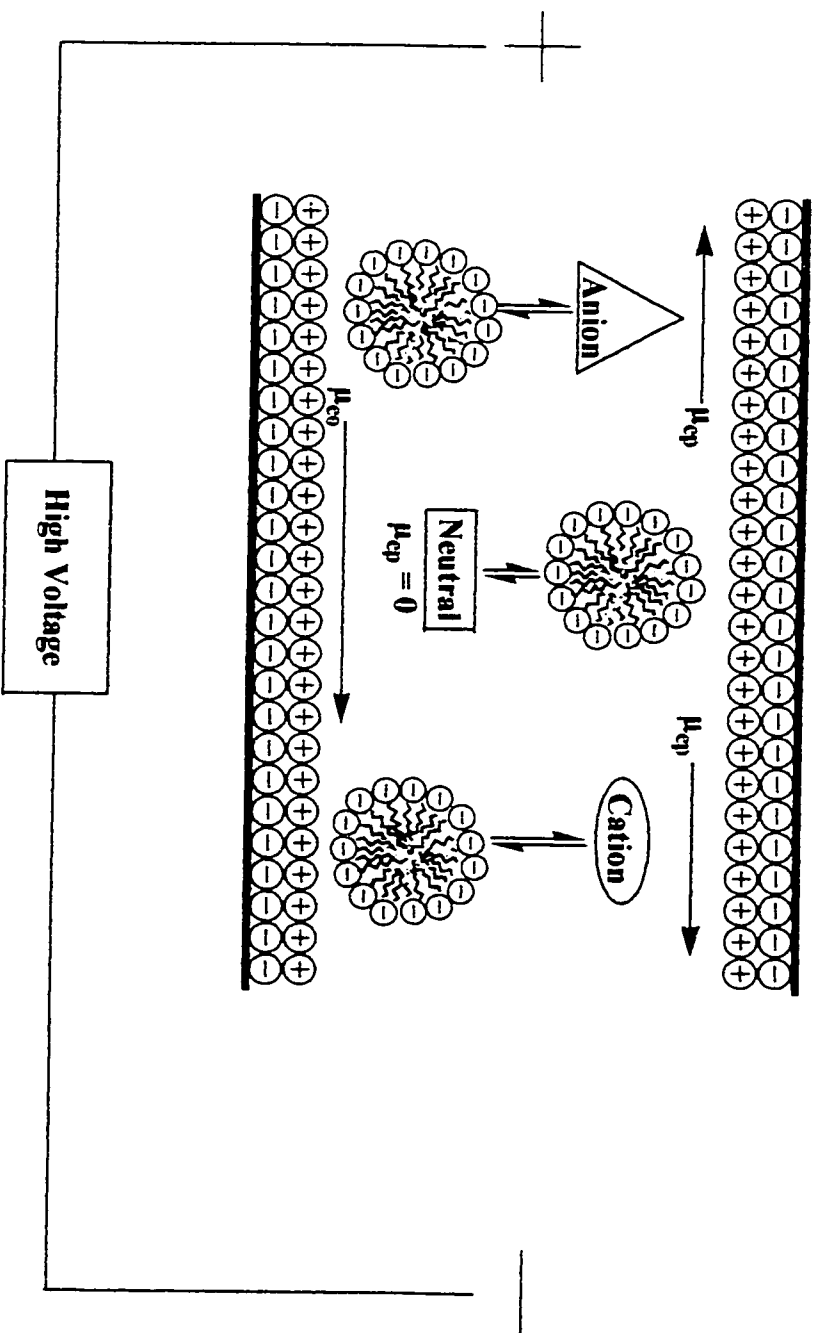
hydrophobic partitioning. MEKC has been used for the analysis of a variety of cationic, neutral, and anionic analytes.[1,51,52,55,100-125] The selectivity of MEKC can be expanded with the introduction of CDs to the micellar electrolyte solution. This technique is called cyclodextrin-modified MEKC (CD-MEKC) and has been used for various enantiomeric separations.[61,126-139]

1.4.4 Nonaqueous CE (NACE)

The majority of CZE separations are performed in aqueous media. The first CE to be described in a nonaqueous system was that of Walbroehl and Jorgenson in 1984.[140] Advantages of organic modifiers in CE are that they can be utilized to improve the selectivity, the resolution and the solubility of analytes, additives or electrolyte salts. They are also employed to reduce wall adsorption of the analytes, and to control EOF. Organic modifiers present in an electrolyte lead to a decrease in electroosmotic mobility. This is attributed to the increase in viscosity and the decrease in dielectric constant of the medium, but also the shifting of the pKa of the silanol groups to higher values. The most pronounced effect on the mobility of the analyte is achieved when an organic solvent is added to a medium whose pH is close to the pKa value of the analyte. Another major advantage of NACE compared to aqueous CE is the possibility of investigating water-insoluble substances. CDs have better solubility in water although lower binding constants between CDs and the enantiomer in the presence of an organic modifier have been observed. Disadvantages of the utilization of organic modifiers include the precipitation of electrolyte salts and erratic migration times. Other disadvantages of organic modifiers are that they exhibit toxicity and UV absorbance that interferes with

absorbance detection. Organic modifiers may also break down micelles and modify the electric double layer on the inner walls of capillaries. Methanol[141-146] is the most commonly used alcohol in NACE but acetonitrile[140,147], formamide[148-151], N-methylformamide[152], N,N-dimethylformamide[153,154], ethanol[155-159], 2-propanol[158-160] and most recently, 1-propanol[161] have been used as well. Investigations into NACE have been recently reviewed.[145,146,157,162,163]

1.5 Thesis overview

This thesis is divided into three parts. In Chapter 2 CZE and CD-CZE are used to analyze the toxin microcystin-LR that was fluorescently tagged at its arginine group with either 5-carboxytetramethylrhodamine, succinimidyl ester or 5-(bromomethyl)-fluorescein. The 5-(bromomethyl)fluorescein labelled microcystin-LR is then used to construct a fluorescent flow displacement immunoassay for the analysis of microcystin-LR.

Chapter 3 involves the development of a novel carbonyl-labelling reaction for use in CE-LIF. This carbonyl-labelling reaction is developed through the application of CZE. In Chapter 4 the developed carbonyl-labelling reaction is utilized to fluorescently derivatize a homologous series of linear saturated free fatty acids which are then analyzed using CZE, CD-CZE, MEKC and NACE.

1.6 References

1. L. Michaelis, *Biochemische Zeitschrift*, 16 (1909) 81.

2. A. Tiselius, *Transactions. Faraday Society*, 33 (1937) 524.

3. J. E. Edstrom, *Nature (London)*, 171 (1953) 908.

4. S. Hjertén, *Chromatographic Reviews*, 9 (1967) 122.

5. F. E. P. Mikkers, F. M. Everaerts, T. P. E. M. Verheggen, *Journal of Chromatography*, 169 (1979) 1.

6. F. E. P. Mikkers, F. M. Everaerts, T. P. E. M. Verheggen, *Journal of Chromatography*, 169 (1979) 11.

7. J. W. Jorgenson, K. D. Lukacs, *Analytical Chemistry*, 53 (1981) 1298.

8. J. W. Jorgenson, K. D. Lukacs, *Science*, 222 (1983) 266.

9. E. Gassman, J. E. Kuo, R. N. Zare, *Science*, 230 (1985) 813.

10. Y. F. Cheng, N. J. Dovichi, *Science*, 242 (1988) 562.

11. A. J. Tüdös, M. M. C. Van Dyck, H. Poppe, W. Th. Kok, *Chromatographia*, 37 (1993) 79.

12. J. Ye, P. Baldwin, *Analytical Chemistry*, 66 (1994) 2669.

13. Y. Guo, L. A. Colon, R. Dadoo, R. N. Zare, *Electrophoresis*, 16 (1995) 493.

14. J. Zhou, S. M. Lunte, *Electrophoresis*, 16 (1995) 98.

15. M. Albin, R. Weinberger, E. Sapp, S. Moring, *Analytical Chemistry*, 63 (1991) 417.

16. W. G. Kuhr, E. S. Yeung, *Analytical Chemistry*, 60 (1988) 1832.

17. S. Wu, N. J. Dovichi, *Journal of Chromatography*, 480 (1989) 141.

18. B. Nickerson, J. W. Jorgenson, *Journal of High Resolution Chromatography and Chromatography Communications*, 11 (1988) 878.

19. J. V. Sweedler, J. B. Shear, H. A. Fishman, R. N. Zare, R. H. Scheller, *Analytical Chemistry*, 63 (1991) 496.

20. H. Swerdlow, R. Gesteland, *Nucleic Acids Research*, 18 (1990) 1415.

21. H. Swerdlow, S. Wu, H. R. Harke, N. J. Dovichi, *Journal of Chromatography*, 516 (1990) 61.

22. H. Swerdlow, J. Z. Zhang, D. Y. Chen, H. R. Harke, R. Grey, S. Wu, N. J. Dovichi, *Analytical Chemistry*, 63 (1991) 2835.

23. J. V. Sweedler, J. B. Shear, H. A. Fishman, R. N. Zare, R. H. Sheller, *Analytical Chemistry*, 63 (1991) 496.

24. H. E. Schwartz, K. J. Ulfelder, F. T. A. Chen, S. L. Pentoney, *Journal of Capillary Electrophoresis*, 1 (1994) 36.

25. S. J. Williams, D. M. Goodall, K. P. Evans, *Journal of Chromatography*, 629 (1993) 379.

26. T. Bergmann, B. Agerberth, H. Jörnvall, *FEBS Letters*, 283 (1991) 100.

27. P. F. Cancalon, *LC-GC*, 11 (1993) 748.

28. P. F. Cancalon, C. R. Bryan, *Journal of Chromatography A*, 652 (1993) 555.

29. M. J. Thornton, C. W. Klampfl, J. S. Fritz, *Journal of High Resolution Chromatography*, 20 (1997) 647.

30. Y. H. Lee, T. I. Lin, *Journal of Chromatography A*, 680 (1994) 287.

31. Y. H. Lee, T. I. Lin, *Journal of Chromatography A*, 716 (1995) 335.

32. D. Y. Chen, N. J. Dovichi, *Journal of Chromatography B*, 657 (1994) 265.

33. D. Y. Chen, K. Adelhelm, X. L. Cheng, N. J. Dovichi, *Analyst*, 119 (1994) 349.

34. J. Y. Zhao, N. J. Dovichi, O. Hindsgaul, S. Gosselin, M. M. Palcic, *Glycobiology*, 4 (1994) 239.

35. A. T. Timperman, K. Khatib, J. V. Sweedler, *Analytical Chemistry*, 67 (1995) 139.

36. D. Y. Chen, N. J. Dovichi, *Analytical Chemistry*, 68 (1996) 690.

37. J. P. Landers, in J. P. Landers (Editor), *Handbook of Capillary Electrophoresis 2nd Edition*, CRC Press, Boca Raton, 1996.

38. T. Wehr, R. Rodríguez-Díaz, M. Zhu, in J. Cazes (Editor), *Capillary Electrophoresis of Proteins. Chromatographic Science Series*, Volume 80, MarcelDekker, New York, 1998.

39. P. Camilleri (Editor), *Capillary Electrophoresis Theory and Practice*, CRC Press, Boca Raton, 1993.

40. H. Z. Helmholtz, *Annalen der Physik und Chemie*, 7 (1879) 337.

41. V. R. Meyer, *Journal of Chromatography*, 334 (1985) 197.

42. J. C. Sternberg, *Advances in Chromatography*, 2 (1996) 206.

43. D. McManigill, S. A. Swedberg, in T. Hugli (Editor), *Techiques In Protein Chemistry*, Academic Press, San Diego, 1989.

44. C. Gelfi, M. Curio, R. G. Righetti, R. Sebastiano, A. Citterio, H. Ahmadzadeh, N. J. Dovichi, *Electrophoresis*, 19 (1998) 1677.

45. L. R. Snyder, J. J. Kirkland, *Introduction to Modern Liquid Chromatography*, Wiley, New York, 1979.

46. L. Krivánková, S. Krásensky, P. Bocek, *Electrophoresis*, 17 (1996) 1959.

47. U. Jegle, *Journal of Chromatography A*, 652 (1993) 495.

48. S. Boonkerd, M. R. Detavernier, Y. Michotte, *Journal of Chromatography A*, 670 (1994) 209.

49. H. L. Shi, Y. F. Ma, J. H. Humphrey, N. E. Craft, *Journal of Chromatography B*, 665 (1995) 89.

50. J. Schiewe, S. Gobel, M. Schwartz, J. Neubert, *Journal of Pharmaceutical and Biomedical Analysis*, 14 (1996) 435.

51. L. Fotsing, M. Fillet, I. Bechet, P. Hubert, J. Crommen, *Journal of Pharmaceutical and Biomedical Analysis*, 15 (1997) 1113.

52. L. Fotsing, M. Fillet, P. Chiap, P. Hubert, J. Crommen, *Journal of Chromatography A*, 853 (1999) 391.

53. S. C. Jacobson, R. Hergenröder, L. B. Koutny, J. M. Ramsey, *Analytical Chemistry*, 66 (1994) 1114.

54. S. C. Jacobson, R. Hergenröder, L. B. Koutny, R. J. Warmack, J. M. Ramsey, *Analytical Chemistry*, 66 (1994) 1107.

55. G. Gutnikov, W. Beck, H. Engelhardt, *Journal of Microcolumn Separations*, 6 (1994) 565.

56. R. Roldan-Assad, P. Gareil, *Journal of Chromatography A*, 708 (1995) 339.

57. L. B. Koutny, D. Schmalzing, T. A. Taylor, M. Fuchs, *Analytical Chemistry*, 68 (1996) 18.

58. J. Collet, P. Gareil, *Journal of Capillary Electrophoresis*, 3 (1996) 77.

59. C. R. McCurdy, T. G. Venkateshwaran, J. W. Beach, J. T. Stewart, *Electrophoresis*, 20 (1999) 212.

60. T. J. Ward, *Analytical Chemistry*, 66 (1994) A633.

61. S. Terabe, *Trends in Analytical Chemistry*, 8 (1989) 129.

62. S. Fanali, P. Bocek, *Electrophoresis*, 11 (1990) 757.

63. A. Guttman, A. Aumatell, S. Brunet, N. Cooke, *American Laboratory*, 27 (1995) 18.

64. Z. Whang, A. Huang, Y. Sun, *Journal of High Resolution Chromatography*, 19 (1996) 478.

65. R. J. Tait, D. J. Skanchy, D. O. Thompson, N. C. Chetwyn, D. A. Dunshee, R. A. Rajewsky, V. J. Stella, J. F. Stobaugh, *Journal of Pharmaceutical and Biomedical Analysis*, 10 (1992) 615.

66. A.M. Stalcup, K. H. Gahm, *Analytical Chemistry*, 68 (1996) 1360.

67. J. B. Vincent, A. D. Sokolowski, T. V. Nguyen, G. Vigh, *Analytical Chemistry*, 69 (1997) 4226.

68. J. B. Vincent, D. Kirby, T. V. Nguygen, G. Vigh, *Analytical Chemistry*, 69 (1997) 4419.

69. H. Cai, T. V. Nguyen, G. Vigh, *Analytical Chemistry*, 70 (1998) 580.

70. F. O'Keeffe, S. A. Shamsi, R. Darcy, P. Schwinte, I. M. Warner, *Analytical Chemistry*, 69 (1997) 4773.

71. J. L. Haynes, S. A. Shamsi, F. O'Keeffe, R. Darcy, I. M. Warner, *Journal of Chromatography A*, 803 (1998) 261.

72. L. J. Jin, Y. Wang, R. Xu, M. L. Go, H. K. Lee, S. F. Y. Li, *Electrophoresis*, 20 (1999) 198.

73. Y. Y. Rawjee, R. L. Williams, L. A. Buckingham, G. Vigh, *Journal of Chromatography A*, 688 (1994) 273.

74. Y. Y. Rawjee, R. L. Williams, G. Vigh, *Journal of Chromatography A*, 680 (1994) 599.

75. A. Guttman, S. Brunet, C. Jurado, N. Cooke, *Chirality*, 7 (1995) 409.

76. B. Chankvetadze, *Journal of Chromatography A*, 792 (1997) 269.

77. L. A. Holland, N. P. Chetwyn, M. D. Perkins, S. M. Lunte, *Pharmaceutical Research*, 14 (1997) 372.

78. J. Bojarski, *Chemia Analityczna (Warsaw)*, 42 (1997) 139.

79. H. Nishi, S. Terabe, *Journal of Chromatography A*, 735 (1996) 3.

80. H. Nishi, *Journal of Chromatography A*, 735 (1996) 57.

81. F. Bressolle, M. Audran, T. N. Pham, J. J. Vallon, *Journal of Chromatography B*, 687 (1996) 303.

82. R. A. Rajewske, V. J. Stella, *Journal of Pharmaceutical Science*, 85 (1996) 1142.

83. S. Topiol, M. Sabio, *Enantiomer*, 1 (1996) 251.

84. M. Novotny, H. Soini, M. Stefansson, *Analytical Chemistry*, 66 (1994) 646A.

85. S. Terabe, K. Otsuka, H. Nishi, *Journal of Chromatography A*, 666 (1994) 295.

86. H. J. Issaq, *Instrumentation Science and Technology*, 22 (1994) 119.

87. R. Kuhn, S. Hoffstetter-Kuhn, *Chromatographia*, 34 (1992) 505.

88. R. L. St. Claire, *Analytical Chemistry*, 68 (1996) 569.

89. S. Fanali, *Journal of Chromatography A*, 735 (1996) 77.

90. B. Chankvetadze, G. Endresz, G. Blaschke, *Chemical Society Reviews*, 25 (1996) 141.

91. R. Vespalec, P. Bocek, *Electrophoresis*, 18 (1997) 843.

92. S. Fanali, *Journal of Chromatography A*, 792 (1997) 227.

93. G. Vigh, A. D. Sokolowski, *Electrophoresis*, 18 (1997) 2305.

94. B. Chankvetadze, *Capillary Electrophoresis in Chiral Analysis*, John Wiley, New York, 1997.

95. H. Engelhardt, W. Beck, T. Schmitt, *Capillary Electrophoresis*, Vieweg, Wiesbaden, 1996.

96. S. Fanali, *An Introduction to Chiral Analysis by Capillary Electrophoresis*, Bio-Rad Laboratories, Richmond, 1995.

97. S. F. Y. Li, *Capillary Electrophoresis, Principles, Practice and Applications*, Elsevier, Amsterdam, 1992.

98. S. Terabe, K. Otsuka, K. Ichikawa, A. Tsuchiyo, T. Ando, *Analytical Chemistry*, 56 (1984) 111.

99. S. Terabe, K. Otsuka, T. Ando, *Analytical Chemistry*, 57 (1985) 834.

100. M. Khaledi, S. Smith, J. Strasters, *Analytical Chemistry*, 63 (1991) 1820.

101. J. Esteve-Romero, I. Escrig-Tena, E. F. Simó-Alfonso, G. Ramis-Ramos, *Analyst*, 124 (1999) 125.

102. D. E. Burton, M. J. Sepaniak, J. Maskarinec, *Journal of Chromatography*, 24 (1986) 347.

103. S. Fujiwara, S. Iwase, S. Honda, *Journal of Chromatography*, 447 (1988) 133.

104. H. Nishi, N. Tsumagari, T. Kakimoto, S. Terabe, *Journal of Chromatography*, 465 (1989) 331.

105. S. Kobayashi, T. Ueda, M. Kikumoto, *Journal of Chromatography*, 480 (1989) 179.

106. C. P. Ong, C. L. Ng, H. K. Lee, S. F. Y. Li, *Journal of Chromatography*, 547 (1991) 419.

107. Y. F. Yik, H. K. Lee, S. F. Y. Li, S. B. Khoo, *Journal of Chromatography*, 585 (1991) 139.

108. S. Boonherd, M. R. Detaevernier, Y. Michotte, *Journal of Chromatography A*, 670 (1994) 209.

109. G. Dinelli, A. Bonetti, *Electrophoresis*, 15 (1994) 1147.

110. S. Terabe, H. Utsumi, K. Otsuka, T. Ando, *Journal of High Resolution Chromatography*, 9 (1986) 666.

111. A. Kunkel, H. Wätzig, *Electrophoresis*, 20 (1999) 2379.

112. J. Collet, P. Gareil, *Journal of Chromatography A*, 792 (1997) 165.

113. I. Rodriguez, H. K. Lee, S. F. Y. Li, *Electrophoresis*, 20 (1999) 118.

114. T. Watanabe, N. Hasegawa, A. Yamamoto, S. Nagai, S. Terabe, *Bunseki Kagaku*, 45 (1996) 765.

115. T. Watanabe, N. Hasegawa, A. Yamamoto, S. Nagai, S. Terabe, *Bioscience, Biotechnology and Biochemistry*, 61 (1997) 1179.

116. T. Watanabe, A. Yamamoto, S. Nagai, S. Terabe, *Analytical Science*, 13 (1997) 571.

117. T. Watanabe, A. Yamamoto, S. Nagai, S. Terabe, *Food Science and Technology International (Tokyo)*, 4 (1998) 54.

118. T. Watanabe, A. Yamamoto, S. Nagai, S. Terabe, *Analytical Science*, 14 (1998) 839.

119. T. Watanabe, A. Yamamoto, S. Nagai, S. Terabe, *Journal of Chromatography A*, 793 (1998) 409.

120. T. Watanabe, R. Nishiyama, A. Yamamoto, S. Nagai, S. Terabe, *Analytical Science*, 14 (1998) 435.

121. T. Watanabe, T. K. Mazumder, A. Yamamoto, S. Nagai, S. Arimoto-Kobayashi, H. Hayatsu, S. Terabe, *Mutation Research*, 444 (1999) 75.

122. M. Idei, E. Györffy, É. Kiss, L. Örfi, J. Seprödi, B. Tamás, F. Hollósy, G. Mészáros, G. Kéri, *Electrophoresis*, 20 (1999) 1561.

123. M. Jussila, S. Sundberg, A. Hopia, M. Mäkinen, M.-L. Riekkola, *Electrophoresis*, 20 (1999) 111.

124. S. Viglio, S. Valentini, G. Zanaboni, G. Cetta, A. De Gregorio, P. Iadarola, *Electrophoresis*, 20 (1999) 138.

125. M. Molina, S. Pérez-Bendito, M. Silva, *Electrophoresis*, 20 (1999) 3439.

126. A. Amini, E. Jäverfalk, S. Bastami, D. Westerlund, *Electrophoresis*, 20 (1999) 204.

127. S. Terabe, Y. Miyashita, O. Shibata, E. R. Barnhart, L. R. Alexander, D. J. Patterson, B. L. Karger, K. Hosoya, N. Tanaka, *Journal of Chromatography*, 516 (1990) 23.

128. H. Nishi, T. Fukuyama, S. Terabe, *Journal of Chromatography*, 553 (1991) 503.

129. L. J. Jin, I. Rodriguez, S. F. Y. Li, *Electrophoresis*, 20 (1999) 1538.

130. T. Ueda, R. Mitchell, F. Kitamura, T. Metcalf, T. Kuwana, A. Nakamoto, *Journal of Chromatography*, 593 (1992) 265.

131. K. DeSilva, T. Kuwana, *Biomedical Chromatography*, 11 (1997) 230.

132. K. C. Chan, G. M. Muschik, H. J. Isaaq, *Electrophoresis*, 16 (1995) 504.

133. H. Wan, P. E. Andersson, A. Engstrom, L. G. Blomberg, *Journal of Chromatography A*, 704 (1996) 179.

134. H. Wan, L. G. Blomberg, *Journal of Chromatographic Science*, 34 (1996) 540.

135. H. Wan, A. Engstrom, L. G. Blomberg, *Journal of Chromatography A*, 731 (1996) 283.

136. S. Terabe, Y. Miyashita, Y. Ishihama, O. Shibata, *Journal of Chromatography*, 636 (1993) 47.

137. C. F. Tsai, C. F. Li, H. M. Chang, *Journal of Agricultural Food Chemistry*, 46 (1998) 979.

138. E. Ban, S. Choi, J. A. Lee, D. S. Lho, Y. S. Yoo, *Journal of Chromatography A*, 853 (1999) 439.

139. K. Otsuka, H. Hayashibara, S. Yamauchi, J. P. Quirino, S. Terabe, *Journal of Chromatography A*, 853 (1999) 413.

140. Y. Walbroehl, J. W. Jorgenson, *Journal of Chromatography*, 315 (1984) 135.

141. M. Chiari, E. Kenndler, *Journal of Chromatography A*, 716 (1995) 303.

142. H. Salimi-Moosavi, R. M. Cassidy, *Analytical Chemistry*, 68 (1996) 293.

143. A. M. Stalcup, K. H. Gham, *Journal of Microcolumn Separations*, 8 (1996) 145.

144. T. Okada, *Journal of Chromatography A*, 695 (1995) 309.

145. I. E. Valkó, H. Sirén, M. L. Riekkola, *LC-GC*, 15 (1997) 560.

146. I. Bjørnsdottir, J. Tjørnelund, S. H. Hansen, *Electrophoresis*, 19 (1998) 2179.

147. S. H. Hansen, J. Tjørnelund, I. Bjørnsdottir, *Trends in Analytical Chemistry*, 5 (1996) 175.

148. R. S. Sahota, M. G. Khaledi, D. Shea, *Analytical Chemistry*, 66 (1994) 1141.

149. I. E. Valkó, H. Sirén, M. L. Riekkola, *Journal of Chromatography A*, 737 (1996) 263.

150. I. E. Valkó, H. Sirén, M. L. Riekkola, Chromatographia, 43 (1996) 242.

151. G. N. W. Leung, H. P. O. Tang, T. S. C. Tso, T. S. M. Wan, *Journal of Chromatography A*, 738 (1996) 141.

152. M. Jansson, J. Roeraade, *Chromatographia*, 40 (1995) 163.

153. H. Salimi-Moosavi, R. M. Cassidy, *Analytical Chemistry*, 67 (1995) 1067.

154. J. Li, J. S. Fritz, *Electrophoresis*, 20 (1999) 84.

155. H. Salimi-Moosavi, R. M. Cassidy, *Journal of Chromatography A*, 790 (1997) 185.

156. I. E. Valkó, S. P. Porras, M. L. Riekkola, *Journal of Chromatography A*, 813 (1998) 179.

157. M. L. Riekkola, S. K. Wiedmer, I. E. Valkó, H. Sirén, *Journal of Chromatography A*, 792 (1997) 13.

158. A. M. Germon, R. D. Edwards, M. R. Euerby, C. M. Johnson, *Pharmaceutical and Pharmacological Communications*, 4 (1998) 189.

159. I. Bjørnsdottir, S. H. Hansen, *Journal of Biochemical and Biophysical Methods*, 38 (1999) 155.

160. K. Raith, R. Wolf, J. Wagner, R. H. H. Neubert, *Journal of Chromatography A*, 802 (1998) 185.

161. I. E. Valkó, H. Sirén, M. L. Riekkola, *Journal of Microcolumn Separations*, 11 (1999) 199.

162. I. E. Valkó, H. Sirén, M. L. Riekkola, *LC-GC International*, 10 (1997) 190.

163. K. Sarmini, E. Kenndler, *Journal of Chromatography A*, 792 (1997) 3.

Chapter 2

The Development of a Fluorescent Flow Displacement Immunoassay for the Analysis of Microcystin-LR and the Development of an Arginine-Labelling Reagent

2.1 Introduction

2.1.1 Microcystins

Eutrophication of freshwater causes the occurrence of water bloom of cyanobacteria in many countries in the world.[1] Since the last century, serious illness and death have been reported amongst domestic and wild animals owing to ingestion of toxins produced by cyanobacteria.[1,2] The most commonly reported toxins that are released to the water column during the collapse of toxic cyanobacterial blooms are the hepatotoxins, the largest group being heptapeptides known as microcystins.[3-7] Microcystins are monocyclic heptapeptides produced by cyanobacteria within the genera *Microcystis, Anabaena, Oscillatoria* or *Nostoc*.[8-13] The structures of the microcystins (Figure 2.1) consist of two variable L-amino acids plus three D-amino acids (alanine, *erythro*-β-methylaspartic acid (*MeASP*) and glutamic acid) plus the two unusual amino acids, *N*-methyldehydroalanine (*Mdha*) and a hydrophobic 20 carbon chain unique to these toxins, 3-amino-9-methoxy-10-phenyl-2,6,8-trimethyldeca-4(*E*)6(*E*)-dienoic acid (*Adda*).[7,8,11,14] There are now over 50 different known microcystins which differ primarily in the two L-amino acids plus methylation and demethylation on the two unusual amino acids.[11,14-16] These microcystins all contain *Adda*, which is essential for expression of their biological activity. The toxins are named using the one-letter abbreviations to indicate the two variable amino acids present.[15] For example, the main toxin responsible for the hepatotoxicity in the blooms of cyanobacteria in the Northern Hemisphere and thus, the most widely studied microcystin, is microcystin-LR which contains the two L-amino acids leucine (L) and arginine (R).[7,15,16]

Figure 2.1 : Structure of microcystin-LR. Besides the two variable L-amino acids, in this case leucine and arginine, the microcystins contain three D-amino acids and the two unusual amino acids N-methyldehydro-alanine (*Mdha*) and 3-amino-9-methoxy-10-phenyl-2,6,8-trimethyldeca-4(E)6(E)-dienoic acid (*Adda*).
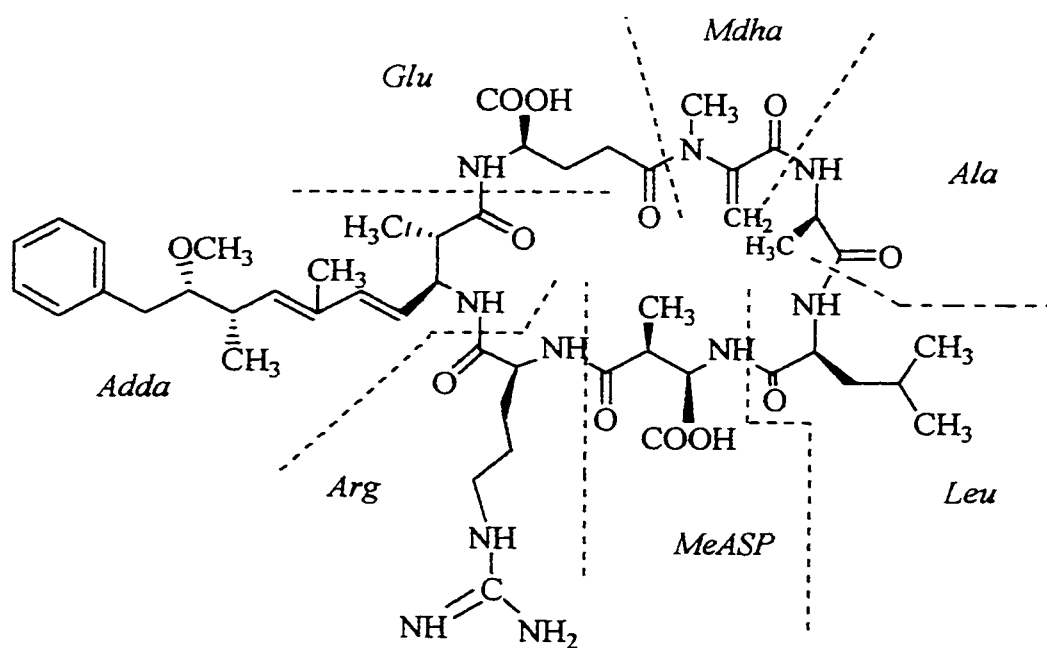
Acute microcystin toxicosis in mammals is characterized histologically by the rounding

and separation of hepatocytes, the disruption of hepatic cords and sinusoidal

endothelium, hepatocyte necrosis and degeneration, and severe intrahepatic

haemorrhaging leading to lethal hypovolemic shock or liver failure.[2,16-23] Among the

species that have died following ingestion of microcystin-containing algae are dogs,

livestock, wild mammals, birds and fish.[17,21,24-26] Hazards to human health and domestic

animals may result from chronic exposure via contaminated water supplies.[21,27]

Microcystins also inhibit strongly and specifically the serine and threonine protein

phosphatases 1 [16,22] and 2A [11,16,28,29] *in vivo* and *in vitro*.[30-33] Protein phosphatases 1 and

2A are two of the major protein phosphatases in the cytosol of mammalian cells and have

been shown to be important in tumour suppression.[7,34] The inhibition of protein

phosphatase 1 and 2A activities by microcystin-LR is similar to that of the known protein

phosphatase inhibitor and tumour promoter okadaic acid.[13,35] This inhibitory action may

explain the effects of microcystins as promoters of primary liver cancer in humans

exposed to long-term low doses of the cyclic peptide toxins through drinking

water.[16,22,23,33] The concentration of microcystin-LR causing 50% inhibition of

recombinant protein phosphatase 1 activity (IC_{50}) is only about 0.1 − 0.3 nM, which is

below the detection limit of most available quantitative analytical methods for these

toxins.[14,28]

Since microcystins are potent hepatotoxins and cancer promoters for humans and

animals, the need for a reliable, rapid and sensitive method for the identification and

quantification of microcystins in the environment has become of great importance. The

analytical methods for the measurement of microcystins fall into three categories:

bioassays, chemical, and biochemical methods. The disadvantages of these methods are as follows: they are not sensitive enough, they are expensive to perform (e.g., the mouse bioassay), and, if they are reasonably sensitive, they require highly sophisticated equipment (HPLC techniques, fast atom bombardment mass spectrometry, etc.).[36,37]

Analytical methods including bioassay, chemical, and biochemical methods as well as the overall analytical strategy have been reviewed.[13,38,39] Bioassays using mouse[13,40] or plant (*Sinapis alba* L.)[13,36] have been used in screening for these hepatotoxins but were found to be non-specific, time consuming (8 days) or did not detect multiple hepatotoxins in one sample.[41] Biochemical methods include enzyme-linked immunosorbent assay (ELISA)[13,14,42] (the most sensitive method to date) and protein phosphatase inhibition assay (PPIA)[14,43]. These are advantageous screening methods due to high sensitivity and the quick treatment of a large number of samples despite the poor identification ability and the potential for false positives.[13] ELISA is insensitive to the different forms of toxins because antibodies that are raised against one form of microcystin recognize the common *Adda* group in microcystins and therefore cross-react with several other microcystins. The sensitivity limit for ELISA was first in the 0.5 - 10 ng/mL[44] range and later was improved to 95 pg/mL[45]. Although the sensitivity of this method has progressively increased, these procedures give no information on the viable biological activity of the toxins.[16]

Chemical analyses of microcystins are usually conducted on reversed-phase high performance liquid chromatography (RP-HPLC) with UV detection at 238 nm.[34,46] The UV detection limit for microcystins is a few nanograms in most HPLC systems.[3,38-40,46] HPLC with diode array detection[7,19,47-50] or electrochemical detection[13,51], LC-mass

46

spectrometry (LC-MS)[13,35,46,52], capillary electrophoresis (CE)[13,52], and CE-MS[13,52] have also been used as chemical methods for the identification and quantification of microcystins.

In this work capillary zone electrophoresis with laser-induced fluorescence detection (CZE-LIF) and with laser-induced fluorescence polarization detection (CZE-LIFP) were investigated as analytical methods for the analysis of microcystin-LR.

2.1.2 Fluorescent labelling

A fluorescent label with an excitation wavelength in the visible region of the spectrum (> 400 nm) is preferable in bioanalysis. This is due to the fact that excitation in the visible spectrum is relatively free of interferences from endogenous compounds present in biological matrices (serum, plasma, etc.)[53,54]. For a fluorescent label to be used in fluorescence polarization the label should have a high quantum yield for sensitive fluorescence detection and a sufficiently long fluorescence lifetime for there to be a detectable difference between the fluorescence depolarizations associated with the free and antibody-bound labelled antigen, respectively.[55] The fluorescent label should also possess acceptable photo- and thermal stabilities when exposed to the laser radiation. High molar absorptivity (ε), quantum yield (ϕ), reasonably high Stokes shift and a single derivatizable functional group are also desirable.[56] The two fluorescent labels that were used in this work were 5-carboxytetramethylrhodamine, succinimidyl ester (5-TAMRA-SE) and 5-(bromomethyl)fluorescein (5-BMF).

The dye 5-TAMRA-SE is a succinimidyl ester and is among the most photostable fluorescent labelling reagents available. The structure of this dye can be found in

47

Figure 2.2. Moreover, its spectrum is not affected by changes in pH between 4 and 10 which is an important advantage over the fluoresceins for many biological applications.[57] 5-TAMRA-SE is an important fluorophore for preparing protein conjugates. Bioconjugates from succinimidyl esters are more stable and often more fluorescent than fluorescein conjugates. This dye is efficiently excited by the 543 nm spectral line of the green He-Ne laser, which is increasingly being used for analytical instrumentation.[57] The absorption and fluorescence emission spectra of 5-TAMRA dissolved in methanol and pH 7 buffer are illustrated in Figure 2.3. These emission spectra are from a product that is closely related, but not identical to 5-TAMRA-SE. Differences between the spectra in Figure 2.3 and those of 5-TAMRA-SE are not expected to be significant according to Molecular Probes.[57] The dye 5-TAMRA-SE has an excitation wavelength at 546 nm and an emission wavelength of 579 nm. The molar absorptivity coefficient of this dye is 89,000 L mol^{-1} cm^{-1} at 546 nm. Unfortunately, the laboratory of our collaborator on this project, Dr. X.C. Le from the Department of Public Health at the University of Alberta, was not equipped with a He-Ne laser. Consequently, the microcystin-LR had to be labelled with a fluorophore that could be excited by an argon ion (Ar$^+$) laser. Ar$^+$ lasers are useful for the quantitation of analytes in biological matrices because of the high power output and the multiple emission lines available in the blue-green region of the spectrum.[54]

The dye that was chosen to label microcystin-LR and that could be excited by an Ar$^+$ laser was the alkyl halide, 5-BMF. The structure of 5-BMF can be found in Figure 2.4. In previous work, 5-BMF has been shown to be a very useful precolumn derivatization reagent suitable for LIF.[54,58] This dye is usually a carboxylic acid labelling

Figure 2.2: Structure of 5-carboxytetramethylrhodamine, succinimidyl ester
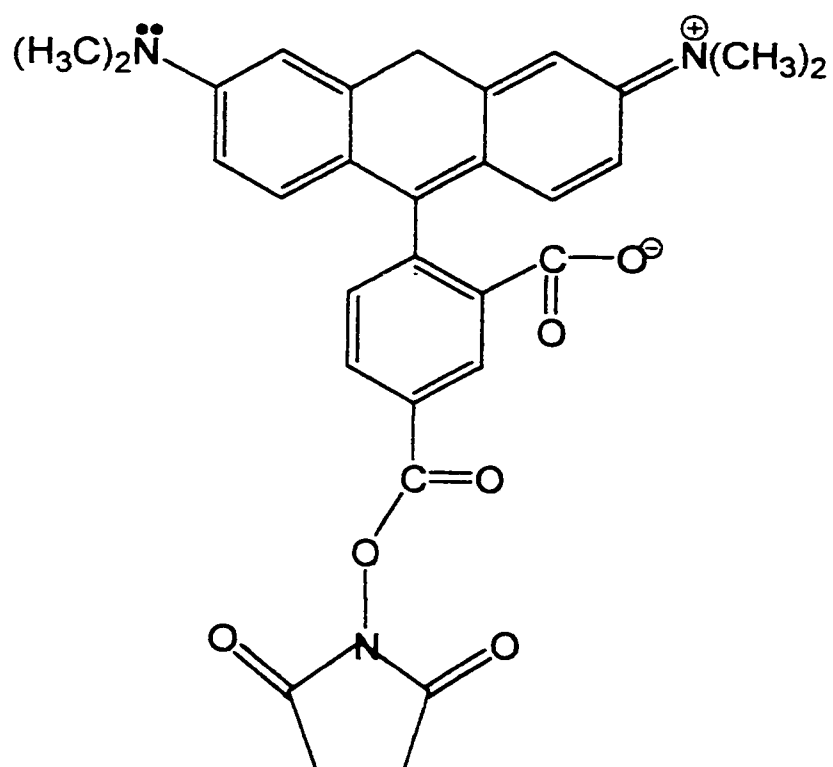
(5-TAMRA-SE).

Figure 2.3: The absorption and fluorescence emission spectra of

5-carboxytetramethylrhodamine (5-TAMRA) in

A) methanol, B) pH 7 buffer.[57]
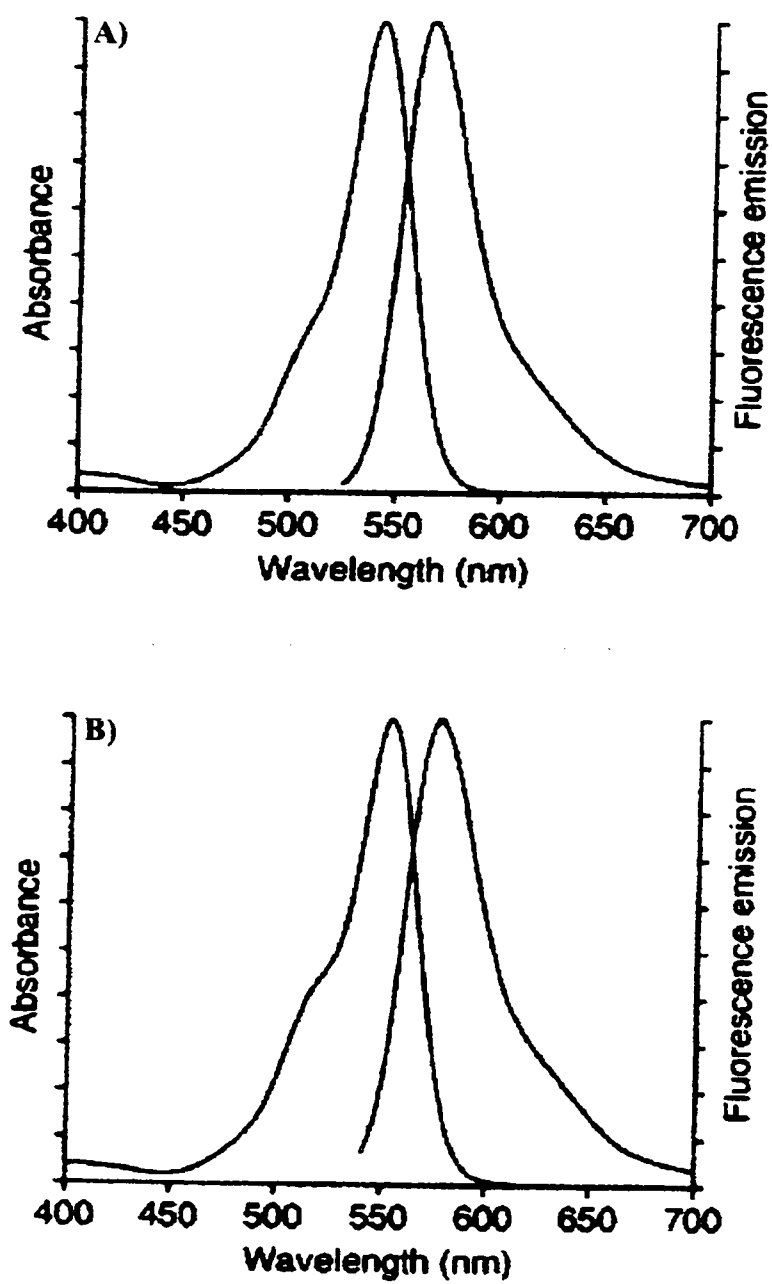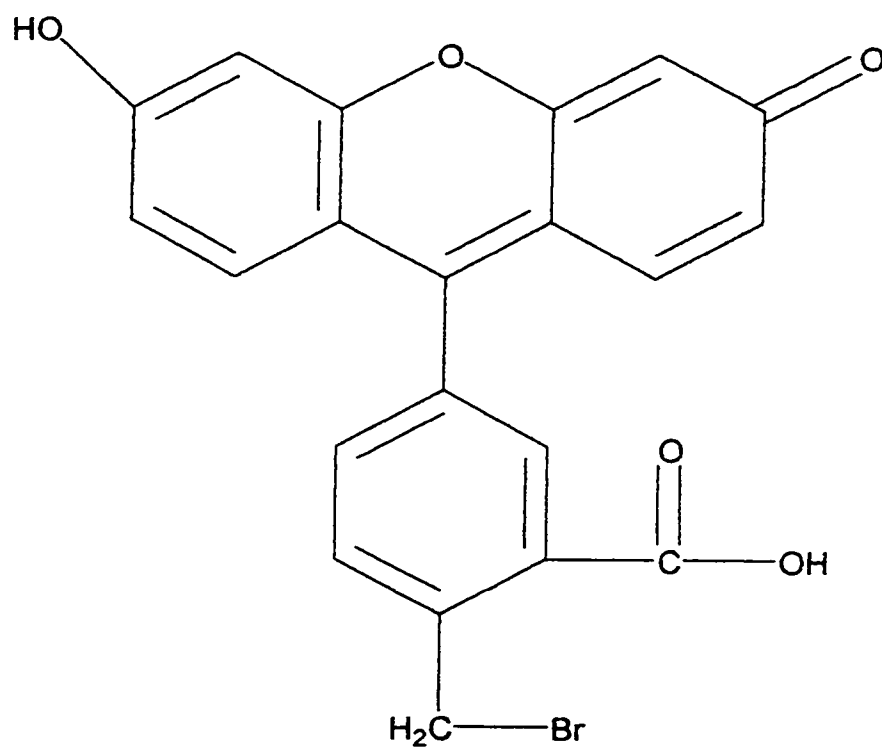
reagent but it can also react with amines of proteins if the pH is in the range 9.0 – 9.5.[59,60]

The absorption and emission spectra of 5-BMF dissolved in methanol are illustrated in

Figure 2.5. The excitation maximum of this dye under basic conditions matches very

well with the intense 488.0 nm emission line of an Ar^+ laser. The excitation wavelength

for 5-BMF is 492 nm and the emission wavelength is 515 nm. The molar absorptivity

coefficient of this dye is 81,000 L mol^{-1} cm^{-1} at 492 nm.

2.1.3 Fluorescence polarization

Perrin[61,62] first developed the principles of fluorescence polarization in the 1920s.

Three decades later the technique was applied to biological systems by Weber[62,63], and its

application to the antigen-antibody reaction was first described in 1961 by Dandliker and

Feigen[62,64]. Fluorescence polarization has been used for the purpose of clinical diagnosis

for more than a decade, but its use has been limited in the research area probably due to

the lack of a sensitive and versatile instrument.[65]

Fluorescence polarization techniques are based on the principle that a

fluorescently labelled compound, when excited by plane polarized light, will emit

polarized fluorescent light. The emitted polarization will differ from the excitation

polarization because the fluorescent molecule is in motion during the time that elapses

between excitation and emission. Polarization of fluorescence depends on the

fluorescence lifetime, which is the time between excitation and emission, and the

rotational relaxation time of the molecule, which is the time required for an oriented

molecule to return to a random orientation in solution. Small molecules will rotate

rapidly in solution resulting in short relaxation times and ultimately low fluorescence

Figure 2.5: The absorption and fluorescence emission spectra of 5-(bromomethyl)fluorescein in methanol.[57]

53
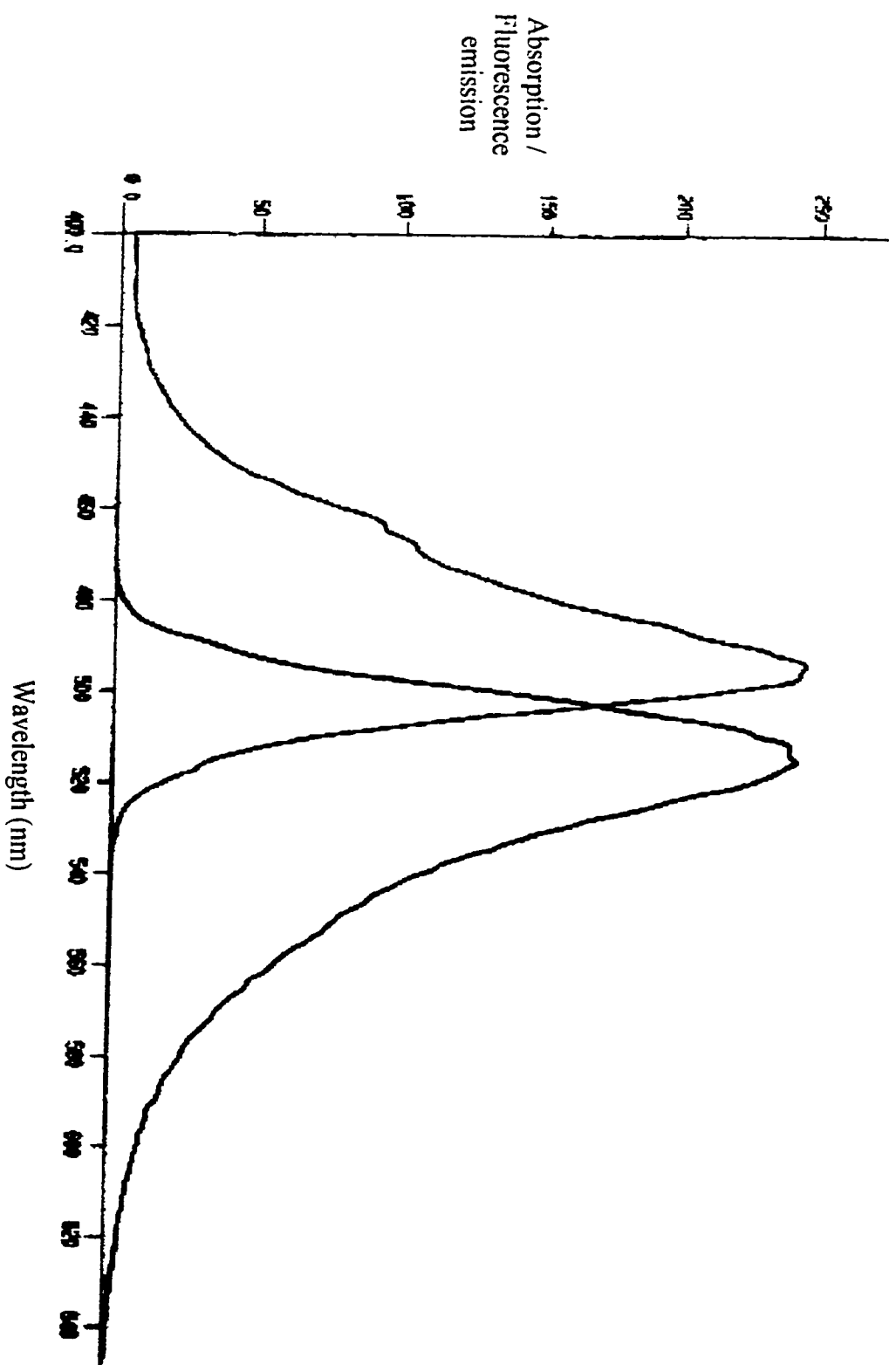
polarization. When a large antibody molecule binds to the small molecule, fluorescence

polarization is considerable because the large molecule rotates slowly in solution and the

relaxation time is prolonged.[66]

The polarization of fluorescence operates differently than the other methods of

detection (e.g. UV, refractive index, electrochemical, etc.) in that it gives a direct

measure of the bound/free molecular ratio instead of simply being a measure of amount

of label present. For a given bound/free molecular ratio the polarization remains constant

over many orders of magnitude of change in the absolute concentrations.[67] This

characteristic provides a definite advantage for some situations in that the essential

measurement can be made without any physical separation of bound and free molecules.

Fluorescence depolarization can be described by fluorescence anisotropy (r), which is

defined as: $r = (I_{vv} - I_{vh})/(I_{vv} + 2I_{vh})$, where I_{vv} and I_{vh} are the emission intensities

detected via a polarizer oriented in parallel and vertically, respectively, to a vertically

polarized monochromatic excitation light.[68]

A capillary electrophoretic (CE) separation of an immunoassay mixture should

reveal two peaks by fluorescence detection, one corresponding to the complex and the

other corresponding to free fluorescently labelled antigen.[69]

2.1.4 Immunoassay technique

Immunoassay is a general analytical technique that relies upon the reaction of an

antigen with a specific antibody, under competitive or non-competitive conditions.[70]

Immunoassays provide valuable tools for applications as diverse as clinical diagnostics,

environmental monitoring, and process control.[71] Based on the extreme specificity of

54

antibody-binding, immunoassay techniques are reliable and well-established.[71] Most immunoassays are based on competitive formats with antibodies of high specificity and low cross-reactivity, thus permitting highly sensitive determinations of the antigen.[72,73] An example of a competitive immunoassay is the flow displacement immunoassay. Displacement is a principle in which either antibodies or antigens are immobilized, whereas the respective interacting antigen (analogue) or antibody is labelled. The antibody displacement consists of washing the sample over these antibody-antigen complexes, releasing labelled molecules from the immobilized site.[74]

Flow displacement immunoassays can be divided into two different categories: one with immobilized antibodies and the other with immobilized antigens. In the case of this work the antibody was immobilized onto the capillary wall as described in Section 2.2.8. When unlabelled antigen is introduced into the CE system, by pressure injection, a proportional amount of labelled antigen is displaced from the binding sites of the immobilized antibodies and is subsequently detected downstream by LIF.[75] The schematic diagram of how this displacement occurs can be found in Figure 2.6. The unique feature of the flow displacement immunoassay is that the bound labelled antigen can be rapidly displaced from the column following the introduction of free antigen.[71] Such a flow displacement of labelled antigens or antigen analogues has been described for small analytes such as cortisol,[76,77] cocaine[78] and trinitrotoluene[79]. In this work spontaneous dissociation, which is the breakage of the bond between an antibody and an antigen due to the association equilibrium (AgAb ↔ Ag + Ab) shifting to the right, was assumed to be minimal. The flow displacement immunoassay performed in this work

Figure 2.6: The schematic diagram of how a displacement immunossay is performed. Legend: �֍ is the labelled antigen, ◉ is the unlabelled antigen and ⋎ is the antibody.

Capillary wall

Capillary wall

+

Detected by LIF
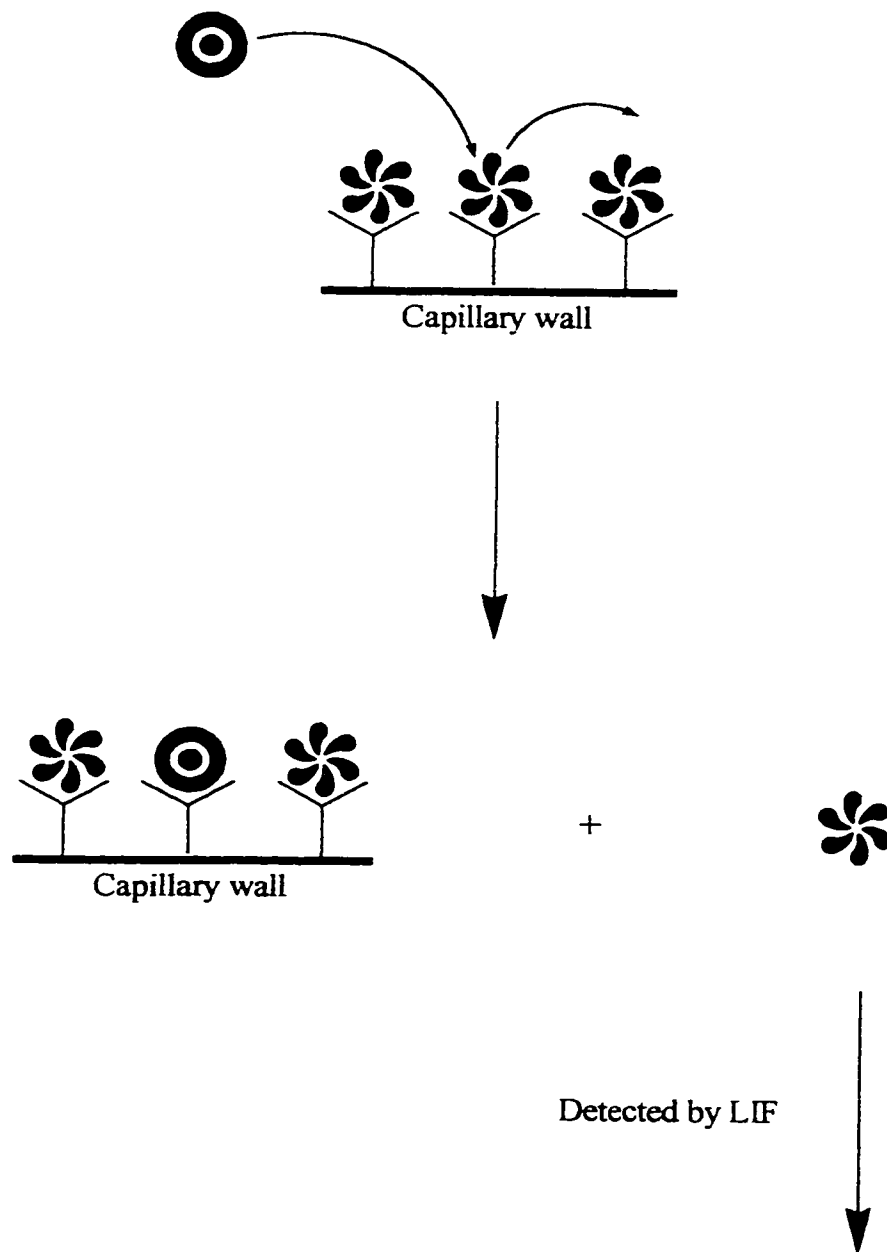
relies on the antigen/antibody dissociation event for the successful detection of the analyte of interest.

2.1.5 Introduction to arginine modification

Chemical modification as an approach to studying the biological function of proteins was an outgrowth of the classical derivatization techniques in organic chemistry.[80] Chemical modification of specific amino-acid residues within enzymes has provided much information on the role of individual residues in enzyme structure and function.[81] Arginyl residues serve a general function as binding sites in a large number of enzymes, particularly those that act on substrates or cofactors carrying a negative charge.[82] Arginine-specific α-dicarbonyl reagents, such as butanedione, phenylglyoxal and cyclohexanedione rapidly inactivate enzymes and the subsequent loss of activity correlates with the modification of one arginine per subunit.[83]

These α-dicarbonyl reagents react more readily with the guanidine groups than with lysine or histidine residues.[84] The reason for this difference lies in the unique chemistry of the guanidinium side chain of arginine, which has a pK_a of 12.5^{80} and is the strongest known organic base. Its two $-NH_2$ functions do not exhibit the same chemical reactivity as the ε-NH_2 group of lysine. This guanidinium group is protonated over the entire pH range of protein stability, unlike the ε-NH_2 of lysine which can be modified under slightly alkaline conditions where some of the free base form is present.[80] The guanidinium ion can be represented by three resonance forms as opposed to the non-equivalent hybrid forms of guanidine. Another feature of the guanidinium group is the coplanarity of the three nitrogens and the central carbon atom brought about by the partial

double bond character of each of the C-N bonds. This feature enables the guanidinium

side chain of arginine to enter into extended patterns of hydrogen bonding that are

unique, thus perhaps explaining the evolutionary selection of arginine as a constituent of

proteins.[80]

In 1966, Yankeelov and coworkers[80,85] reported that 2,3-butanedione solutions

react with guanidinium salts. Their evidence suggested that an initial self-condensation

of the reagent was necessary before it would react. Subsequently, Yankeelov was able to

prepare the crystalline dimer and trimer of butanedione and demonstrated their reactivity

with arginine, both free and in proteins.[80,86] Monomeric butanedione was found to react

faster than either the dimer or the trimer.

The schematic diagram of the reaction mechanism of the α-dicarbonyl reagent,

2,3-butanedione, with the guanidinium group of arginine can be found in Figure 2.7. The

reaction of 2,3-butanedione with the guanidinium side chain of arginine proceeds via the

formation of 4,5-dimethyl-4,5-dihydroxy-2-imidazole (intermediate I) which is

moderately stable. If this reaction is carried out for an hour in the absence of borate,

followed by the addition of borate, intermediate II is formed instantaneously. At this

point if the reaction mixture is gel-filtered to remove excess reagent, the intermediate will

dissociate and thus, arginine is regenerated and the native enzyme activity is restored. If

the reaction of 2,3-butanedione with the guanidinium group of arginine is allowed to

proceed for longer than an hour, intermediate III is formed. This intermediate cannot be

reactivated by gel-filtration and the addition of borate to this intermediate has no effect.

The rearrangement of intermediate I into intermediate III is thought to occur by a

pinacoltype process.[80] Under the acidic conditions used for protein hydrolysis, prior to

Figure 2.7: The schematic diagram of the reaction mechanism of the α-dicarbonyl reagent, 2,3-butanedione, with the guanidinium group of arginine.
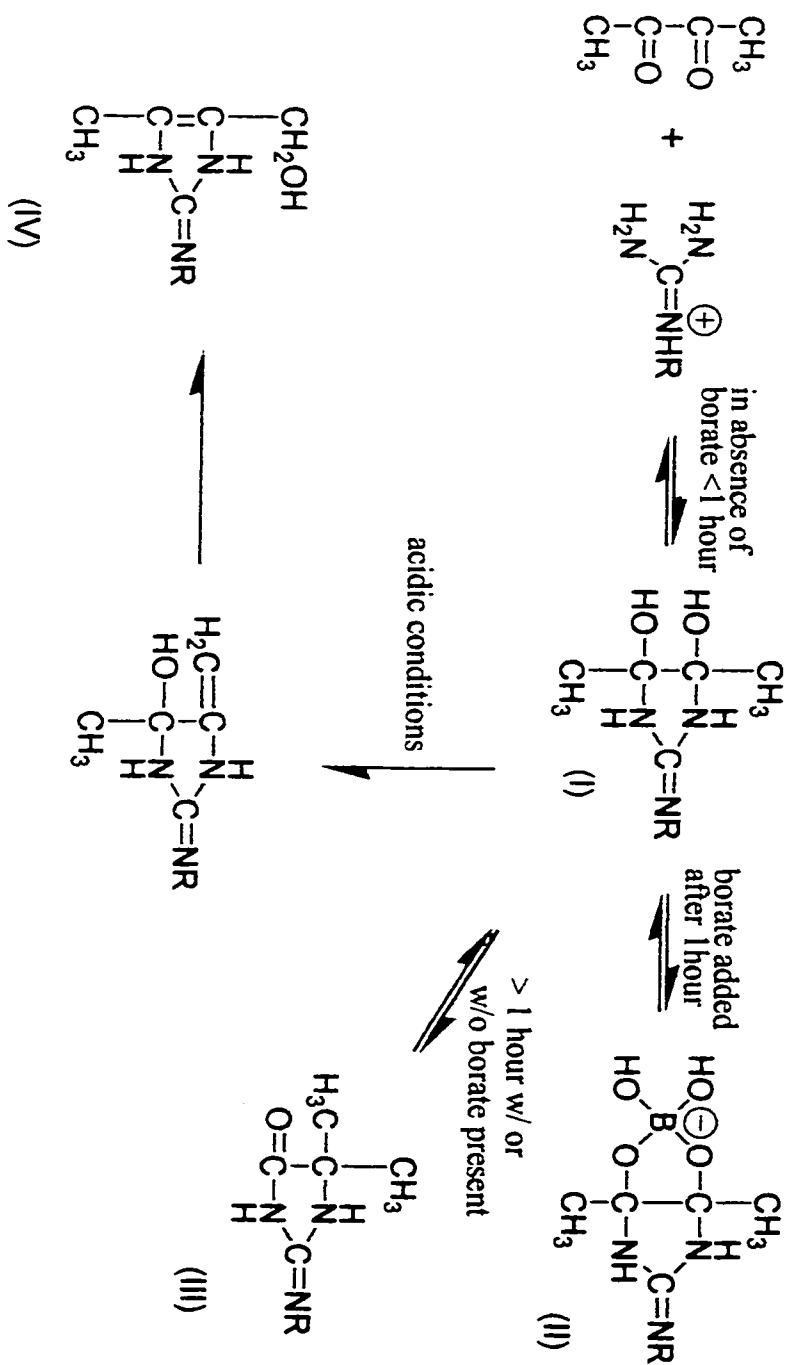
amino acid analysis, intermediate I dehydrates to form the methylene species which then undergoes an anionotropic shift to give intermediate IV, which is hydroxylmethyl-imidazoline. The specific enhancement effect of borate buffer together with the reversibility of the modification (within the time limitations mentioned) and the prevention of reversibility by borate provide a convenient means to recognize arginine-modified proteins.[80]

The goal of this work was to develop a fluorescent-labelling reagent that would react with the guanidinium side chain of an arginine residue. This labelling reagent was synthesized by reacting 5-(bromomethyl)fluorescein with the α-dicarbonyl reagent 2,3-butanedione.

2.2 Experimental

2.2.1 Reagents

Microcystin-LR was purchased from Calbiochem (La Jolla, CA, USA). N,N-Dimethylformamide (DMF) and Molecular Sieve Type 4A beads were obtained from Caledon (Georgetown, Ontario, Canada). The DMF was dried with Molecular Sieve Type 4A beads in a dry glass bottle, septum-capped to prevent moisture from entering. Toluene and N_α-acetyl arginine were purchased from Sigma (St. Louis, MO, USA). 5-Carboxytetramethylrhodamine, succinimidyl ester (5-TAMRA-SE) and 5-(bromomethyl)fluorescein (5-BMF) were acquired from Molecular Probes (Eugene, OR, USA). Fused-silica capillary (50 μm inner diameter (I.D.), 140 μm outer diameter (O.D.)) was obtained from PolyMicro Technologies (Phoenix, AZ, USA). 2,3-Butanedione was purchased from Lancaster (Georgetown, ON, Canada). Di-sodium

tetraborate and potassium carbonate (K_2CO_3) were bought from BDH Chemicals (Toronto, ON, Canada). The Bio-Gel P-4 Gel for gel permeation chromatography was purchased from Bio Rad Laboratories (Richmond, CA, USA). Sodium phosphate monobasic (NaH_2PO_4) was purchased from Anachemia Chemicals (Champlain, NY, USA). Sodium phosphate dibasic (Na_2HPO_4) and calcium chloride ($CaCl_2$) were obtained from Fisher Scientific (Fair Lawn, NJ, USA). Sodium hydride (NaH), 2,5-dihydroxybenzoic acid (DHB), 6-aza-2-thiothyamine, β-cyclodextrin, sodium hydroxide (NaOH), and ethanol were purchased from Aldrich (Milwaukee, WI, USA). The mercaptopropyltrimethoxysilane (MTS) and N-succinimidyl-4-maleimidobutyrate (GMBS) were bought from Fluka Chemika (Switzerland). The antibodies against microcystin-LR were prepared by Dr. Chu at the University of Wisconsin-Madison, in collaboration with Dr. Carmichael at Wright State University.[87] They obtained the anti-microcystin antibody from rabbit serum after immunizing rabbits with a bovine serum albumin-microcystin-LR conjugate. Dr. Carmichael provided this anti-microcystin antibody to Dr. Xc. Le from the Department of Public Health at the University of Alberta. Dr. Xc. Le then provided the anti-microcystin antibody to our group.

2.2.2 Instruments

Matrix assisted laser desorption ionization mass spectrometry (MALDI-MS) was performed with a commercial KRATOS-MALDI instrument. The CE-LIF instrument is a home-built instrument that was described in Chapter 1. The SpeedVac for solvent evaporation was purchased from Savant (Farmingdale, NY, USA).

The schematic diagram of the set-up used for fluorescence polarization can be found in Figure 2.8 and was described in detail elsewhere.[66] The LIFP system was constructed on an optical breadboard and is very similar to the CE-LIF set-up described in Chapter 1. The electrophoresis was driven by a high-voltage power supply (CZE1000R, Spellman High Voltage Electronics, Plainview, NY, USA). A 65-mW Ar^+ laser (Model 2214-65ml, Uniphase, San Jose, CA, USA) with a wavelength of 488 nm was used as the excitation source. Fluorescence was collected at a right angle with respect to both the laser beam and the sample stream by using a high-numerical aperture microscope objective (60X, 0.7 NA, Universe Kogaku, Oyster Bay, NY, USA). The fluorescence was then spectrally filtered with a bandpass filter (515DF20) to reject scattered laser light. A 200-μm radius pinhole was placed in the reticle position of the microscope objective to restrict the field of view of the photomultiplier tubes (PMTs) to the illuminated sample stream. The fluorescent light was split, by using a polarizing beamsplitter (Melles Griot, Nepean, ON, Canada), to two PMTs (R1477, Hamamatsu Photonics, Japan) for measuring horizontally and vertically polarized light, respectively. A PCI data acquisition board and LabVIEW software (National Instruments) in a Power PC Macintosh computer digitized the output from the two PMTs.

The schematic diagram of the set-up used for the microcystin-LR fluorescent flow displacement immunoassay can be found in Figure 2.9. The set-up for the flow displacement immunoassay was the same as the CE-LIF set-up described in Chapter 1 except the sample was pressure injected using gravity as a siphon and the flow for separation was sustained via a Harvard Apparatus syringe pump.

Figure 2.8: A schematic diagram showing CE separation with LIFP detection.
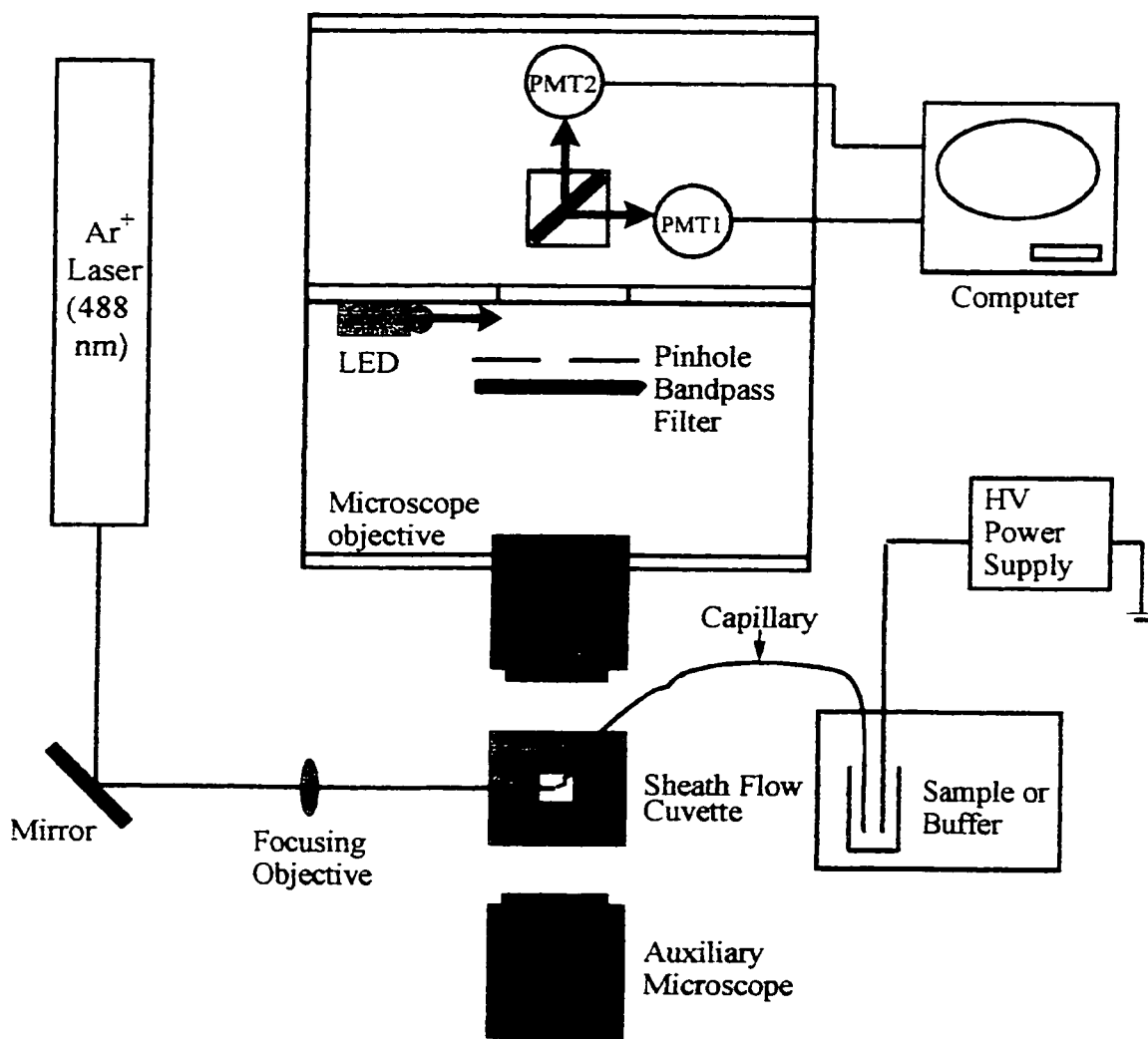
Figure 2.9: The schematic diagram of the fluorescent flow displacement

immunoassay with LIF detection used in the analysis of microcystin-LR.
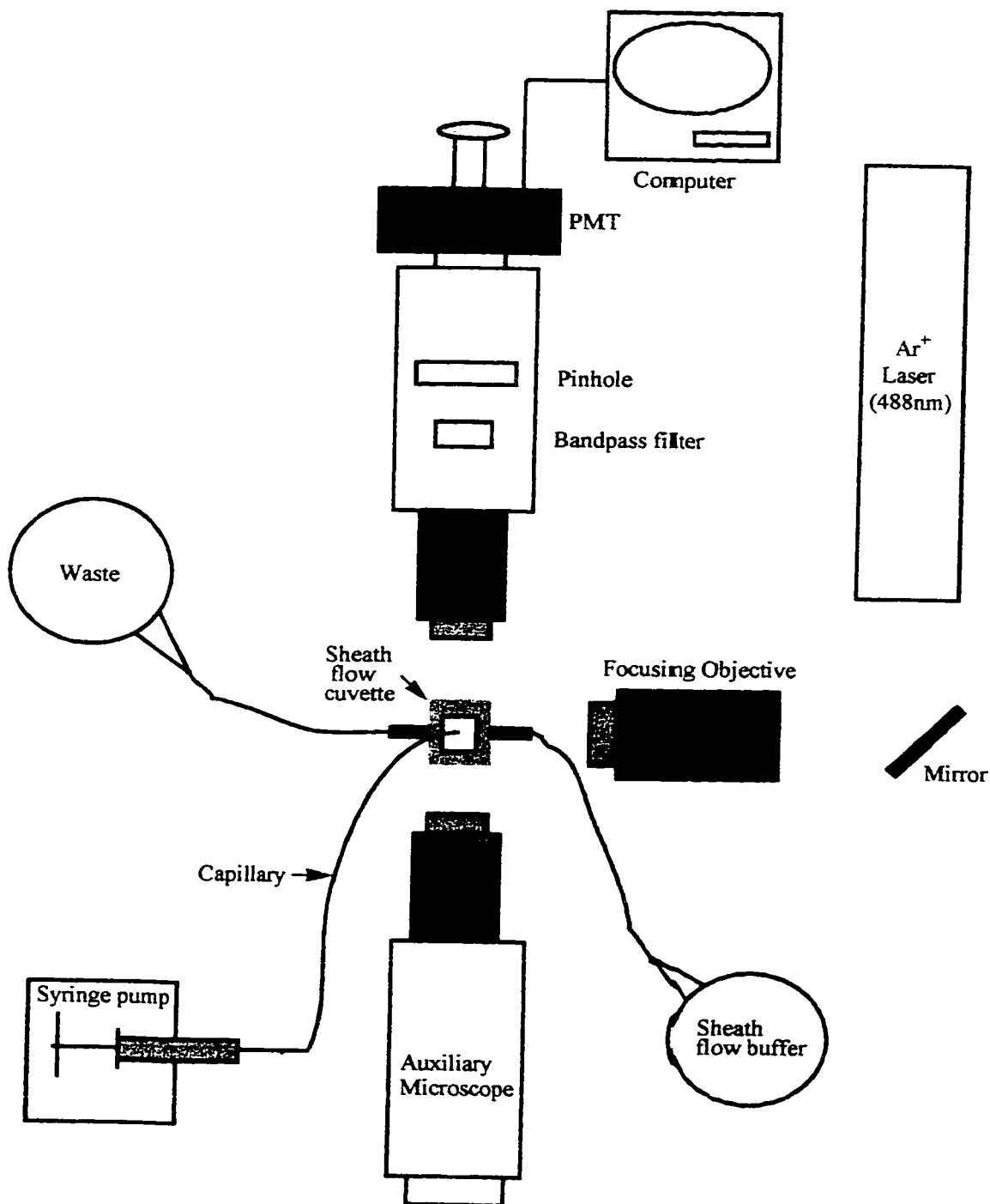
The electrospray ionization mass spectrometry (ESI-MS) analysis was performed by positive mode electrospray ionization on a Micromass ZabSpec Hybrid Sector-TOF. The liquid carrier (in this case HPLC grade acetonitrile, Fisher) was infused into the electrospray source by means of a Harvard syringe pump at a flow rate of 15 μL/minute. The sample solution, diluted with the same solvent, was introduced via a 1-μL loop injector. Prepurified nitrogen was used as a spray pneumatic aid and filtered air as the bath gas, heated at ca. 80 °C. For low resolution, the mass spectra were acquired by magnetic scan at a rate of 5 seconds/10 m/z units at ca. 1000 resolution. Data acquisition and processing were achieved by using the OPUS software package on a Digital Alpha station with VMS operating system.

2.2.3 Microcystin-LR labelling with 5-TAMRA-SE using NaH deprotonation

Graduate student Hossein Ahmadzadeh first developed the procedure for this labelling reaction. The schematic diagram of the apparatus used in this reaction can be found in Figure 2.10. 500 μg of microcystin-LR was dissolved in 1 mL of DMF and then transferred to a 5-mL three-neck round bottom flask. Next, decanted 60 % NaH in excess and 250 μL of a 5 mg/mL solution of 5-TAMRA-SE were added to the reaction flask. The 60 % NaH was decanted with DMF to remove as much oil as possible. The final volume was 1.25 mL and the ratio of dye to analyte was 5:1. The reaction mixture was heated at 70 - 75 °C in an oil bath under reflux for 3 - 4 hours. The reaction mixture was performed under a dry argon atmosphere with a CaCl₂ guard column placed on top of the reflux system.

Figure 2.10: The schematic diagram of the apparatus used for the arginine-labelling

reaction of microcystin-LR. 1) 5-mL three-neck flask, 2) septum,

3) 250 °C thermometer, 4) condenser, 5) syringe with needle, 6) calcium

chloride guard column, 7) three-way connector, 8) tubing.
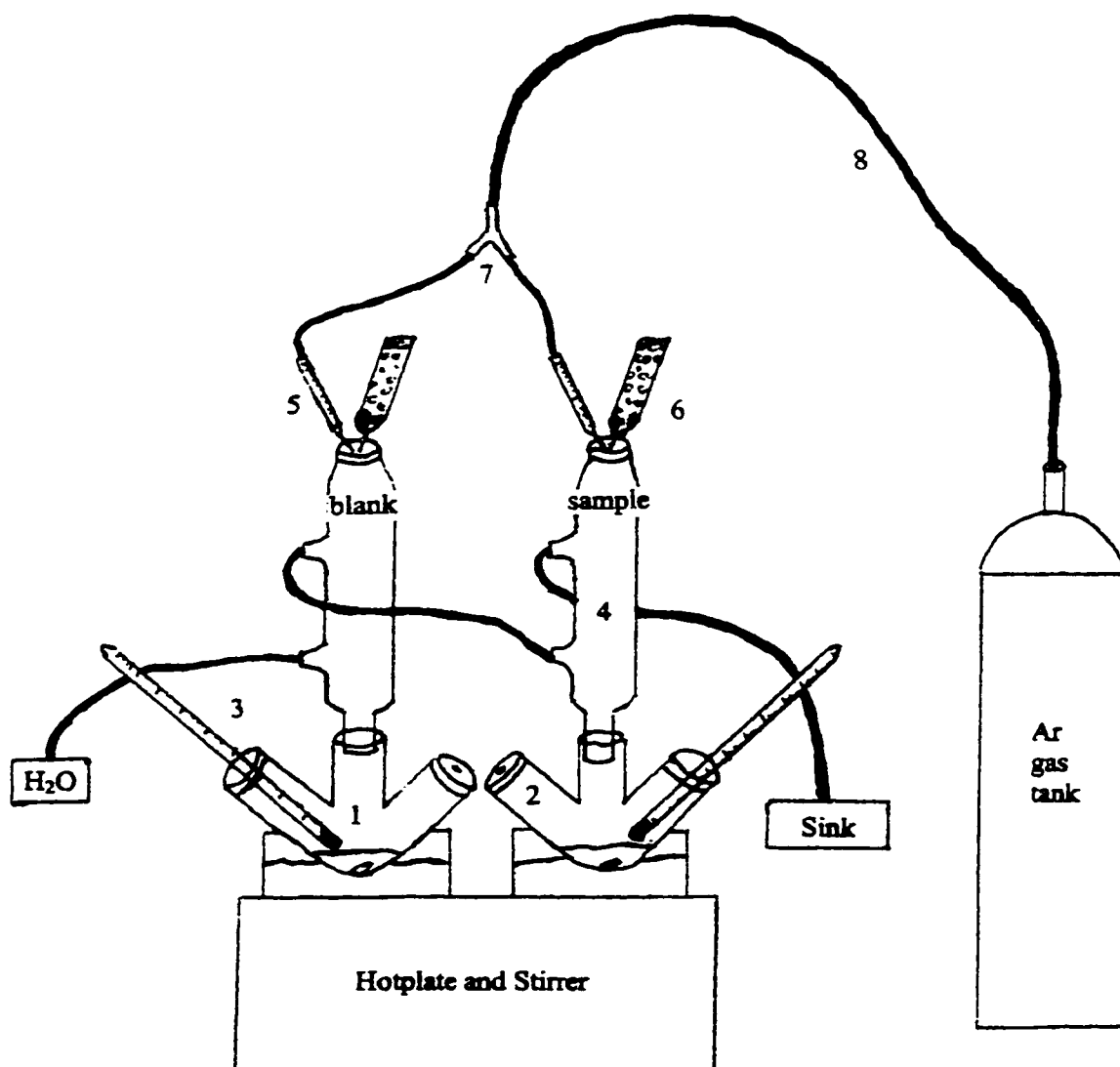
MALDI-MS and CZE-LIF were used to check for the presence of the product. When using CZE-LIF the labelled microcystin-LR (M*-LR) solution and the blank solution were serially diluted down to concentrations of $5*10^{-6}$ M with 10 mM borate at pH 9 as the dilution buffer. The fused-silica capillary used for the separation was 29.5 cm in length with an O.D. of 140 μm and an I.D. of 50 μm. A 543 nm He-Ne laser beam was used to excite the sample which had 5 mW of power. The interference filter used was 590DF35 and the run and sheath flow buffers were 10 mM borate with a pH of 9. The injections were done at 3000 V for 5 s and the separation voltage was at 14 kV. The PMT used for detection was biased to 1000 V.

2.2.4 Two-layer sample deposition for MALDI

The MALDI probe consisted of a 1 x 10 cm stainless steel plate with 20 linearly arranged platinum-coated sample wells. The sample preparation and the two-layer sample deposition method were adapted from Kalbag and Roeske.[88] The matrix solution used in the positive-ion mode was DHB and in the negative-ion mode was 6-aza-2-thiothyamine. The matrix solution concentration was ~10 mg/mL using 30 % acetonitrile/water as the solvent. The matrix solution was first vortexed and then centrifuged to separate out as much undissolved matrix as possible. Next, 0.5 μL aliquots of the centrifuged matrix solution supernatant were placed on the MALDI plate deposition spots and allowed to dry. This step was performed twice. This procedure was also used for analysing samples with the exception that the centrifuged matrix solution supernatant was mixed with sample. When every deposition spot had completely dried

the MALDI probe was inserted into the KRATOS-MALDI instrument and using a computer program each deposition spot was targeted one by one for analysis.

2.2.5 Separation of the labelled microcystin-LR

Size-exclusion chromatography or gel permeation chromatography was first used to try to separate the components of the microcystin-LR labelling reaction. A glass column was filled with polyacrylamide gel (Bio-Gel P-4 Gel Fine Resin) and the reaction mixture was applied to the top of the column and eluted by using water as the mobile phase at a rate of 5 - 10 cm/h. The column was equipped with a fraction collector and an UV detector. All fractions were 2 mL in volume and were collected until the effluent was colourless.

In a second attempt to isolate the labelled microcystin-LR from the other reaction components reversed-phase chromatography with a Sep-Pak® cartridge was used. To perform reversed-phase chromatography with Sep-Pak® cartridges a gradient of strongly to weakly polar solvents (water and methanol, respectively) with nonpolar C_{18} as the sorbent were used. First the bonded phase was solvated with six to ten cartridge hold-up volumes of methanol. The cartridge was then flushed with six to ten hold-up volumes of water. Next, the sample reaction mixture dissolved in water was loaded on to the cartridge. Then, the cartridge was flushed with water until the effluent was colourless to remove all the unwanted reactants like 5-BMF and sodium hydride. This step should leave only the labelled microcystin-LR on the C_{18} sorbent. Next, the cartridge was washed with methanol to remove the labelled microcystin-LR from the sorbent. The washings collected were then concentrated using a rotary evaporator.

2.2.6 Microcystin-LR labelling with 5-BMF using NaH deprotonation

This process is the same as the procedure described in Section 2.2.3 except that the fluorescent dye used was 5-BMF. The blank and sample reaction mixtures were purified using a C_{18} Sep-Pak® cartridge as described in Section 2.2.5. MALDI-MS and ESI-MS were used to check for the presence of labelled microcystin-LR.

2.2.7 Fluorescence polarization

The first CZE-LIFP experiment was performed under the following conditions. The capillary was 35 cm in length and had an I.D. of 50 µm and an O.D. of 140 µm. The run and sheath flow buffers were 10 mM borate at pH 9. The separation voltage was 14 kV and the injections were done at 3000 V for 5 s. The PMT was biased at 750 V and the Ar^+ laser beam had 4 mW of power at 488 nm. The interference filter used was 515DF20.

The second CZE-LIFP experiment had the same run conditions with the following exceptions. The capillary was 36 cm in length, the run buffer was 10 mM borate with 1 mM β-cyclodextrin at pH 9 and the voltage used for separation was 23 kV.

2.2.8 Antibody immobilization on a capillary

A 5 m long capillary (50 µm I.D., 140 µm O.D.) was cut and connected to a nitrogen gas tank by using various connections and fittings. Molecular sieve Type 4A beads were used to filter the nitrogen gas to ensure the gas was anhydrous. First the capillary was cleaned by flowing 10 mM NaOH, distilled deionized water and then nitrogen gas through the capillary 1 hour each under 20 PSI of pressure. The actual

coating procedure started with passing a 4 % solution of mercatopropyltrimethoxysilane (MTS) in toluene through the capillary using 20 PSI of pressure for 1 hour. Next, the capillary was flushed with toluene for 1 hour and then a 2 mM GMBS solution (cross-linker) was drawn through it for 1 hour. Then the capillary was rinsed with distilled deionized water and a 1 mg/mL antibody-microcystin-LR solution was passed through for 1 hour. Next, the capillary was rinsed three times with distilled deionized water and then the labelled microcystin-LR reaction mixture was passed through the capillary for one hour. At the end of the coating procedure the ends of the capillary were capped with a GC septum and refrigerated for a minimum of 12 hours. Before use in an experiment, the excess labelled microcystin-LR in the antibody-immobilized capillary was flushed out with run buffer.

2.2.9 Microcystin-LR fluorescent flow displacement immunoassay

The capillary used in this immunoassay experiment was 50 cm long with a 50 µm I.D. and a 140 µm O.D.. The PMT was biased at 1000 V. The run buffer was 10 mM NaH_2PO_4 with 2.5 % ethanol at pH 7.6. The sheath flow was 0.05 M Na_2HPO_4 and 0.025 M K_2SO_4 at pH 10.2. The injection flow pump was run at 0.2 µL/min and had a 500 µL syringe (diameter 3.26 mm) which contained the run buffer. A 488 nm Ar^+ laser beam with 12.1 mW of power was used for excitation. The interference filter was 518DF25. All injections were performed by pressure injection using gravity as a siphon. The injections were performed holding the capillary in the standard solutions at a height of 21 cm for 10 s. Based on the Poiseuille Equation these conditions produce a 6 nL injection which results in a 0.6 % plug length.

2.2.10 Synthesis of arginine-labelling reagent

60 % NaH in oil was decanted with DMF to remove as much of the oil as possible. Then, 5 mg of 5-BMF dissolved in DMF was placed into the sample reaction flask under anhydrous argon gas. The reaction flask was then placed in an ice bath. Then, 3 molar equivalents of decanted 60 % NaH were added to the reaction flask. Next, 1 mg of 2,3-butanedione was added dropwise to the entire reaction mixture. Once the reaction was complete the unreacted NaH was removed by filtration. The remaining reaction mixture was concentrated by rotary evaporation.

ESI-MS was used to check for the presence of product.

2.2.11 Reaction of arginine-labelling reagent and N_α-acetyl arginine

5 μmol of N_α-acetyl arginine was placed into a 5-mL three-neck round bottom flask. Next, 5 molar equivalents of arginine-labelling reagent synthesized in Section 2.2.10 were added to the reaction flask. The final volumes were made to 1 mL by adding 100 mM borate at pH 9. The reaction mixture was allowed to react for 1 hour in the dark at room temperature.

CZE-LIF was used to check the success of the reaction. The capillary used was 30 cm in length and had an I.D. of 50 μm and an O.D. of 140 μm. The laser beam used for excitation was Ar^+ with a wavelength of 488 nm and a power of 12.1 mW. The run and sheath flow buffers were 10 mM borate at pH 9. The separation voltage was 17 kV and the injections were performed at 3000 V for 5 s. The PMT was biased at 1000 V. The interference filter used was 518DF25.

71

2.3 Results and Discussion

2.3.1 Microcystin-LR labelling with 5-TAMRA-SE using NaH deprotonation

The labelling procedure was performed under the conditions described in Section 2.2.3. The reaction apparatus included two 5-mL three-neck flasks, one for the labelling reaction (sample flask) and one for the blank reaction, which contained all reactants except for microcystin-LR. The reaction was performed under anhydrous argon gas and two calcium chloride guard columns were placed on top of the reflux apparatus so that the hydrolysis of NaH to NaOH was eliminated as much as possible. If the NaH is hydrolysed, the hydroxide ion produced displaces the succinimidyl ester group in 5-TAMRA-SE, leaving the dye unreactive.

Figure 2.11 shows the microcystin-LR (M-LR) labelling reaction with 5-TAMRA-SE using NaH for deprotonation, which is a nucleophilic substitution reaction. The dye 5-TAMRA-SE is an ester and the toxin microcystin-LR has one free amine group and two carboxyl groups. This labelling reaction involves aminolysis which occurs when the dye ester is reacted with the free amine group of microcystin-LR (found in the arginine side residue) to yield an amide. If the dye ester reacts with the carbonyl groups of microcystin-LR an acid anhydride is formed. This reaction is unfavourable since converting a less polar acid derivative (carboxylic acid) into a more polar acid derivative (acid anhydride) is theoretically improbable. Therefore, one expected product from this labelling reaction is the microcystin-LR with its guanidinium group of the arginine side chain attached to the fluorescent dye. Other labelling products could be formed due to the lone pair of the dye's amide group reacting with the carboxyl

72

Figure 2.11: The schematic diagram of the arginine-labelling reaction of

microcystin-LR with 5-TAMRA-SE which involves aminolysis.
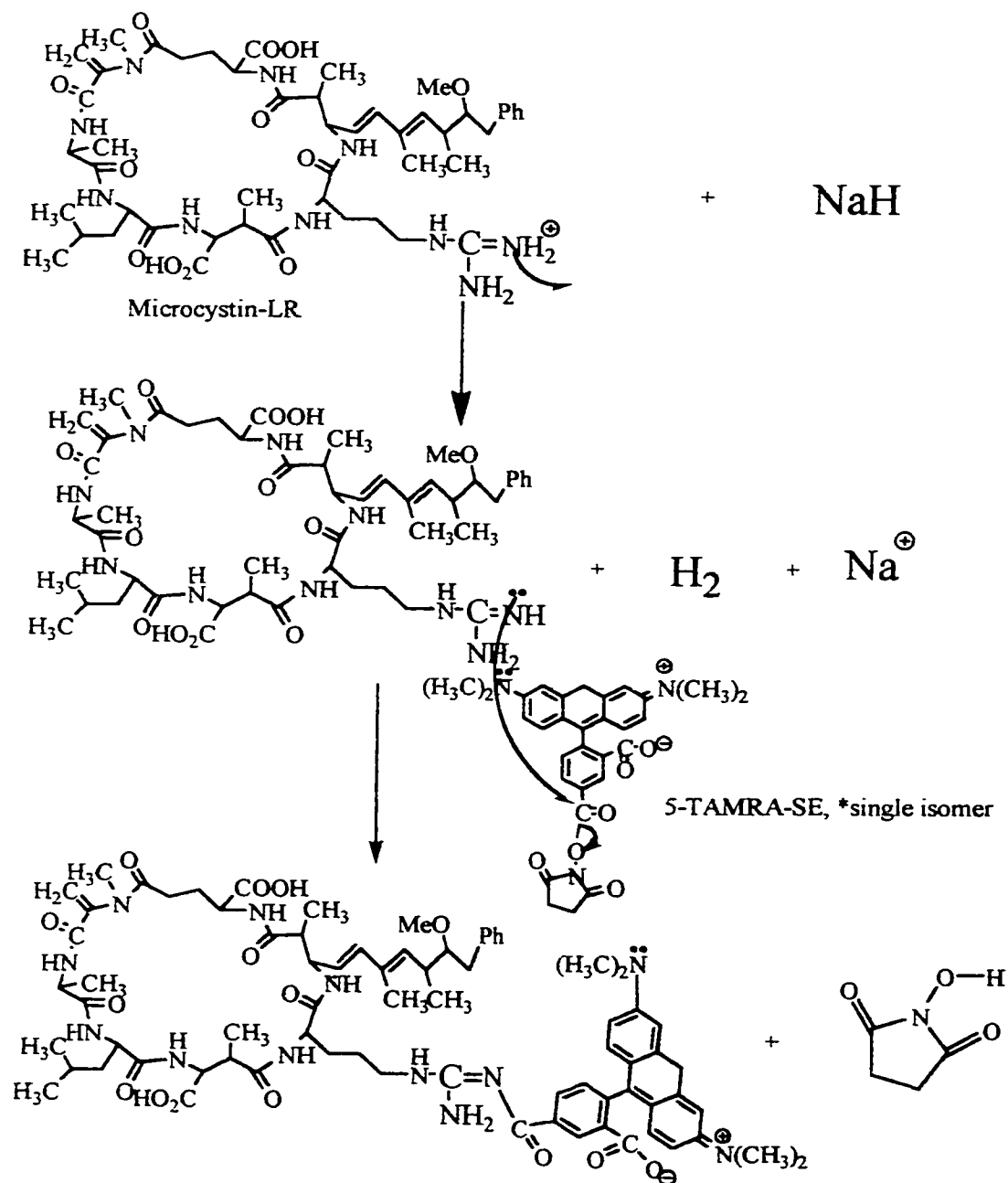
functional groups in microcystin-LR. The labelling reaction mixtures were checked for product using MALDI-MS and CZE-LIF.

MALDI-MS using the two-layer deposition method described in Sections 2.2.4 was used to check the reaction mixture for the presence of labelled microcystin-LR. Figure 2.12 shows the positive-ion mode MALDI-MS spectra of the matrix, dye, unlabelled microcystin-LR and sample labelling reaction, which should contain the fluorescently labelled microcystin-LR. The positive-ion mode MALDI-MS spectrum for the matrix (Figure 2.12A) reveals peaks at 154 amu and 137 amu which correspond to the hydrogen adduct of DHB and the DHB with a loss of a hydroxide ion respectively. These two peaks are characteristic of the matrix DHB and can be found in any MALDI-MS spectrum using DHB. The positive-ion mode MALDI-MS spectrum for the dye 5-TAMRA-SE (Figure 2.12B) reveals major peaks at 522 amu, which is assigned as the hydrogen adduct of the dye, and at 550 amu, which is assigned as the sodium adduct of the dye. The unlabelled microcystin-LR positive-ion mode MALDI-MS spectrum (Figure 2.12C) reveals only one major peak at 996 amu, which is the hydrogen adduct of the toxin. This single major peak suggests that the microcystin-LR in the labelling reaction was pure. The positive-ion mode MALDI-MS spectra for the labelling reaction mixture (Figures 2.12D and 2.12E) show numerous small peaks of which correspond not only to the hydrogen adduct of the labelled microcystin-LR (1406 amu) but also various salt adducts of the product. The salt adducts found in Figure 2.12D are at 1428 amu, 1444 amu, 1460 amu, 1472 amu and 1483 amu and are assigned as the $(M*+Na)^+$, $(M*+K)^+$, $(M*+Na+K)^+$, $(M*+3Na)^+$ and $(M*+2K)^+$ adducts, respectively. Peaks for the unlabelled microcystin-LR (Figure 2.12E) in the labelling reaction mixture are found at

Figure 2.12: The positive-ion mode MALDI-MS spectra of A) 2,5-dihydroxy-

benzoic acid (DHB) used as the matrix, B) 5-TAMRA-SE used as the

labelling reagent, C) unlabelled microcystin-LR and D) 5-TAMRA-SE

labelled microcystin-LR range m/z 1400 - 1500 E) 5-TAMRA-SE

labelled microcystin-LR range m/z 900 - 1100.
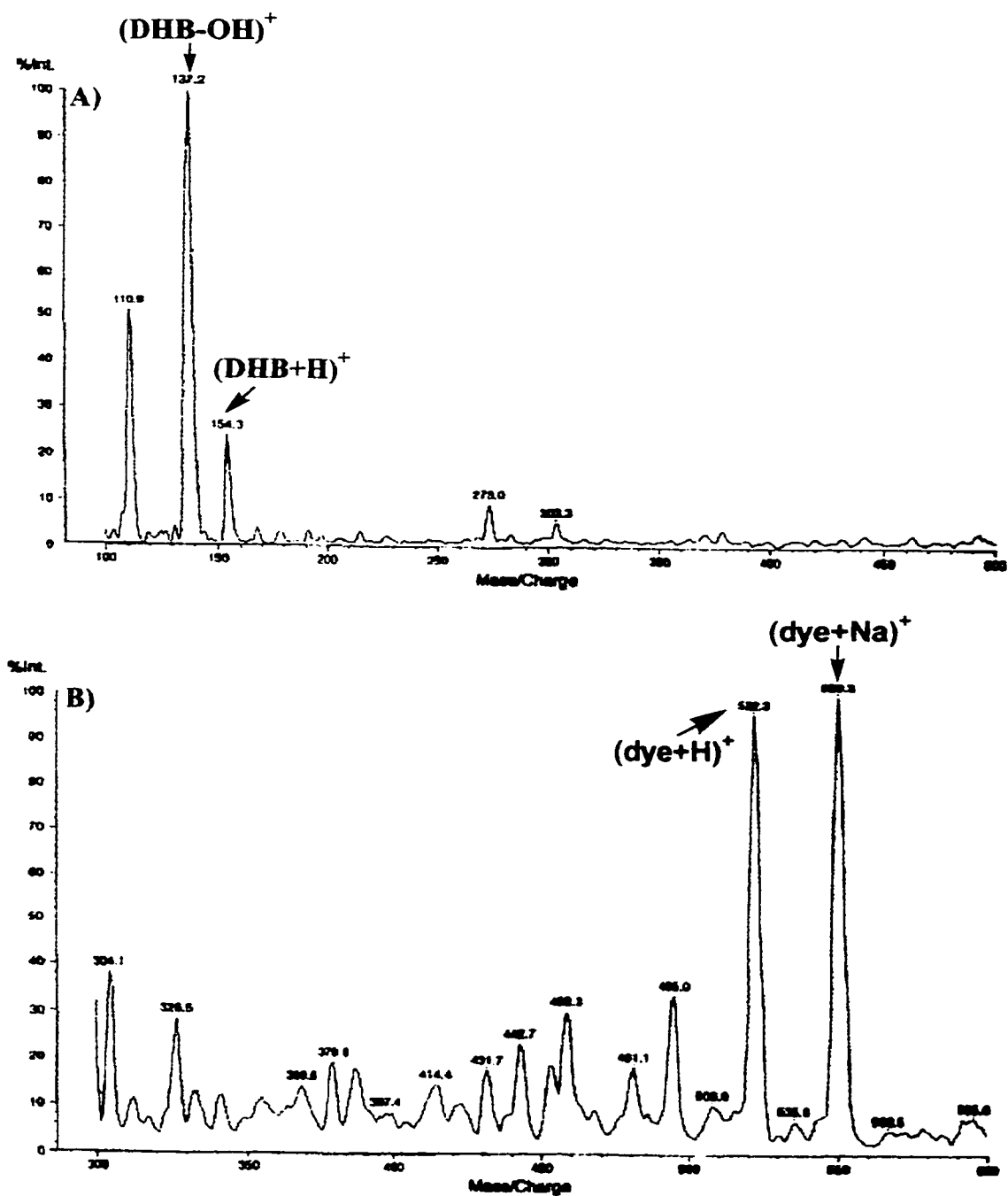
Figure 2.12: (continued)
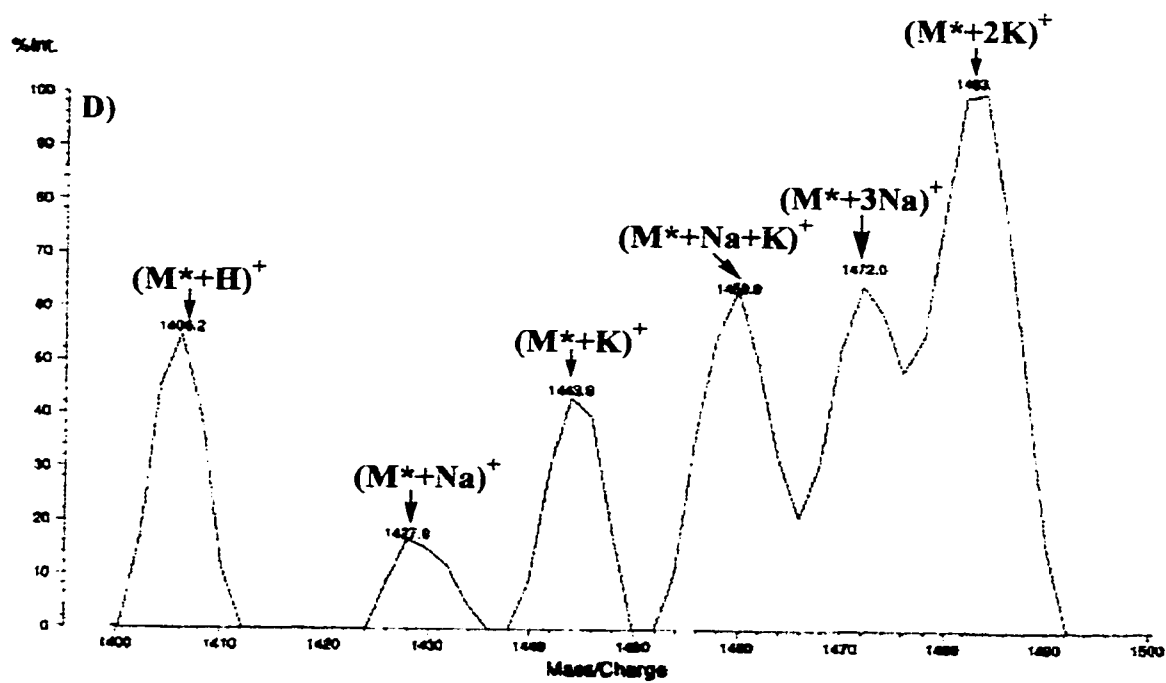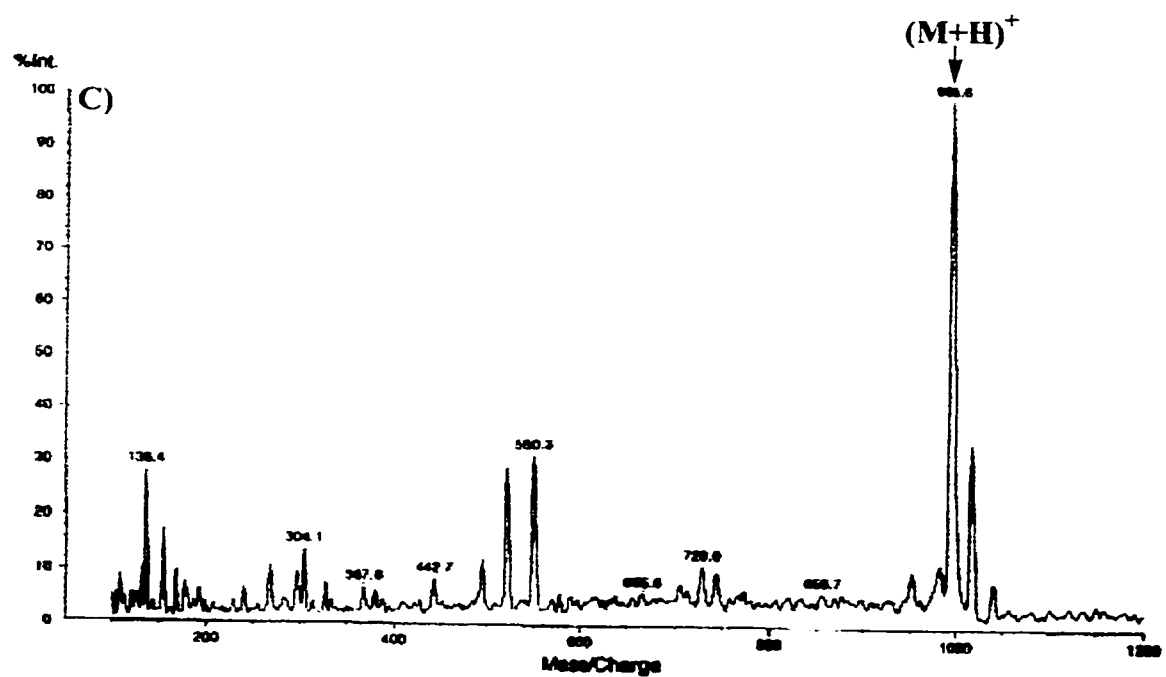
Figure 2.12: (continued)
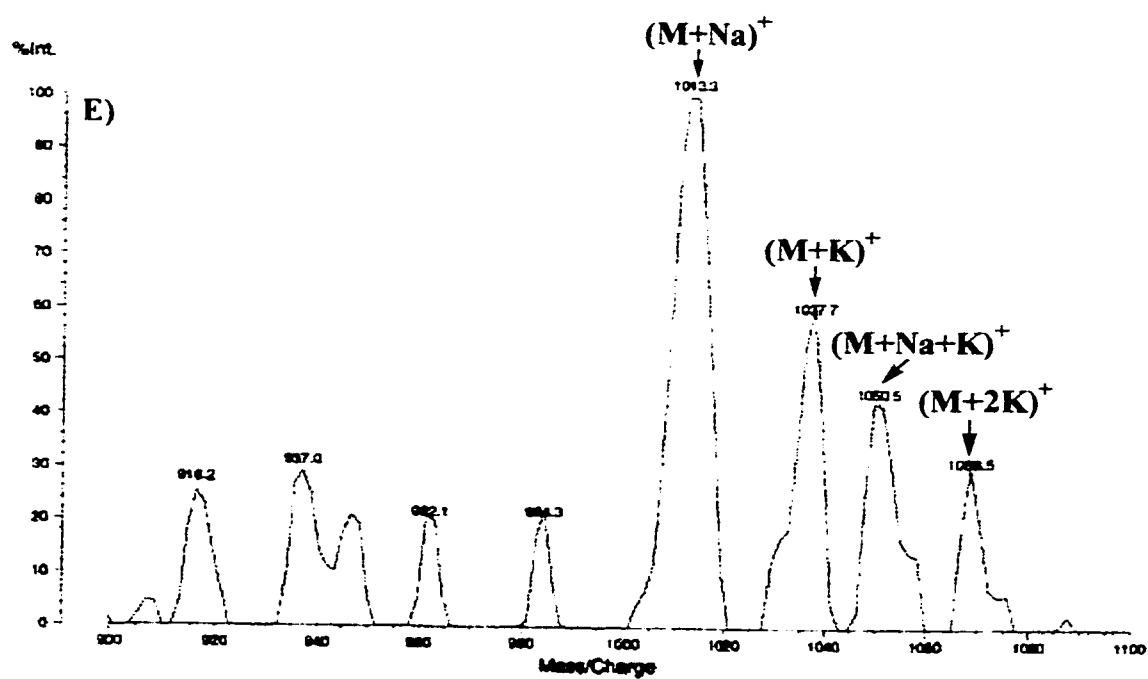
1013 amu, 1038 amu, 1051 amu and 1069 amu and are the $(M+Na)^+$, $(M+K)^+$,

$(M+Na+K)^+$ and $(M+2K)^+$ adducts, respectively. These results suggest that the labelling

reaction was successful but not going to completion.

Figure 2.13 shows the CZE-LIF electropherograms of the blank and sample

reaction mixtures run under the conditions described in Section 2.2.3. At least four

product peaks are present for labelled microcystin-LR (M*-LR) and are at migration

times between 96 – 108 s when both the blank and sample mixtures were run at a

concentration of $5*10^{-6}$ M. These peaks show the result of multiple labelling. This

means that the fluorescent dye not only reacted with the arginine group in microcystin-

LR but also the two carbonyl groups. Microcystin-LR antibody was then added

(2 – 10 μL) to the labelled microcystin-LR mixture and then run on the CE-LIF

instrument. The run conditions for this experiment are described in Section 2.2.3. The

effect of the added antibody can be seen in Figure 2.14. A peak for the antibody-antigen

complex of microcystin-LR was not found. It is suspected that an antibody complex peak

was not seen due to the complex adhering to the capillary wall. The labelled microcystin-

LR peak area as calculated using the Igor Pro macro Append Cursor Integration was

found to decrease linearly with the addition of the antibody. A working curve was

constructed (Figure 2.15) by graphing the peak area versus the amount of added

microcystin-LR antibody and the correlation coefficient was found to be r = -0.9906. The

correlation coefficient is used to test the hypothesis that there is no relationship between

two dependent and independent variables. A correlation coefficient close to ±1 shows

that there is a relationship between the peak area of the labelled microcystin-LR and the

Figure 2.13: The CZE-LIF electropherograms for the arginine-labelling reaction of microcystin-LR with 5-TAMRA-SE.

Capillary: 29.5 cm, 50 μm I.D., 140 μm O.D.. Run: 10 mM borate, pH 9, 14 kV. Injections: 3000 V, 5 s.

PMT: 1000 V. Laser: He-Ne (543 nm), 5 mW. Interference filter: 590DF35. Concentration: $5*10^{-6}$ M.
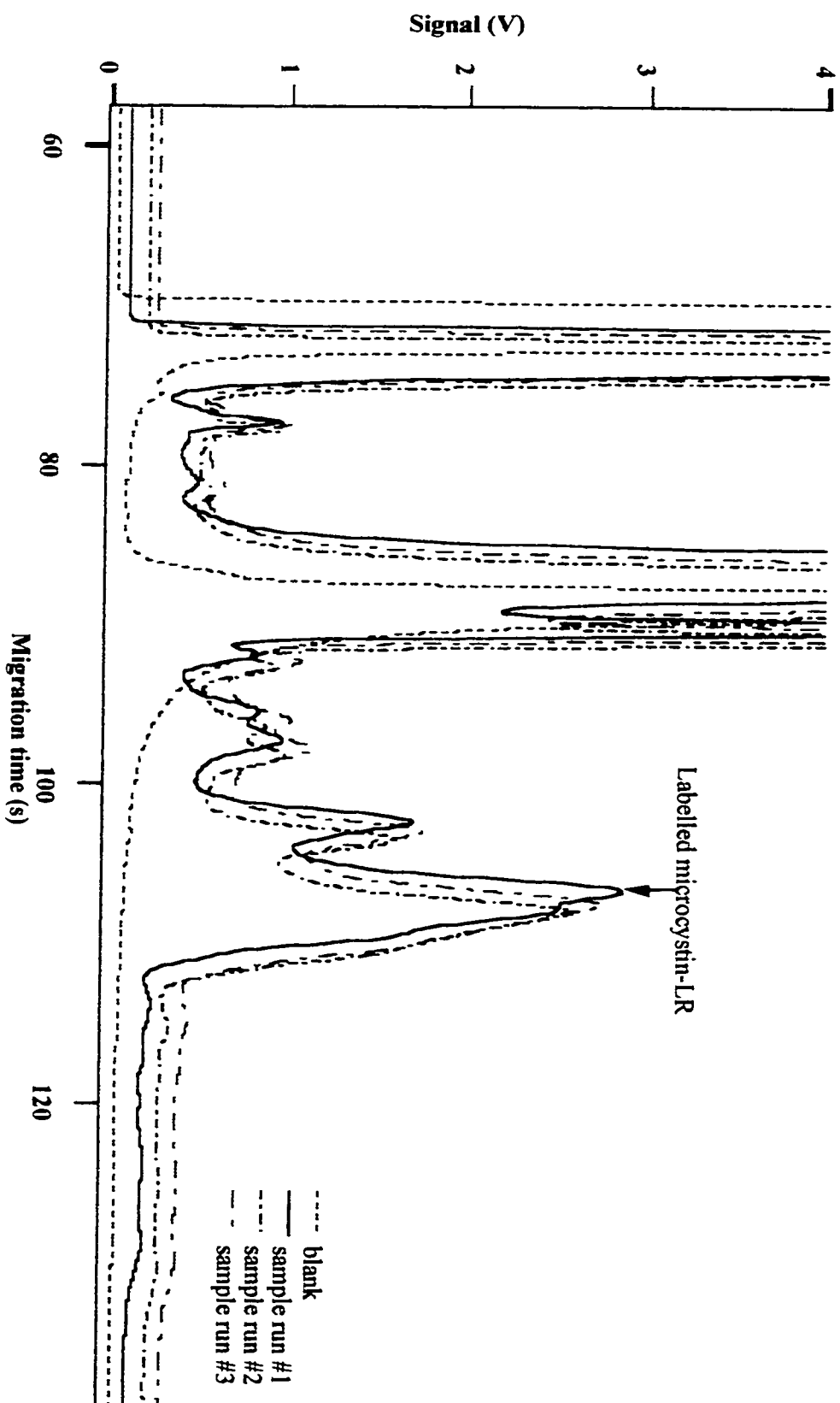
Figure 2.14: The results of added antibody to the 5-TAMRA-SE labelled microcystin-LR. Capillary: 29.5 cm, 50 μm I.D., 140 μm O.D.. Run: 10 mM borate, pH 9, 14 kV. Injections: 3000 V, 5 s. PMT: 1000 V. Laser: He-Ne (543 nm), 5 mW. Interference filter: 590DF35. Concentration: 10^{-6} M.

80
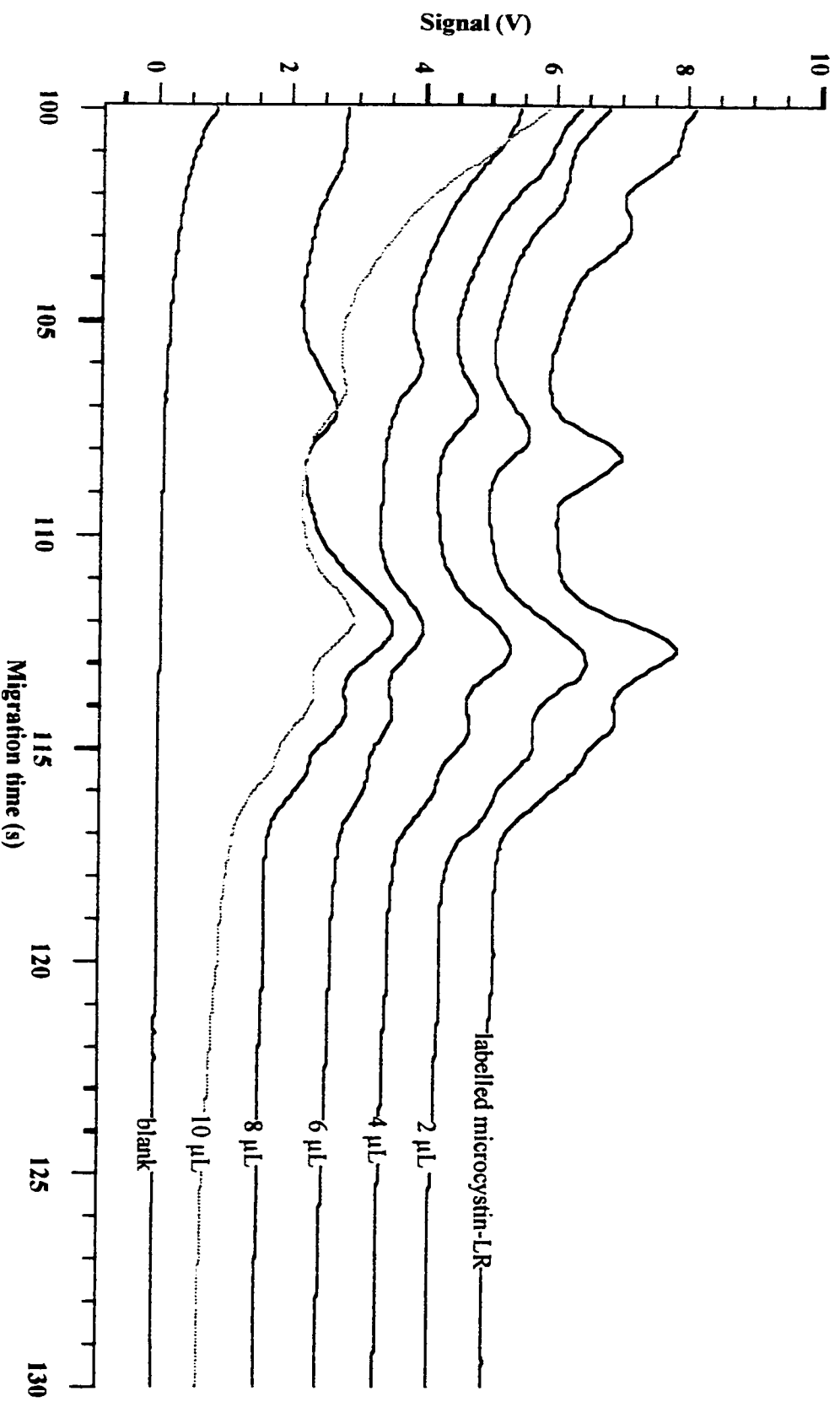
Figure 2.15: The calibration curve of added microcystin-LR antibody versus the peak area of the 5-TAMRA-SE labelled microcystin-LR peak.

81
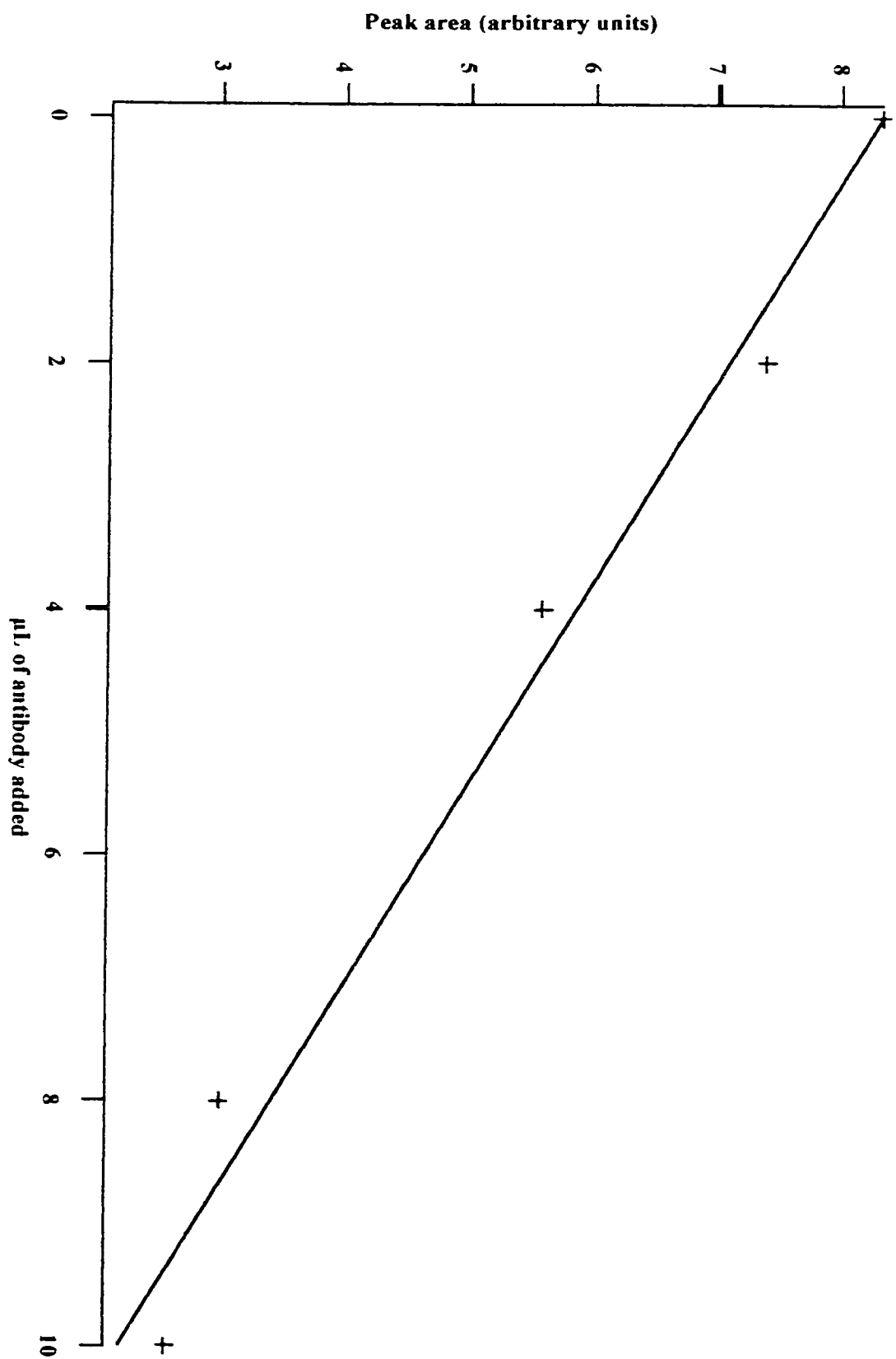
amount of microcystin antibody added however, it does not necessarily mean that the data are linear.

Next, gel permeation chromatography was used in an attempt to isolate the labelled microcystin-LR from the reaction mixture as described in Section 2.2.5. The resulting UV chromatogram showed three peaks (data not shown) which corresponded to fractions 22 – 36 for peak one, fractions 37 – 38 for peak two and fractions 41 – 48 for peak three. In size-exclusion chromatography theory the labelled microcystin-LR should elute first followed by unlabelled microcystin-LR and the uncomplexed dye. Each set of fractions was concentrated using a rotary evaporator. The concentrated fractions for the first and second peaks on the UV chromatogram (data not shown) were then analysed using MALDI-MS as described in Section 2.2.4. For both modes the concentrated fractions were dissolved in 4 µL of distilled deionized water and then 2 µL of the fraction solution was mixed with matrix solution and placed on the MALDI probe. The resulting spectra can be found in Figures 2.16 and 2.17. In the positive-ion mode of the first set of fractions (Figure 2.16 A) three major peaks for the dye are found at 494 amu, 522 amu and 549 amu, which are the hydrolysed dye, hydrogen, and sodium adducts, respectively. These results show that even though the labelling reaction worked some dye was hydrolysed due to water somehow present during the reaction. Three major peaks for the labelled product in the first set of fractions (Figure 2.16 B) are found at 1432 amu, 1448 amu and 1482 amu which correspond to the $(M^*+Na)^+$, $(M^*+K)^+$ and $(M^*+K+Na)^+$ adducts, respectively. The positive-ion mode spectrum of the second set of fractions (Figure 2.16 C) shows that just hydrolysed dye was present. The negative-ion mode of the first set of fractions (Figure 2.17 A) shows a major peak at 470 amu, which

Figure 2.16: The positive-ion mode MALDI-MS spectra of A) the first peak

(fractions 22-36) m/z 400 - 700, B) the first peak (fractions 22-36)

m/z 1400 - 1500, C) the second peak (fractions 37-38).
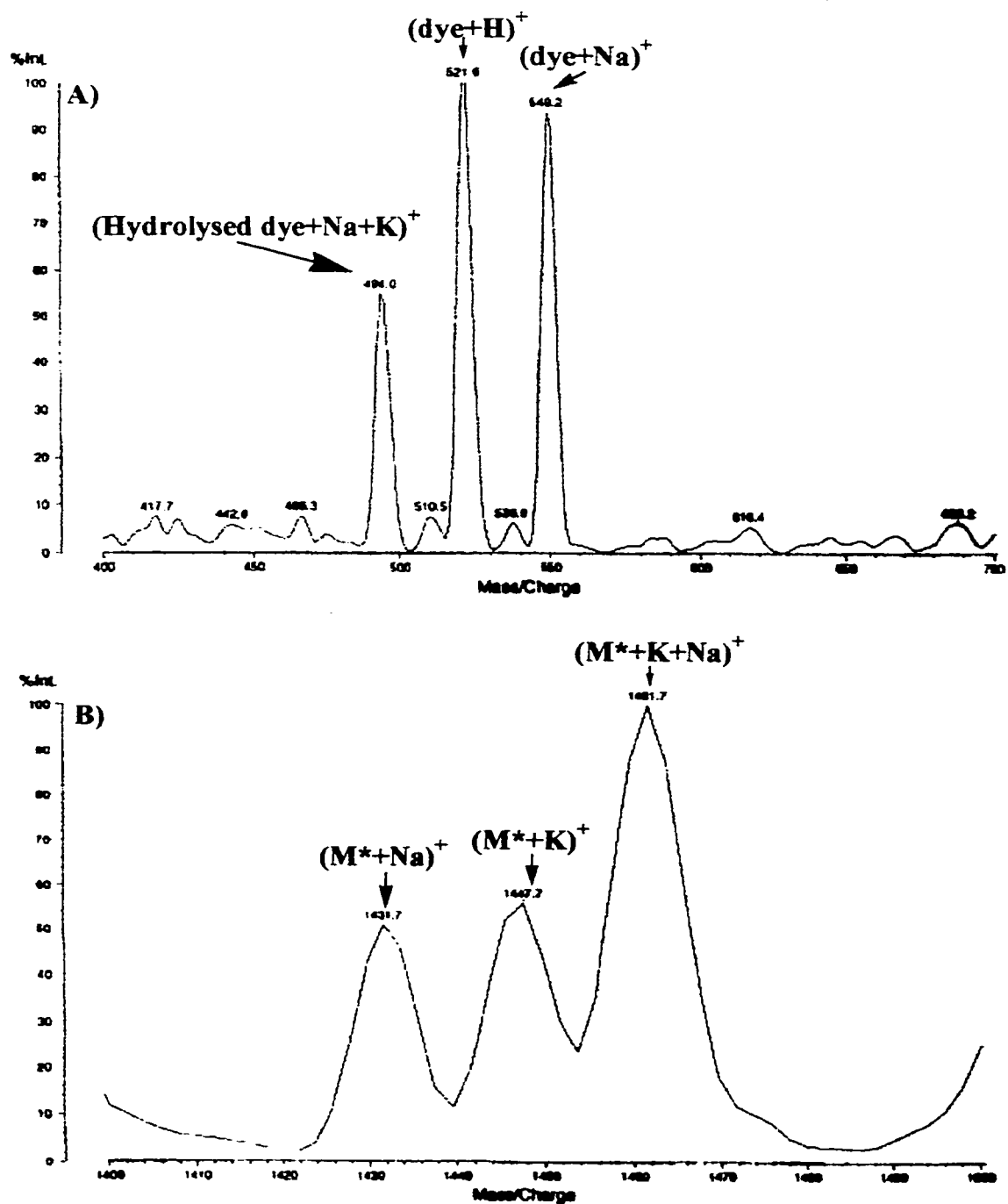
Figure 2.16: (continued)
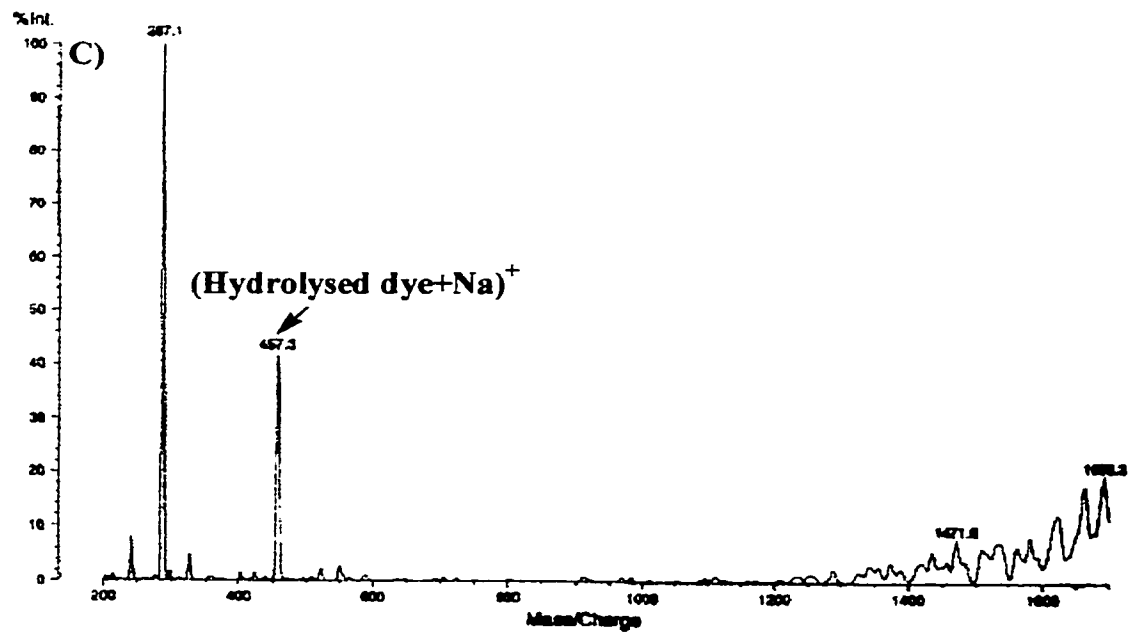
Figure 2.17: The negative-ion mode MALDI-MS spectra of A) the first peak

(fractions 22-36) m/z 400 - 1600, B) the first peak (fractions 22-36)

m/z 1380 - 1560, C) the second peak (fractions 37-38).
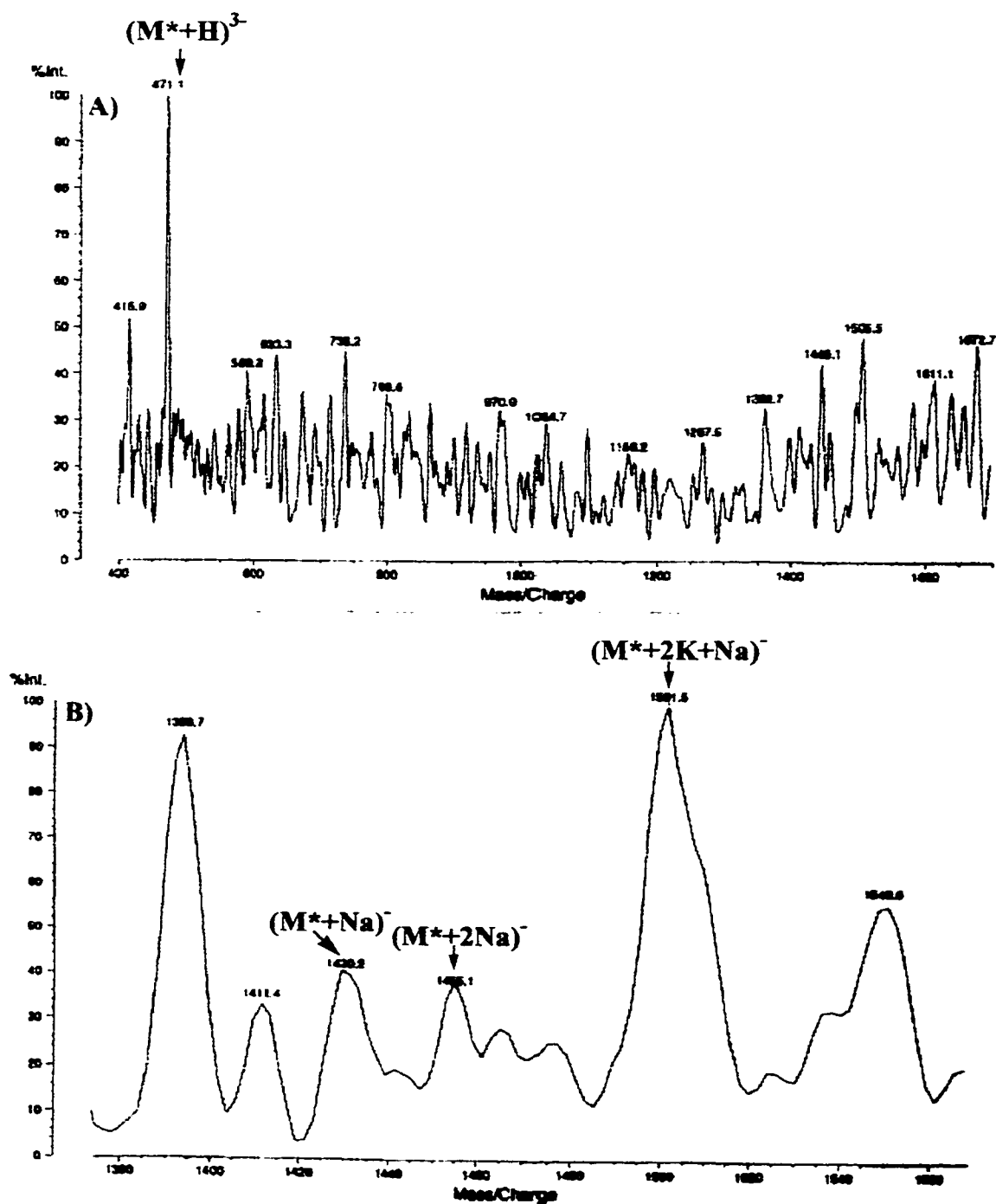
Figure 2.17: (continued)

86
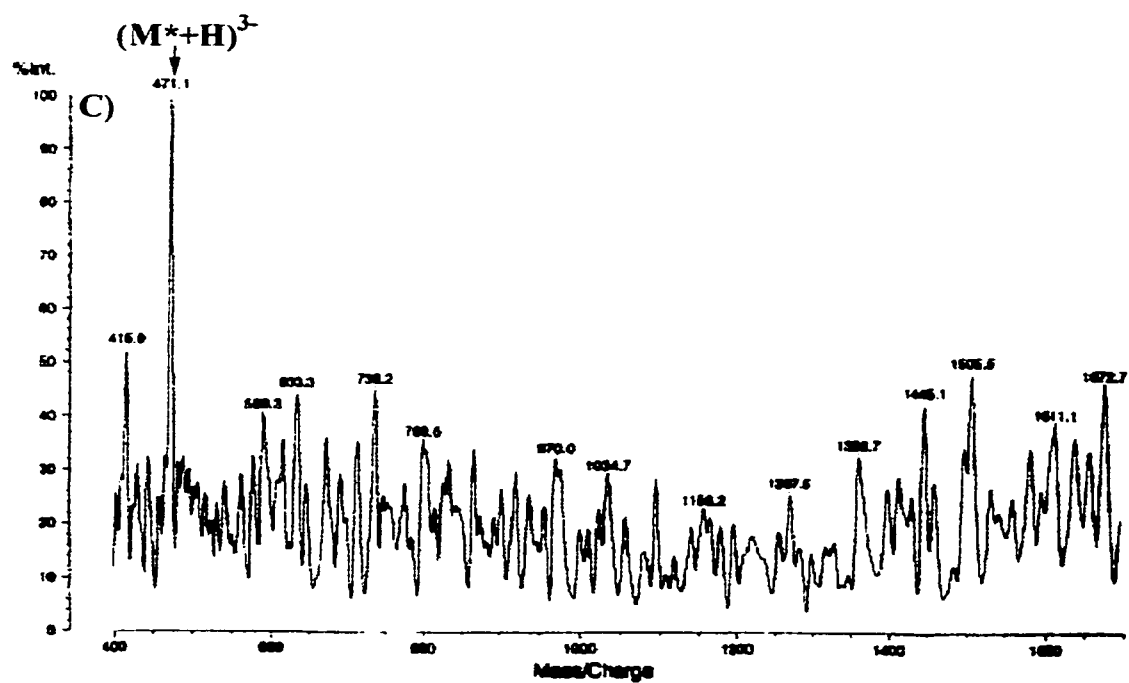
corresponds to the triply-charged hydrogen adduct of the labelled microcystin-LR. The

negative-ion mode of the first set of fractions (Figure 2.17 B) also shows small peaks at

1430 amu, 1455 amu, and 1502 amu which are assigned as $(M^*+Na)^-$, $(M^*+2Na)^-$ and

$(M^*+2K+Na)^-$, respectively. The negative-ion mode of the second set of fractions

(Figure 2.17 C) shows one major peak at 471 amu, which is the triply-charged hydrogen

adduct of the labelled microcystin-LR. These results show that gel permeation

chromatography was unsuccessful in completely separating the labelled microcystin-LR

from the unreacted reagents.

2.3.2 Microcystin-LR labelling with 5-BMF using NaH deprotonation

The next step was to label the microcystin-LR with 5-BMF as described in

Section 2.2.6. The same reaction apparatus was used as before. The reaction mechanism

for this labelling reaction using 5-BMF can be found in Figure 2.18. This nucleophilic

substitution reaction occurs via a S_N2 mechanism, which takes place in a single step

without intermediates. The entering nucleophile (amine group of arginine) attacks the

substrate (5-BMF) at 180° from the leaving group (bromide ion). As the nucleophile

comes in on one side of the molecule, the leaving group departs from the opposite side.

Microcystin-LR contains one free amine group found on the arginine residue plus two

carbonyl groups that can react with the dye. Since the carbonyl group is a better leaving

group than the amine group, it is assumed that the preferential product will have its amine

group reacting with the dye even though both functional groups will react with the alkyl

halide dye to some extent. As a result, there are many possible labelling products that

can be formed in this labelling reaction.

Figure 2.18: The schematic diagram of the arginine-labelling reaction of microcystin-LR with 5-BMF, which involves a nucleophilic substitution reaction via a S_N2 mechanism.
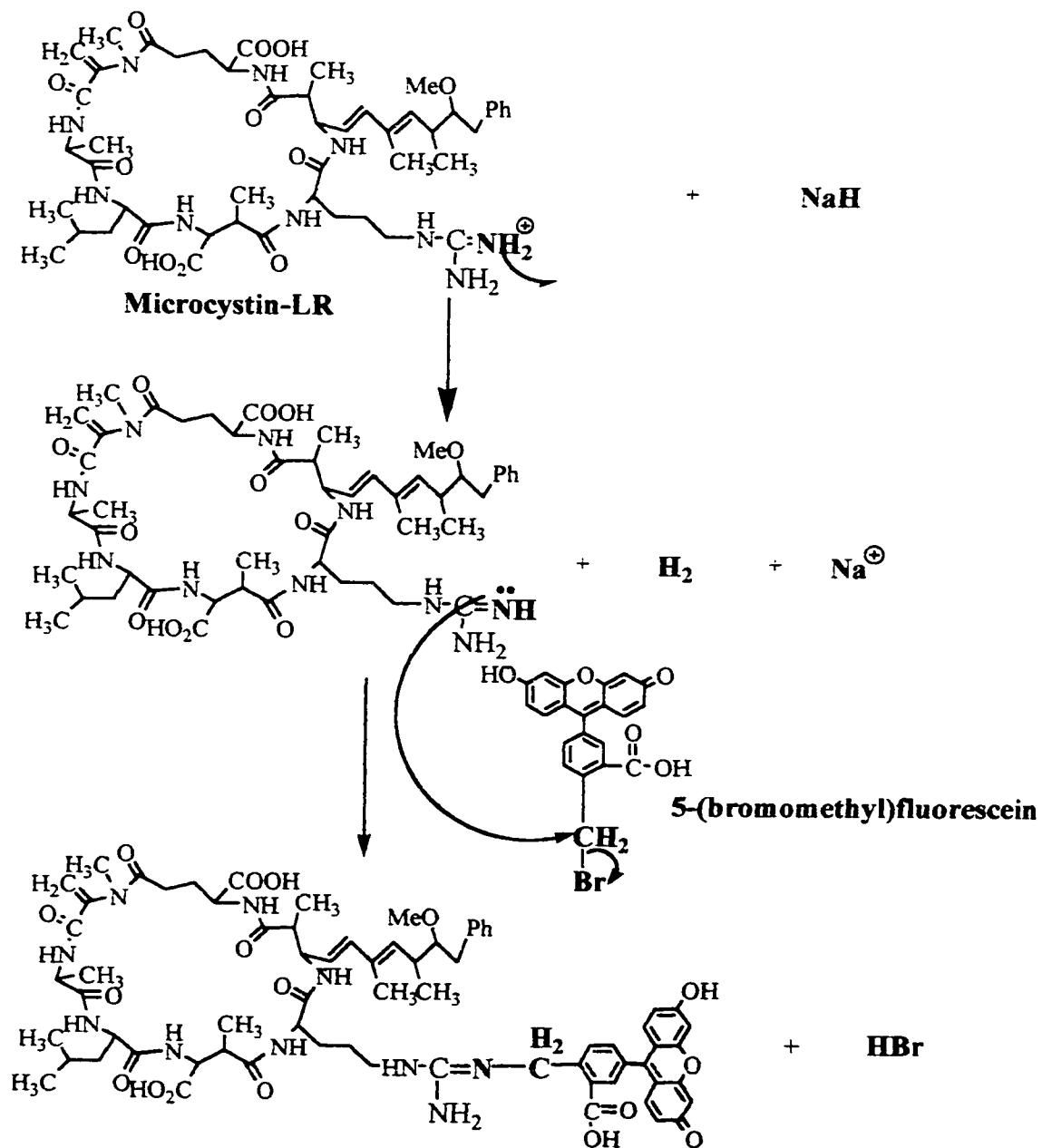
The blank and sample reaction mixtures were purified using a C_{18} Sep-Pak[R]

cartridge as described in Section 2.2.5. Next, the purified sample reaction mixture was

analysed using MALDI-MS in both the positive-ion mode and the negative-ion mode.

The resulting spectra can be found in Figure 2.19. Using the positive-ion mode a number

of salt adduct peaks are found for the labelled microcystin-LR (M*). The peaks are at

1344 amu, 1363 amu, 1375 amu, 1410 amu, 1428 amu, 1450 amu and 1474 amu and are

assigned as $(M*+H)^+$, $(M*+Na)^+$, $(M*+K)^+$, $(M*+3Na)^+$, $(M*+4Na)^+$, $(M*+3Na+K)^+$ and

$(M*+3K+Na)^+$, respectively. In the negative-ion mode only one major peak is found for

the labelled microcystin-LR which is at 1361 amu and is assigned as $(M*+Na)^+$. These

results indicate that the labelling reaction was successful.

Next, the purified sample reaction mixture was analysed using positive-ion mode

ESI-MS as described in Section 2.2.2 and the resulting spectrum is found in Figure 2.20.

The relevant peaks found in the positive-ion mode ESI-MS spectra are at 346 amu, 689

amu, 996 amu, 1033 amu and 1377 amu and are assigned as $(dye-Br + H)^+$, (dimer of

dye-Br + $H)^+$, $(M+H)^+$, $(M+K)^+$, and $(M*+K)^+$, respectively. This positive-ion mode

ESI-MS spectrum shows that the labelling reaction was successful, since labelled

microcystin-LR (M*) is present, yet was not going to completion since unlabelled

microcystin-LR (M) is found.

Next, the purified blank and sample reaction mixtures were analysed using CZE-

LIFP. The CZE-LIFP set-up is found in Figure 2.8 and is described in Section 2.2.2. The

CZE-LIFP electropherograms of the blank and sample labelling reaction mixtures with

added antibody are found in Figure 2.21 and were performed under the conditions

described in Section 2.2.7. The resulting CZE-LIFP electropherograms showed that there

Figure 2.19: The MALDI-MS spectra of the arginine-labelling reaction of

microcystin-LR with 5-BMF using NaH deprotonation.

A) positive-ion mode B) negative-ion mode.
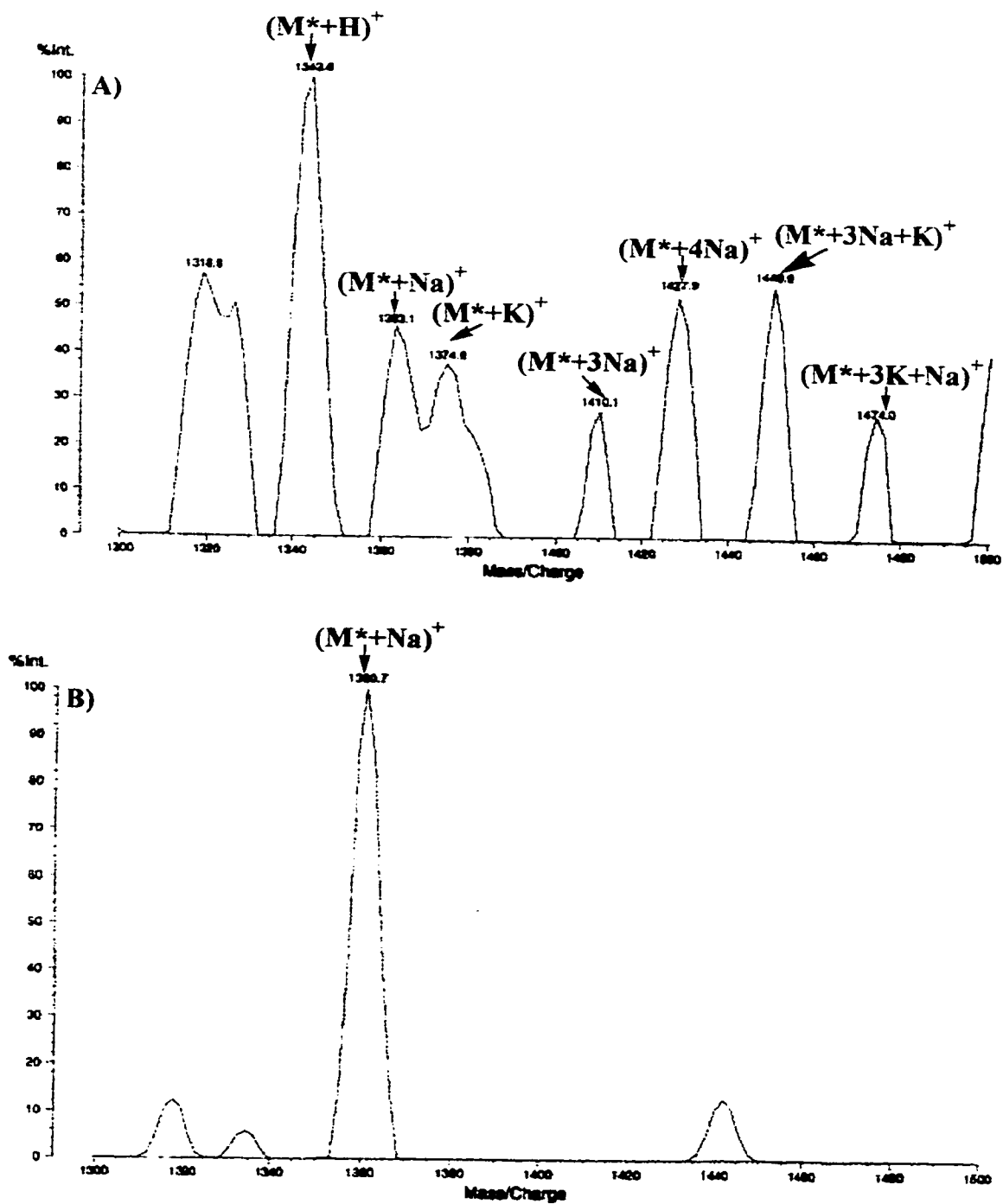
Figure 2.20: The positive-ion mode ESI-MS spectrum of the purified 5-BMF labelled microcystin-LR reaction mixture.

91
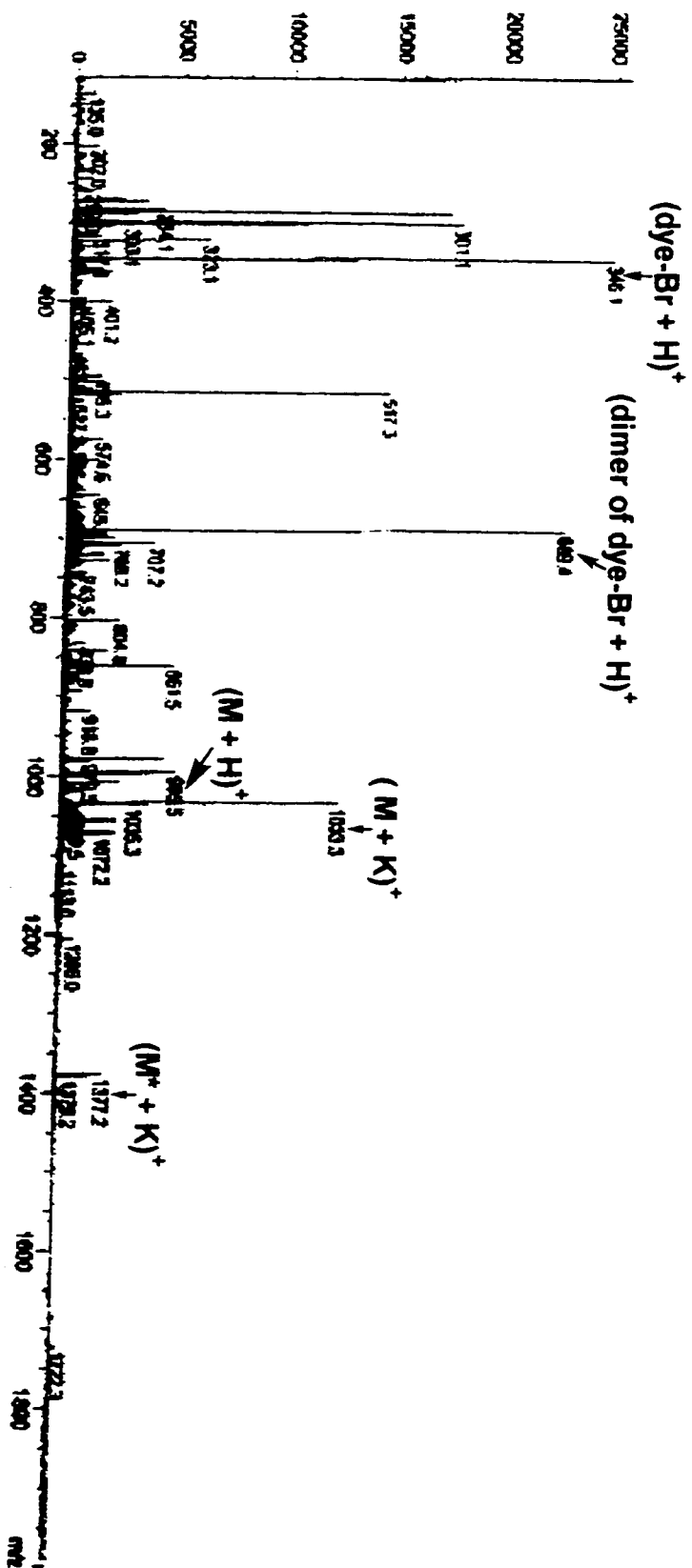
Figure 2.21: The CZE-LIFP electropherograms of the 5-BMF labelled microcystin-LR with 0 and 5 μL added antibody, at the two channels. Capillary: 35 cm, 50 μm I.D., 140 μm O.D.. Run: 10 mM borate, pH 9, 14 kV. Injections: 3000 V, 5 s. PMT: 750 V. Laser: 488 nm Ar⁺, 4 mW. Interference filter: 515DF20. Concentration: post-column ~10⁻⁶ M.
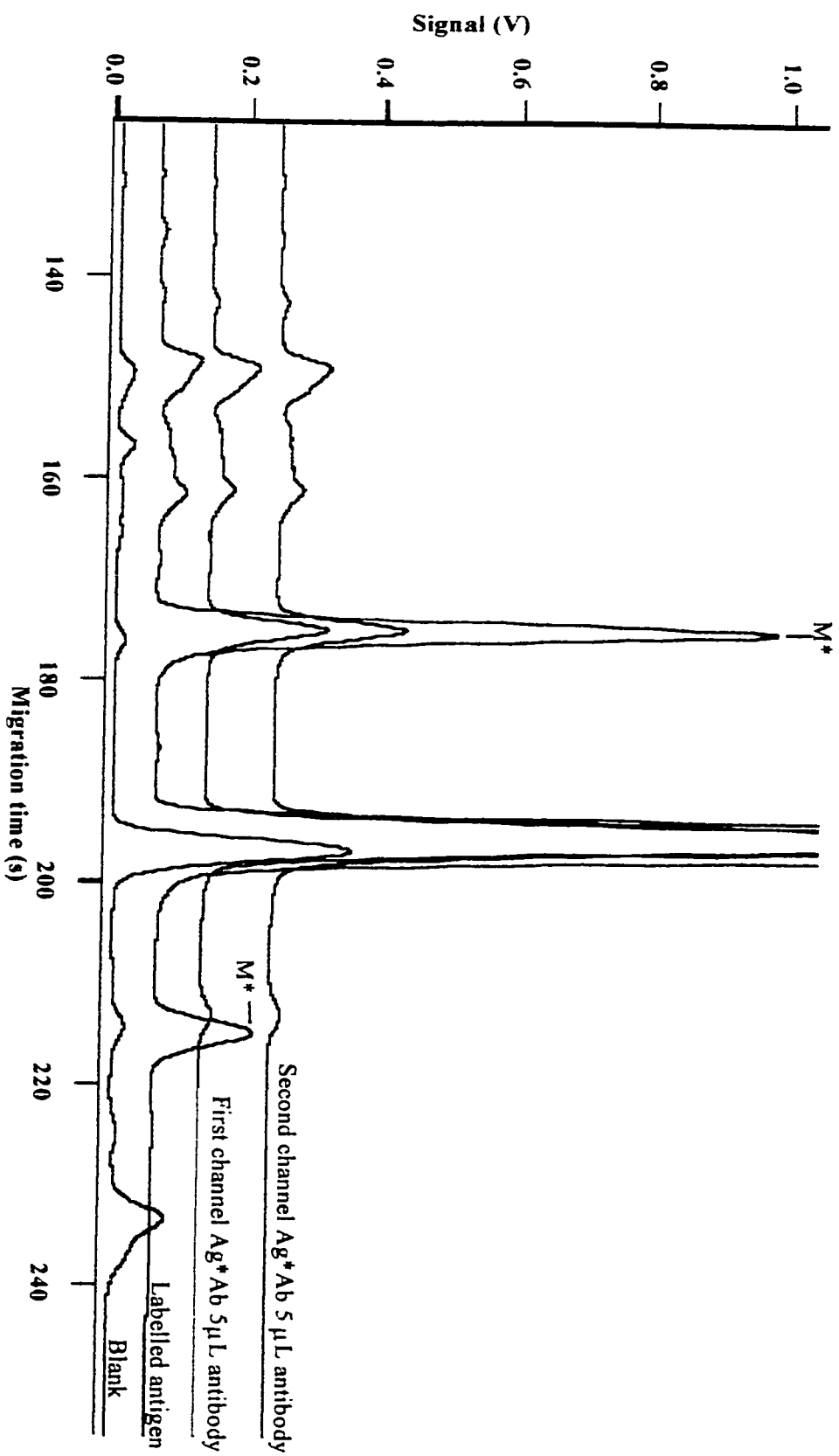
are two peaks that could be the labelled microcystin-LR but a peak for the antibody-microcystin-LR complex was not found. The CZE-LIFP electropherograms also showed that there was no difference in signal between the first and second channel PMTs which confirms that an antibody complex was not present. The antibody complex was probably stuck to the capillary wall so that is why a complex peak was not found. The presence of two product peaks shows that multiple labelling has occurred.

The conditions for the second CZE-LIFP experiment are described in Section 2.2.7. For the purpose of monitoring the effect of added antibody (0 – 5 μL) the second product peak was observed (Figure 2.22). Once again a peak for the antibody complex was not found and this is thought to be due to adherence to the capillary wall. Another working curve was constructed by plotting the peak area of the second product peak as calculated by the Igor Pro macro Append Cursor Integration versus the amount of added antibody and can be found in Figure 2.23. The resulting curve was linear with a correlation coefficient of r = -0.9932. This working curve was similar to the one constructed in Figure 2.15 and proves the reproducibility of the added antibody experiment. To try to find the antibody-microcystin-LR complex peak a Grignard-poly-acryloylaminopropanol (poly-AAP)-coated capillary was used to analyze the blank and sample reaction mixtures but a complex peak was still not found (data not shown). Next, a microcystin-LR fluorescent flow displacement immunoassay was attempted using the labelled microcystin-LR reaction mixture.

Figure 2.22: Monitoring of the second 5-BMF labelled microcystin-LR peak from Figure 2.21 to see the effect of added antibody. Capillary: 36 cm, 50 µm I.D., 140 µm O.D.. Run: 10 mM borate with 1 mM β-cyclodextrin, 23 kV. Injections: 3000 V, 5 s. PMT: 750 V. Laser: 488 nm Ar⁺, 4 mW. Interference filter: 515DF20. Concentration: post-column ~ 10^{-6} M.
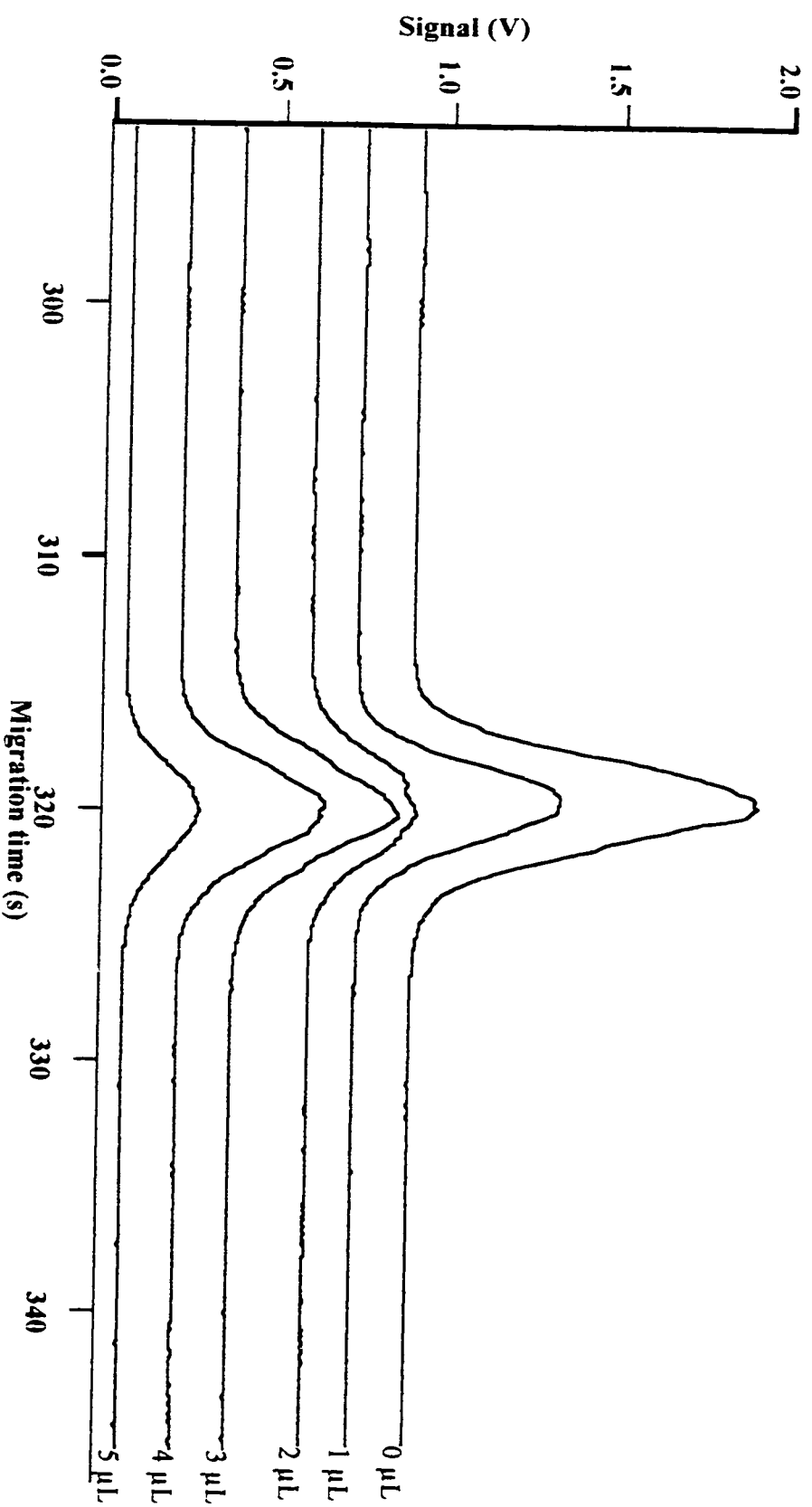
Figure 2.23: The CZE-LIFP working curve of added antibody versus the peak area of the second 5-BMF labelled microcystin-LR peak.
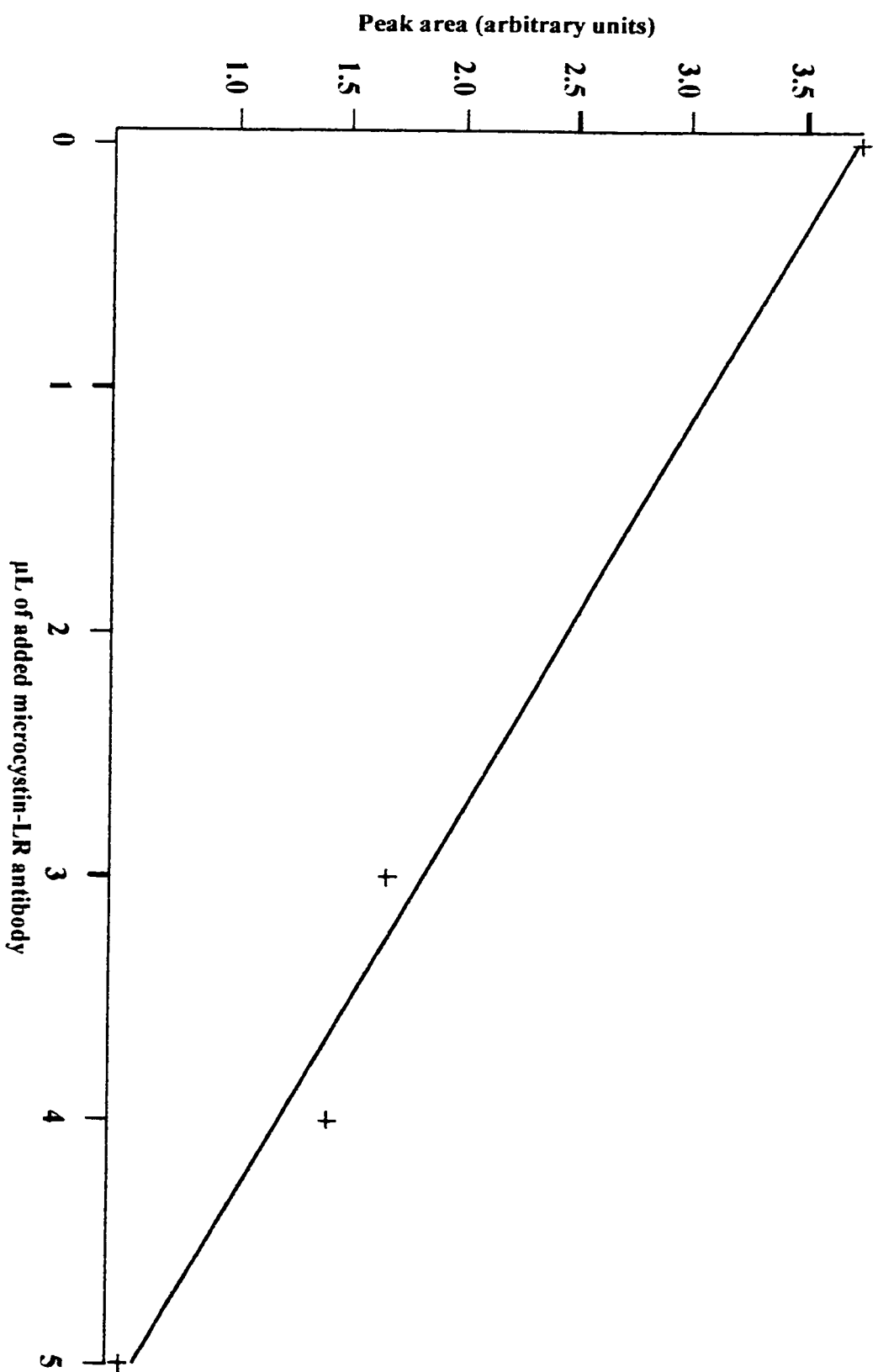
2.3.3 Microcystin-LR fluorescent flow displacement immunoassay

The description of how the microcystin-LR fluorescent flow displacement immunoassay works was described in Section 2.1.4. The procedure for immobilizing the microcystin-LR antibody on the capillary wall is described in Section 2.2.8. The conditions under which the flow displacement immunoassay was performed are described in Section 2.2.9. The standards were made using purchased unlabelled microcystin-LR dissolved in run buffer. The resulting spectrum for the 1 nM standard run on the microcystin-LR fluorescent flow displacement immunoassay can be found in Figure 2.24. A calibration curve constructed from all standards (0 – 5 nM) run using flow injection and LIF detection can be found in Figure 2.25. The peak areas of each of the resulting 5-BMF labelled microcystin-LR peaks were calculated using the Igor Pro macro Append Cursor Integration. This calibration curve was exponential in nature. Peak area was plotted against the logarithm of concentration to linearize the calibration curve and the resulting curve had a correlation coefficient of r = +0.9922. This calibration curve can be found in Figure 2.26. At this time, it was desirable that the microcystin-LR fluorescent flow displacement immunoassay be checked for reproducibility but unfortunately additional antibody to microcystin-LR was unavailable so further investigation into this procedure was unable to be performed.

2.3.4 Arginine-labelling reagent

The arginine-labelling reagent was synthesized as described in Section 2.2.10. The schematic diagram of the mechanism of this synthesis reaction can be seen in Figure 2.27 and occurs via a S_N2 reaction. The reaction mixture was checked for product by

Figure 2.24: The peak for the 10^{-9} M unlabelled microcystin-LR standard using the microcystin-LR fluorescent flow displacement immunoassay. Capillary: 50 cm, 50 μm I.D., 140 μm O.D.. Run: 10 mM NaH₂PO₄, 2.5 % ethanol, pH 7.6. Injections: 21 cm pressure injection using gravity as a siphon for 10 s, rate 0.2 μL/min. Sheath flow buffer: 0.05 M Na₂HPO₄, 0.025 M K₂SO₄, pH 10.2. PMT: 1000 V. Laser: 488 nm Ar⁺, 12.1 mW. Interference filter: 518DF25.

97
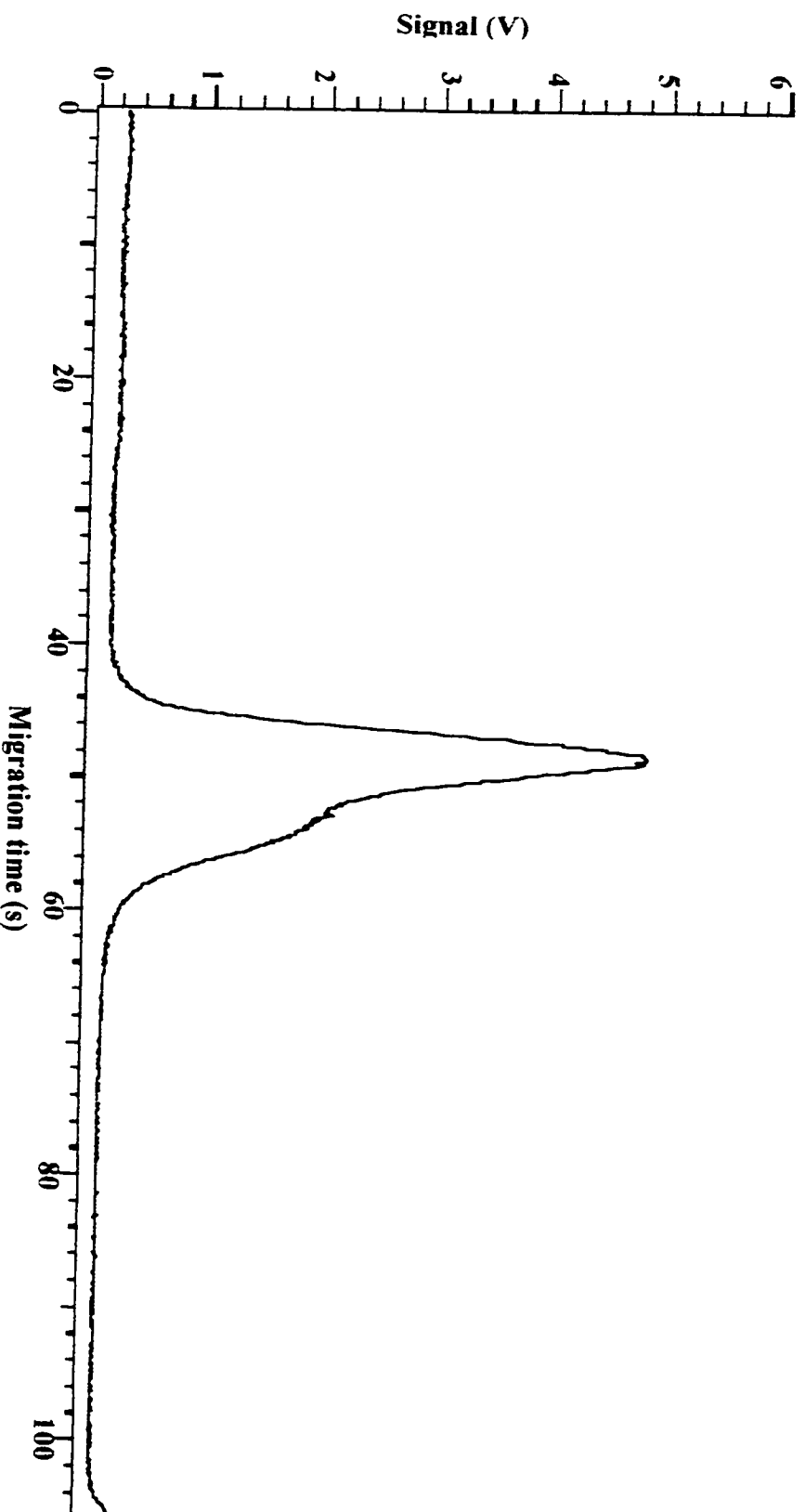
Figure 2.25: The exponential calibration curve for the microcystin-LR fluorescent flow displacement immunoassay.
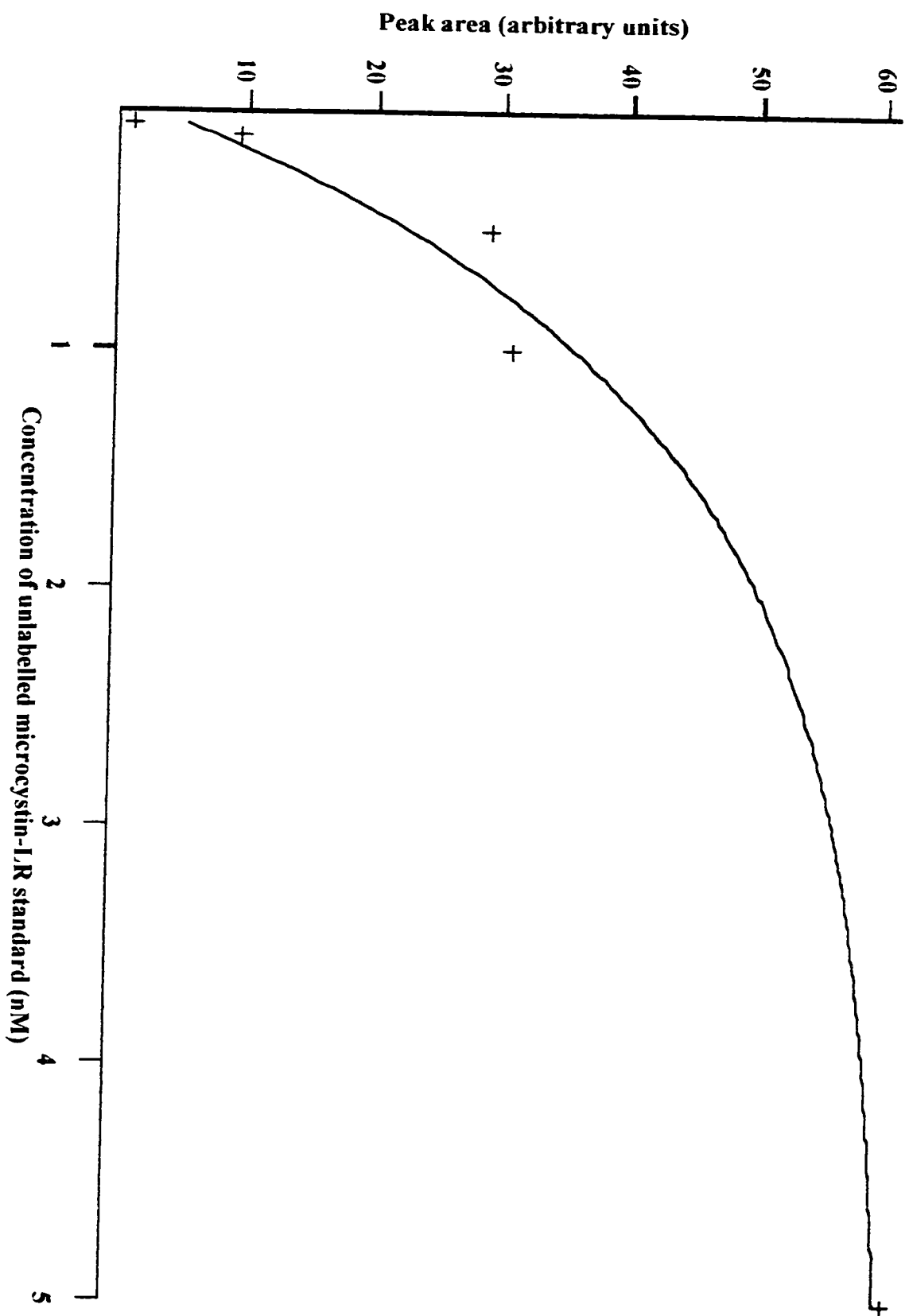
Figure 2.26: The logarithm of the exponential calibration curve for the microcystin-LR fluorescent flow displacement immunoassay.
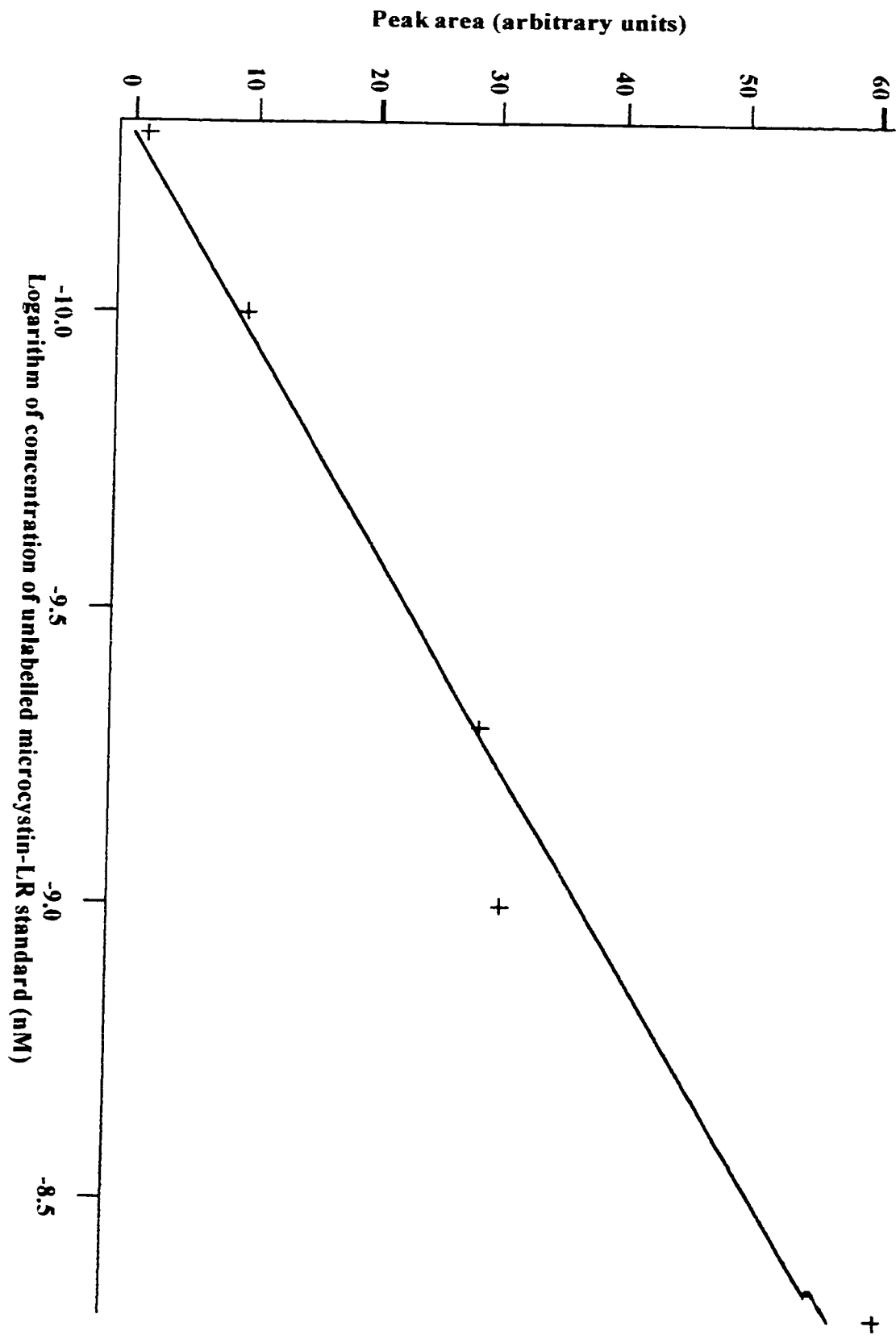
Figure 2.27: The schematic diagram of the synthesis of the arginine-labelling reagent which involves a nucleophilic substitution reaction which occurs via a S_N2 mechanism.

2,3-butanedione
MW= 86.09 g/mol

5-(bromomethyl)fluorescein
MW= 425.23 g/mol

MW= 430.42 g/mol
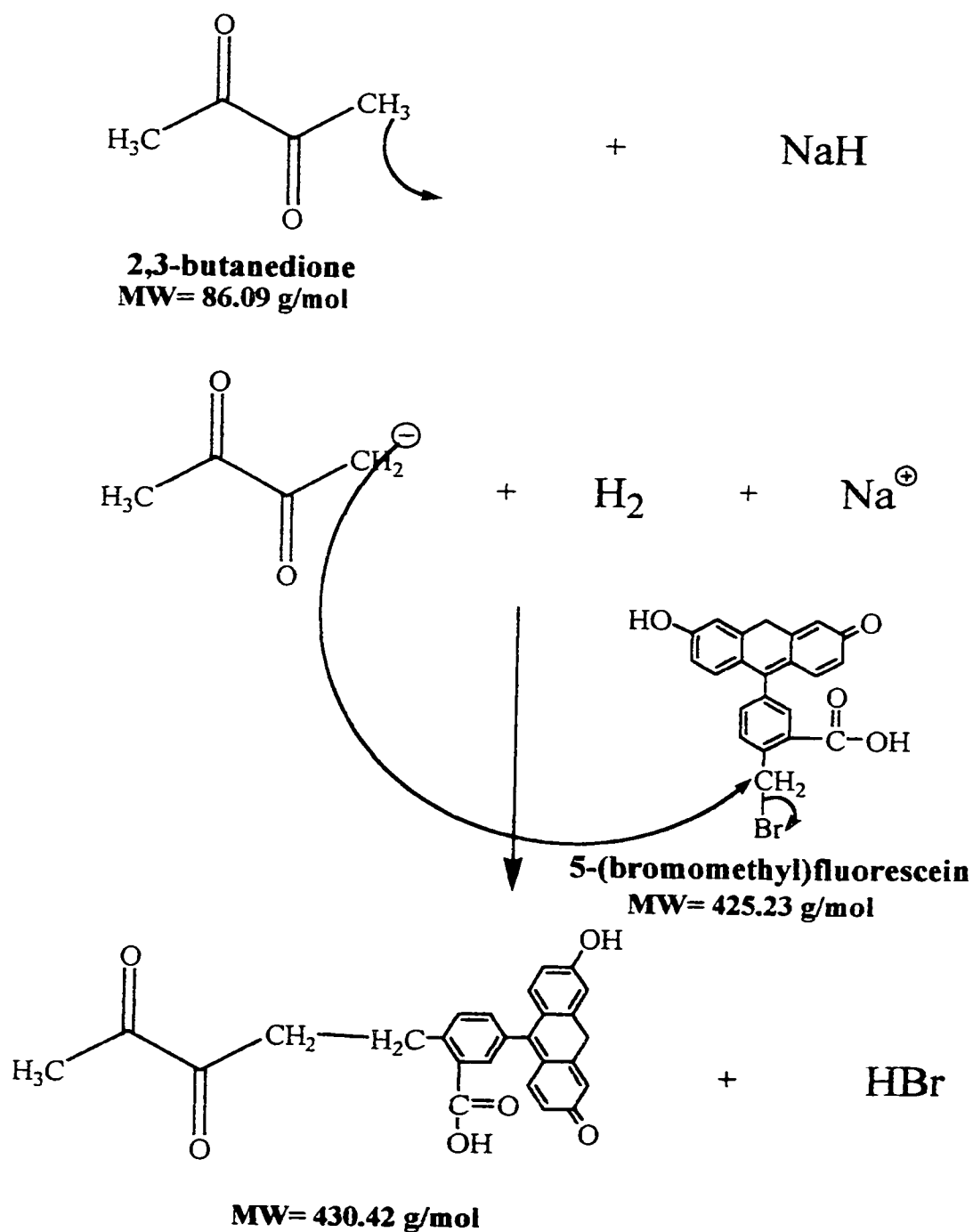
positive-ion mode ESI-MS and the resulting spectrum can be found in Figure 2.28. The resulting positive-ion mode ESI-MS spectrum shows a product peak at 469 amu, which was assigned as the potassium adduct of the desired product. The presence of this peak proved that the synthesis was successful.

Next, the arginine-labelling reagent was reacted with N_α-acetyl arginine as described in Section 2.2.11. The schematic diagram of this reaction can be found in Figure 2.7 and is explained in detail in Section 2.1.5. The blank and sample reaction mixtures were then analysed using CZE-LIF under the conditions described in Section 2.2.10 and the resulting electropherograms can be found in Figure 2.29. A peak for labelled arginine was not found and therefore this arginine-labelling reaction was unsuccessful. A possible explanation for the unsuccessful binding of the labelling reagent to arginine is that the nucleophilic group introduced onto the diketone to displace the bromide ion of 5-BMF will destroy the diketone functional group faster than the displacement reaction can occur. If this degradation of the diketone functional group occurs the labelling reagent is unable to react with the guanidinium group of arginine. Graduate student Hans Osthoff will do further investigation into this project.

2.4 Conclusions

The hepatotoxin microcystin-LR was successfully fluorescently labelled with two labelling reagents, 5-carboxytetramethylrhodamine, succinimidyl ester (5-TAMRA-SE) and 5-(bromomethyl)fluorescein (5-BMF). The monocyclic peptide microcystin-LR has one free amine group and two carbonyl groups that can react with the fluorescent derivatization reagents.

Figure 2.28: The positive-ion mode ESI-MS spectrum of the synthesized arginine-labelling reagent.
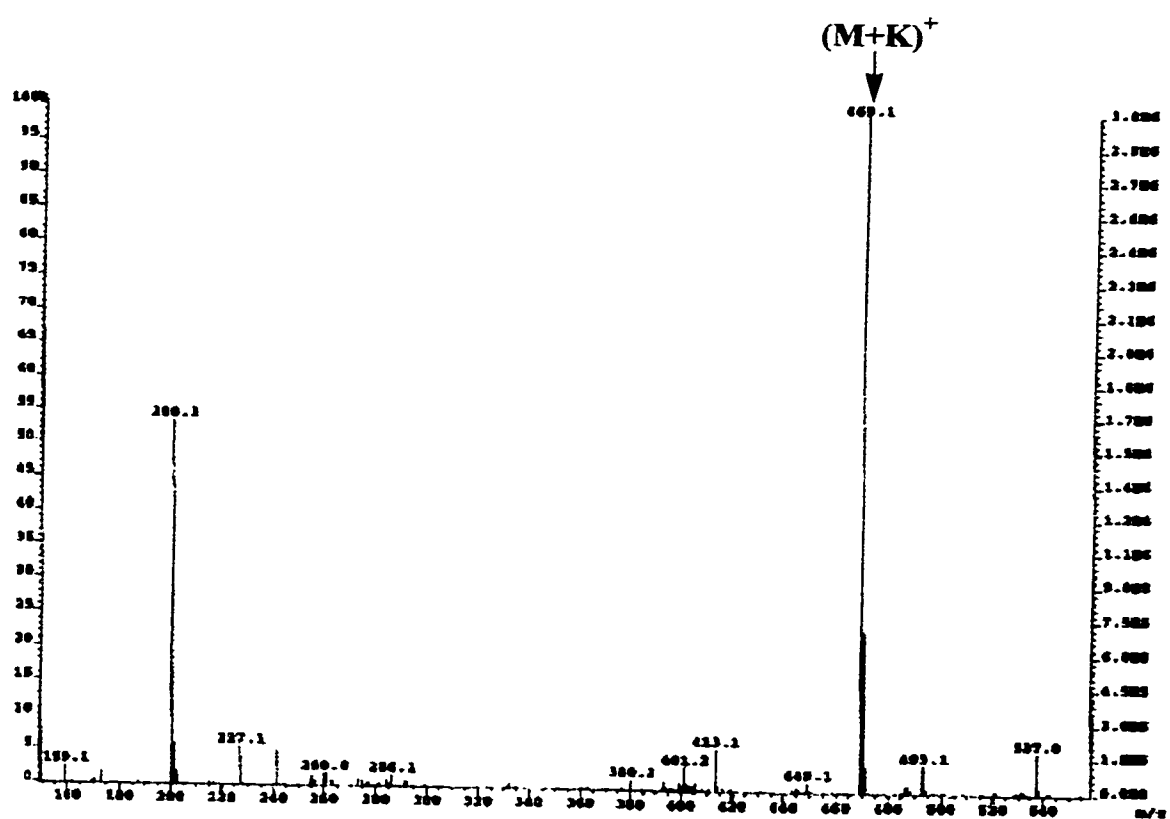
Figure 2.29: The CZE-LIF electropherograms of the reaction of N_α-acetyl arginine with the synthesized arginine-labelling reagent. Capillary: 30 cm, 50 μm I.D., 140 μm O.D.. Run: 10 mM borate, pH 9, 17 kV. Injections: 3000 V, 5 s. Laser: 488 nm Ar^+, 12.1 mW. PMT: 1000 V. Interference filter: 518DF25. Concentration: 10^{-8} M.

blank
sample run #1
sample run #2
5-BMF
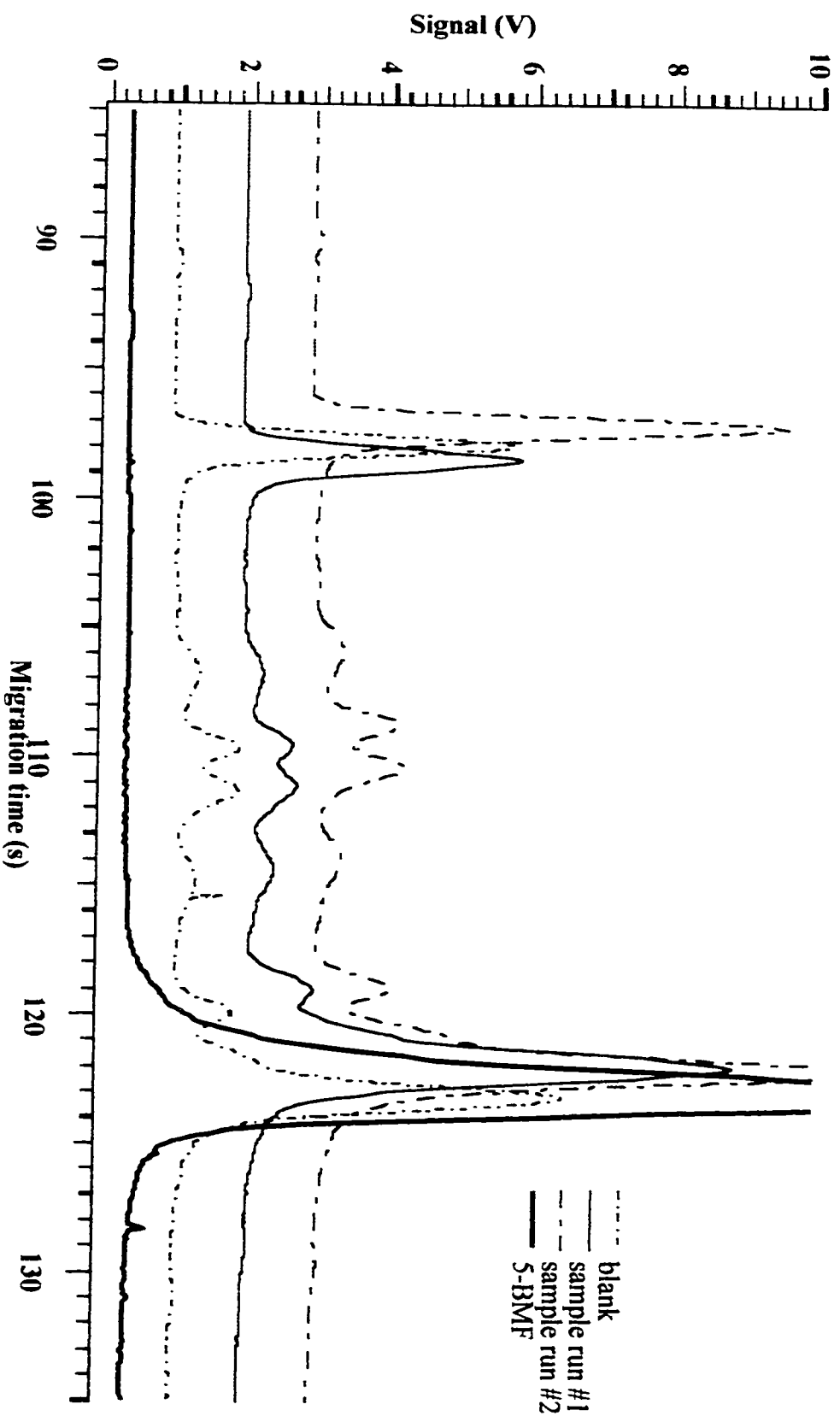
The MALDI-MS spectrum of the labelling reaction mixture involving the fluorescent dye 5-TAMRA-SE revealed peaks for labelled and unlabelled microcystin-LR, which proved that the labelling reaction was successful but did not go to completion. The CZE-LIF electropherograms of the reaction mixture revealed four product peaks for labelled microcystin-LR when 5-TAMRA-SE was used as the fluorescent tag. These results show that multiple labelling occurred in the labelling reaction. A working curve of the effect of adding microcystin antibody to the labelling reaction mixture was constructed using CZE-LIF and the resulting curve had a correlation coefficient of $r = -0.9906$. The fluorescent dye, 5-TAMRA-SE, can only be excited by the 543 nm emission line of a He-Ne laser. Unfortunately our collaborator's laboratory is not equipped with a He-Ne laser therefore, the microcystin-LR was labelled with 5-BMF. The 488 nm emission line of an Ar^+ laser can excite this dye.

The MALDI-MS and ESI-MS spectra of the 5-BMF labelling reaction mixture of microcystin-LR proved that the labelling reaction was successful but did not go to completion. The CZE-LIFP electropherograms of 5-BMF labelled microcystin-LR revealed two product peaks. A working curve was constructed to observe the effect of adding microcystin antibody to the labelling reaction mixture and the resulting curve had a correlation coefficient of $r = -0.9932$.

Next, a fluorescent flow displacement assay was developed for the analysis of microcystin-LR. This immunoassay involved immobilizing the microcystin antibody to the capillary wall and then saturating the recognition sites with the 5-BMF labelled microcystin-LR. The resulting displacement immunoassay curve was exponential in nature. This curve was linearized and had a correlation coefficient of $r = +0.9922$.

104

Further investigation into this microcystin-LR fluorescent flow displacement immunoassay was not performed since the antibody was unavailable for purchase.

The synthesis of an arginine-labelling reagent was proposed based on arginine modification techniques that were already established. Hossein Ahmadzadeh first proposed the synthesis of this arginine-labelling reagent. The synthesis for the labelling reagent was proven to be successful through analysis by ESI-MS under the conditions described in Section 2.2.2. The ESI-MS spectrum revealed only one major peak at 469 amu which was the potassium adduct of our desired product. This synthesized labelling reagent was reacted with N_α-acetyl arginine but was found to be unsuccessful through CZE-LIF analysis. Graduate student Hans Osthoff will do further investigation into the synthesis of an arginine-labelling reagent.

2.5 References

1. M. F. Watanabe, H. D. Park, F. Kondo, K. i. Harada, H. Hayashi, T. Okino, *Natural Toxins*, 5 (1997) 31.

2. W. W. Carmichael, United States Environmental Protection Agency/600/R-92/079, (1992) 1.

3. K. Berg, O. M. Skulberg, R. Skulberg, *Archives of Hydrobiology*, 108 (1987) 549.

4. J. Kiviranta, K. Sivonen, K. Lahti, R. Luukkainen, S. I. Niemelä, *Archives of Hydrobiology*, 121 (1991) 281.

5. M. F. Watanabe, K. Tsuji, Y. Watanabe, K. i. Harada, M. Suzuki, *Natural Toxins*, 1 (1992) 48.

6. K. Christoffersen, *Natural Toxins*, 4 (1996) 215.

7. L. A. Lawton, C. Edwards, G. A. Codd, *Analyst* (London), 119 (1994) 1525.

8. D. P. Botes, H. Kruger, C. C. Viljoen, *Toxicon*, 20 (1982) 945.

9. D. P. Botes, P. L. Wessels, H. Kruger, M. T. C. Runnegar, S. Santikarn, R. J. Smith, J. C. J. Barna, D. H. Williams, *Journal of the Chemical Society Perkin Transactions*, 1(1985) 2747.

10. K. i. Harada, K. Matsuura, M. Suzuki, M. F. Watanabe, S. Oishi, A. M. Dahlem, V. R. Beasley, W. W. Carmichael, *Toxicon*, 28 (1990) 55.

11. K. L. Rinehart, M. Namikoshi, B. W. Choi, *Journal of Applied Phycology*, 6 (1994) 159.

12. D. P. Botes, A. A. Tuinman, P. L. Wessels, C. C. Viljoen, H. Kruger, D. H. Williams, S. Santikarn, R. J. Smith, S. J. Hammond, *Journal of the Chemical Society Perkin Transactions*, 1 (1984) 2311.

13. H. S. Lee, C. K. Jeong, H. M. Lee, S. J. Choi, K. S. Do, K. Kim, Y. H. Kin, *Journal of Chromatography A*, 848 (1999) 179.

14. J. An, W. W. Carmichael, *Toxicon*, 34 (1994) 1495.

15. W. W. Carmichael, in A.T. Tu (editor), *Handbook of Natural Toxins*, Marcel Dekker, New York, 1988.

16. O. I. Fontal, M. R. Vieytes, J. M. V. Baptista de Sousa, M. C. Louzao, L. M. Botana, *Analytical Biochemistry*, 269 (1999) 289.

17. F. D. Galey, V. R. Beasley, W. W. Carmichael, G. Kleppe, S. B. Hooser, W. M. Haschek, *American Journal of Veterinary Research*, 48 (1987) 1415.

18. S. B. Hooser, V. R. Beasley, R. A Lovell, W. W. Carmichael, W. M. Haschek, *Veterinary Pathology*, 26 (1989) 246.

19. R. A. Lovell, D. J. Schaeffer, S. B. Hooser, W. M. Haschek, A. M. Dahlem, W. W. Carmichael, V. R. Beasley, *Journal of Environmental Pathology, Toxicology, and Oncology*, 9 (1989) 221.

20. W. C. Theiss, W. W. Carmichael, J. Wyman, R. Bruner, *Toxicon*, 26 (1988) 603.

21. M. Wickstrom, W. Haschek, G. Henningsen, L. A. Miller, J. Wyman, V. R. Beasley, *Natural Toxins*, 4 (1996) 195.

22. I. R. Falconer, A. R. B. Jackson, J. Langley, M. T. C. Runnegar, *Australian Journal of Biological Science*, 34 (1981) 179.

23. J. E. Eriksson, D. M. Toivola, J. A. O. Meriluoto, H. Haiki, Y. Han, D. Hartshorne, *Biochemical and Biophysical Research Communications*, 173 (1990) 1347.

24. R. J. Andersen, H. A. Luu, D. Z. X. Chen, C. F. B. Holmes, M. L. Kent, M. LeBlanc, F. J. R. Taylor, D. E. Williams, *Toxicon*, 31 (1993) 1315.

25. V. R. Beasley, R. A. Lovell, A. M. Dahlem, W. M. Haschek, S. B. Hooser in A. T. Tu (Editor), *Handbook of Natural Toxins*, Marcel Dekker, New York, 1991.

26. S. E. DeVries, F. D. Galey, M. Namikoshi, J. C. Woo, *Journal of Veterinary Diagnostic Investigation*, 5 (1993) 403.

27. W. W. Carmichael, I.R. Falconer, in I.R. Falconer (Editor), *Algal Toxins in Seafood and Drinking water*, Academic Press, London, 1993.

28. C. MacKintosh, K. A. Beattie, S. Klumpp, P. Cohen, G. A. Codd, *FEBS Letters*, 264 (1990) 187.

29. R. E. Honkanen, J. Zwiller, R. E. Moore, S. L. Daily, B. S. Khatra, M. Dukelow, A. L. Boynton, *Journal of Biological Chemistry*, 265 (1990) 19401.

30. S. Yoshizawa, R. Matsushima, M. F. Watanabe, *Journal of Cancer Research and Clinical Oncology*, 116 (1990) 609.

31. R. Matsushima, S. Yoshizawa, M. F. Watanabe, K. i. Harada, M. Furusawa, W. W. Carmichael, H. Fujiki, *Biochemical and Biophysical Research Communications*, 171 (1990) 867.

32. M. Runnegar, N. Berndt, S. M. Kong, E. Y. C. Lee, L. Zhang, *Biochemical and Biophysical Research Communications*, 216 (1995) 162.

33. R. Nishiwaki-Matsushima, T. Ohta, S. Nishiwaki, M. Suganuma, K. Kohyama, T. Ishikawa, W. W. Carmichael, H. Fujiki, *Journal of Cancer Research and Clinical Oncology*, 118 (1992) 420.

34. P. Cohen, *Annual Review of Biochemistry*, 58 (1989) 453.

35. F. Kondo, Y. Ikai, H. Oka, H. Matsumoto, S. Yamada, N. Ishikawa, L. Tsuji, K. i. Harada, T. Shimada, M. Oshikata, M. Suzuki, *Natural Toxins*, 3 (1995) 41.

36. P. Kós, G. Gorzó, G. Surányi, G. Borbély, *Analytical Biochemistry*, 225(1995) 49.

37. G. A. Codd, G. K. Poon, in L. J. Rogers and J. G. Gallon (Editors), *Biochemistry of the Algae and Cyanobacteria*, Clarendon Press, Oxford, 1988.

38. J. Meriluoto, *Analytica Chimica Acta*, 352 (1997) 277.

39. J. Meriluoto, A. S. Härmälä-Braskén, J. Eriksson, D. Toivola, T. Lindholm, *Phycologia*, 35 (Suppl. 6) (1996) 125.

40. W. P. Brooks, G. A. Codd, *Letters in Applied Microbiology*, 2 (1986) 1.

41. J. A. O. Meriluoto, J. E. Eriksson, K.-i. Harada, A. M. Dahlem, K. Sivonen, W. W. Carmichael, *Journal of Chromatography*, 509 (1990) 390.

42. S. Nagata, T. Tsutsumi, F. Yoshida, Y. Ueno, M. F. Watanabe, *Journal of AOAC International*, 80 (1997) 408.

43. T. W. Lambert, M. P. Boland, C. F. B. Holmes, S. E. Hrudey, *Environmental Science and Technology*, 28 (1994) 753.

44. F. S. Chu, X. Huang, R. D. Wei, *Journal of the Association of Official Analytical Chemists*, 73 (1990) 451.

45. C. M. McDermott, R. Feola, J. Plude, *Toxicon*, 33 (1995) 1433.

46. F. Kondo, Y. Ikai, H. Oka, N. Ishikawa, M. F. Watanabe, M. Watanabe, K.-i. Harada, M. Suzuki, *Toxicon*, 30 (1992) 591.

47. K.-i. Harada, K. Matsuura, M. Suzuki, H. Oka, M. F. Watanabe, S. Oishi, A. M. Dahlem, V. R. Beasley, W. W. Carmichael, *Journal of Chromatography*, 448 (1988) 275.

48. R.W. Moollan, B. Rae, A. Verbeek, *Analyst*, 121 (1996) 233.

109

49. C. Rivasseau, S. Martins, M. C. Hennion, *Journal of Chromatography A*, 799 (1998) 155.

50. K. Tsuji, S. Naito, F. Kondo *et al.*, *Toxicon*, 32 (1994) 1251.

51. J. Meriluoto, B. Kincaid, M. R. Smyth, M. Wasberg, *Journal of Chromatography A*, 810 (1998) 226.

52. K. P. Bateman, P. Thibault, D. J. Douglas, R. L. White, *Journal of Chromatography A*, 712 (1995) 253.

53. C. M. B. Van Den Beld, H. Lingeman, G. J. Van Ringer, V. R. Tjaden, J. Van Der Greef, *Analytica Chimica Acta*, 205 (1988) 15.

54. P. S. Mukherjee, K. H. DeSilva, H. T. Karnes, *Pharmaceutical Research*, 12 (1995) 930.

55. B. Desfosses, P. Urios, N. Christeff, K. M. Rajowski, N. Cittanova, *Analytical Biochemistry*, 159 (1986) 179.

56. P. S. Mukherjee, *Analyst*, 121 (1996) 1573.

57. R. P. Haugland, *Handbook of Fluorescent Probes and Research Chemicals*, Molecular Probes, 6th Edition, 1996.

58. P. S. Mukherjee, H. T. Karnes, *Analytical Chemistry*, 68 (1996) 327.

59. F. R. N. Gurd, *Methods in Enzymology*, 11 (1967) 532.

60. M. Brinkley, *Bioconjugate Chemistry*, 3 (1992) 2.

61. F. Perrin, *Journal de Physique et le Radium*, 7 (1926) 390.

62. M. E. Jolley, S. D. Stroupe, K. S. Schwenzer, C. J. Wang, M. Lu-Steffes, H. D. Hill, S. R. Popelka, J. T. Holen, D. M. Kelso, *Clinical Chemistry*, 27 (1981) 1575.

63. G. Weber, *Advances in Protein Chemistry*, 8 (1953) 415.

64. W. B. Dandliker, G. A. Feigen, *Biochemical Research Communications*, 5 (1961) 299.

65. Y. Oda, M. Kinoshita, K. Nakayama, K. Kakehi, *Biological and Pharmaceutical Bulletin*, 21 (1998) 1215.

66. L. Ye, X. C. Le, J. Z. Xing, M. Mingsheng, R. Yatscoff, *Journal of Chromatography B*, 714 (1998) 59.

67. W. B. Dandliker, M. L. Hsu, J. Levin, B. R. Rao, *Methods in Enzymology*, 74 (1981) 3.

68. X. Zhang, J. K. Jackson, H. M. Burt, *Journal of Biochemical and Biophysical Methods*, 31 (1996) 145.

69. N. M. Schultz, R. T. Kennedy, *Analytical Chemistry*, 65 (1993) 3161.

70. E. P. Diamandis, *Clinical Biochemistry*, 21 (1988) 139.

71. G. A. Wemhoff, S. Y. Rabbany, A.W. Kusterbeck, R. A. Ogert, R. Bredehorst, F. S. Ligler, *Journal of Immunological Methods*, 156 (1992) 223.

72. M. Gerdes, M. Meusel, F. Spener, *Journal of Immunological Methods*, 223 (1999) 217.

73. M. P. Byfield, R. A. Abukneshs, *Biosensors and Bioelectronics*, 9 (1994) 373.

74. W. A. Kapstein, J. Korf, S. Cheng, M. Yang, J. F. C. Glatz, R. Renneberg, *Journal of Immunological Methods*, 217 (1998) 103.

75. H. Yu, A. W. Kusterbeck, M. J. Hale, F. S. Ligler, J. P. Whelan, *Biosensors and Bioelectronics*, 11 (1996) 725.

76. M. Aizawa, *Advances in Clinical Chemistry*, 31 (1994) 247.

77. K. Kronkvist, U. Lovgren, J. Svenson, L. E. Edholm, G. Johansson, *Journal of Immunological Methods*, 200 (1997) 145.

78. R. A. Ogert, A. W. Klusterbeck, G. A. Wemhoff, R. Burke, F. S. Ligler, *Analytical Letters*, 25 (1992) 1999.

79. J. P. Whelan, A. W. Klusterbeck, G. A. Wemhoff, R. Bredehorst, F. S. Ligler, *Analytical Chemistry*, 65 (1993) 3561.

80. J. F. Riordan, *Molecular & Cellular Biochemistry*, 26 (1979) 71.

81. S. G. Powers, J. F. Riordan, *Proceedings of the National Academy of Sciences USA*, 72 (1975) 2616.

82. J. F. Riordan, R. Scandurra, *Biochemical and Biophysical Research Communications*, 66 (1975) 417.

83. C. L. Borders, J. F. Riordan, *Biochemistry*, 14 (1975) 4699.

84. R. R. Lobb, A. M. Stokes, A. O. Hill, J. F. Riordan, *European Journal of Biochemistry*, 70 (1976) 517.

85. J. A. Yankeelov, M. Kochert, J. Page, A. Westphal, *Federation Proceedings*, 25 (1966) 590.

86. J. A. Yankeelov, *Biochemistry*, 9 (1970) 2433.

87. F. S. Chu, X. Huang, R. D. Wei, W. W. Carmichael, *Applied & Environmental Microbiology*, 55 (1989) 1928.

88. S. M. Kalbag, W. Roeske, *Journal of the American Chemical Society*, 97 (1975) 441.

Chapter 3

The Development of a Novel Carbonyl-Labelling Reaction for Use with Capillary Electrophoresis with Laser-Induced Fluorescence Detection

3.1 Introduction

3.1.1 Carboxylic Acids

Approximately 8% of biologically interesting analytes including amino acids, peptides and fatty acids possess a carboxyl group.[1] Carboxylic acids are hydrophilic weak electrolytes. Carboxylic acids can be found as natural compounds or preservatives in food and beverages, are extensively used for manufacturing products in the pharmaceutical industry and are used as antioxidants, acidifiers and drug adsorption modifiers. Consequently, it is of great interest to develop suitable techniques for the quantitative determination of carboxylic acids even at very low concentrations.

The analysis of carboxylic acids is often complicated by the fact that conventional separation and detection methods do not always provide sufficient selectivity or sensitivity for low level quantitation. The detection of these compounds at trace levels using absorptiometry is difficult because of their weak absorption in the ultraviolet-visible (UV-Vis) region.[2] Carboxylic acids that possess native fluorescence are rare. Mass spectrometric (MS) detection of carboxylic acids has been shown to provide limited sensitivity.[3] Application of chemiluminescence detection to the analysis of carboxylic acids is limited and radioimmunological detection is time-consuming and laborious.[4] The problems encountered in the quantitative analysis of carbonyl-containing analytes using UV absorbance, fluorescence, chemiluminescence, radioimmunoassay, MS and gas chromatography-electron capture detection modes have been previously discussed in detail.[3-6] Since many biologically important carboxylic acids do not exhibit efficient absorption (UV-Vis), luminescent properties (fluorescence or chemiluminescence) or electrochemical activity, chemical derivatization is utilized for detection purposes.

114

Several criteria are important in the development of a precolumn derivatization reagent: commercial availability; moderate derivatization conditions; no interferences in derivatization or detection; stability; and suitability for the detection of low analyte levels.[7] Various tagging reagents have been developed for the determination of carboxylic acids which address only some of these issues.

Tagging of carboxylic acids with reagents that produce chromophores having ultraviolet and visible bands has become quite common in the past two decades. Some of the UV-Vis tagging reagents include phenacylbromide (PB)[2,8-10], p-bromophenacyl bromide (BPB), p-phenylphenacyl bromide (PPB)[2,11-12], p-nitrophenacyl bromide (NPB)[2,13], α-bromo-2'-acetonaphthone (BAN)[2,14,15], 2-nitrophenylhydrazine (NPH)[2,16,17], pyridinium dichromate (PDC)[2,18,19], hydroxamic acid (HA)[2,20], poly(4-nitrobenzyl p-styrenesulfonate) (PS-NB)[2,21], poly[(2-phthalimino)ethyl p-styrenesulfonate] (PS-PE)[2,21], 3,5-dinitrophenyl isocyanate (DNPI)[2,22] and (-)-phenylethylamine (S(-)-PEA)[2,23]. Fluorescent tagging reagents include 4-bromomethyl-7-methoxycoumarin (BrMMC)[2,24-40], 4-bromomethyl-7-acetoxycoumarin (BrMAC)[2,41-44], 3-bromoacetyl-6,7-methylenedioxycoumarin (BrAMDC)[2,45], 3-bromoacetyl-7-methoxycoumarin (BrAMC)[2,46], p-(9-anthroyloxy)phenacyl bromide (PBr)[2,47-54], 9-anthryldiazomethane (ADAM)[2,55-62], 3-bromomethyl-6,7-dimethoxy-1-methyl-2(1H)-quinoxalinone (BrDMEQ)[2,63-70], 3-bromomethyl-6,7-methylenedioxy-1-methyl-2(1H)-quinoxalinone (BrMMEQ)[2,63-70], 6,7-dimethoxy-1-methyl-2(1H)-quinoxalinone-3-propionylcarboxylic acid hydrazide (DMEQ-Hz)[2,63-70], 2-(4-hydrazinocarbonylphenyl)-4,5-diphenylimidazole (HCPI)[2,71], 5-(dimethylamino)naphthalene-1-sulfonhydrazide (DNS-Hz)[2,72,73],

5-(dimethylamino)-1-naphthalenesulfonyl-semipiperazide (DNS-PZ)[2,74], monodansyl

cadaverine (MDC) and 2-(2,3-naphthalimino)ethyl trifluoromethanesulfonate (NE-

OTf)[2,75]. The tagging reagents for electrochemical detection are few in number and

include p-aminophenol (AP)[2,76], 2,4-dimethoxyaniline (DMA)[2,77], ferrocene

derivatives[2,78], 3,5-dinitrobenzoyl chloride (DNBC), 2-bromo-2'-nitroacetophenone

(NPA), p-nitrobenzyloxyamine hydrochloride (PNBA) and 2,4-dinitrophenylhydrazine

(DNPH)[2,79]. Tagging reagents used for chemiluminescence detection include luminol

and its analogs[2,80], N-(4-aminobutyl)-N-ethylisoluminol (ABEI)[2,81], N-(4-aminobutyl)-N-

methylisoluminol (ABMI)[2,81], luminarin-4[2,82], 4-(N,N-dimethylminosulfonyl)-7-(5-

aminopentylamino)-2,1,3-benzoxadiazole (DBD-CD), 4-(N,N-dimethylminosulfonyl)-7-

(1-piperazinyl)-2,1,3-benzoxadiazole (DBD-PZ)[2,83] and (+)- and (-)-4-(N,N-dimethyl-

minosulfonyl)-7-(3-aminopyrrolidin-1-yl)-2,1,3-benzoxadiazole (DBD-APy)[2,84]. The

excitation wavelengths of all the tagging reagents mentioned are in the range of

210 – 390 nm. The best limit of detection achieved using these derivatization reagents

was in the femtomole range.

Laser light sources in conjunction with fluorescence detection have been utilized

to achieve detection limits at low femtomole and attomole ranges for compounds of

pharmaceutical and biomedical interest.[5,85-88] An argon ion (Ar$^+$) laser provides high-

power output and multiple emission lines in the blue-green region (450 – 550 nm) of the

spectrum. An excitation wavelength in this region is preferable in bioanalysis due to the

fact that excitation in the blue-green region is relatively free of interferences from

endogenous compounds present in biological matrices (serum, plasma, etc.). Most

carbonyl-group derivatization reagents cannot be utilized with an Ar$^+$ laser which is the

case of the fluorescent tagging reagents listed above. A suitable tagging reagent should possess acceptable photo- and thermal stabilities when exposed to laser radiation and should have high molar absorptivity (ε), quantum yield (ϕ), reasonably high Stokes shift, and a single derivatizable functional group. 5-(Bromomethyl)fluorescein (5-BMF) has been shown to possess the strongest fluorescence among potential carboxylic acid derivatization reagents that are suitable for the Ar^+ laser-induced fluorescence detection (LIF) of carboxylic acids.[89] The excitation wavelength maximum of this reagent under basic conditions matches very well with the intense 488.0 nm emission line of an Ar^+ laser. The combination of 5-BMF as a fluorophore with LIF detection has the potential for achieving low limits of detection for carbonyl-containing analytes.[90]

In this work, a novel carbonyl-labelling procedure using 5-BMF as the derivatization reagent has been developed. The derivatized carboxylic acid was analysed using capillary zone electrophoresis with LIF detection (CZE-LIF), which is a powerful technique among separative analysis. Graduate student Hossein Ahmadzadeh completed the initial experiments of this project.

3.2 Experimental

3.2.1 Reagents

5-(Bromomethyl)fluorescein (5-BMF) was purchased from Molecular Probes (Eugene, OR, USA). *N,N*-Dimethylformamide (DMF) was obtained from Caledon (Georgetown, ON, Canada) and was dried with Molecular Sieve Type 4A beads (Caledon, Georgetown, ON, Canada) in a dry glass bottle, septum-capped to prevent

moisture entry. Fused-silica capillary (50 µm inner diameter (I.D.), 140 µm outer

diameter (O.D.)) was acquired from PolyMicro Techologies (Phoenix, AZ, USA).

Di-sodium tetraborate and anhydrous solid potassium carbonate were bought from BDH

Chemicals (Toronto, ON, Canada). 1,4-Diazabicyclo[2.2.2]octane (triethylenediamine,

TED) and 18-Crown-6 were purchased from Fluka Chemika (Switzerland). Penicillin-G

(PEN-G) potassium salt was obtained from Calbiochem (La Jolla, CA, USA). HPLC

grade methanol (MeOH) was acquired from B & J Brand (Muskegon, MI, USA). Lauric

acid sodium salt and lauric acid were bought from Sigma (St. Louis, MO, USA).

Acetone and acetonitrile were purchased from Aldrich (Milwaukee, WI, USA).

3.2.2 Instruments

The CE-LIF instrument is a home-built instrument that was described in

Chapter 1. The electrospray ionization mass spectrometry (ESI-MS) instrument was

described in detail in Chapter 2 in Section 2.2.2.

3.2.3 Carbonyl-labelling reaction of Penicillin-G performed in the presence of TED

The schematic diagram of the set-up apparatus used for this reaction can be found

in Chapter 2 (Figure 2.10). Penicillin-G (PEN-G) was chosen as the model carboxylic

acid because it is inexpensive and has an antibody that is commercially available for

future immunoassay experiments. 1 µmol of PEN-G dissolved in DMF was transferred

into a 5-mL three-neck round bottom flask. Next, two molar equivalents of 5-BMF and

one molar equivalent of triethylenediamine (TED) were added to the reaction flask. The

final reaction volumes were 1 mL. The reaction mixture was heated at 80 °C under

reflux for 2 hours. The blank reaction mixture contained all reactants except the carboxylic acid to be labelled.

The blank and sample reaction mixtures were checked for product using CZE-LIF with the following conditions. The blank and sample reaction mixtures were diluted to a concentration of 10^{-7} M with 10 mM borate at pH 9. The run and sheath flow buffers were 10 mM borate at pH 9. The capillary used was 30 cm in length and had an O.D. of 140 μm and an I.D. of 50 μm. The injections were done at 3000 V for 5 s and the separation voltage was 20 kV. The PMT was biased at 500 V and the Ar^+ laser beam used for excitation had 12.1 mW of power at 488 nm. The interference filter used was 518DF25. A calibration curve for labelled PEN-G was constructed by running each standard concentration three times each (n = 3) on the CE-LIF instrument with the same run conditions except that the separation voltage was 12 kV.

The reaction mixtures were also checked for product using ESI-MS.

3.2.4 Carbonyl-labelling reaction of Penicillin-G performed in the absence of TED

This labelling reaction was the same as in Section 3.2.1 only the one molar equivalent of TED was not present.

The reaction mixtures were checked for the presence of product using CZE-LIF. The resulting blank and sample mixtures were diluted to a concentration of 10^{-9} M with 10 mM borate at pH 9. The capillary used was 30 cm in length and had an O.D. of 140 μm and an I.D. of 50 μm. The run and sheath flow buffers were 10 mM borate at pH 9. The injections were performed at 1000 V for 5 s and the separation voltage was

12 kV. The PMT was biased at 1000 V and the Ar^+ laser beam used for excitation had 12.1 mW of power at 488 nm. The interference filter used was 518DF25. A calibration curve for labelled PEN-G was constructed by running each standard concentration three times (n = 3) on the CE-LIF instrument under the same run conditions.

The reaction mixtures were also checked for product using ESI-MS.

3.2.5 Carbonyl-labelling reaction of lauric acid sodium salt

1 μmol of lauric acid sodium salt was dissolved in DMF and placed into a 5-mL three-neck round bottom flask. Next, 2 molar equivalents of 5-BMF were added to the reaction flask. The reaction mixture was then heated at 80 °C under reflux for 2 hours. All reaction mixtures had a final volume of 1 mL.

The blank and sample reaction mixtures were checked for the presence of product using CZE-LIF. The reaction mixtures were diluted to a concentration of 10^{-8} M with 10 mM borate at pH 9. The sample reaction mixture was run three times (n = 3) on the CE-LIF instrument. The capillary used was 30 cm in length with an I.D. of 50 μm and an O.D. of 140 μm. The run and sheath flow buffers were 10 mM borate at pH 9. The injections were performed at 1000 V for 5 s and the separation voltage was 12 kV. The PMT was biased at 1000 V and the Ar^+ laser beam used for excitation had a power of 12.1 mW at 488 nm. The interference filter used was 518DF25.

3.2.6 Mukherjee's labelling reaction[5]

300 µL of lauric acid (100 µg/mL in acetone), 250 µL of 5-BMF (125 µg/mL in acetonitrile), 200 µL of 18-Crown-6 (700 µg/mL in acetonitrile), and 20-25 mg of anhydrous solid potassium carbonate were placed in a 5-mL three-neck round bottom flask and mixed together. The reaction mixture was heated at 87 °C for 1.5 hours. This reaction was performed twice.

The reaction mixtures were diluted to a concentration of 10^{-8} M with 10 mM borate at pH 9. The sample reaction mixture was run three times (n = 3) on the CE-LIF instrument. The capillary used was 30 cm in length and had an O.D. of 140 µm and an I.D. of 50 µm. The run and sheath flow buffers were 10 mM borate at pH 9. The injections were performed at 1000 V for 5 s and the separation voltage was 12 kV. The PMT was biased at 1000 V and the Ar^+ laser beam used for excitation had 12.1 mW of power at 488 nm. The interference filter used was 518DF25. For the repeated experiment the sample reaction mixture was run two times (n = 2) on the CE-LIF instrument.

3.2.7 Carbonyl-labelling reaction of lauric acid sodium salt performed in the presence of TED & 18-Crown-6

1 µmol of lauric acid sodium salt dissolved in DMF (or a 4:1 mixture of DMF:MeOH) was placed into a 5-mL three-neck round bottom flask. Next, one molar equivalents of 18-Crown-6 and TED were added to the reaction flask. Then, two molar equivalents of 5-BMF were added to the reaction flask. The reaction mixture was then

heated at 80°C under reflux for two hours. The blank and sample reaction mixtures had a final volume of 1 mL.

CZE-LIF was used to check for the presence of product. The blank and sample reaction mixtures were diluted to a concentration of 10^{-8} M with 10 mM borate at pH 9. The sample reaction mixture was run three times (n = 3) on the CE-LIF instrument. The capillary used was 30 cm in length and had an O.D. of 140 μm and an I.D. of 50 μm. The sheath flow and run buffers were 10 mM borate at pH 9. The injections were performed at 1000 V for 5 s and the separation voltage was 12 kV. The PMT was biased at 1000 V and the Ar^+ laser beam used for excitation had 12.1 mW of power at 488 nm. The interference filter used was 518DF25.

3.2.8 Carbonyl-labelling reaction of lauric acid sodium salt performed in the presence of 18-Crown-6

1 μmol of lauric acid sodium salt was dissolved with a 4:1 mixture of DMF:MeOH and placed into a 5-mL three-neck round bottom flask. Next, one molar equivalent of 18-Crown-6 and two molar equivalents of 5-BMF were added to the reaction flask. The reaction mixture was then heated at 80°C under reflux for two hours. The blank and sample reaction mixtures had a final volume of 1 mL.

CZE-LIF was used to check for the presence of product. The blank and sample reaction mixtures were diluted to a concentration of 10^{-8} M with 10 mM borate at pH 9. The capillary used was 30 cm in length and had an O.D. of 140 μm and an I.D. of 50 μm. The sheath flow and run buffers were 10 mM borate at pH 9. The injections were performed at 1000 V for 5 s and the separation voltage was 12 kV. The PMT was

biased at 1000 V and the Ar^+ laser beam used for excitation had 12.1 mW of power at 488 nm. The interference filter used was 518DF25.

3.2.9 Carbonyl-labelling reaction of lauric acid sodium salt performed in the presence of TED

1 µmol of lauric acid sodium salt was dissolved with a 4:1 mixture of DMF:MeOH and placed into a 5-mL three-neck round bottom flask. Next, 2 molar equivalents of 5-BMF and one molar equivalent of TED were added to the reaction flask. The reaction mixture was then heated at 80 °C under reflux for 2 hours. All reaction mixtures had a final volume of 1 mL.

The blank and sample reaction mixtures were then checked for product using CZE-LIF. The blank and sample reaction mixtures were diluted to a concentration of 10^{-8} M with 10 mM borate at pH 9. The sample reaction mixture was run two times (n = 2) on the CE-LIF instrument. The capillary used was 30 cm in length and had an O.D. of 140 µm and an I.D. of 50 µm. The sheath flow and run buffers were 10 mM borate at pH 9. The injections were performed at 1000 V for 5 s and the separation voltage was 12 kV. The PMT was biased at 1000 V and the Ar^+ laser beam used for excitation had 12.1 mW of power at 488 nm. The interference filter used was 518DF25.

3.2.10 Optimization of the dye to analyte ratio

1 µmol of lauric acid sodium salt was dissolved with a 4:1 mixture of DMF:MeOH and then transferred to a 5-mL three-neck round bottom flask. Next, 1, 2, 3, 4 or 5 molar equivalents of 5-BMF dissolved in DMF were added to the reaction flask.

The final volume was made to be 1 mL by adding DMF. The reaction mixture was then

heated at 80 °C under reflux for 2 hours.

All resulting reaction mixtures were diluted to a concentration of 10^{-8} M with

10 mM borate at pH 9 as the dilution buffer. The sample reaction mixture was run three

times (n = 3) on the CE-LIF instrument to check for the presence of product. The

capillary used was 30 cm in length with an I.D. of 50 μm and an O.D. of 140 μm. The

run and sheath flow buffers were 10 mM borate at pH 9. The injections were done at

1000 V for 5 sec and the separation voltage was 12 kV. The PMT was biased at 1000 V

and the Ar^+ laser beam used for excitation had 12.1 mW of power at 488 nm. The

interference filter used was 518DF25.

3.2.11 Reactant limitation

10^{-7} (or 10^{-8} or 10^{-9}) moles of lauric acid sodium salt were dissolved with a 4:1

mixture of DMF:MeOH and then transferred to a 5-mL three-neck round bottom flask.

Next, two molar equivalents of 5-BMF dissolved in DMF were placed into the reaction

flask. The reaction mixture was then heated at 80 °C under reflux for 2 hours. The final

reaction volumes were made to be 1 mL (or 100 μL) by adding DMF.

The reaction mixtures were checked for the presence of product using CZE-LIF.

The blank and sample reaction mixtures were diluted to a concentration of 10^{-8} M with

10 mM borate at pH 9. The sample reaction mixtures were run on the CE-LIF instrument

three times (n = 3). The capillary used was 30 cm in length and had an O.D. of 140 μm

and an I.D. of 50 μm. The injections were performed at 1000 V for 5 s and the separation

voltage was 12 kV. The PMT was biased at 1000 V and the Ar^+ laser beam used for excitation had 12.1 mW of power at 488 nm. The interference filter used was 518DF25.

3.2.12 Reaction time optimization

1 μmol of lauric acid sodium salt was dissolved with a 4:1 mixture of DMF:MeOH and then transferred to a 5-mL three-neck round bottom flask. Next, two molar equivalents of 5-BMF dissolved in DMF were added to the reaction flask. The reaction mixture was then heated at 80 °C under reflux. The final reaction volume was made to be 1 mL by adding DMF.

20 μL aliquots of the blank and sample reaction mixtures were taken every ten minutes for 3 hours. The blank and sample reaction mixtures were diluted to a concentration of 10^{-8} M using 10 mM borate at pH 9 as the dilution buffer. The sample reaction mixture was run three times (n = 3) on the CE-LIF instrument. The capillary was 30 cm in length and had an I.D. of 50 μm and an O.D. of 140 μm. The run and sheath flow buffers were 10 mM borate at pH 9. The injections were done at 1000 V for 5 s and the separation voltage was 12 kV. The PMT was biased at 1000 V and the Ar^+ laser beam used for excitation had 12.1 mW of power at 488 nm. The interference filter used was 518DF25.

This reaction time optimization procedure was repeated with the exception that the 20 μL aliquots were taken every ten minutes for only 2 hours. The 20 μL aliquots were then run on the CE-LIF instrument at a concentration of $5*10^{-8}$ M using 10 mM borate at pH 9 as the dilution buffer. All other CZE-LIF run conditions for this reaction time optimization experiment were the same as in the first experiment. A calibration

125

curve was constructed for labelled lauric acid using the 120-min aliquot. Each standard concentration of labelled lauric acid was run three times (n = 3) on the CE-LIF instrument.

3.3 Results and Discussion

3.3.1 Carbonyl-labelling reaction of PEN-G performed in the presence of TED

The carbonyl-labelling reaction was carried out as described in Section 3.2.3. The carbonyl-labelling reaction was performed in the presence of the strong base TED instead of other strong bases such as potassium carbonate or sodium hydride under the advice of Dr. Vederas at the University of Alberta. The base TED was used because it will completely dissolve in the aprotic solvent DMF, unlike potassium carbonate or sodium hydride. The incomplete dissolution of potassium carbonate or sodium hydride in the reaction mixture results in a heterogeneous mixture leaving the acid unable to be fully deprotonated. This heterogeneity results in the acid being in equilibrium between its protonated and deprotonated forms. Conversely, the strong base TED dissolves completely in DMF resulting in a homogeneous mixture where the acid is completely deprotonated. Hence, the base TED is preferred over other bases for this reaction.

The mechanism of this carbonyl-labelling reaction involves a nucleophilic substitution, which occurs via a S_N2 mechanism, which is similar to the one described in detail in Chapter 2 under Section 2.3.2. The mechanism for the carbonyl-labelling reaction is illustrated in Figure 3.1. The blank and sample reaction mixtures were checked for the presence of product using CZE-LIF with the run conditions described in Section 3.2.3. The resulting CZE-LIF electropherogram can be found in Figure 3.2. A

Figure 3.1: The reaction mechanism for the carbonyl-labelling reaction of a
carboxylic acid salt.

1 μmol carboxylic acid /
carboxylate anion

2 molar equivalents of 5-BMF

S_N2 nucleophilic
substitution

80 °C
2 hours
$(V_f = 1 \text{ mL})$

5-BMF labelled carboxylic acid
(ester)

NaBr or KBr

bromide salt

Figure 3.2: The CZE-LIF electropherogram of the carbonyl-labelling reaction of PEN-G performed in the presence of TED.

Capillary: 30 cm, 50 μm I.D., 140 μm O.D. Run: 10 mM borate, pH 9, 20 kV. Injection: 3000 V, 5 s.

Laser: 488 nm Ar⁺, 12.1 mW. PMT: 500 V. Interference filter: 518DF25. Concentration: 10^{-7} M.

128
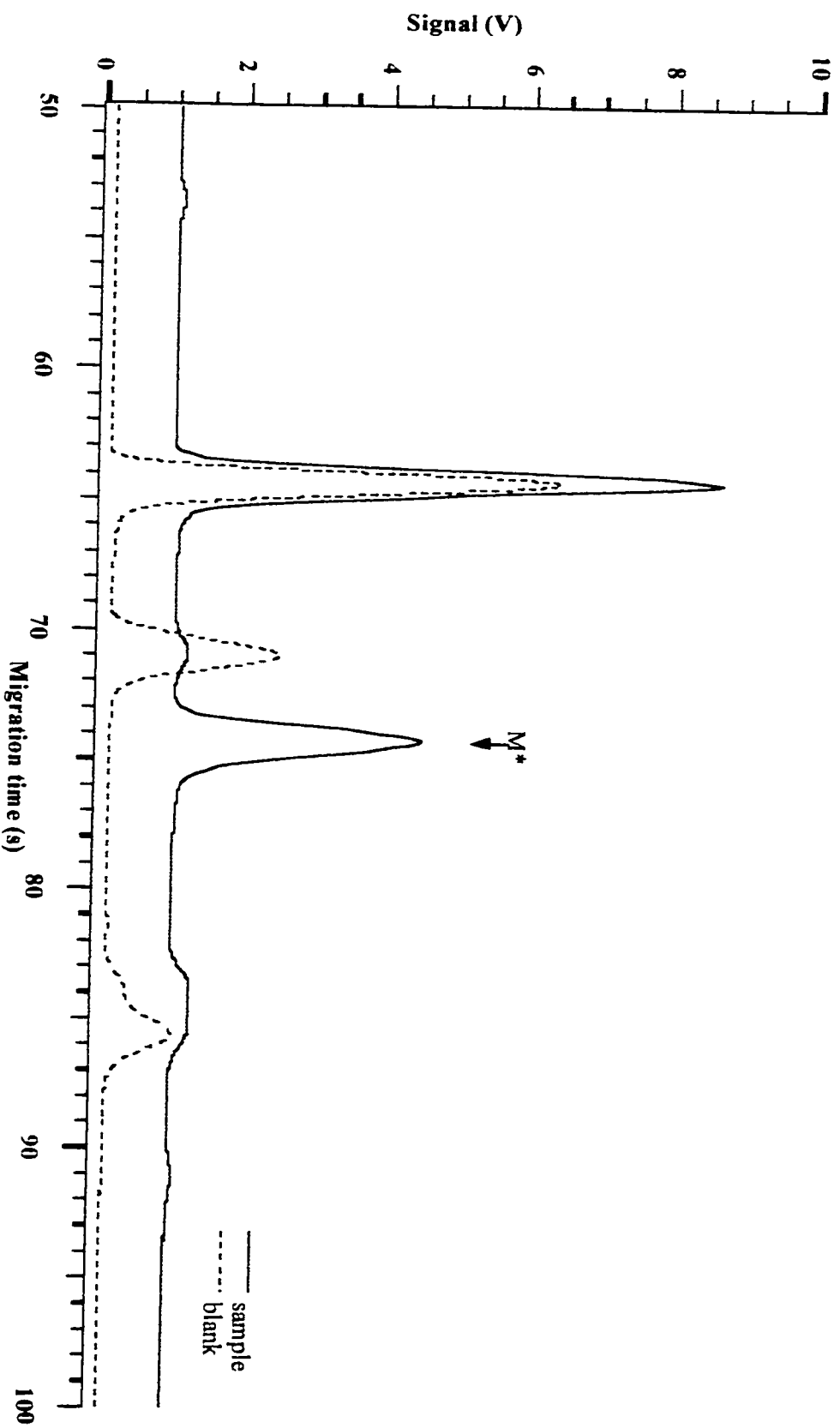
peak for the labelled PEN-G (M*) appears at ~74 s. A calibration curve for the labelled

PEN-G was constructed as described in Section 3.2.3 and can be found in Figure 3.3.

The peak areas for each of the standard concentrations of labelled PEN-G were calculated

using the Igor Pro macro Append Cursor Integration. The error bars on the calibration

curve represent ±1 standard deviation of the average peak area found for each standard

labelled PEN-G concentration. The resulting calibration curve had a correlation

coefficient of $r = +0.9953$ and a limit of detection (LOD) of 0.2 attomoles or 38 pM when

5.9 nL of sample was injected ($n = 3$).

Next, ESI-MS was used to analyze the blank and sample reaction mixtures. The

positive-ion mode ESI-MS spectra for this labelling reaction can be found in Figure 3.4.

The positive-ion mode ESI-MS spectrum for the blank reaction showed peaks at 390 amu

and 457 amu which correspond to $(dye-Br+2Na)^+$ and $(dye+MeOH+H)^+$, respectively.

The positive-ion mode ESI-MS spectrum for the sample reaction showed peaks at

457 amu and 701 amu which were assigned as $(dye+MeOH+H)^+$ and $(M*+Na)^+$,

respectively. A peak for unlabelled PEN-G was not found. These results show that the

carbonyl-labelling reaction of PEN-G performed in the presence of TED was successful.

Next, this carbonyl-labelling reaction of PEN-G was repeated in the absence of

the base TED. The procedure used for this reaction can be found in Section 3.2.4. The

reaction mixtures were checked for the presence of product using CZE-LIF with the run

conditions described in Section 3.2.4. The CZE-LIF electropherogram of this labelling

reaction can be found in Figure 3.5. A peak for the labelled PEN-G (M*) appears at a

migration time of ~117 s. The migration time found for labelled PEN-G is larger than the

earlier value of ~74 s due to the lower voltage used for separation. A calibration

Figure 3.3: The calibration curve of labelled PEN-G which was fluorescently tagged in the presence of TED. Capillary: 30 cm, 50 μm I.D., 140 μm O.D.. Run: 10 mM borate, pH 9, 12 kV. Injection: 3000 V, 5 s. Laser: 488 nm Ar⁺, 12.1 mW. PMT: 500 V. Interference filter: 518DF25. (n = 3)

130

Figure 3.4: The positive-ion mode ESI-MS spectra of the carbonyl-labelling reaction
of PEN-G performed in the presence of TED. A) blank reaction mixture;
B) sample reaction mixture.

$(dye + MeOH + H)^+$

A)

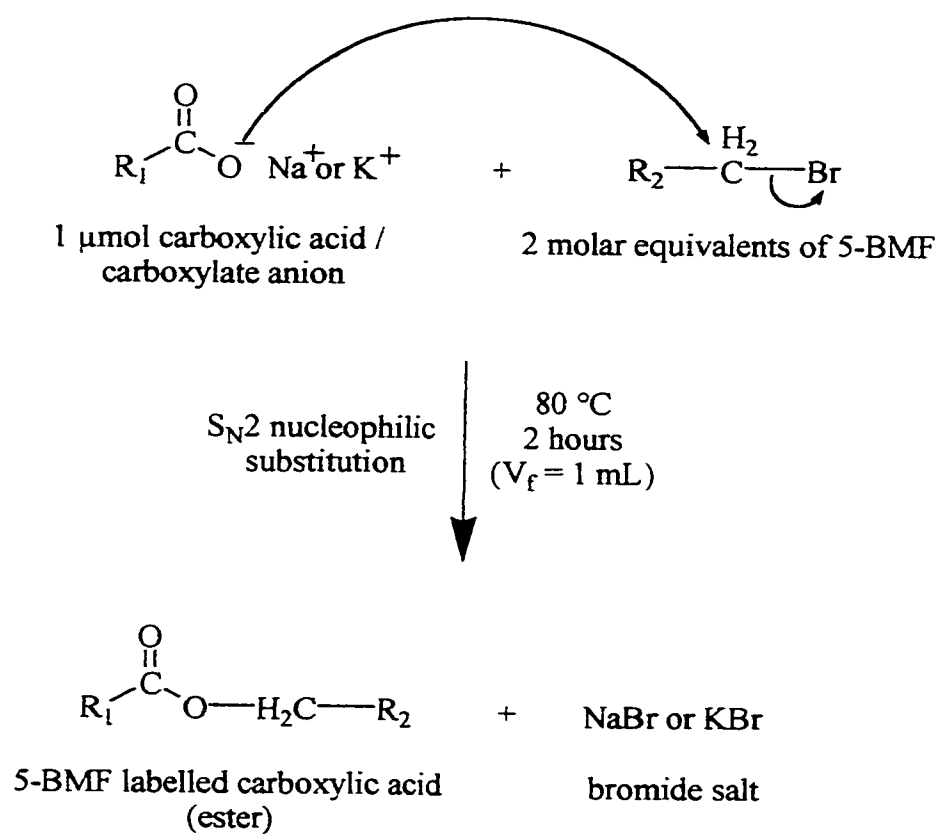$(dye-Br + 2Na)^+$

$(dye + MeOH + H)^+$

B)

$(M^* + Na)^+$

Figure 3.5: The CZE-LIF electropherogram of the carbonyl-labelling reaction of PEN-G performed in the absence of TED.

Capillary: 30 cm, 50 μm I.D., 140 μm O.D.. Run: 10 mM borate, pH 9, 12 kV. Injection: 1000 V, 5 s. Laser: 488 nm Ar$^+$, 12.1 mW. PMT: 1000 V. Interference filter: 518DF25. Concentration: 10^{-9} M.
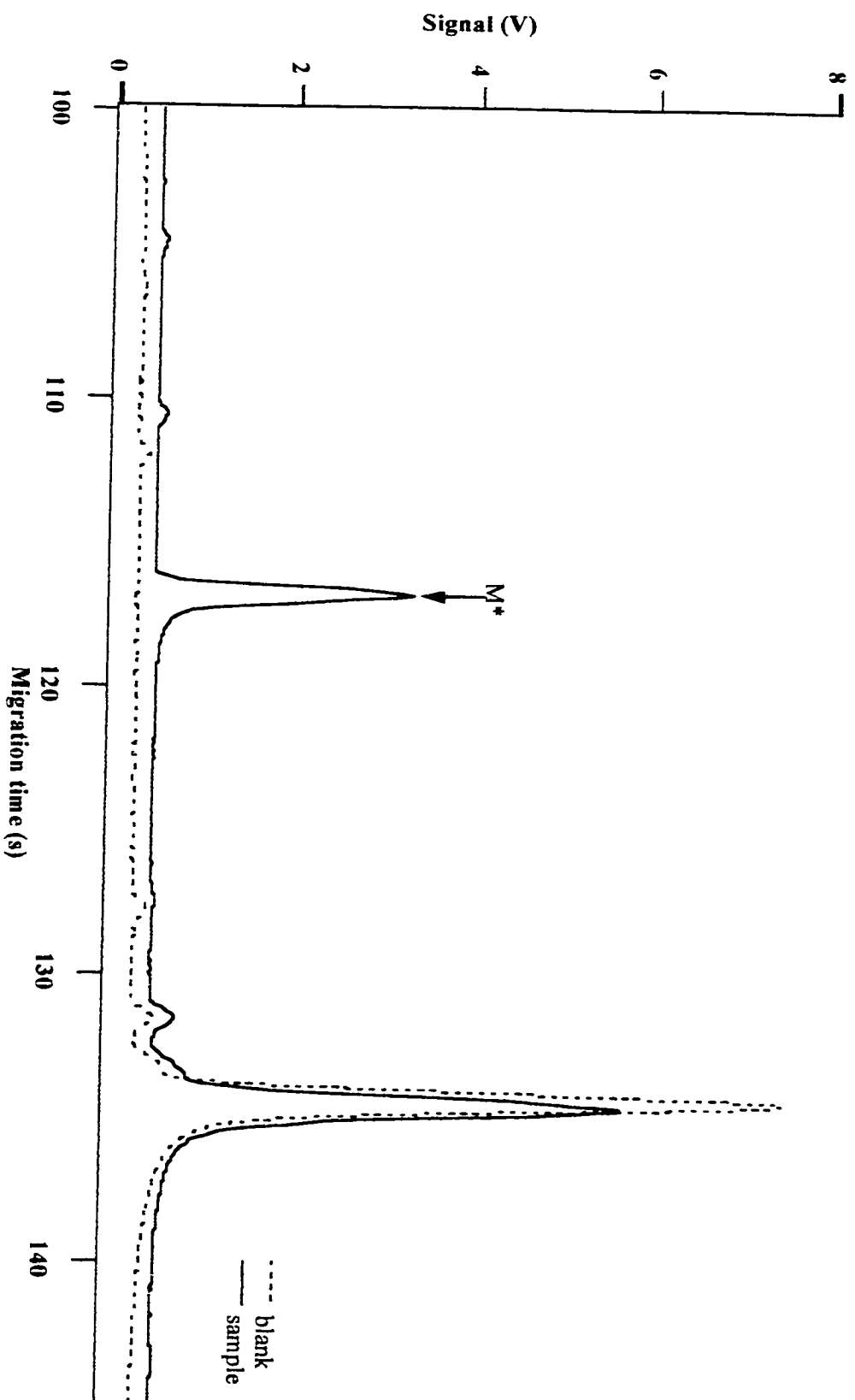
curve was constructed for the labelled PEN-G as described in Section 3.2.4 and can be found in Figure 3.6. The peak areas for each of the standard concentrations of labelled PEN-G were calculated using the Igor Pro macro Append Cursor Integration. The error bars on the calibration curve represent ± 1 standard deviation of the average peak area found for each standard labelled PEN-G concentration. This calibration curve had a correlation coefficient of $r = +0.9854$ and a limit of detection (LOD) of $6*10^{-21}$ moles or 3 pM where 2 nL of sample was injected (n = 3). The LOD is lower for this carbonyl-labelling reaction than the previous one therefore the carbonyl-labelling reaction must work better in the absence of the base TED.

Next, ESI-MS was used to analyze the blank and sample reaction mixtures. The positive-ion mode ESI-MS for this labelling reaction can be found in Figure 3.7. The positive-ion mode ESI-MS spectrum of the blank reaction mixture revealed peaks at 343 amu, 365 amu, 391 amu and 734 amu which correspond to $(dye-Br+H)^+$, $(dye-Br+Na)^+$, $(dye-Br+2Na)^+$, and $(dye\ dimer+2Na)^+$, respectively. The positive-ion mode ESI-MS spectrum of the sample reaction mixture revealed peaks at 347 amu, 390 amu, 679 amu, 681 amu, and 717 amu which correspond to $(dye-Br+H)^+$, $(dye-Br+2Na)^+$, $(M^*+H)^+$, $(M^*+Na)^+$ and $(M^*+K)^+$, respectively. These results show that the carbonyl-labelling reaction of PEN-G performed in the absence of TED was successful. In comparing the positive-ion mode ESI-MS spectra in Figures 3.4 and 3.7 it is confirmed that the efficiency of the carbonyl-labelling reaction is decreased by the presence of the base TED since there are larger product peaks found in Figure 3.7. Next, this carbonyl-labelling reaction was used to try to label the linear saturated free fatty acid, lauric acid.

Figure 3.6: The calibration curve of labelled PEN-G which was fluorescently tagged in the absence of TED. Capillary: 30 cm, 50 μm I.D., 140 μm O.D.. Run: 10 mM borate, pH 9, 12 kV. Injection: 1000 V, 5 s. Laser: 488 nm Ar$^+$, 12.1 mW. PMT: 1000 V. Interference filter: 518DF25. (n = 3)
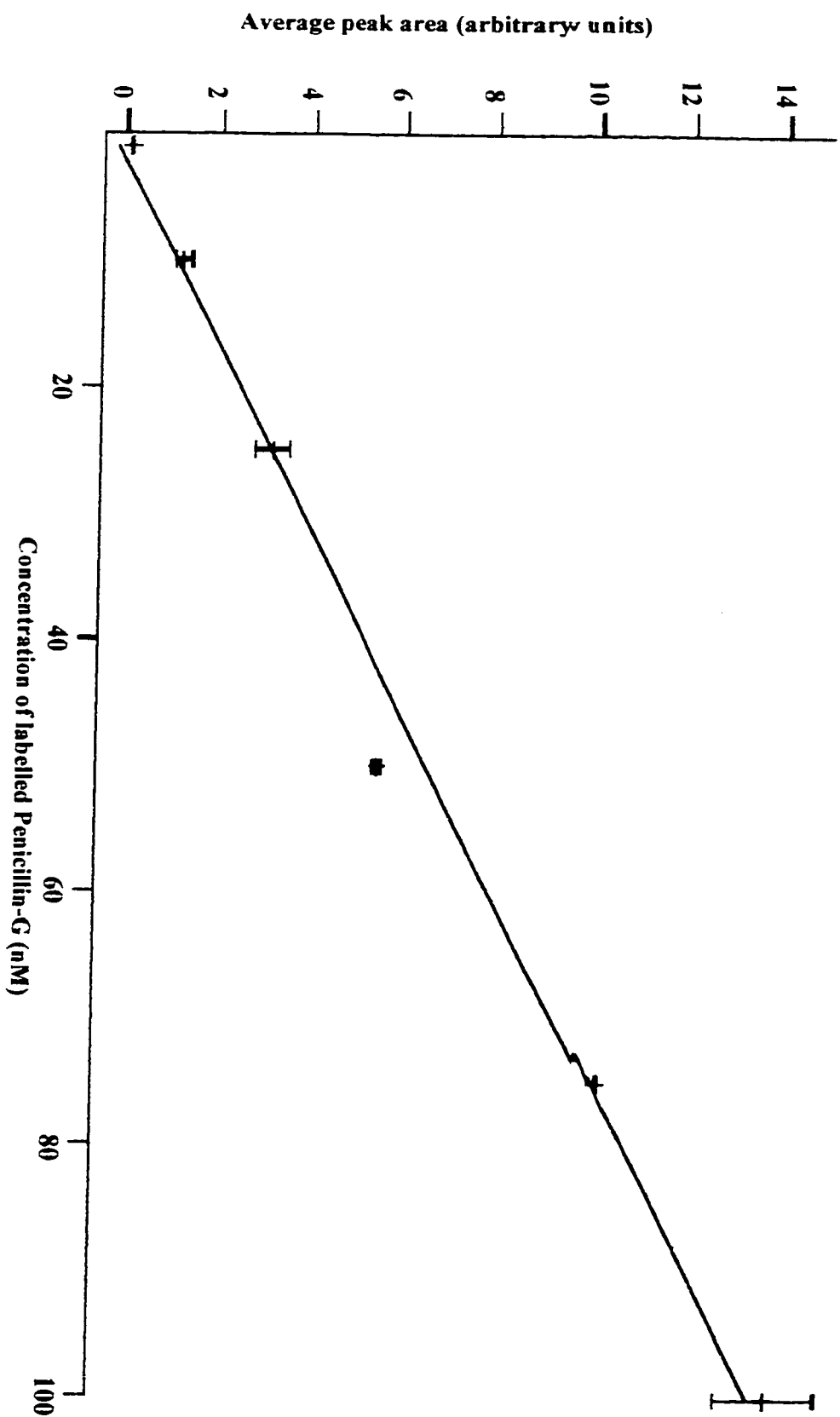
134

Figure 3.7: The positive-ion mode ESI-MS spectra of the carbonyl-labelling reaction of PEN-G performed in the absence of TED. A) blank reaction mixture; A) sample reaction mixture.
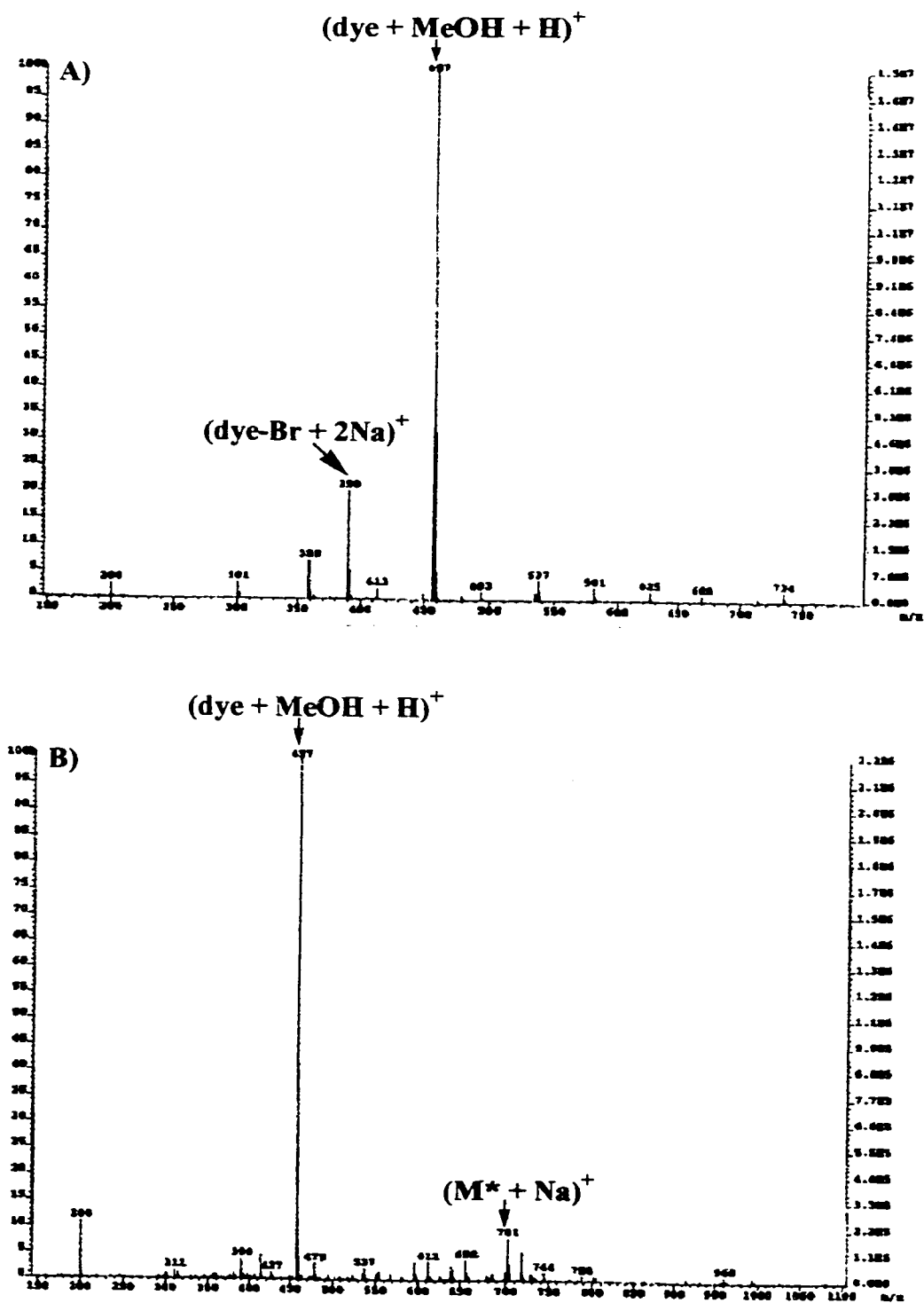
3.3.2 Carbonyl-labelling reaction of lauric acid sodium salt

The carbonyl-labelling reaction was performed as described in Section 3.2.5. It should be noted that the lauric acid sodium salt did not dissolve readily in DMF but required both sonication and heat for complete dissolution to occur. This difficulty in dissolution will be addressed later in the chapter. The blank and sample reaction mixtures were checked for the presence of product using CZE-LIF with the run conditions described in Section 3.2.5 and the resulting electropherograms can be found in Figure 3.8. A peak for labelled lauric acid (M*) appears at an average migration time of ~121 s with an average peak area of 2.546 as calculated using the Igor Pro macro Append Cursor Integration (n = 3). To confirm that the carbonyl-labelling reaction worked, positive-ion mode ESI-MS was used to analyze the blank and sample reaction mixtures. The resulting mass spectra can be found in Figure 3.9. The positive-ion mode ESI-MS blank spectrum showed peaks at 347 amu, 363 amu, 392 amu, 427 amu and 734 amu. These peaks were assigned as $(dye-Br+H)^+$, $(dye-Br+Na)^+$, $(dye-Br+K)^+$, $(dye+H)^+$ and $(dye\ dimer+2Na)^+$, respectively. The positive-ion mode ESI-MS sample spectrum showed peaks at 347 amu, 391 amu, 545 amu and 734 amu. The peak at 545 amu corresponded to the $(M*+H)^+$ peak. These results show that the carbonyl-labelling reaction of lauric acid sodium salt was successful. Next, this labelling reaction was compared to the Mukherjee labelling reaction.

3.3.3 Mukherjee's labelling reaction[5]

The Mukherjee labelling reaction was performed as described in Section 3.2.6 using lauric acid so that the results could be compared with the results of the carbonyl-

136

Figure 3.8: The CZE-LIF electropherograms of the carbonyl-labelling reaction of lauric acid sodium salt.

Capillary: 30 cm, 50 μm I.D., 140 μm O.D. Run: 10 mM borate, pH 9, 12 kV. Injection: 1000 V, 5 s.

Laser: 488 nm Ar⁺, 12.1 mW. PMT: 1000 V. Interference filter: 518DF25. Concentration: 10^{-8} M.
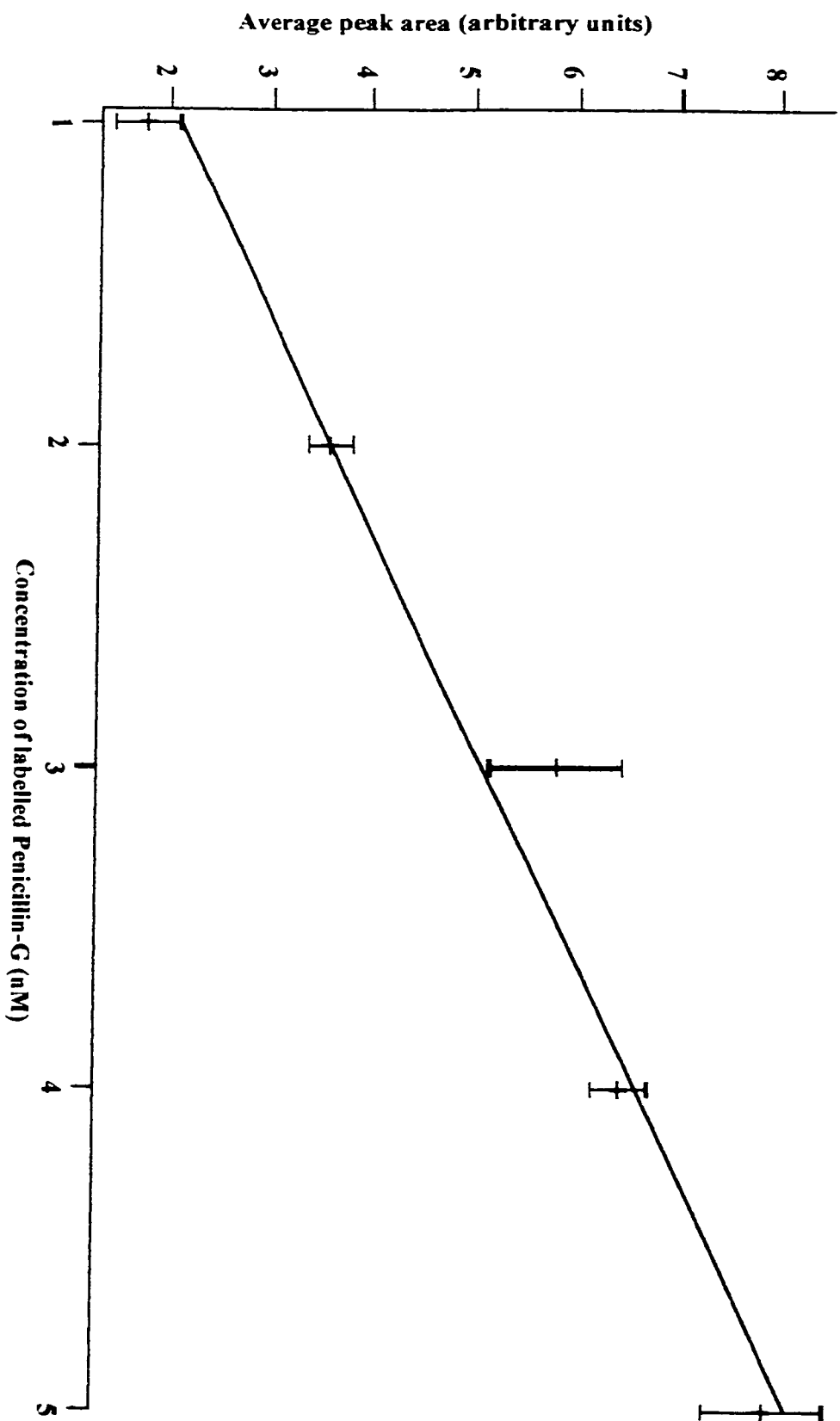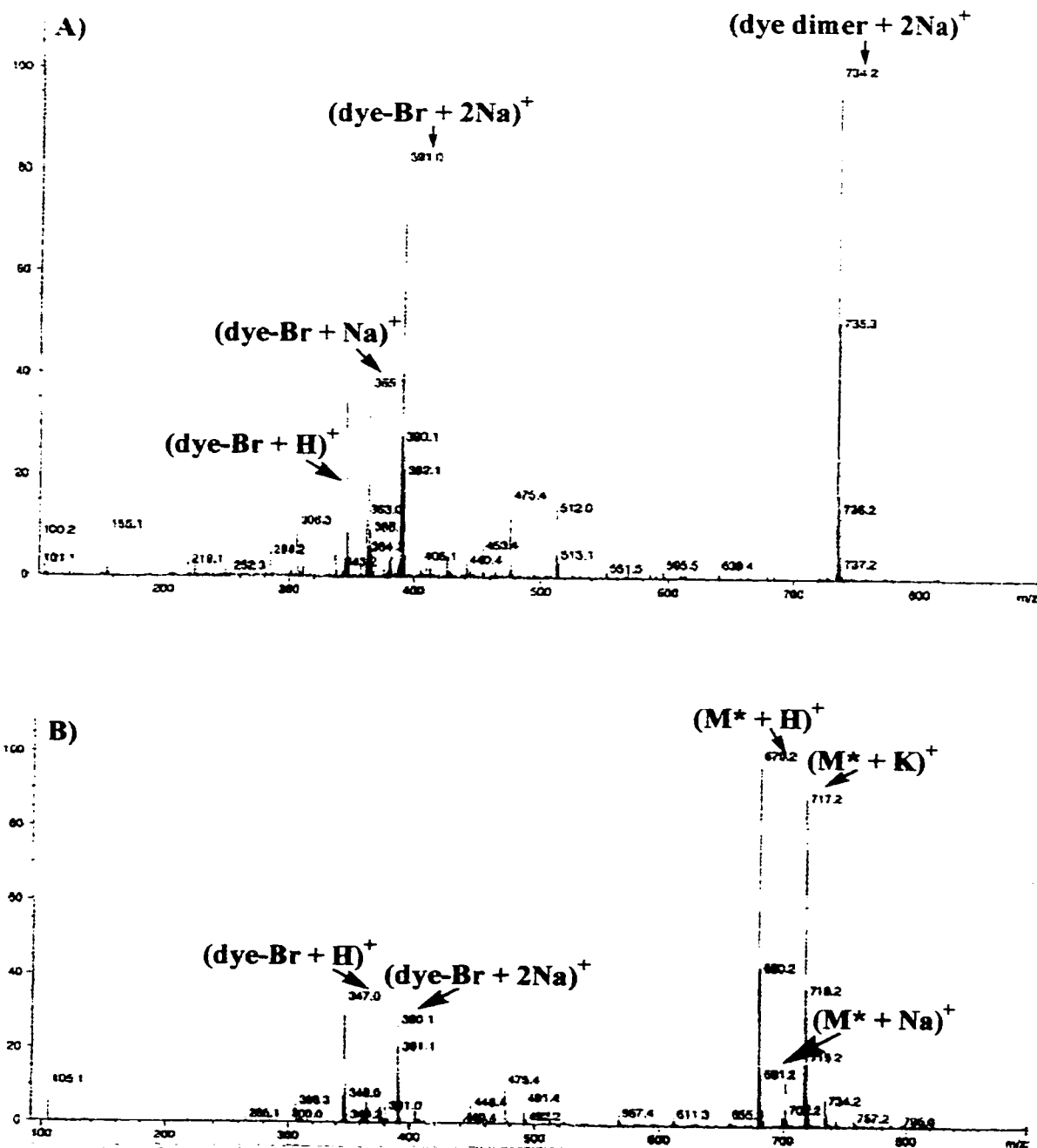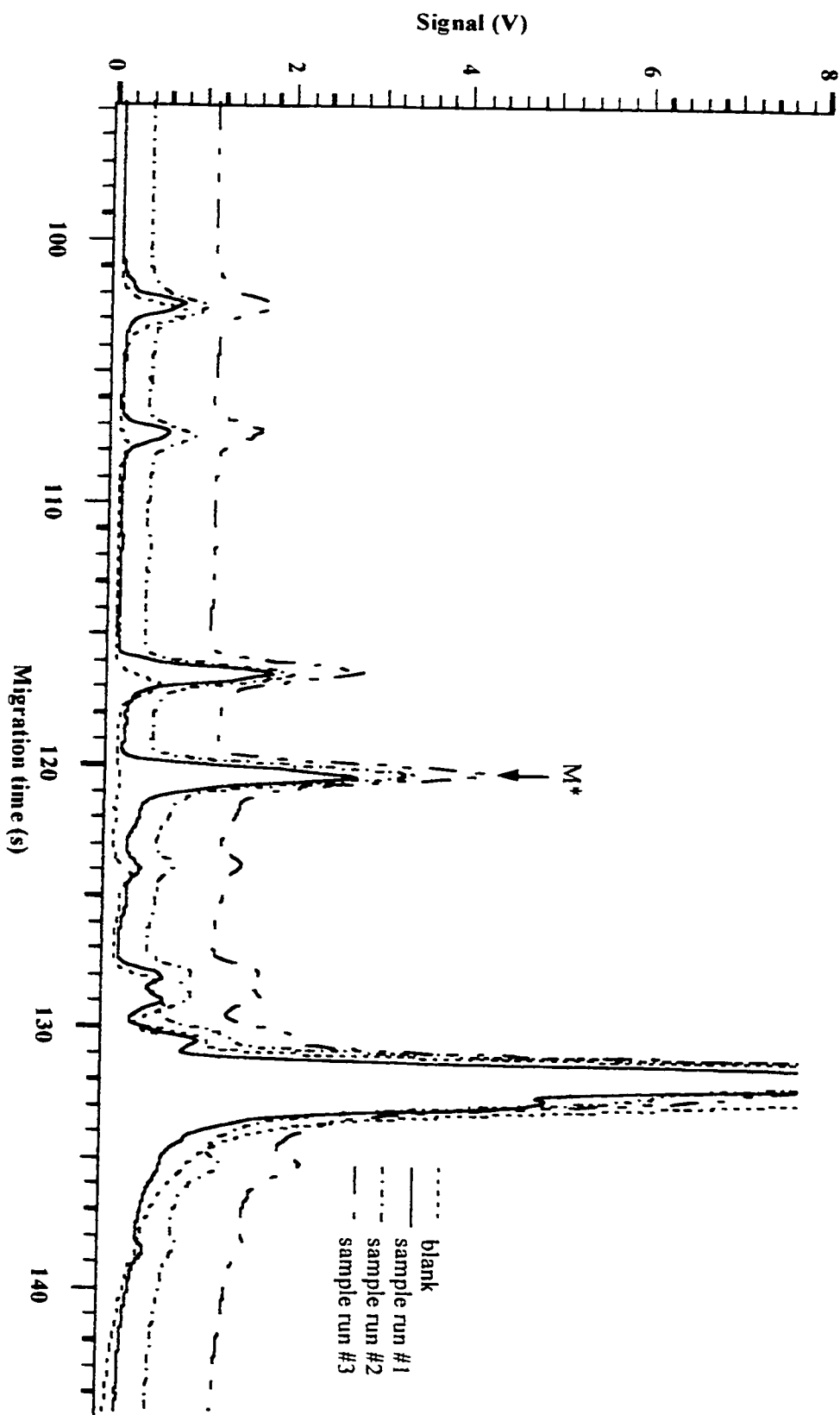
Figure 3.9: The positive-ion mode ESI-MS spectra for the carbonyl-labelling reaction of lauric acid sodium salt. A) blank reaction mixture; B) sample reaction mixture.
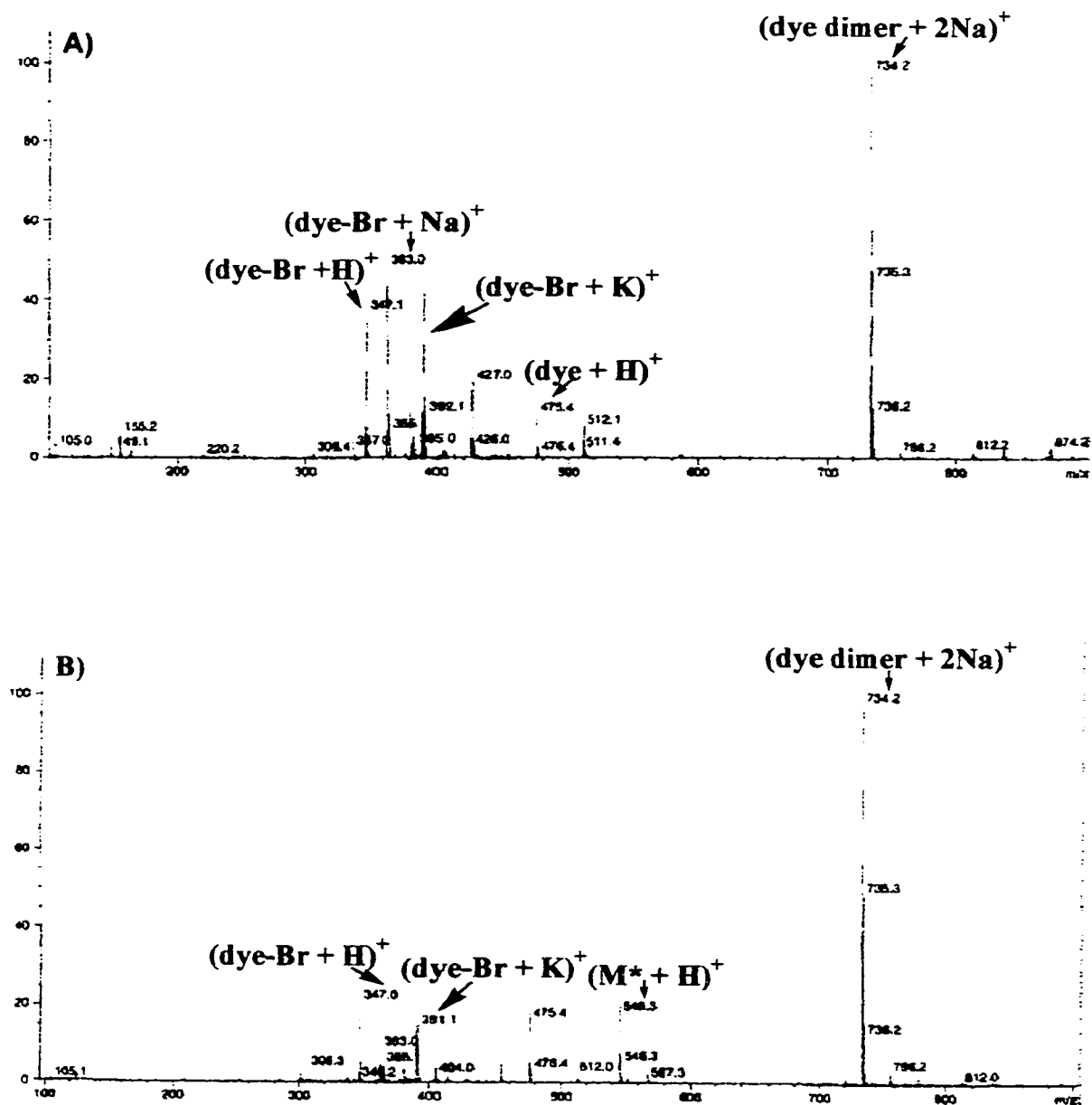
labelling reaction of lauric acid using the procedure described in Section 3.2.5. The reaction mixtures were checked for the presence of product using CZE-LIF under the conditions described in Section 3.2.6. The CZE-LIF electropherograms of this labelling reaction can be found in Figure 3.10. A peak for the labelled lauric acid (M*) appears at an average migration time of ~122 s with an average peak area of 0.684 as calculated using the Igor Pro macro Append Cursor Integration (n = 3). This labelling reaction was repeated to ensure reproducibility and the resulting reaction mixtures were checked for the presence of product using CZE-LIF with the run conditions described in Section 3.2.6. The resulting CZE-LIF electropherograms can be found in Figure 3.11. A peak for labelled lauric acid (M*) appear at an average migration time of ~124 s with an average peak area of 0.250 as calculated using the Igor Pro macro Append Cursor Integration (n = 2). This labelled lauric acid peak area is much lower than the peak area found in the first Mukherjee labelling reaction which could be due to low reproducibility of the labelling reaction, differences in injection volumes, or differences in the serial dilutions of the reaction mixtures. The last two variables can be controlled through the use of an internal standard. In comparing the CZE-LIF electropherograms in Figures 3.8, 3.10 and 3.11 it is evident that the carbonyl-labelling reaction developed in this work is more efficient than the Mukherjee reaction since the product peak is much larger in Figure 3.8. There are many reasons why the Mukherjee labelling reaction is less efficient. First, the Mukherjee labelling reaction involves the base potassium carbonate, which does not completely dissolve in DMF and results in a heterogeneous reaction mixture. This heterogeneity is undesirable as explained earlier in Section 3.3.1. Secondly, the Mukherjee reaction involves acetone, which is not an aprotic solvent like

Figure 3.10: The CZE-LIF electropherograms of the Mukherjee labelling reaction of lauric acid. Capillary: 30 cm, 50 μm I.D., 140 μm O.D.. Run: 10 mM borate, pH 9, 12 kV. Injection: 1000 V, 5 s. Laser: 488 nm Ar^{+}, 12.1 mW. PMT: 1000 V. Interference filter: 518DF25. Concentration: 10^{-8} M.
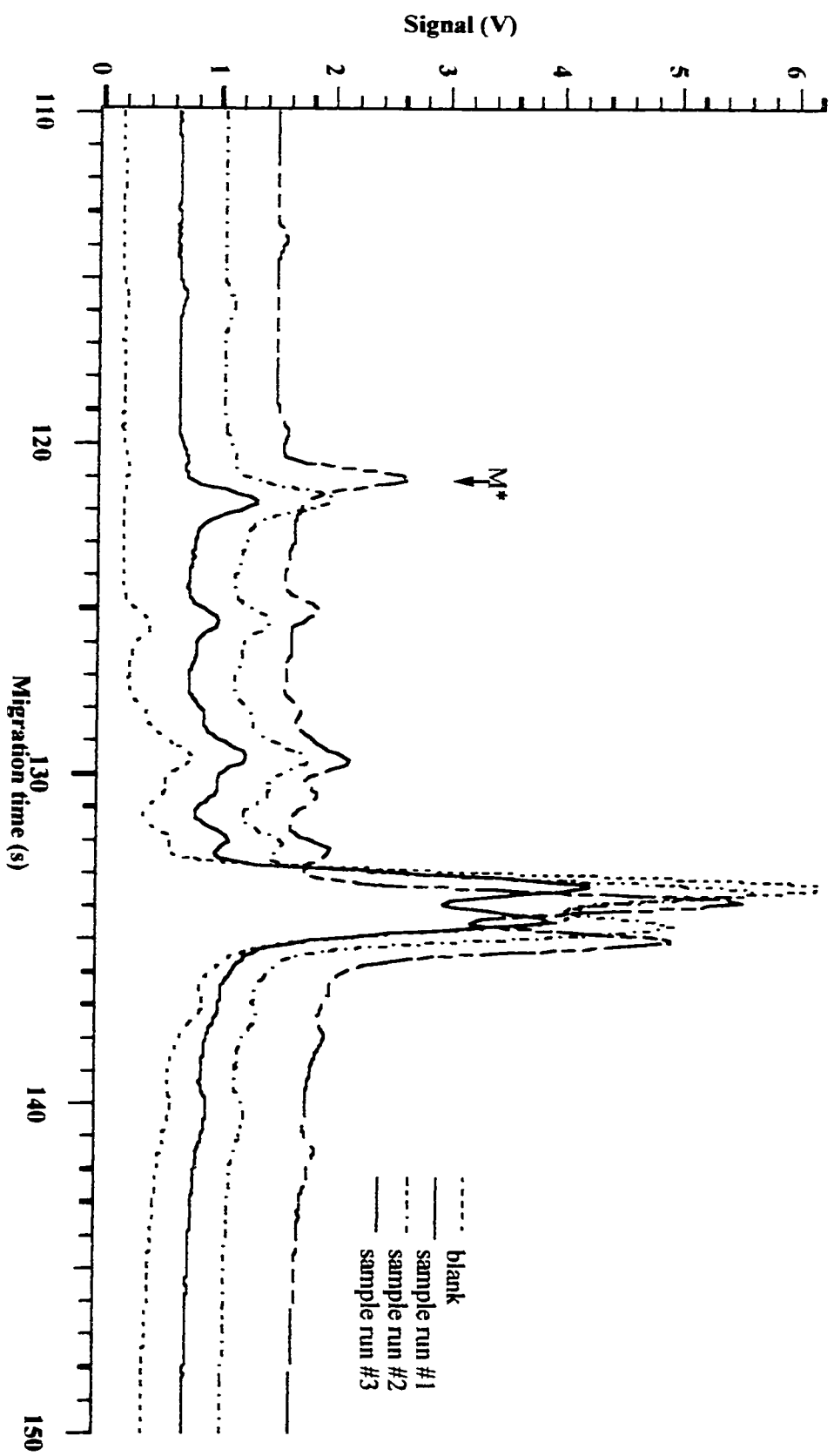
Figure 3.11: The CZE-LIF electropherograms of the repeated Mukherjee labelling reaction of lauric acid. Capillary: 30 cm, 50 μm I.D., 140 μm O.D.. Run: 10 mM borate, pH 9, 12 kV. Injection: 1000 V, 5 s. Laser: 488 nm Ar⁺, 12.1 mW. PMT: 1000 V. Interference filter: 518DF25. Concentration: 10^{-8} M.

141
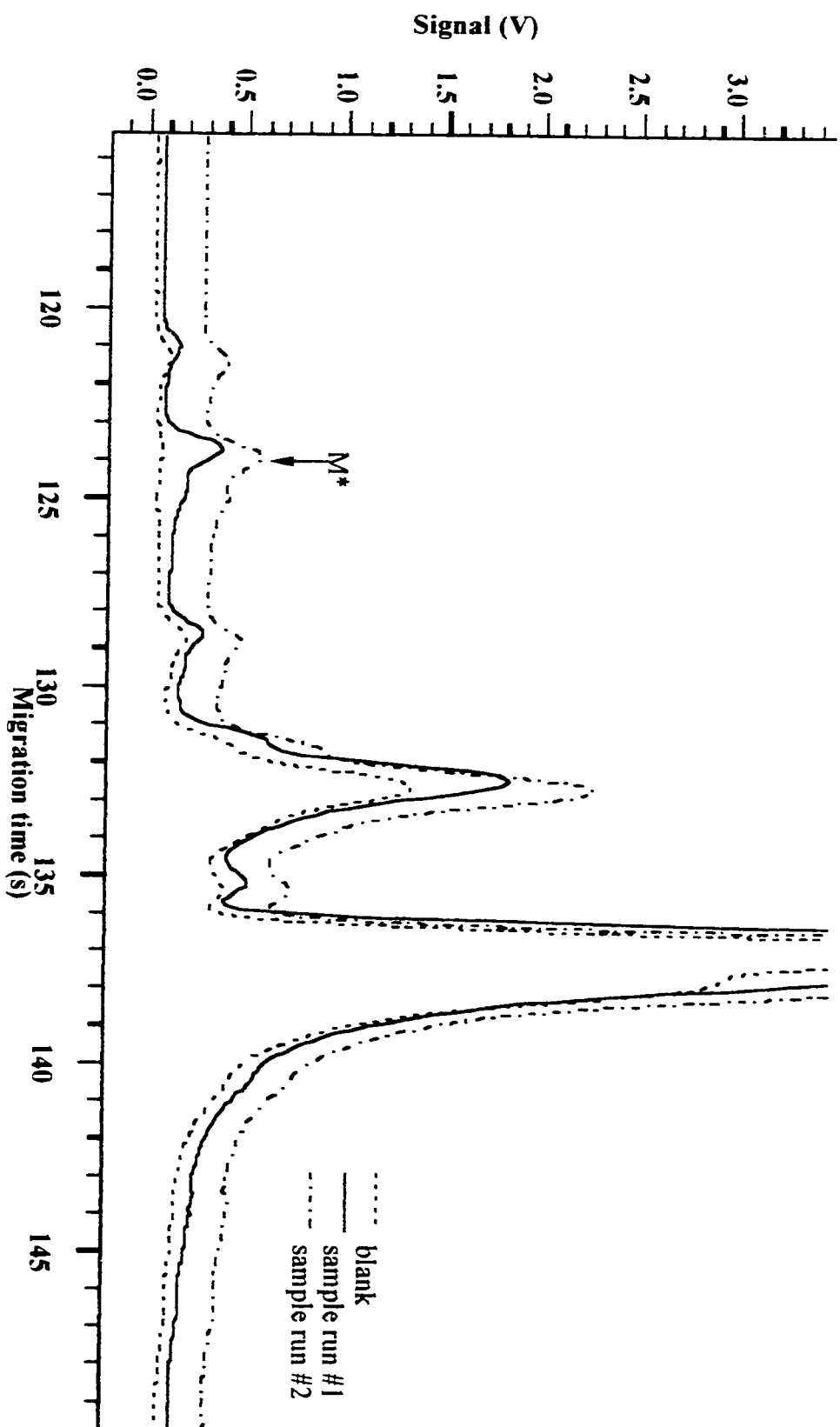
DMF. In the presence of a base, such as potassium carbonate, acetone will be in its enolate form and can react as a nucleophile and displace the bromide ion of 5-BMF leaving the 5-BMF unreactive. The last reason for the poor efficiency of the Mukherjee reaction is that it is required to be performed at 87 °C which turns out to be detrimental to the labelling reaction since the dye 5-BMF is not thermally stable at temperatures above 80 °C.[91]

3.3.4 Further revisions of the carbonyl-labelling reaction of lauric acid sodium salt

Next, the carbonyl-labelling reaction of lauric acid sodium salt was performed in the presence of the base TED and the catalyst 18-Crown-6 to investigate if these reagents would improve the carbonyl-labelling reaction efficiency. The reaction was carried out as described in Section 3.2.7. The reaction mixtures were checked for the presence of product using CZE-LIF with the run conditions described in Section 3.2.7. The resulting CZE-LIF electropherograms can be found in Figure 3.12. A peak for the labelled lauric acid (M*) appears at an average migration time of ~114 s and had an average peak area of 0.536 as calculated by the Igor Pro macro Append Cursor Integration (n = 3). The presence of this peak indicates the success of the carbonyl-labelling reaction of lauric acid sodium salt. Although the carbonyl-labelling reaction was successful when the base TED and the catalyst 18-Crown-6 were present in the reaction mixture it cannot be said that they improved the reaction since the labelling procedure also worked without their presence as shown in Figure 3.8. In comparing Figures 3.8 and 3.12 it is evident that the presence of TED and 18-Crown-6 in the carbonyl-labelling reaction did not improve the labelling efficiency but actually degraded it since the area for labelled lauric acid peak in

Figure 3.12: The CZE-LIF electropherograms of the carbonyl-labelling reaction of lauric acid sodium salt performed in the presence of both the catalyst 18-Crown-6 and the base TED. Capillary: 30 cm, 50 μm I.D., 140 μm O.D.. Run: 10 mM borate, pH 9, 12 kV. Injection: 1000 V, 5 s. Laser: 488 nm Ar⁺, 12.1 mW. PMT: 1000 V. Interference filter: 518DF25. Concentration: 10^{-8} M.

143
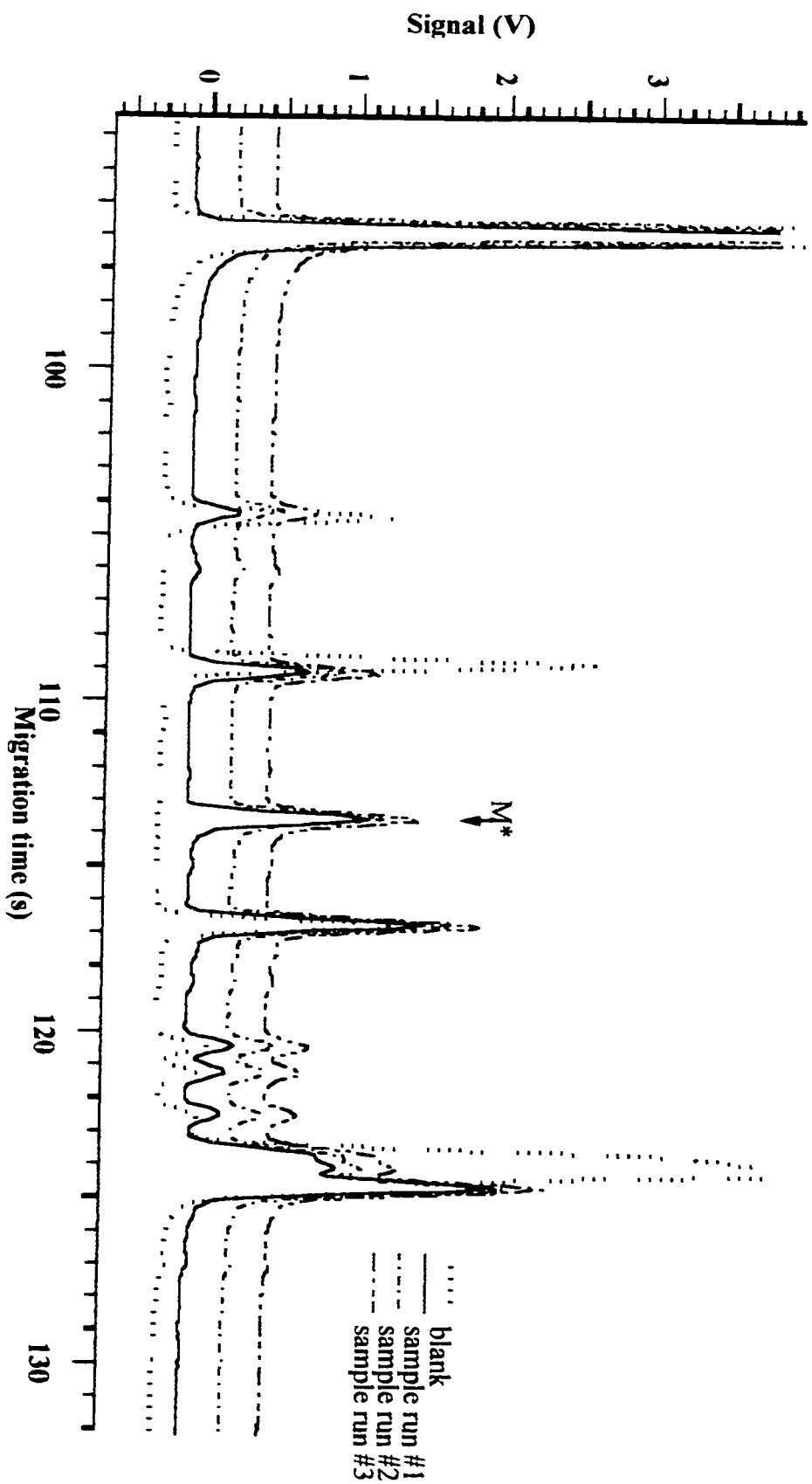
Figure 3.8 is larger than in Figure 3.12. Next, the carbonyl-labelling reaction of lauric acid sodium salt dissolved in a mixture of methanol and DMF was performed in order to investigate the effect the presence of methanol has on the carbonyl-labelling reaction efficiency.

The dissolution of fatty acids in DMF is not complete so a mixture of methanol and DMF was required. The effect of methanol present in the carbonyl-labelling reaction has not been addressed thus far. The carbonyl-labelling reaction of lauric acid sodium salt dissolved in a 4:1 mixture of DMF:MeOH was performed as described in Section 3.2.7. The reaction mixtures were checked for the presence of product using CZE-LIF with the run conditions described in Section 3.2.7. The resulting CZE-LIF electropherograms can be found in Figure 3.13. A peak for labelled lauric acid (M*) appears at an average migration time of ~114 s with an average peak area of 0.492 as calculated by the Igor Pro macro Append Cursor Integration (n = 3). In comparing the CZE-LIF electropherograms in Figures 3.12 and 3.13 one can see that the presence of methanol in the carbonyl-labelling reaction decreased the labelling efficiency only slightly. This degradation was expected since the methoxide ion can react as a nucleophile and displace the bromide ion of 5-BMF, leaving the dye unreactive. Next, the carbonyl-labelling reaction of lauric acid sodium salt was performed in the presence of only the catalyst 18-Crown-6 to see if it would increase the reaction efficiency.

The carbonyl-labelling reaction of lauric acid sodium salt was performed in the presence of the catalyst 18-Crown-6 as described in Section 3.2.8. This reaction mixture was then checked for the presence of product using CZE-LIF under the run conditions described in Section 3.2.8. The resulting CZE-LIF electropherogram can be found in

144

Figure 3.13: The CZE-LIF electropherograms of the carbonyl-labelling reaction of lauric acid sodium salt dissolved in a 4:1 mixture of DMF:MeOH performed in the presence of both the catalyst 18-Crown-6 and the base TED. Capillary: 30 cm, 50 μm I.D., 140 μm O.D.. Run: 10 mM borate, pH 9, 12 kV. Injection: 1000 V, 5 s. Laser: 488 nm Ar⁺, 12.1 mW. PMT: 1000 V. Interference filter: 518DF25. Concentration: 10^{-8} M.

Figure 3.14. A peak for labelled lauric acid (M*) appears a migration time of ~121 s and had a peak area of 0.867 as calculated using the Igor Pro macro Append Cursor Integration. If the CZE-LIF electropherograms in Figures 3.8 and 3.14 are compared one can see that the presence of the catalyst 18-Crown-6 decreases the efficiency of the carbonyl-labelling reaction since the area for the labelled lauric acid peak in Figure 3.14 is much lower than in Figure 3.8. Next, the carbonyl-labelling reaction of lauric acid sodium salt was performed in the presence of the base TED to again try to improve reaction efficiency.

The carbonyl-labelling reaction was performed in the presence of TED as described in Section 3.2.9. The reaction mixtures were checked for the presence of product using CZE-LIF with the run conditions described in Section 3.2.9. The CZE-LIF electropherograms for this reaction can be found in Figure 3.15. A peak for labelled lauric acid (M*) appears at an average migration time of ~122 s and had an average peak area of 0.218 as calculated using the Igor Pro macro Append Cursor Integration (n = 2). When the CZE-LIF electropherograms in Figures 3.8 and 3.15 are compared one can see that the presence of the base TED in the carbonyl-labelling reaction decreases the labelling efficiency since the peak area of labelled lauric acid in Figure 3.8 is much larger than in Figure 3.15. A summary of all the data found for the various reaction conditions used for the carbonyl-labelling reaction of lauric acid sodium salt can be found in Table 3.1. These results prove that the presence of the base TED and/or the catalyst 18-Crown-6 did not improve the efficiency of the carbonyl-labelling reaction. Next, the carbonyl-labelling reaction of lauric acid sodium salt was optimized for the molar ratio of dye to analyte.

Figure 3.14: The CZE-LIF electropherogram of the carbonyl-labelling reaction of lauric acid sodium salt performed in the presence of the catalyst 18-Crown-6. Capillary: 30 cm, 50 μm I.D., 140 μm O.D.. Run: 10 mM borate, pH 9, 12 kV. Injection: 1000 V, 5 s. Laser: 488 nm Ar$^+$, 12.1 mW. PMT: 1000 V. Interference filter: 518DF25. Concentration: 10^{-8} M.
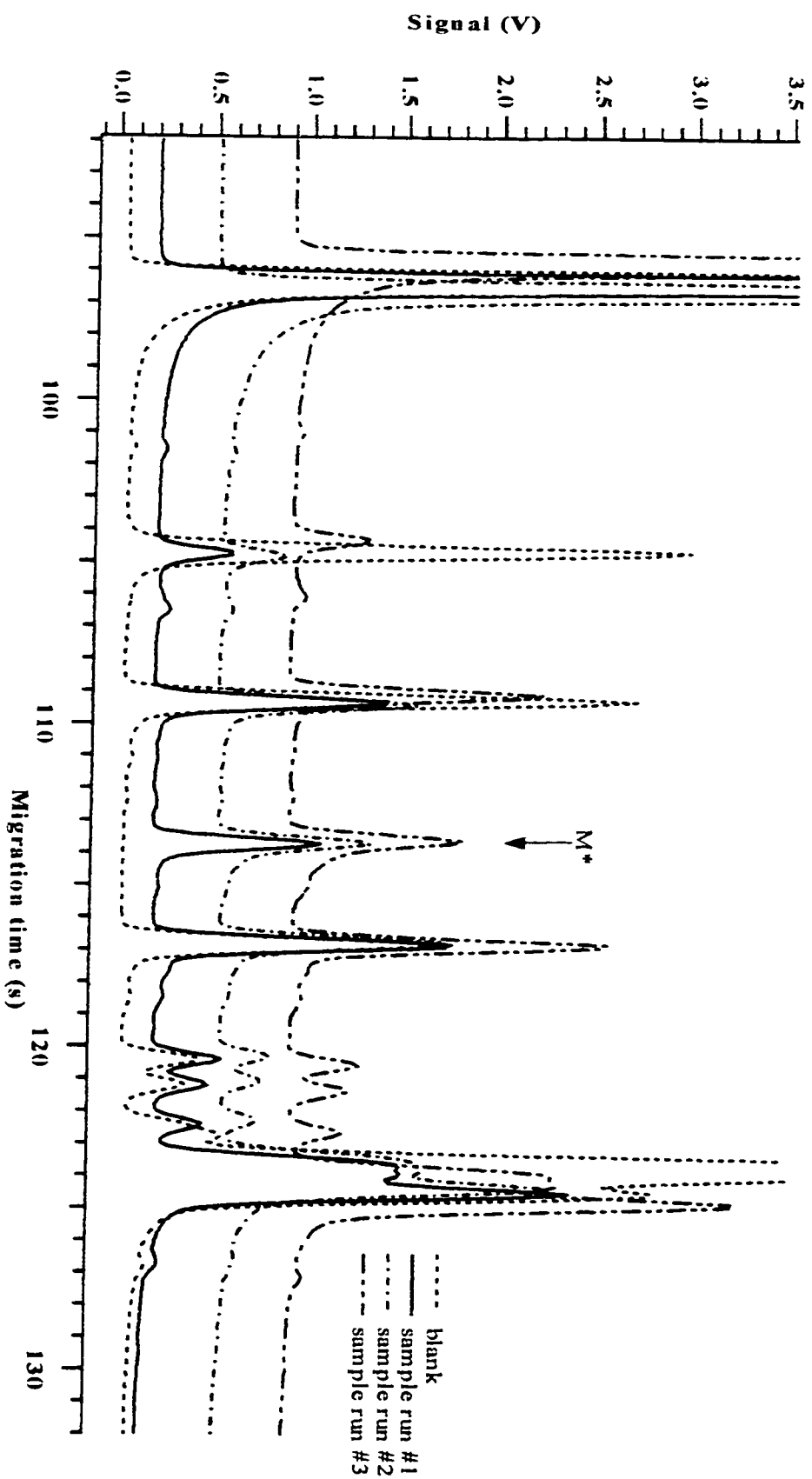
Figure 3.15: The CZE-LIF electropherograms of the carbonyl-labelling reaction of lauric acid sodium salt performed in the presence of the base TED. Capillary: 30 cm, 50 μm I.D., 140 μm O.D.. Run: 10 mM borate, pH 9, 12 kV. Injection: 1000 V, 5 s. Laser: 488 nm Ar⁺, 12.1 mW. PMT: 1000 V. Interference filter: 518DF25. Concentration: 10^{-8} M.

148
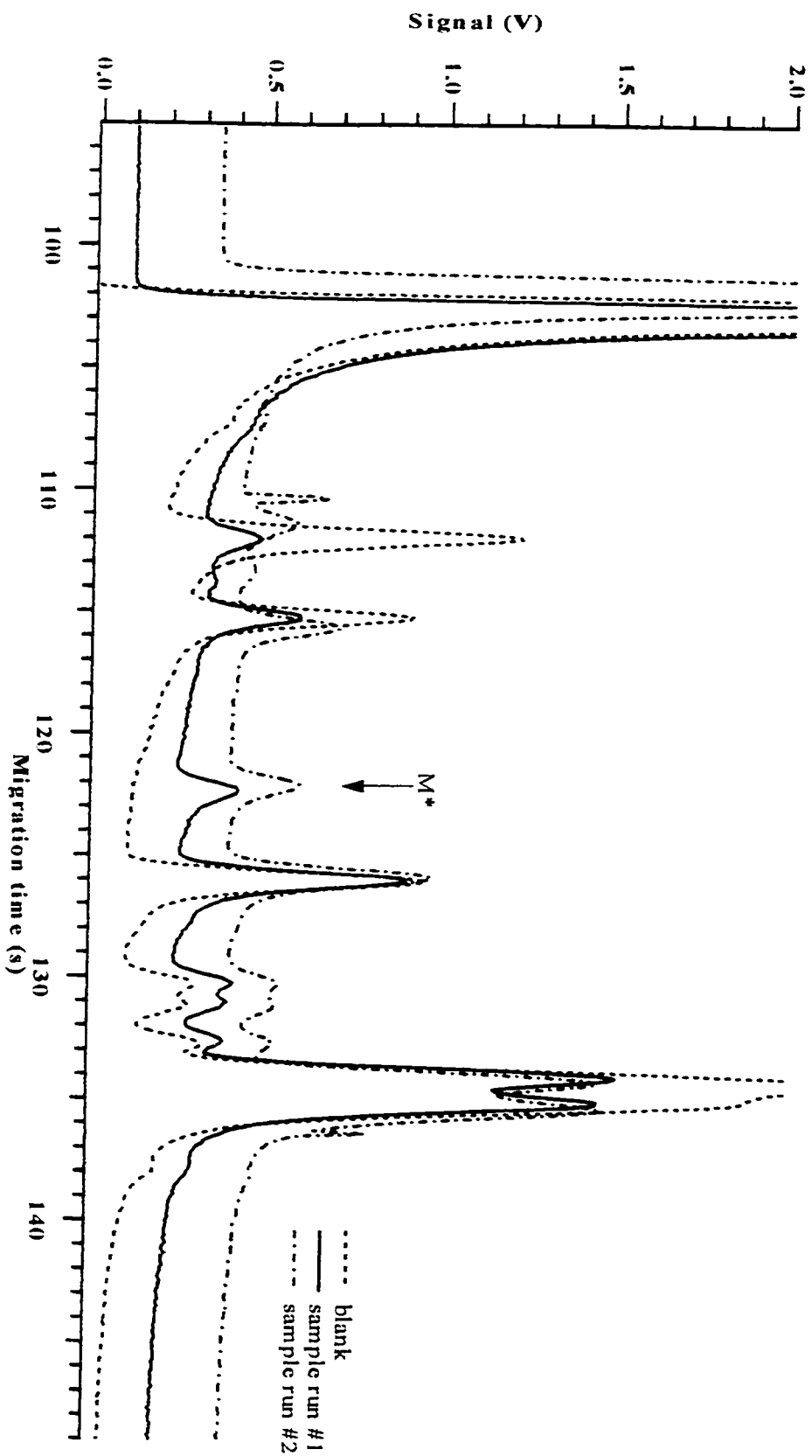
Table 3.1: A summary of all the data found for the various reaction conditions used for

the carbonyl-labelling reaction of lauric acid sodium salt.

Reaction conditions	Average peak area (arbitrary units)
1 μmol lauric acid sodium salt and 2 eqs 5-BMF (dissolved in DMF)	2.546
1 μmol lauric acid sodium salt, 2 eqs 5-BMF, 1 eq TED and 1 eq 18-Crown-6 (dissolved in DMF)	0.536
1 μmol lauric acid sodium salt, 2 eqs 5-BMF, 1 eq TED and 1 eq 18-Crown-6 (dissolved in a 4: 1 mixture of DMF:MeOH)	0.492
1 μmol lauric acid sodium salt, 2 eqs 5-BMF, and 1 eq 18-Crown-6 (dissolved in a 4: 1 mixture of DMF:MeOH)	0.867
1 μmol lauric acid sodium salt, 2 eqs 5-BMF, and 1 eq TED (dissolved in a 4: 1 mixture of DMF:MeOH)	0.218

3.3.5 Optimization of the carbonyl-labelling reaction of lauric acid sodium salt

The dye (5-BMF) to analyte ratio optimization procedure was performed as described in Section 3.2.10. The resulting CZE-LIF electropherograms can be found in Figure 3.16 – 3.20. A peak for labelled lauric acid (M*) appears at an average migration time of 121 s (n = 15). An optimization curve was constructed using these results and can be found in Figure 3.21. The error bars on the optimization curve represent ±1 standard deviation of the average peak areas calculated for the labelled lauric acid peaks found using the various dye to analyte ratios in the carbonyl-labelling reaction of lauric acid sodium salt. These results show that the carbonyl-labelling reaction is optimized when two molar equivalents of 5-BMF are reacted in the procedure.

Next, the reactant limitation of the carbonyl-labelling reaction was investigated as described in Section 3.2.11. In experiments thus far only 1 μmol of lauric acid sodium salt was present in the carbonyl-labelling reaction. The amount of lauric acid sodium salt present in the carbonyl-labelling reaction was scaled down to find its limitation. All resulting reaction mixtures were checked for the presence of product using CZE-LIF with the run conditions described in Section 3.2.11. The carbonyl-labelling reaction was carried out as described in Section 3.2.11 where only 10^{-7} moles of lauric acid sodium salt were reacted and the final volume was 1 mL. The resulting CZE-LIF electropherograms can be found in Figure 3.22. A peak for the labelled lauric acid (M*) appears at an average migration time of ~129 s (n = 3). This labelling procedure was then repeated using a final volume of 100 μL as described in Section 3.2.11. The resulting CZE-LIF electropherograms can be found in Figure 3.23. A peak for the

Figure 3.16: The CZE-LIF electropherograms of the carbonyl-labelling reaction of lauric acid sodium salt performed with one molar equivalent of 5-BMF present. Capillary: 30 cm, 50 μm I.D., 140 μm O.D.. Run: 10 mM borate, pH 9, 12 kV. Injection: 1000 V, 5 s. Laser: 488 nm Ar$^+$, 12.1 mW. PMT: 1000 V. Interference filter: 518DF25. Concentration: 10^{-8} M.
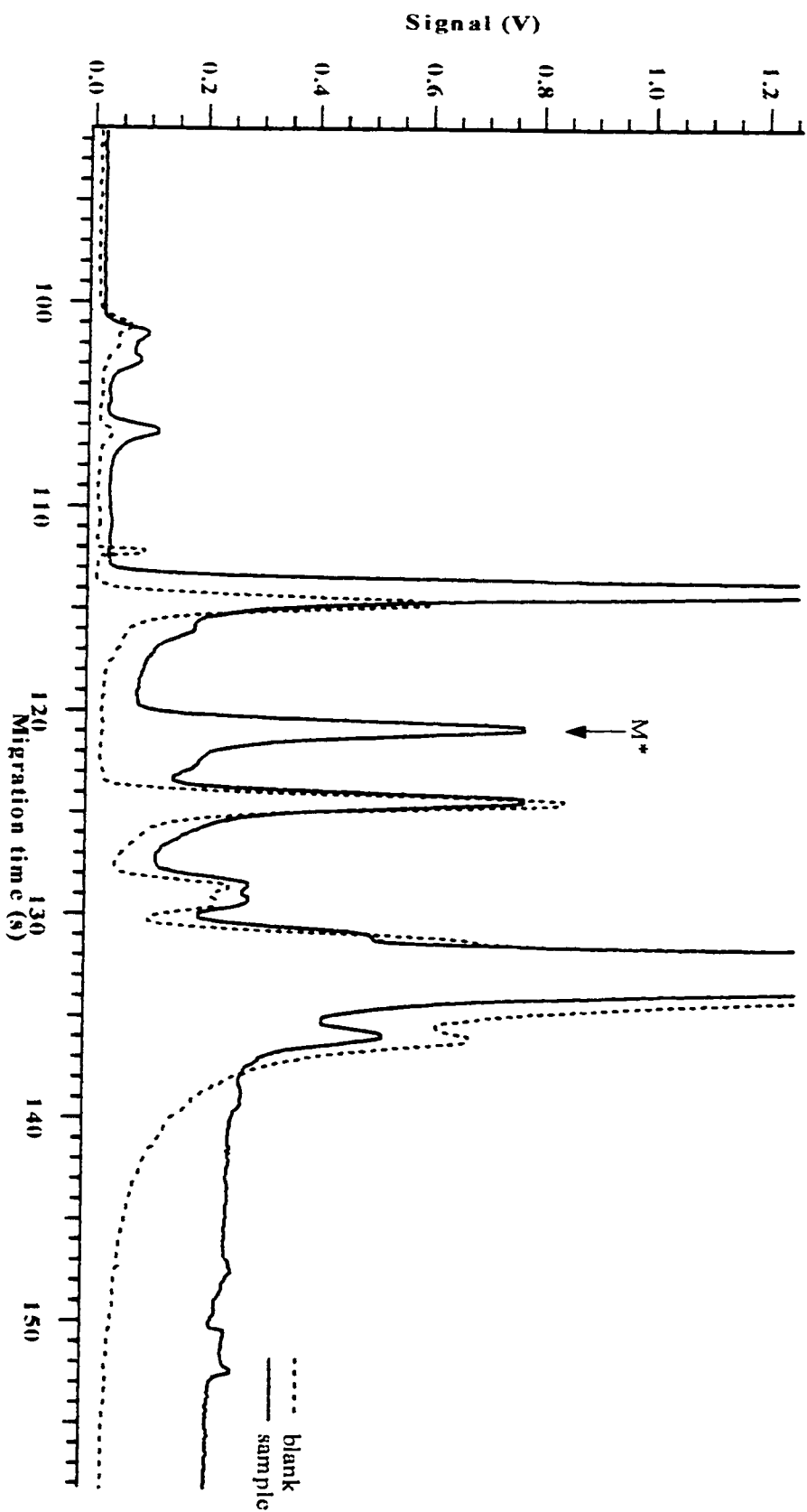
151
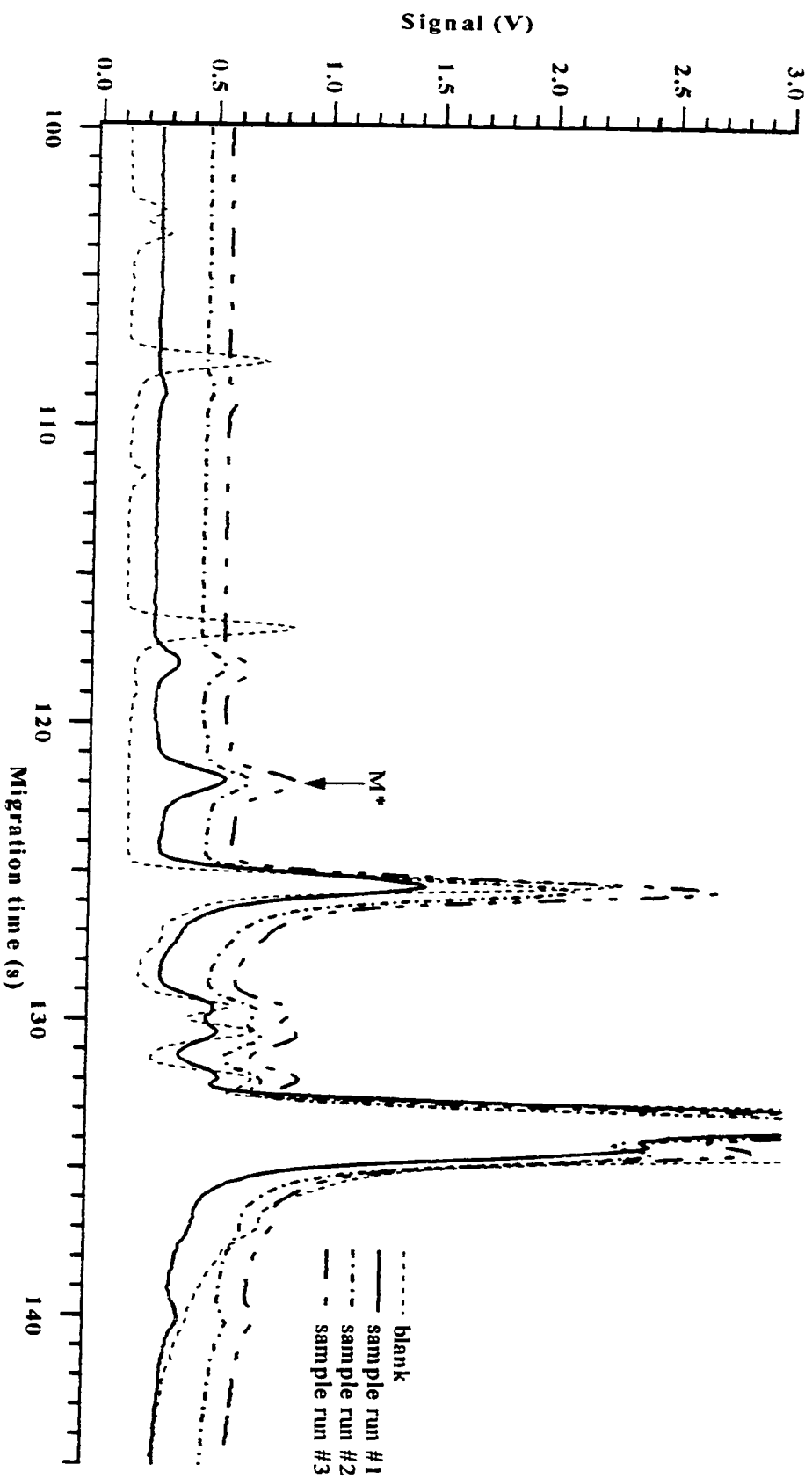
Figure 3.17: The CZE-LIF electropherograms of the carbonyl-labelling reaction of lauric acid sodium salt performed with two molar equivalents of 5-BMF present. Capillary: 30 cm, 50 μm I.D., 140 μm O.D. Run: 10 mM borate, pH 9, 12 kV. Injection: 1000 V, 5 s. Laser: 488 nm Ar⁺, 12.1 mW. PMT: 1000 V. Interference filter: 518DF25. Concentration: 10^{-8} M.

152

Figure 3.18: The CZE-LIF electropherograms of the carbonyl-labelling reaction of lauric acid sodium salt performed with three molar equivalents of 5-BMF present. Capillary: 30 cm, 50 μm I.D., 140 μm O.D.. Run: 10 mM borate, pH 9, 12 kV. Injection: 1000 V, 5 s. Laser: 488 nm Ar$^+$, 12.1 mW. PMT: 1000 V. Interference filter: 518DF25. Concentration: 10^{-8} M.

153
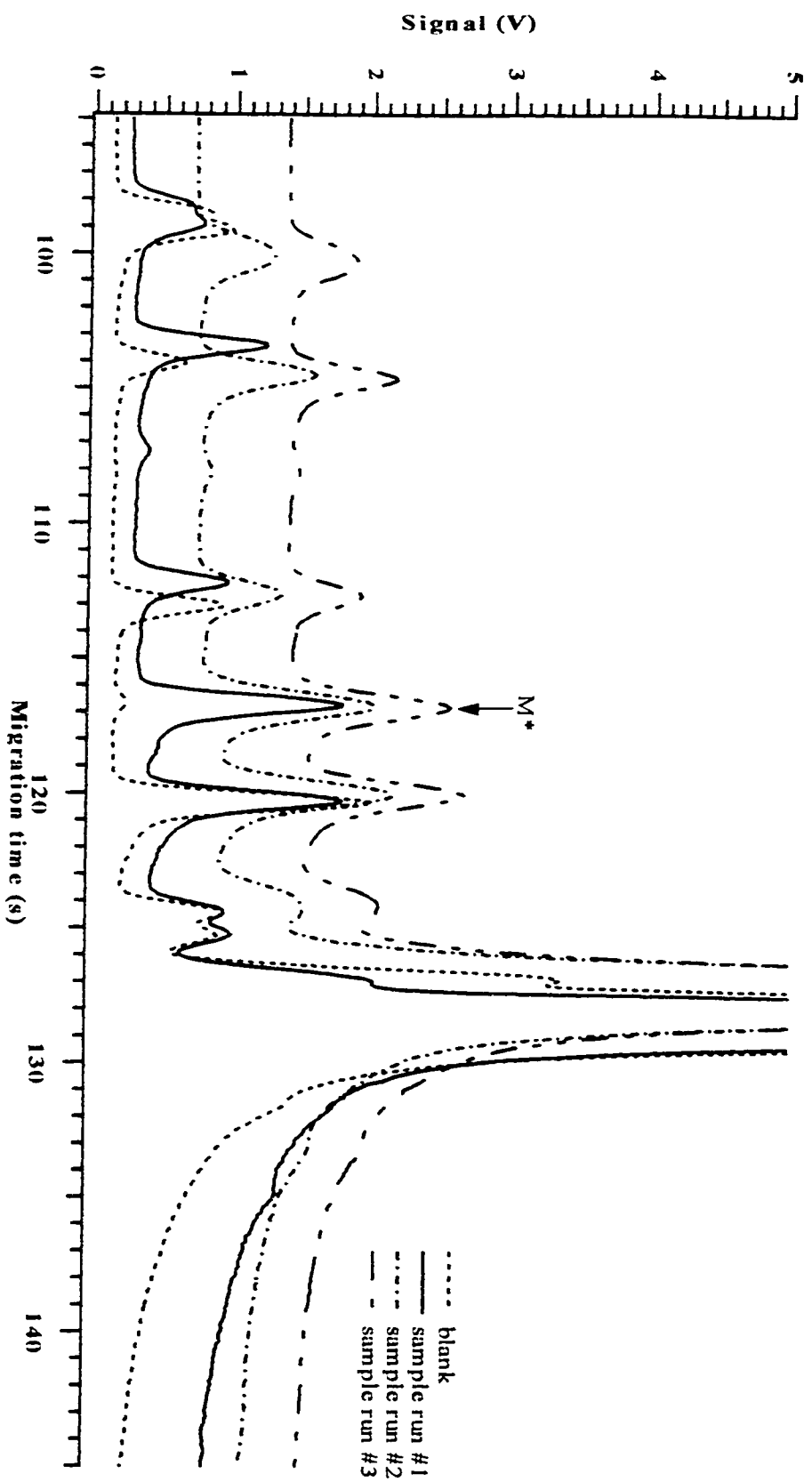
Figure 3.19: The CZE-LIF electropherograms of the carbonyl-labelling reaction of lauric acid sodium salt performed with four molar equivalents of 5-BMF present. Capillary: 30 cm, 50 μm I.D., 140 μm O.D.. Run: 10 mM borate, pH 9, 12 kV. Injection: 1000 V, 5 s. Laser: 488 nm Ar$^+$, 12.1 mW. PMT: 1000 V. Interference filter: 518DF25. Concentration: 10^{-8} M.
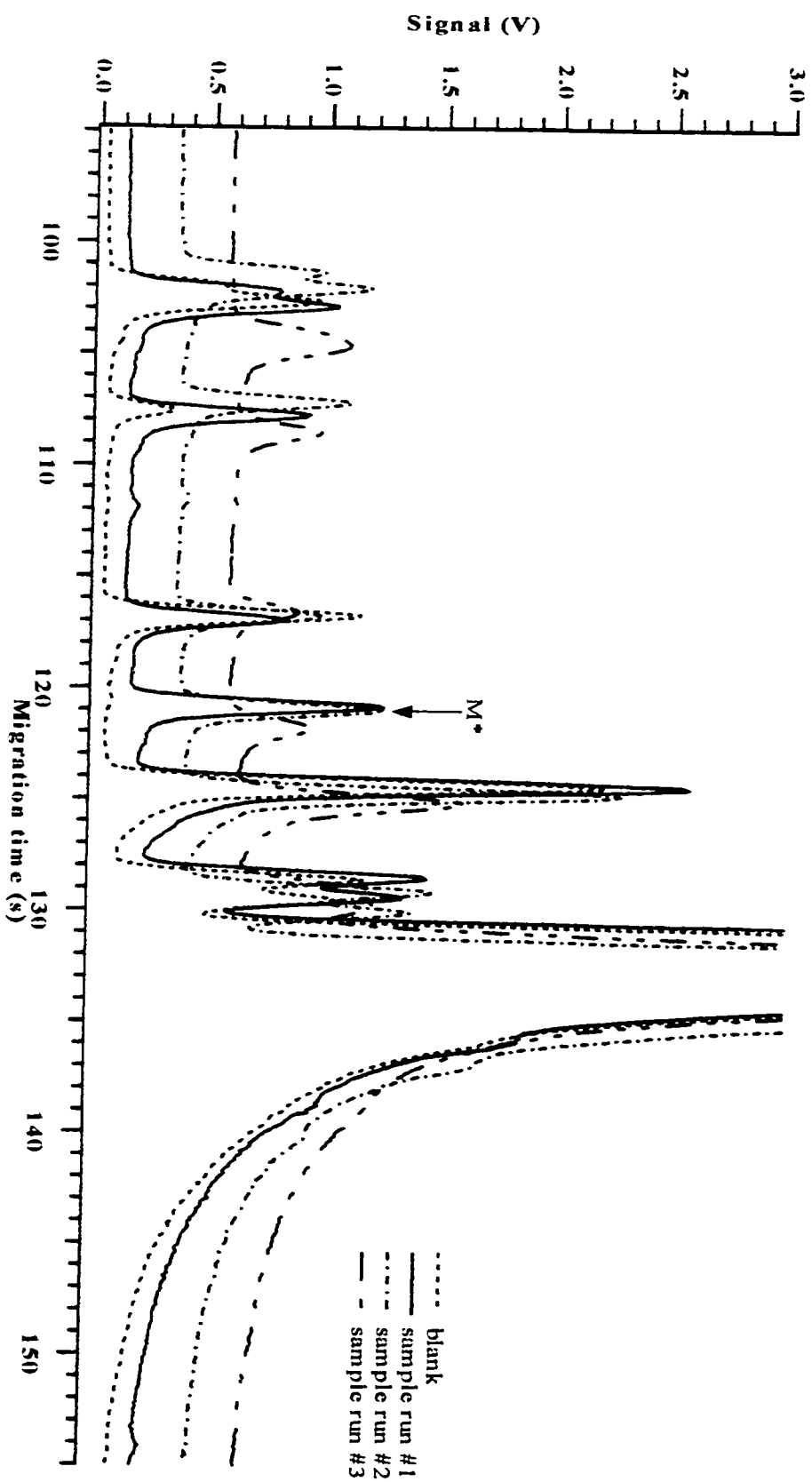
Figure 3.20: The CZE-LIF electropherograms of the carbonyl-labelling reaction of lauric acid sodium salt performed with five molar equivalents of 5-BMF present. Capillary: 30 cm, 50 μm I.D., 140 μm O.D.. Run: 10 mM borate, pH 9, 12 kV. Injection: 1000 V, 5 s. Laser: 488 nm Ar⁺, 12.1 mW. PMT: 1000 V. Interference filter: 518DF25. Concentration: 10^{-8} M.

155
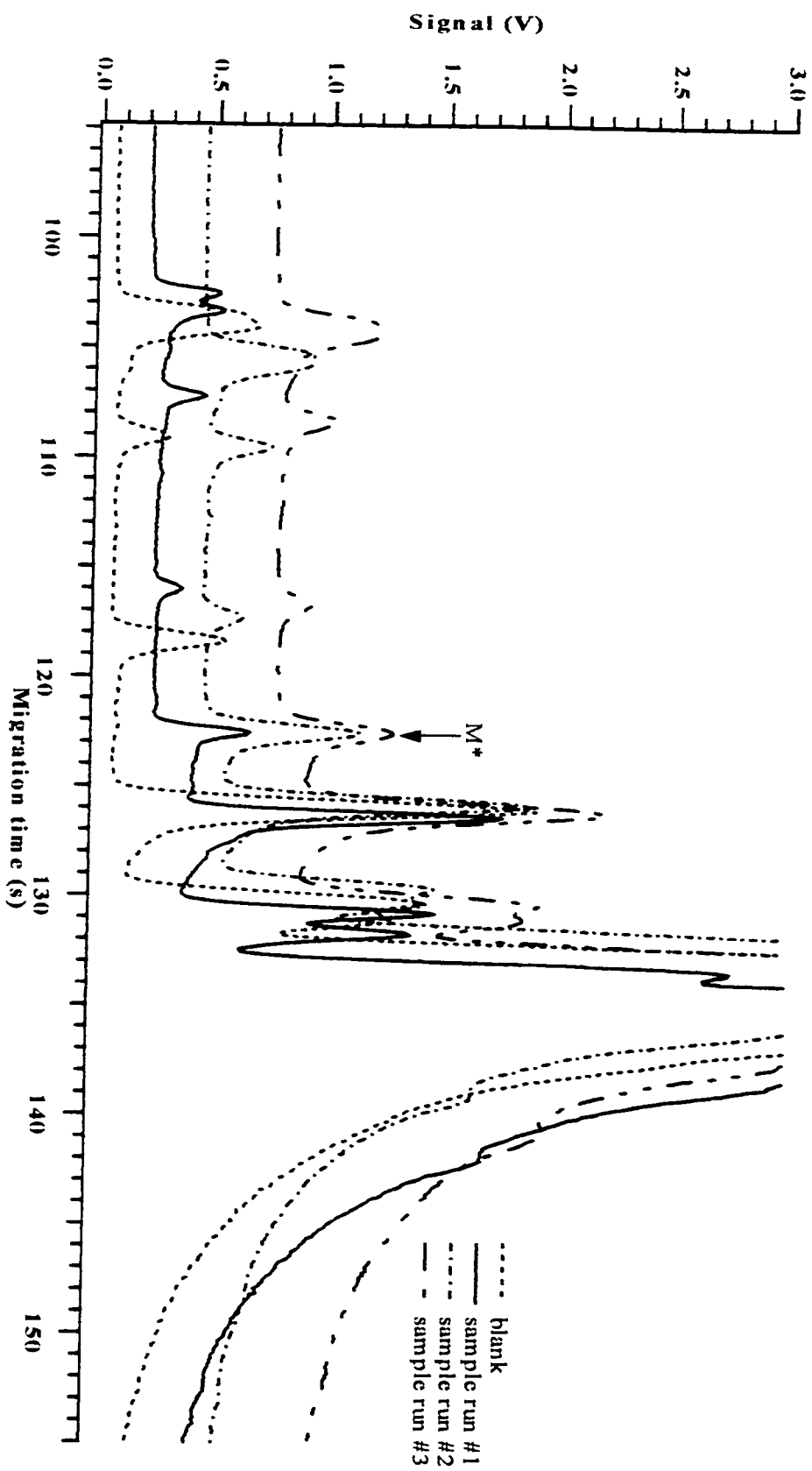
Figure 3.21: The dye to analyte ratio optimization curve for the carbonyl-labelling reaction of lauric acid sodium salt.

Capillary: 30 cm, 50 μm I.D., 140 μm O.D.. Run: 10 mM borate, pH 9, 12 kV. Injection: 1000 V, 5 s.

Laser: 488 nm Ar$^+$, 12.1 mW. PMT: 1000 V. Interference filter: 518DF25. Concentration: 10^{-8} M. (n = 3)

Figure 3.22: The reactant limitation of the carbonyl-labelling reaction. The CZE-LIF electropherograms of the carbonyl-labelling reaction using 10^{-7} moles of lauric acid sodium salt. The final volume was 1 mL. Capillary: 30 cm, 50 μm I.D., 140 μm O.D.. Run: 10 mM borate, pH 9, 12 kV. Injection: 1000 V, 5 s. Laser: 488 nm Ar⁺, 12.1 mW. PMT: 1000 V. Interference filter: 518DF25. Concentration: 10^{-8} M.
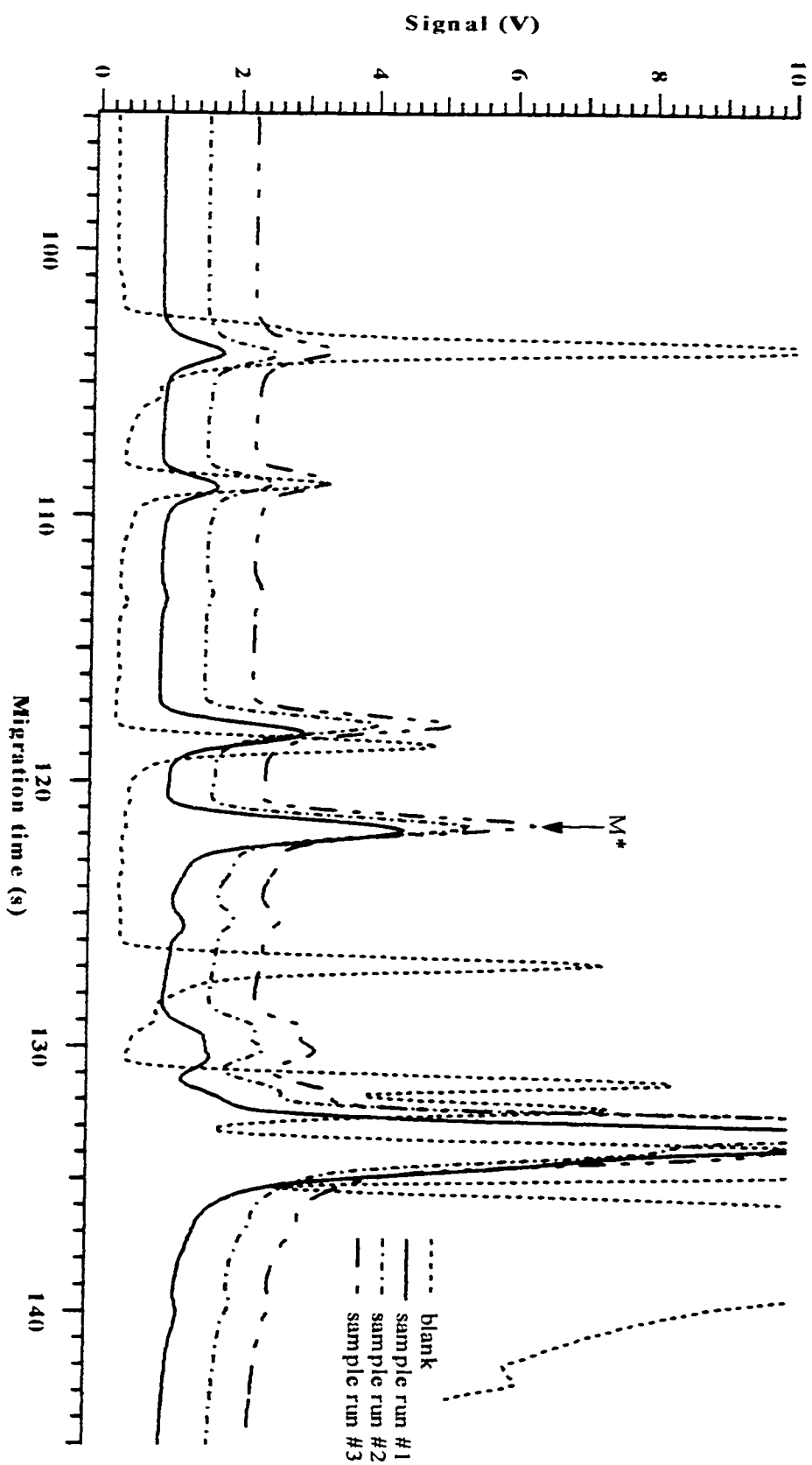
157

Figure 3.23: The reactant limitation of the carbonyl-labelling reaction. The CZE-LIF electropherograms of the carbonyl-labelling reaction using 10^{-7} moles of lauric acid sodium salt. The final volume was 100 µL. Capillary: 30 cm, 50 µm I.D., 140 µm O.D., Run: 10 mM borate, pH 9, 12 kV. Injection: 1000 V, 5 s. Laser: 488 nm Ar⁺, 12.1 mW. PMT: 1000 V. Interference filter: 518DF25. Concentration: 10^{-8} M.

158

labelled lauric acid (M*) appears at an average migration time of ~130 s (n = 3). Next, the carbonyl-labelling reaction was repeated using only 10^{-8} moles of lauric acid sodium salt with a final volume of 1 mL as described in Section 3.2.11. The resulting CZE-LIF electropherograms can be found in Figure 3.24. A small peak for labelled lauric acid (M*) appears at an average migration time of ~132 s (n = 3). This labelling procedure was repeated as described in Section 3.2.11 only the final volume was 100 µL. The resulting CZE-LIF electropherograms can be found in Figure 3.25. A peak for labelled lauric acid (M*) appears at an average migration time of ~116 s (n = 3). The labelling procedure was repeated again as described in Section 3.2.11 only 10^{-9} moles of lauric acid sodium salt were reacted and the final volume was 1 mL. The resulting CZE-LIF electropherograms can be found in Figure 3.26. A peak for labelled lauric acid is not present. The labelling procedure was then repeated as described in Section 3.2.11 only the final volume was 100 µL. The resulting CZE-LIF electropherograms can be found in Figure 3.27. A peak for labelled lauric acid is not present. These results show that the limitation of the carbonyl-labelling reaction is when 10^{-8} moles of lauric acid sodium salt were reacted. Next, the carbonyl-labelling reaction of lauric acid sodium salt was optimized for reaction time.

The reaction time optimization of the carbonyl-labelling reaction using lauric acid sodium salt was performed as described in Section 3.2.12. All resulting reaction mixtures were check for the presence of product using CZE-LIF with the run conditions described in Section 3.2.12. The resulting CZE-LIF electropherograms can be found in Figures 3.28 – 3.38. These CZE-LIF electropherograms were then used to build a reaction time optimization curve, which can be found in Figure 3.39. The error bars on the
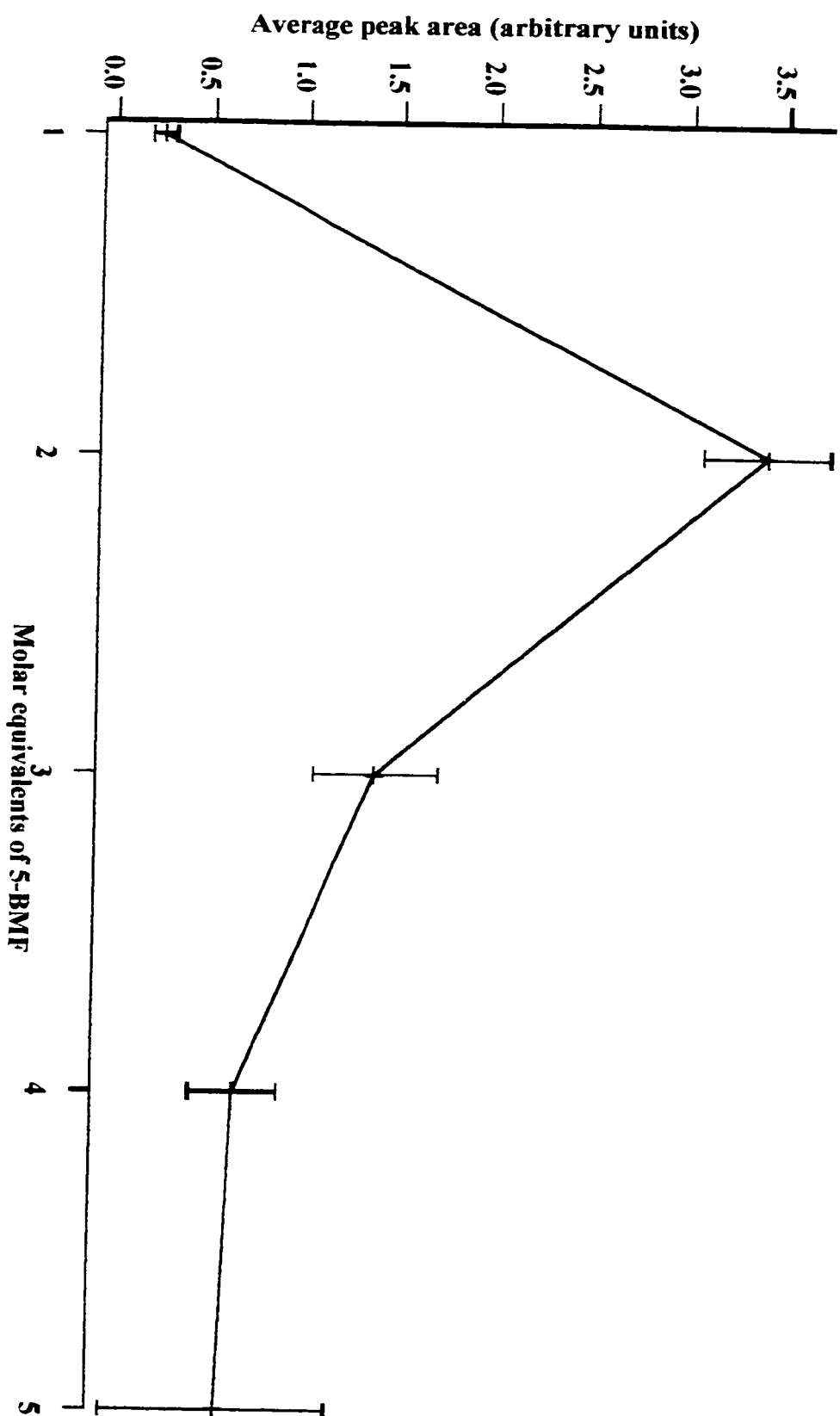
159

Figure 3.24: The reactant limitation of the carbonyl-labelling reaction. The CZE-LIF electropherograms of the carbonyl-labelling reaction using 10^{-8} moles of lauric acid sodium salt. The final volume was 1 mL. Capillary: 30 cm, 50 μm I.D., 140 μm O.D.. Run: 10 mM borate, pH 9, 12 kV. Injection: 1000 V, 5 s. Laser: 488 nm Ar$^+$, 12.1 mW. PMT: 1000 V. Interference filter: 518DF25. Concentration: 10^{-8} M.
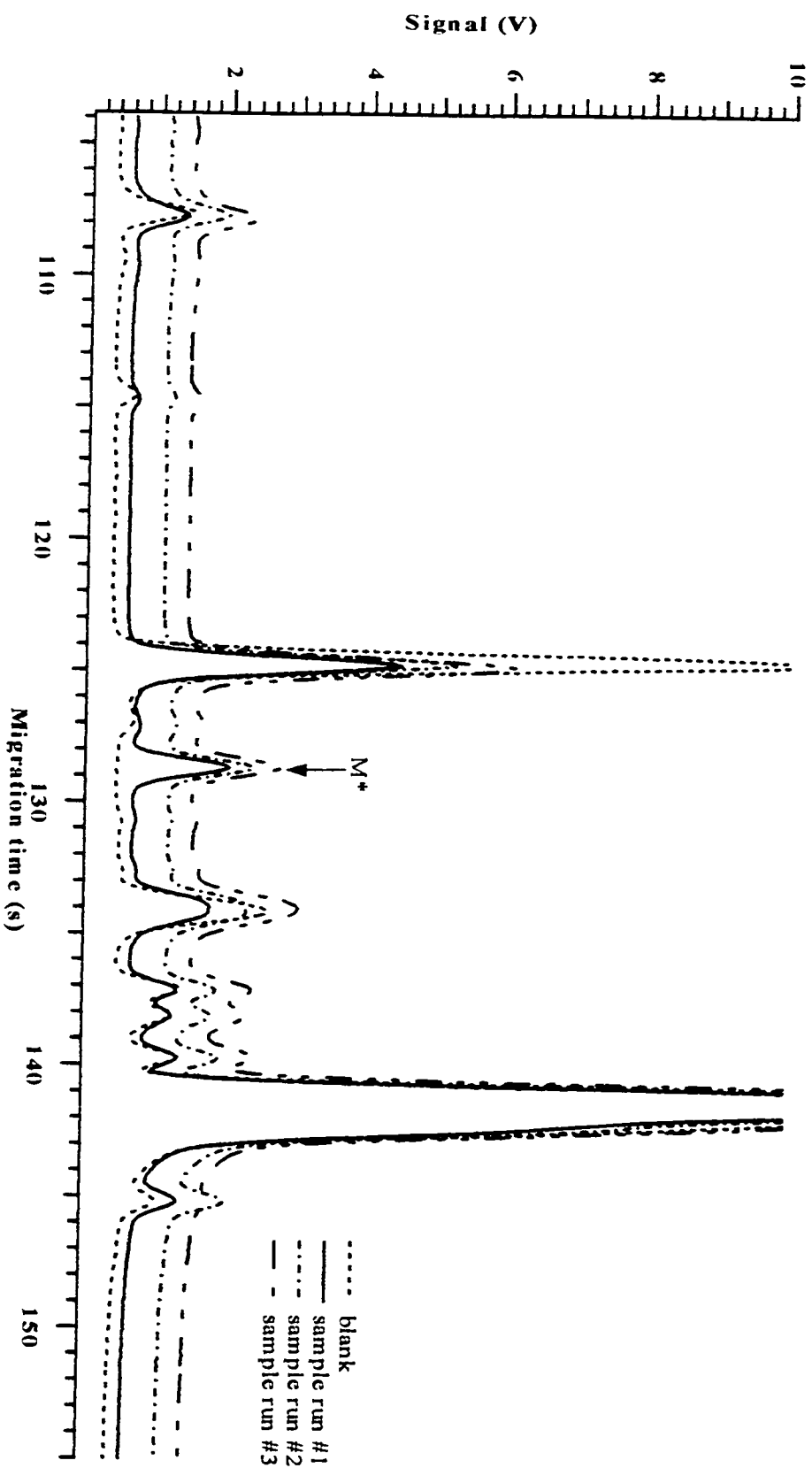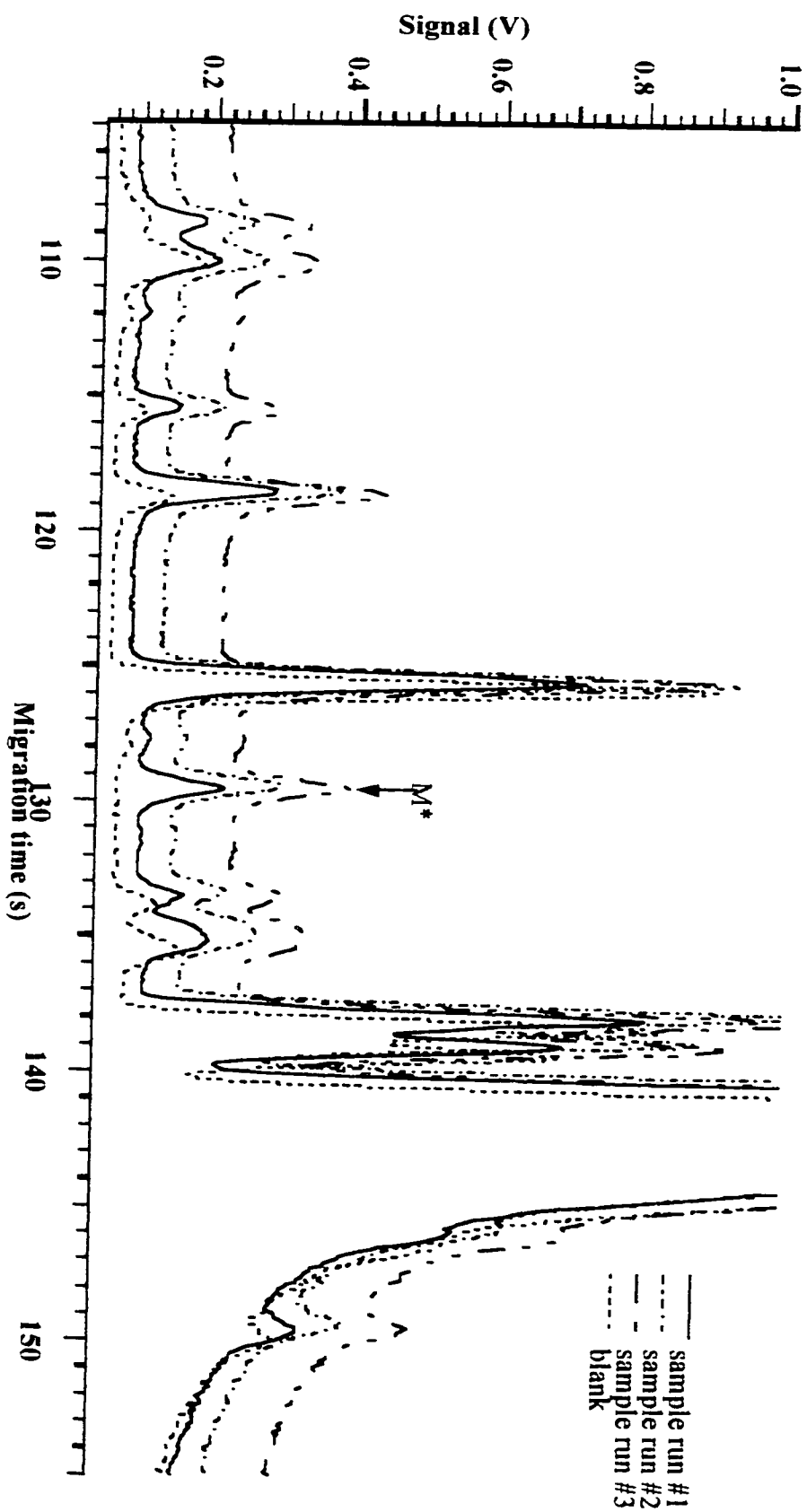
Figure 3.25: The reactant limitation of the carbonyl-labelling reaction. The CZE-LIF electropherograms of the carbonyl-labelling reaction using 10^{-8} moles of lauric acid sodium salt. The final volume was 100 µL. Capillary: 30 cm, 50 µm I.D., 140 µm O.D.. Run: 10 mM borate, pH 9, 12 kV. Injection: 1000 V, 5 s. Laser: 488 nm Ar⁺, 12.1 mW.

PMT: 1000 V. Interference filter: 518DF25. Concentration: 10^{-8} M.

Figure 3.26: The reactant limitation of the carbonyl-labelling reaction. The CZE-LIF electropherograms of the carbonyl-labelling reaction using 10^{-9} moles of lauric acid sodium salt. The final volume was 1 mL. Capillary: 30 cm, 50 µm I.D., 140 µm O.D.. Run: 10 mM borate, pH 9, 12 kV. Injection: 1000 V, 5 s. Laser: 488 nm Ar$^+$, 12.1 mW. PMT: 1000 V. Interference filter: 518DF25. Concentration: 10^{-8} M.

162

Figure 3.27: The reactant limitation of the carbonyl-labelling reaction. The CZE-LIF electropherograms of the carbonyl-labelling reaction using 10^{-9} moles of lauric acid sodium salt. The final volume was 100 μL. Capillary: 30 cm, 50 μm I.D., 140 μm O.D.. Run: 10 mM borate, pH 9, 12 kV. Injection: 1000 V, 5 s. Laser: 488 nm Ar$^+$, 12.1 mW. PMT: 1000 V. Interference filter: 518DF25. Concentration: 10^{-8} M.

Figure 3.28: The reaction time optimization of the carbonyl-labelling reaction. The CZE-LIF electropherograms of the carbonyl-labelling reaction of lauric acid sodium salt immediately after mixing the acid and the 5-BMF together.

Capillary: 30 cm, 50 μm I.D., 140 μm O.D.. Run: 10 mM borate, pH 9, 12 kV. Injection: 1000 V, 5 s.

Laser: 488 nm Ar$^+$, 12.1 mW. PMT: 1000 V. Interference filter: 518DF25. Concentration: 10^{-8} M.

164

Figure 3.29: The reaction time optimization of the carbonyl-labelling reaction. The CZE-LIF electropherograms of the carbonyl-labelling reaction of lauric acid sodium salt after 10 min. Capillary: 30 cm, 50 μm I.D., 140 μm O.D.. Run: 10 mM borate, pH 9, 12 kV. Injection: 1000 V, 5 s. Laser: 488 nm Ar⁺, 12.1 mW. PMT: 1000 V. Interference filter: 518DF25. Concentration: 10⁻⁸ M.
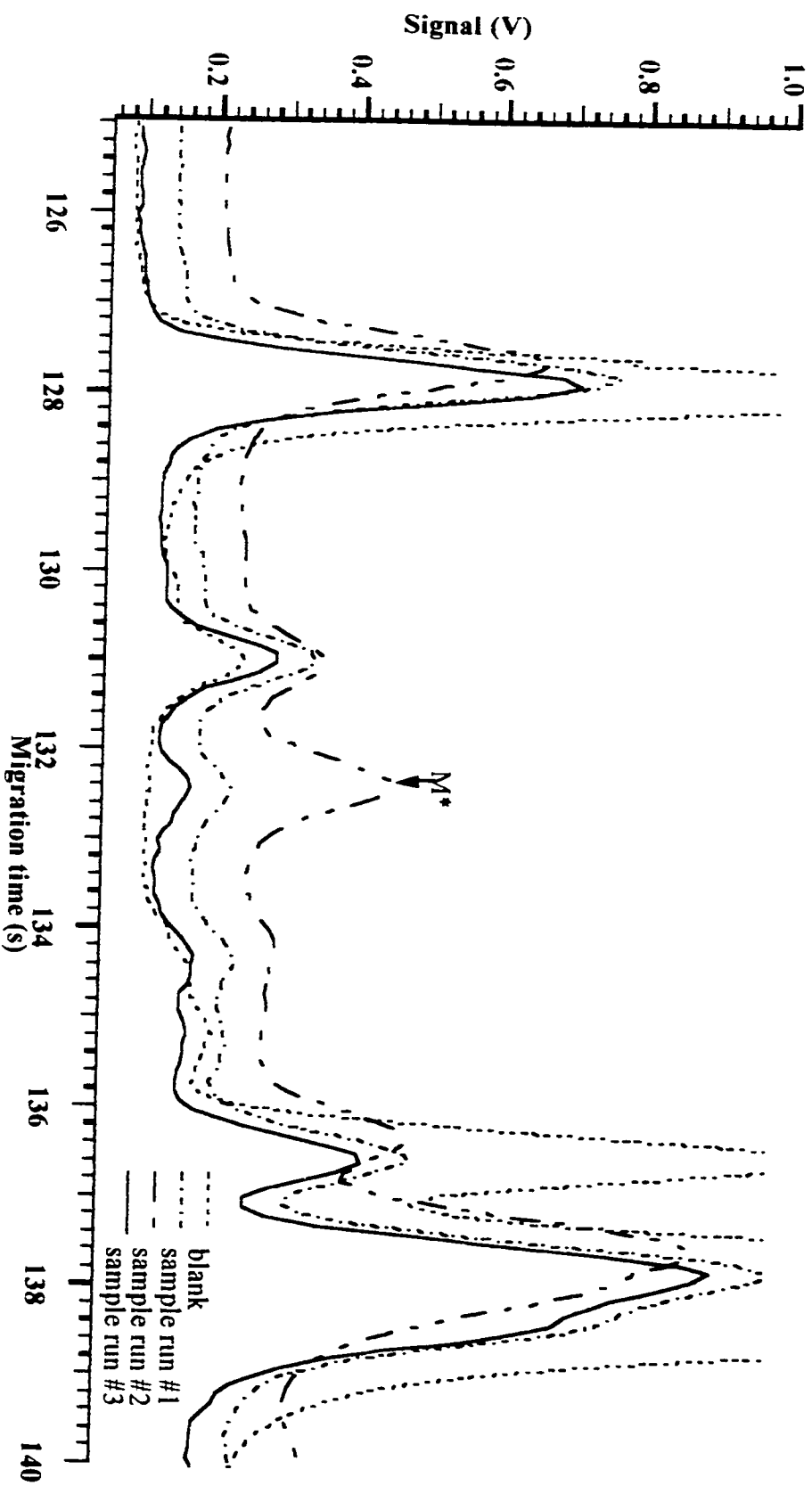
Figure 3.30: The reaction time optimization of the carbonyl-labelling reaction. The CZE-LIF electropherograms of the carbonyl-labelling reaction of lauric acid sodium salt after 20 min. Capillary: 30 cm, 50 µm I.D., 140 µm O.D.. Run: 10 mM borate, pH 9, 12 kV. Injection: 1000 V, 5 s. Laser: 488 nm Ar$^+$, 12.1 mW. PMT: 1000 V. Interference filter: 518DF25. Concentration: 10^{-8} M.
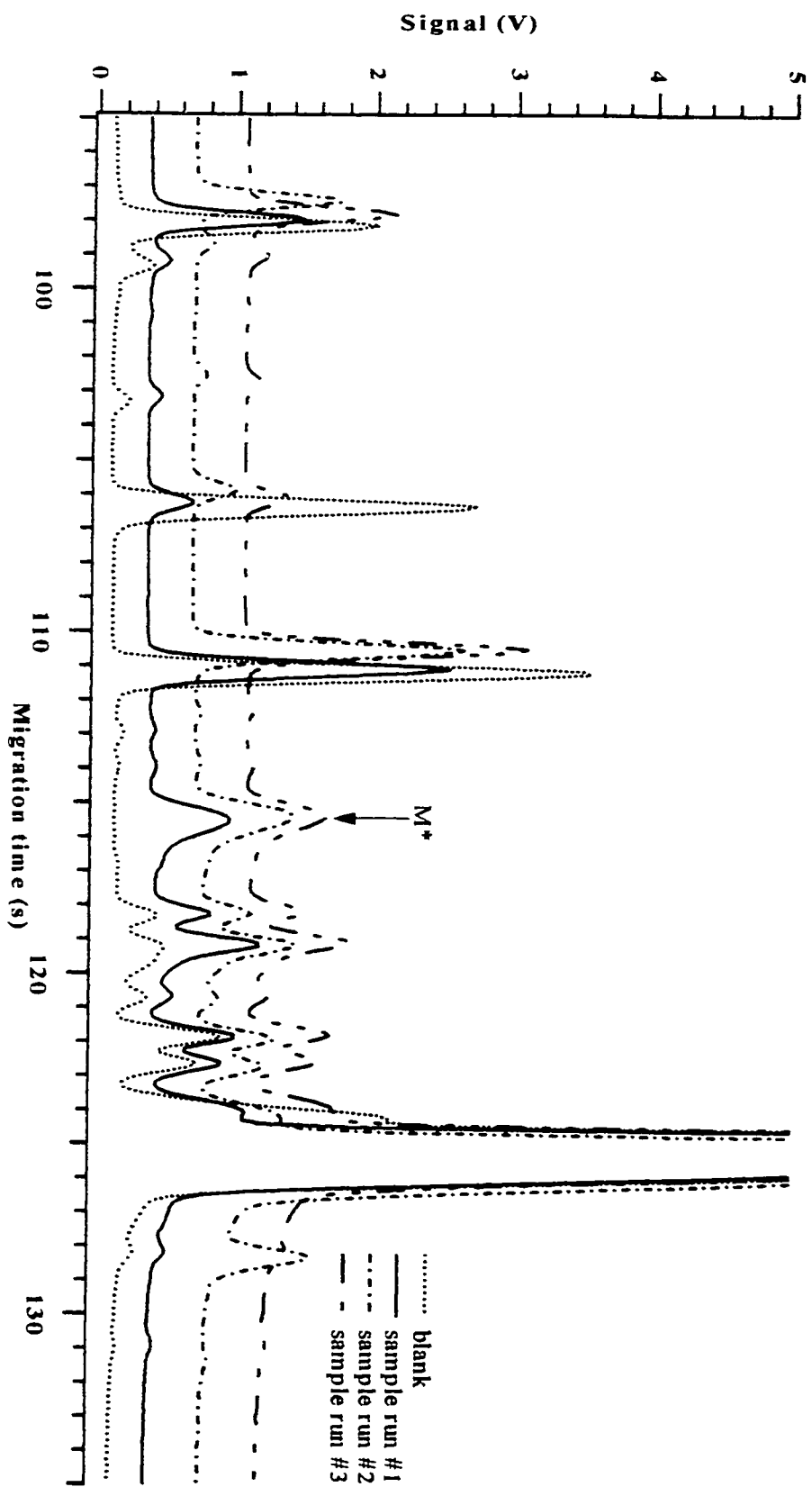
166

Figure 3.31: The reaction time optimization of the carbonyl-labelling reaction. The CZE-LIF electropherograms of the carbonyl-labelling reaction of lauric acid sodium salt after 30 min. Capillary: 30 cm, 50 µm I.D., 140 µm O.D.. Run: 10 mM borate, pH 9, 12 kV. Injection: 1000 V, 5 s. Laser: 488 nm Ar⁺, 12.1 mW. PMT: 1000 V. Interference filter: 518DF25. Concentration: 10^{-8} M.
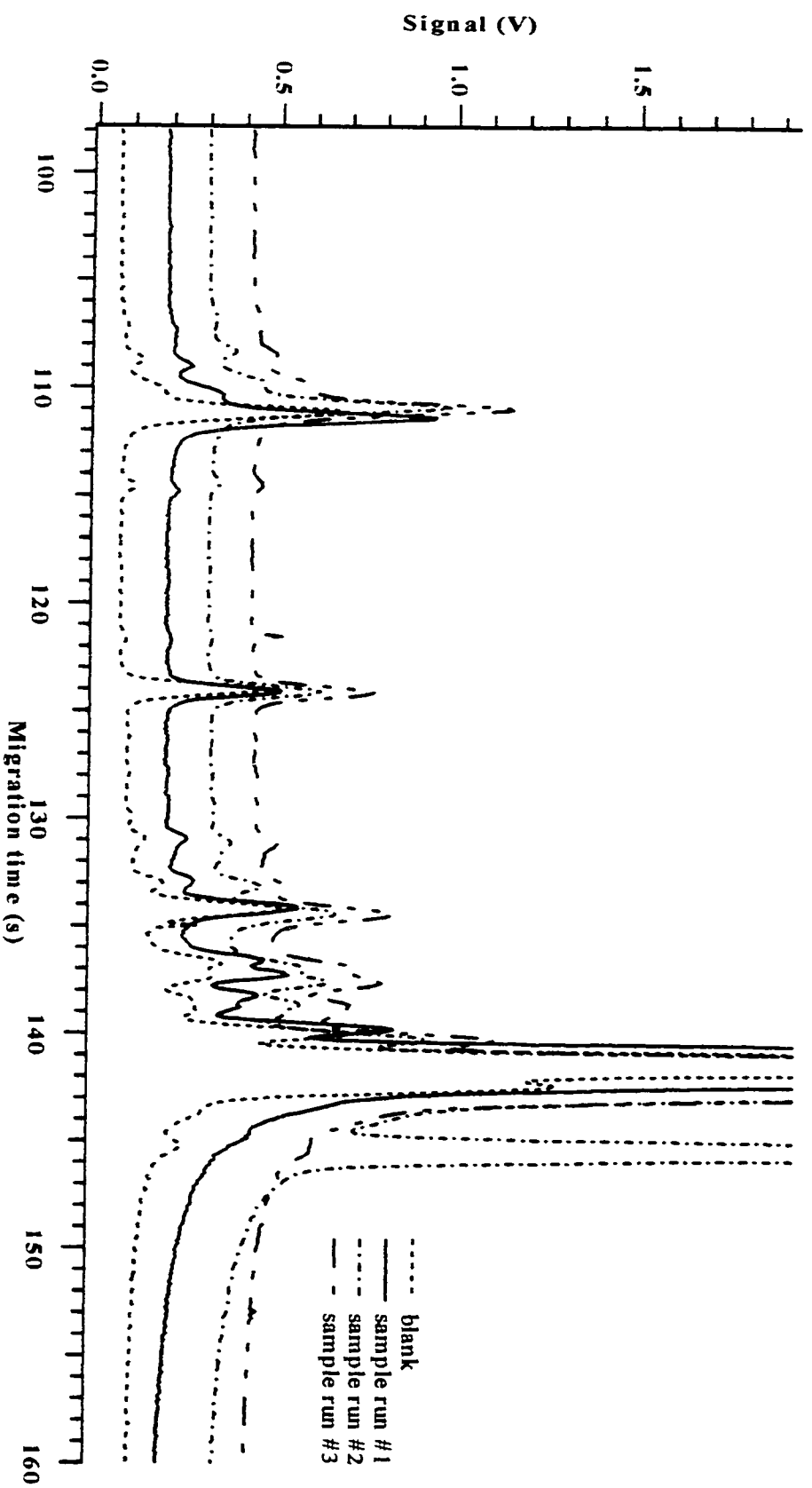
Figure 3.32: The reaction time optimization of the carbonyl-labelling reaction. The CZE-LIF electropherograms of the carbonyl-labelling reaction of lauric acid sodium salt after 40 min. Capillary: 30 cm, 50 μm I.D., 140 μm O.D.. Run: 10 mM borate, pH 9, 12 kV. Injection: 1000 V, 5 s. Laser: 488 nm Ar⁺, 12.1 mW. PMT: 1000 V. Interference filter: 518DF25. Concentration: 10^{-8} M.
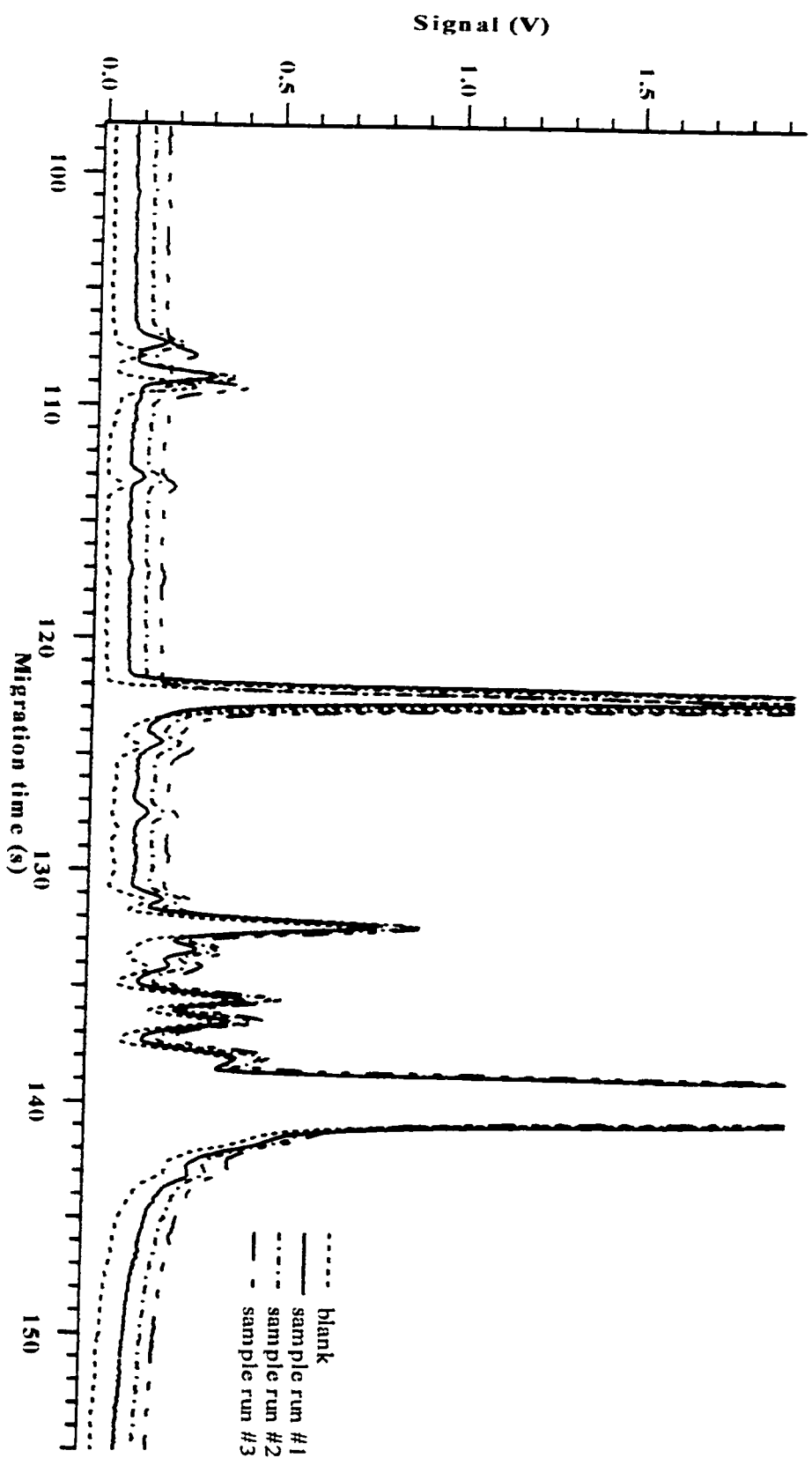
168

Figure 3.33: The reaction time optimization of the carbonyl-labelling reaction. The CZE-LIF electropherograms of the carbonyl-labelling reaction of lauric acid sodium salt after 50 min. Capillary: 30 cm, 50 μm I.D., 140 μm O.D.. Run: 10 mM borate, pH 9, 12 kV. Injection: 1000 V, 5 s. Laser: 488 nm Ar+, 12.1 mW. PMT: 1000 V. Interference filter: 518DF25. Concentration: 10^{-8} M.
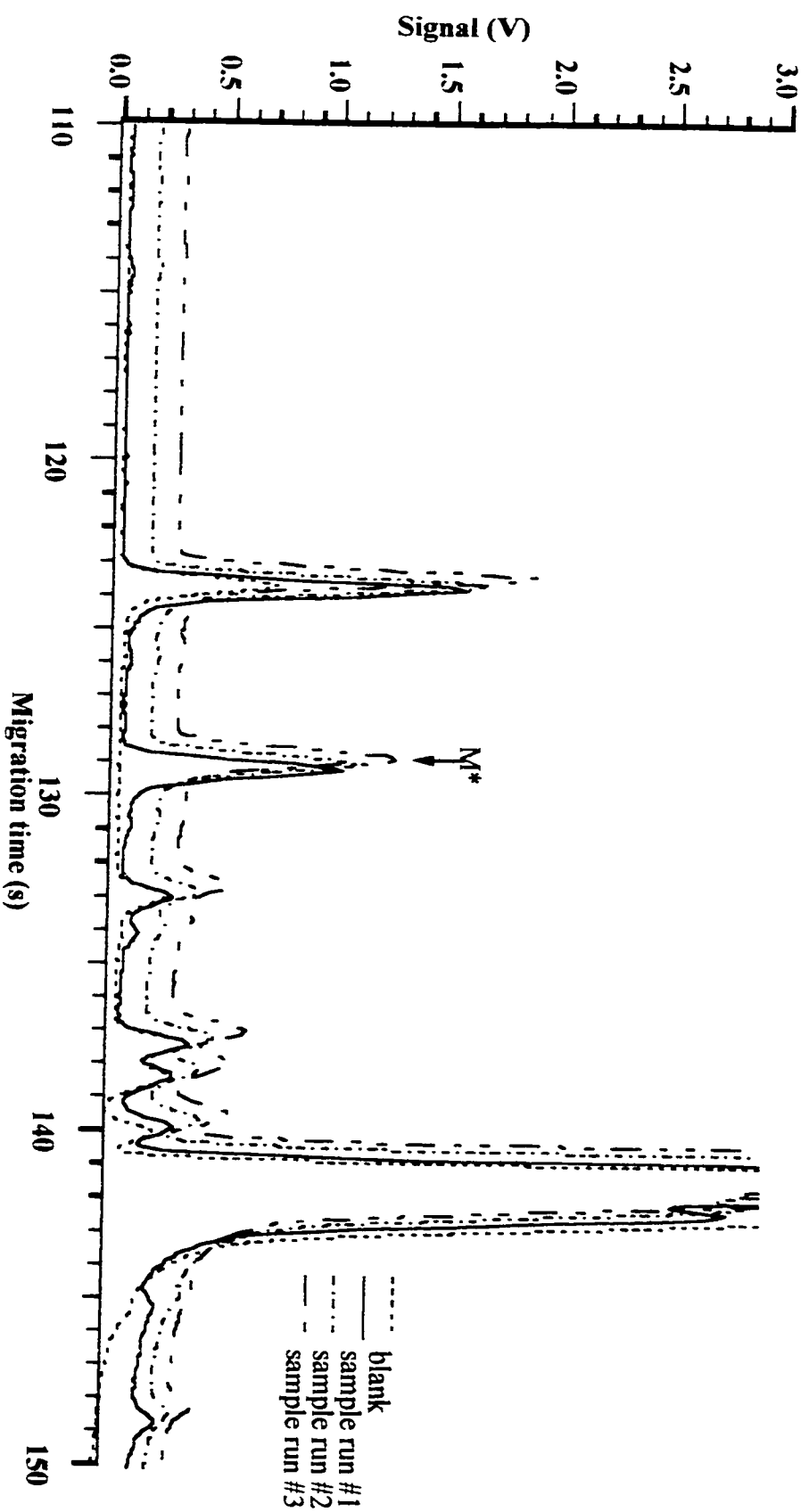
169
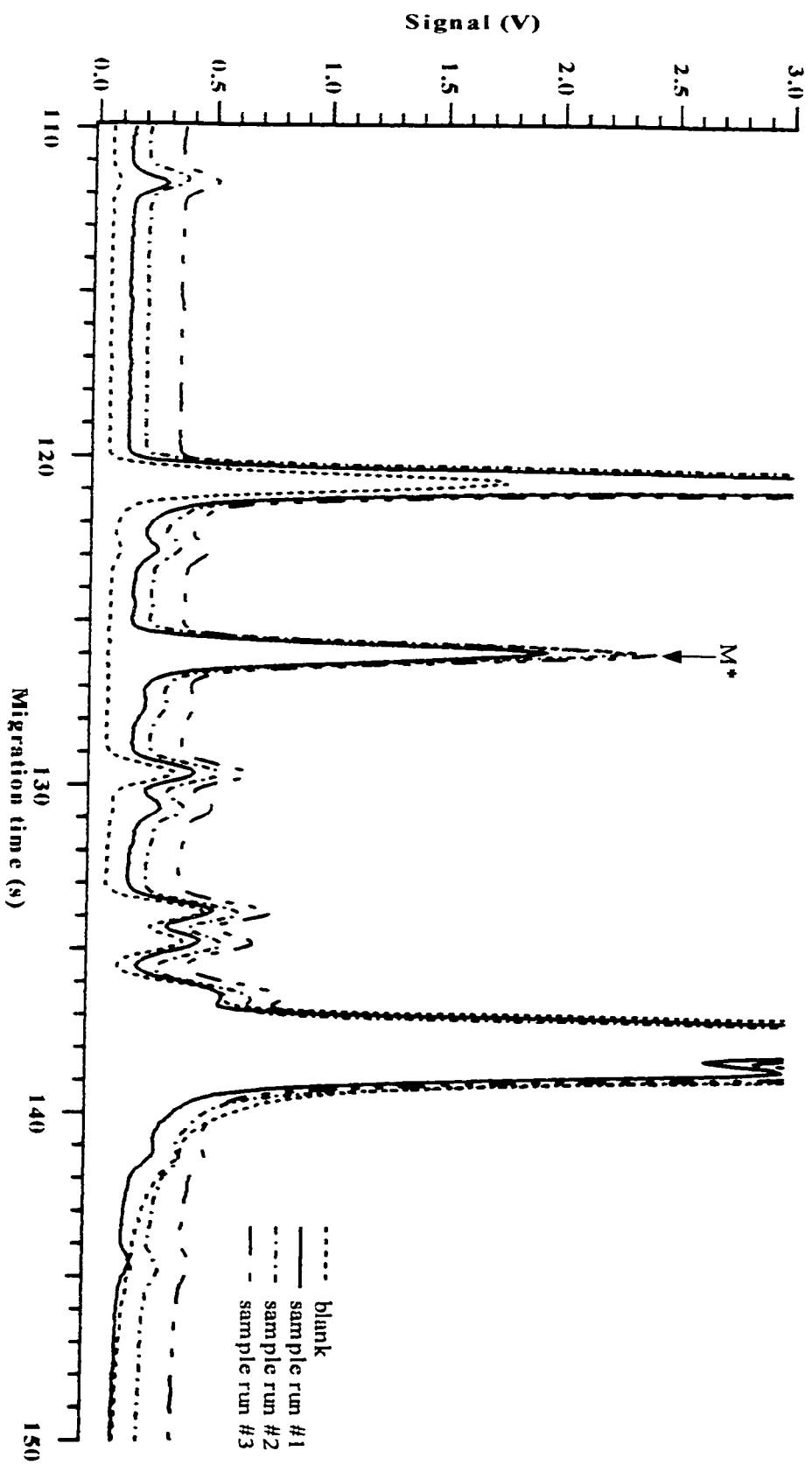
Figure 3.34: The reaction time optimization of the carbonyl-labelling reaction. The CZE-LIF electropherograms of the carbonyl-labelling reaction of lauric acid sodium salt after 60 min. Capillary: 30 cm, 50 µm I.D., 140 µm O.D.. Run: 10 mM borate, pH 9, 12 kV. Injection: 1000 V, 5 s. Laser: 488 nm Ar+, 12.1 mW. PMT: 1000 V. Interference filter: 518DF25. Concentration: 10⁻⁸ M.
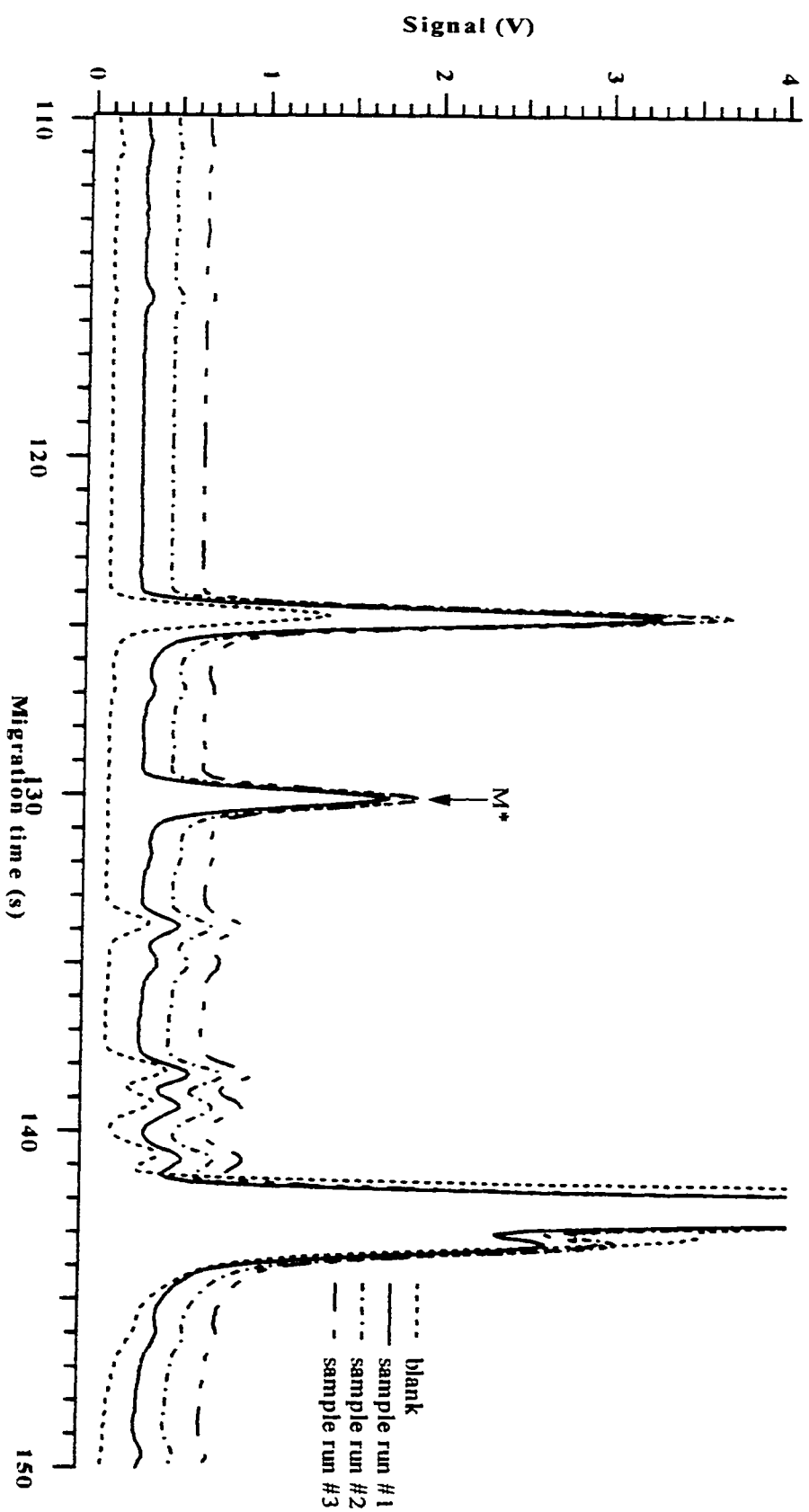
170
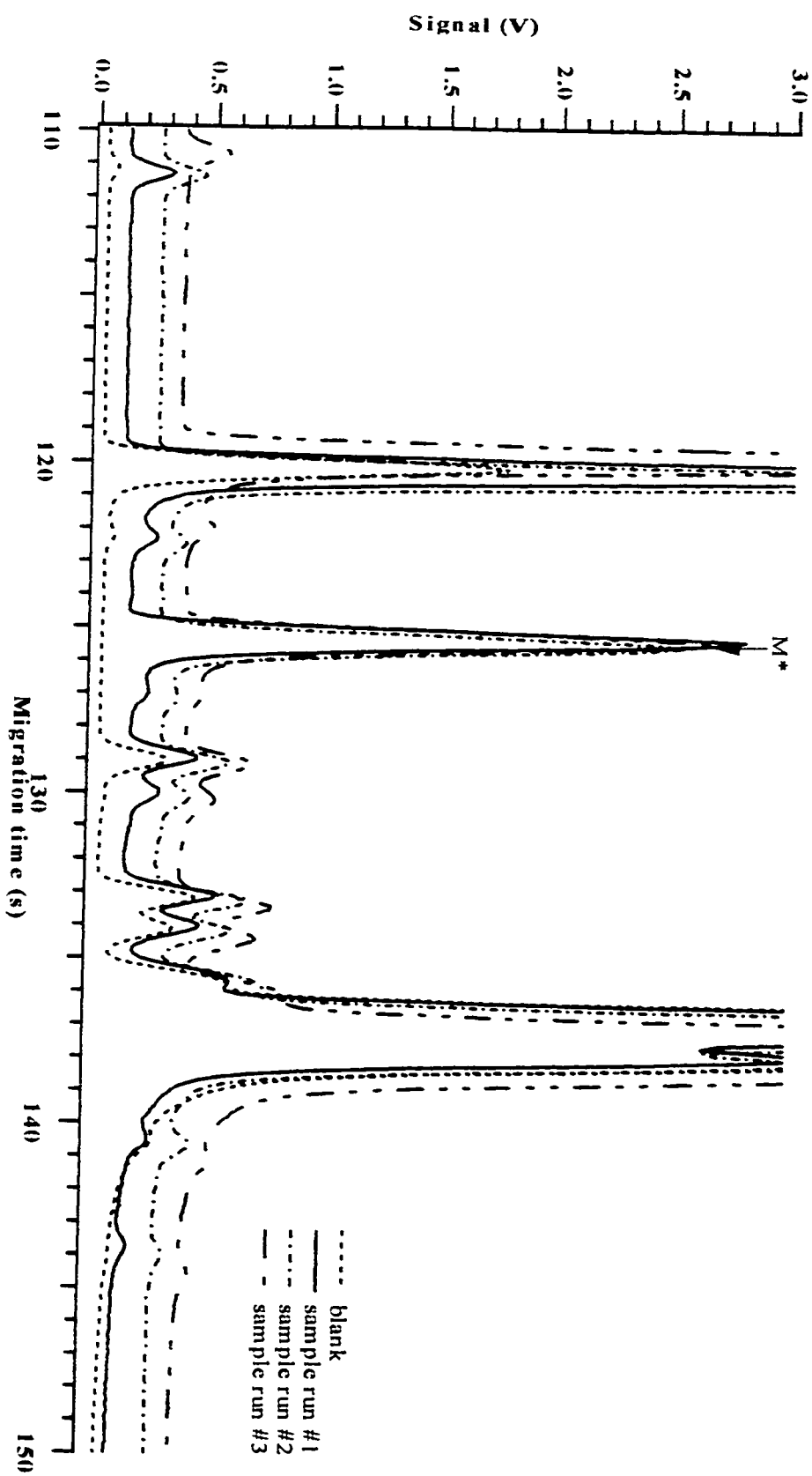
Figure 3.35: The reaction time optimization of the carbonyl-labelling reaction. The CZE-LIF electropherograms of the carbonyl-labelling reaction of lauric acid sodium salt after 90 min. Capillary: 30 cm, 50 μm I.D., 140 μm O.D.. Run: 10 mM borate, pH 9, 12 kV. Injection: 1000 V, 5 s. Laser: 488 nm Ar$^+$, 12.1 mW. PMT: 1000 V. Interference filter: 518DF25. Concentration: 10^{-8} M.
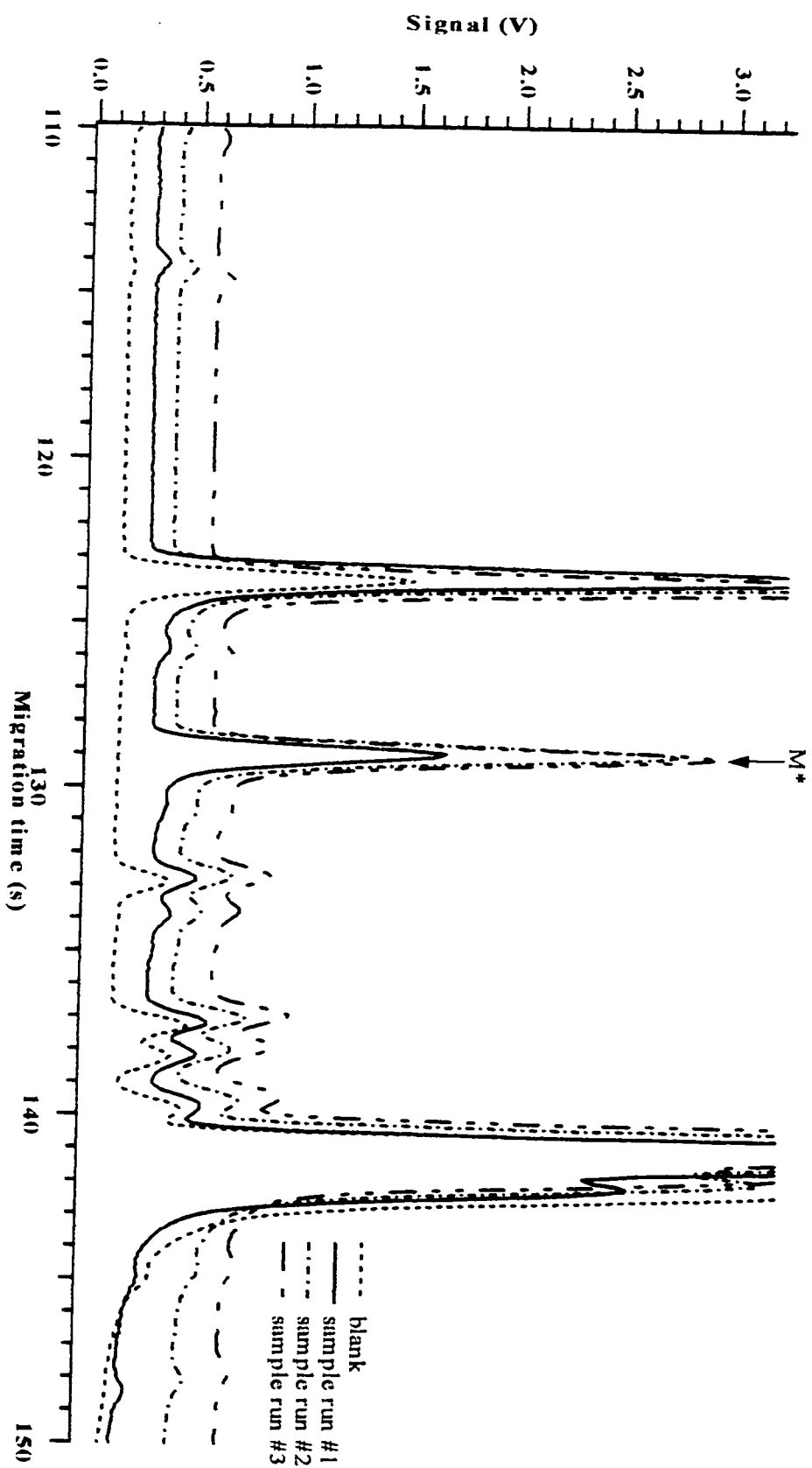
171
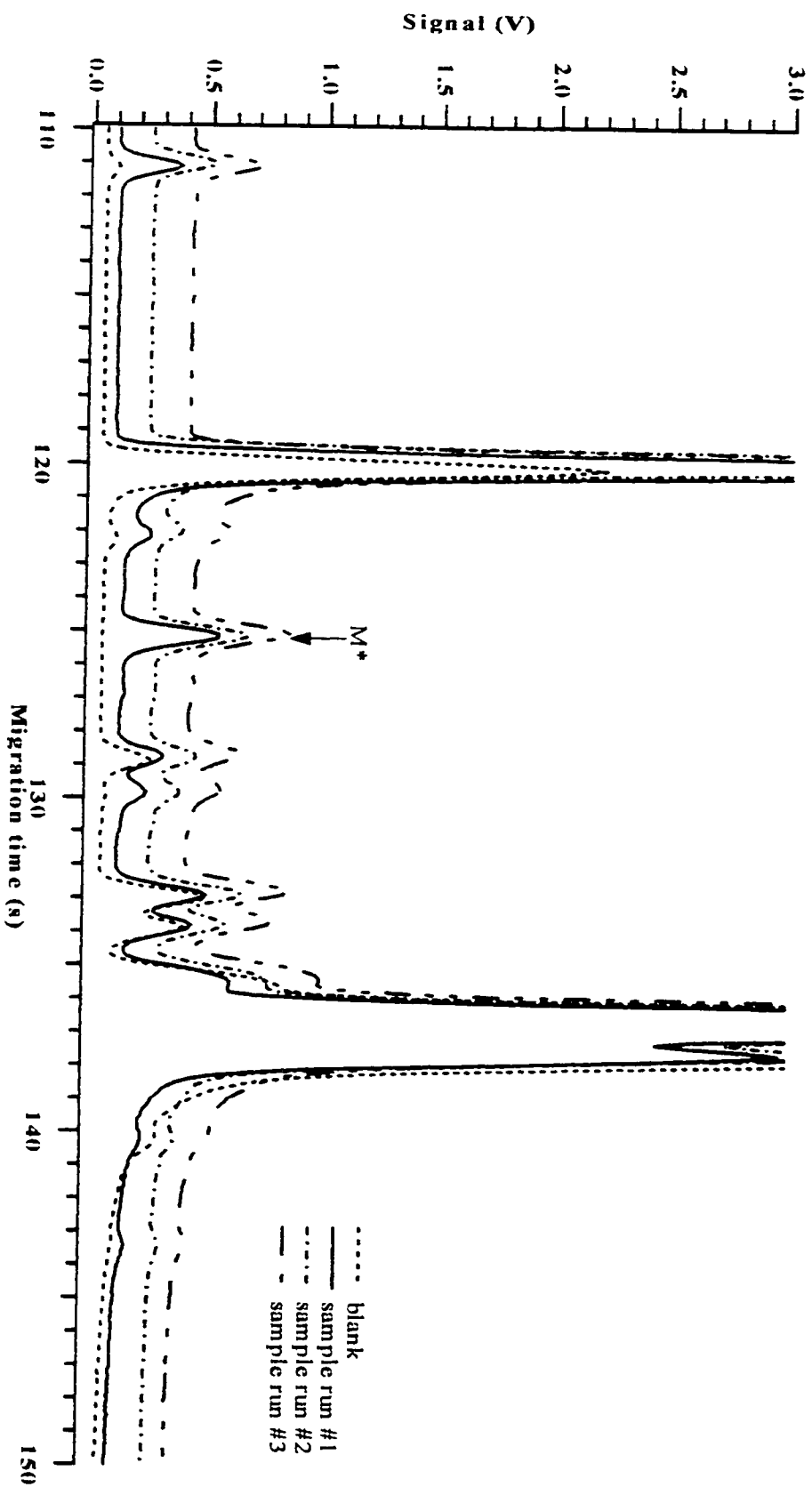
Figure 3.36: The reaction time optimization of the carbonyl-labelling reaction. The CZE-LIF electropherograms of the carbonyl-labelling reaction of lauric acid sodium salt after 120 min. Capillary: 30 cm, 50 µm I.D., 140 µm O.D..

Run: 10 mM borate, pH 9, 12 kV. Injection: 1000 V, 5 s. Laser: 488 nm Ar$^+$, 12.1 mW. PMT: 1000 V.

Interference filter: 518DF25. Concentration: 10^{-8} M.

Signal (V)

Migration time (s)

M*

······ blank
——— sample run #1
····· sample run #2
– – – sample run #3

Figure 3.37: The reaction time optimization of the carbonyl-labelling reaction. The CZE-LIF electropherograms of the carbonyl-labelling reaction of lauric acid sodium salt after 150 min. Capillary: 30 cm, 50 μm I.D., 140 μm O.D.. Run: 10 mM borate, pH 9, 12 kV. Injection: 1000 V, 5 s. Laser: 488 nm Ar⁺, 12.1 mW. PMT: 1000 V. Interference filter: 518DF25. Concentration: 10^{-8} M.
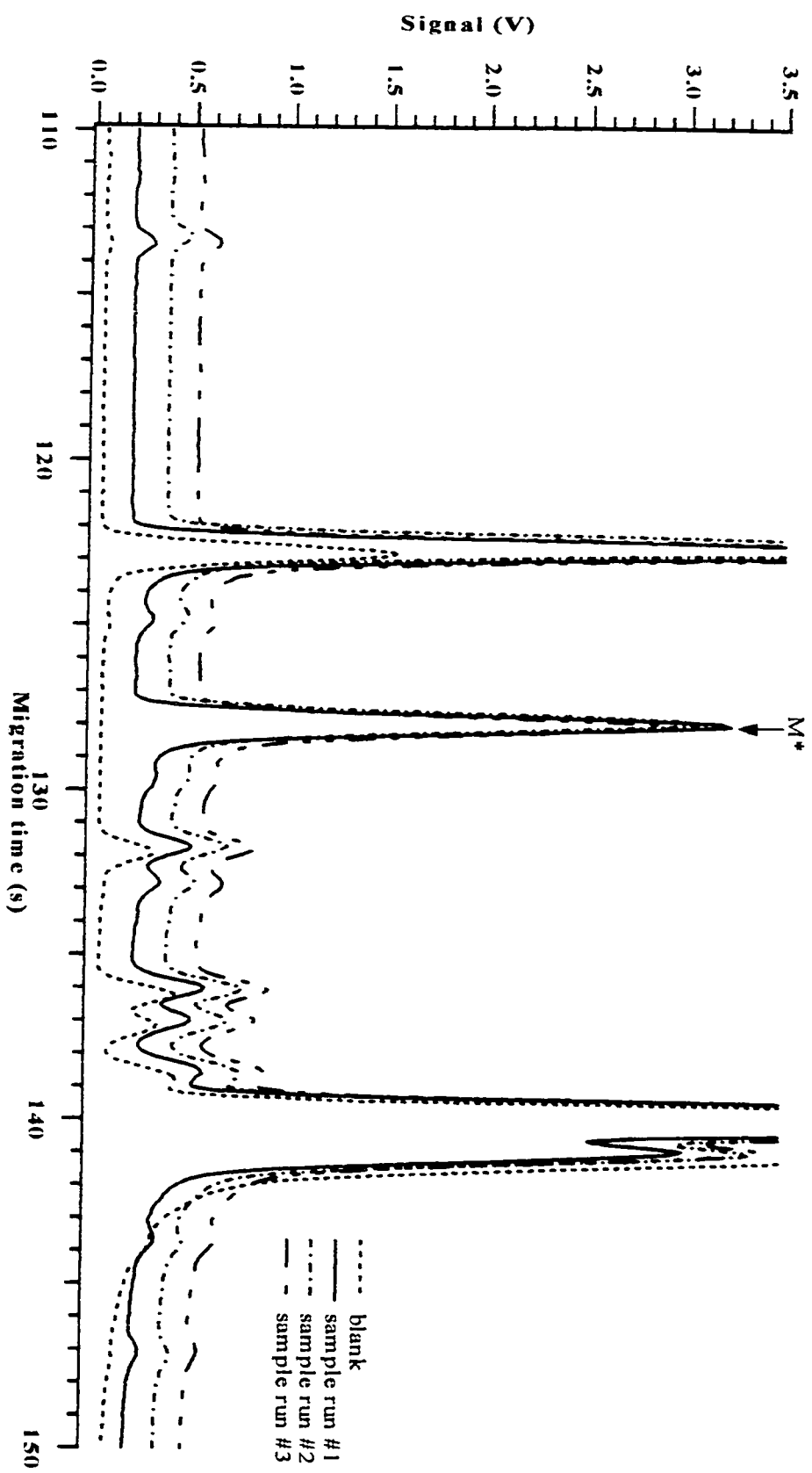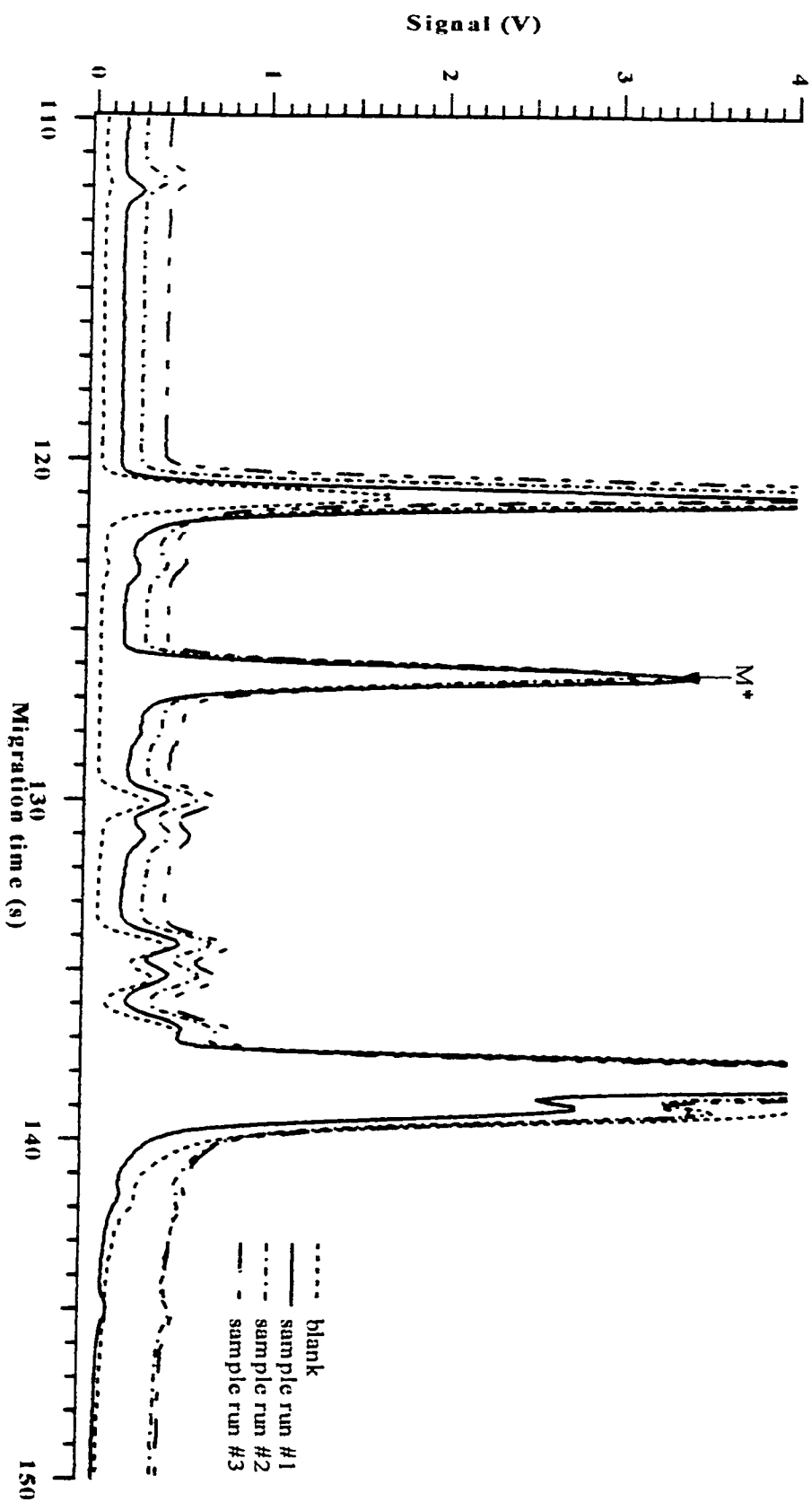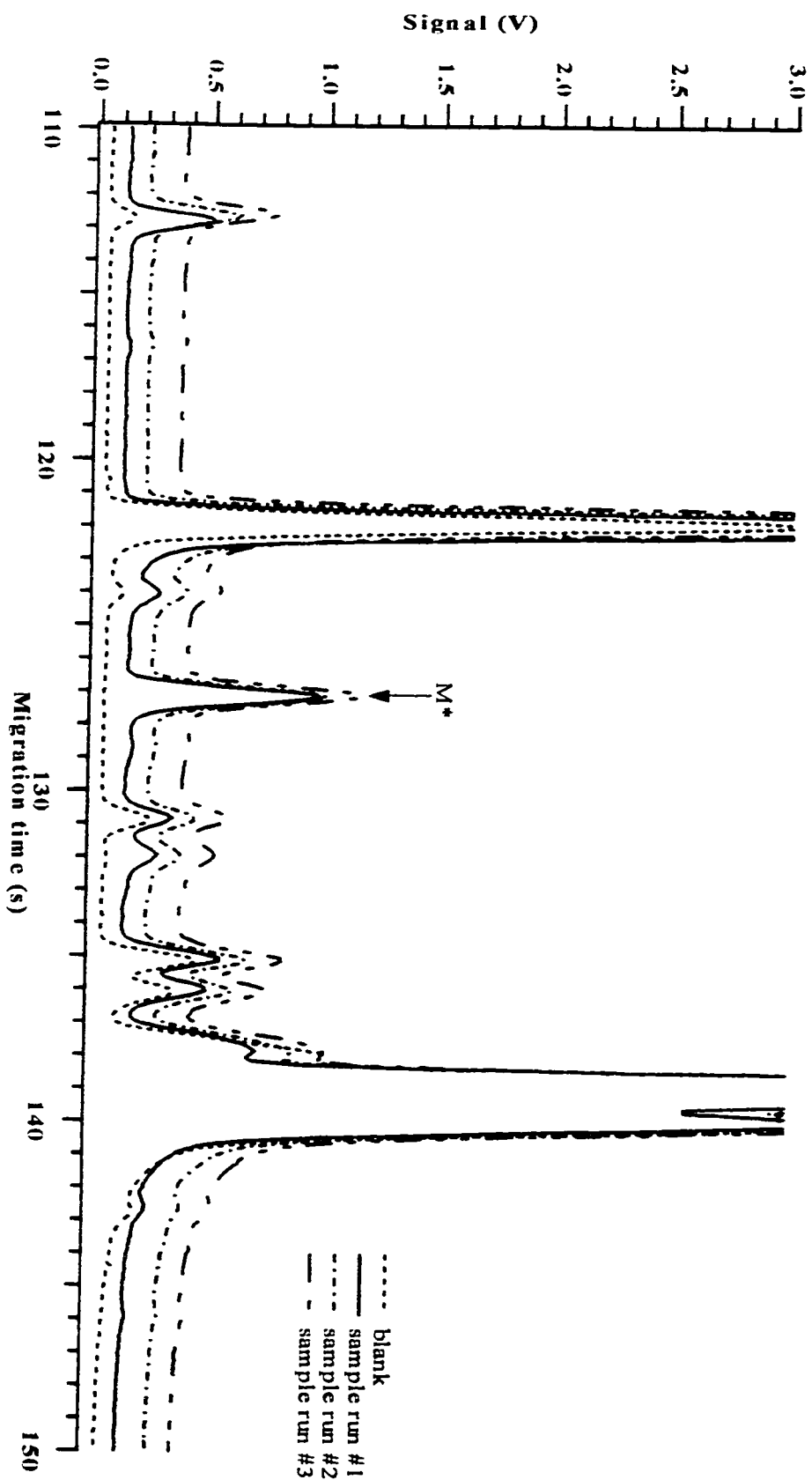
Figure 3.38: The reaction time optimization of the carbonyl-labelling reaction. The CZE-LIF electropherograms of the carbonyl-labelling reaction of lauric acid sodium salt after 180 min. Capillary: 30 cm, 50 μm I.D., 140 μm O.D.. Run: 10 mM borate, pH 9, 12 kV. Injection: 1000 V, 5 s. Laser: 488 nm Ar⁺, 12.1 mW. PMT: 1000 V. Interference filter: 518DF25. Concentration: 10⁻⁸ M.

174

Figure 3.39: The reaction time optimization curve of the carbonyl-labelling reaction of lauric acid sodium salt. Capillary: 30 cm, 50 μm I.D., 140 μm O.D.. Run: 10 mM borate, pH 9, 12 kV. Injection: 1000 V, 5 s. Laser: 488 nm Ar$^+$, 12.1 mW. PMT: 1000 V. Interference filter: 518DF25. Concentration: 10^{-8} M. (n = 3)
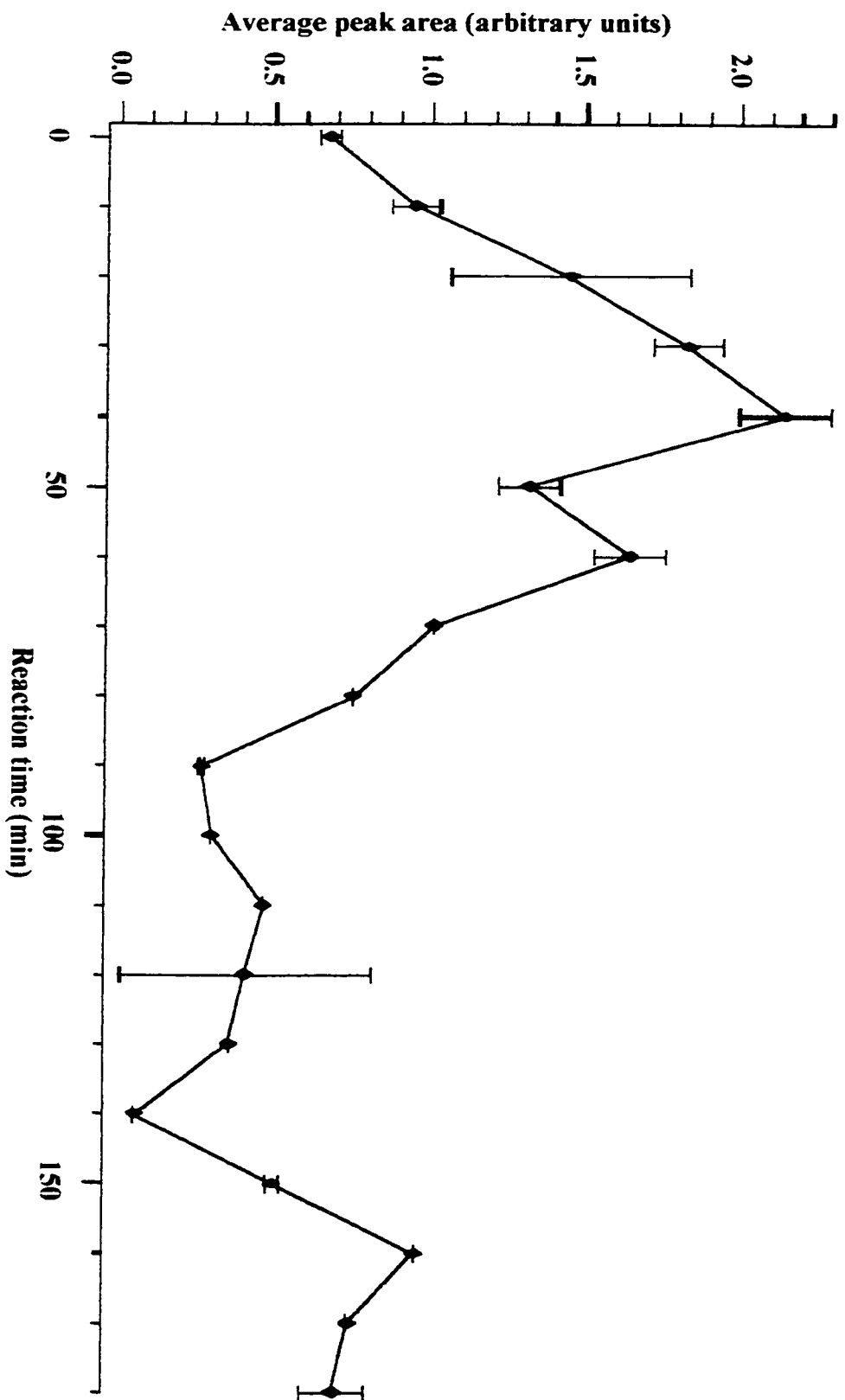
optimization curve represent ±1 standard deviation of the average peak area for labelled lauric acid at each reaction time. The carbonyl-labelling reaction was optimized when let to react for 40 minutes. It is interesting to note that a peak for labelled lauric acid (M*) was found immediately after mixing the acid and the 5-BMF together. This result suggests that the carbonyl-labelling reaction has a high reaction rate since the variations in the peak area at each time could be due to variations in injections since an internal standard was not used. This reaction time optimization procedure was performed again to ensure reproducibility as described in Section 3.2.12. The resulting reaction time optimization curve can be found in Figure 3.40. This time the carbonyl-labelling reaction was optimized when it was allowed to react for 90 minutes. Once again a peak for labelled lauric acid (M*) was found immediately after mixing the acid and the 5-BMF together. As mentioned earlier this could mean that the carbonyl-labelling reaction has a high reaction rate and the variations of the labelled lauric acid peak area at different reaction times is due to injection variations that have not been corrected since an internal standard was not used. Since the results of the reaction time optimization were non-conclusive any further carbonyl-labelling reactions should be reacted for the same time period (2 hours) as the previous reactions. Further investigation into the reaction time optimization with the use of an internal standard is needed. Next, a calibration curve was constructed as described in Section 3.2.12 using the 120-min sample reaction mixture aliquot. This calibration curve can be found in Figure 3.41. The error bars on the calibration curve represent ±1 standard deviation of the average peak area for each standard labelled lauric acid concentration. The correlation coefficient was r = +0.9964 and the LOD was 34 attograms or 34 pM when 2 nL of sample was injected (n = 3).

Figure 3.40: The repeated reaction time optimization curve of the carbonyl-labelling reaction of lauric acid sodium salt.

Capillary: 30 cm, 50 μm I.D., 140 μm O.D.. Run: 10 mM borate, pH 9, 12 kV. Injection: 1000 V, 5 s.

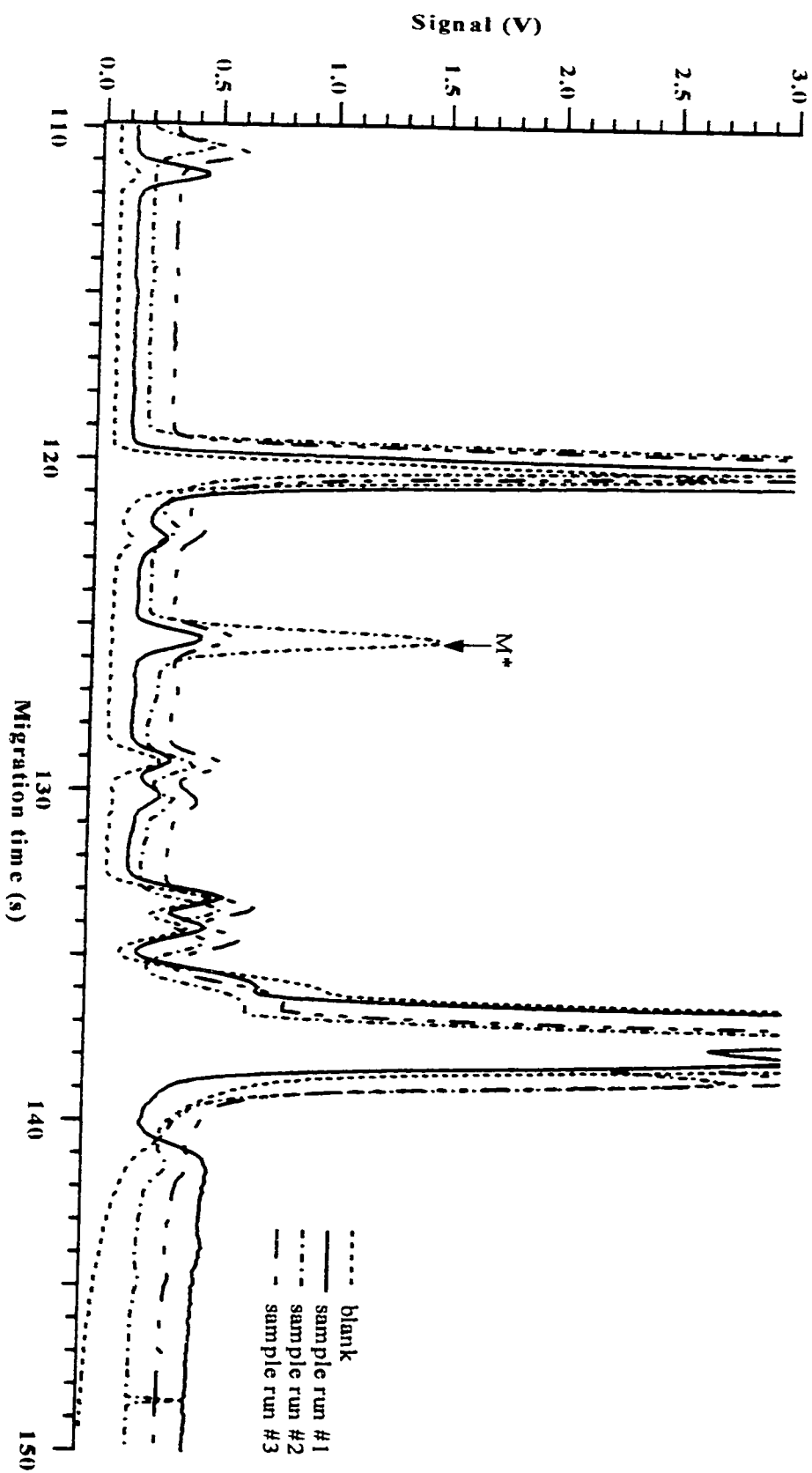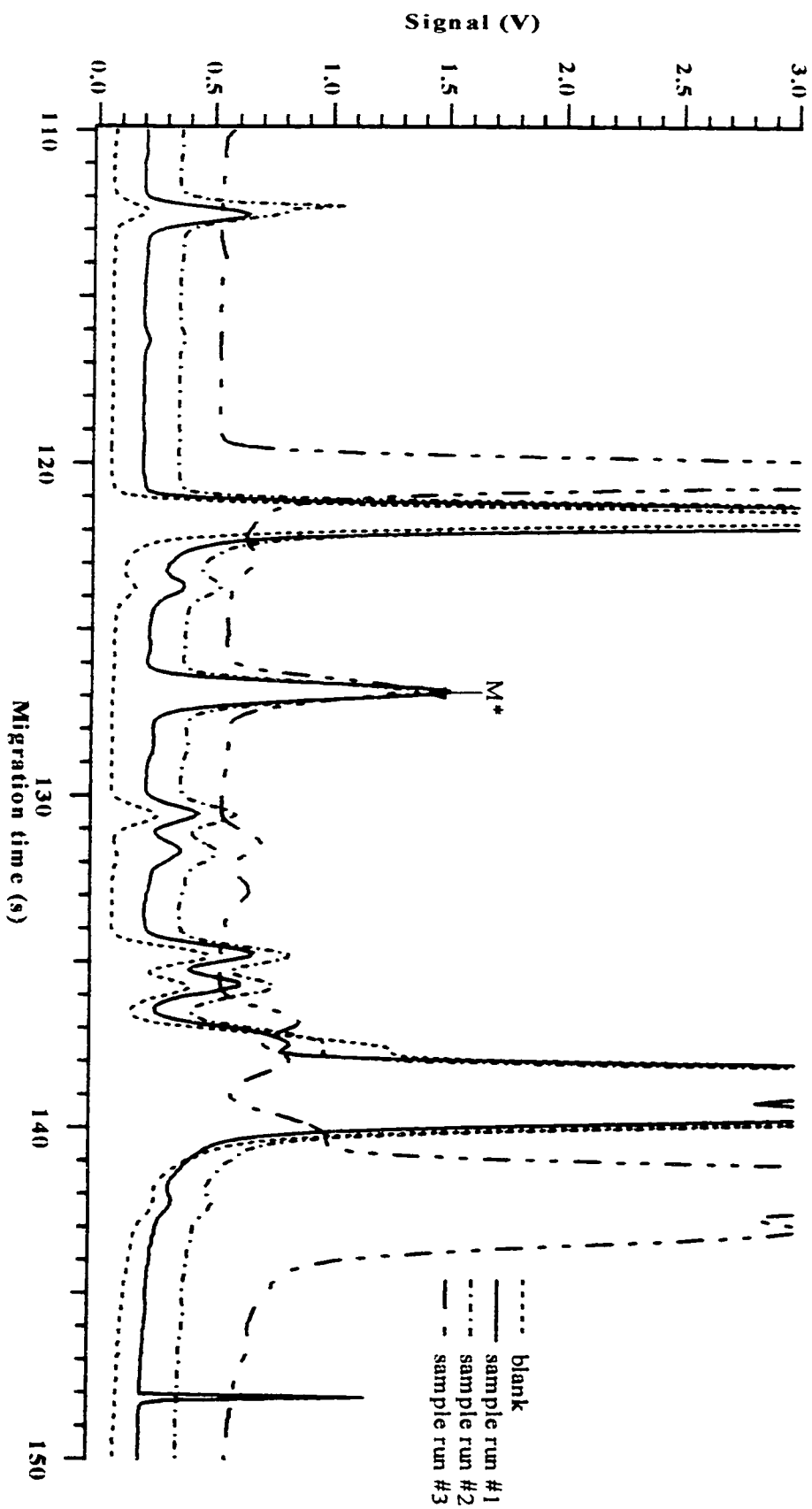Laser: 488 nm Ar$^+$, 12.1 mW. PMT: 1000 V. Interference filter: 518DF25. Concentration: 5*10^{-8} M. (n = 1)
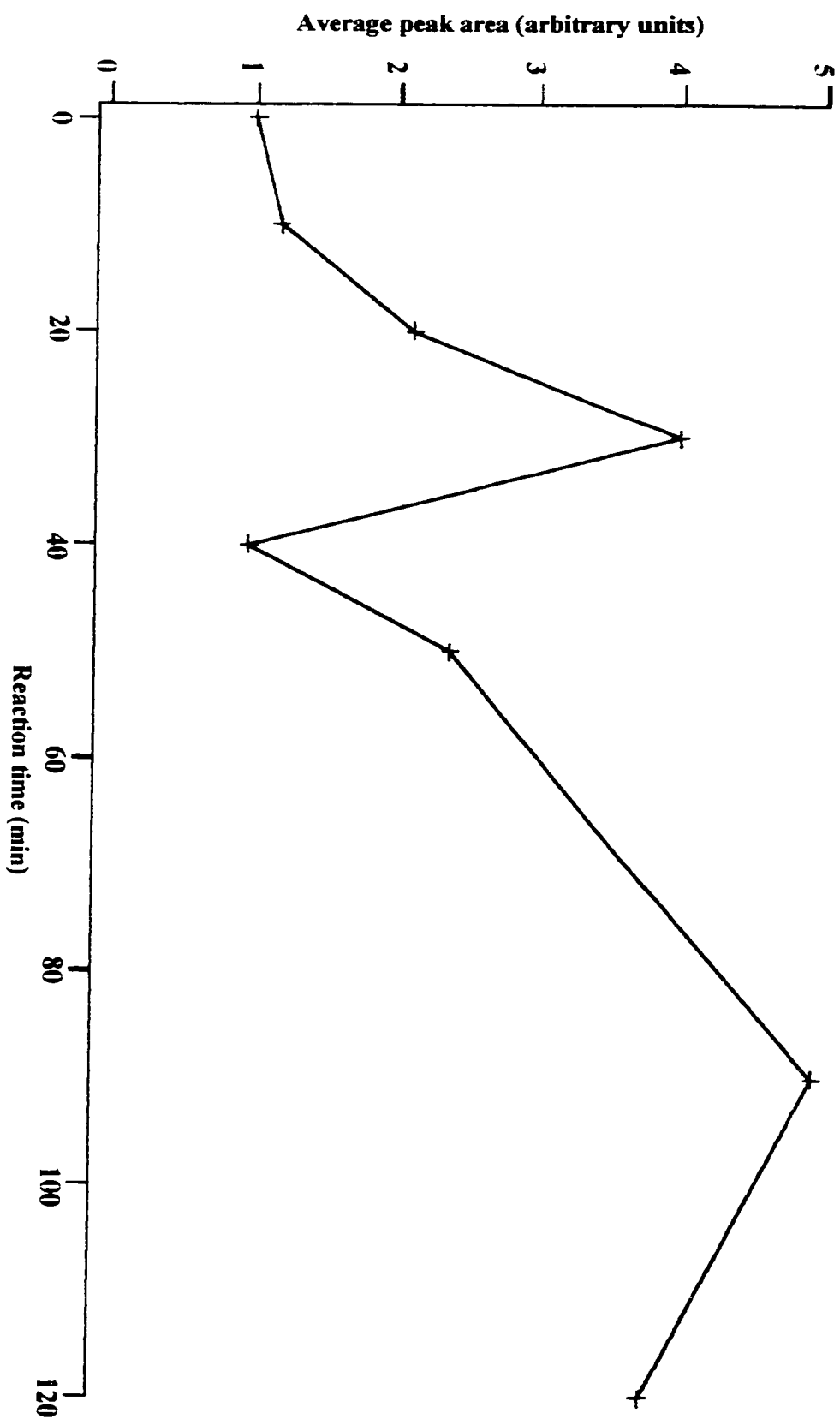
Figure 3.41: The calibration curve for labelled lauric acid using the 120-min sample reaction mixture from the second reaction time optimization experiment. Capillary: 30 cm, 50 μm I.D., 140 μm O.D.. Run: 10 mM borate, pH 9, 12 kV. Injection: 1000 V, 5 s. Laser: 488 nm Ar$^+$, 12.1 mW. PMT: 1000 V. Interference filter: 518DF25. ($n = 3$)

178
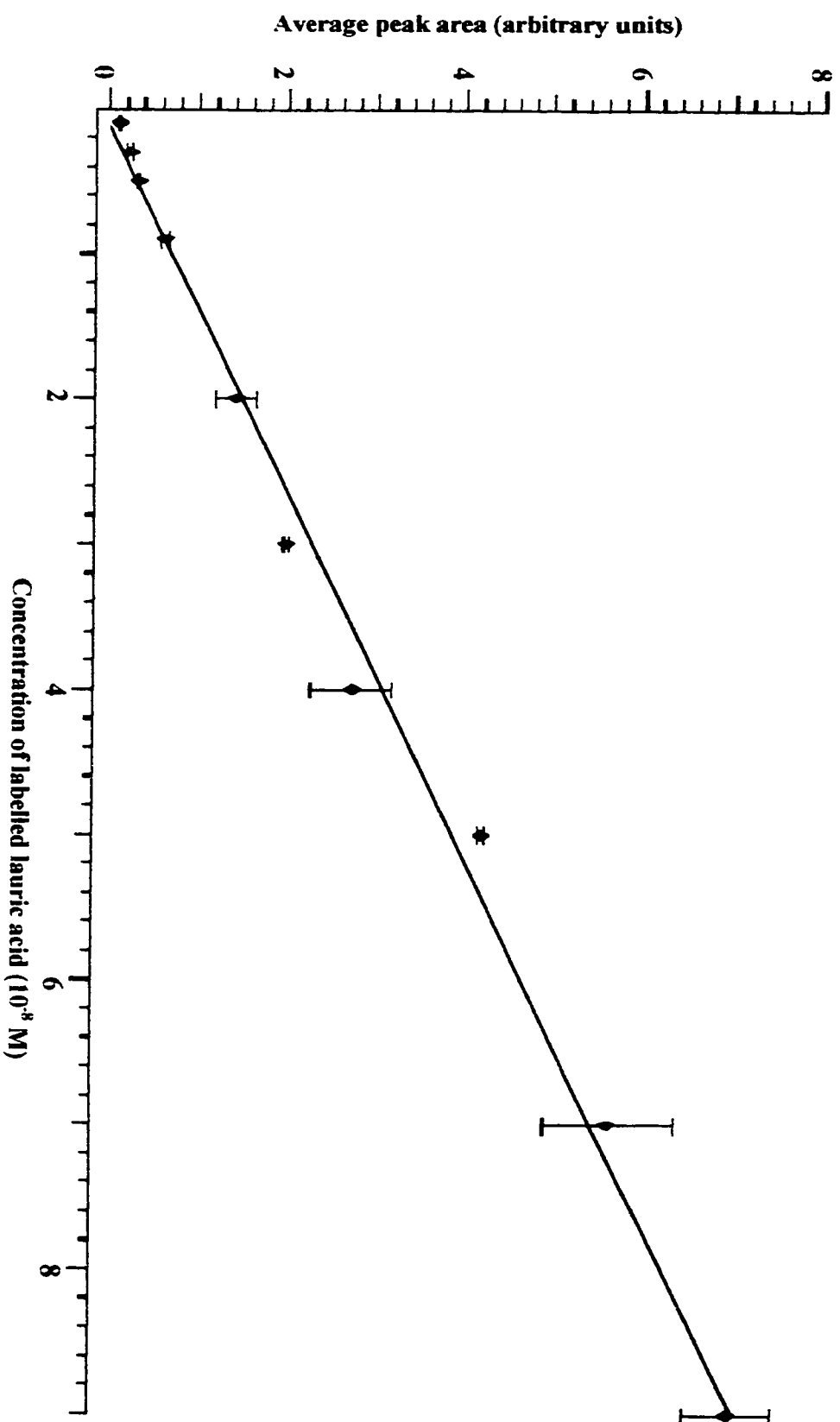
In the next chapter, a homologous series of linear saturated free fatty acids will be labelled using this optimized carbonyl-labelling reaction.

3.4 Conclusions

The model carboxylic acid PEN-G was fluorescently labelled with the derivatization reagent 5-BMF using a carbonyl-labelling reaction performed in the presence of the base TED. This carbonyl-labelling reaction was checked for the presence of product using CZE-LIF and ESI-MS. The CZE-LIF electropherogram revealed one product peak at a migration time of ~74 s indicating the reaction's success. A calibration curve was constructed and the resulting curve had a correlation coefficient of $r = +0.9953$ and a limit of detection of 38 pM (n = 3). The positive-ion mode ESI-MS spectrum also showed that the reaction was successful. This carbonyl-labelling reaction of PEN-G was then performed in the absence of the base TED and the resulting reaction mixtures were analysed using CZE-LIF and ESI-MS. The CZE-LIF electropherogram showed a product peak at a migration time of ~117 s indicating the reaction's success. A calibration curve was constructed and the resulting curve had a correlation coefficient of $r = +0.9854$ and a limit of detection of 3 pM (n = 3). The positive-ion mode ESI-MS spectra also proved that the carbonyl-labelling reaction of PEN-G was successful. The positive-ion mode ESI-MS spectra showed that more labelled PEN-G was produced when the base TED was absent from the carbonyl-labelling reaction. Next, the carbonyl-labelling reaction performed in the absence of TED was used to fluorescently label the linear saturated free fatty acid, lauric acid.

179

The carbonyl-labelling reaction of lauric acid sodium salt was performed and then analysed using CZE-LIF and ESI-MS. The CZE-LIF electropherograms showed a product peak at an average migration time of ~121 s (n = 3) indicating the reaction's success. The positive-ion mode ESI-MS spectrum confirmed that the carbonyl-labelling reaction of lauric acid sodium salt was successful. Next, the carbonyl-labelling reaction of lauric acid sodium salt was repeated in the presence of the base TED and/or the catalyst 18-Crown-6 to investigate the effect these reagents had on the carbonyl-labelling reaction efficiency. Each reaction mixture was checked for the presence of product using CZE-LIF. The resulting CZE-LIF electropherograms revealed that the presence of these reagents decreased the efficiency of carbonyl-labelling reaction. The effect of the presence of methanol in the carbonyl-labelling reaction was also investigated and was found to have little or no effect on the efficiency of the reaction. The ratio of dye to analyte in the carbonyl-labelling reaction was optimized and was found to be most efficient when two molar equivalents of 5-BMF were reacted. The carbonyl-labelling reaction was also optimized for reaction time but unfortunately the results were not reproducible or therefore conclusive. The reactant limitation of this carbonyl-labelling reaction was found to be 10^{-8} moles of lauric acid sodium salt. A calibration curve for the labelled lauric acid (120 min aliquot) was constructed and the resulting curve had a correlation coefficient of r = +0.9964 and a limit of detection of 34 pM (n = 3).

This carbonyl-labelling reaction of lauric acid sodium salt was also compared to the established Mukherjee labelling reaction and it was shown that the carbonyl-labelling reaction that was developed in this work is far more efficient. In the next chapter, the

optimized carbonyl-labelling reaction will be used to label a homologous series of linear

saturated free fatty acids.

3.5 References

1. W. Dunges, *Analytical Chemistry*, 49 (1977) 442.

2. T. Toyo'oka, *Journal of Chromatography B*, 671 (1995) 91.

3. D. Pilosof, H. Y. Kim, D. F. Dyckes, M. L. Vestal, *Analytical Chemistry*, 56 (1984) 1236.

4. A. MacDonald, T. A. Nieman, *Analytical Chemistry*, 57 (1985) 936.

5. P. S. Mukherjee, K. H. DeSilva, H. T. Karnes, *Pharmaceutical Research*, 12 (1995) 930.

6. C. M. B. Van Den Beld, H. Lingeman, G. J. Van Ringer, V. R. Tjaden, J. Van Der Greef, *Analytica Chimica Acta*, 205 (1988) 15.

7. B. W. Sandmann, M. L. Grayeski, *Journal of Chromatography B*, 653 (1994) 123.

8. G. J. Engelmann, E. L. Esmans, F. C. Alderweireldt, *Journal of Chromatography*, 432 (1988) 29.

9. T. Haniš, M. Smrz, P. Klír, K. Macek, J. Klíma, J. Baše, Z. Deyl, *Journal of Chromatography*, 452 (1988) 443.

10. W. W. Christie, G. H. McG. Breckenridge, *Journal of Chromatography*, 469 (1989) 261.

11. C. Osterroht, *Fresenius' Journal of Analytical Chemistry*, 345 (1993) 773.

12. F. A. Fitzpatrick, *Analytical Chemistry*, 48 (1976) 499.

13. F. E. Callahan, H. A. Norman, T. Srinath, J. B. St. John, R. Dhar, A. K. Mattoo, *Analytical Biochemistry*, 183 (1989) 220.

14. P. H. Zoutendam, P. B. Bowman, J. L. Rumph, T. M. Ryan, *Journal of Chromatography*, 283 (1984) 281.

15. L. D. Kissinger, R. H. Robins, *Journal of Chromatography*, 321 (1985) 353.

16. H. Miwa, M. Yamamoto, *Journal of Chromatography*, 351 (1986) 275.

17. H. Miwa, M. Yamamoto, *Journal of Chromatography*, 421 (1987) 33.

18. J. Doehl, T. Greibrokk, *Journal of Chromatography*, 349 (1985) 431.

19. J. Doehl, T. Greibrokk, *Journal of Chromatography*, 529 (1990) 21.

20. G. Gutnikov, J. R. Streng, *Journal of Chromatography*, 587 (1991) 292.

21. Y. Yasaka, M. Tanaka, T. Matsumoto, K. Funazo, T. Shono, *Analytical Sciences*, 5 (1989) 611.

22. T. Takagi, Y. Itabashi, *Journal of Chromatographic Science*, 27 (1989) 574.

23. C. P. Clark, B. G. Snider, P. B. Bowman, *Journal of Chromatography*, 408 (1987) 275.

24. S. Yoshida, S. Hirose, M. Iwamoto, *Journal of Chromatography*, 383 (1986) 61.

25. J. B. F. Lloyd, *Journal of Chromatography*, 178 (1979) 249.

26. J. H. Wolf, J. Korf, *Journal of Chromatography*, 502 (1990) 423.

27. J. S. Yoo, V. L. McGuffin, *Journal of Chromatography*, 627 (1992) 87.

28. J. H. Wolf, J. Korf, *Journal of Chromatography*, 436 (1988) 437.

29. J. H. Wolf, L. Veenma, V. Duin, J. Korf, *Journal of Chromatography*, 487 (1989) 496.

30. F. A. L. Horst, G. G. Eikelboom, J. J. M. Holthuis, *Journal of Chromatography*, 456 (1988) 191.

31. W. Voelter, R. Huber, K. Zech, *Journal of Chromatography*, 217 (1981) 491.

32. H. Cisse, R. Farinotti, S. Kirkiacharian, A. Dauphin, *Journal of Chromatography*, 225 (1981) 509.

33. J. H. Wolf, L. Veenma, V. Duin, J. Korf, *Journal of Pharmacy and Pharmacology*, 43 (1991) 101.

34. S. Lam, E. Grushka, *Journal of Chromatography*, 158 (1978) 207.

35. V. L. McGuffin, R. N. Zare, *Applied Spectroscopy*, 39 (1985) 847.

36. K. Hayashi, J. Kawase, K. Yoshimura, K. Ara, K. Tsuji, *Analytical Biochemistry*, 136 (1984) 314.

37. K. A. Hordijk, T. E. Cappenberg, *Applied and Environmental Microbiology*, 46 (1983) 361.

38. W. Elbert, S. Breitenbach, A. Neftel, J. Hahn, *Journal of Chromatography*, 328 (1985) 111.

39. R. Wintersteiger, H. Juan, *Prostaglandins, Leukotrienes and Medicine*, 14 (1984) 25.

40. R. B. Gueddour, M. Matt, A. Nicolas, *Analytical Letters*, 26 (1993) 429.

41. H. Tsuchiya, T. Hayashi, H. Naruse, N. Takagi, *Journal of Chromatography*, 234 (1982) 121.

42. H. Tsuchiya, T. Hayashi, H. Naruse, N. Takagi, *Journal of Chromatography*, 231 (1982) 247.

43. H. Tsuchiya, T. Hayashi, M. Sato, M. Tatsumi, N. Takagi, *Journal of Chromatography*, 309 (1984) 43.

44. R. A. Kelly, D. S. O'Hara, V. Kelley, *Journal of Chromatography*, 416 (1987) 247.

45. A. Takadate, T. Masuda, C. Murata, C. Haratake, A. Isobe, M. Irikura, S. Goya, *Analytical Sciences*, 8 (1992) 695.

46. A. Takadate, T. Masuda, C. Tajima, C. Murata, M. Irikura, S. Goya, *Analytical Sciences*, 8 (1992) 663.

47. R. H. Pullen, J. A. Howell, J. W. Cox, *Prostaglandins, Leukotrienes and Medicine*, 29 (1987) 205.

48. W. D. Watkins, M. B. Peterson, *Analytical Biochemistry*, 125 (1982) 30.

49. J. S. Hawkes, M. J. James, L. G. Cleland, *Prostaglandins*, 42 (1991) 355.

50. G. A. Cordis, D. K. Das, *Journal of Chromatography*, 536 (1991) 309.

51. C. E. Morreal, D. K. Sinha, C. J. White, D. T. Nemoto, *Journal of Chromatography*, 345 (1985) 380.

52. W. Engels, M. A. F. Kamps, P. J. M. R. Lemmens, G. J. van der Vusse, R. S. Reneman, *Journal of Chromatography*, 427 (1988) 209.

53. T. A. Stein, L. Angus, E. Borrero, L. J. Auguste, L. Wise, *Journal of Chromatography*, 395 (1987) 591.

54. J. W. Cox, R. H. Pullen, *Analytical Chemistry*, 56 (1984) 1866.

55. Y. Yamaguchi, T. Tomita, M. Senda, A. Hirai, T. Terano, Y. Tamura, S. Yoshida, *Journal of Chromatography*, 357 (1986) 199.

56. K. Kiyomiya, K. Yamaki, N. Nimura, T. Kinoshita, S. Oh-ishi, *Prostaglandins*, 31 (1986) 71.

57. T. Yoshida, A. Uetaka, H. Yamaguchi, N. Nimura, T. Kinoshita, *Analytical Biochemistry*, 173 (1988) 70.

58. K. Tohyama, S. Manabe, H. Yanagisawa, O. Wada, *Japanese Journal of Hygiene*, 42 (1988) 1064.

59. N. Ichinose, S. Abe, K. Adachi, R. Kato, *Nihon Kagakukaishi*, (1986) 1011.

60. M. Hatsumi, S. Kimata, K. Hirosawa, *Journal of Chromatography*, 253 (1982) 271.

61. S. A. Barker, J. A. Monti, S. T. Christian, F. Benington, R. D. Morin, *Analytical Biochemistry*, 107 (1980) 116.

62. N. Nimura, T. Kinoshita, *Analytical Letters*, 13 (1980) 191.

63. M. Yamaguchi, S. Hara, R. Matsunaga, M. Nakamura, Y. Ohkura, *Analytical Sciences*, 1 (1985) 295.

64. M. Yamaguchi, S. Hara, R. Matsunaga, M. Nakamura, Y. Ohkura, *Journal of Chromatography*, 346 (1985) 227.

65. M. Yamaguchi, R. Matsunaga, S. Hara, M. Nakamura, Y. Ohkura, *Journal of Chromatography*, 375 (1986) 27.

66. M. Yamaguchi, K. Fukuda, S. Hara, M. Nakamura, Y. Ohkura, *Journal of Chromatography*, 380 (1986) 257.

67. M. Yamaguchi, O. Takehiro, S. Hara, M. Nakamura, Y. Ohkura, *Chemical and Pharmaceutical Bulletin*, 36 (1988) 2263.

68. M. Yamaguchi, O. Takehiro, J. Ishida, M. Nakamura, *Chemical and Pharmaceutical Bulletin*, 37 (1989) 2846.

69. M. Yamguchi, T. Iwata, K. Inoue, S. Hara, M. Nakamura, *Analyst*, 115 (1990) 1363.

70. T. Iwata, K. Inoue, M. Nakamura, M. Yamaguchi, *Biomedical Chromatography*, 6 (1992) 120.

71. K. Nakashima, Y. Taguchi, N. Kuroda, S. Akiyama, *Journal of Chromatography*, 619 (1993) 1.

72. K. Yamada, M. Onodera, Y. Aizawa, *Journal of Pharmacological Methods*, 9 (1983) 93.

73. V. V. Bezuglov, N. M. Gretskaya, G. S. Kogteva, E. M. Manevich, E. M. Koroleva, B. G. Belen'kii, Y. E. Lille, L. D. Bergel'son, *Doklady Akademii Nauk SSSR*, 308 (1989) 231.

74. I. Yanagisawa, M. Yamane, T. Urayama, *Journal of Chromatography*, 345 (1985) 229.

75. Y. Yasaka, M. Tanaka, T. Shono, T. Tetsumi, J. Katakawa, *Journal of Chromatography*, 508 (1990) 133.

76. S. Ikenoya, O. Hiroshima, M. Ohmae, K. Kawabe, *Chemical and Pharmaceutical Bulletin*, 28 (1980) 2941.

77. J. Knospe, D. Steinhilber, T. Herrmann, H. J. Roth, *Journal of Chromatography*, 442 (1988) 444.

78. K. Shimada, C. Sakayori, T. Nambara, *Journal of Liquid Chromatography*, 10 (1987) 2177.

79. G. M. Beck, D. A. Roston, B. Jaselskis, *Talanta*, 36 (1989) 373.

80. H. Karatani, *Bulletin. Chemical Society of Japan*, 60 (1987) 2023.

81. T. Kawasaki, M. Maeda, A. Tsuji, *Journal of Chromatography*, 328 (1985) 121.

82. M. Tod, M. Prevot, J. Chalom, R. Farinotti, F. Mahuzier, *Journal of Chromatography*, 542 (1991) 295.

83. T. Toyo'oka, M. Ishibashi, Y. Takeda, K. Nakashima, S. Akiyama, S. Uzu, K. Imai, *Journal of Chromatography*, 588 (1991) 61.

84. T. Toyo'oka, M. Ishibashi, T. Terao, *Journal of Chromatography*, 627 (1992) 75.

85. S. A. Soper, S. M. Lunte, T. Kuwana, *Analytical Sciences*, 5 (1989) 23.

86. T. Higashijima, T. Fuchigami, T. Imasaka, N. Ishibashi, *Analytical Chemistry*, 64 (1992) 711.

87. L. Hernandez, J. Escalona, N. Joshi, N. Guzman, *Journal of Chromatography*, 559 (1991) 182.

88. C. Toulas, L. Hernandez, *LC-GC*, 10 (1993) 471.

89. R. P. Haugland, K. D. Larison, *Handbook of Fluorescent Probes and Research Chemicals*, 5th Ed., Molecular Probes Inc., Eugene, OR, 1992.

90. P. S. Mukherjee, H. T. Karnes, *Analytical Chemistry*, 68 (1996) 327.

91. P. S. Mukherjee, H. T. Karnes, *Analyst*, 121 (1996) 1573.

Chapter 4

Application of the Optimized Carbonyl-Labelling Reaction

to a Homologous Series of Linear Saturated

Free Fatty Acids ($C_6 - C_{24}$)

4.1 Introduction

4.1.1 Free fatty acids

Fatty acids are defined as all saturated and unsaturated aliphatic carboxylic acids with a carbon chain length in the range of $C_6 - C_{24}$.[1] Fatty acids and their esters constitute an important part of most lipids that are found in plants and animals. Free fatty acids (FFAs) differ by their chain length and branching, degree of unsaturation, and position and configuration of their double bonds. FFAs are formed as a result of lipolytic enzyme action on glycerides, are naturally present in food, and are functional groups of many surface active agents presently used as food additives.[2] The separation and analysis of fatty acid metal salts, e.g. those of sodium or calcium, are important in the study of the biodegradation of fatty acids in biological fluids.[3] Due to the importance of their analysis in biochemical and clinical investigations, linear saturated FFAs $C_6 - C_{24}$ were chosen as model compounds in this work.

Either gas chromatography (GC)[4-8] or high-performance liquid chromatography (HPLC)[4,9-18] is currently used to determine FFAs and their metal salts. In the GC determination of FFAs a number of difficulties are encountered, the most important being the low volatility of acids. This problem necessitates operation at temperatures close to the maximal operating temperature of most known stationary liquid phases (SLP).[19] Other problems include the intermolecular association of acids in the vapour phase and adsorption of the acids in the injector and separation column. To overcome these problems methyl, butyl or silyl esters are formed to enhance the analyte volatility prior to introduction into the GC. FFAs do not possess a chromophoric or fluorophoric group therefore derivatization for satisfactory separation and sensitivity in HPLC analysis is

needed. Many precolumn derivatization reagents have been proposed for absorbance or fluorescence detection. UV-absorbing labels include phenacyl[4,10,20-29] and its p-bromo[4,10,20,22,30-34] or methoxy analogue[4,10,20,35,36], naphthacyl esters[4,10,20,21,37,38], p-methoxyacetanilides[4,10,39], 1-chloromethylisantin[4,10,40], naphthyldiazoalkanes[4,10,41] and naphthylamine[4,20,42,43]. Fluorescent labels include 4-bromomethyl-7-methoxy-coumarin[4,10,44,45] and its 7-acetoxy analogue[4,10,20,46,47], 9-anthryldiazomethane[4,10,48-50], 9-chloromethylanthracene[4,51], 9-aminophenanthrene[4,10,20,43], 9,10-diaminophen-anthrene[4,10,20,52], 2-nitrophenylhydrazides[4,10,20,53], dansyl ethanolamine[4,54] and 5-(bromo-methyl)fluorescein (5-BMF)[55-57]. Other analytical techniques used for the separation of FFAs include thin-layer chromatography[58], supercritical fluid chromatography[59-61], liquid chromatography-mass spectrometry[62] and capillary electrophoresis.

Capillary electrophoresis (CE) has found increasingly more applications for separations of a wide variety of compounds during the past decade. The key advantages of CE derive from its simplicity, high efficiency, fast analyses, and small sample volumes, which are desirable in biological sample analysis. Separation of FFAs has been performed using capillary zone electrophoresis (CZE)[63-67], micellar electrokinetic capillary chromatography (MEKC)[1,55] and nonaqueous CE[68,69]. Capillary electrophoretic analysis of FFAs, especially of carbon numbers greater than twelve[68], is difficult due to the fact that the solubility of FFAs in aqueous solutions decreases rapidly as alkyl chain length increases. Increase in the alkyl chain length of FFAs in aqueous media also causes intermolecular association due to the hydrophobic character of their alkyl groups. This hydrophobicity causes the FFAs to adsorb to the separation column, and leads to a

decrease in selectivity.[68] Introduction of organic solvents and/or surfactants into the

aqueous media can partially alleviate such problems. Various CZE separations of

$C_7 - C_{18}$ saturated FFAs with an electrolyte containing a cyclodextrin and/or an organic

modifier have been performed successfully and usually result in a limit of detection

(LOD) on the order of 10^{-6} M.[63-67] In the presence of the cyclodextrin (CD), analyte

solubility is enhanced through the inclusion of the acid's alkyl chain in the CD cavity,

while separation selectivity will be improved because the stability constants of the

inclusion complexes increase with increasing chain length of the acid. Roldan-Assad and

Gareil used CZE with indirect absorbance detection for the separation of $C_7 - C_{18}$

saturated FFAs with an electrolyte containing 60 % methanol, the additive trimethyl-β-

cyclodextrin and a chromogenic species for detection.[63] Collet and Gareil used CZE with

indirect UV detection with an electrolyte containing 50 % methanol and the additive

dimethyl-β-cyclodextrin to separate a mixture of $C_7 - C_{18}$ saturated FFAs.[64] Gutnikov

and co-workers performed a CE with indirect UV detection (CE-IUVD) separation of a

standard mixture of $C_3 - C_{18}$ saturated FFAs with a 60 % acetonitrile buffer.[65] Desbene

and co-workers used CE with indirect laser-induced fluorescence (LIF) to analyze a

mixture of $C_7 - C_{18}$ saturated FFAs using a 40 % ethanol buffer.[66,67]

Various MEKC techniques for the separation of FFAs have been applied

successfully.[1,55] A micellar surfactant is used to solubilize compounds that are insoluble

or slightly soluble in aqueous phases, such as FFAs. Erim and co-workers used MEKC-

IUVD for the separation of $C_8 - C_{20}$ fatty acids using a water-acetonitrile medium with

added sodium dodecyl benzenesulfonate as micellar surfactant and the non-ionic

detergent Brij® 35 as a solubilizing agent.[1] Zuriguel and co-workers used MEKC-LIF

for the analysis of FFAs however resolution of only the $C_8 - C_{11}$ acids could be achieved.[55] This technique resulted in a LOD in the 10^{-10} M range. Fatty acids with a carbon number greater than 20 can not be satisfactorily analysed using CZE or MEKC due to poor solubility in aqueous media. It is believed that a nonaqueous medium is required for the electrophoretic separation of long-chain FFAs. Wang, Wei, and Li used nonaqueous CE with indirect fluorescence detection for the separation of FFAs $C_6 - C_{26}$ which utilized an electrolyte containing 2.8 mM KOH, 60 % methanol and 40 % acetonitrile.[68] The LOD was reported to be 0.01 – 0.02 mM. Advantages of nonaqueous media include better solubility for hydrophobic analytes and modifiers, different acid-base chemistries and potential enhancement of selectivity due to changes in solvation and ion interaction.[68]

In this work a homologous series of linear saturated FFAs of carbon number 6 to 24 was labelled with the only fluorescent reagent that can be excited by an argon ion (Ar^+) laser, 5-BMF, using the optimized carbonyl-labelling reaction developed in Chapter 3. 5-BMF has been shown to be a very useful labelling reagent suitable for the LIF detection of carboxylic acids.[70] The resulting labelled linear saturated FFA reaction mixtures were analysed using CZE-LIF, MEKC-LIF, and ESI-MS. CZE and MEKC separations of a mixture of the labelled linear saturated FFAs were performed.

4.2 Experimental

4.2.1 Reagents

Caproic acid sodium salt, caprylic acid sodium salt, nonanoic acid sodium salt, capric acid sodium salt, undecanoic acid, lauric acid sodium salt, tridecanoic acid,

myristic acid sodium salt, pentadecanoic acid, palmitic acid sodium salt, heptadecanoic acid, stearic acid sodium salt, nonadecanoic acid, arachidic acid, heneicosanic acid, behenic acid, tricosanic acid, and lignoceric acid were purchased from Sigma (St. Louis, MO, USA). 5-BMF was obtained from Molecular Probes (Eugene, OR, USA). Dimethyl-β-cyclodextrin and trimethyl-β-cyclodextrin were bought from Aldrich (Milwaukee, MI, USA). Anhydrous methanol (MeOH), N,N-dimethylformamide (DMF), and sodium dodecyl sulfate (SDS) were acquired from Caledon (Georgetown, ON, Canada). Sodium hydroxide (NaOH), potassium hydroxide (KOH) and sodium tetraborate were purchased from BDH (Toronto, ON, Canada). Fused-silica capillary (50 μm I.D., 140 μm O.D.) was obtained from PolyMicro Technologies (Phoenix, AZ, USA). Tris was bought from Gibco BRL (Grand Island, NY). Acetonitrile (ACN) was acquired from Em Science (Gibbstown, NJ, USA). The 1.11 cm diameter filter paper was purchased from Whatman (Maidstone, England).

4.2.2 Instruments

The CE-LIF instrument that was used is a home-built instrument that was described in Chapter 1. The electrospray ionization mass spectrometry (ESI-MS) instrument used was described in Chapter 2 in Section 2.2.2.

4.2.3 Optimized carbonyl-labelling reaction

The apparatus used to perform this reaction was described earlier in Chapter 2 in Section 2.2.3 and is illustrated in Figure 2.10. 1 μmol of FFA sodium salt was dissolved in a 4:1 mixture of DMF:MeOH and then transferred to a 5-mL three-neck round bottom

194

flask. Next, two molar equivalents of 5-BMF dissolved in DMF were added to the reaction flask and the reaction mixture was then heated at 80 °C under reflux for 2 hours. The final reaction volume was made to be 1 mL by adding DMF. The blank reaction mixture contained all reactants except the FFA. This carbonyl-labelling reaction was applied to the following homologous series of linear saturated FFAs: caproic acid (C_6), caprylic acid (C_8), nonanoic acid (C_9), capric acid (C_{10}), undecanoic acid (C_{11}), lauric acid (C_{12}), tridecanoic acid (C_{13}), myristic acid (C_{14}), pentadecanoic acid (C_{15}), palmitic acid (C_{16}), heptadecanoic acid (C_{17}), stearic acid (C_{18}), nonadecanoic acid (C_{19}), arachidic acid (C_{20}), heneicosanic acid (C_{21}), behenic acid (C_{22}), tricosanic acid (C_{23}) and lignoceric acid (C_{24}).

4.2.4 CZE-LIF separations of a homologous series of labelled FFAs

The CZE-LIF separations of a homologous series of labelled linear saturated FFAs (C_6 – C_{24}) were performed at concentrations of 10^{-8} M using 10 mM borate at pH 9 as the dilution buffer. The sample reaction mixture of each labelled linear saturated FFA was run two times on the CE-LIF instrument (n = 2). The capillary used was 30 cm in length and had an outer diameter (O.D.) of 140 μm and an inner diameter (I.D.) of 50 μm. The run and sheath flow buffers were 10 mM borate at pH 9. The injections were performed at 1000 V for 5 s and the separation voltage was 12 kV. The Ar^+ laser beam used for excitation had 12.1 mW of power at 488 nm and the PMT was biased at 1000 V. The interference filter used was 518DF25. The calibration curves were constructed and the CZE-LIF separations of a labelled linear saturated FFA mixture were performed under the same run conditions.

4.2.5 Conversion of linear saturated FFAs into sodium salts

An arbitrary amount of linear saturated FFA was dissolved in methanol in a 25-mL round bottom flask and then 0.5 M NaOH was added dropwise to precipitate out the FFA sodium salt. The salt was collected by vacuum filtration using Whatman 1.11 cm diameter filter paper. The isolated FFA sodium salt was then dried using a lyophilizer. The remaining FFA sodium adduct was used in the carbonyl-labelling reaction as described in Section 4.2.3. This conversion procedure was performed for undecanoic acid (C_{11}), tridecanoic acid (C_{13}), pentadecanoic acid (C_{15}), heptadecanoic acid (C_{17}), nonadecanoic acid (C_{19}), arachidic acid (C_{20}), heneicosanic acid (C_{21}), behenic acid (C_{22}), tricosanic acid (C_{23}) and lignoceric acid (C_{24}).

4.2.6 CZE-LIF separations of a labelled FFA mixture using a coated capillary

The CZE-LIF separations of a labelled linear saturated FFA mixture using a Grignard-poly-acryloylaminopropanol (poly-AAP)-coated capillary were performed using the blank and sample reaction mixtures at concentrations of 10^{-7} M using 10 mM borate at pH 9 as the dilution buffer. The Grignard-poly-AAP-coated capillary used for separation was 40 cm in length with an I.D. of 50 µm and an O.D. of 140 µm. The capillary was coated with poly-AAP as described in reference 71. The run and sheath flow buffers were 10 mM borate at pH 9. The injections were performed at -1000 V for 5 s and the electric field used for separation was -16 kV. The Ar^+ laser beam used for excitation had 12.1 mW of power at 488 nm and the PMT was biased at 1000 V. The interference filter used was 518DF25.

4.2.7 CZE-LIF separations using a cyclodextrin

The aqueous CZE-LIF separations using an electrolyte containing dimethyl-β-cyclodextrin or trimethyl-β-cyclodextrin were performed using the blank and sample caproic acid reaction mixtures at concentrations of 10^{-8} M using 10 mM borate at pH 9 as the dilution buffer. The capillary used was 30 cm in length and had an I.D. of 50 μm and an O.D. of 140 μm. The run and sheath flow buffers were 10 mM borate at pH 9. The injections were performed at 1000 V for 5 s and the separation voltage was 12 kV. The Ar$^+$ laser beam used for excitation had 12.1 mW of power at 488 nm and the PMT was biased at 1000 V. The interference filter used was 518DF25.

4.2.8 CZE-LIF separations using a cyclodextrin and an organic modifier

The CZE-LIF separations of labelled undecanoic acid using an electrolyte containing a cyclodextrin and an organic modifier were performed at a concentration of 10^{-8} M using 10 mM borate as the dilution buffer. The capillary used was 30 cm in length and had an I.D. of 50 μm and an O.D. of 140 μm. The run buffer was 10 mM Tris and 1 mM dimethyl-β-cyclodextrin in 50 % methanol at pH 10 or 10 mM Tris and 1 mM trimethyl-β-cyclodextrin in 60 % methanol at pH 10. The sheath flow buffer was 10 mM borate at pH 9 and the separation voltage was 30 kV. Injections were performed at 1000 V for 5 s. The Ar$^+$ laser beam used for excitation had 12.1 mW of power at 488 nm and the PMT was biased at 1000 V. The interference filter used was 518DF25.

197

4.2.9 Nonaqueous CE-LIF separations

The nonaqueous CE-LIF separations of labelled undecanoic acid were performed at a concentration of 10^{-8} M using 10 mM borate at pH 9 as the dilution buffer. The capillary used was 30 cm in length and had an I.D. of 50 μm and an O.D. of 140 μm. The run buffer was 2.8 mM KOH made in 60 % methanol and 40 % acetonitrile at pH 13. The sheath flow buffer was 10 mM borate at pH 9. The injections were performed at 1000 V for 5 s and the separation voltage was 24 kV. The Ar^{+} laser beam used for excitation had 12.1 mW of power at 488 nm and the PMT was biased at 1000 V. The interference filter used was 518DF25.

4.2.10 MEKC-LIF separations using SDS

The MEKC-LIF separations of labelled caproic acid were performed using the micelle surfactant SDS at a concentration of 10^{-8} M using 10 mM borate at pH 9 as the dilution buffer. The capillary used was 40 cm in length and had an I.D. of 50 μm and an O.D. of 140 μm. The run buffers were 10 mM borate containing 10, 20, 30, 40, or 50 mM SDS at pH 9. The sheath flow buffer was 10 mM borate at pH 9. The separation voltages used were 16 kV for the 10, 20, and 30 mM SDS buffers, 12 kV for the 40 mM SDS buffer and 8 kV for the 50 mM SDS buffer. Injections were performed at 3000 V for 5 s. The Ar^{+} laser beam used for excitation had 12.1 mW of power at 488 nm and the PMT was biased at 1000 V. The interference filter used was 518DF25.

4.2.11 MEKC-LIF separations of a homologous series of labelled FFAs

The MEKC-LIF separations of the homologous series of labelled linear saturated FFAs ($C_6 - C_{24}$) were done at a concentration of 10^{-7} M using 10 mM borate at pH 9 as the dilution buffer. The capillary used was 40 cm in length had an I.D. of 50 μm and an O.D. of 140 μm. The run buffer was 10 mM borate and 50 mM SDS at pH 9 and the sheath flow buffer was 10 mM borate at pH 9. Injections were performed at 1000 V for 5 s and the separation voltage was 12 kV. The Ar^+ laser beam used for excitation had 12.1 mW of power at 488 nm and the PMT was biased at 1000 V. The interference filter used was 518DF25. The MEKC-LIF separations of a labelled linear saturated FFA mixture were performed using the same run conditions.

4.2.12 CZE-LIF separations of labelled caprylic acid

The CZE-LIF separations of the repeated carbonyl-labelling reaction involving caprylic acid sodium salt were done at a concentration of 10^{-8} M using 10 mM borate at pH 9 as the dilution buffer. The sample reaction mixture was run two times on the CE-LIF instrument (n = 2). The capillary used was 30 cm in length and had an I.D. of 50 μm and an O.D. of 140 μm. The run and sheath flow buffers were 10 mM borate at pH 9. The injections were performed at 1000 V for 5 s and the separation voltage was 12 kV. The Ar^+ laser beam used for excitation had 12.1 mW of power at 488 nm and the PMT was biased at 1000 V. The interference filter used was 518DF25.

All CE electropherograms were analysed using IgorPro. The peak areas of each of the product peaks found were calculated using the IgroPro macro Append Cursor Integration.

4.3 Results and Discussion

4.3.1 CZE-LIF separations of a homologous series of labelled FFAs

The first linear saturated FFA in the homologous series ($C_6 - C_{24}$) to be labelled with 5-BMF using the optimized carbonyl-labelling reaction that was developed in Chapter 3 was caprylic acid sodium salt (C_8). The carbonyl-labelling reaction was performed as described in Section 4.2.3. The resulting blank and sample reaction mixtures were checked for the presence of product using CZE-LIF with run conditions described in Section 4.2.4. The resulting CZE-LIF electropherograms can be found in Figure 4.1. A peak for labelled caprylic acid appears at an average migration time of ~123.9 s (n = 2). The limit of detection (LOD) was calculated to be on average 14 pM or 0.03 attomoles when 2 nL of sample was injected. The number of theoretical plates (N) was calculated to be $3*10^5$ plates. A calibration curve was constructed for labelled caprylic acid and can be found in Figure 4.2. Each standard concentration of labelled caprylic acid was run three times of the CE-LIF instrument (n = 3). The resulting calibration curve had a correlation coefficient of r = +0.9946. The error bars on the calibration curve represent ±1 standard deviation of the average peak area calculated for each concentration of labelled caprylic acid.

Next, nonanoic acid sodium salt was labelled with 5-BMF using the procedure described in Section 4.2.3. The blank and sample reaction mixtures were checked for the presence of product using CZE-LIF with the run conditions described in Section 4.2.4. The resulting CZE-LIF electropherograms can be found in Figure 4.3. A peak for labelled nonanoic acid appears at an average migration time of ~125.0 s (n = 2). The LOD was calculated to be 8 pM or 0.01 attomoles when 2 nL of sample was injected.

Figure 4.1: The CZE-LIF electropherograms of labelled caprylic acid (C_8). Capillary: 30 cm, 50 μm I.D., 140 μm O.D.. Run: 10 mM borate, pH 9, 12 kV. Injection: 1000 V, 5 s. Laser: 488 nm Ar$^+$, 12.1 mW. PMT: 1000 V. Interference filter: 518DF25. Concentration: 10^{-8} M.
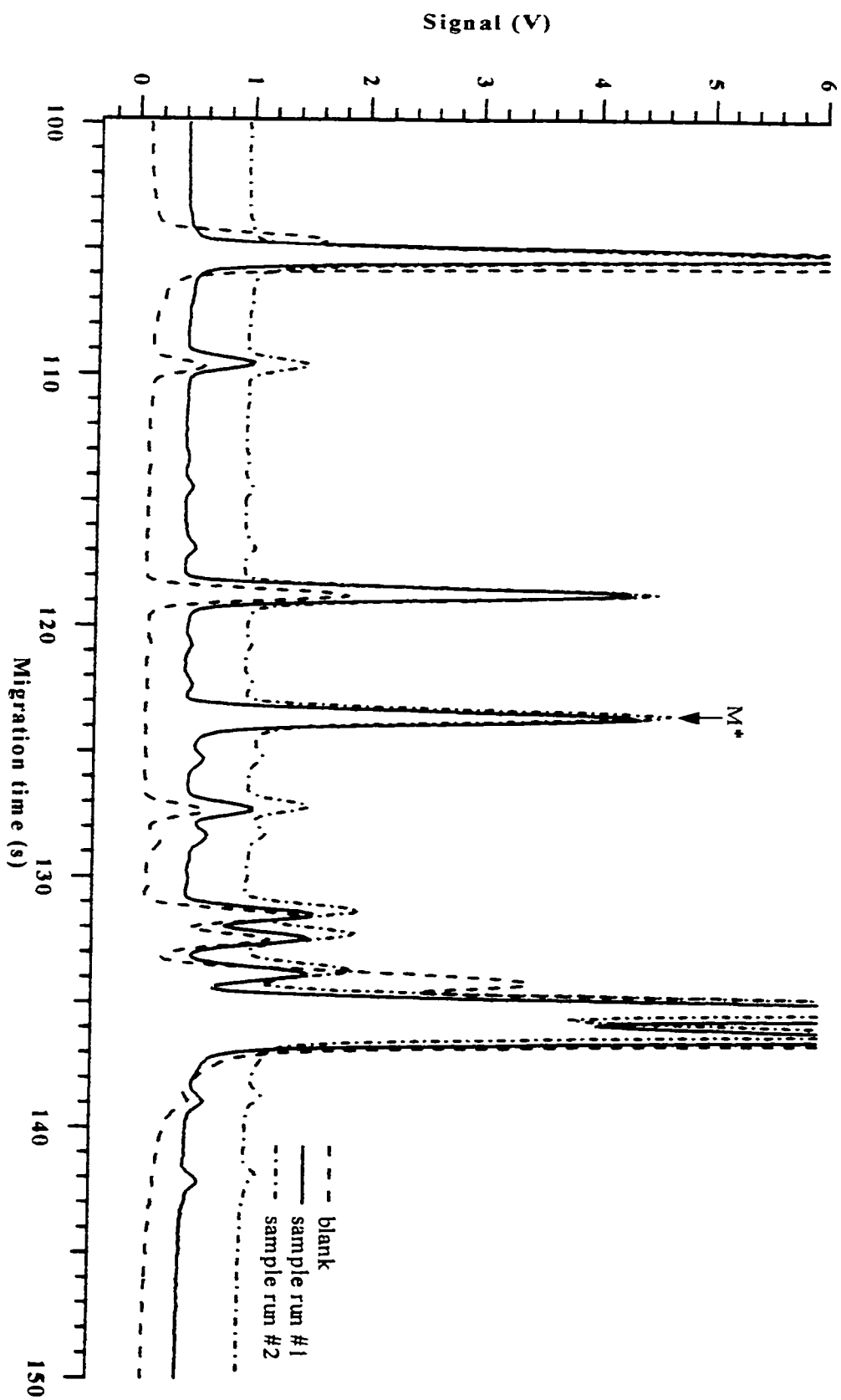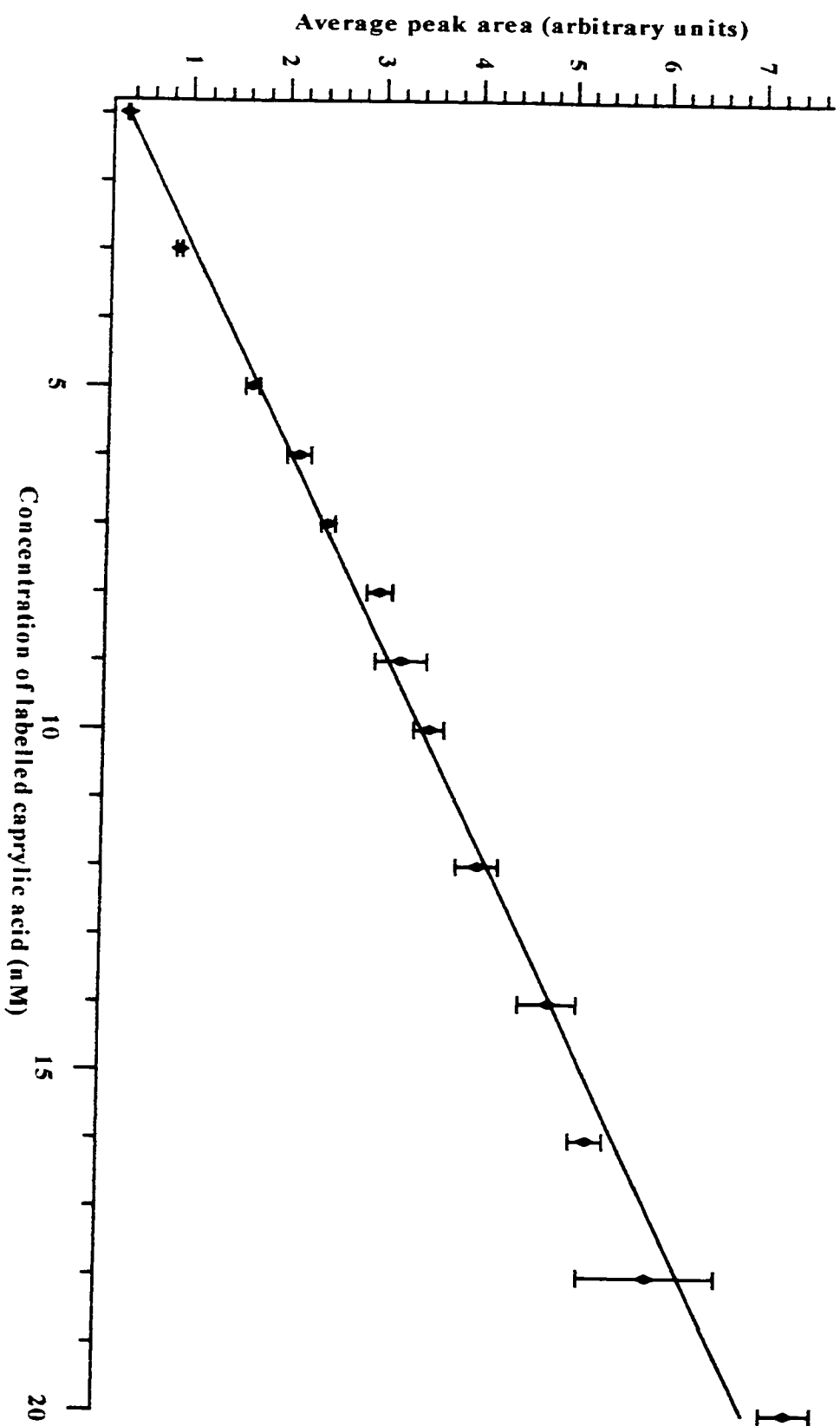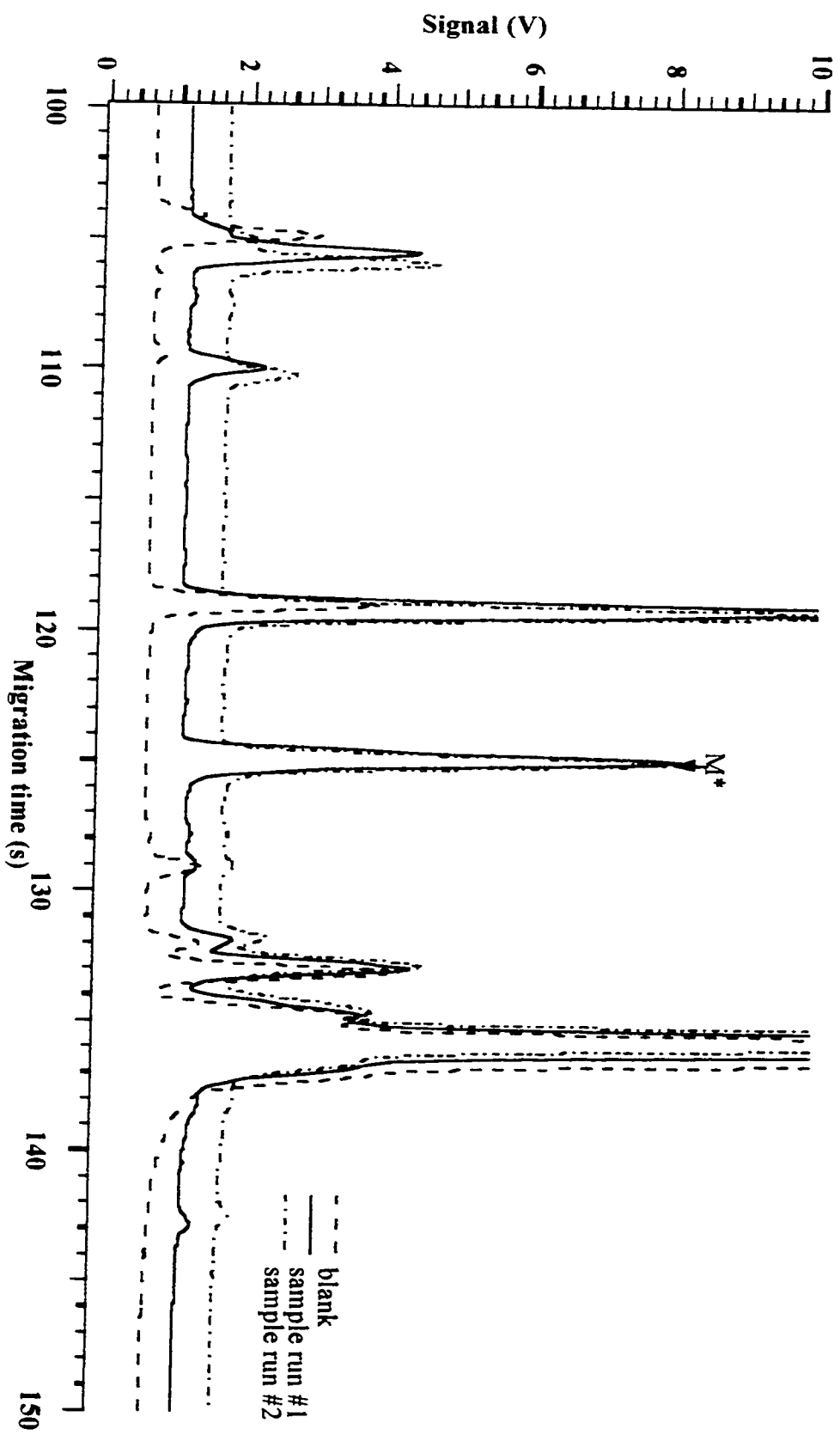
Figure 4.2: The calibration curve of labelled caprylic acid (C_8). Capillary: 30 cm, 50 μm I.D., 140 μm O.D..

Run: 10 mM borate, pH 9, 12 kV. Injection: 1000 V, 5 s. Laser: 488 nm Ar$^+$, 12.1 mW. PMT: 1000 V.

Interference filter: 518DF25 ($n = 3$).

202

Figure 4.3: The CZE-LIF electropherograms of labelled nonanoic acid (C_9). Capillary: 30 cm, 50 μm I.D., 140 μm O.D.. Run: 10 mM borate, pH 9, 12 kV. Injection: 1000 V, 5 s. Laser: 488 nm Ar+, 12.1 mW. PMT: 1000 V. Interference filter: 518DF25. Concentration: 10^{-8} M.

The value of N was calculated to be $2*10^5$ plates. A calibration curve was constructed for the labelled nonanoic acid and can be found in Figure 4.4. Each standard concentration of labelled nonanoic acid was run three times on the CE-LIF instrument (n = 3). The resulting calibration curve had a correlation coefficient of r = +0.9910. The error bars on the calibration curve represent ±1 standard deviation of the average peak area calculated for each concentration of labelled nonanoic acid.

Next, caproic acid sodium salt (C_6) was labelled with 5-BMF using the procedure described in Section 4.2.3. The blank and sample reaction mixtures were checked for the presence of product using CZE-LIF with the run conditions described in Section 4.2.4. The resulting CZE-LIF electropherograms can be found in Figure 4.5. A peak for the labelled caproic acid appears at an average migration time of ~126.6 s (n = 2). The LOD was found to be on average 6 pM or 0.01 attomoles when 2 nL of sample was injected. The value of N for this CE-LIF separation was calculated to be $2*10^5$ plates.

Next, the remaining linear saturated FFAs in the homologous series ($C_{10} - C_{24}$) were labelled with 5-BMF as described in Section 4.2.3. The undecanoic, tridecanoic, pentadecanoic, heptadecanoic, nonadecanoic, arachidic, heneicosanic, behenic, tricosanic and lignoceric acids were converted into sodium salts using the procedure described in Section 4.2.5. The blank and sample reaction mixtures for each linear saturated FFA were checked for the presence of product using CZE-LIF with the run conditions described in Section 4.2.4. The resulting CZE-LIF electropherograms can be found in Figures 4.6 – 4.20.

The CZE-LIF electropherograms for labelled capric acid can be found in Figure 4.6. A peak for labelled capric acid appears at an average migration time of

Figure 4.4: The calibration curve of labelled nonanoic acid (C_9). Capillary: 30 cm, 50 μm I.D., 140 μm O.D.. Run: 10 mM borate, pH 9, 12 kV. Injection: 1000 V, 5 s. Laser: 488 nm Ar^+, 12.1 mW. PMT: 1000 V. Interference filter: 518DF25 (n = 3).
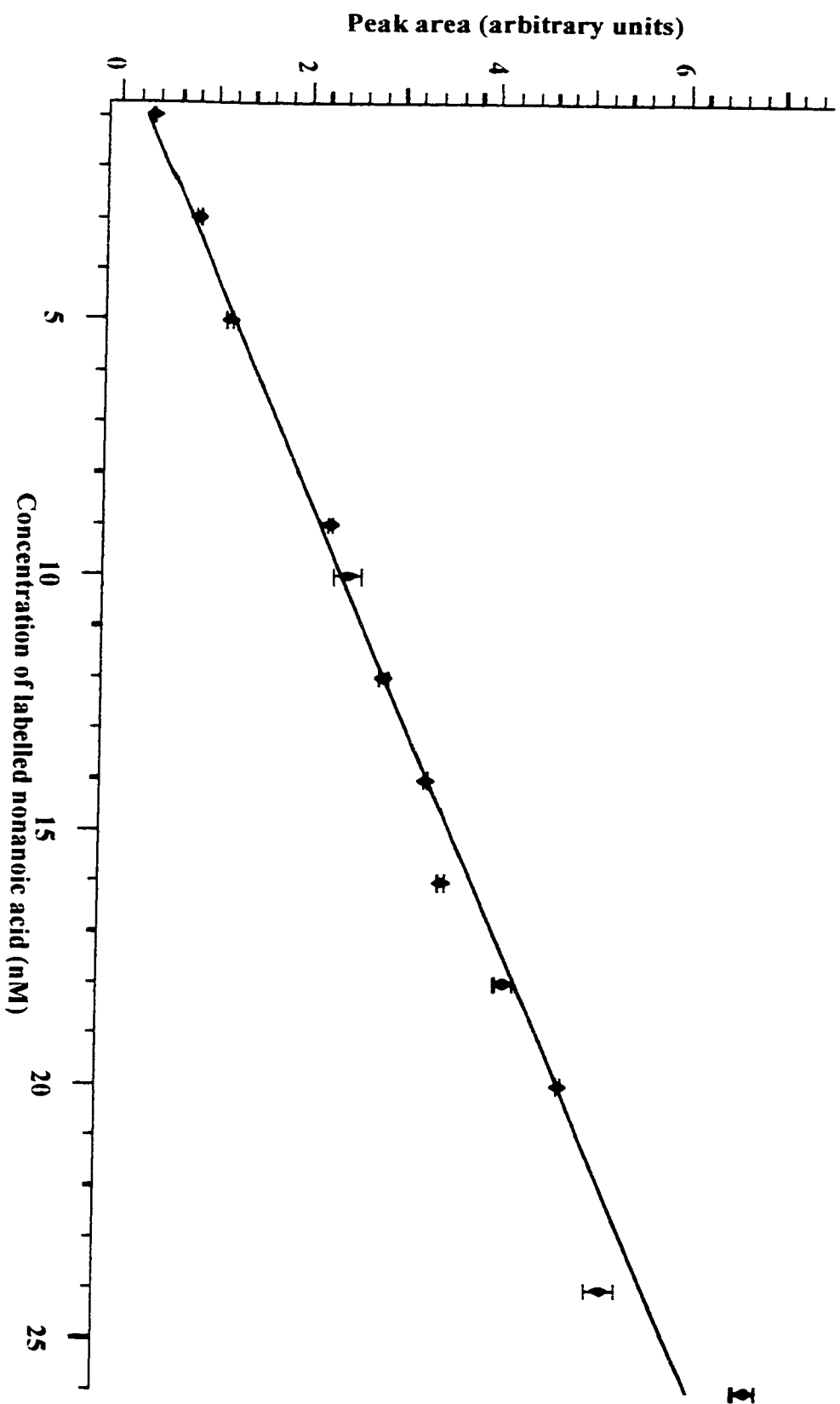
Figure 4.5: The CZE-LIF electropherograms of labelled caproic acid (C_6). Capillary: 30 cm, 50 μm I.D., 140 μm O.D.. Run: 10 mM borate, pH 9, 12 kV. Injection: 1000 V, 5 s. Laser: 488 nm Ar$^+$, 12.1 mW. PMT: 1000 V. Interference filter: 518DF25. Concentration: 10^{-8} M.
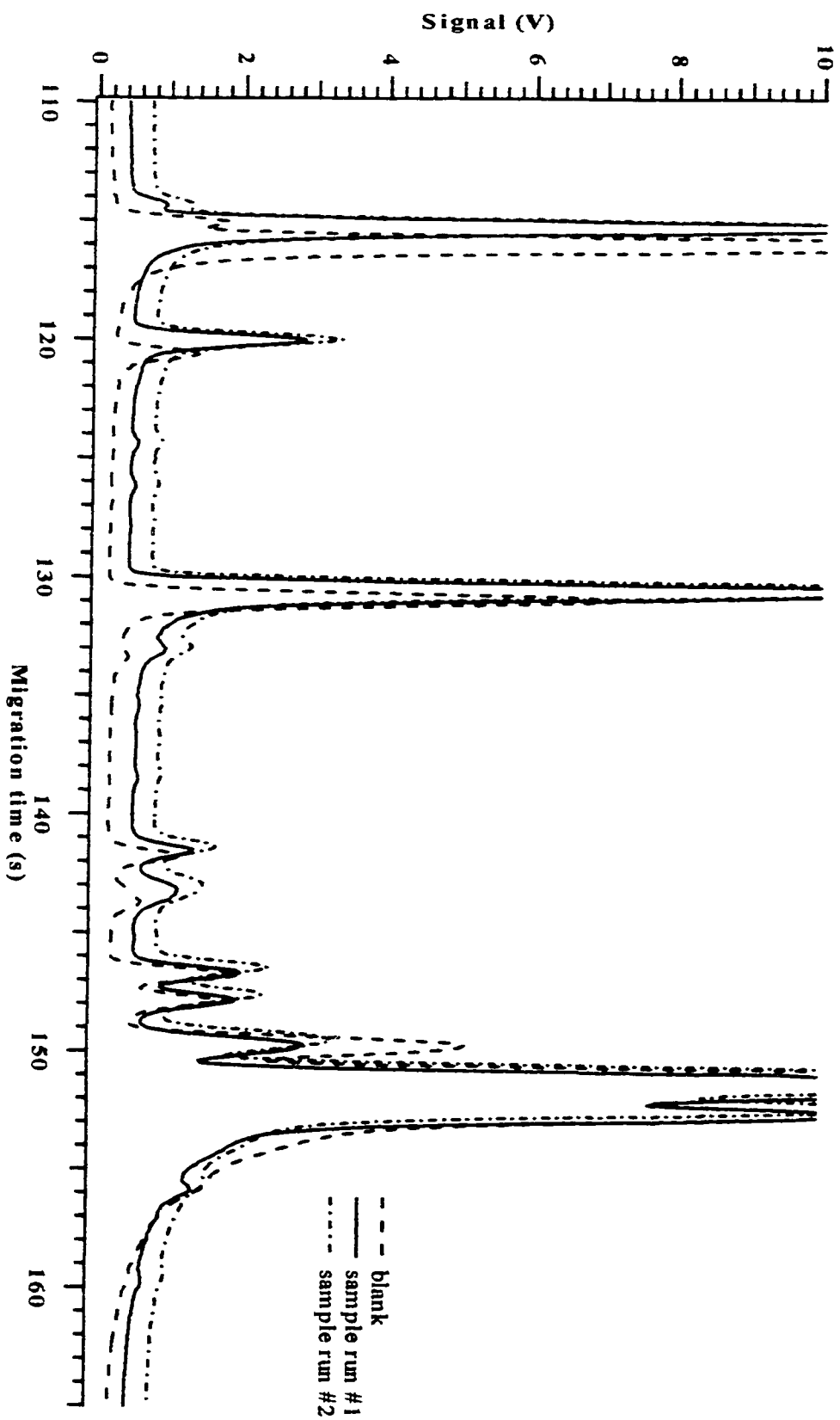

206
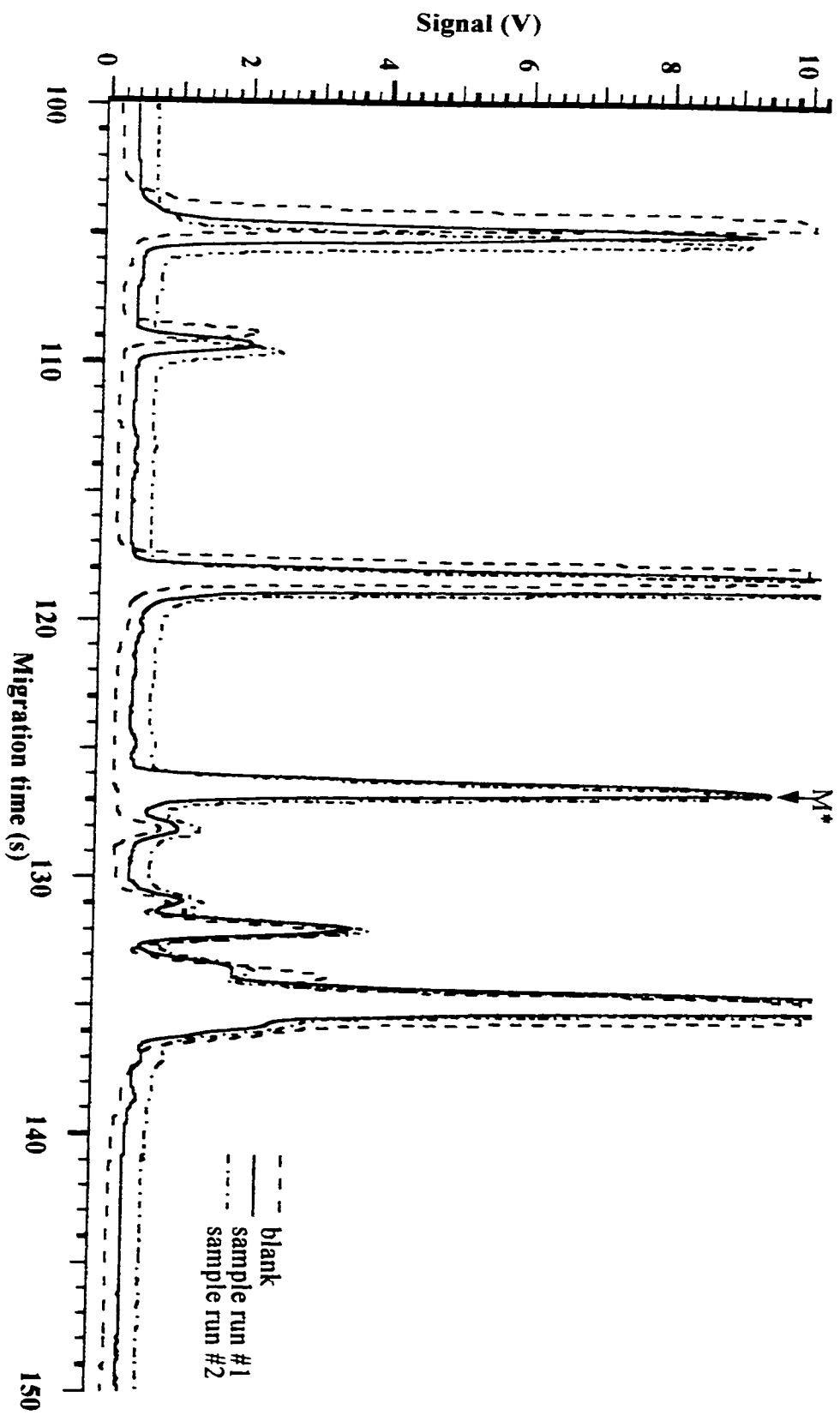
Figure 4.6: The CZE-LIF electropherograms of labelled capric acid (C_{10}). Capillary: 30 cm, 50 μm I.D., 140 μm O.D..

Run: 10 mM borate, pH 9, 12 kV. Injection: 1000 V, 5 s. Laser: 488 nm Ar$^+$, 12.1 mW. PMT: 1000 V.
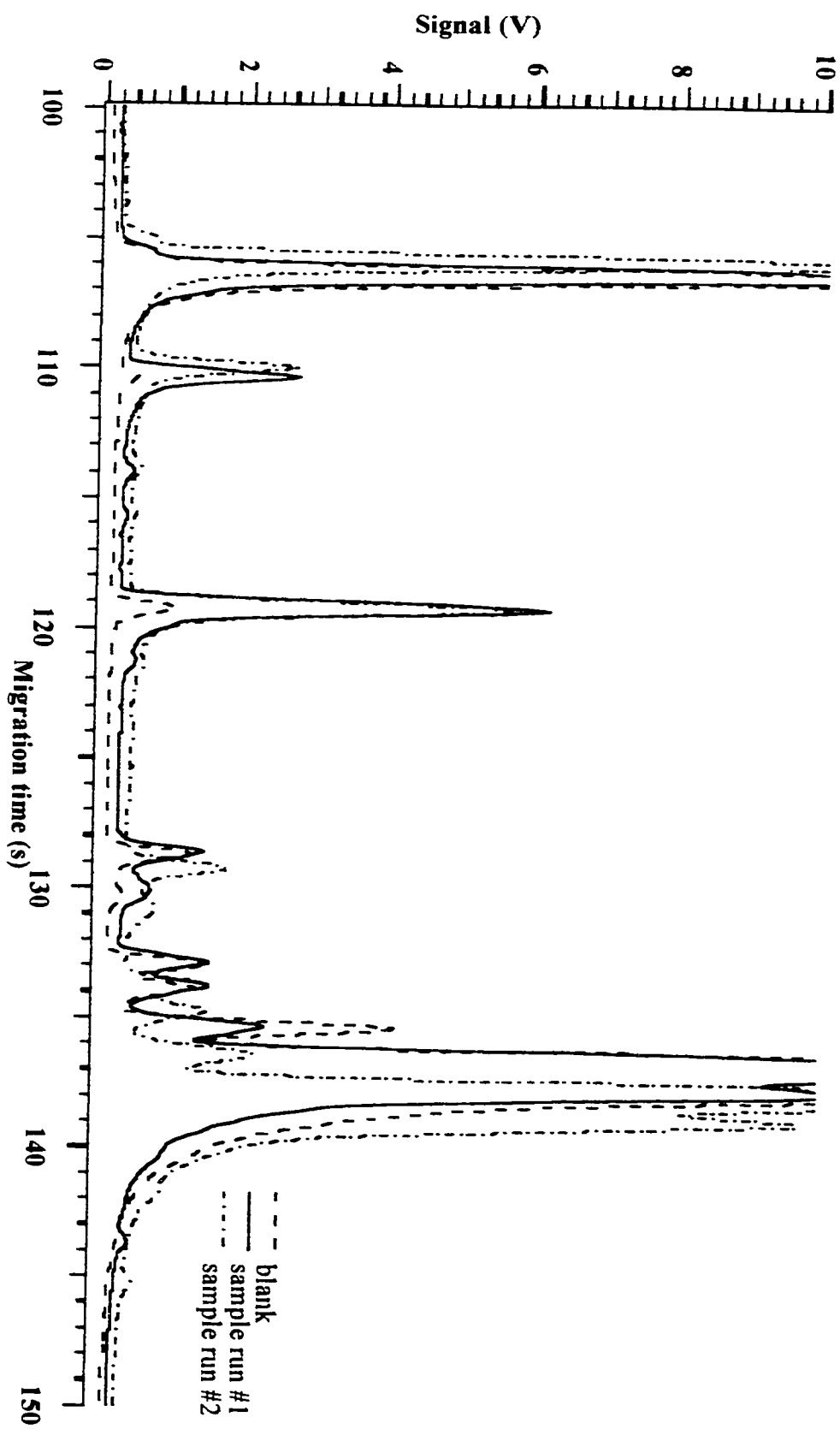
Interference filter: 518DF25. Concentration: 10^{-8} M.
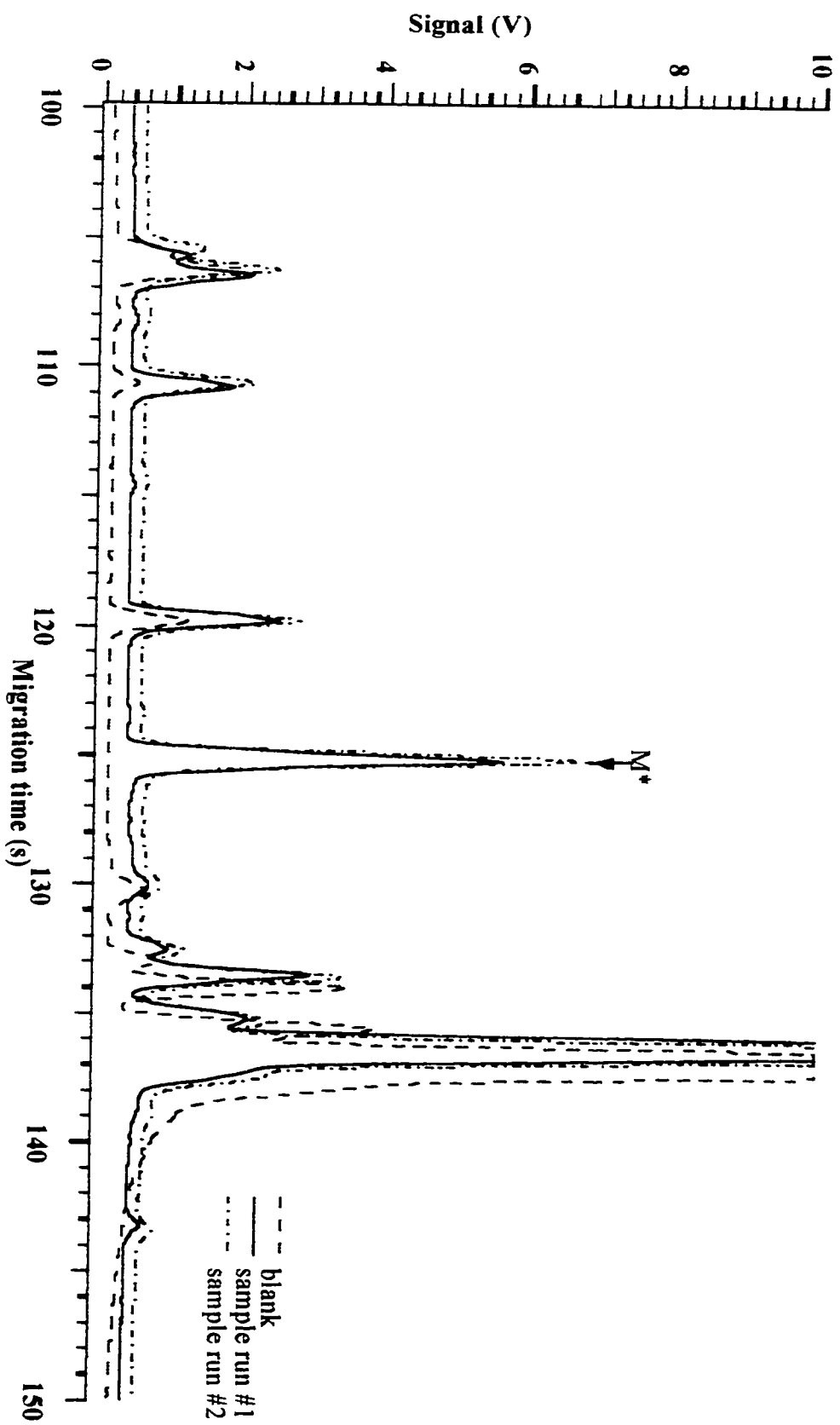
Figure 4.7: The CZE-LIF electropherograms of labelled undecanoic acid (C$_{11}$). Capillary: 30 cm, 50 µm I.D., 140 µm O.D..

Run: 10 mM borate, pH 9, 12 kV. Injection: 1000 V, 5 s. Laser: 488 nm Ar$^+$, 12.1 mW. PMT: 1000 V.
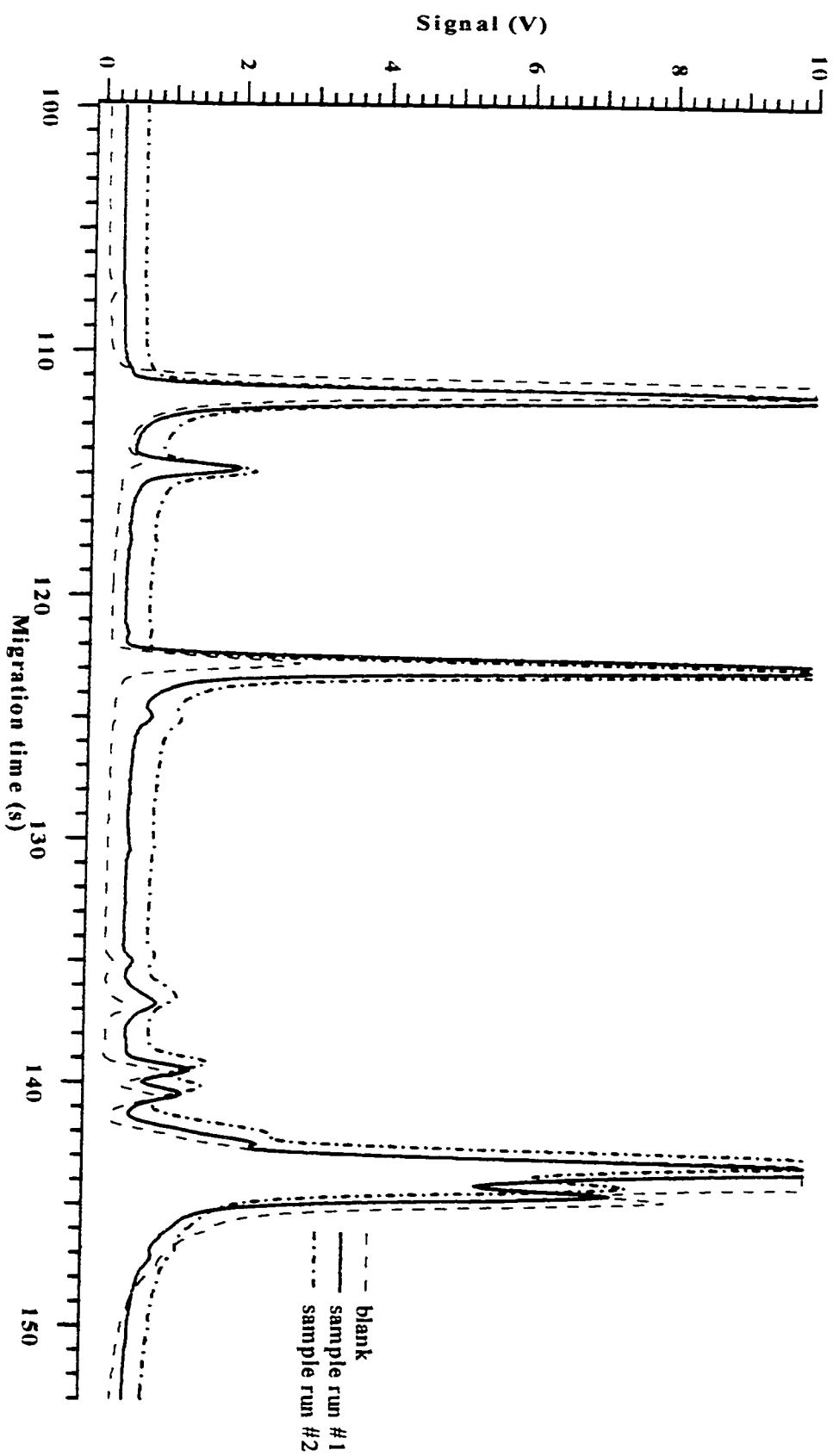
Interference filter: 518DF25. Concentration: 10^{-8} M.
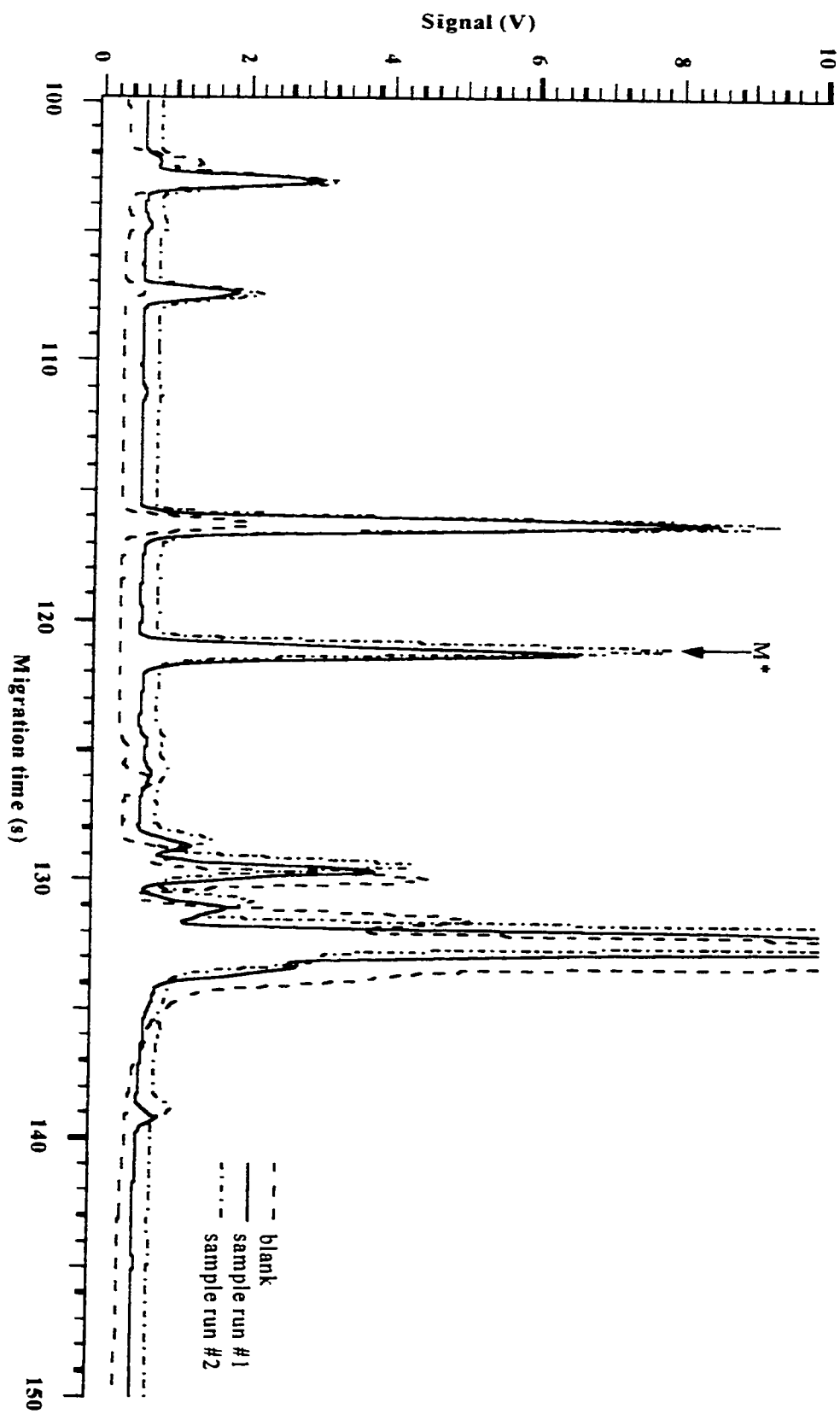
Figure 4.8: The CZE-LIF electropherograms of labelled lauric acid (C_{12}). Capillary: 30 cm, 50 μm I.D., 140 μm O.D.. Run: 10 mM borate, pH 9, 12 kV. Injection: 1000 V, 5 s. Laser: 488 nm Ar$^+$, 12.1 mW. PMT: 1000 V. Interference filter: 518DF25. Concentration: 10^{-8} M.
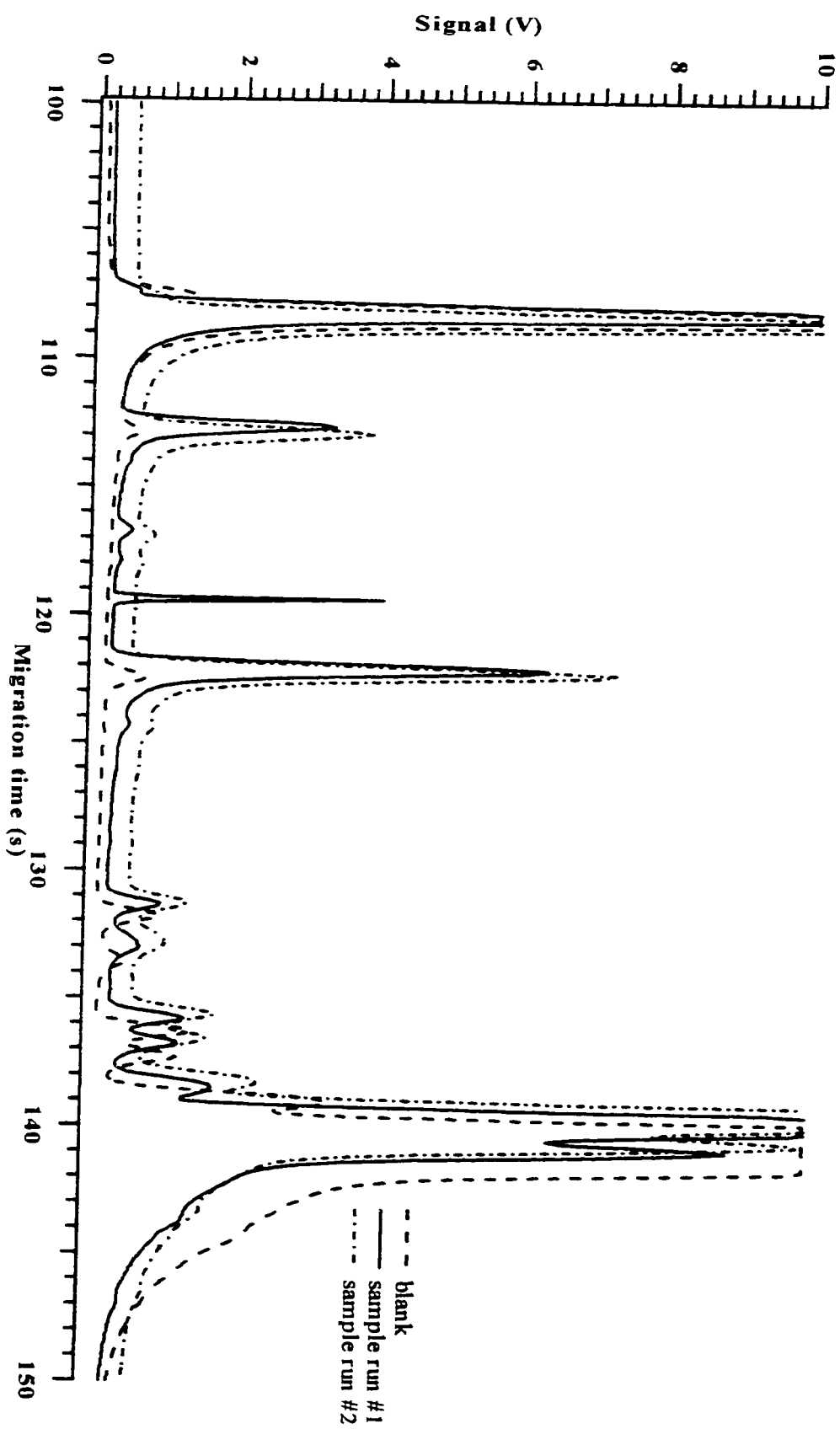
209
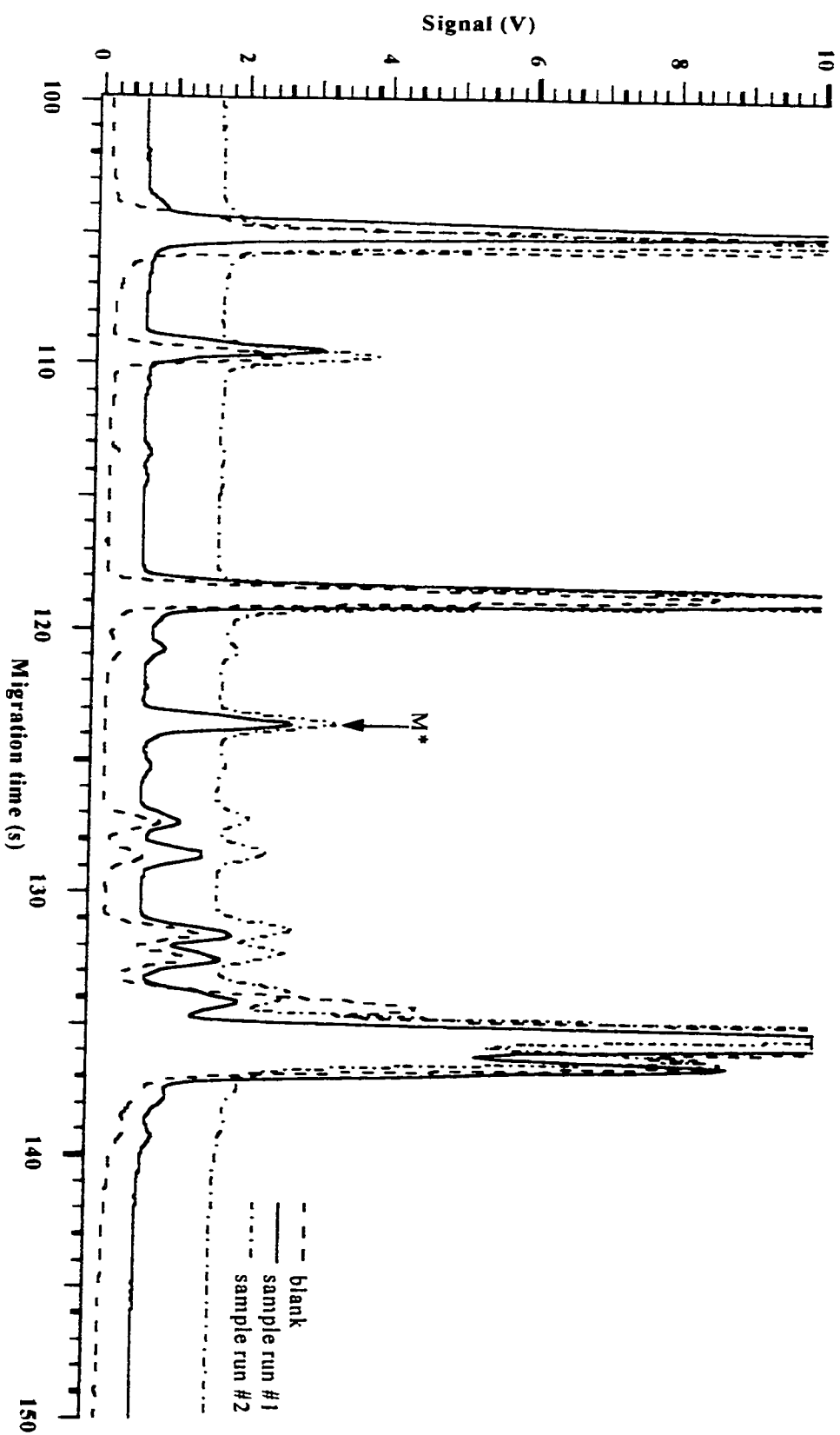
Figure 4.9: The CZE-LIF electropherograms of labelled tridecanoic acid (C_{13}). Capillary: 30 cm, 50 μm I.D., 140 μm O.D..
Run: 10 mM borate, pH 9, 12 kV. Injection: 1000 V, 5 s. Laser: 488 nm Ar^+, 12.1 mW. PMT: 1000 V.
Interference filter: 518DF25. Concentration: 10^{-8} M.
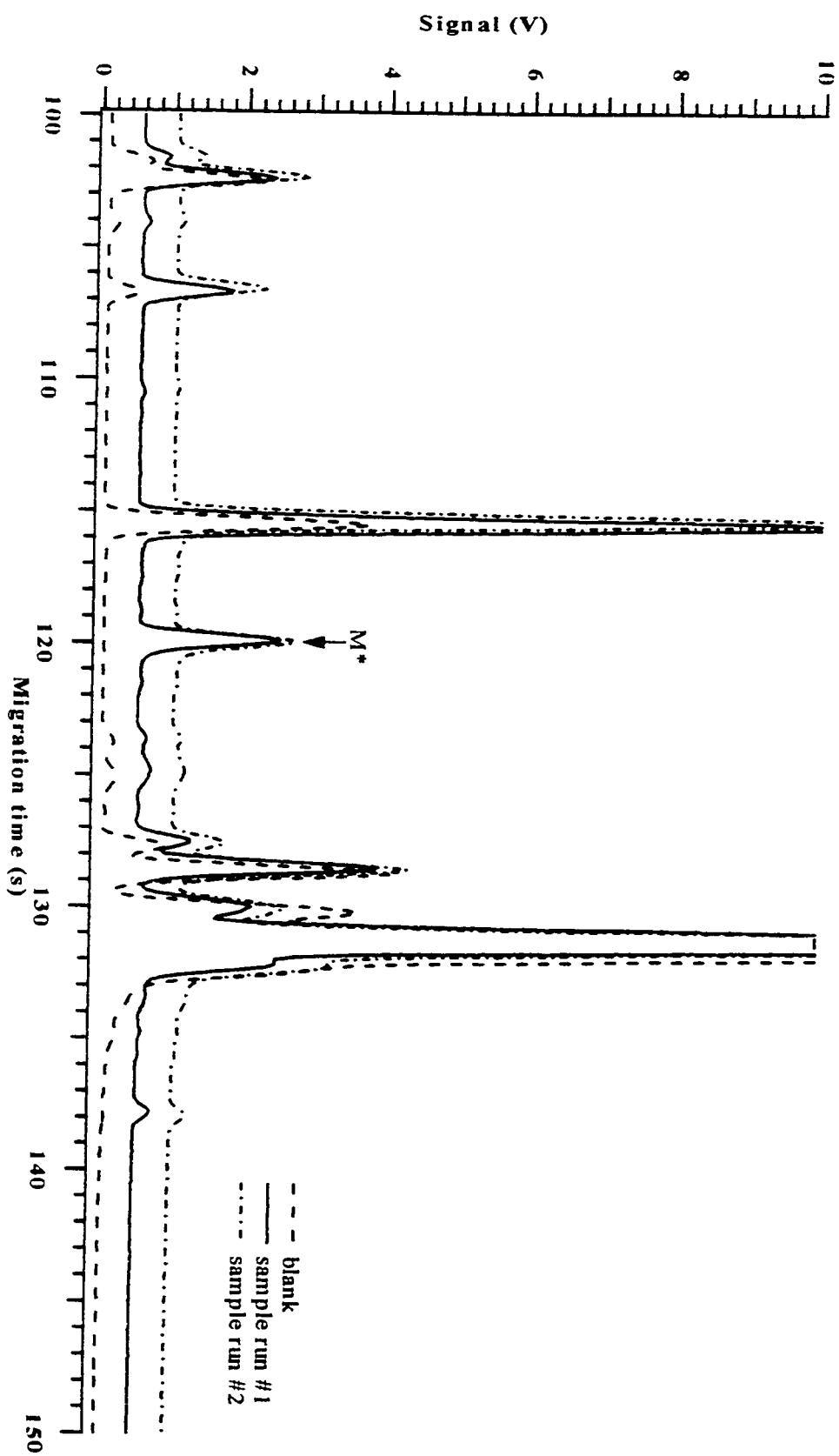
Figure 4.10: The CZE-LIF electropherograms of labelled myristic acid (C_{14}). Capillary: 30 cm, 50 μm I.D., 140 μm O.D.. Run: 10 mM borate, pH 9, 12 kV. Injection: 1000 V, 5 s. Laser: 488 nm Ar$^+$, 12.1 mW. PMT: 1000 V. Interference filter: 518DF25. Concentration: 10^{-8} M.
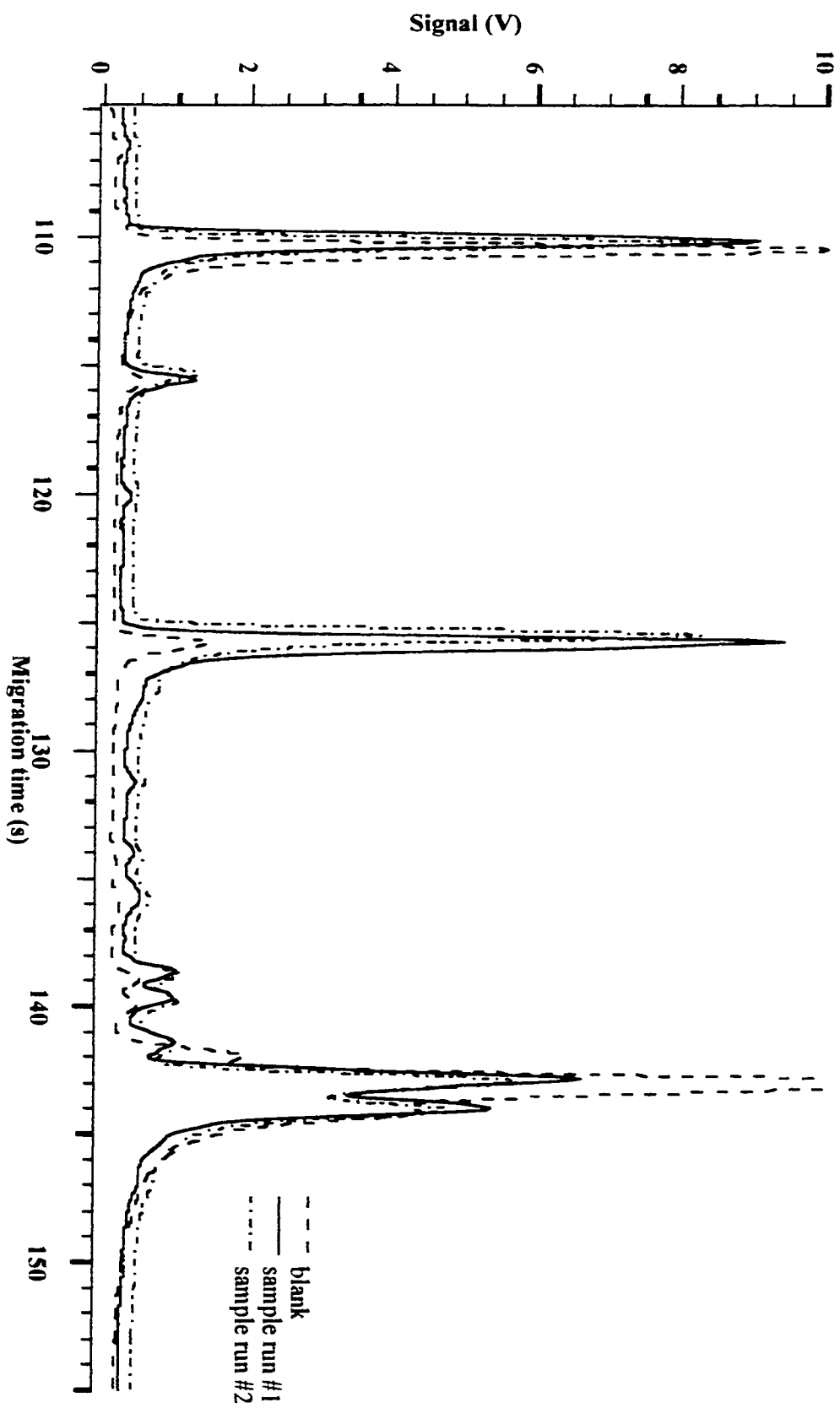
Figure 4.11: The CZE-LIF electropherograms of labelled pentadecanoic acid (C_{15}). Capillary: 30 cm, 50 μm I.D., 140 μm O.D.. Run: 10 mM borate, pH 9, 12 kV. Injection: 1000 V, 5 s. Laser: 488 nm Ar^+, 12.1 mW. PMT: 1000 V. Interference filter: 518DF25. Concentration: 10^{-8} M.
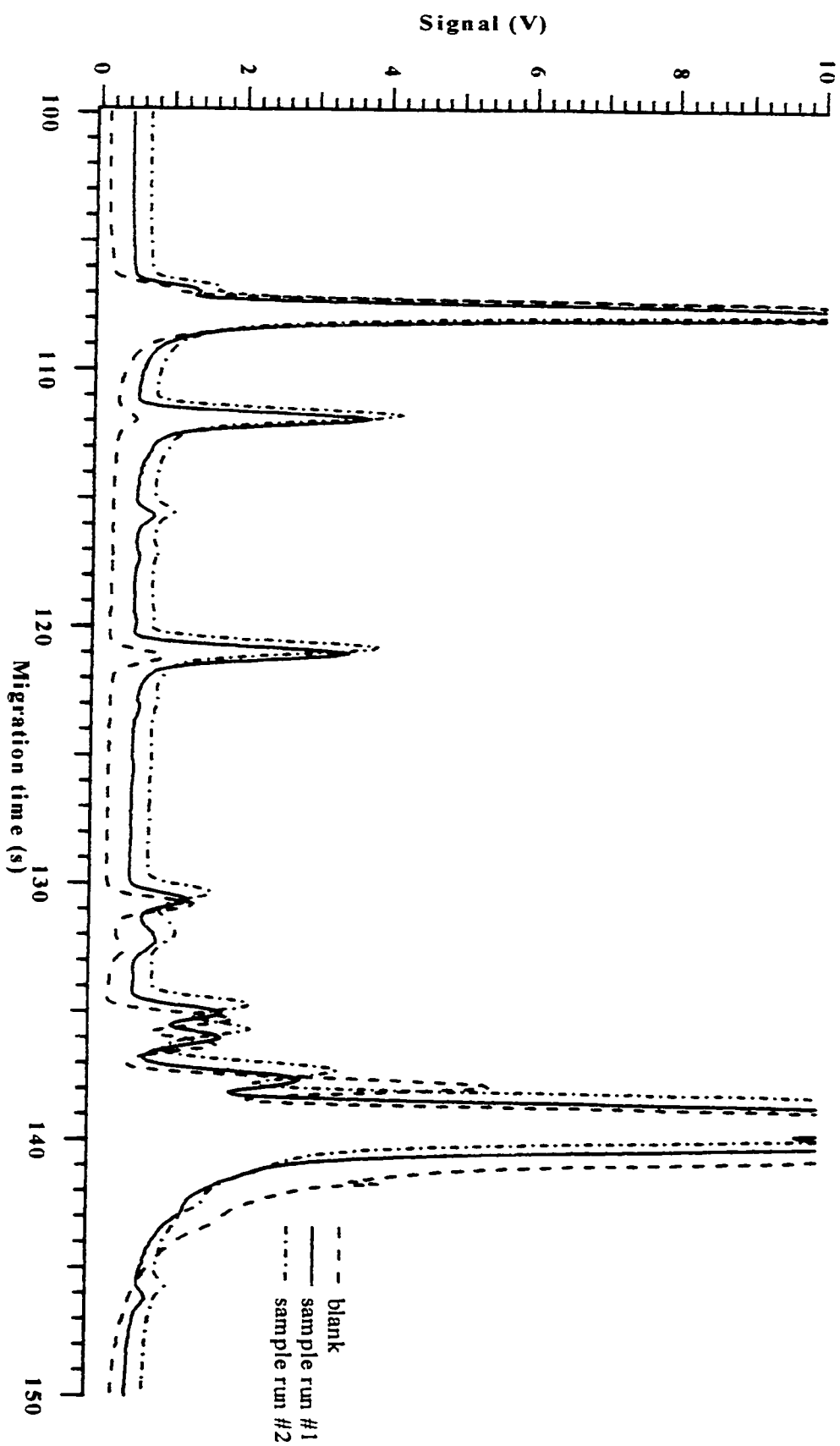
Figure 4.12: The CZE-LIF electropherograms of labelled palmitic acid (C_{16}). Capillary: 30 cm, 50 μm I.D., 140 μm O.D.. Run: 10 mM borate, pH 9, 12 kV. Injection: 1000 V, 5 s. Laser: 488 nm Ar$^+$, 12.1 mW. PMT: 1000 V. Interference filter: 518DF25. Concentration: 10^{-8} M.


blank
sample run #1
sample run #2

213

Figure 4.13: The CZE-LIF electropherograms of labelled heptadecanoic acid (C_{17}). Capillary: 30 cm, 50 μm I.D., 140 μm O.D.. Run: 10 mM borate, pH 9, 12 kV. Injection: 1000 V, 5 s. Laser: 488 nm Ar^+, 12.1 mW. PMT: 1000 V. Interference filter: 518DF25. Concentration: 10^{-8} M.
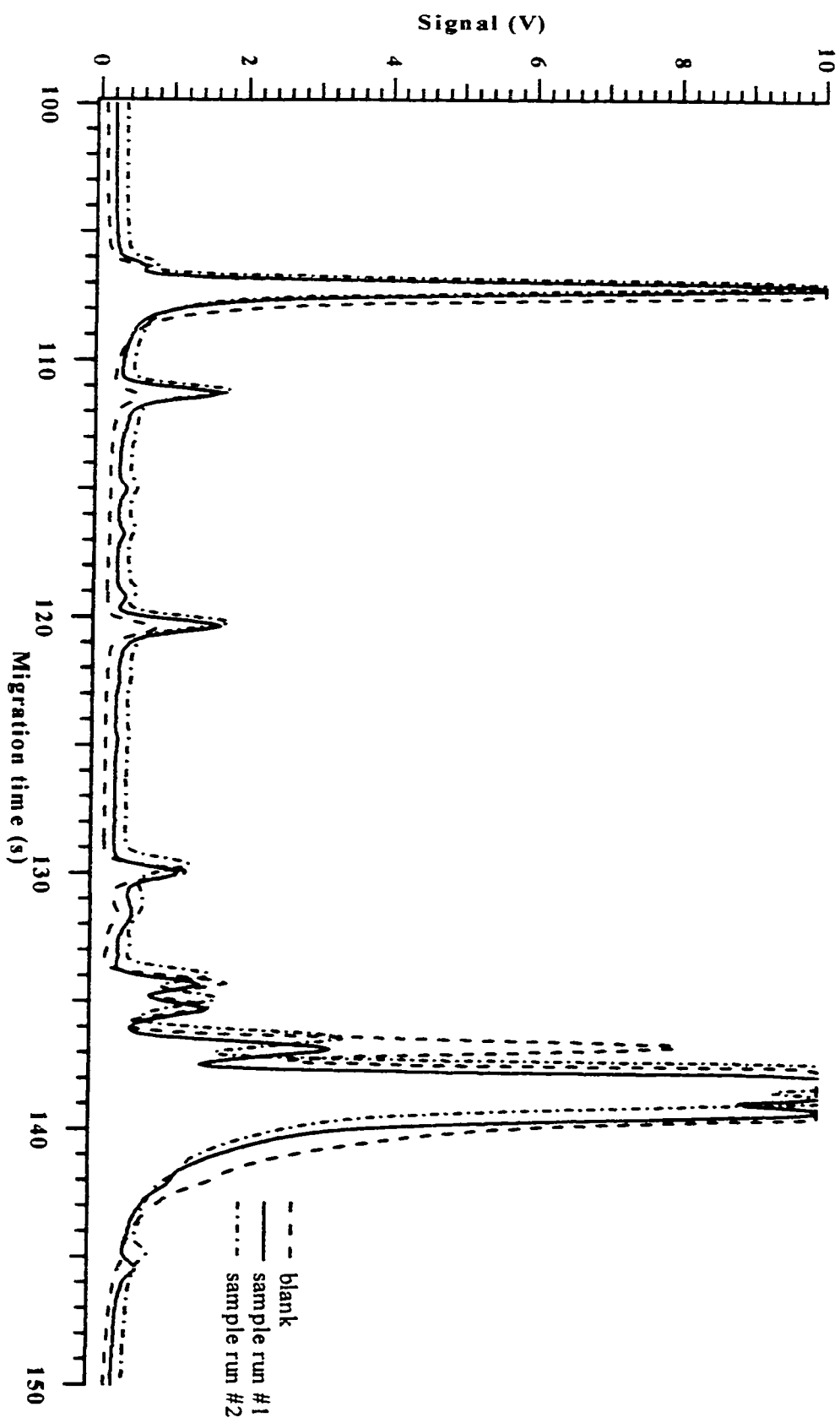
Figure 4.14: The CZE-LIF electropherograms of labelled stearic acid (C_{18}). Capillary: 30 cm, 50 µm I.D., 140 µm O.D.. Run: 10 mM borate, pH 9, 12 kV. Injection: 1000 V, 5 s. Laser: 488 nm Ar^+, 12.1 mW. PMT: 1000 V. Interference filter: 518DF25. Concentration: 10^{-8} M.

215

Figure 4.15: The CZE-LIF electropherograms of labelled nonadecanoic acid (C_{19}). Capillary: 30 cm, 50 μm I.D., 140 μm O.D.. Run: 10 mM borate, pH 9, 12 kV. Injection: 1000 V, 5 s. Laser: 488 nm Ar^+,12.1 mW. PMT: 1000 V. Interference filter: 518DF25. Concentration: 10^{-8} M.
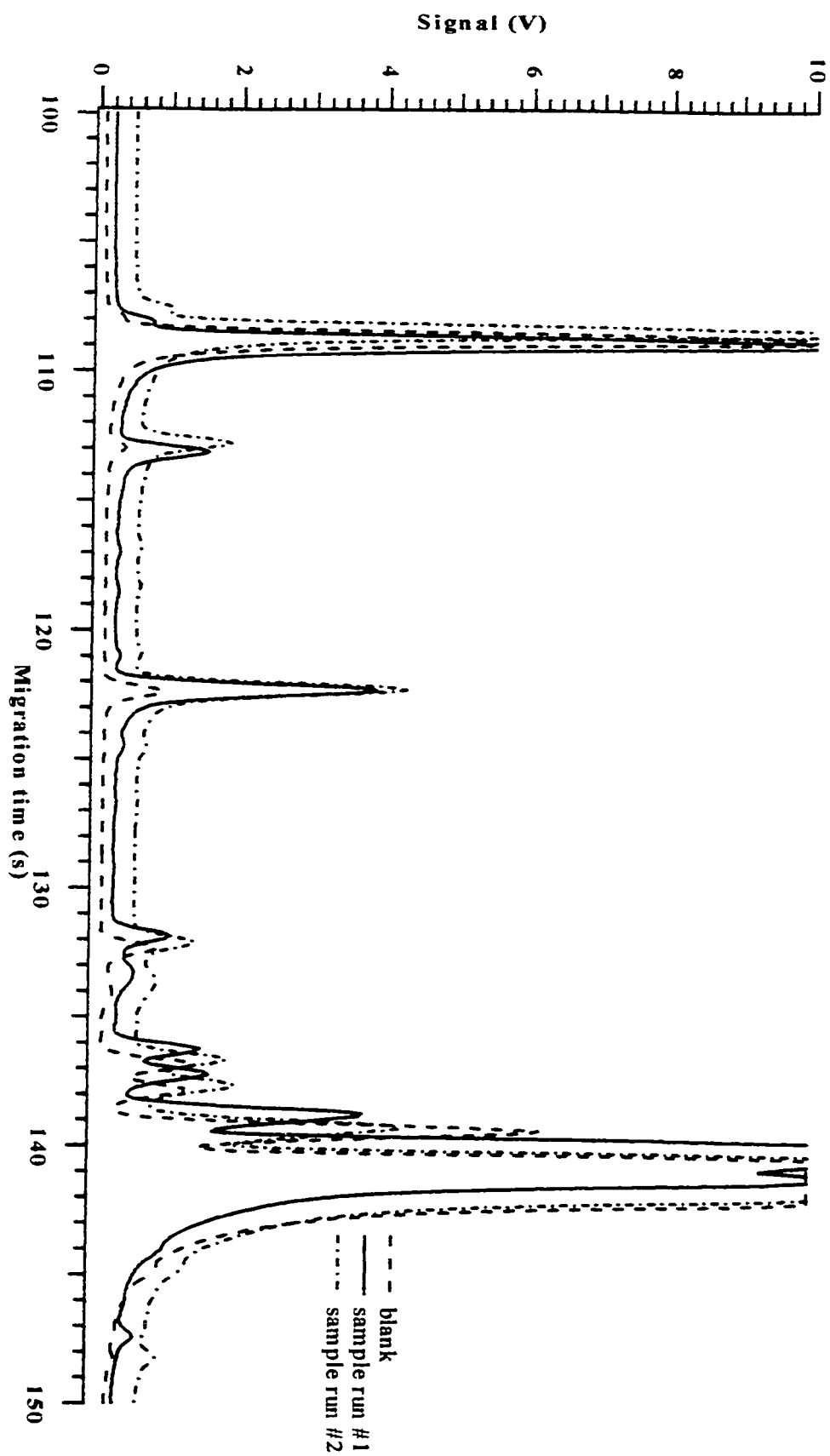
Figure 4.16: The CZE-LIF electropherograms of labelled arachidic acid (C_{20}). Capillary: 30 cm, 50 µm I.D., 140 µm O.D.. Run: 10 mM borate, pH 9, 12 kV. Injection: 1000 V, 5 s. Laser: 488 nm Ar^+, 12.1 mW. PMT: 1000 V. Interference filter: 518DF25. Concentration: 10^{-8} M.
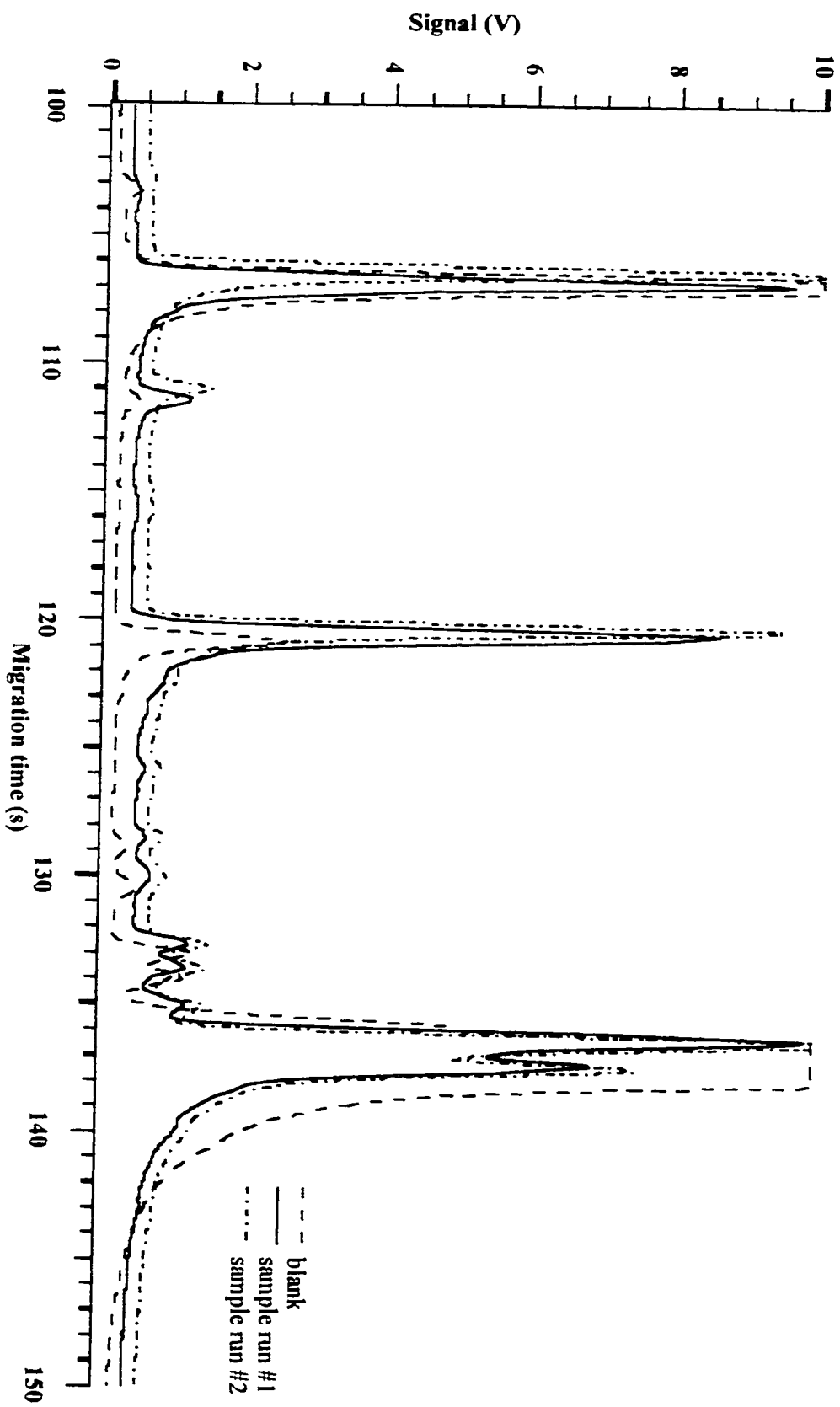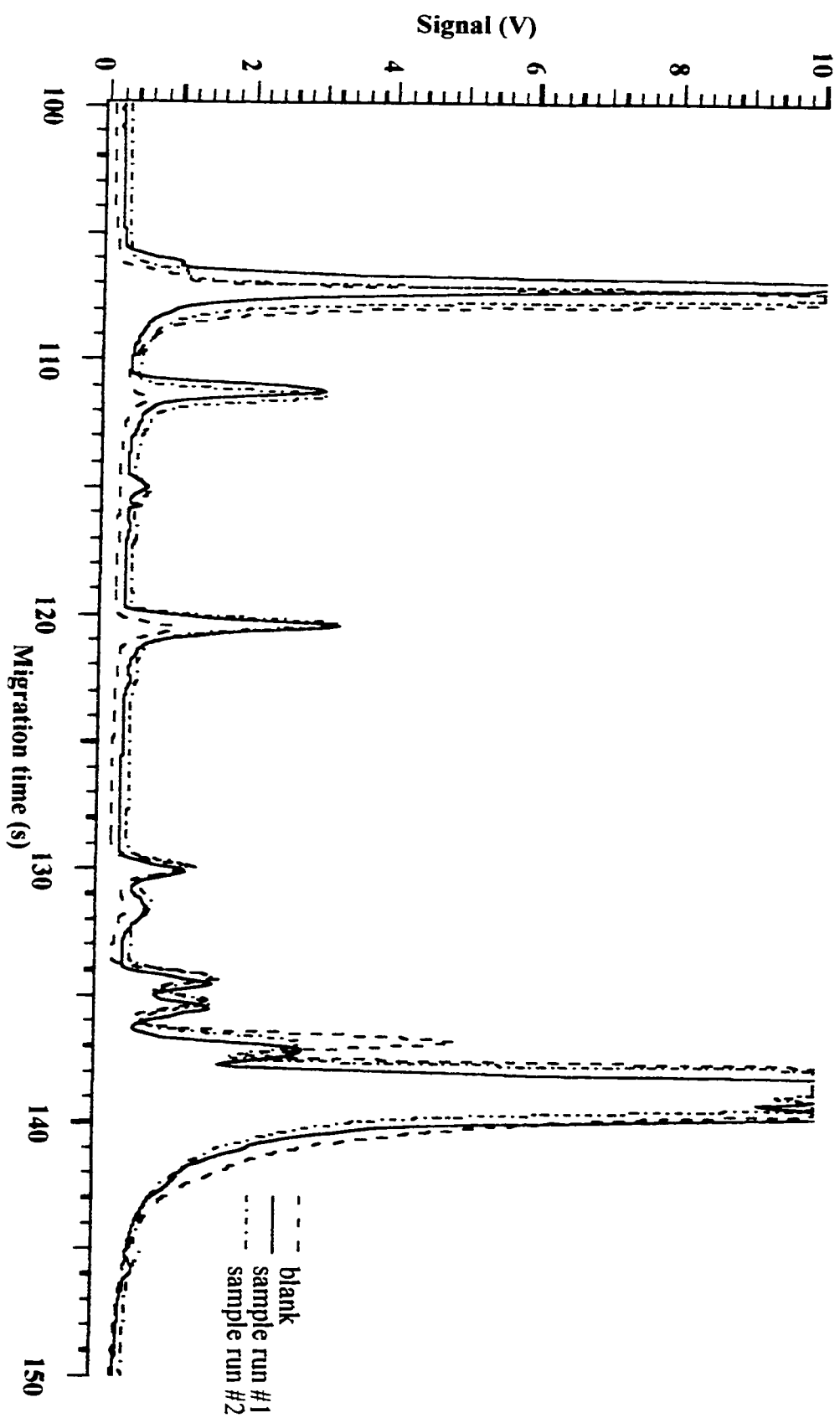
Figure 4.17: The CZE-LIF electropherograms of labelled heneicosanic acid (C_{21}). Capillary: 30 cm, 50 μm I.D., 140 μm O.D.. Run: 10 mM borate, pH 9, 12 kV. Injection: 1000 V, 5 s. Laser: 488 nm Ar$^+$, 12.1 mW. PMT: 1000 V. Interference filter: 518DF25. Concentration: 10^{-8} M.

218

Figure 4.18: The CZE-LIF electropherograms of labelled behenic acid (C₂₂). Capillary: 30 cm, 50 μm I.D., 140 μm O.D.. Run: 10 mM borate, pH 9, 12 kV. Injection: 1000 V, 5 s. Laser: 488 nm Ar⁺, 12.1 mW. PMT: 1000 V. Interference filter: 518DF25. Concentration: 10⁻⁸ M.

Figure 4.19: The CZE-LIF electropherograms of labelled tricosanic acid (C_{23}). Capillary: 30 cm, 50 μm I.D., 140 μm O.D..
Run: 10 mM borate, pH 9, 12 kV. Injection: 1000 V, 5 s. Laser: 488 nm Ar$^+$, 12.1 mW. PMT: 1000 V.
Interference filter: 518DF25. Concentration: 10^{-8} M.

Signal (V)

Migration time (s)

-- -- blank
------ sample run #1
······· sample run #2

220

Figure 4.20: The CZE-LIF electropherograms of labelled lignoceric acid (C_{24}). Capillary: 30 cm, 50 μm I.D., 140 μm O.D.. Run: 10 mM borate, pH 9, 12 kV. Injection: 1000 V, 5 s. Laser: 488 nm Ar$^+$, 12.1 mW. PMT: 1000 V. Interference filter: 518DF25. Concentration: 10^{-8} M.

221
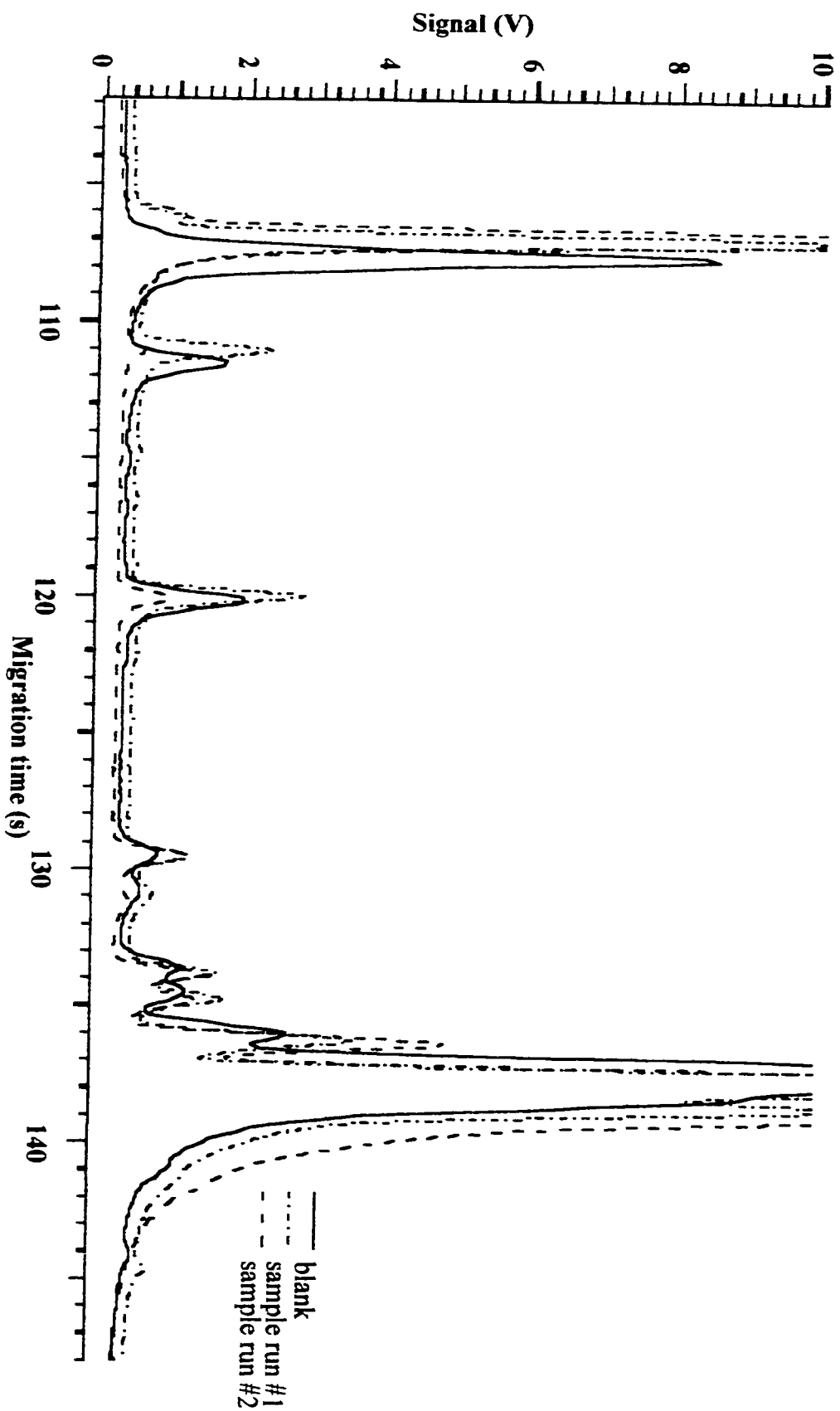
~124.5 s (n = 2). The LOD was calculated to be 9 pM or 0.02 attomoles when 2 nL of

sample was injected. The value of N was calculated to be $2*10^5$ plates.

The CZE-LIF electropherograms for labelled undecanoic acid can be found in

Figure 4.7. A peak for labelled undecanoic acid appears at an average migration time of

~121.0 s (n = 2). The LOD was calculated to be 5 pM or 0.01 attomoles when 2 nL of

sample was injected. The value of N was calculated to be $3*10^5$ plates.

The CZE-LIF electropherograms for labelled lauric acid can be found in

Figure 4.8. A peak for labelled lauric acid appears at an average migration time of

~124.0 s (n = 2). The LOD was calculated to be 29 pM or 0.06 attomoles when 2 nL of

sample was injected. The value of N was calculated to be $3*10^5$ plates.

The CZE-LIF electropherograms for labelled tridecanoic acid can be found in

Figure 4.9. A peak for labelled tridecanoic acid appears at an average migration time of

~120.0 s (n = 2). The LOD was calculated to be 23 pM or 0.05 attomoles when 2 nL of

sample was injected. The value for N was calculated to be $3*10^5$ plates.

The CZE-LIF electropherograms for the linear saturated FFAs with carbon

numbers 14 to 24 can be found in Figures 4.10 – 4.20. Product peaks for the labelled

FFAs C_{14} to C_{24} were not found which indicates that either the carbonyl-labelling

reactions for these FFAs were unsuccessful or the labelled FFA peaks are co-migrating

with a dye peak. A summary of all the data for the CZE-LIF separations of the

homologous series of labelled linear saturated FFAs ($C_6 - C_{24}$) can be found in Table 4.1.

Data plots of average migration time, peak height, peak area, LOD and number of

theoretical plates versus carbon number were constructed for the labelled purchased

FFAs to determine if there are any relationships between the variables and can be found

Table 4.1: A summary of all the data for the CZE-LIF separations of the homologous series of labelled linear saturated

FFAs ($C_6 - C_{24}$) (*n = 2).

Name of acid	Carbon number (n)	Average migration time (s)*	Average peak height (V)*	Average peak area (arbitrary units)*	Average limit of detection (pM)*	Number of theoretical plates (*10^5 plates)*
caproic	6	126.6	8.970	5.870	6	2
caprylic	8	123.9	3.804	2.302	14	3
nonanoic	9	125.0	6.621	4.168	8	2
capric	10	124.5	5.716	3.546	9	2
undecanoic	11	121.0	6.582	3.576	5	3
lauric	12	124.0	1.827	1.102	29	3
tridecanoic	13	120.0	1.792	1.062	23	3

223

in Figure 4.21. These data plots do not include the data from the CZE-LIF separations of the labelled synthesized FFAs because the efficiency of the procedure described in Section 4.3.5, in which the linear saturated FFAs are converted into their sodium salts, is not known. Therefore, combining the data points of the CZE-LIF separations of labelled purchased and synthesized FFAs is not valid. Data plots for the CZE-LIF separations of the labelled synthesized FFAs were not constructed because only two data points existed. This is not enough data points for any statistically valid plot. The data plots of average migration time, peak height, peak area, LOD or number of theoretical plates versus carbon number did not reveal any relationships between the variables.

Next, the separation of a mixture of labelled linear saturated FFAs $C_6 - C_{13}$ was attempted using CZE-LIF under the run conditions described in Section 4.2.4. The CZE-LIF electropherograms of the separation of a mixture of labelled linear saturated FFAs $C_6 - C_{13}$ can be found in Figure 4.22. Only the FFAs of carbon number 6 to 9 could be separated under these aqueous CZE-LIF conditions. The FFAs of carbon number greater than 9 were found to co-migrate.

Next, a Grignard-poly-AAP-coated capillary, provided by graduate student Dawn Richards, was used to try to improve the separation of the labelled linear saturated FFA mixture and the resulting CZE-LIF electropherograms performed under the run conditions described in Section 4.2.6 can be found in Figure 4.23. In this separation a peak for the labelled FFA C_{10} could be found which could not be seen in the CZE-LIF separation of the mixture without a coated capillary. In addition the peak for the labelled FFA C_8 found in the CZE-LIF separation of the mixture without a coated capillary could not be found in this separation which perhaps illustrates degradation in separation. Peaks

Figure 4.21: The data plots of average A) migration time, B) peak height, C) peak area, D) limit of detection, and E) number of theoretical plates versus carbon number for the CZE-LIF separations of the labelled purchased FFAs (n = 2).
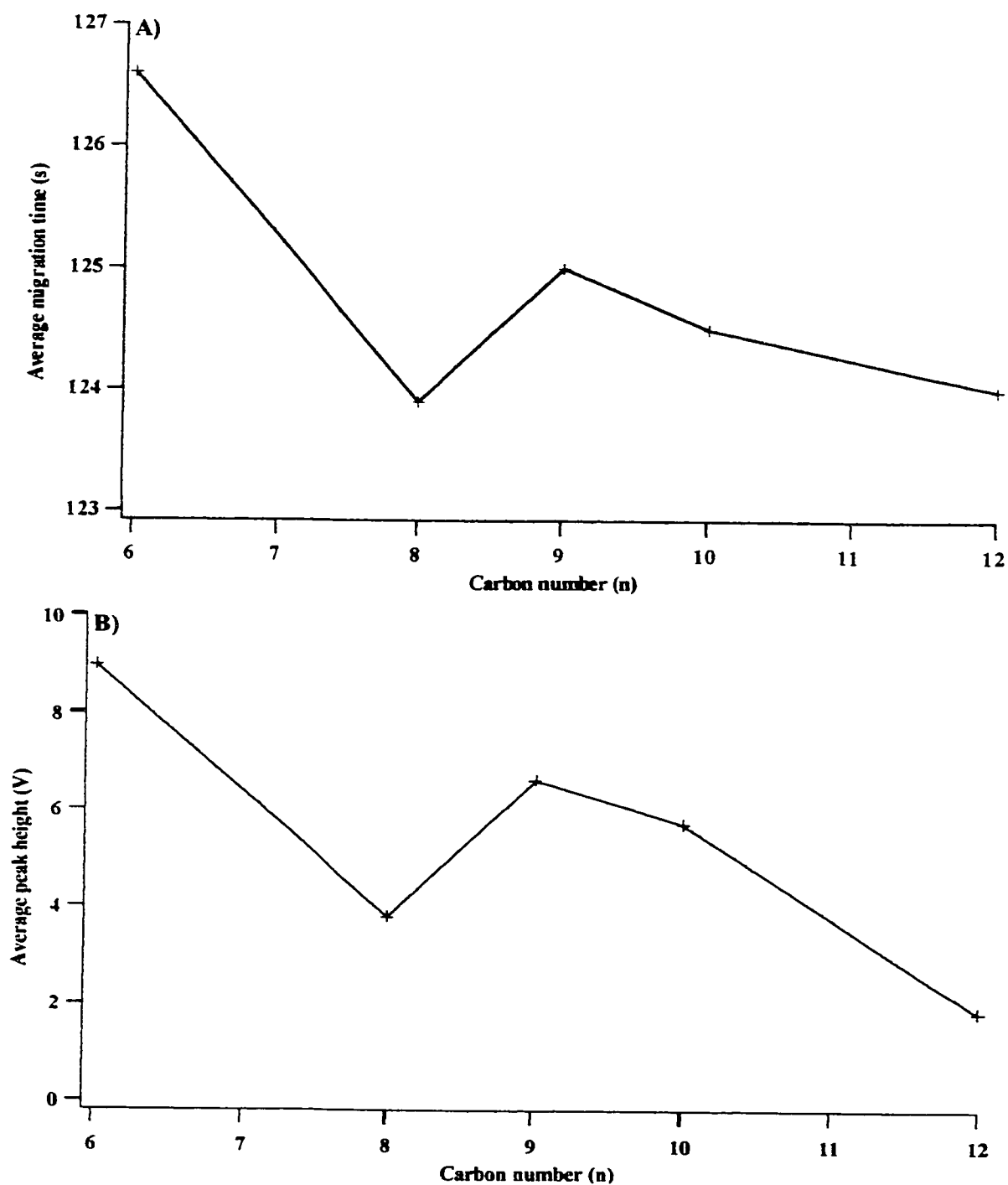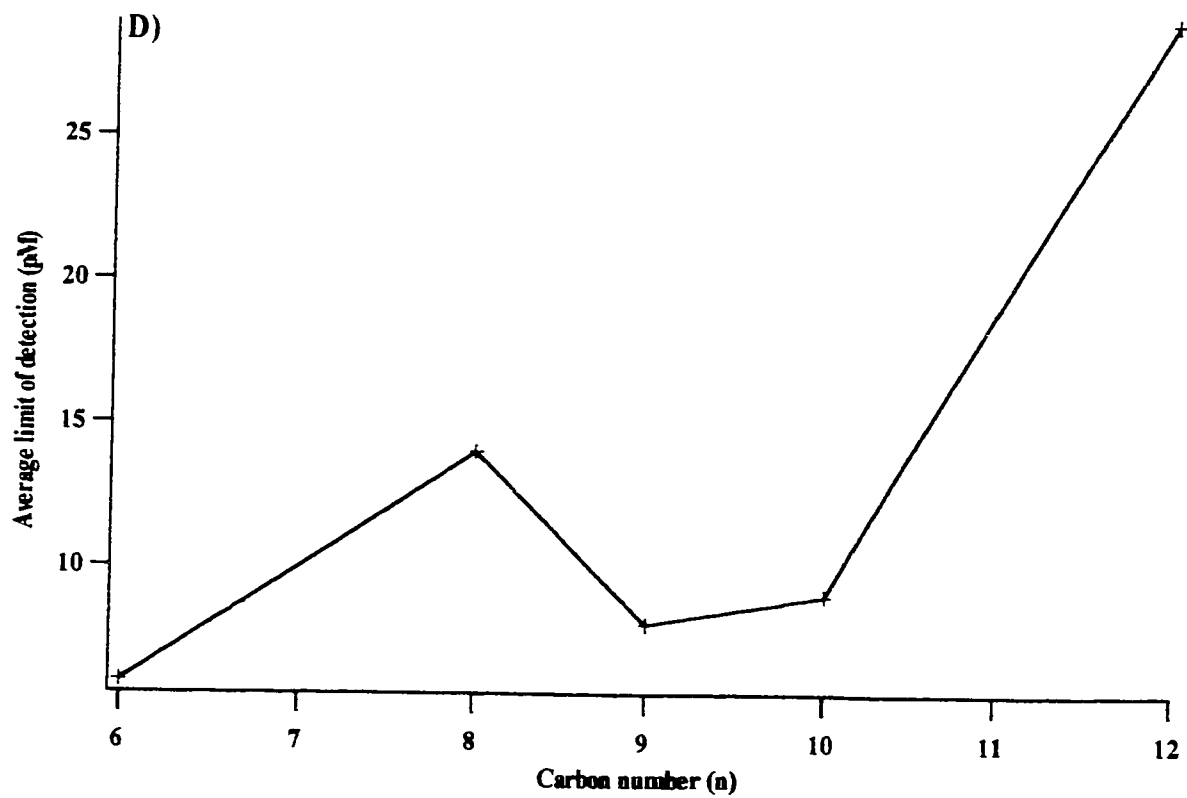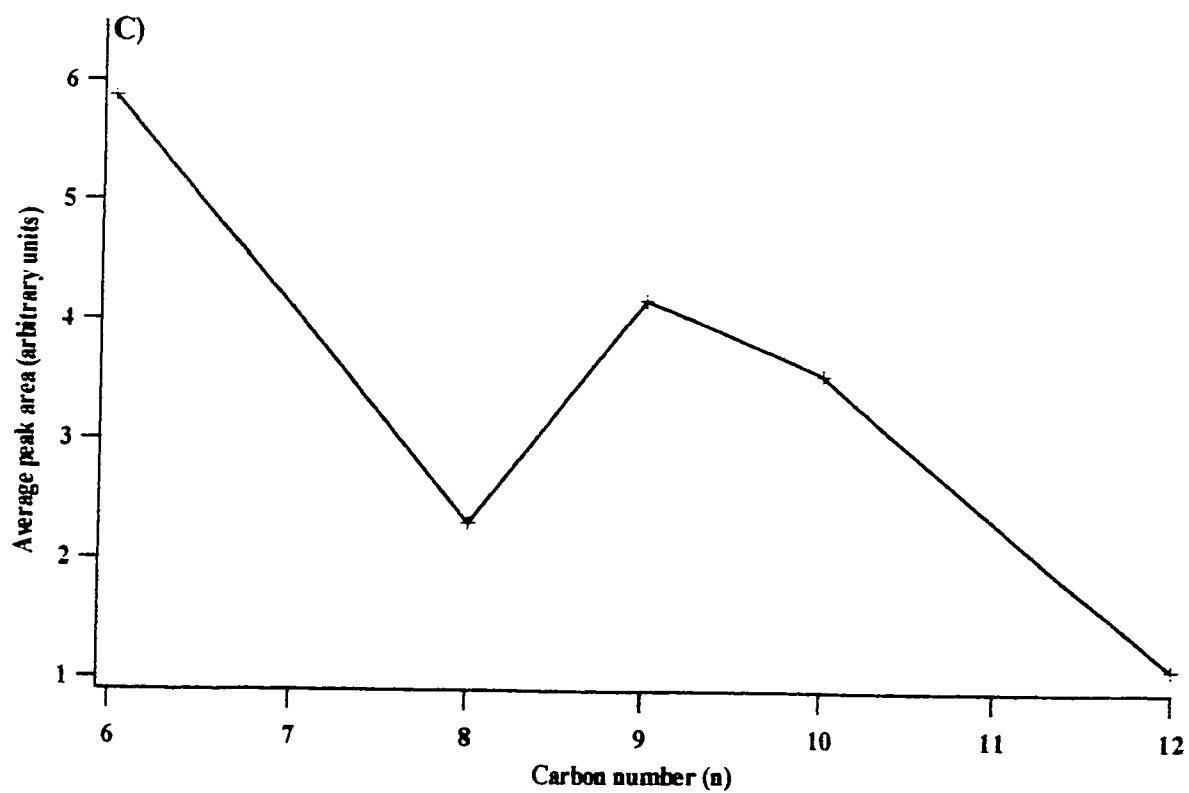
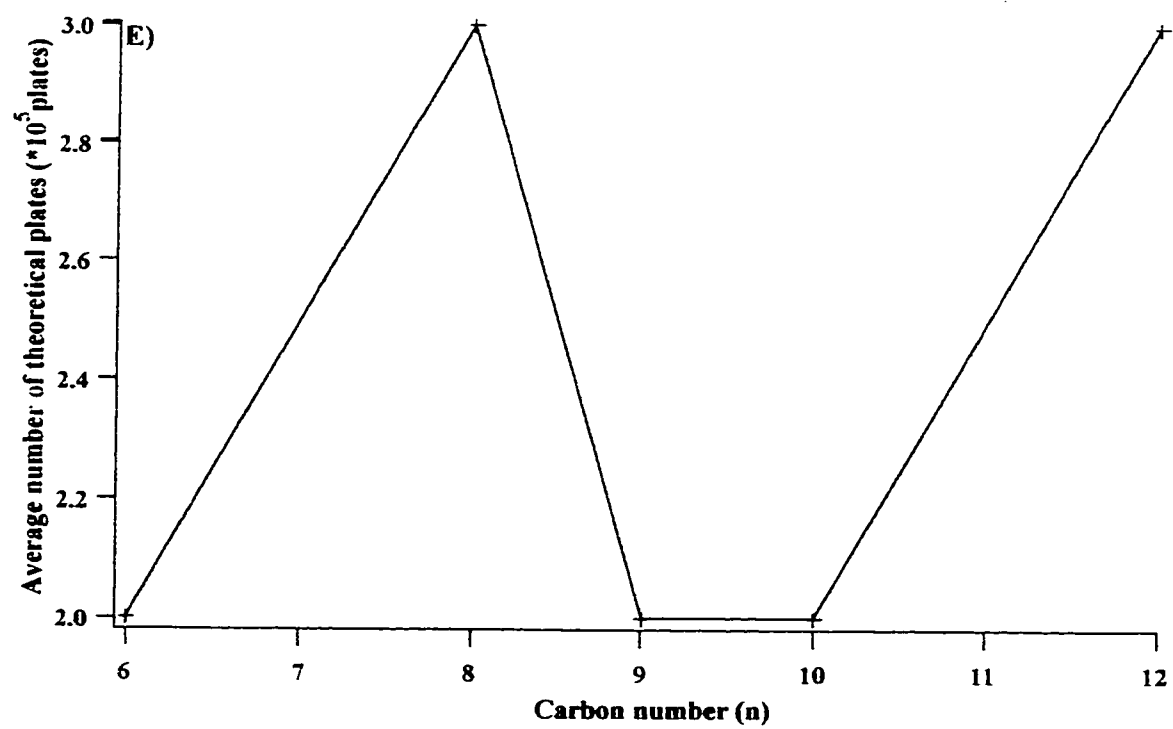**Figure 4.21:** (continued)

Figure 4.21: (continued)

E)

Carbon number (n)

Average number of theoretical plates ($*10^5$ plates)

3.0
2.8
2.6
2.4
2.2
2.0

6   7   8   9   10   11   12

Figure 4.22: The CZE-LIF electropherograms of the separation of a labelled linear saturated FFA mixture ($C_6 - C_{13}$).

Capillary: 30 cm, 50 μm I.D., 140 μm O.D.. Run: 10 mM borate, pH 9, 12 kV. Injection: 1000 V, 5 s.

Laser: 488 nm Ar$^+$, 12.1 mW. PMT: 1000 V. Interference filter: 518DF25. Concentration: 10^{-8} M. The CZE-LIF

electropherogram contains A) FFA C_6; B) FFAs C_6, C_8; C) FFAs C_6, C_8, C_9; D) FFAs C_6, C_8, C_9, C_{10};

E) FFAs C_6, C_8, C_9, C_{10}, C_{11}; F) FFAs C_6, C_8, C_9, C_{10}, C_{11}, C_{12}; G) FFAs C_6, C_8, C_9, C_{10}, C_{11}, C_{12}, C_{13}.

228

Figure 4.22: (continued)

229
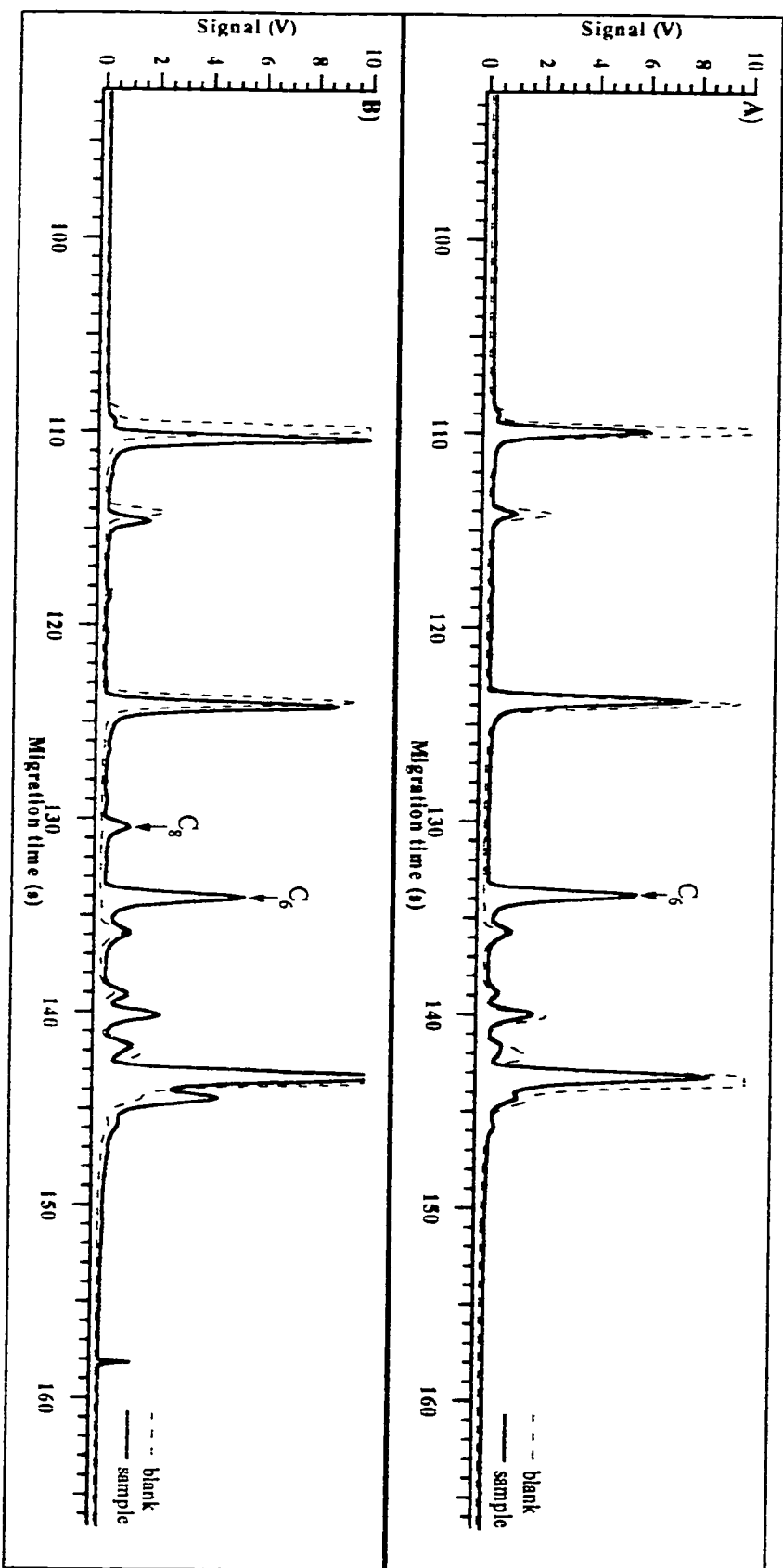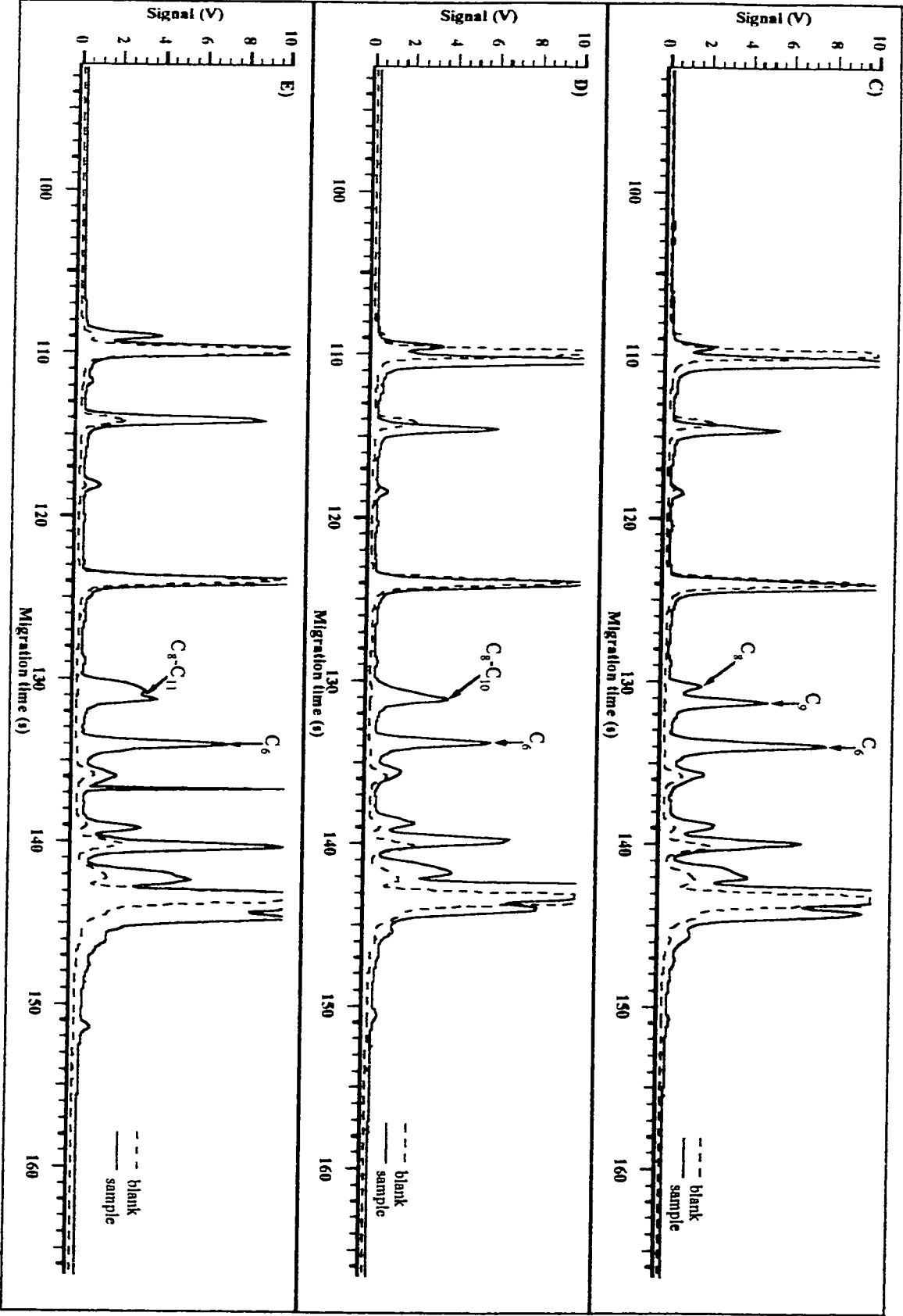
Figure 4.22: (continued)
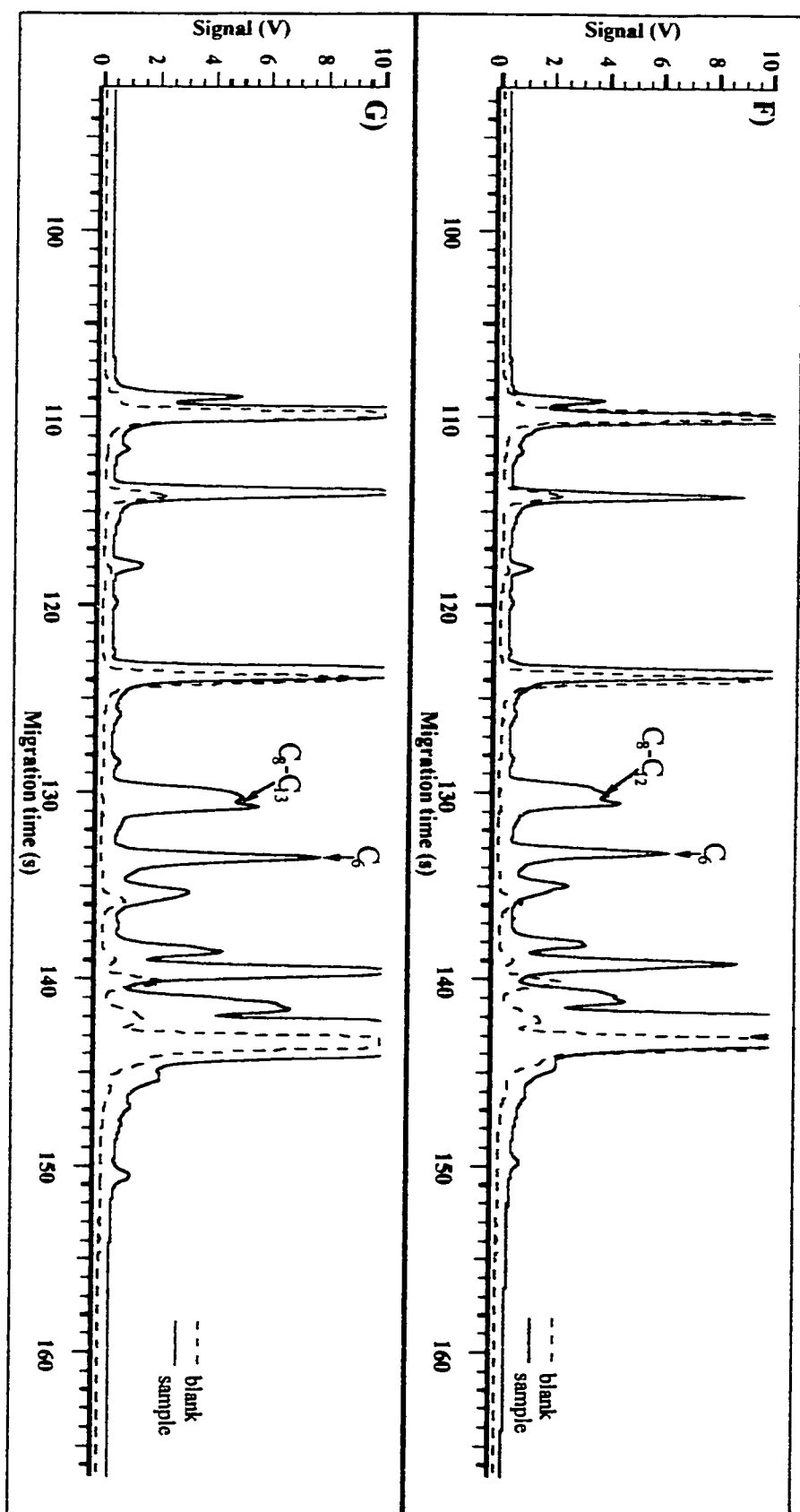
Figure 4.23: The CZE-LIF electropherograms of the separation of a labelled linear saturated FFA mixture ($C_6 - C_{13}$) using a Grignard-poly-AAP-coated capillary. Capillary: 40 cm, 50 μm I.D., 140 μm O.D.. Run: 10 mM borate, pH 9, -16 kV. Injection: -1000 V, 5 s. Laser: 488 nm Ar$^+$, 12.1 mW. PMT: 1000 V. Interference filter: 518DF25. Concentration: 10^{-7} M. The CZE-LIF electropherogram contains A) FFA C_6; B) FFAs C_6, C_8; C) FFAs C_6, C_8, C_9; D) FFAs C_6, C_8, C_9, C_{10}; E) FFAs C_6, C_8, C_9, C_{10}, C_{11}; F) FFAs C_6, C_8, C_9, C_{10}, C_{11}, C_{12}; G) FFAs C_6, C_8, C_9, C_{10}, C_{11}, C_{12}, C_{13}.

231

Figure 4.23: (continued)

232

Figure 4.23: (continued)

233
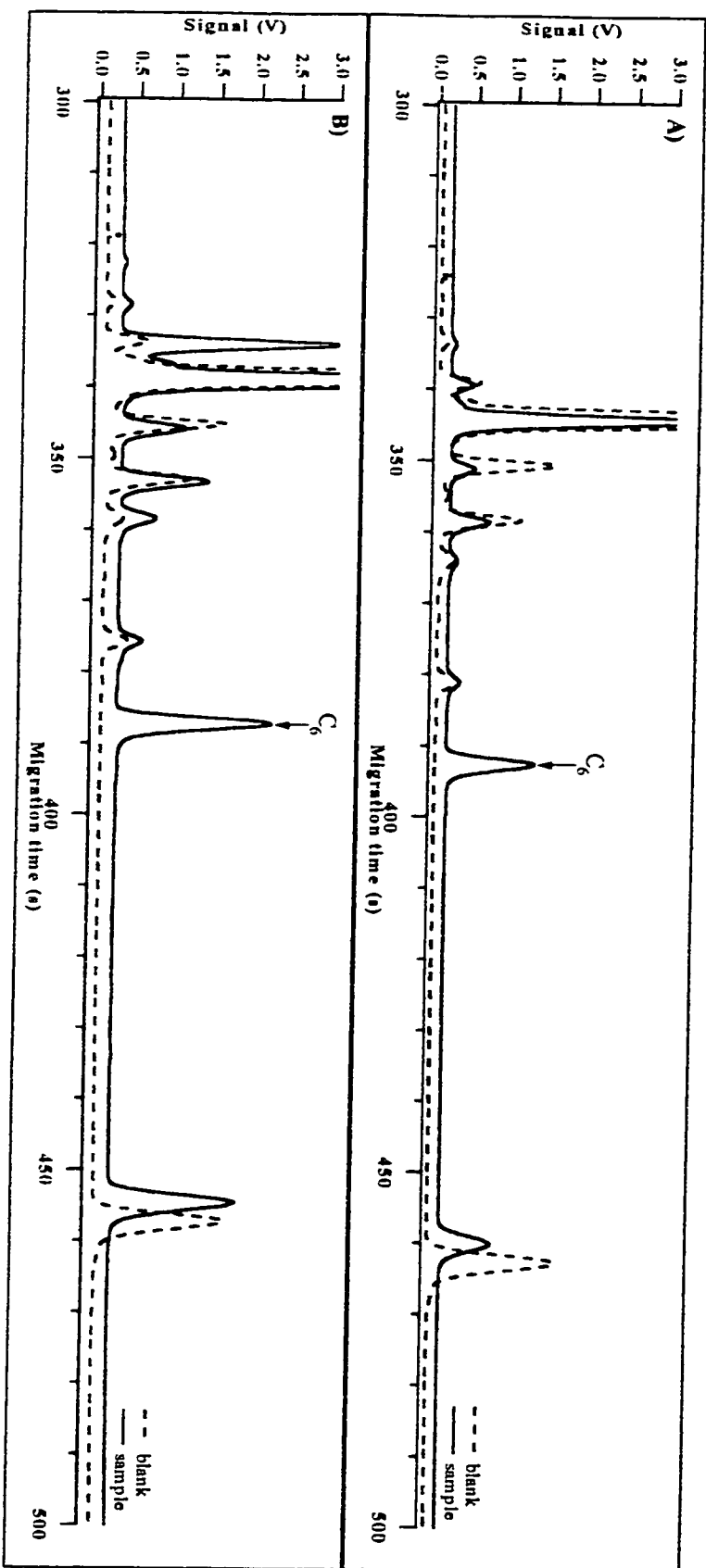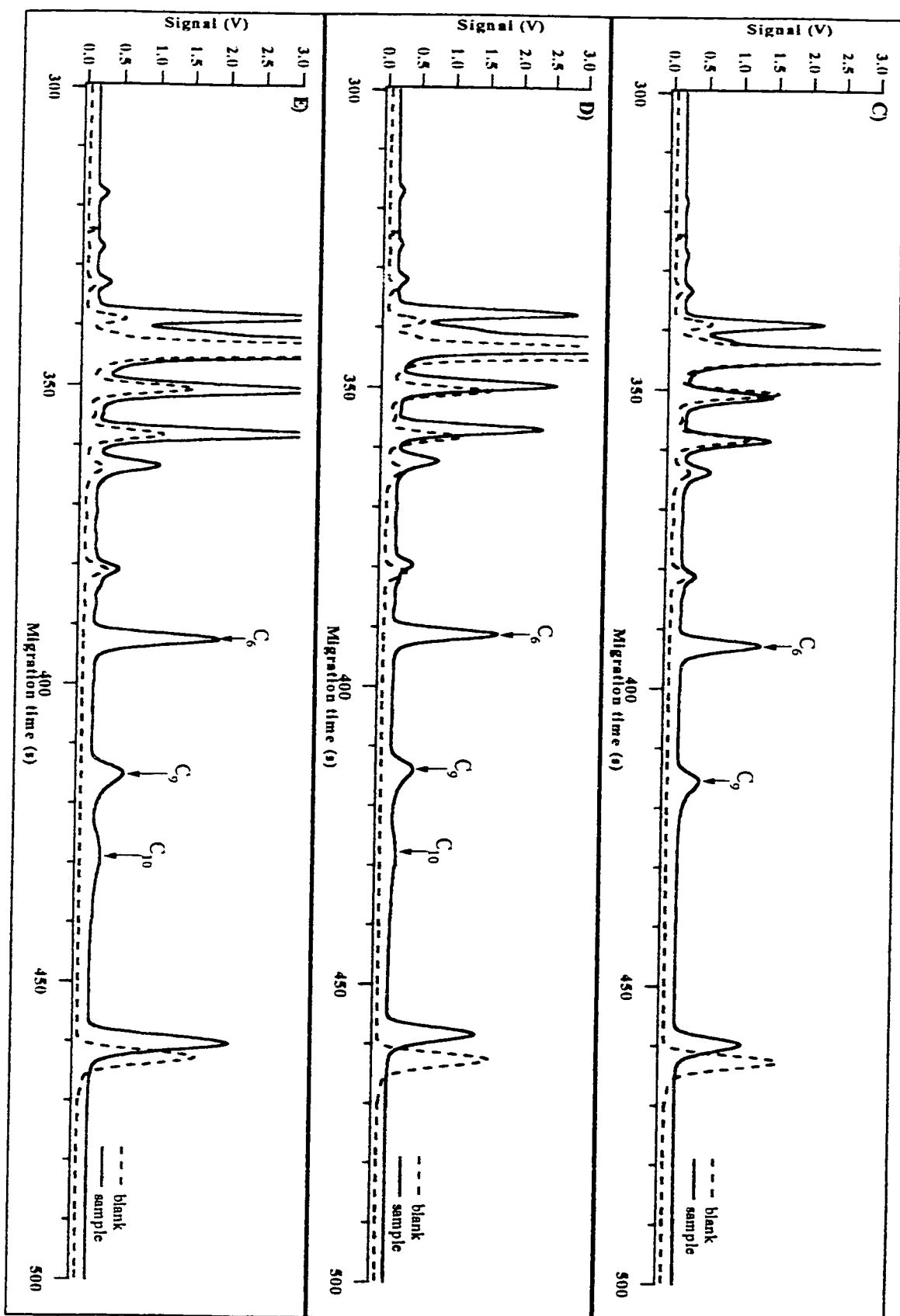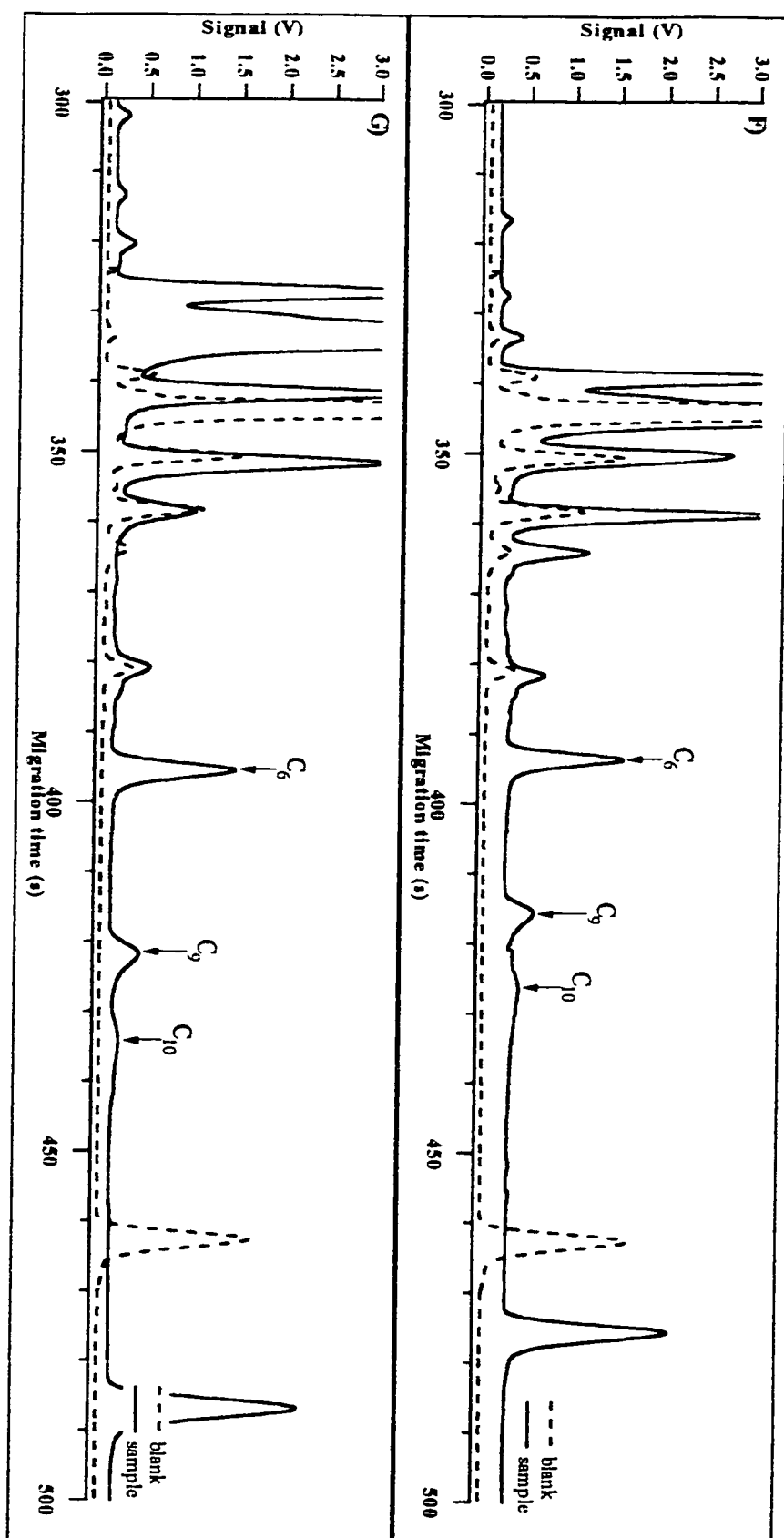
for the labelled FFAs with an alkyl chain length greater than C_{10} were not found in the CE separation using a Grignard-poly-AAP-coated capillary. Overall, it was concluded that the use of a Grignard-poly-AAP-coated capillary did not help in the separation of the mixture of FFAs.

4.3.2 CZE-LIF separations using a cyclodextrin

Next, CZE-LIF separations using an electrolyte containing a cyclodextrin as used in references 63 and 64 were performed in attempts to enhance separation selectivity and separate the labelled FFA peaks from the excess dye peaks. The chiral CZE-LIF run conditions for the separation of labelled caproic acid are described in Section 4.2.7. Labelled caproic acid was used to examine what effects adding dimethyl-β-cyclodextrin or trimethyl-β-cyclodextrin to the electrolyte has on the CZE separation. The effect of dimethyl-β-cyclodextrin in the CZE electrolyte was investigated using concentrations of 1 mM and 10 mM in 10 mM borate buffer. The resulting chiral CZE-LIF electropherograms can be found in Figures 4.24 and 4.25, respectively. When the electropherogram in Figure 4.24 is compared to the one in Figure 4.5 it is evident that the presence of 1 mM dimethyl-β-cyclodextrin in the electrolyte shortens the migration time of the labelled caproic acid peak. When 10 mM dimethyl-β-cyclodextrin was added to the running buffer the peak for labelled caproic acid could not be found. Thus it can be concluded that the peak for labelled caproic acid is co-migrating with a dye peak. Next, the effect of trimethyl-β-cyclodextrin present in the electrolyte was investigated using concentrations of 1 mM and 5 mM in 10 mM borate buffer. The resulting chiral CZE-LIF electropherograms can be found in Figures 4.26 and 4.27, respectively. In

Figure 4.24: The CZE-LIF electropherograms of labelled caproic acid (C_6). Capillary: 30 cm, 50 μm I.D., 140 μm O.D.. Run: 10 mM borate and 1 mM dimethyl-ß-cyclodextrin, pH 9, 12 kV. Injection: 1000 V, 5 s. Laser: 488 nm Ar$^+$, 12.1 mW. PMT: 1000 V. Interference filter: 518DF25. Concentration: 10^{-8} M.
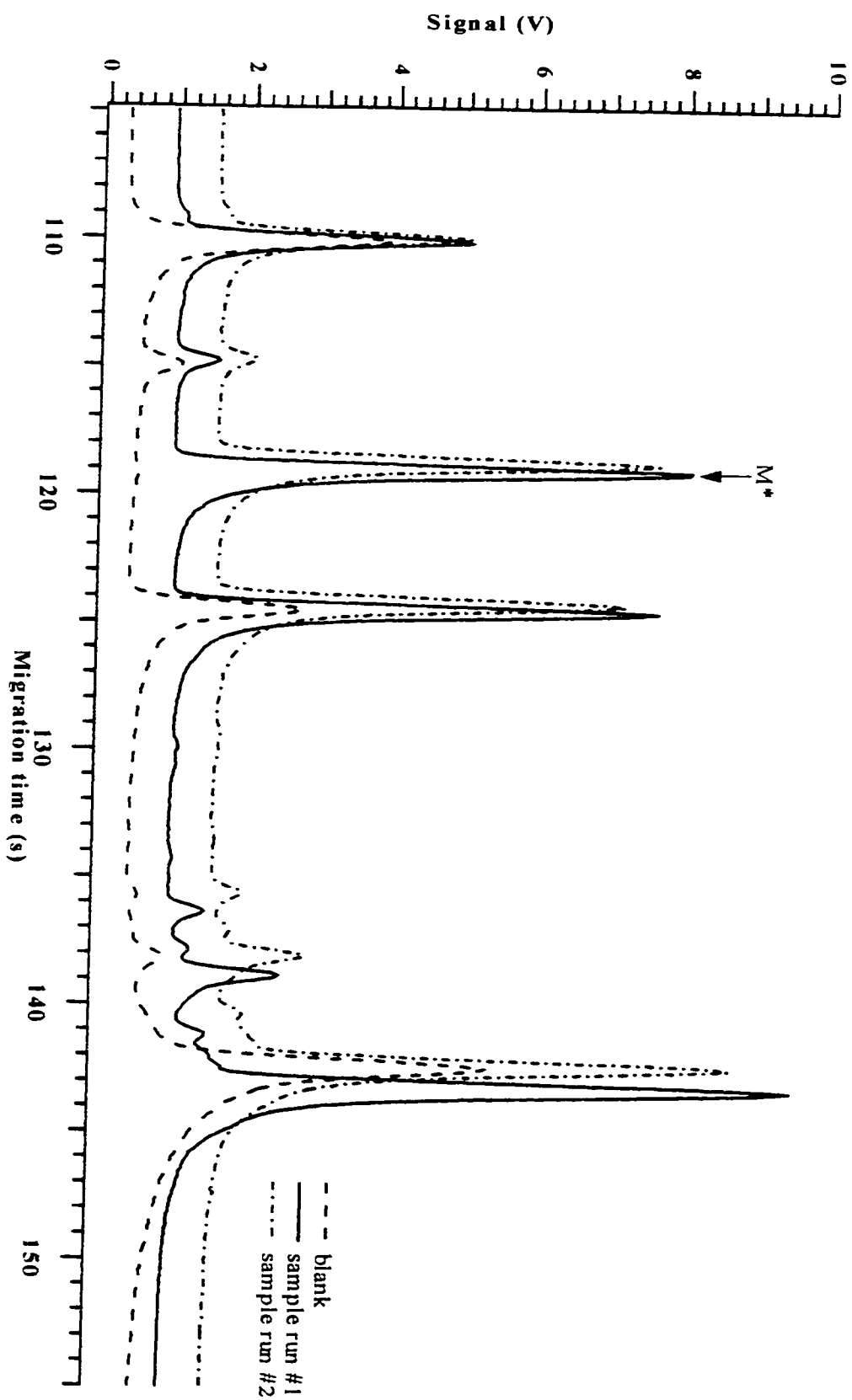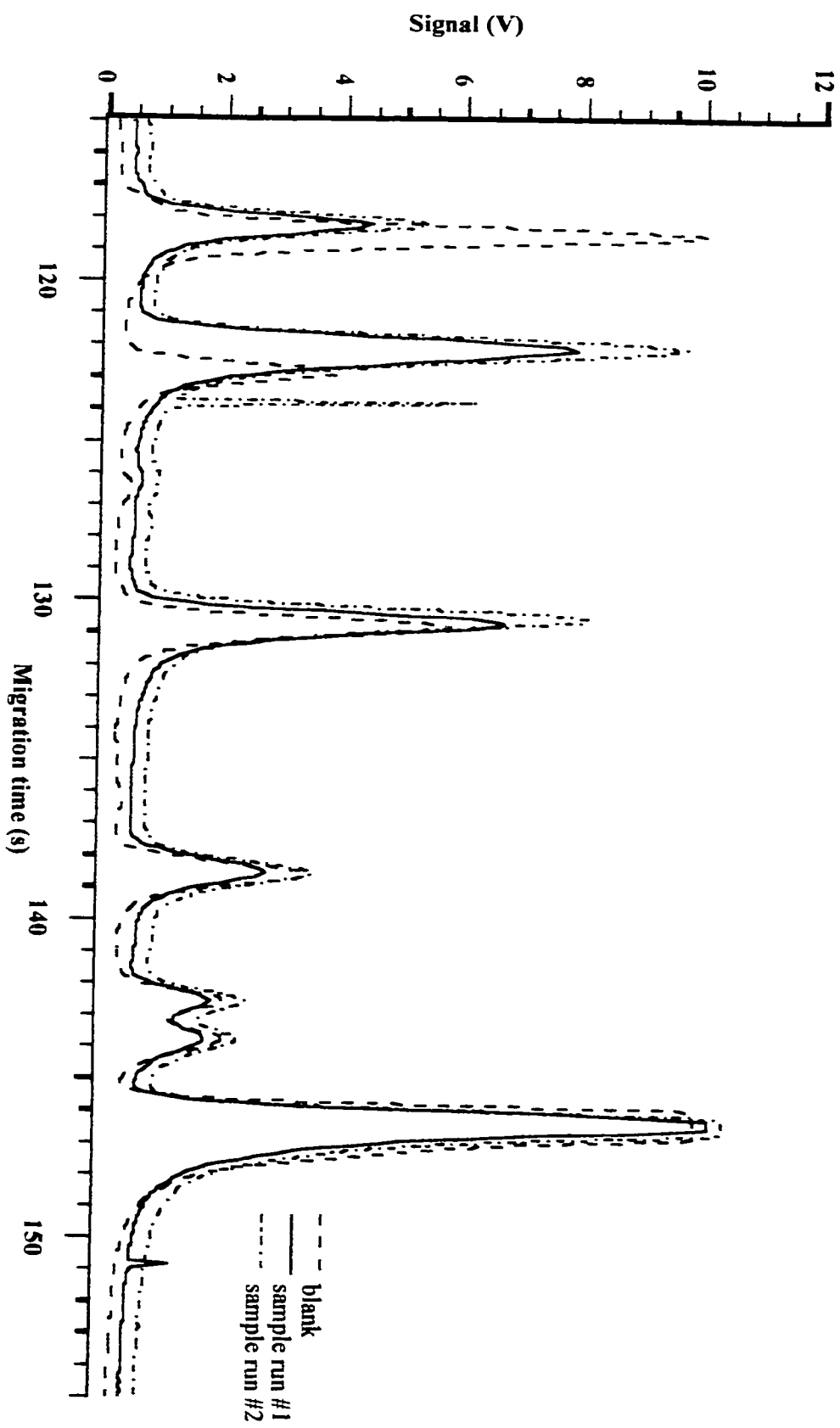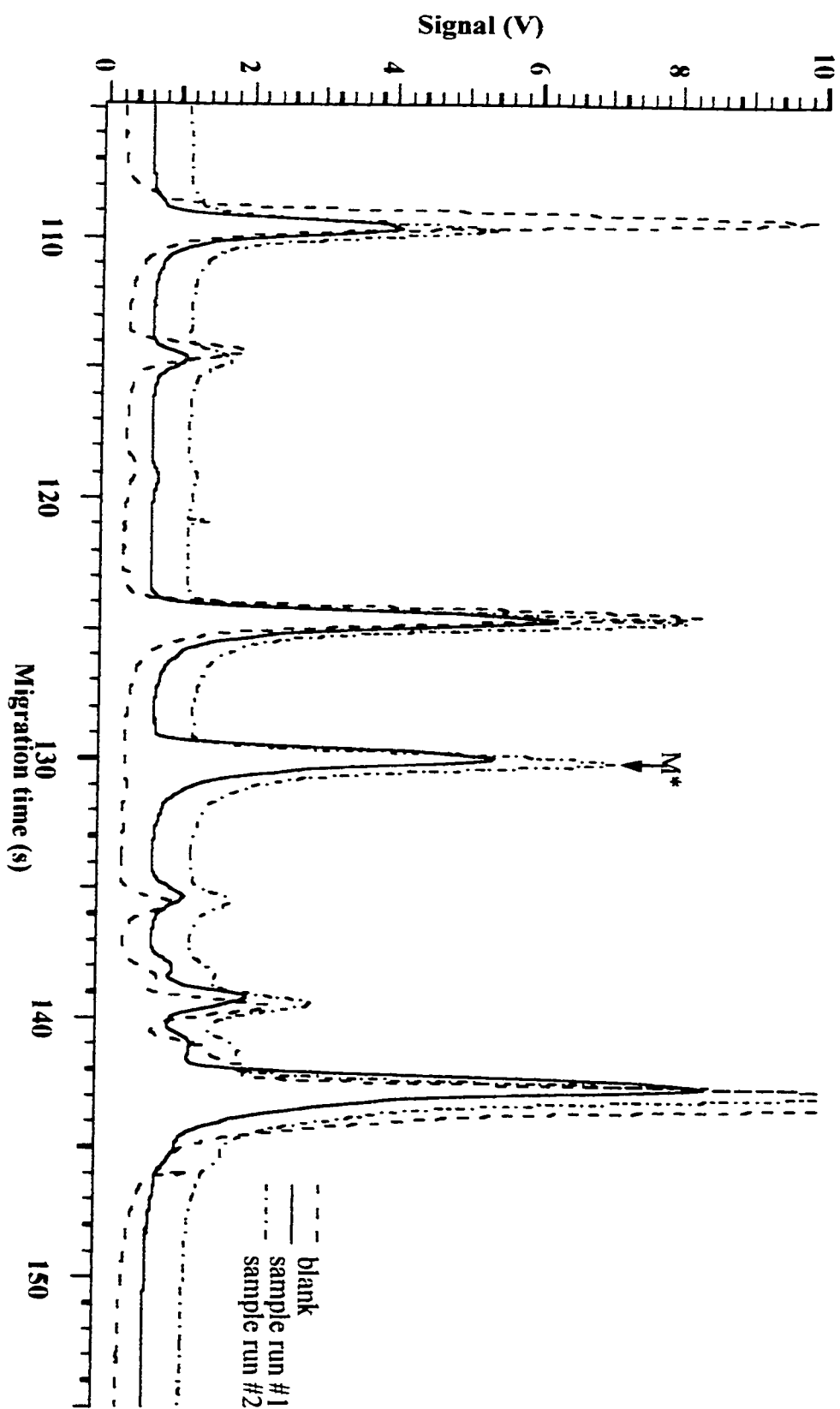
Figure 4.25: The CZE-LIF electropherograms of labelled caproic acid (C_6). Capillary: 30 cm, 50 μm I.D., 140 μm O.D..

Run: 10 mM borate and 10 mM dimethyl-ß-cyclodextrin, pH 9, 12 kV. Injection: 1000 V, 5 s.

Laser: 488 nm Ar^+, 12.1 mW. PMT: 1000 V. Interference filter: 518DF25. Concentration: 10^{-8} M.

Figure 4.26: The CZE-LIF electropherograms of labelled caproic acid (C_6). Capillary: 30 cm, 50 µm I.D., 140 µm O.D.. Run: 10 mM borate and 1 mM trimethyl-β-cyclodextrin, pH 9, 12 kV. Injection: 1000 V, 5 s. Laser: 488 nm Ar^+, 12.1 mW. PMT: 1000 V. Interference filter: 518DF25. Concentration: 10^{-8} M.

237

Figure 4.27: The CZE-LIF electropherograms of labelled caproic acid (C_6). Capillary: 30 cm, 50 μm I.D., 140 μm O.D..
Run: 10 mM borate and 5 mM trimethyl-ß-cyclodextrin, pH 9, 12 kV. Injection: 1000 V, 5 s.
Laser: 488 nm Ar^+, 12.1 mW. PMT: 1000 V. Interference filter: 518DF25. Concentration: 10^{-8} M.
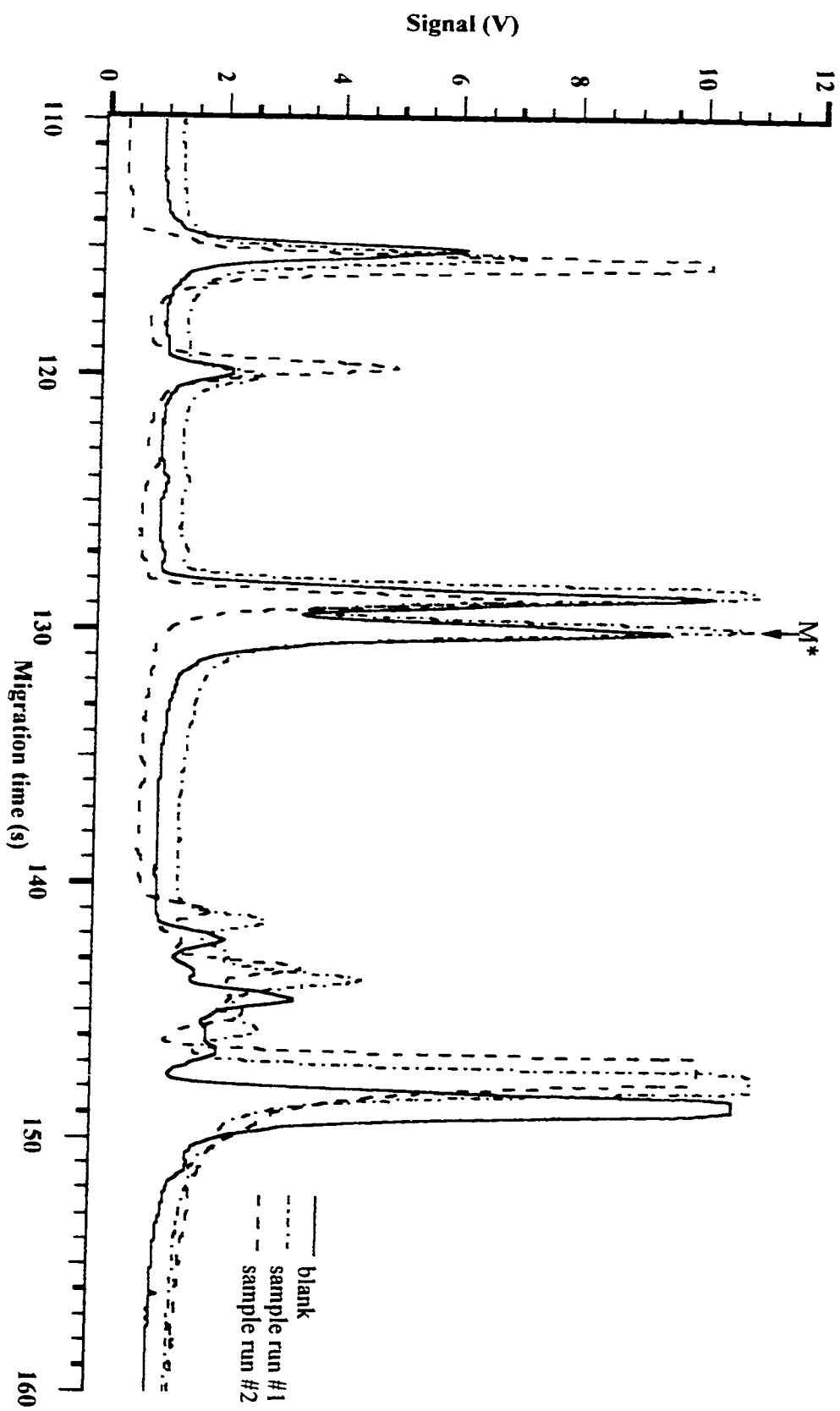
comparing Figures 4.5, 4.24, and 4.26 it is apparent that the presence of 1 mM trimethyl-β-cyclodextrin in the electrolyte does shorten the migration time of the labelled caproic acid peak but not as much as the electrolyte containing 1 mM dimethyl-β-cyclodextrin. At a higher concentration of 5 mM trimethyl-β-cyclodextrin in 10 mM borate buffer the migration time for labelled caproic acid peak shortens even more but unfortunately starts to co-migrate with a dye peak as shown when Figures 4.5 and 4.27 are compared. These investigations into CZE using electrolytes that contain cyclodextrin show that the most promising method for separating the labelled caproic acid peak from the dye peaks is when dimethyl-β-cyclodextrin is present at a concentration higher than 10 mM in the 10 mM borate buffer. When dimethyl-β-cyclodextrin is present in 10 mM borate at a concentration greater than 10 mM the labelled caproic acid peak's migration time should shorten enough so that it is the first component to migrate out. However, performing a CZE separation with dimethyl-β-cyclodextrin at a high concentration is expensive so other potential separation conditions using additives such as organic modifiers or micelle surfactants were investigated.

4.3.3 CZE-LIF separations using a cyclodextrin and an organic modifier

Next, various CZE-LIF techniques using electrolytes that contain organic modifiers were investigated using labelled undecanoic acid. The first technique investigated was used by Collet and Gareil[64] and involved an electrolyte containing 10 mM Tris, 50 % MeOH and 1 mM dimethyl-β-cyclodextrin. The nonaqueous chiral CZE-LIF electropherogram for labelled undecanoic acid performed under the run conditions described in Section 4.2.8 can be found in Figure 4.28. A peak for labelled

Figure 4.28: The CZE-LIF electropherogram of labelled undecanoic acid (C_{11}). Capillary: 30 cm, 50 μm I.D., 140 μm O.D..
Run: 10 mM Tris and 1 mM dimethyl-ß-cyclodextrin 50/50 MeOH/H₂O, pH 10, 30 kV. Injection: 1000 V, 5 s.
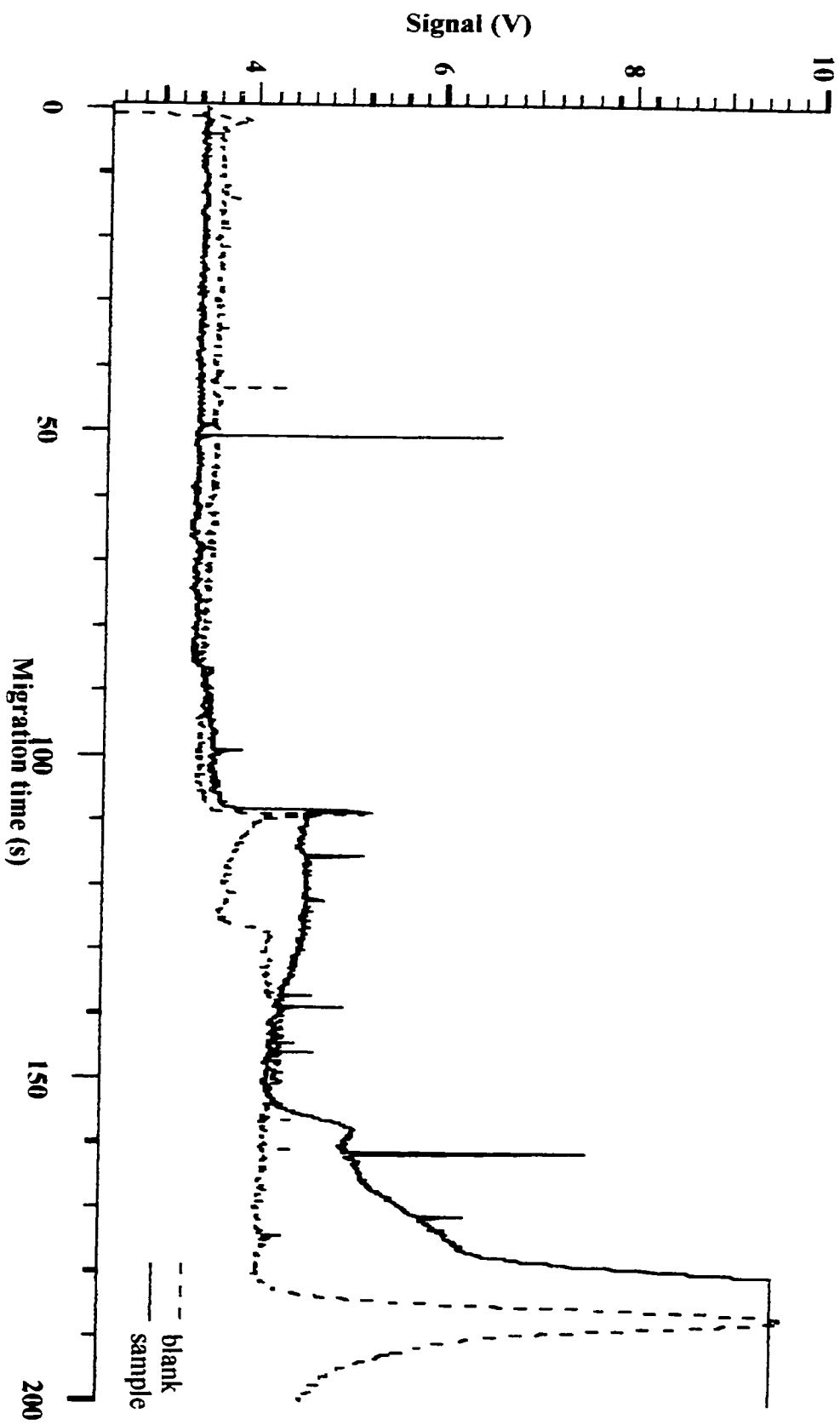Laser: 488 nm Ar⁺, 12.1 mW. PMT: 1000 V. Interference filter: 518DF25. Concentration: 10⁻⁸ M.

240
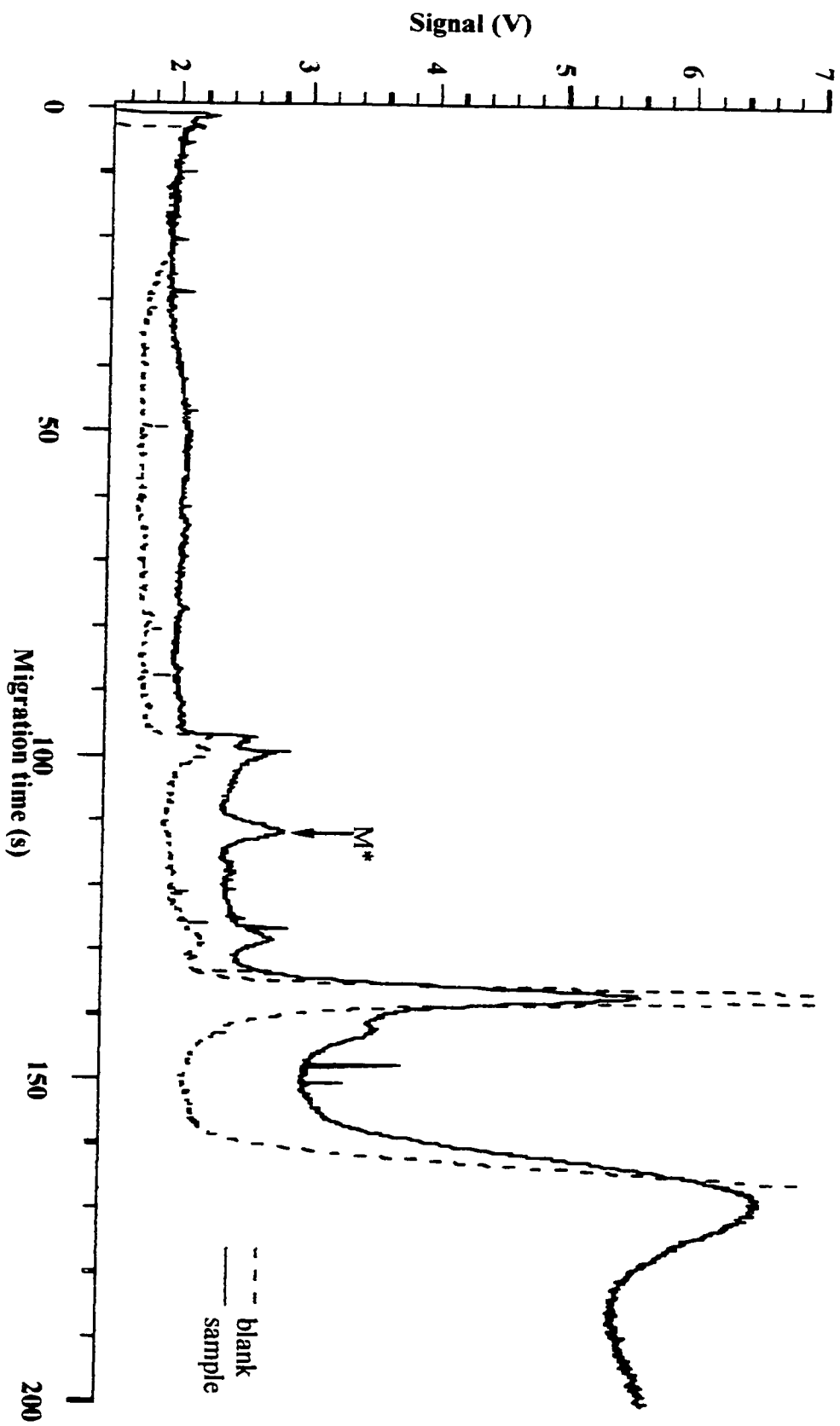
undecanoic acid was found but the presence of MeOH in the separation was shown to cause an increase in background signal, a decrease in peak area and a decrease in resolution which is visible when Figures 4.7 and 4.28 are compared. Next, the CZE technique used by Roldan-Assad and Gareil[63] involving an electrolyte containing 10 mM Tris, 60 % MeOH, and 1 mM of trimethyl-β-cyclodextrin was investigated. The resulting nonaqueous chiral CZE-LIF electropherogram performed under the run conditions described in Section 4.2.8 can be found in Figure 4.29. A peak for labelled undecanoic acid was not found and the background signal was seen to increase.

4.3.4 Nonaqueous CE-LIF separations

Next, a nonaqueous CE separation was performed on labelled undecanoic acid using the electrolyte that was used by Wang[68], which contained 2.8 mM KOH in 60 % MeOH / 40 % ACN. The resulting nonaqueous CE-LIF electropherogram performed under the run conditions described in Section 4.2.9 can be found in Figure 4.30. A peak for labelled undecanoic acid was not found and the background signal and the baseline noise were found to increase. The results found in Figures 4.28, 4.29 and 4.30 show that the presence of an organic modifier in an electrolyte used for CE separation does not improve separation or selectivity as expected but actually degrades them. Next, the effect of a micelle surfactant present in the electrolyte used in a MEKC separation will be investigated.

Figure 4.29: The CZE-LIF electropherogram of labelled undecanoic acid (C_{11}). Capillary: 30 cm, 50 μm I.D., 140 μm O.D.. Run: 10 mM Tris and 1 mM trimethyl-β-cyclodextrin 60/40 MeOH/H_2O, pH 10, 30 kV. Injection: 1000 V, 5 s. Laser: 488 nm Ar^+, 12.1 mW. PMT: 1000 V. Interference filter: 518DF25. Concentration: 10^{-8} M.
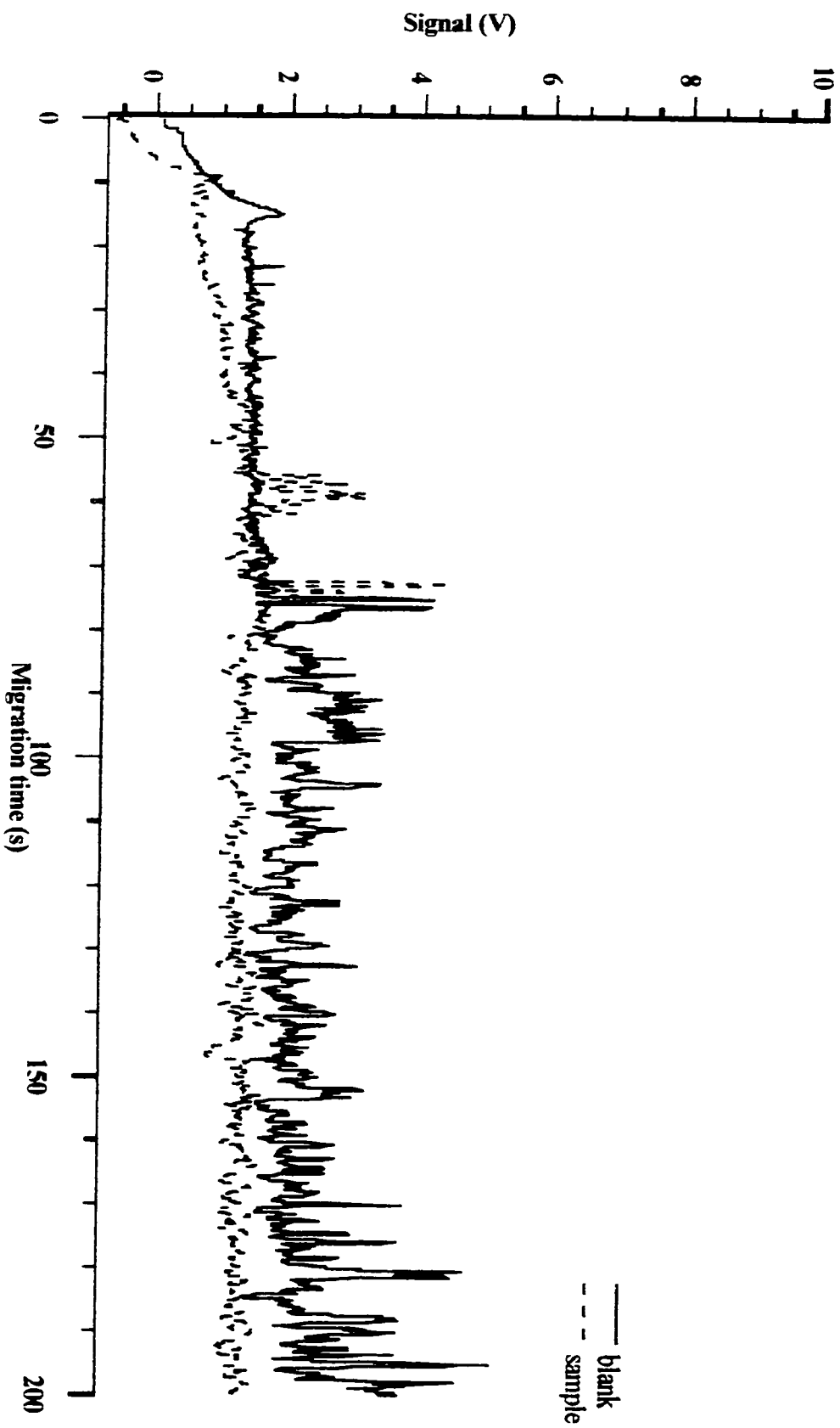
242

Figure 4.30: The nonaqueous CE-LIF electropherogram of labelled undecanoic acid (C_{11}). Capillary: 30 cm, 50 μm I.D., 140 μm O.D.. Run: 2.8 mM KOH, 60/40 MeOH/ACN, pH 13, 24 kV. Injection: 1000 V, 5 s. Laser: 488 nm Ar$^+$, 12.1 mW. PMT: 1000 V. Interference filter: 518DF25. Concentration: 10^{-8} M.

4.3.5 MEKC-LIF separations using SDS

For the investigations into the effect micelle surfactant present in the electrolyte has on CE separation labelled caproic acid was used. The run conditions for the MEKC-LIF separations of labelled caproic acid are described in Section 4.2.10. The first MEKC separations of labelled caproic acid were performed using an electrolyte similar to the ones used in references 1 and 55. The MEKC-LIF electropherogram of labelled caproic acid using an electrolyte that contained 10 mM SDS in 10 mM borate at pH 9 can be found in Figure 4.31. A peak for labelled caproic acid was found but was co-migrating with a dye peak. In comparing Figures 4.5 and 4.31 it is evident that the presence of SDS in the electrolyte increases the migration time of the labelled caproic acid peak. Next, MEKC-LIF separations of labelled caproic acid were performed using 20 mM, 30 mM, 40 mM and 50 mM SDS in 10 mM borate and the resulting MEKC-LIF electropherograms can be found in Figures 4.32 – 4.35, respectively. The best separation of the labelled caproic acid peak from the dye peaks was achieved when 50 mM SDS was used in the electrolyte.

4.3.6 MEKC-LIF separations of a homologous series of labelled FFAs

Next, MEKC-LIF using an electrolyte that contained 50 mM SDS in 10 mM borate at pH 9 was used to separate the remaining labelled linear saturated FFAs in the homologous series. The run conditions for these MEKC-LIF separations are described in Section 4.2.11. The resulting MEKC-LIF electropherograms can be found in Figures 4.36 – 4.53. A summary of all the data for the MEKC-LIF separations of the homologous series of labelled linear saturated FFAs ($C_6 - C_{24}$) can be found in Table 4.2.

Figure 4.31: The MEKC-LIF electropherogram of labelled caproic acid (C_6). Capillary: 40 cm, 50 μm I.D., 140 μm O.D..
Run: 10 mM borate and 10 mM SDS, pH 9, 16 kV. Injection: 3000 V, 5 s. Laser: 488 nm Ar⁺, 12.1 mW.
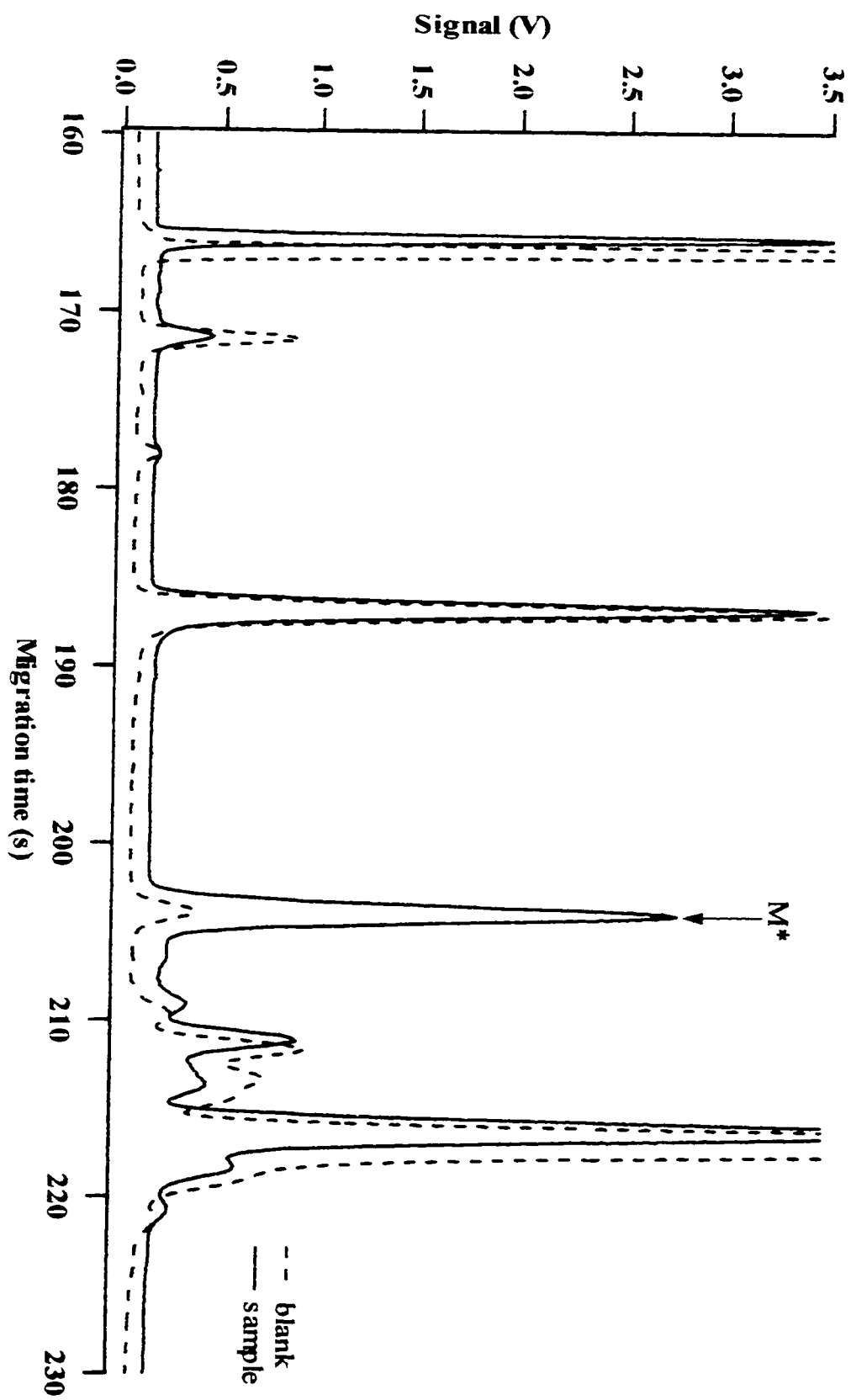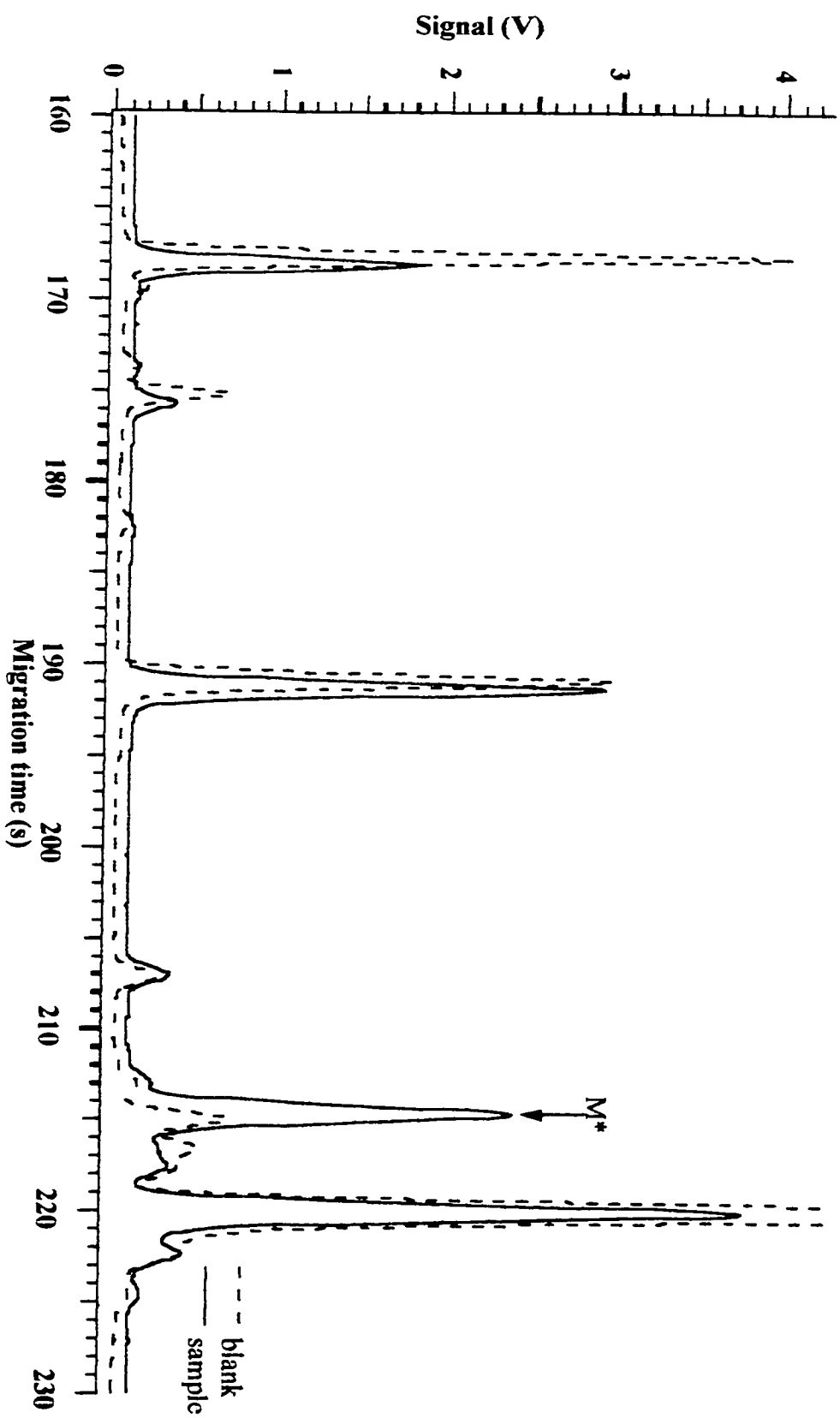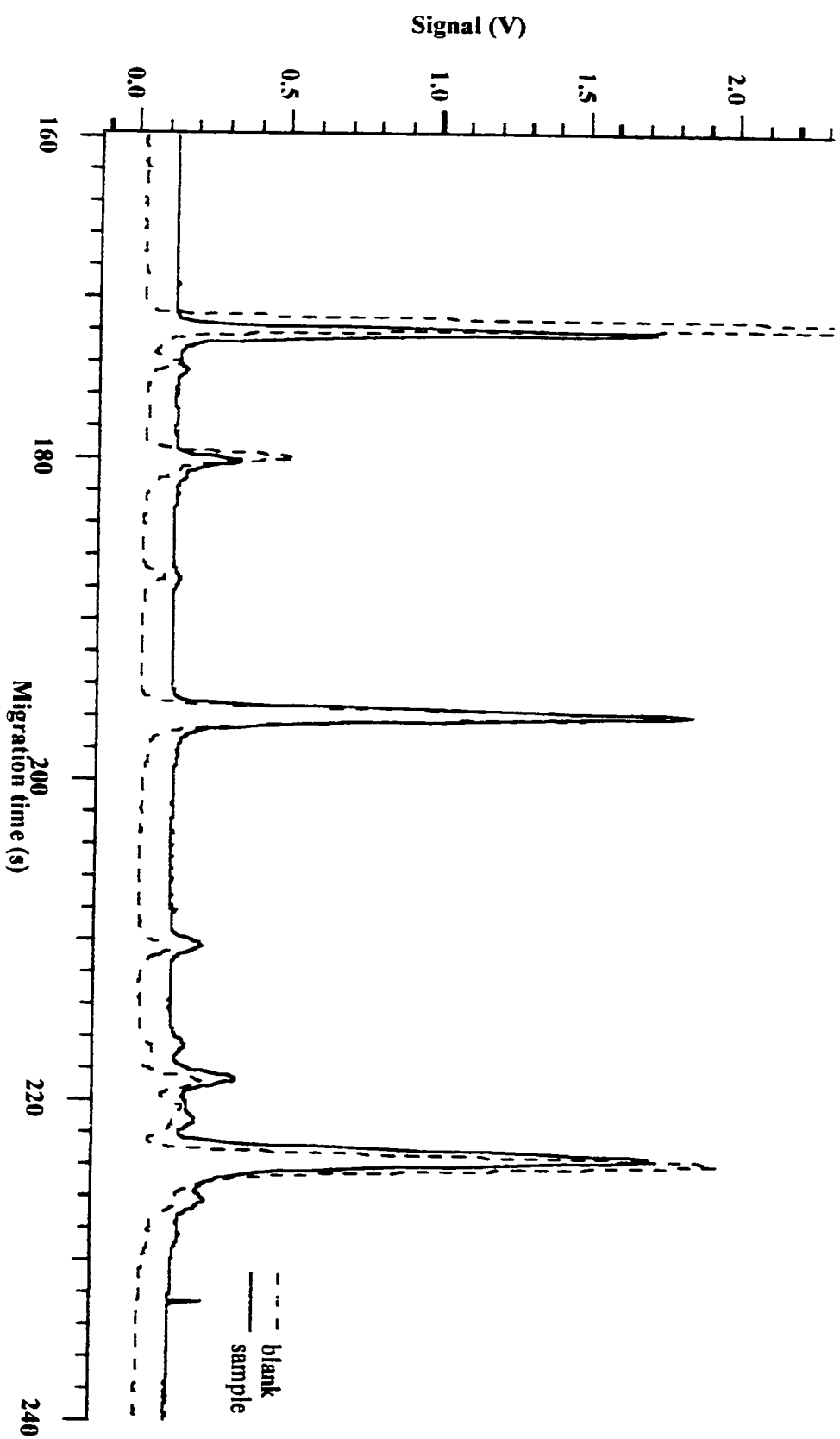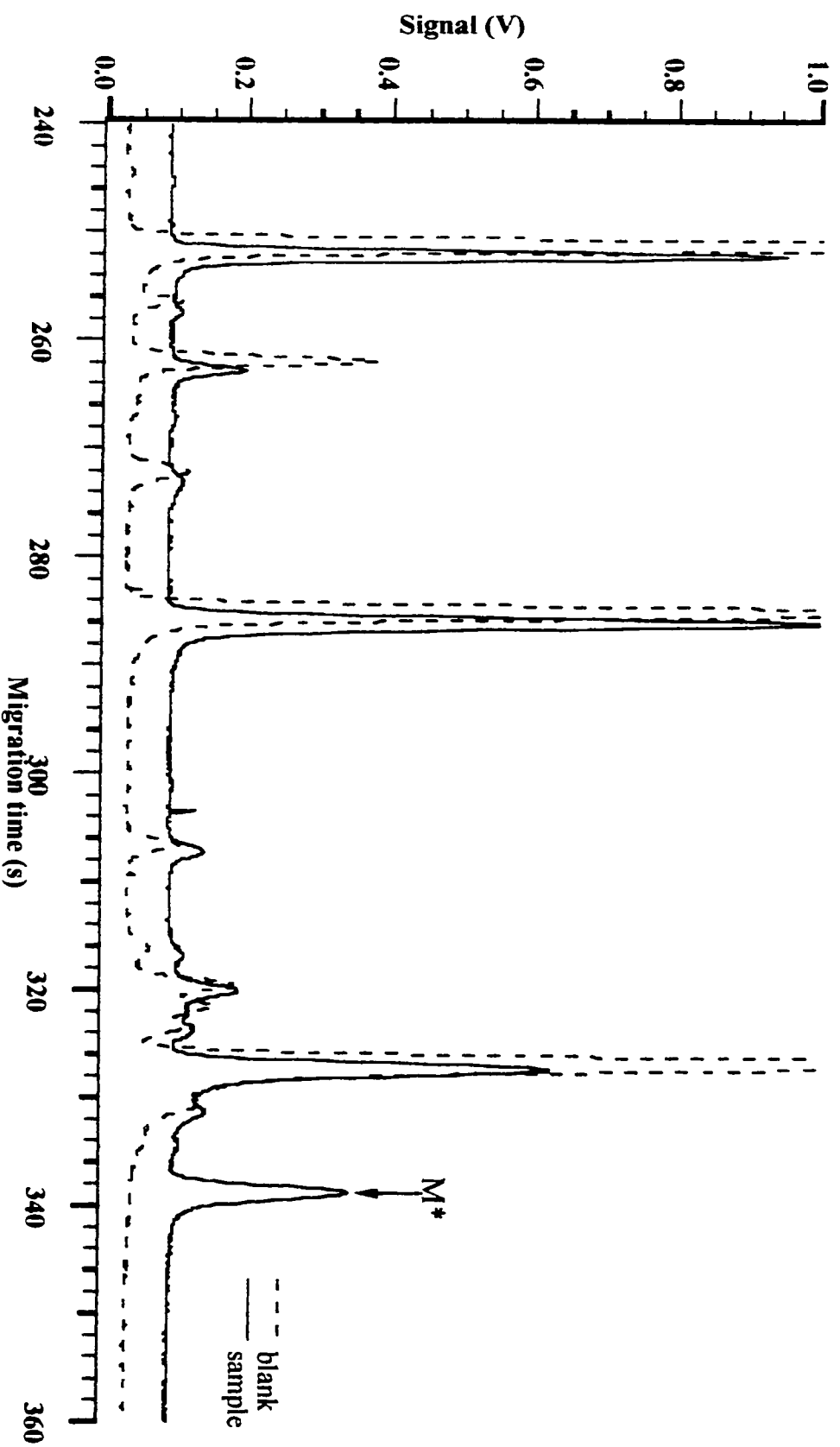PMT: 1000 V. Interference filter: 518DF25. Concentration: 10^{-8} M.

Figure 4.32: The MEKC-LIF electropherogram of labelled caproic acid (C_6). Capillary: 40 cm, 50 μm I.D., 140 μm O.D..

Run: 10 mM borate and 20 mM SDS, pH 9, 16 kV. Injection: 3000 V, 5 s. Laser: 488 nm Ar$^+$, 12.1 mW.

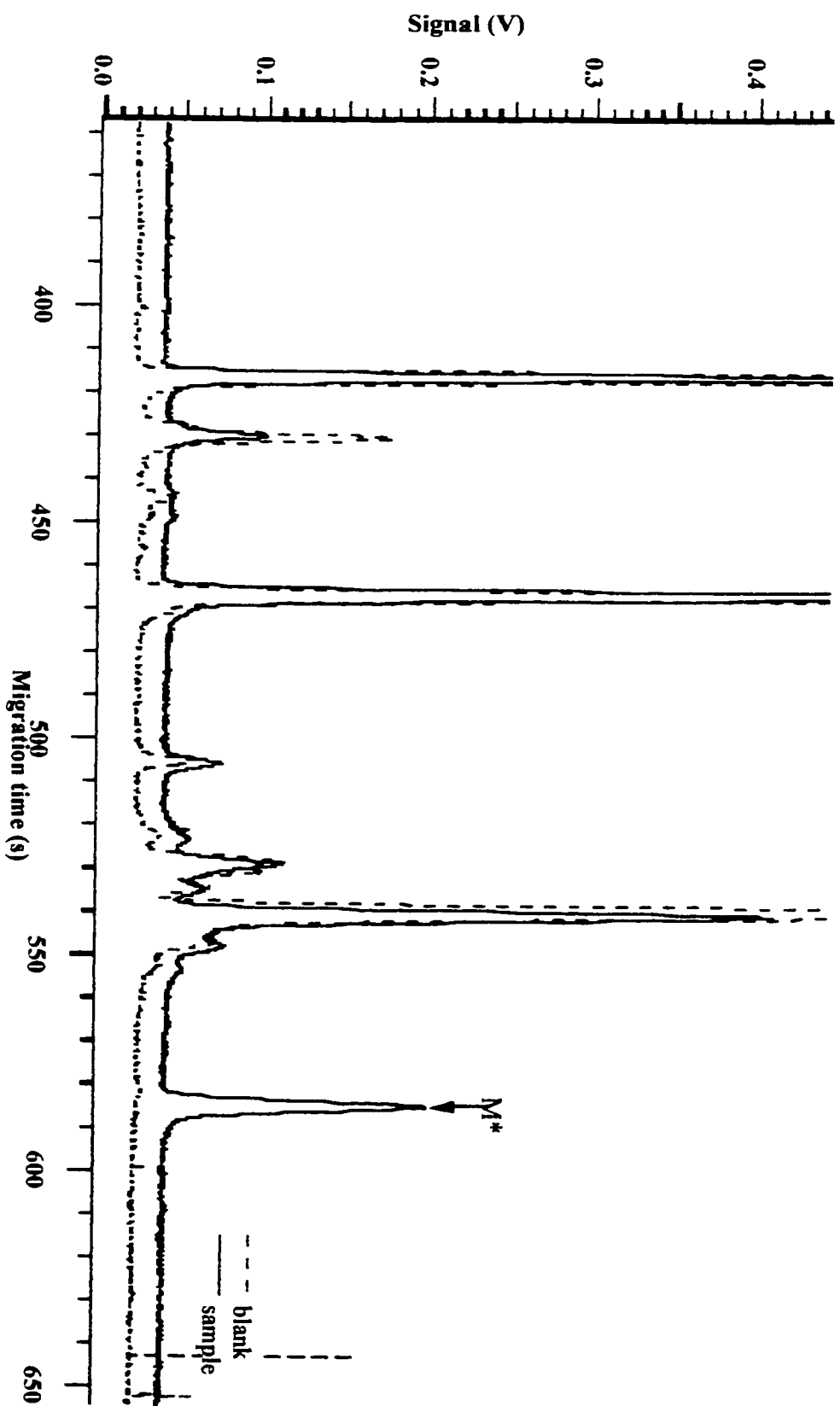PMT: 1000 V. Interference filter: 518DF25. Concentration: 10^{-8} M.

Figure 4.33: The MEKC-LIF electropherogram of labelled caproic acid (C_6). Capillary: 40 cm, 50 μm I.D., 140 μm O.D..

Run: 10 mM borate and 30 mM SDS, pH 9, 16 kV. Injection: 3000 V, 5 s. Laser: 488 nm Ar$^+$, 12.1 mW.

PMT: 1000 V. Interference filter: 518DF25. Concentration: 10^{-8} M.
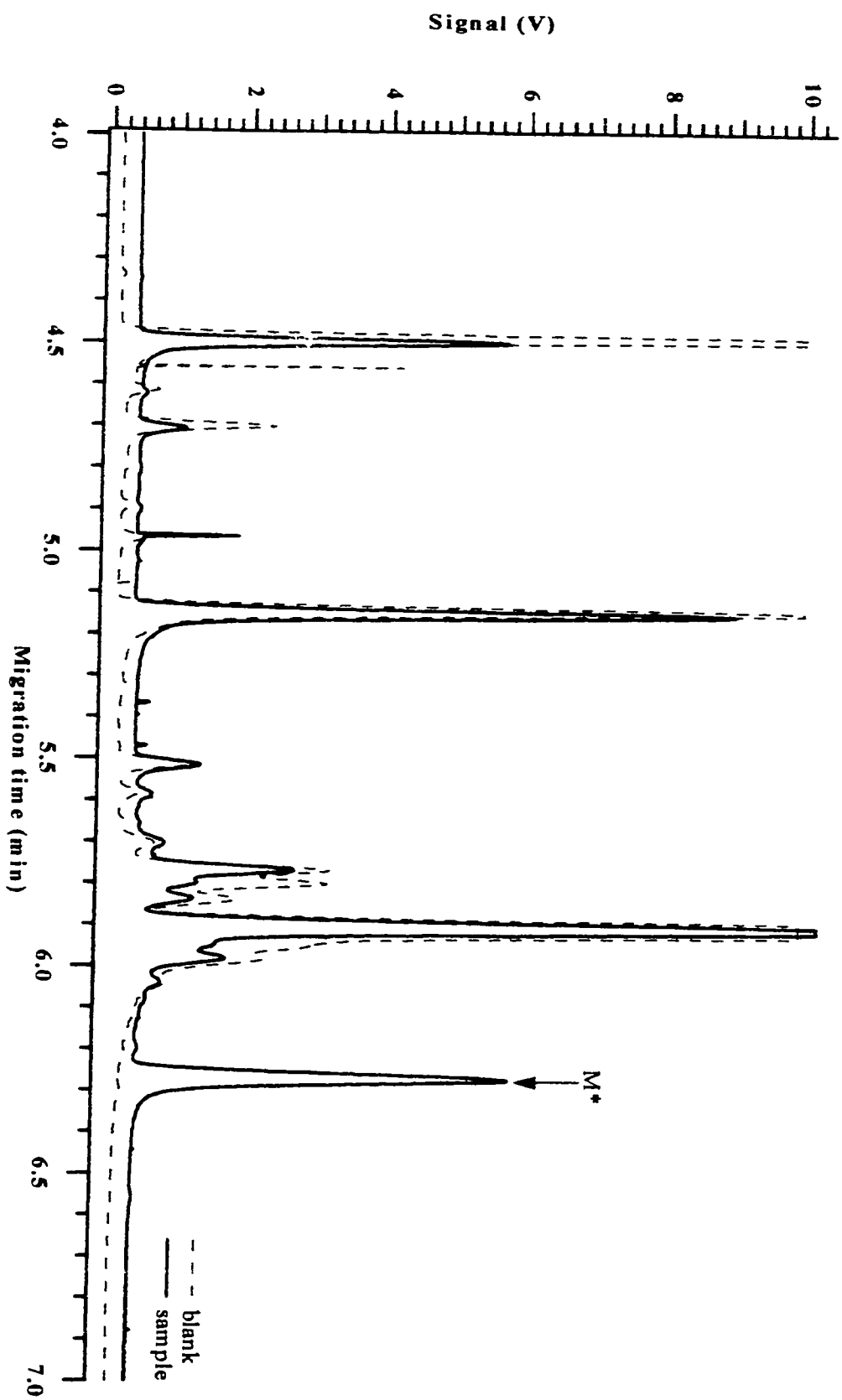
247

Figure 4.34: The MEKC-LIF electropherogram of labelled caproic acid (C_6). Capillary: 40 cm, 50 μm I.D., 140 μm O.D..

Run: 10 mM borate and 40 mM SDS, pH 9, 12 kV. Injection: 3000 V, 5 s. Laser: 488 nm Ar$^+$, 12.1 mW.

PMT: 1000 V. Interference filter: 518DF25. Concentration: 10^{-8} M.

Figure 4.35: The MEKC-LIF electropherogram of labelled caproic acid (C_6). Capillary: 40 cm, 50 μm I.D., 140 μm O.D.. Run: 10 mM borate and 50 mM SDS, pH 9, 8 kV. Injection: 3000 V, 5 s. Laser: 488 nm Ar$^+$, 12.1 mW. PMT: 1000 V. Interference filter: 518DF25. Concentration: 10^{-8} M.
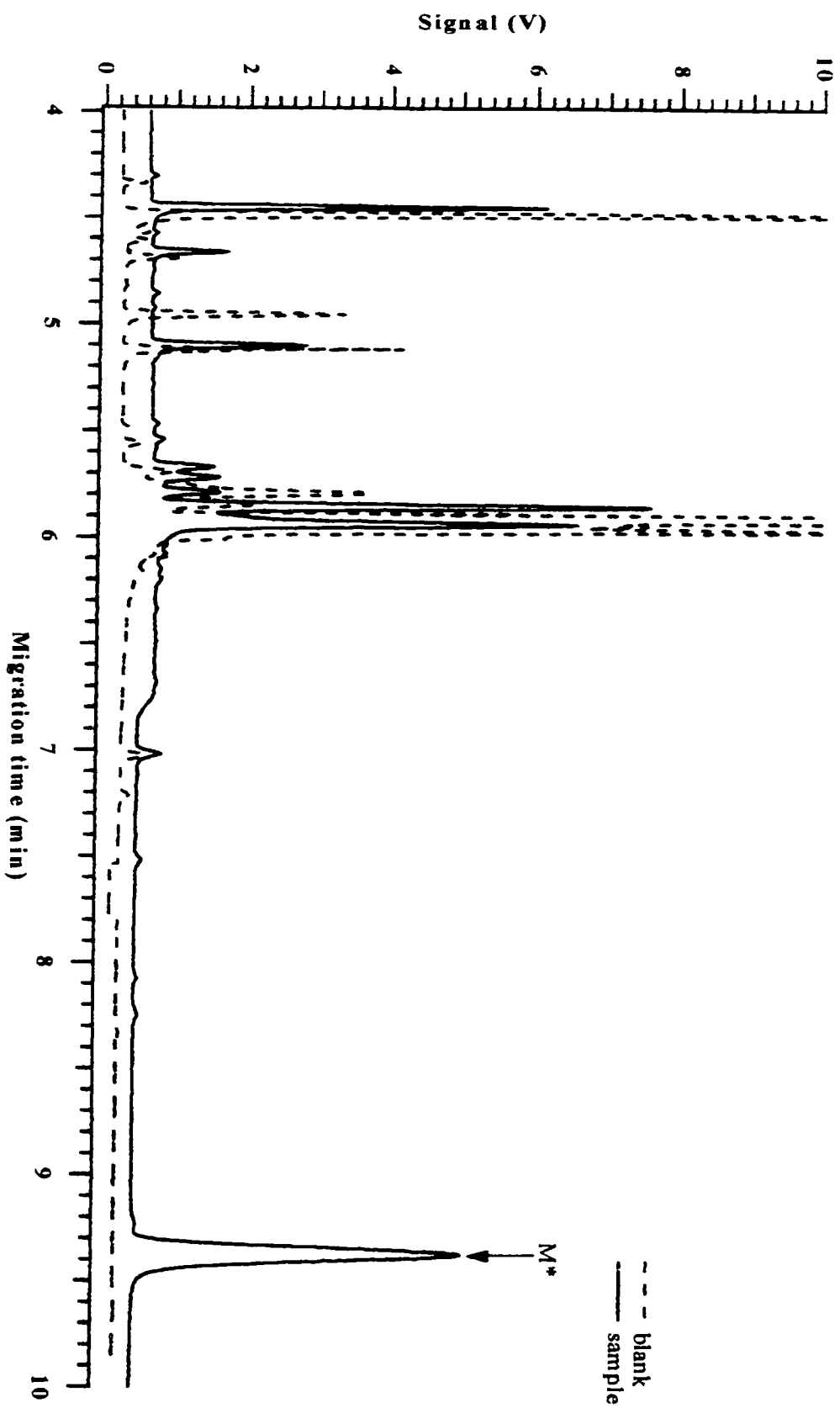
Figure 4.36: The repeated MEKC-LIF electropherogram of labelled caproic acid (C_6). Capillary: 40 cm, 50 μm I.D., 140 μm O.D.. Run: 10 mM borate and 50 mM SDS, pH 9, 12 kV. Injection: 1000 V, 5 s. Laser: 488 nm Ar^+, 12.1 mW. PMT: 1000 V. Interference filter: 518DF25. Concentration: 10^{-7} M.
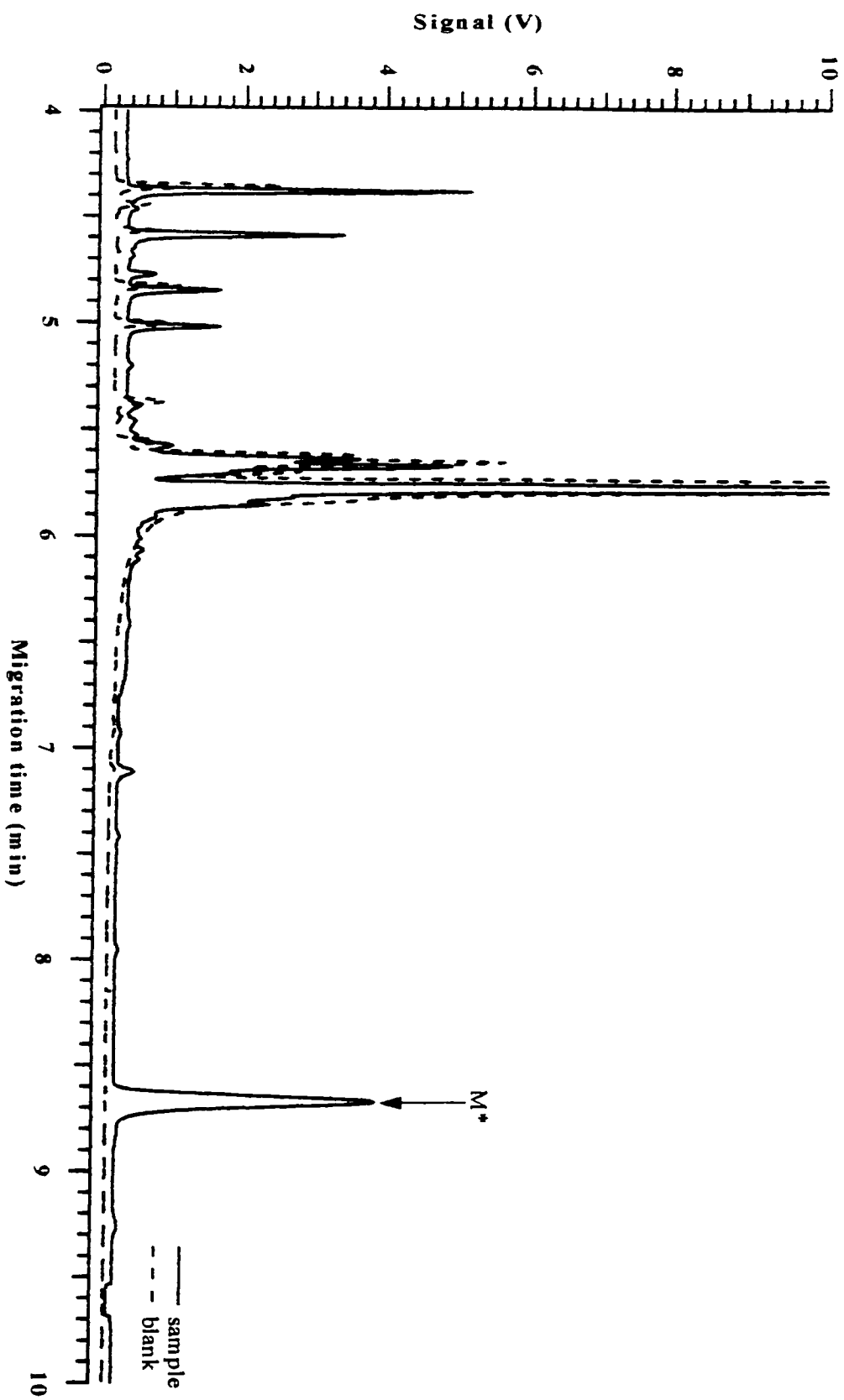
Figure 4.37: The MEKC-LIF electropherogram of labelled caprylic acid (C_8). Capillary: 40 cm, 50 μm I.D., 140 μm O.D..

Run: 10 mM borate and 50 mM SDS, pH 9, 12 kV. Injection: 1000 V, 5 s. Laser: **488** nm Ar^+, 12.1 mW.

PMT: 1000 V. Interference filter: 518DF25. Concentration: 10^{-7} M.

Figure 4.38: The MEKC-LIF electropherogram of labelled nonanoic acid (C₉). Capillary: 40 cm, 50 μm I.D., 140 μm O.D..

Run: 10 mM borate and 50 mM SDS, pH 9, 12 kV. Injection: 1000 V, 5 s. Laser: 488 nm Ar⁺, 12.1 mW.

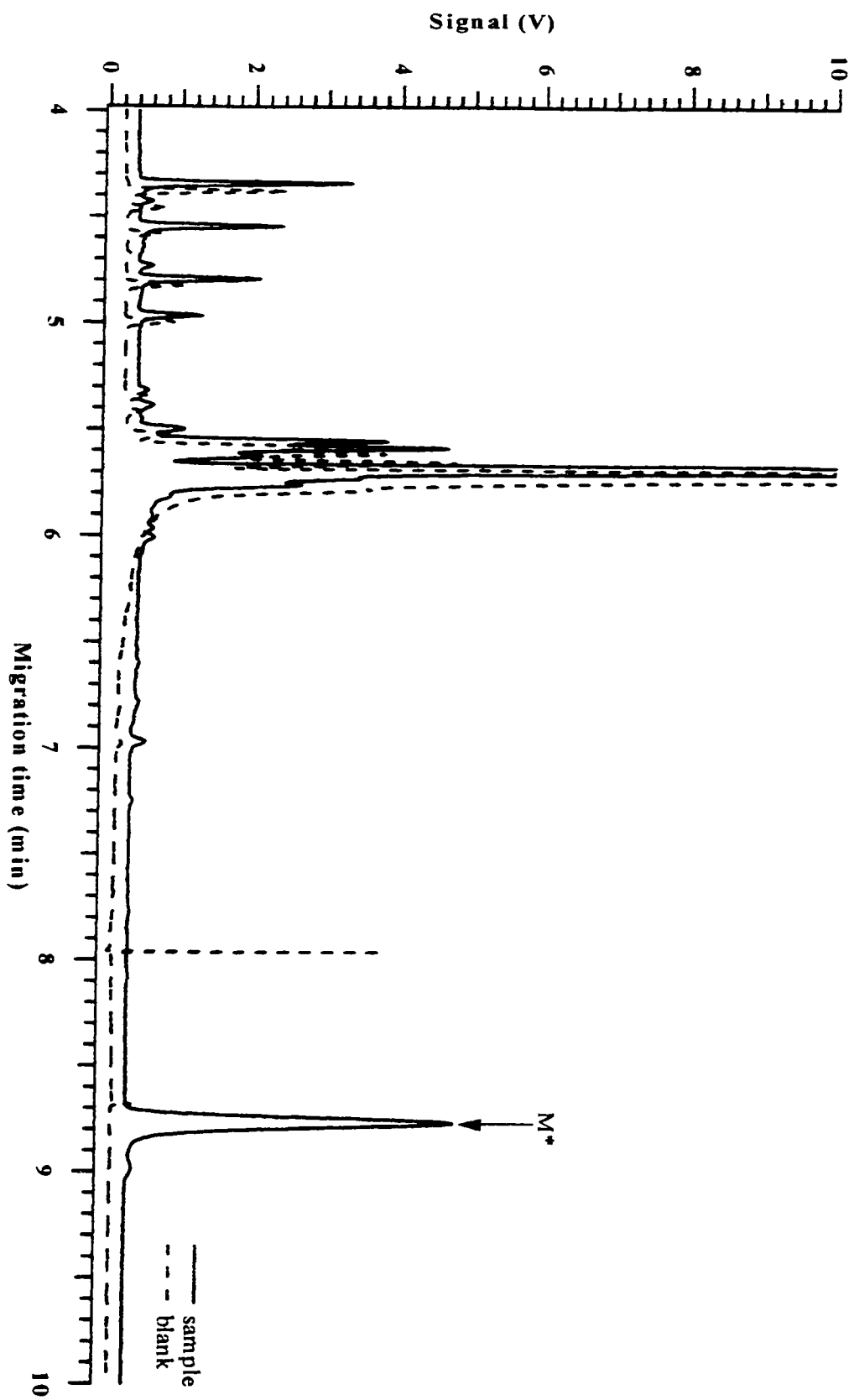PMT: 1000 V. Interference filter: 518DF25. Concentration: 10^{-7} M.

Figure 4.39: The MEKC-LIF electropherogram of labelled capric acid (C_{10}). Capillary: 40 cm, 50 μm I.D., 140 μm O.D..

Run: 10 mM borate and 50 mM SDS, pH 9, 12 kV. Injection: 1000 V, 5 s. Laser: 488 nm Ar$^+$, 12.1 mW.

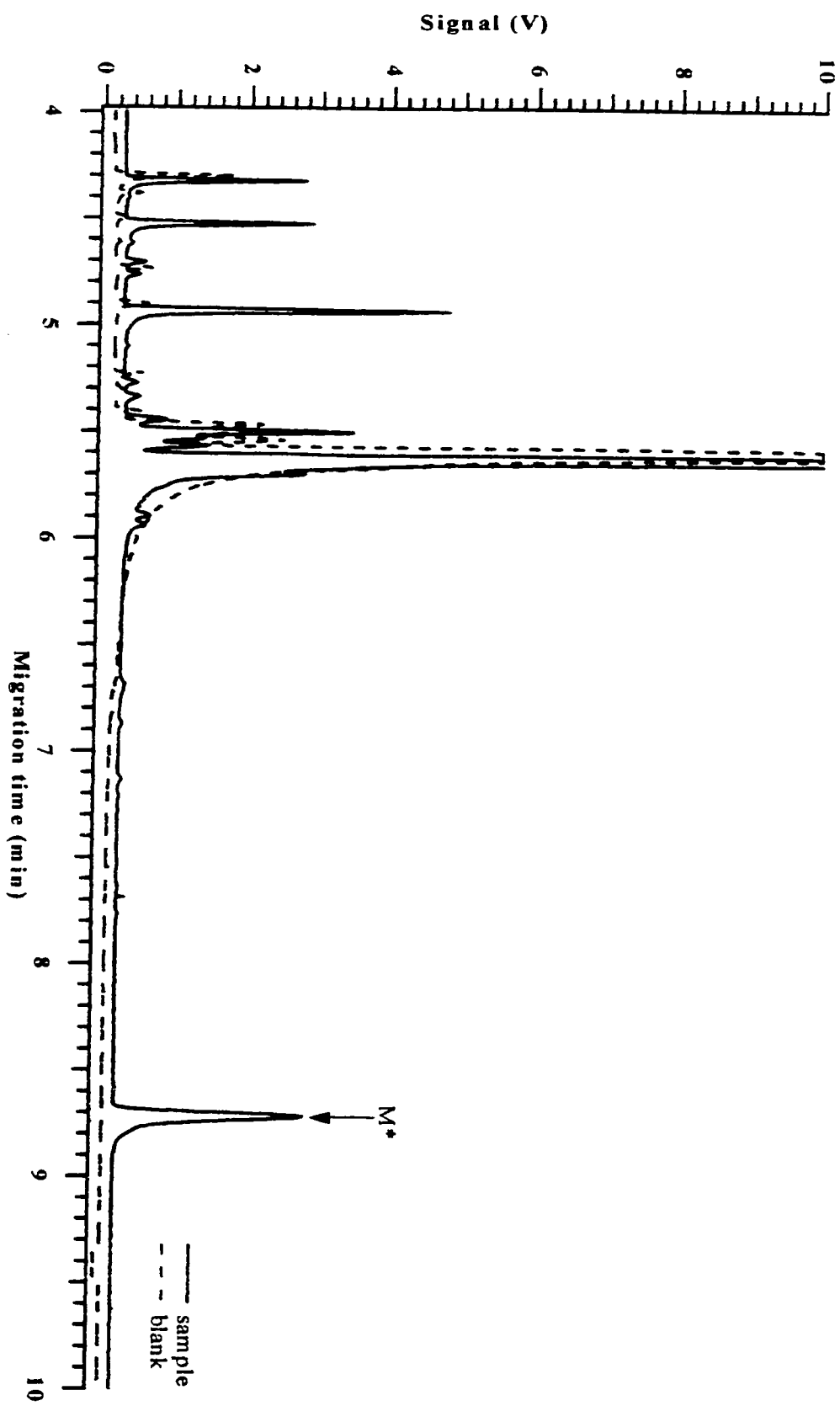PMT: 1000 V. Interference filter: 518DF25. Concentration: 10^{-7} M.

Figure 4.40: The MEKC-LIF electropherogram of labelled undecanoic acid (C_{11}). Capillary: 40 cm, 50 μm I.D., 140 μm O.D..
Run: 10 mM borate and 50 mM SDS, pH 9, 12 kV. Injection: 1000 V, 5 s. Laser: 488 nm Ar⁺, 12.1 mW.

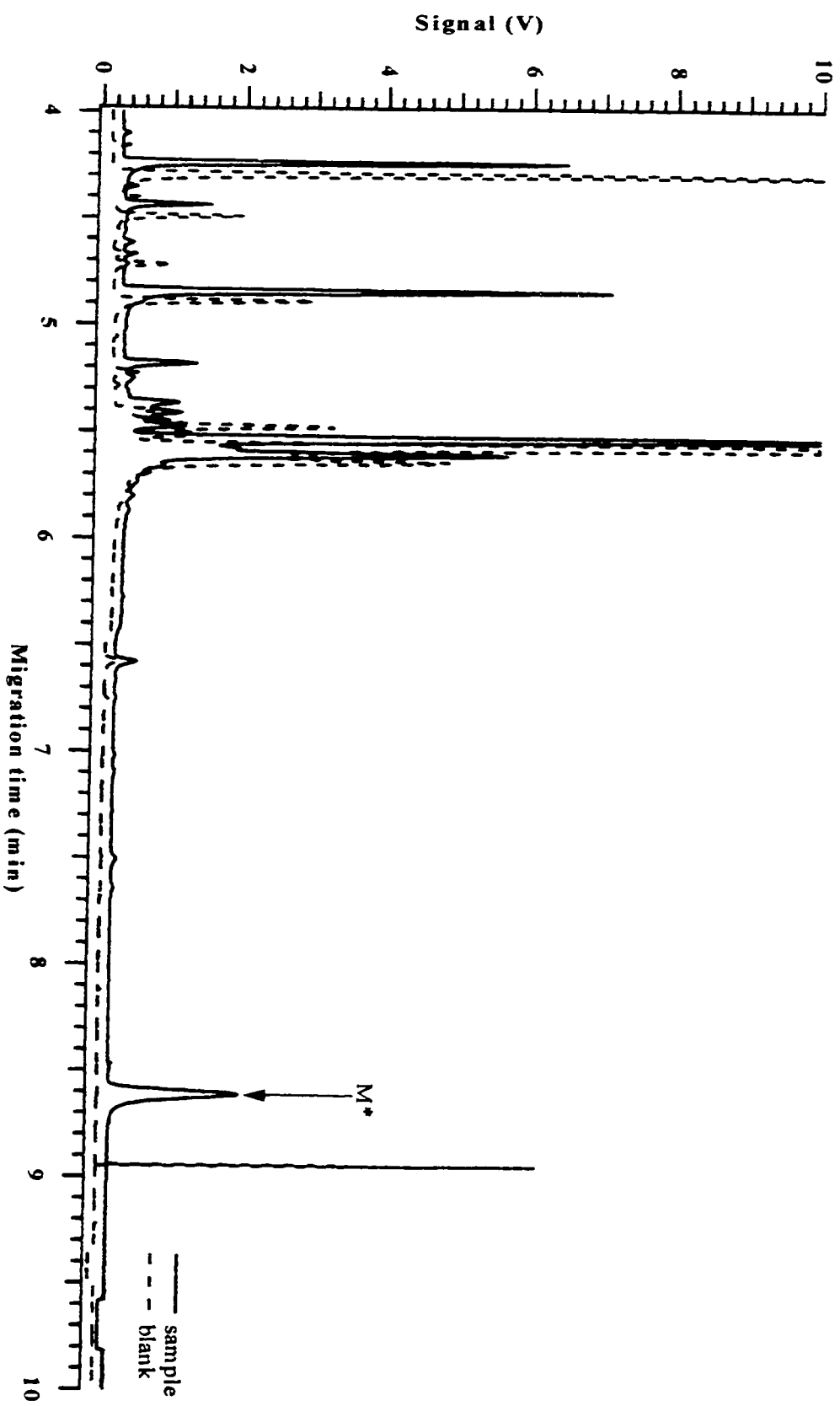PMT: 1000 V. Interference filter: 518DF25. Concentration: 10^{-7} M.

254

Figure 4.41: The MEKC-LIF electropherogram of labelled lauric acid (C_{12}). Capillary: 40 cm, 50 µm I.D., 140 µm O.D..

Run: 10 mM borate and 50 mM SDS, pH 9, 12 kV. Injection: 1000 V, 5 s. Laser: 488 nm Ar^+, 12.1 mW.

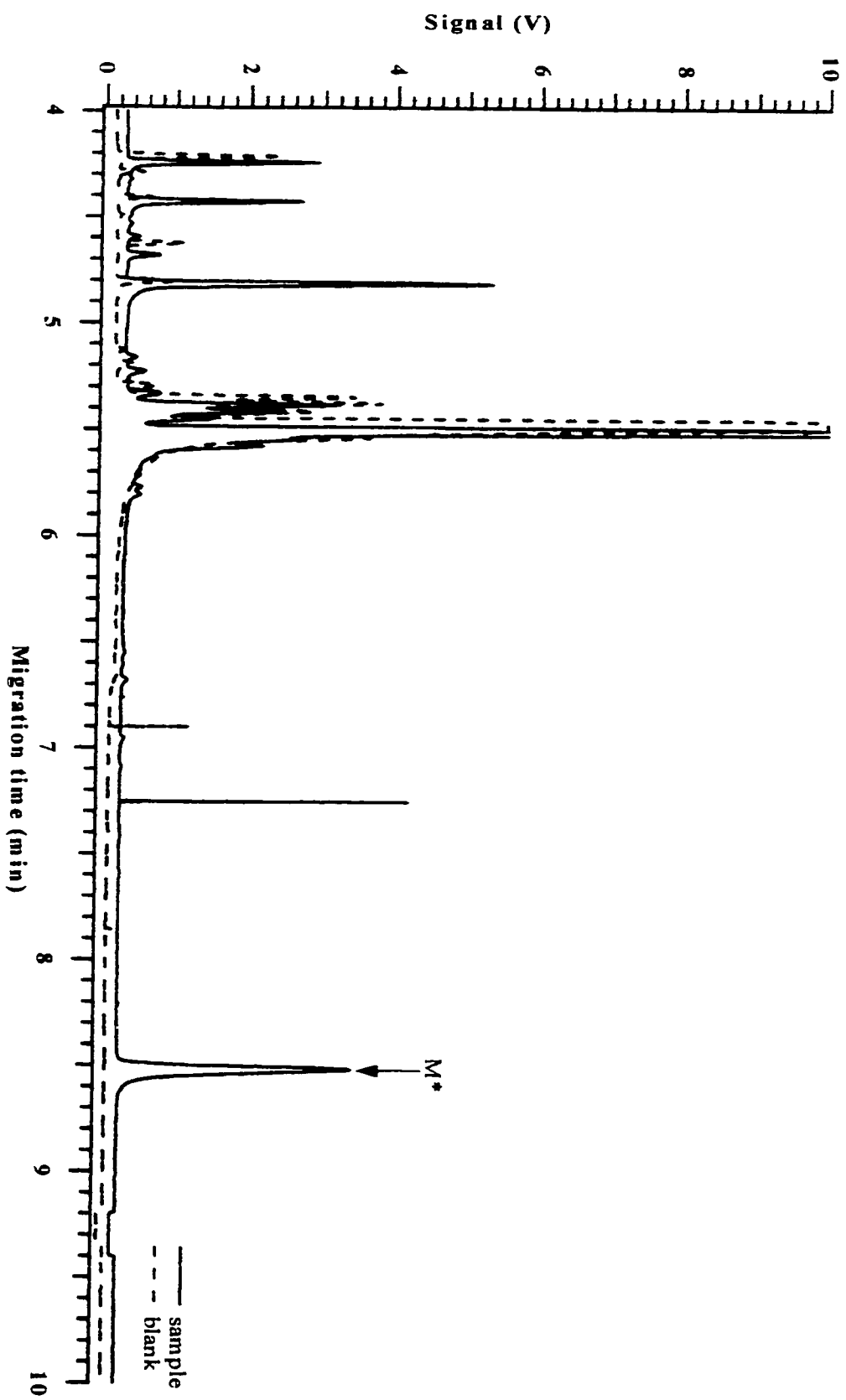PMT: 1000 V. Interference filter: 518DF25. Concentration: 10^{-7} M.

Figure 4.42: The MEKC-LIF electropherogram of labelled tridecanoic acid (C_{13}). Capillary: 40 cm, 50 μm I.D., 140 μm O.D.. Run: 10 mM borate and 50 mM SDS, pH 9, 12 kV. Injection: 1000 V, 5 s. Laser: 488 nm Ar⁺, 12.1 mW. PMT: 1000 V. Interference filter: 518DF25. Concentration: 10^{-7} M.

Figure 4.43: The MEKC-LIF electropherogram of labelled myristic acid (C_{14}). Capillary: 40 cm, 50 μm I.D., 140 μm O.D..

Run: 10 mM borate and 50 mM SDS, pH 9, 12 kV. Injection: 1000 V, 5 s. Laser: 488 nm Ar⁺, 12.1 mW.

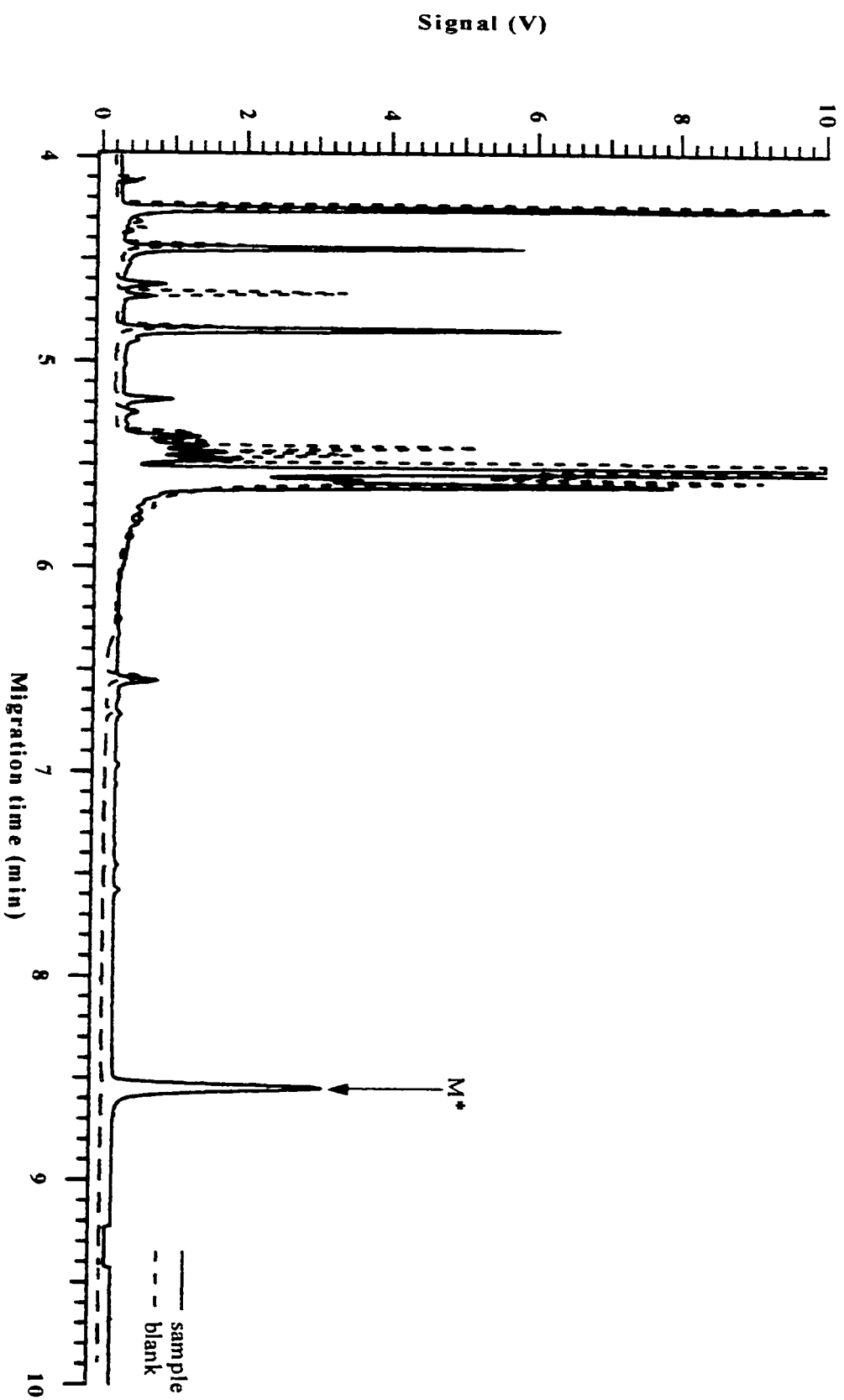PMT: 1000 V. Interference filter: 518DF25. Concentration: 10^{-7} M.

Figure 4.44: The MEKC-LIF electropherogram of labelled pentadecanoic acid (C_{15}). Capillary: 40 cm, 50 μm I.D., 140 μm O.D.. Run: 10 mM borate and 50 mM SDS, pH 9, 12 kV. Injection: 1000 V, 5 s. Laser: 488 nm Ar^+, 12.1 mW. PMT: 1000 V. Interference filter: 518DF25. Concentration: 10^{-7} M.
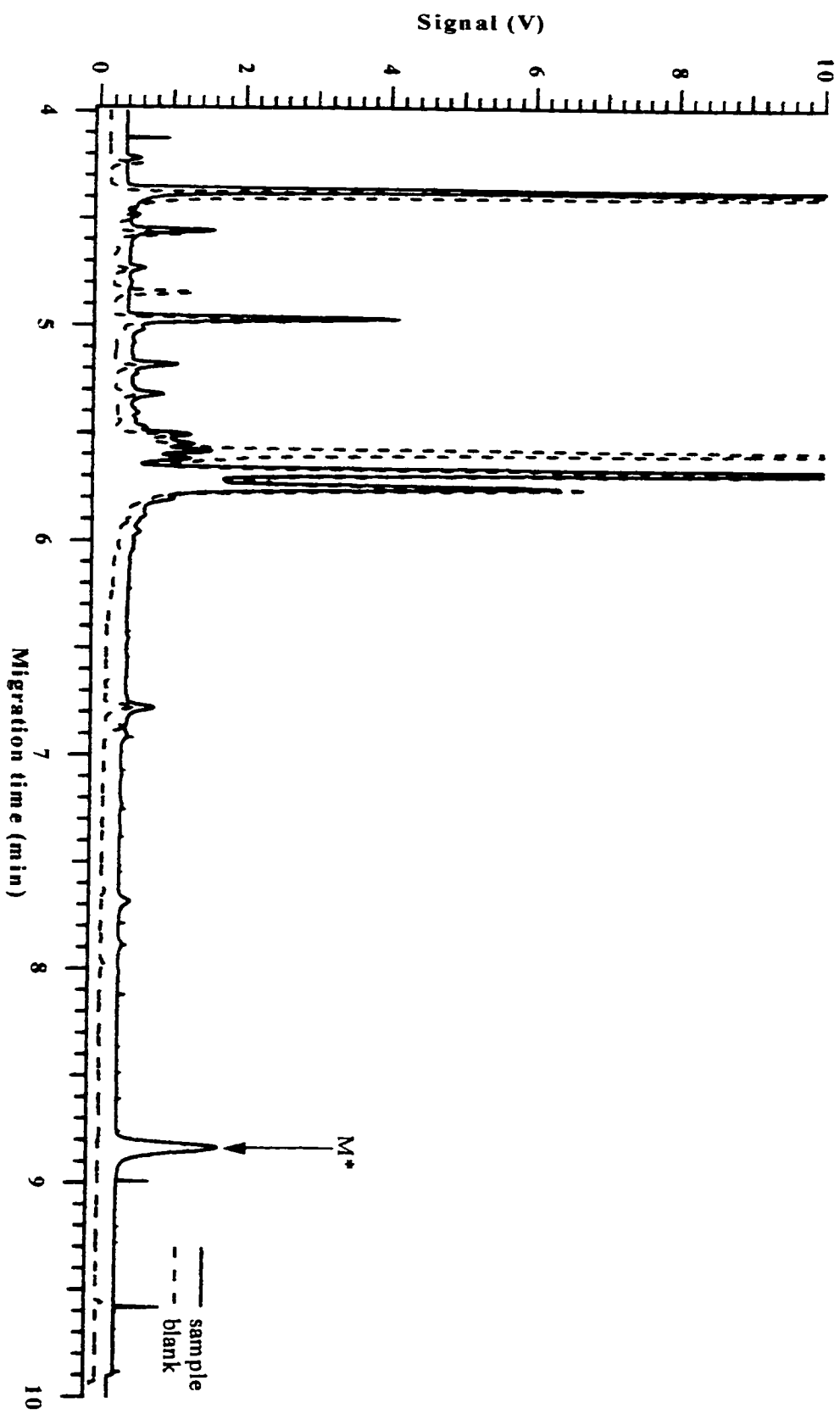
Figure 4.45: The MEKC-LIF electropherogram of labelled palmitic acid (C_{16}). Capillary: 40 cm, 50 μm I.D., 140 μm O.D..

Run: 10 mM borate and 50 mM SDS, pH 9, 12 kV. Injection: 1000 V, 5 s. Laser: 488 nm Ar$^+$, 12.1 mW.

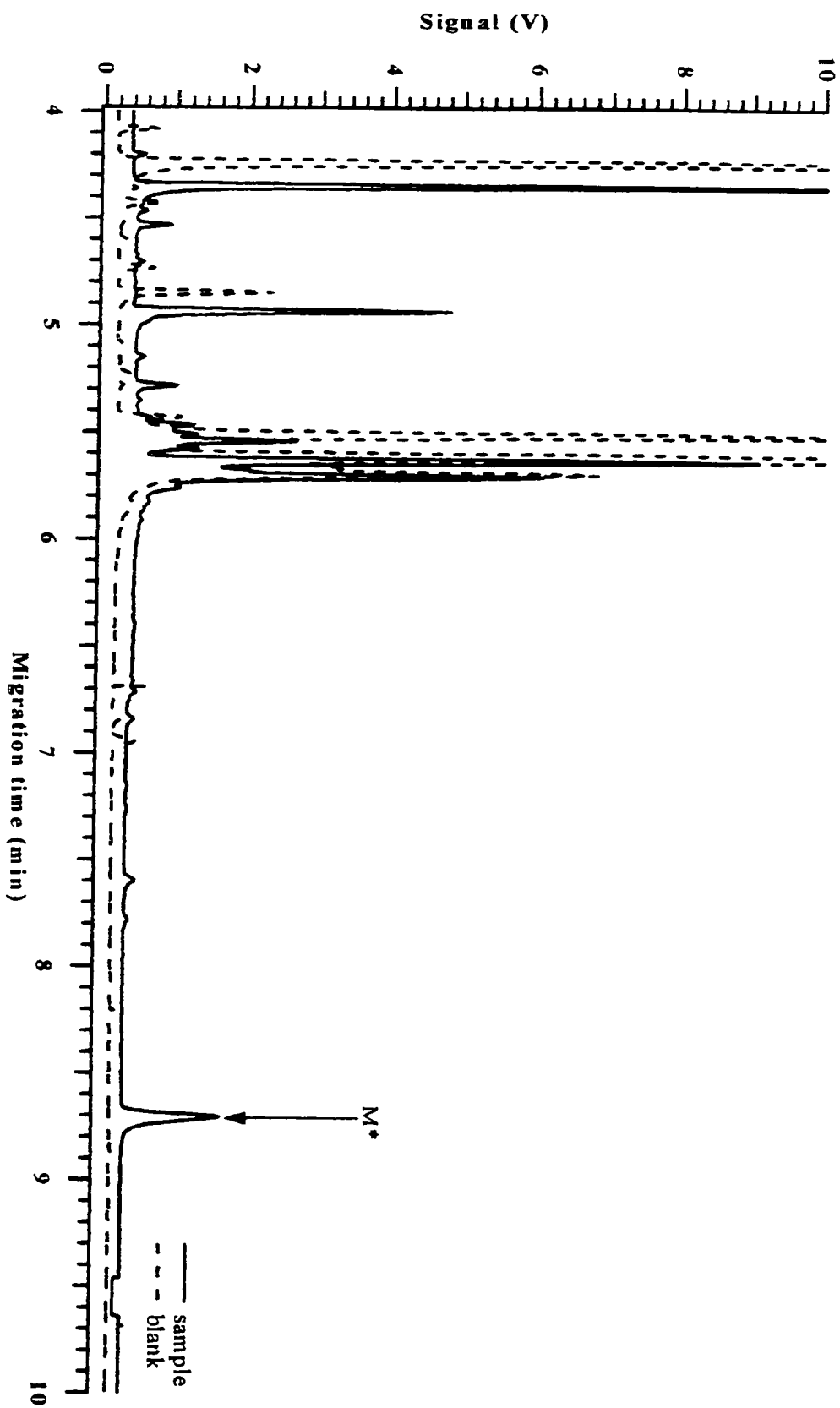PMT: 1000 V. Interference filter: 518DF25. Concentration: 10^{-7} M.

Figure 4.46: The MEKC-LIF electropherogram of labelled heptadecanoic acid (C_{17}). Capillary: 40 cm, 50 μm I.D., 140 μm O.D..

Run: 10 mM borate and 50 mM SDS, pH 9, 12 kV. Injection: 1000 V, 5 s. Laser: 488 nm Ar^+, 12.1 mW.

PMT: 1000 V. Interference filter: 518DF25. Concentration: 10^{-7} M.

sample
blank

M*

Signal (V)

Migration time (min)

260

Figure 4.47: The MEKC-LIF electropherogram of labelled stearic acid (C_{18}). Capillary: 40 cm, 50 μm I.D., 140 μm O.D..

Run: 10 mM borate and 50 mM SDS, pH 9, 12 kV. Injection: 1000 V, 5 s. Laser: 488 nm Ar$^+$, 12.1 mW.

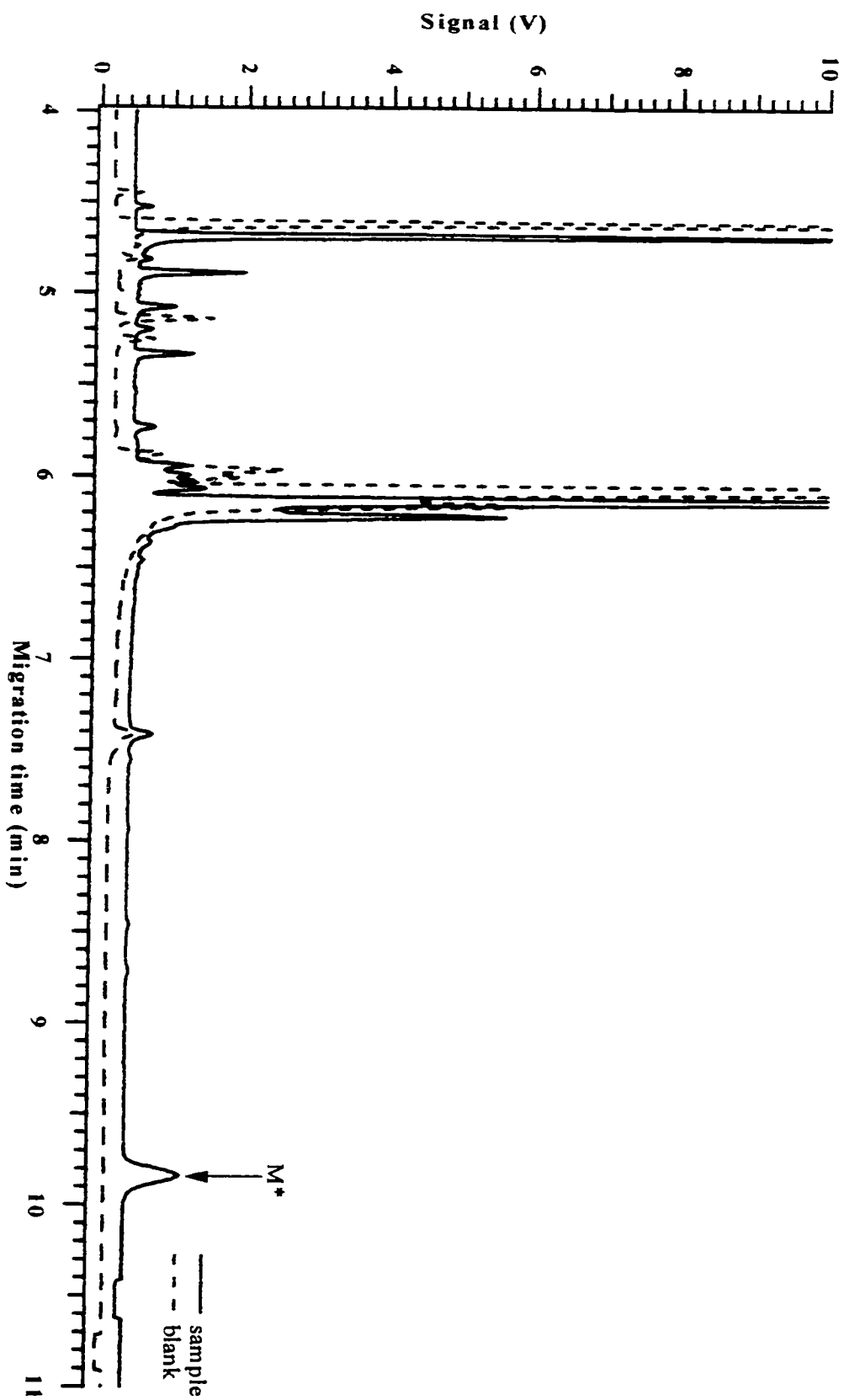PMT: 1000 V. Interference filter: 518DF25. Concentration: 10^{-7} M.

Figure 4.48: The MEKC-LIF electropherogram of labelled nonadecanoic acid (C_{19}). Capillary: 40 cm, 50 µm I.D., 140 µm O.D. Run: 10 mM borate and 50 mM SDS, pH 9, 12 kV. Injection: 1000 V, 5 s. Laser: 488 nm Ar$^+$, 12.1 mW. PMT: 1000 V. Interference filter: 518DF25. Concentration: 10^{-7} M.
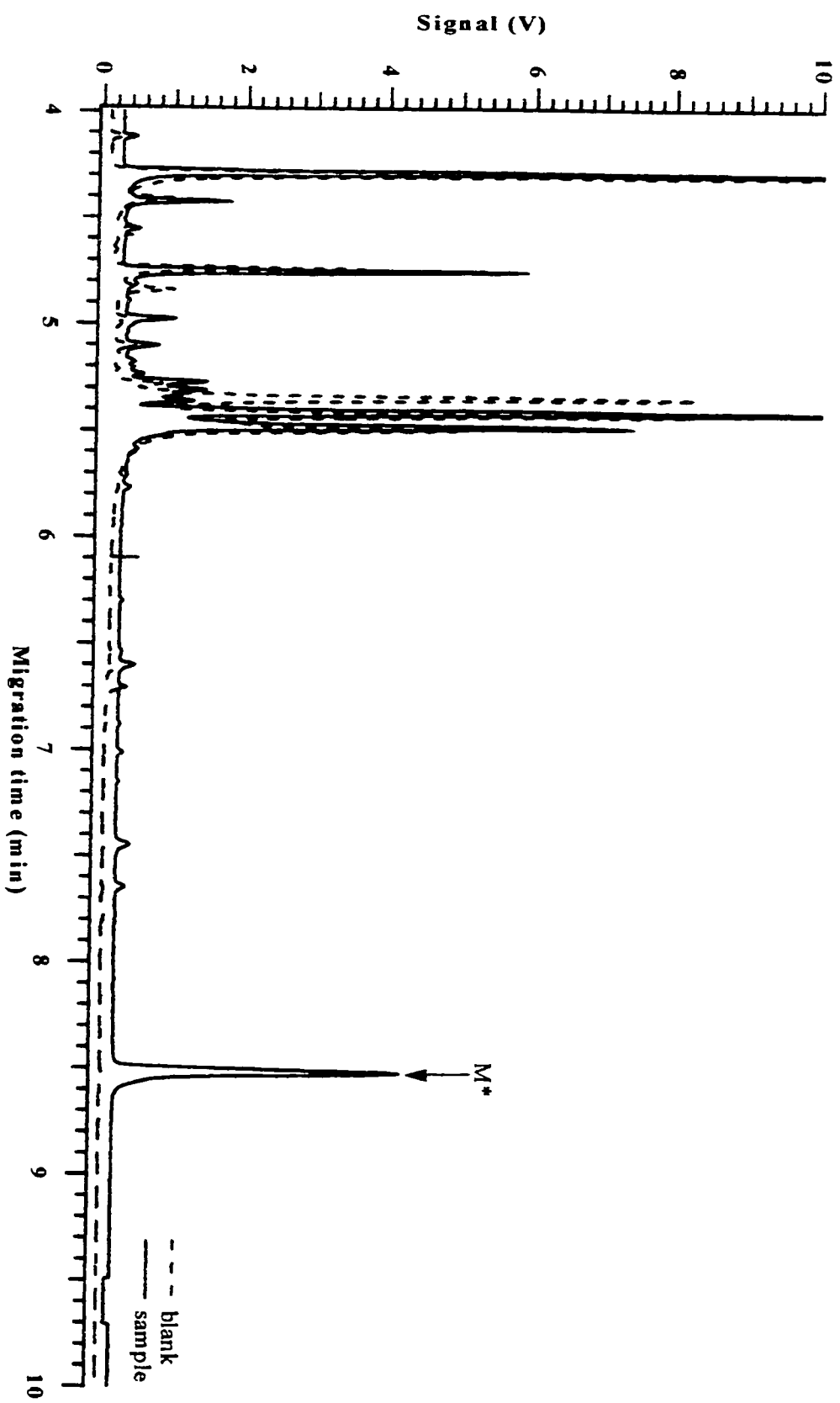
Figure 4.49: The MEKC-LIF electropherogram of labelled arachidic acid (C_{20}). Capillary: 40 cm, 50 μm I.D., 140 μm O.D..

Run: 10 mM borate and 50 mM SDS, pH 9, 12 KV. Injection: 1000 V, 5 s. Laser: 488 nm Ar^+, 12.1 mW.

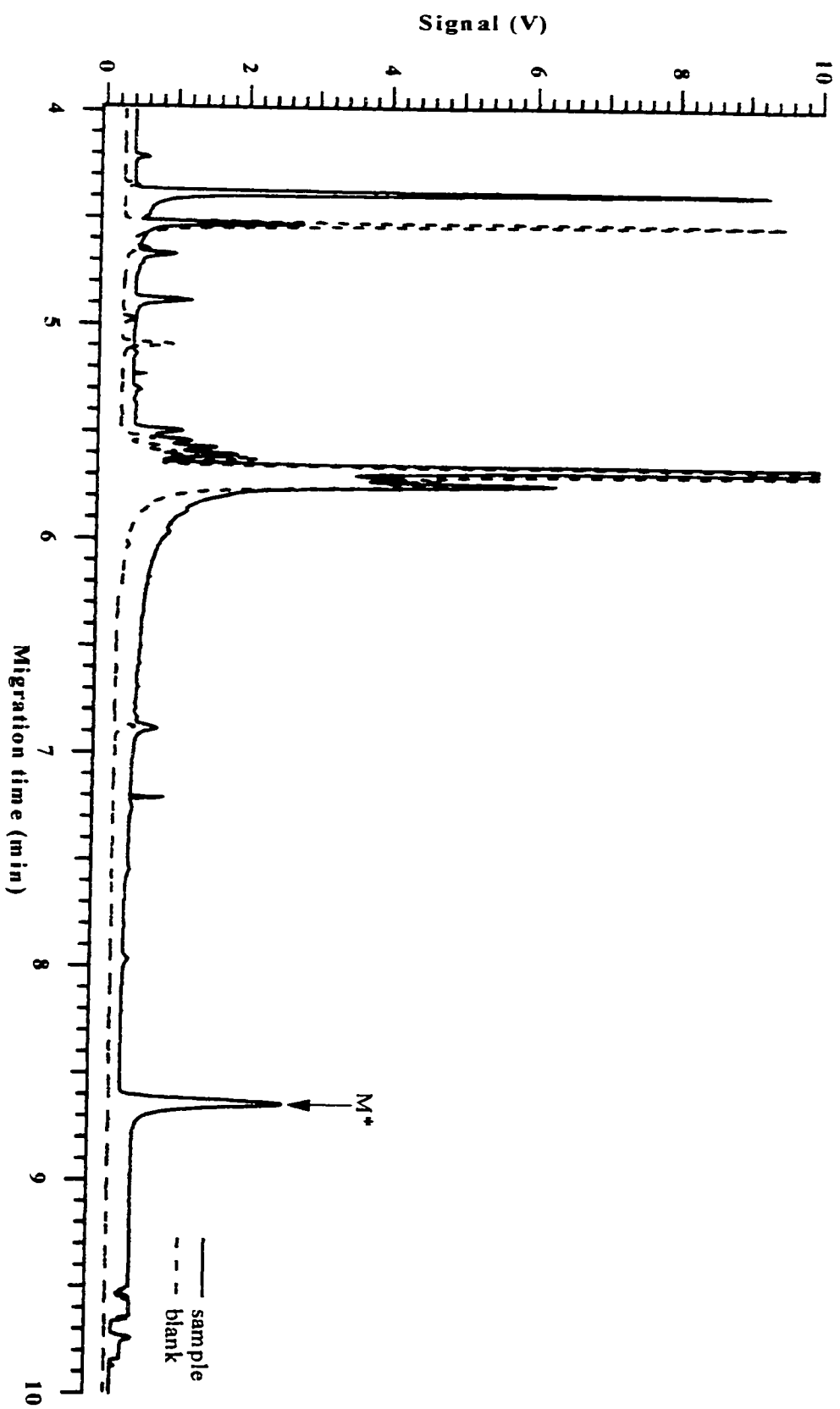PMT: 1000 V. Interference filter: 518DF25. Concentration: 10^{-7} M.

Figure 4.50: The MEKC-LIF electropherogram of labelled heneicosanic acid (C_{21}). Capillary: 40 cm, 50 µm I.D., 140 µm O.D..

Run: 10 mM borate and 50 mM SDS, pH 9, 12 kV. Injection: 1000 V, 5 s. Laser: 488 nm Ar^+, 12.1 mW.

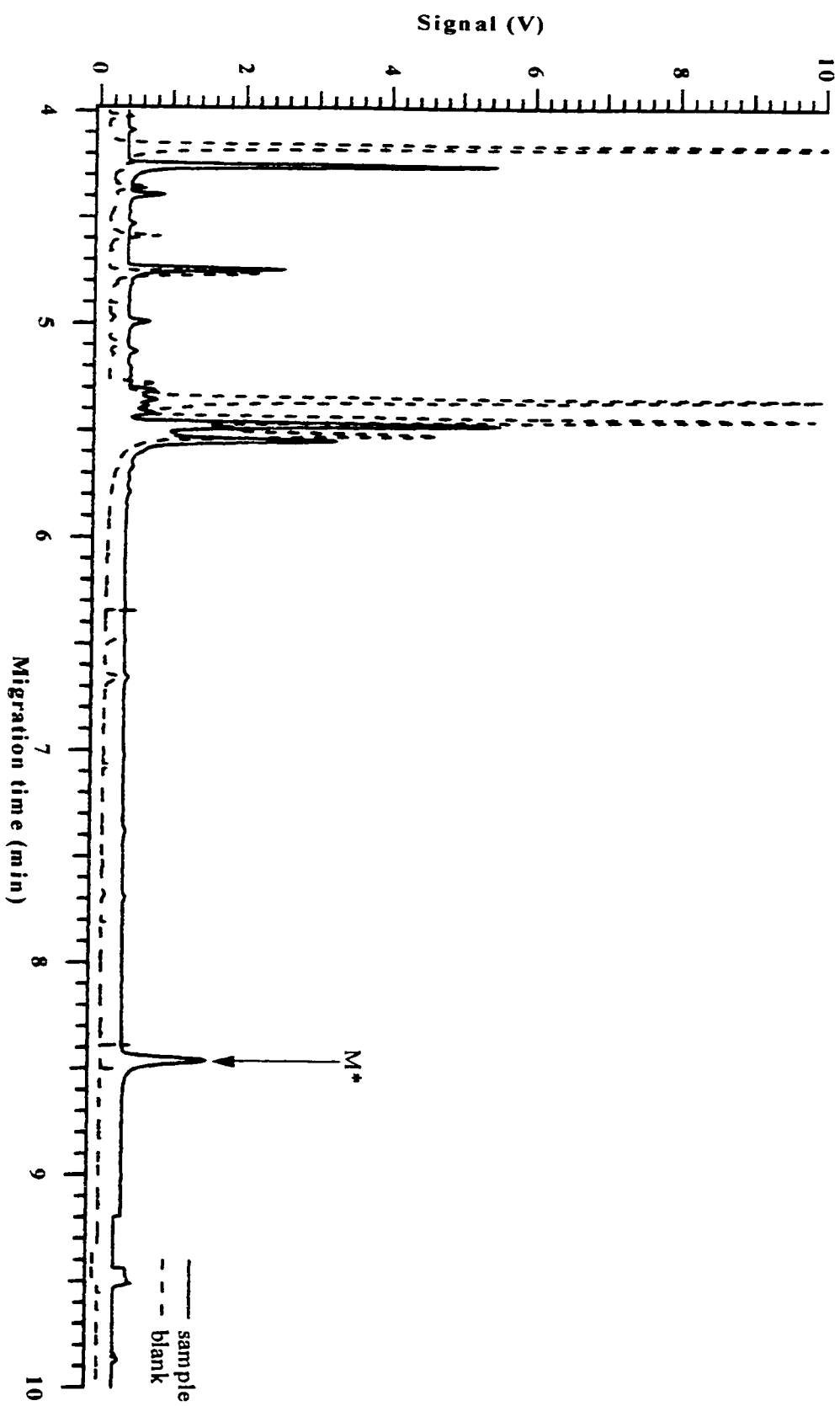PMT: 1000 V. Interference filter: 518DF25. Concentration: 10^{-7} M.

Figure 4.51: The MEKC-LIF electropherogram of labelled behenic acid (C_{22}). Capillary: 40 cm, 50 μm I.D., 140 μm O.D.

Run: 10 mM borate and 50 mM SDS, pH 9, 12 kV. Injection: 1000 V, 5 s. Laser: 488 nm Ar^+, 12.1 mW.

PMT: 1000 V. Interference filter: 518DF25. Concentration: 10^{-7} M.
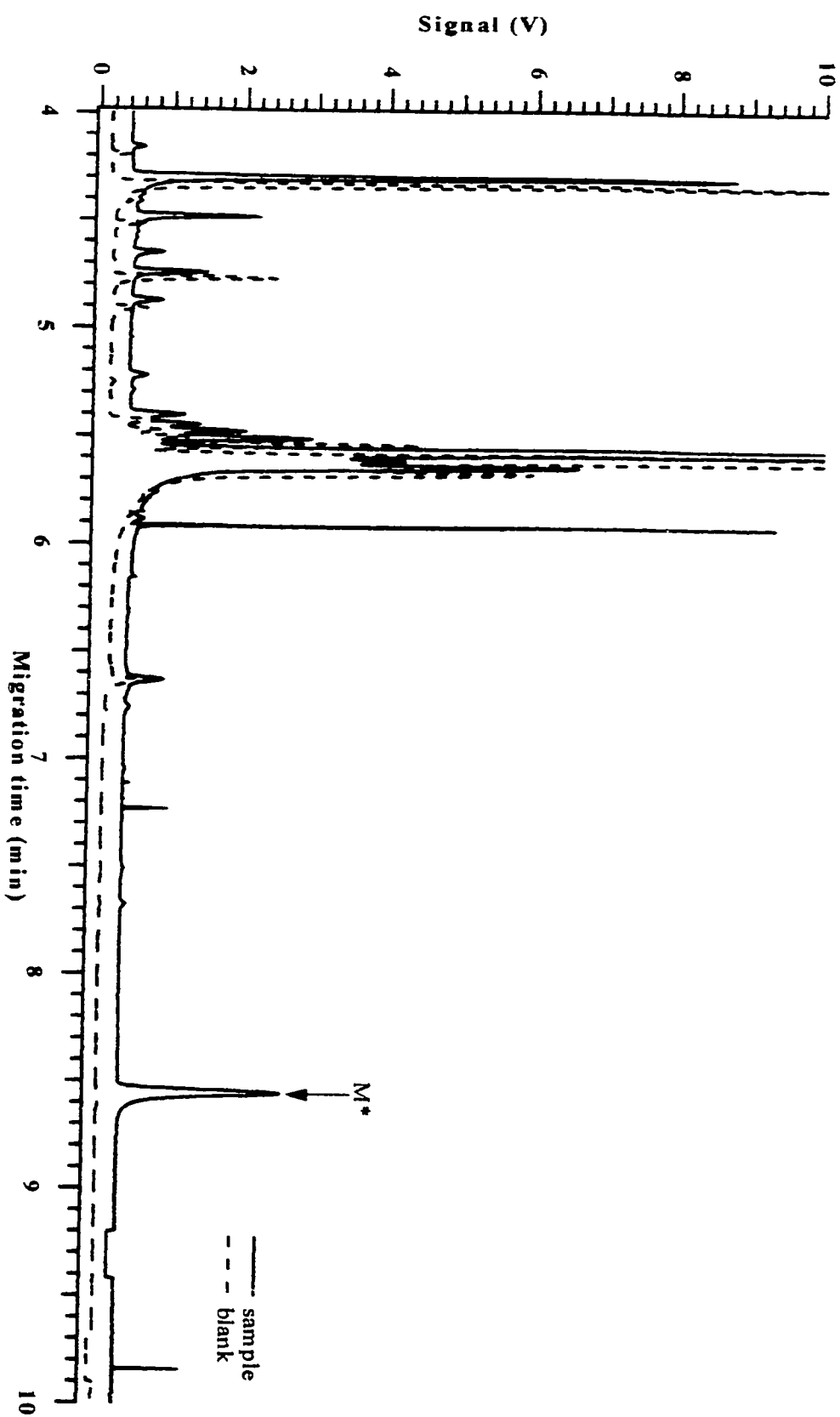
Figure 4.52: The MEKC-LIF electropherogram of labelled tricosanic acid (C_{23}). Capillary: 40 cm, 50 μm I.D., 140 μm O.D.. Run: 10 mM borate and 50 mM SDS, pH 9, 12 kV. Injection: 1000 V, 5 s. Laser: 488 nm Ar^+, 12.1 mW. PMT: 1000 V. Interference filter: 518DF25. Concentration: 10^{-7} M.
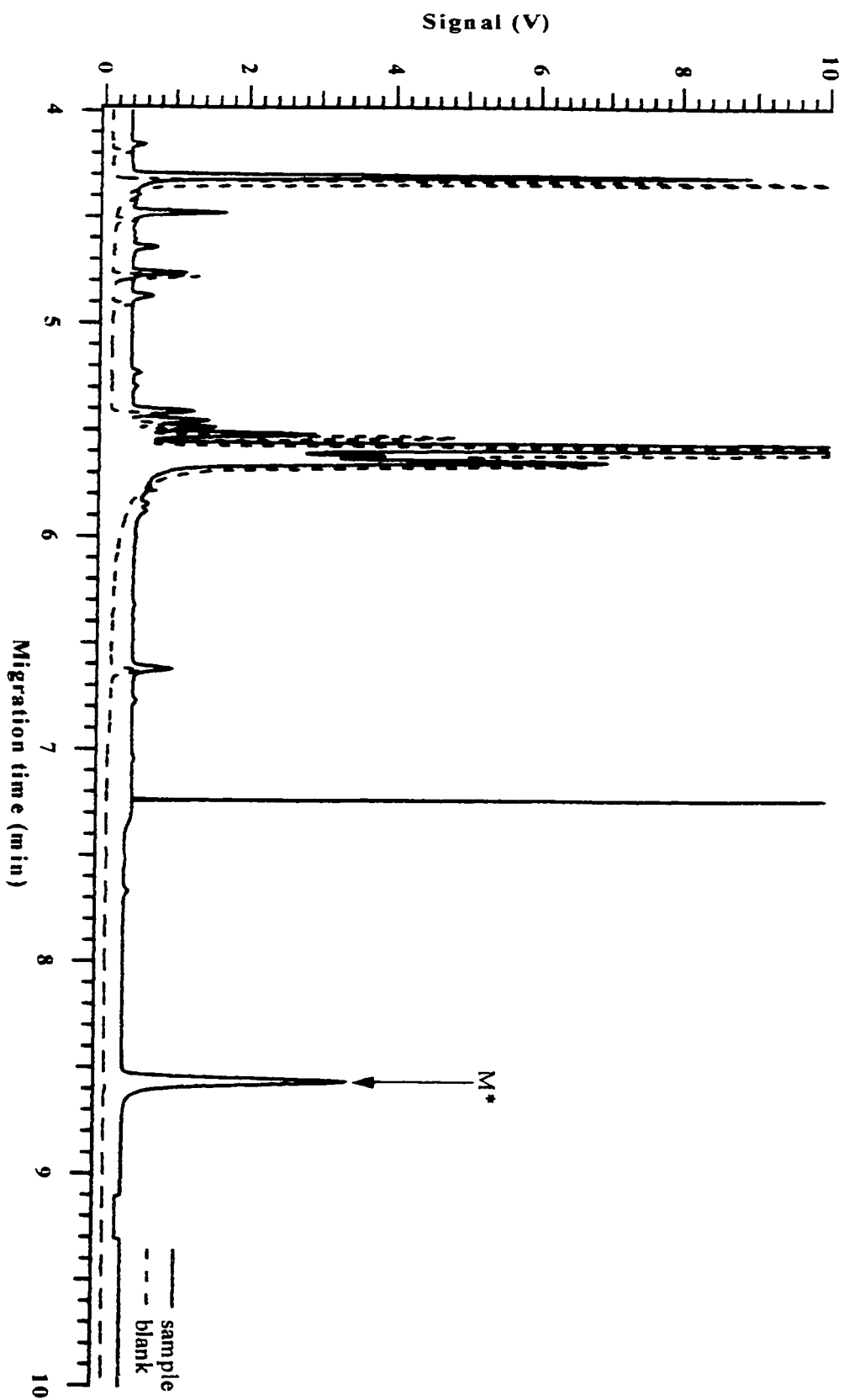
Figure 4.53: The MEKC-LIF electropherogram of labelled lignoceric acid (C_{24}). Capillary: 40 cm, 50 μm I.D., 140 μm O.D.. Run: 10 mM borate and 50 mM SDS, pH 9, 12 kV. Injection: 1000 V, 5 s. Laser: 488 nm Ar^+, 12.1 mW. PMT: 1000 V. Interference filter: 518DF25. Concentration: 10^{-7} M.
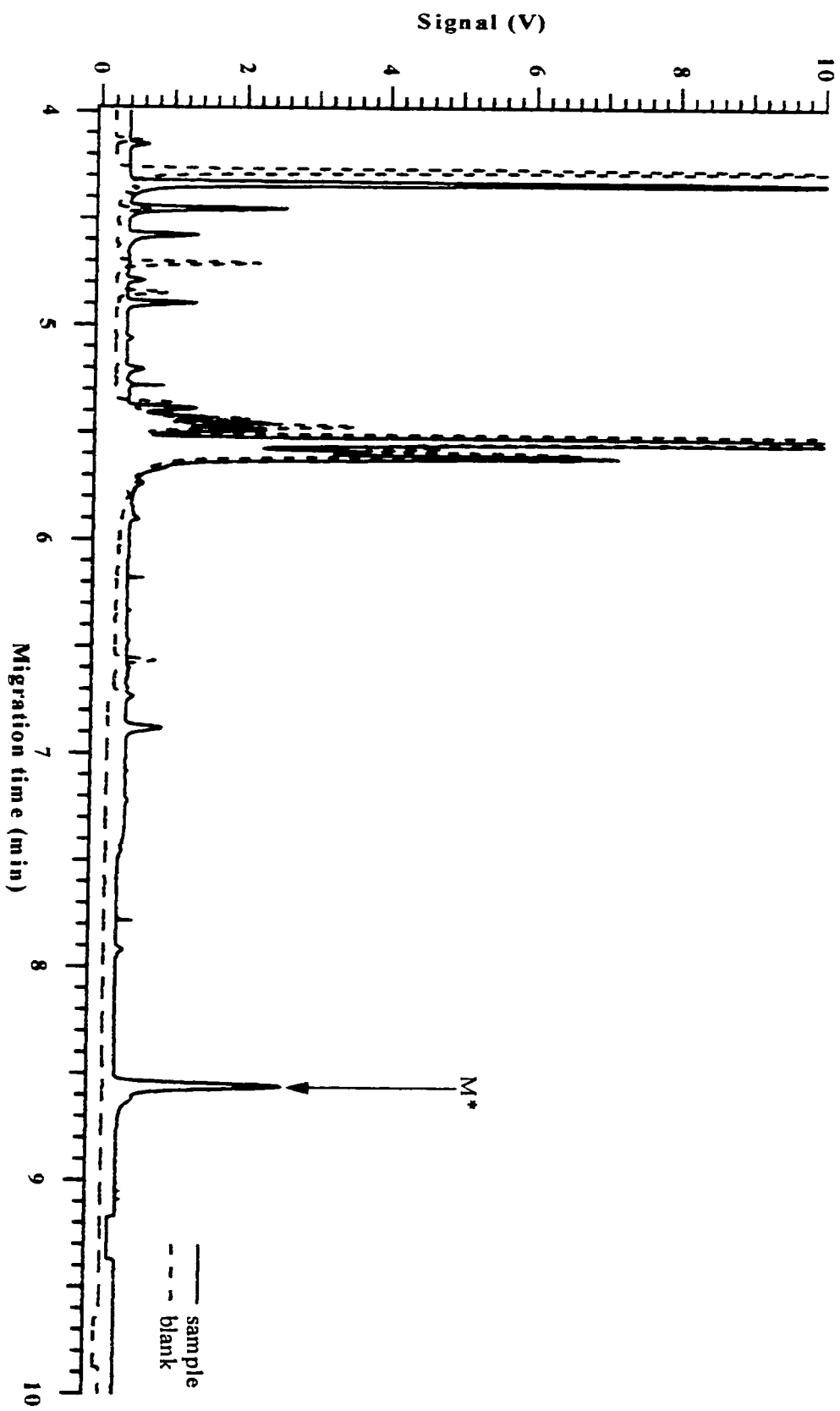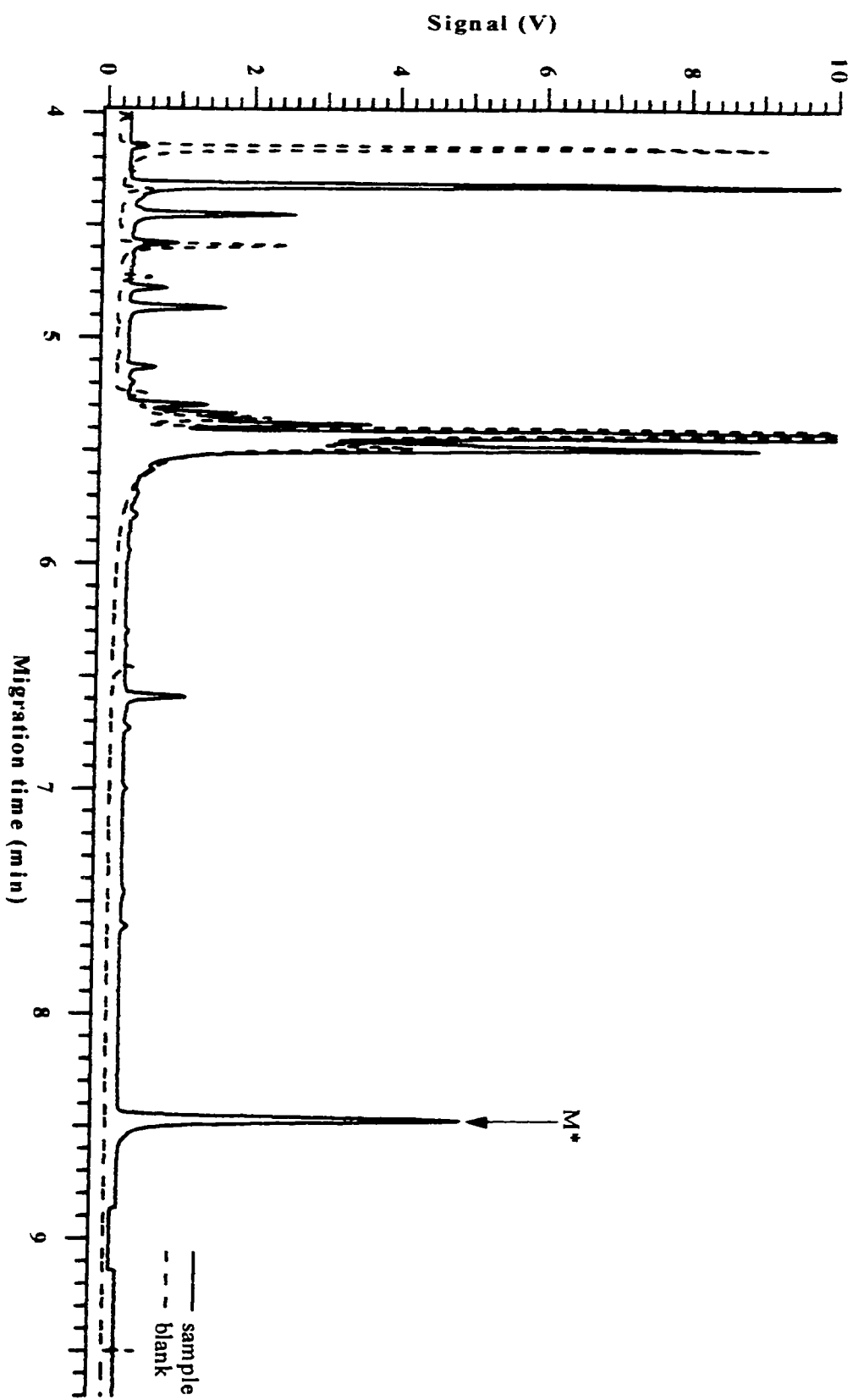
Table 4.2: A summary of all the data for the MEKC-LIF separations of the homologous series of labelled linear saturated FFAs ($C_6 - C_{24}$) (n = 1).

Name of acid	Carbon number (n)	Migration time (min)	Peak height (V)	Peak area (arbitrary units)	Injected volume (nL)	Limit of detection (nM)	Number of theoretical plates (*10^5 plates)
caproic	6	6.3	5.456	0.178	0.87	0.3	2.7
caprylic	8	9.4	4.539	0.359	0.58	0.1	0.9
nonanoic	9	8.7	3.450	0.231	0.63	0.5	1.3
capric	10	8.8	4.483	0.286	0.62	0.4	1.3
undecanoic	11	8.7	2.605	0.137	0.63	0.2	2.2
lauric	12	8.6	1.749	0.091	0.63	0.7	2.0
tridecanoic	13	8.5	3.189	0.141	0.64	0.2	2.6
myristic	14	8.6	2.876	0.130	0.64	0.7	2.6
pentadecanoic	15	8.8	1.385	0.081	0.62	0.4	1.8
palmitic	16	8.7	1.319	0.065	0.63	0.4	2.2
heptadecanoic	17	9.8	0.567	0.065	0.55	2.2	0.5
stearic	18	8.5	3.984	0.151	0.64	0.2	4.4
nonadecanoic	19	8.7	1.658	0.084	0.63	0.7	2.3
arachidic	20	8.5	1.149	0.048	0.64	0.4	3.2
heneicosanoic	21	8.5	3.073	0.128	0.64	0.4	3.1
behenic	22	8.6	2.228	0.093	0.64	0.4	3.4
tricosanic	23	8.6	2.284	0.086	0.64	0.5	4.0
lignoceric	24	8.5	2.204	0.083	0.64	0.2	4.0

When the LOD values in Table 4.1 and 4.2 are compared it is evident that the LOD values calculated for the MEKC-LIF separations of the homologous series of labelled linear saturated FFAs are much higher than the values found using CZE-LIF. This degradation in LOD in the MEKC-LIF separations could be due to the presence of micelle surfactant in the electrolyte or it could be due to the degradation of the product with time. Data plots of migration time, peak height, peak area, volume injected, LOD and number of theoretical plates versus carbon number were constructed for the labelled purchased and synthesized FFAs to determine if there are any relationships between the variables. The data from the MEKC-LIF separations of the labelled purchased FFAs and the labelled synthesized FFAs were not plotted together in order to ensure validity as explained earlier in Section 4.3.1. The data plots for labelled purchased and synthesized FFAs can be found in Figures 4.54 and 4.55, respectively. The data plots of peak height, peak area, LOD and number of theoretical plates versus carbon number for the labelled purchased FFAs did not reveal any relationships between the variables. The data plots of migration time and volume injected versus carbon number for the labelled purchased FFAs revealed that the migration time exponentially increased and the volume injected exponentially decreased with an increase in carbon number. The data plots for the labelled synthesized FFAs in Figure 4.54 did not reveal any relationships between migration time, peak height, peak area, volume injected, LOD or number of theoretical plates and carbon number.

Next, a mixture of the labelled linear saturated FFAs ($C_6 - C_{24}$) was separated using MEKC-LIF under the run conditions described in Section 4.2.11 and the resulting electropherograms can be found in Figure 4.56. The MEKC-LIF electropherograms

Figure 4.54: The data plots of A) migration time, B) peak height, C) peak area,

D) volume injected, E) limit of detection, and F) number of theoretical

plates versus carbon number for the MEKC-LIF separations of the labelled
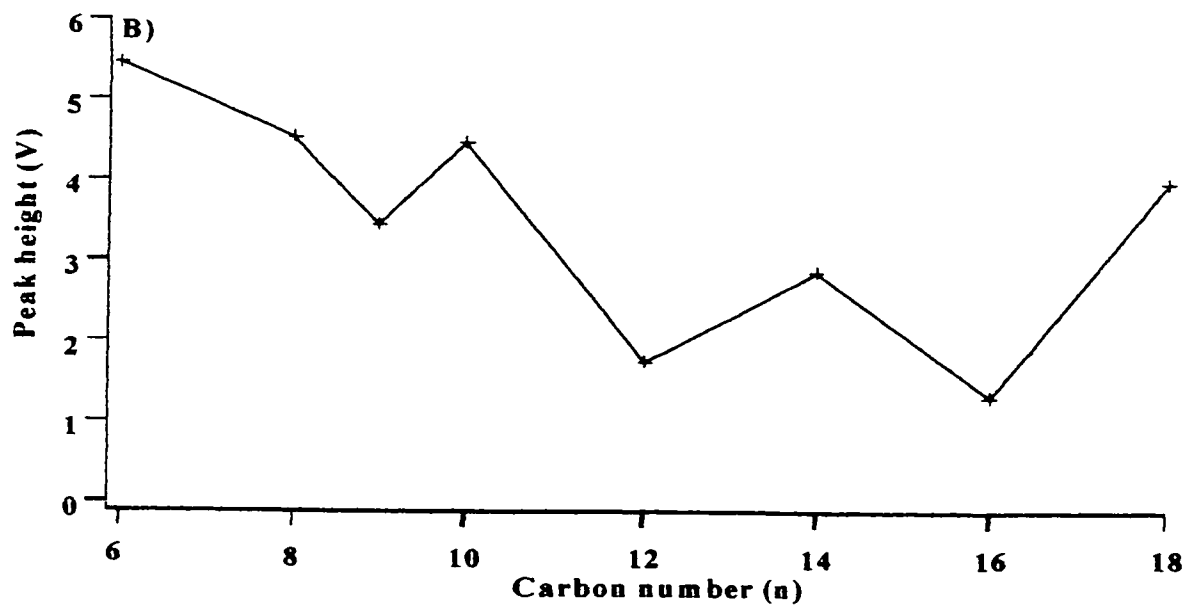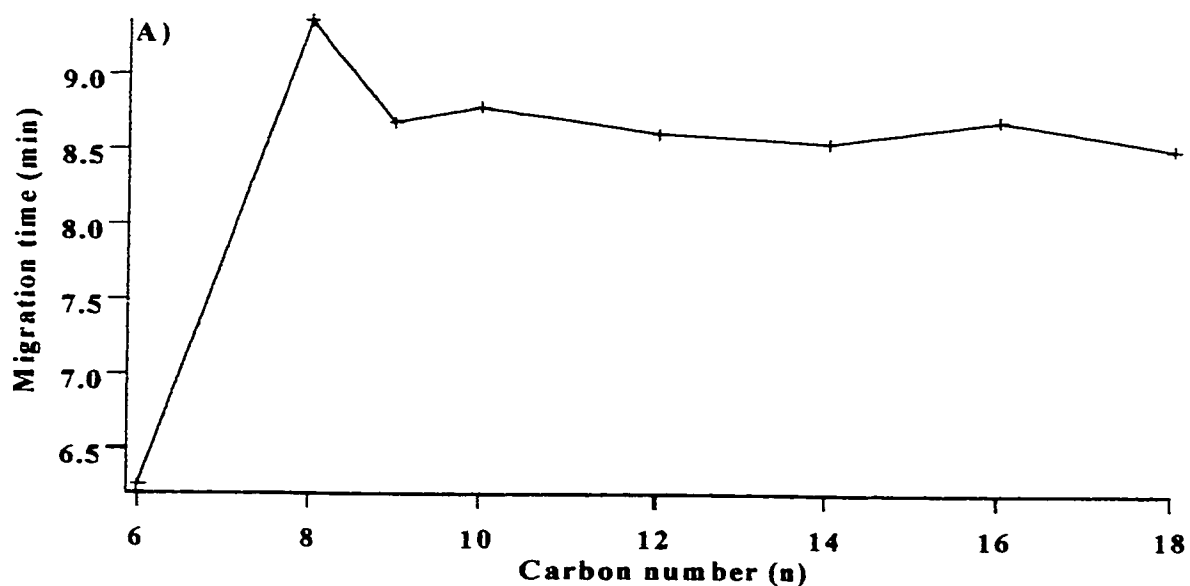
purchased FFAs (n = 1).
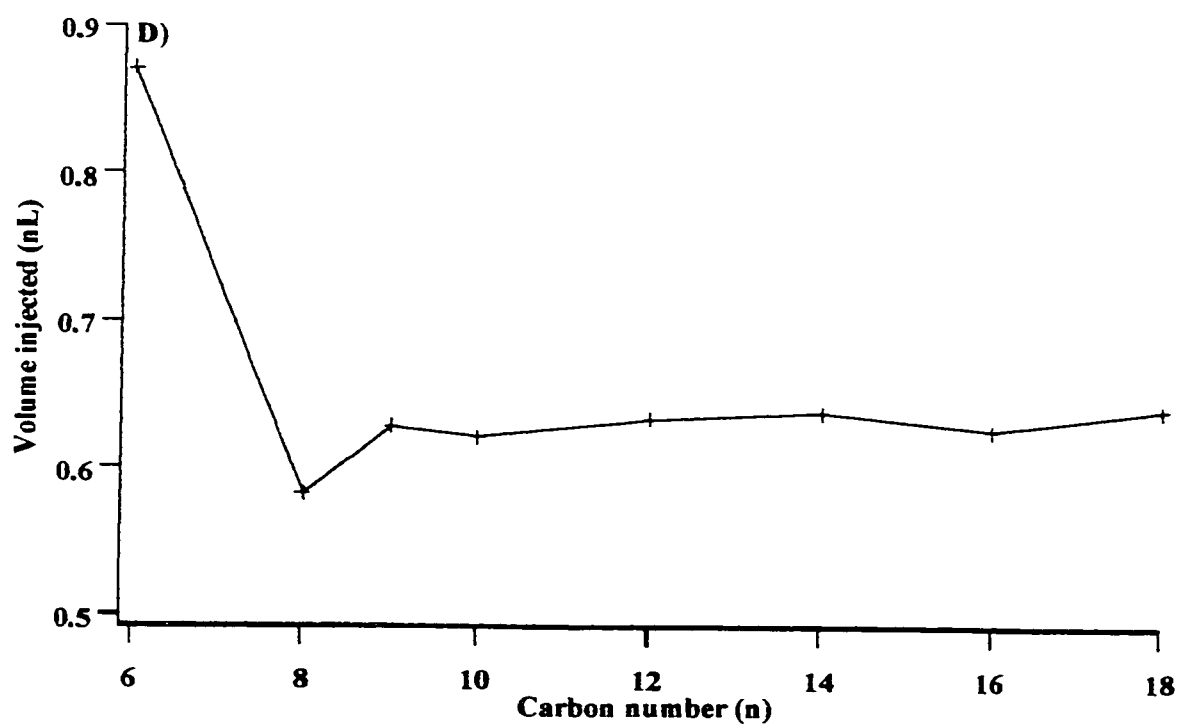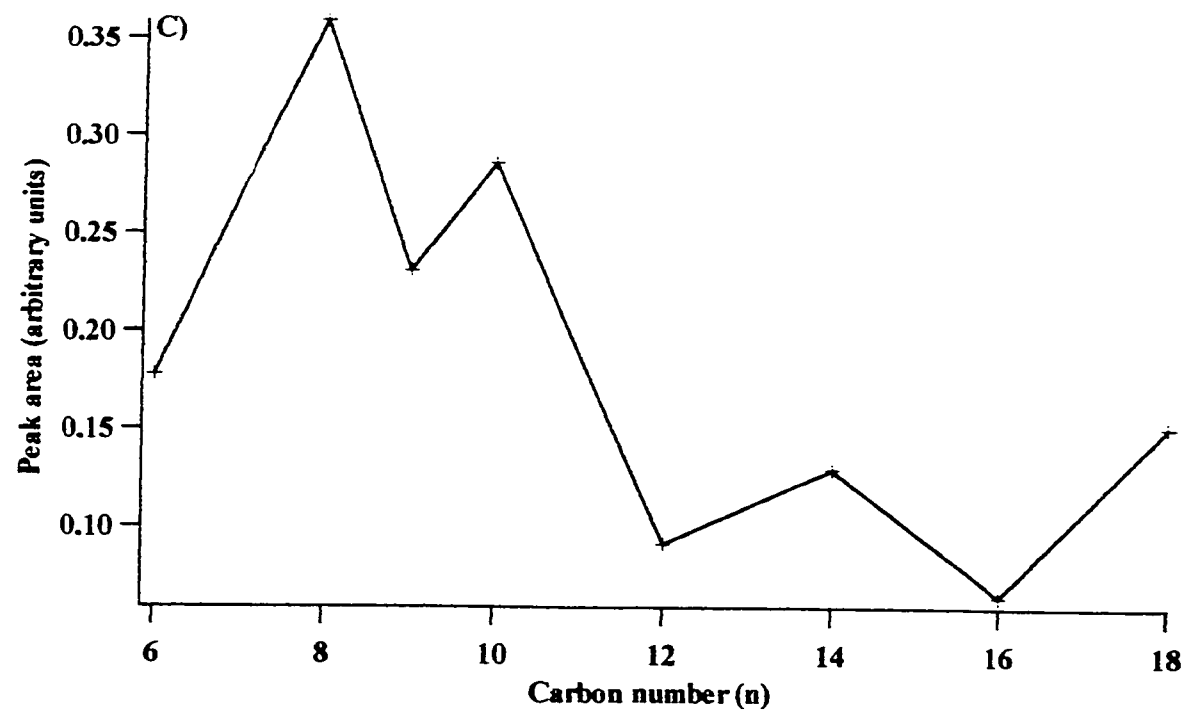
Figure 4.54: (continued)

E)

Limit of detection (nM)

Carbon number (n)

F)

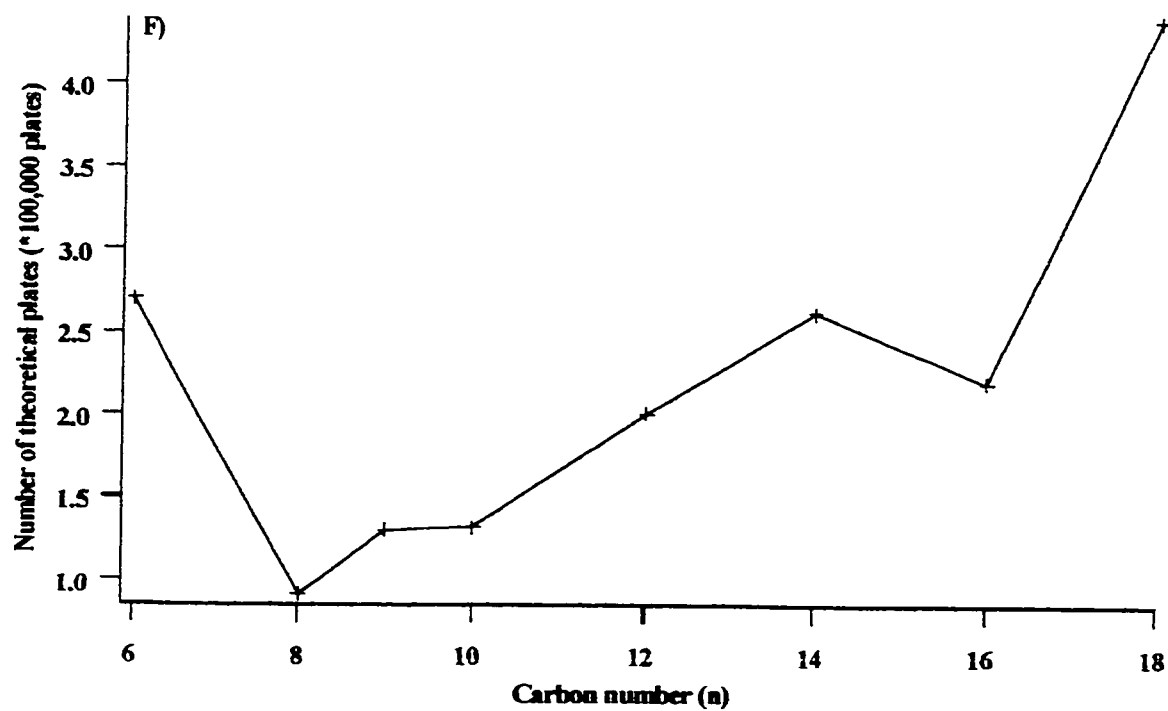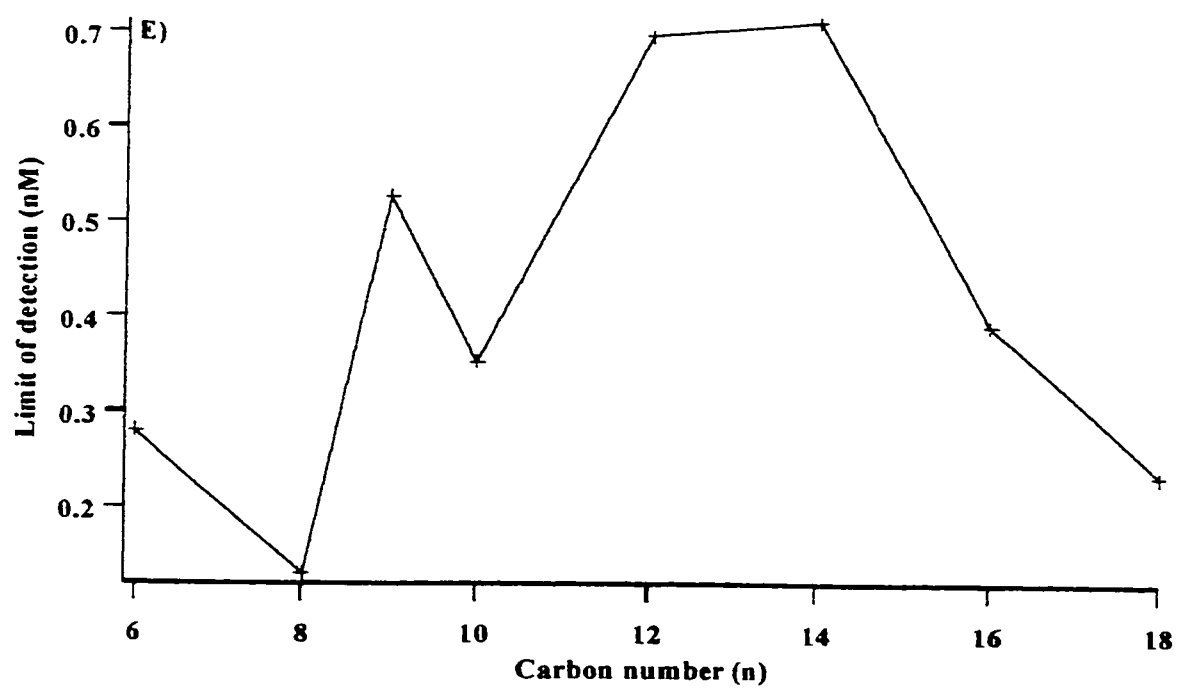Number of theoretical plates (*100,000 plates)

Carbon number (n)

Figure 4.55: The data plots of A) migration time, B) peak height, C) peak area, D) volume injected, E) limit of detection, and F) number of theoretical plates versus carbon number for the MEKC-LIF separations of the labelled synthesized FFAs (n = 1).
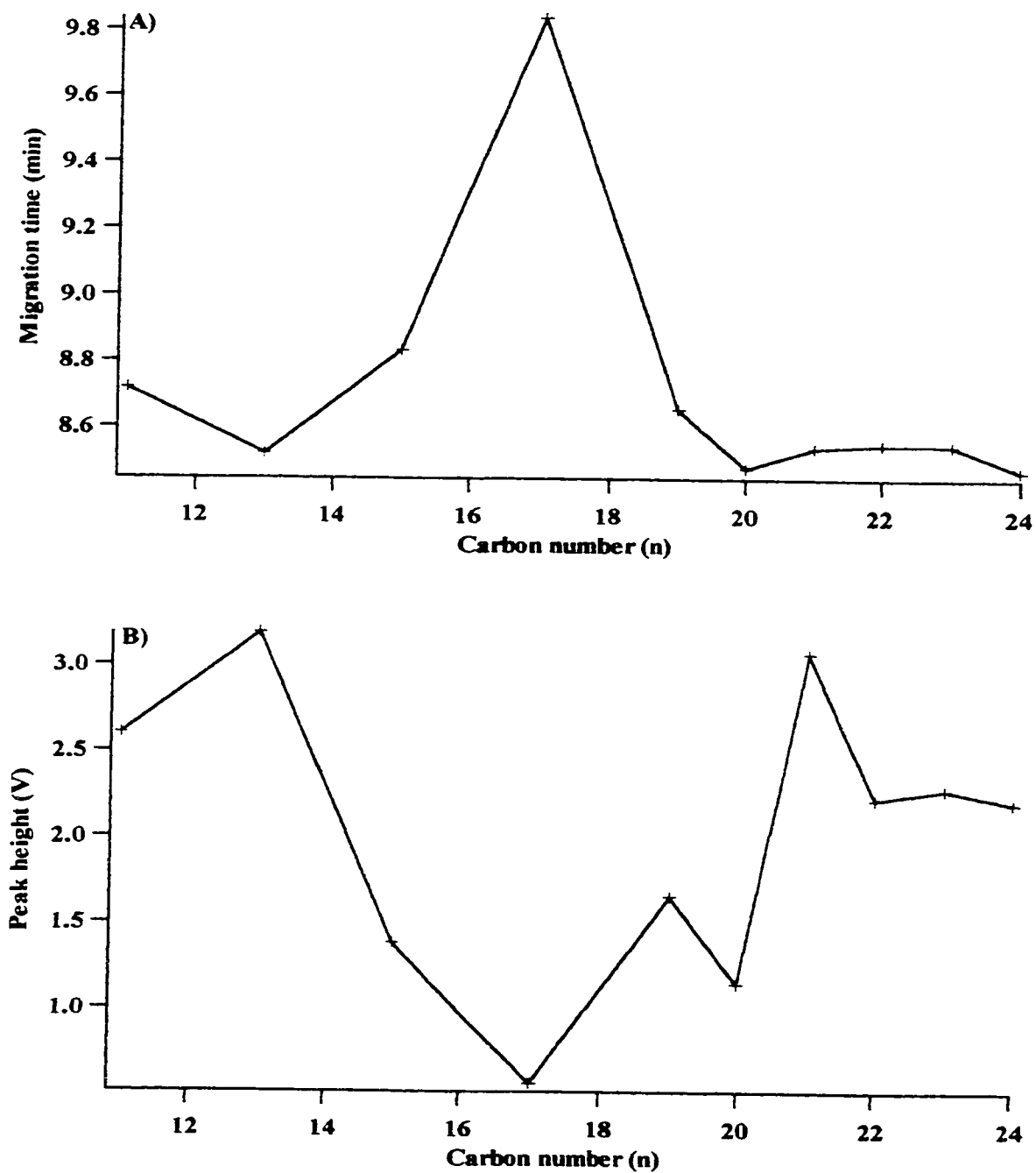
Figure 4.55: (continued)
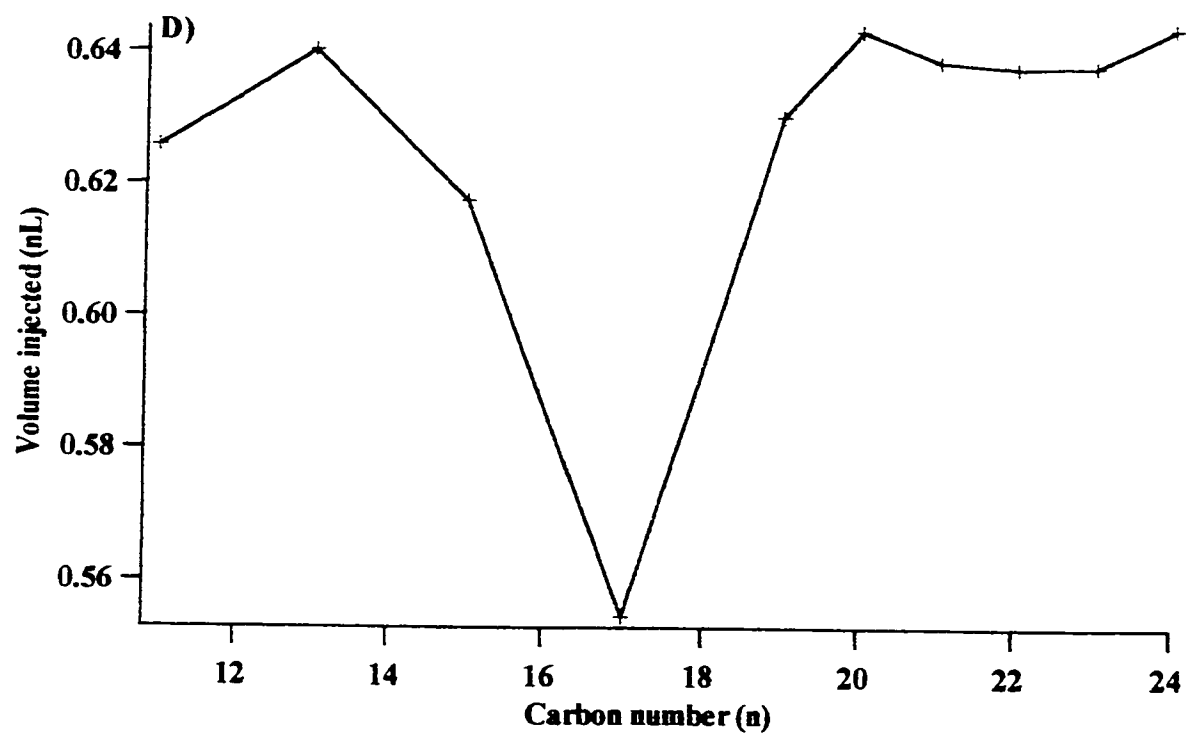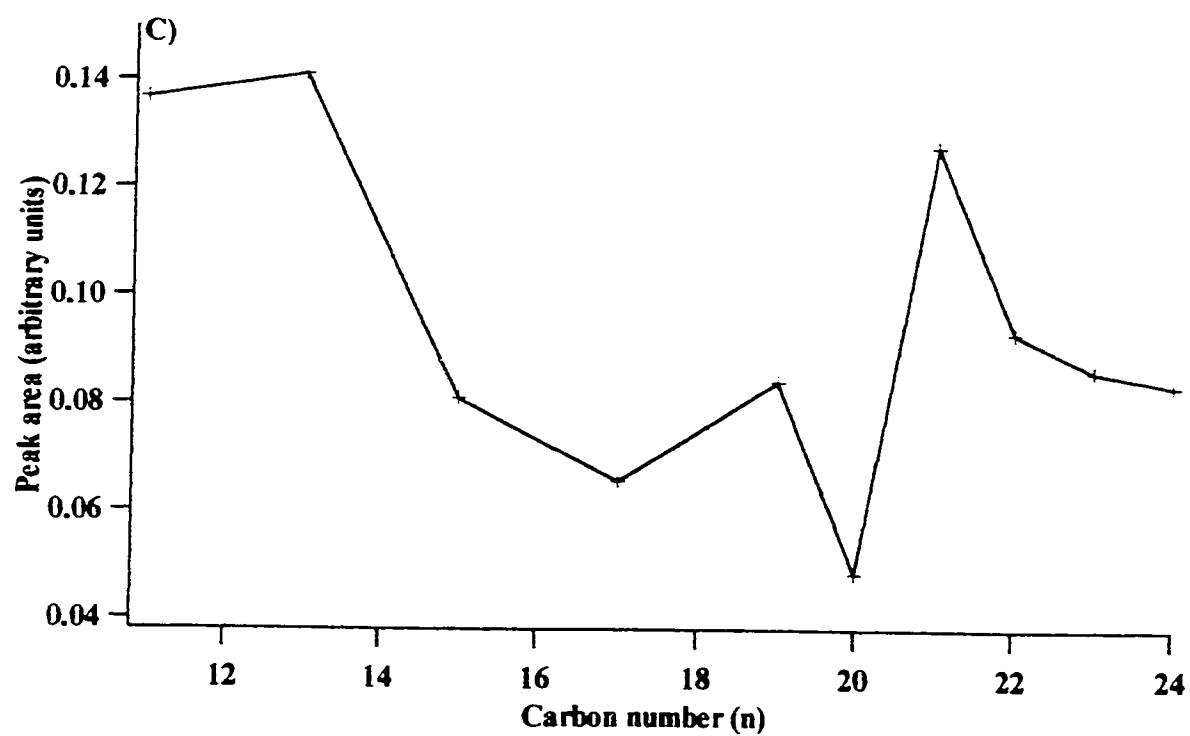
Figure 4.55: (continued)
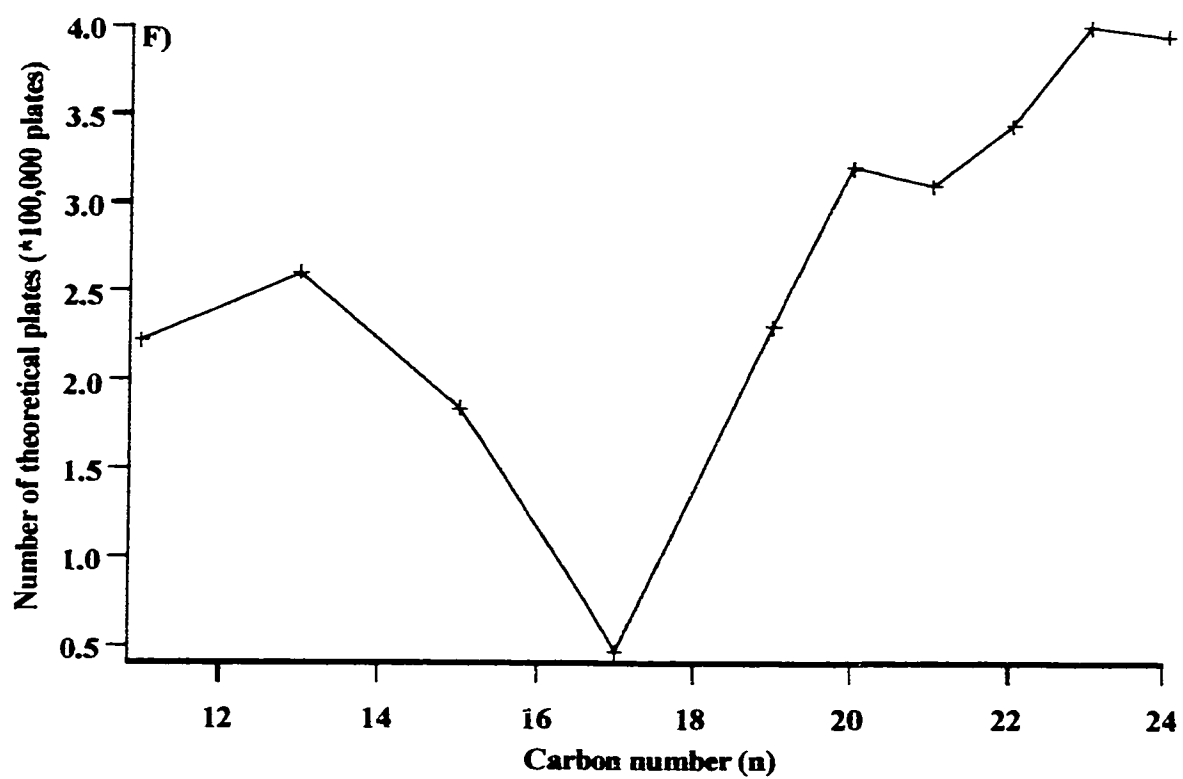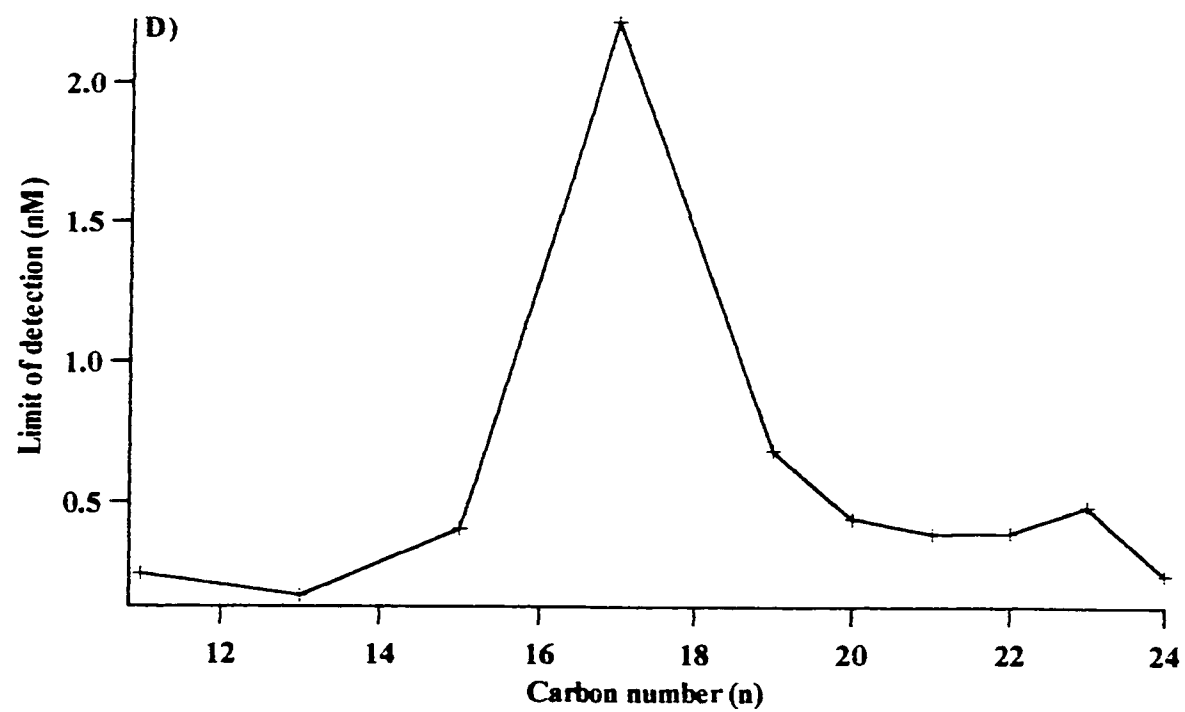
Figure 4.56: The MEKC-LIF electropherograms of the separation of a labelled linear saturated FFA mixture ($C_6 - C_{14}$).

Capillary: 40 cm, 50 μm I.D., 140 μm O.D.. Run: 10 mM borate and 50 mM SDS, pH 9, 12 kV. Injection: 1000 V, 5 s.

Laser: 488 nm Ar$^+$, 12.1 mW. PMT: 1000 V. Concentration: 10^{-7} M. The MEKC-LIF electropherogram contains

A) FFA C_6; B) FFAs C_6, C_8; C) FFAs C_6, C_8, C_9; D) FFAs C_6, C_8-C_{10}; E) FFAs C_6, $C_8 - C_{11}$; F) FFAs C_6, $C_8 - C_{12}$;

G) FFAs C_6, $C_8 - C_{13}$; and H) FFAs C_6, $C_8 - C_{14}$.

Figure 4.56: (continued)

Figure 4.56: (continued)

278

show that there is some improvement in separation compared to Figure 4.22 since labelled linear saturated FFAs of carbon number up to 11 can now be resolved. This 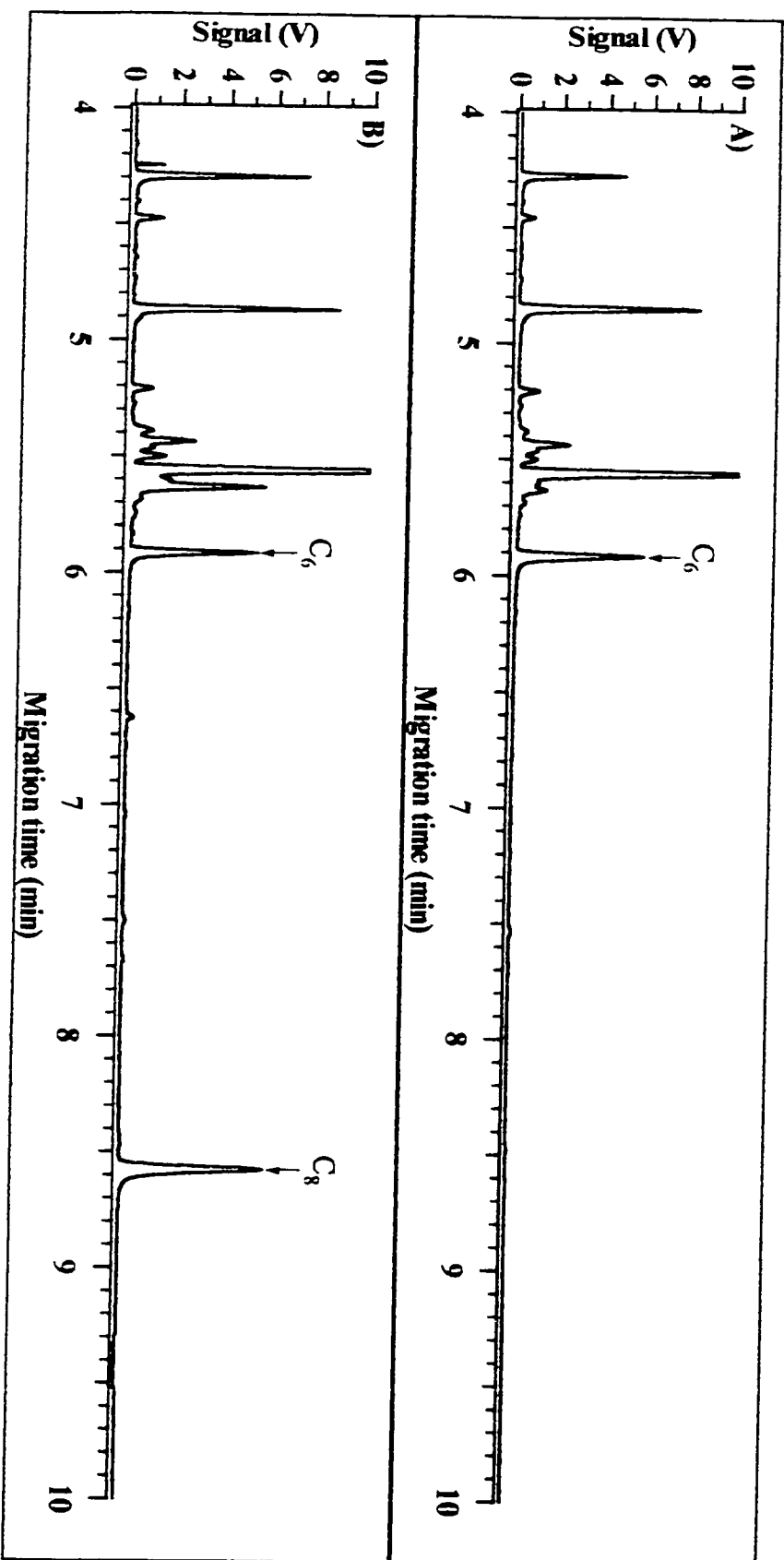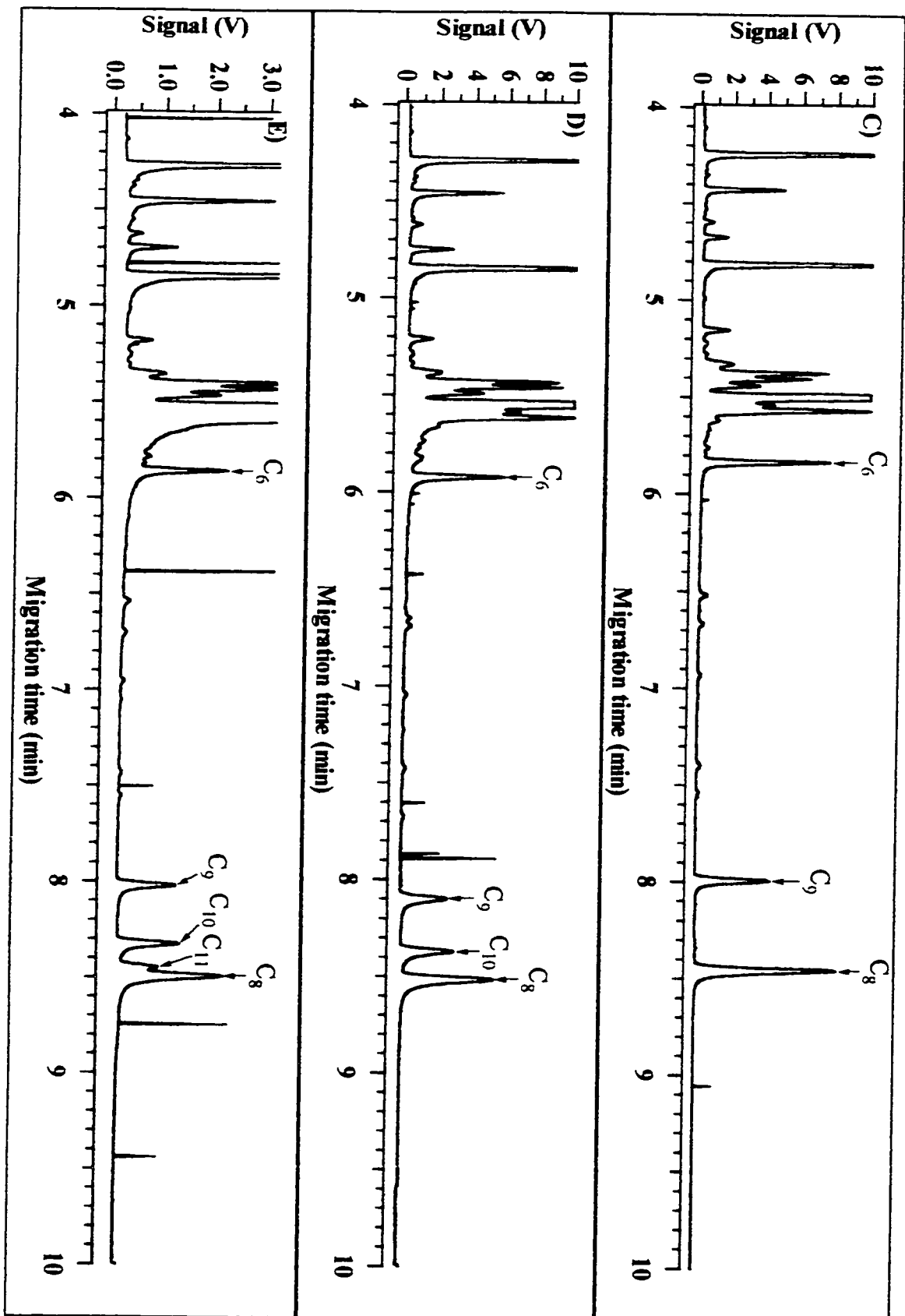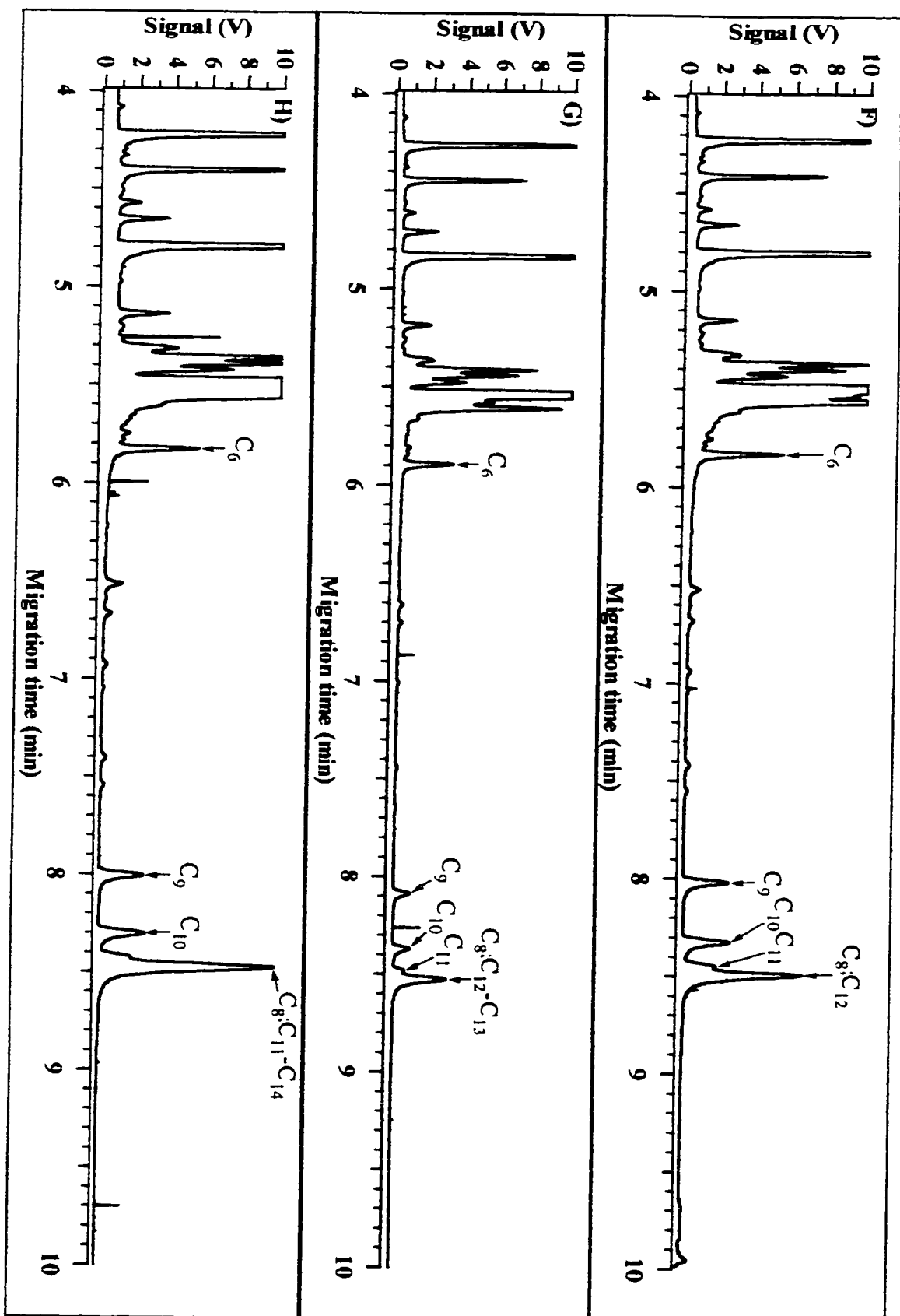result illustrates that the presence of micelle surfactant in the electrolyte used for CE separation does help separation resolution.

4.3.7 Positive-ion mode ESI-MS spectra of a homologous series of labelled FFAs

Next, the sample reaction mixtures of each linear saturated FFA in the homologous series were checked for the presence of product using positive-ion mode ESI-MS to confirm that the carbonyl-labelling reactions were successful. The positive-ion mode ESI-MS spectra of the homologous series of linear saturated FFAs can be found in Figures 4.57 – 4.65. These positive-ion mode ESI-MS spectra show that all the carbonyl-labelling reactions performed, with the exception of the reaction that involved caprylic acid sodium salt, were successful since product peaks for all the labelled linear saturated FFAs were found as hydrogen adducts. The positive-ion mode ESI-MS spectrum for labelled caprylic acid, which can be found in Figure 4.57, reveals a $(M^* + H)^+$ peak, which corresponds to labelled lauric acid not labelled caprylic acid and thus, it was concluded that a systematic error must have occurred during the carbonyl-labelling reaction. As a result of this systematic error, the CZE-LIF and MEKC-LIF data found in the respective separations of labelled caprylic acid are not valid and therefore, should not be included in the data plots. This error also explains why a peak for FFA C_8 (really C_{12}) was not found in the CZE separation involving a Grignard-poly-AAP-coated capillary (Figure 4.23) since peaks for FFAs with carbon numbers greater than C_{10} could not be resolved.

279

Figure 4.57: The positive-ion mode ESI–MS spectra of labelled A) caproic acid C_6 and B) caprylic acid C_8.
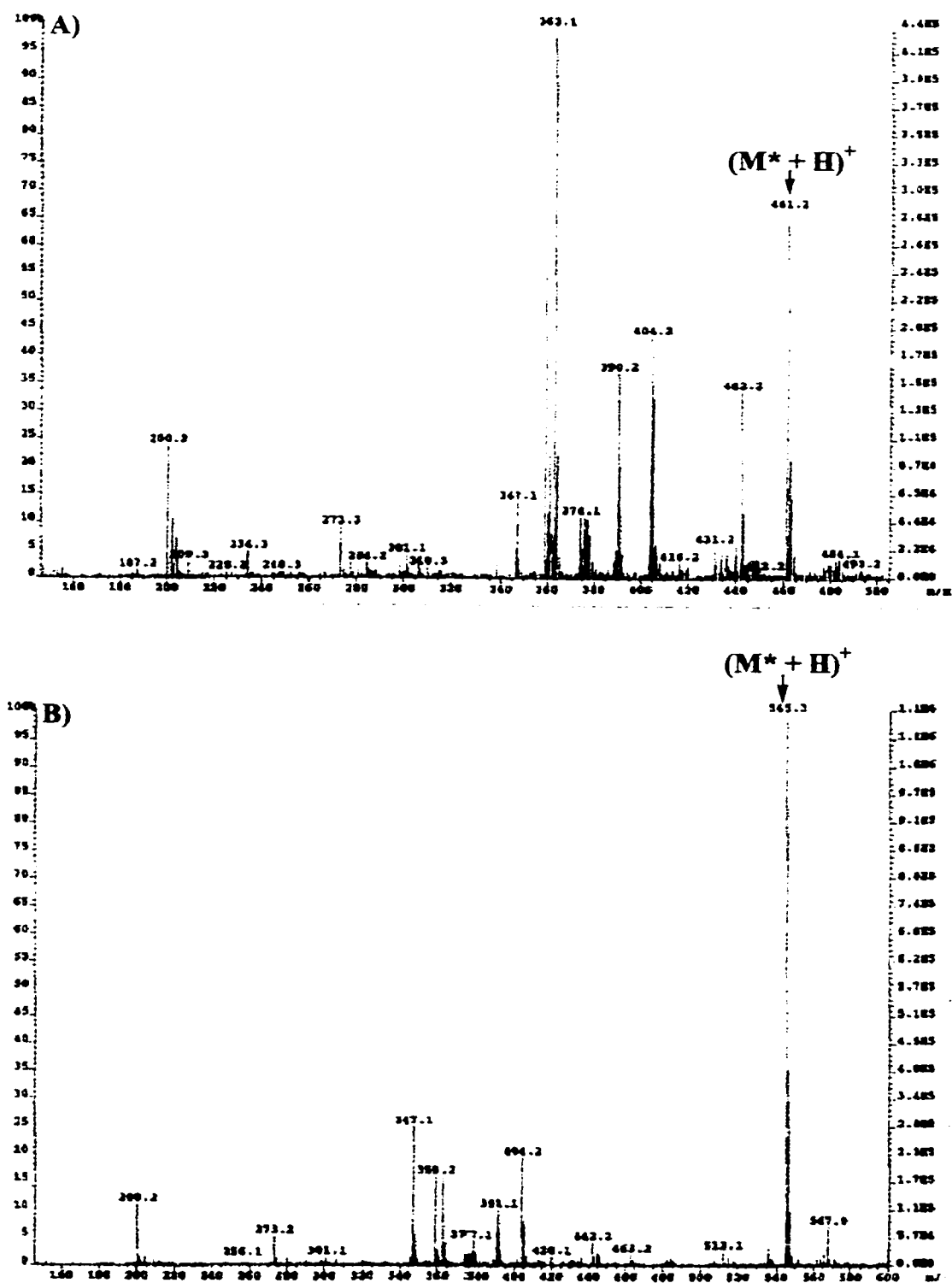
Figure 4.58: The positive-ion mode ESI-MS spectra of labelled A) nonanoic acid C_9 and B) capric acid C_{10}.

Figure 4.59: The positive-ion mode ESI-MS spectra of labelled A) undecanoic

acid C_{11} and B) lauric acid C_{12}.
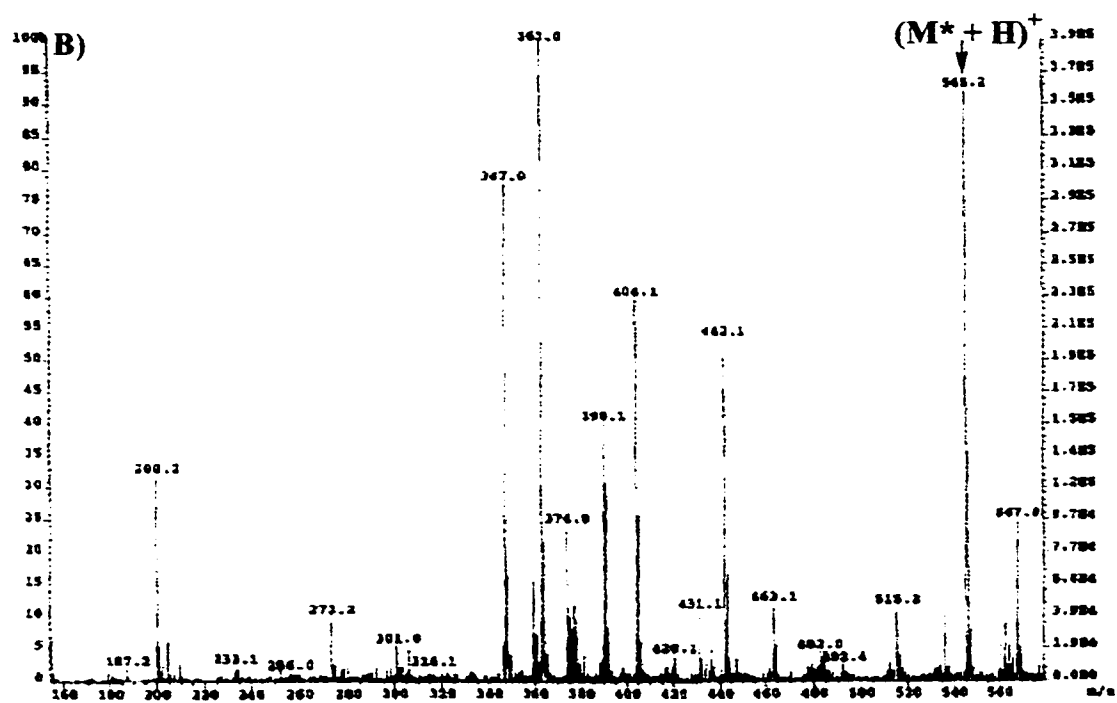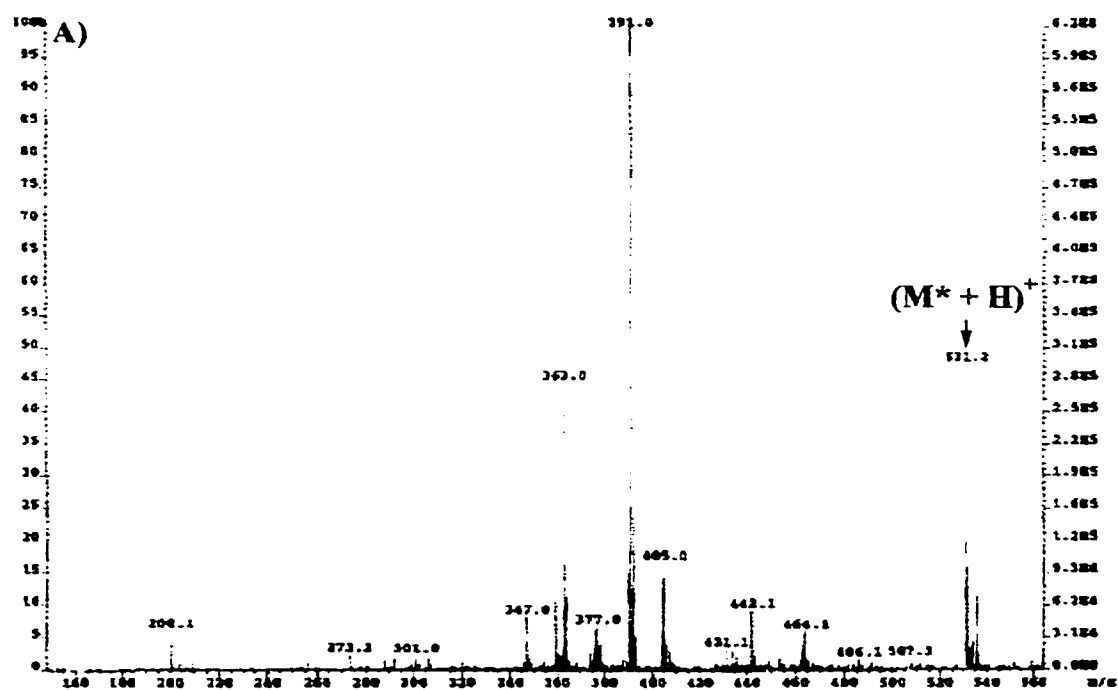
Figure 4.60: The positive-ion mode ESI-MS spectra of labelled A) tridecanoic

acid C_{13} and B) myristic acid C_{14}.

Figure 4.61: The positive-ion mode ESI-MS spectra of labelled A) pentadecanoic

acid C_{15} and B) palmitic acid C_{16}.
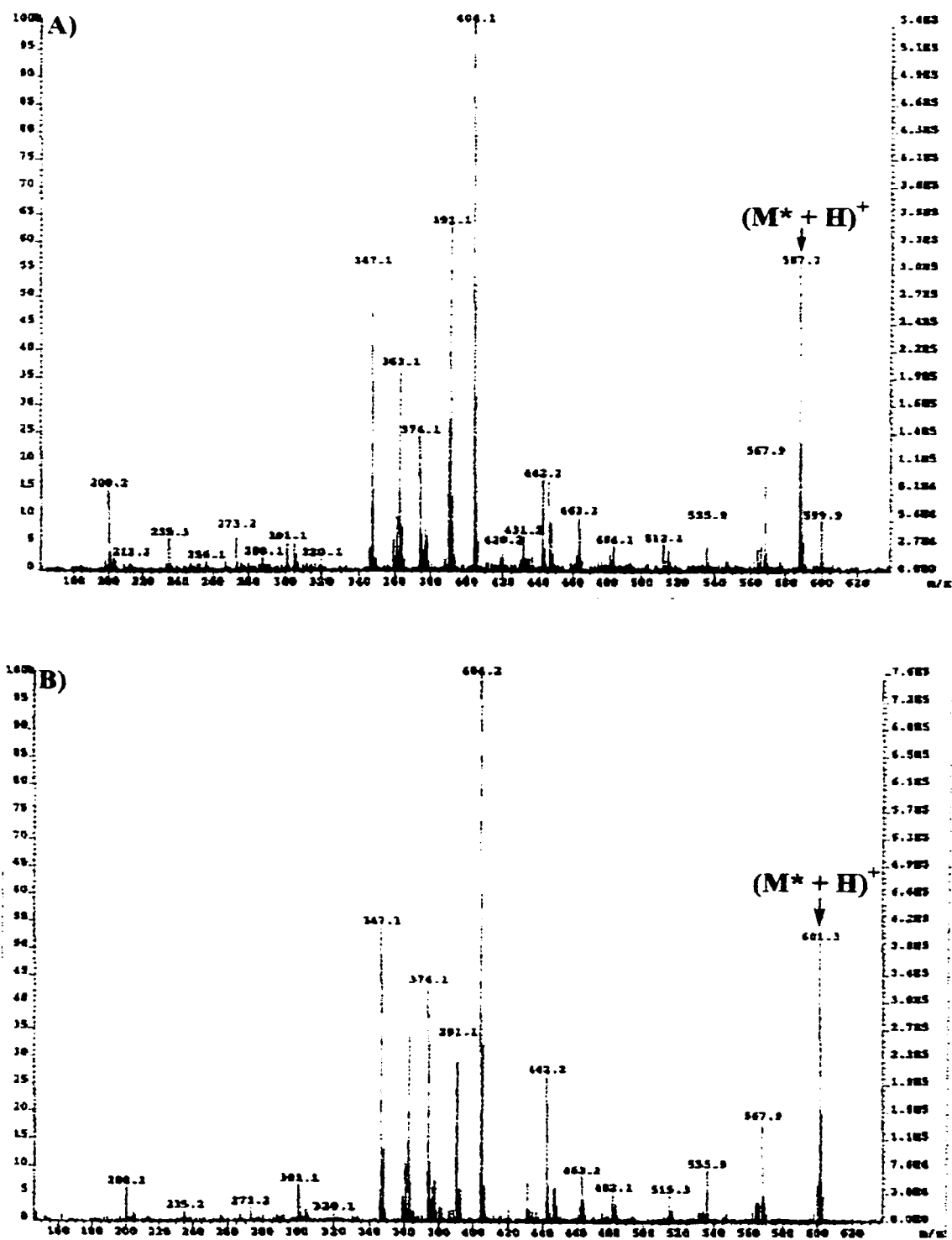
Figure 4.62: The positive-ion mode ESI-MS spectra of labelled A) heptadecanoic acid C_{17} and B) stearic acid C_{18}.
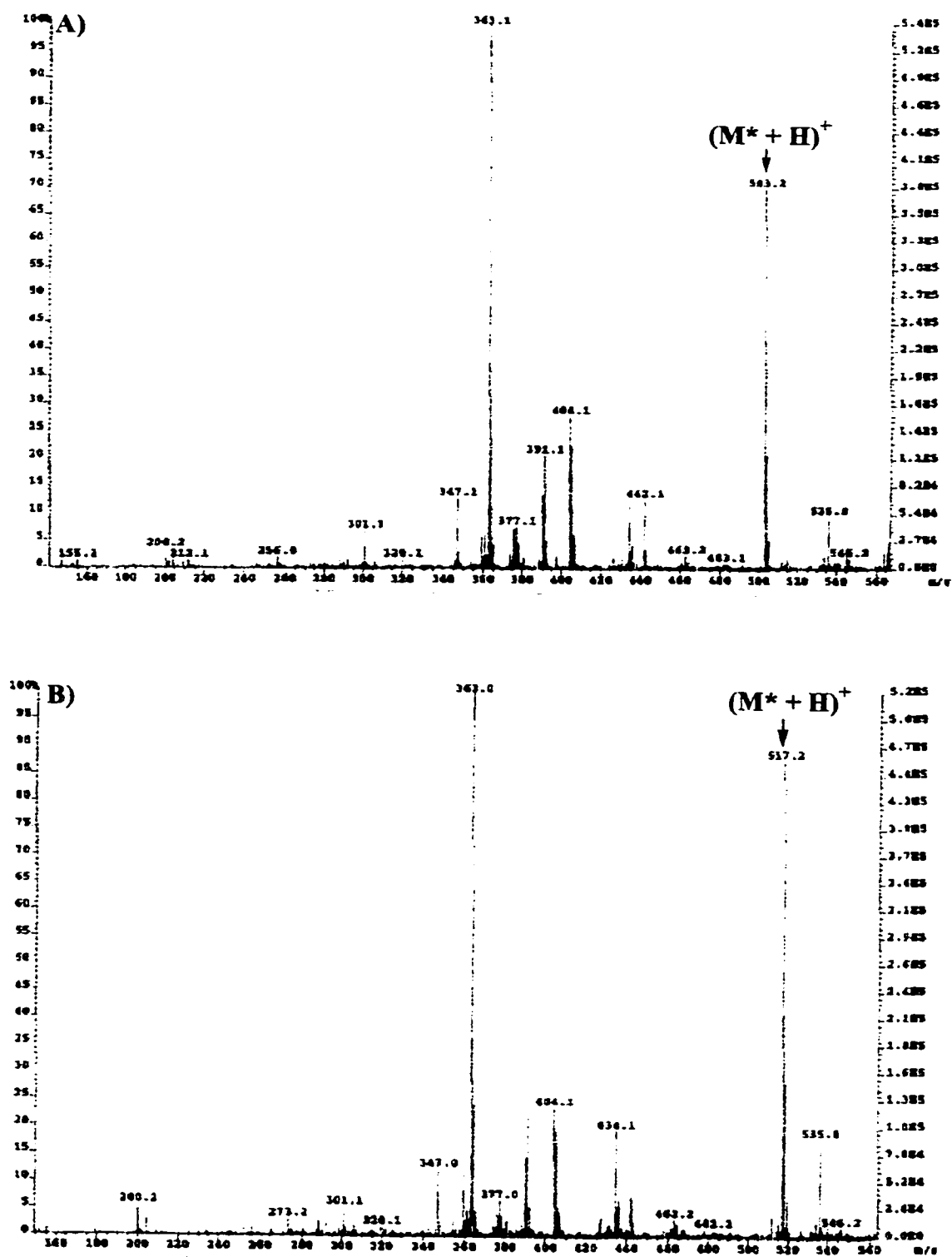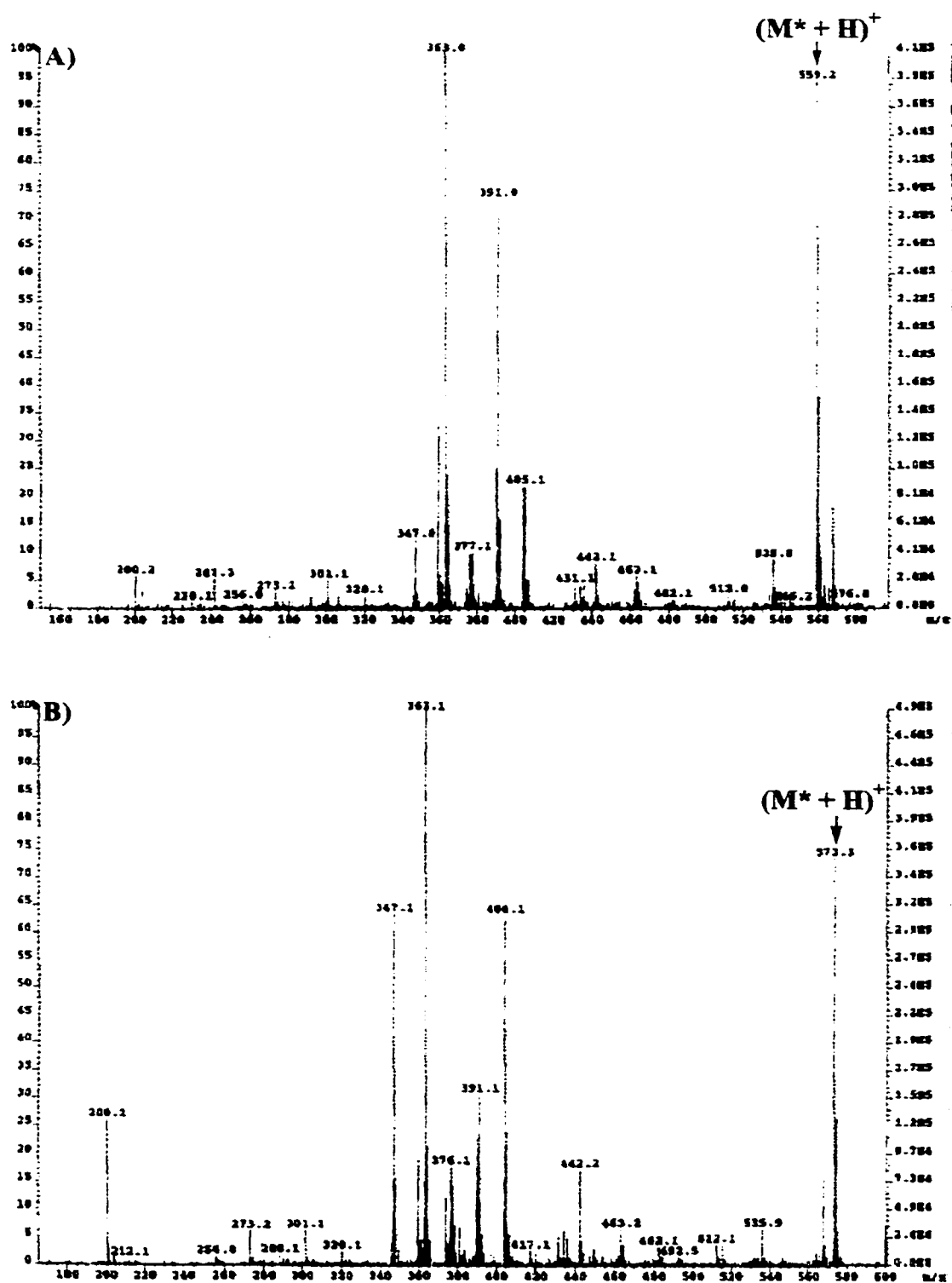
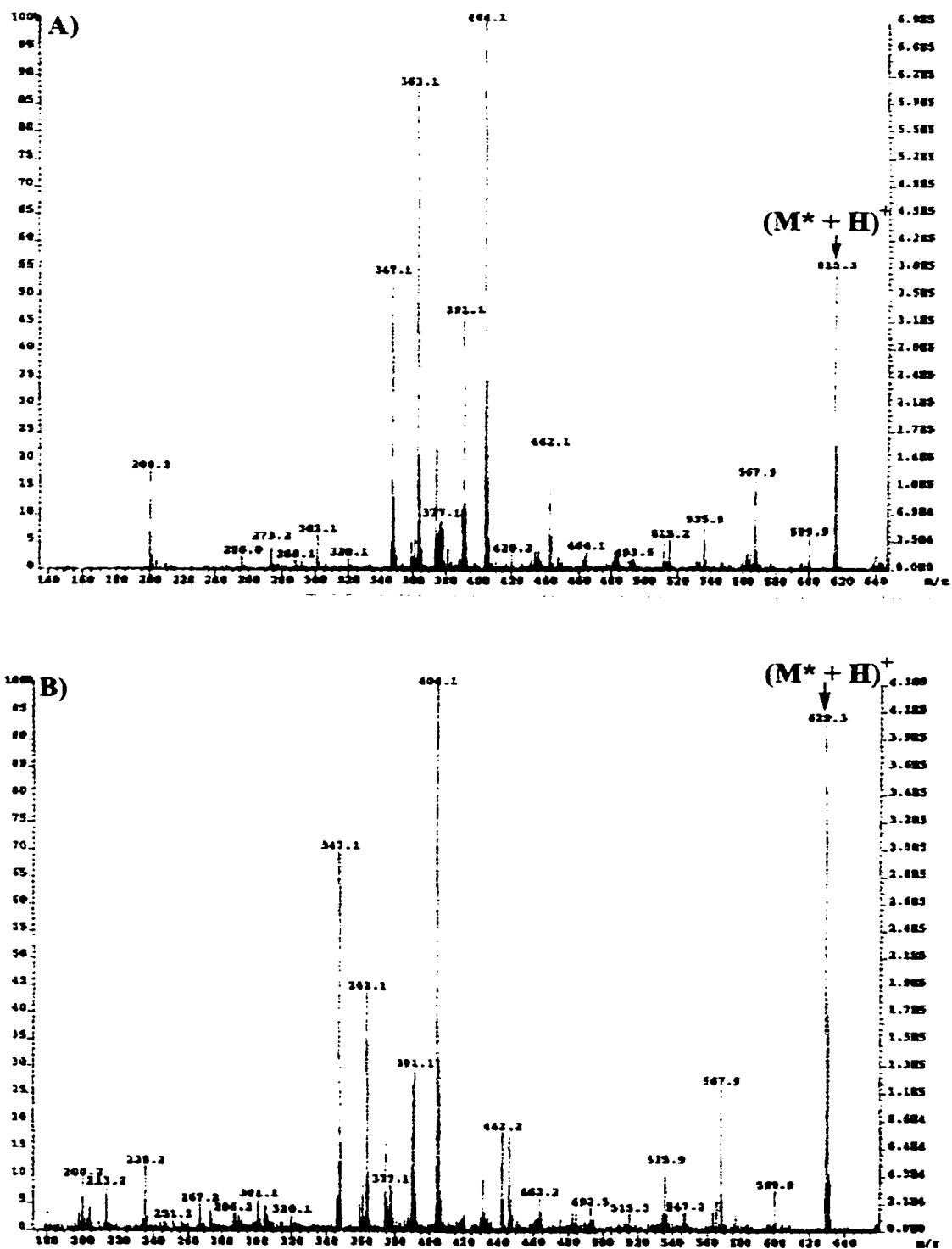**Figure 4.63:** The positive-ion mode ESI-MS spectra of labelled A) nonadecanoic

acid C_{19} and B) arachidic acid C_{20}.
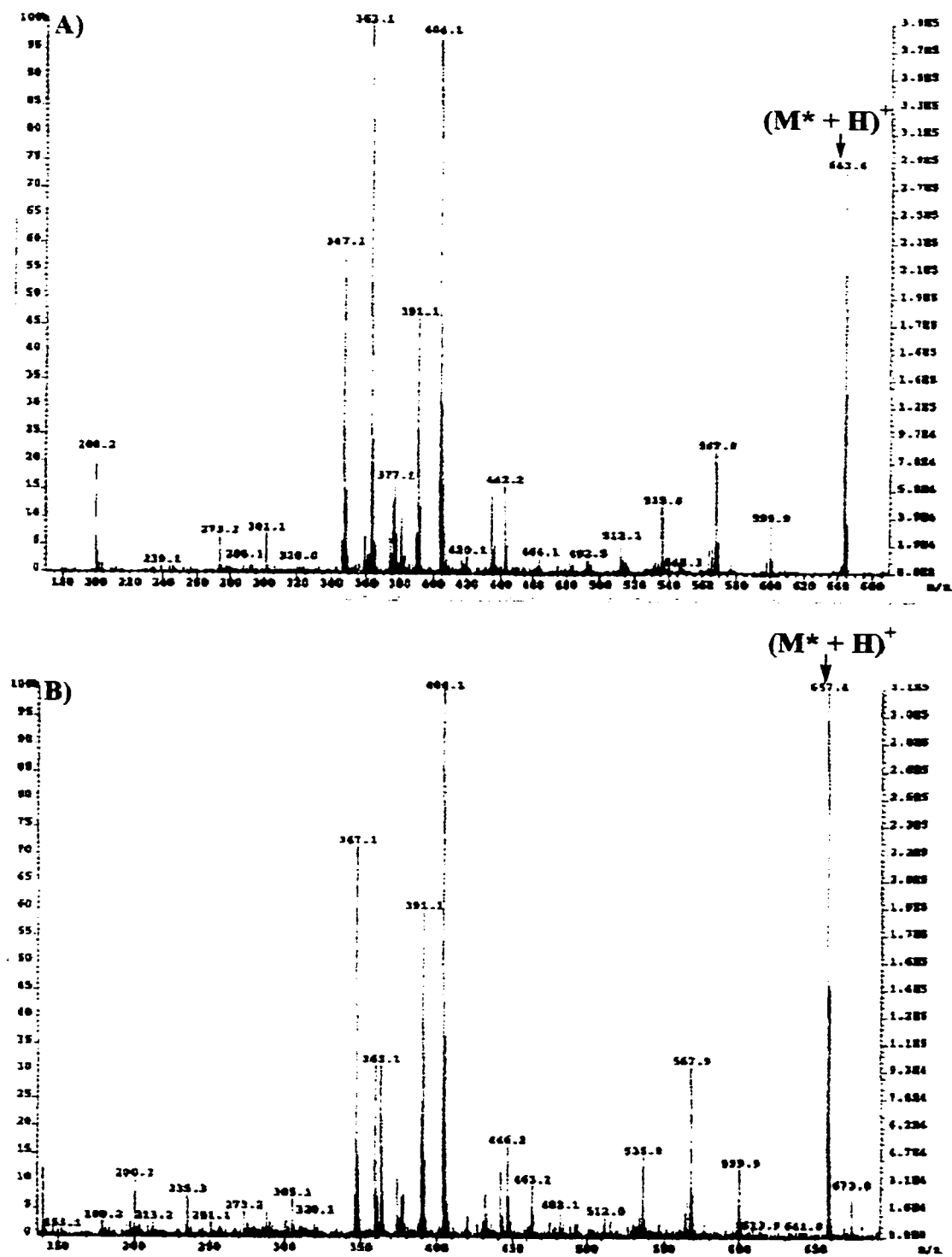
Figure 4.64: The positive-ion mode ESI-MS spectra of labelled A) heneicosanic

acid C_{21} and B) behenic acid C_{22}.
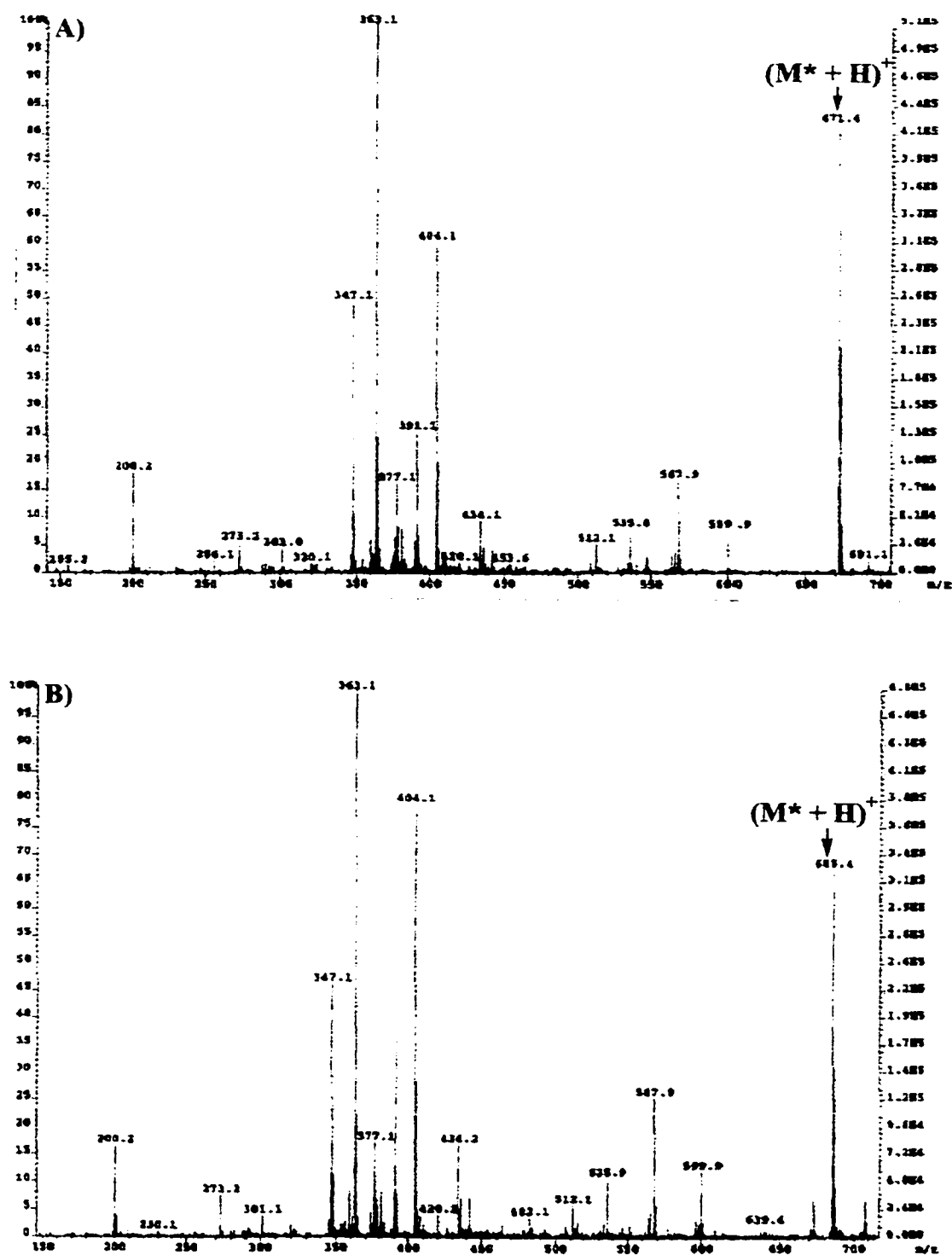
Figure 4.65: The positive-ion mode ESI-MS spectra of labelled A) tricosanic acid C_{23} and B) lignoceric acid C_{24}.
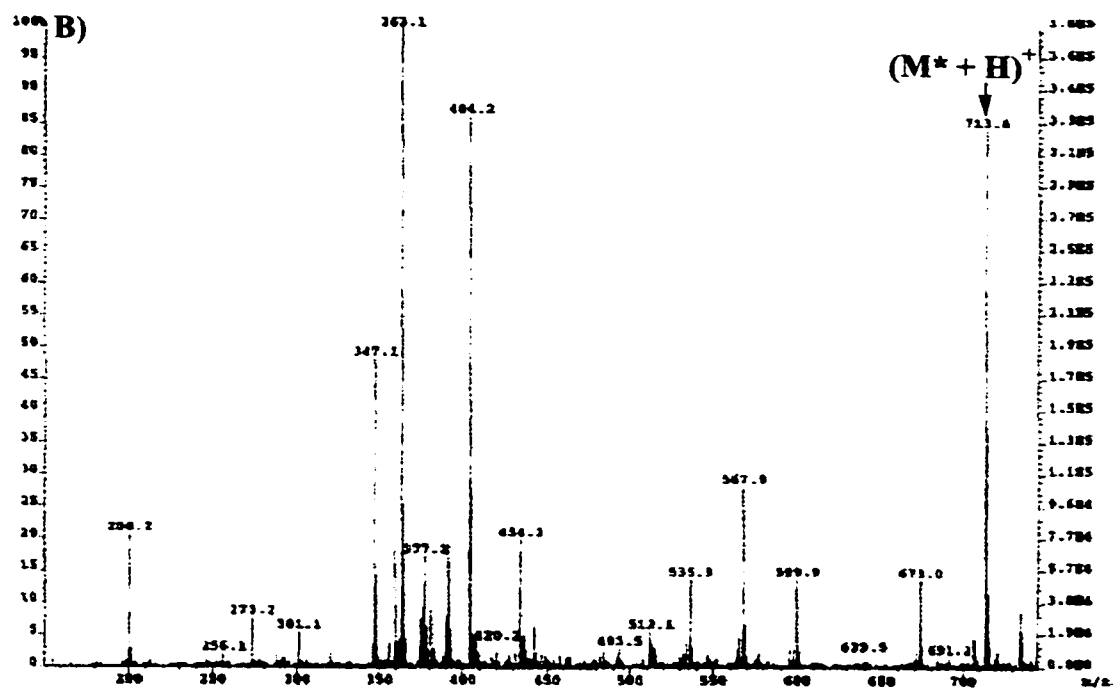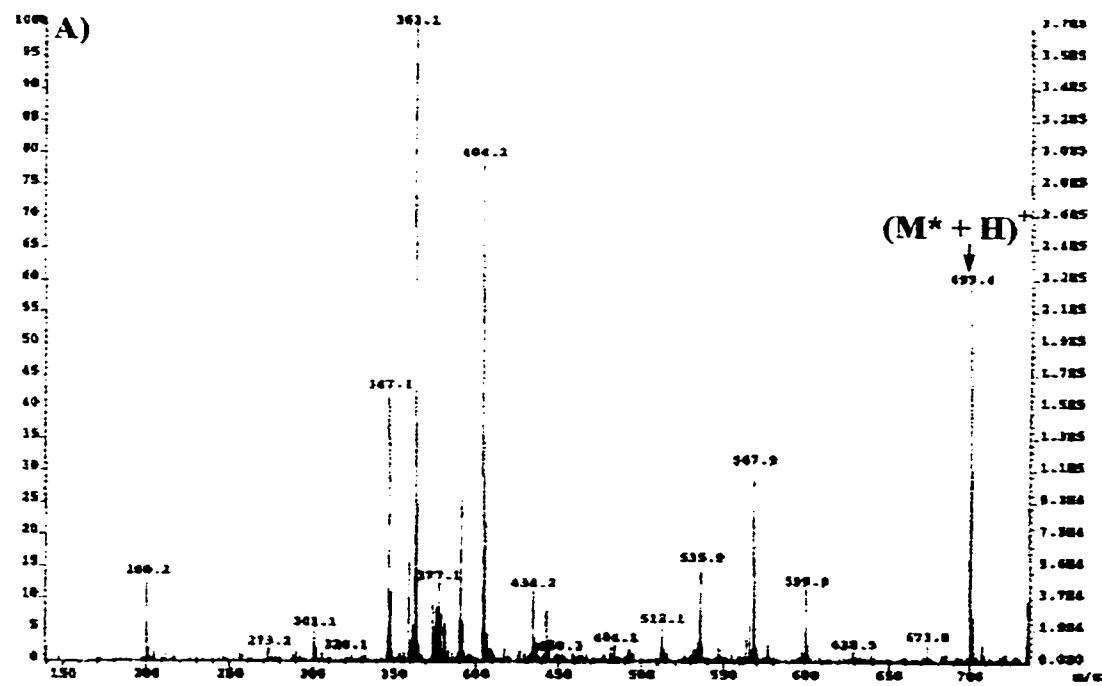
4.3.8 Repeated carbonyl-labelling reaction of caprylic acid sodium salt

The carbonyl-labelling reaction of caprylic acid sodium salt was repeated as described in Section 4.2.3 and the resulting sample reaction mixture was checked for the presence of product using CZE-LIF under the run conditions described in Section 4.2.12 and ESI-MS. The resulting CZE-LIF electropherograms for labelled caprylic acid can be found in Figure 4.66. A peak for labelled caprylic acid was found at an average migration time of ~126 s (n = 2). The LOD was calculated to be on average 21 pM or 0.05 attomoles. The value of N was found to be $0.6 * 10^5$ plates. The positive-ion mode ESI-MS spectrum for labelled caprylic acid can be found in Figure 4.67. This positive-ion mode ESI-MS spectra showed a hydrogen adduct peak corresponding to labelled caprylic acid. Product peaks were found for labelled caprylic acid using both CZE-LIF and ESI-MS and thus, it can be concluded that the carbonyl-labelling reaction was successful. The data plots for the CZE-LIF separations of the labelled purchased FFAs (Figure 4.21) were reconstructed using these new data points for labelled caprylic acid and can be found in Figure 4.68. The revised data plots of average peak height, peak area, LOD and number of theoretical plates versus carbon number for the labelled purchased FFAs did not reveal any relationships between the variables. The data plot of average migration time versus carbon number for the labelled purchased FFAs had a correlation coefficient of r = −0.9730. A correlation coefficient close to ±1 means that there is a relationship between carbon number and migration time but the data are not necessarily linear.

Figure 4.66: The CZE-LIF electropherograms of labelled caprylic acid (C_8). Capillary: 30 cm, 50 µm I.D., 140 µm O.D..

Run: 10 mM borate, pH 9, 12 kV. Injection: 1000 V, 5 s. Laser: 488 nm Ar^+, 12.1 mW. PMT: 1000 V.

Interference filter: 518DF25. Concentration: 10^{-8} M
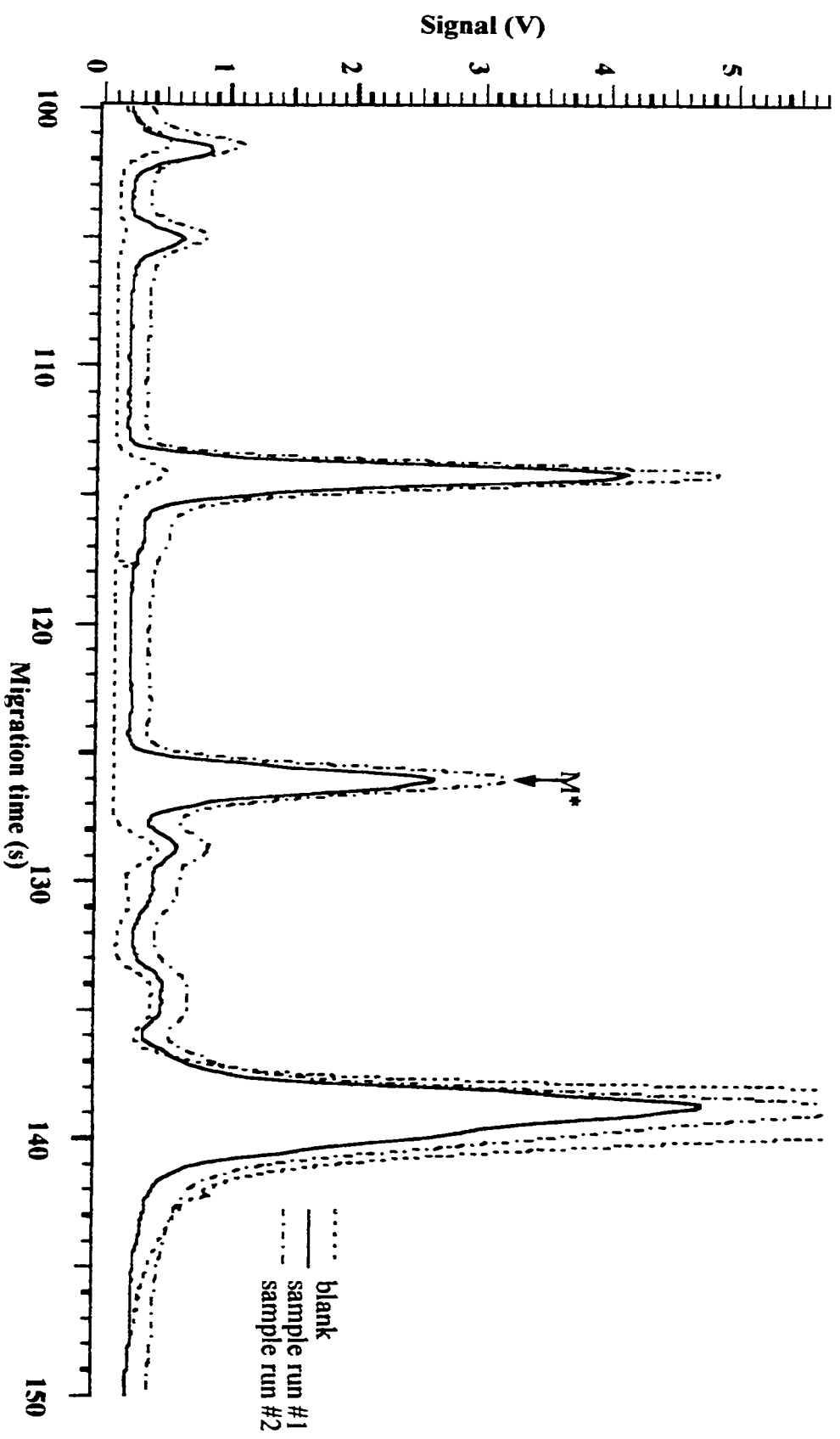
Figure 4.67: The positive-ion mode ESI-MS spectrum of the second carbonyl-labelling reaction involving caprylic acid sodium salt.
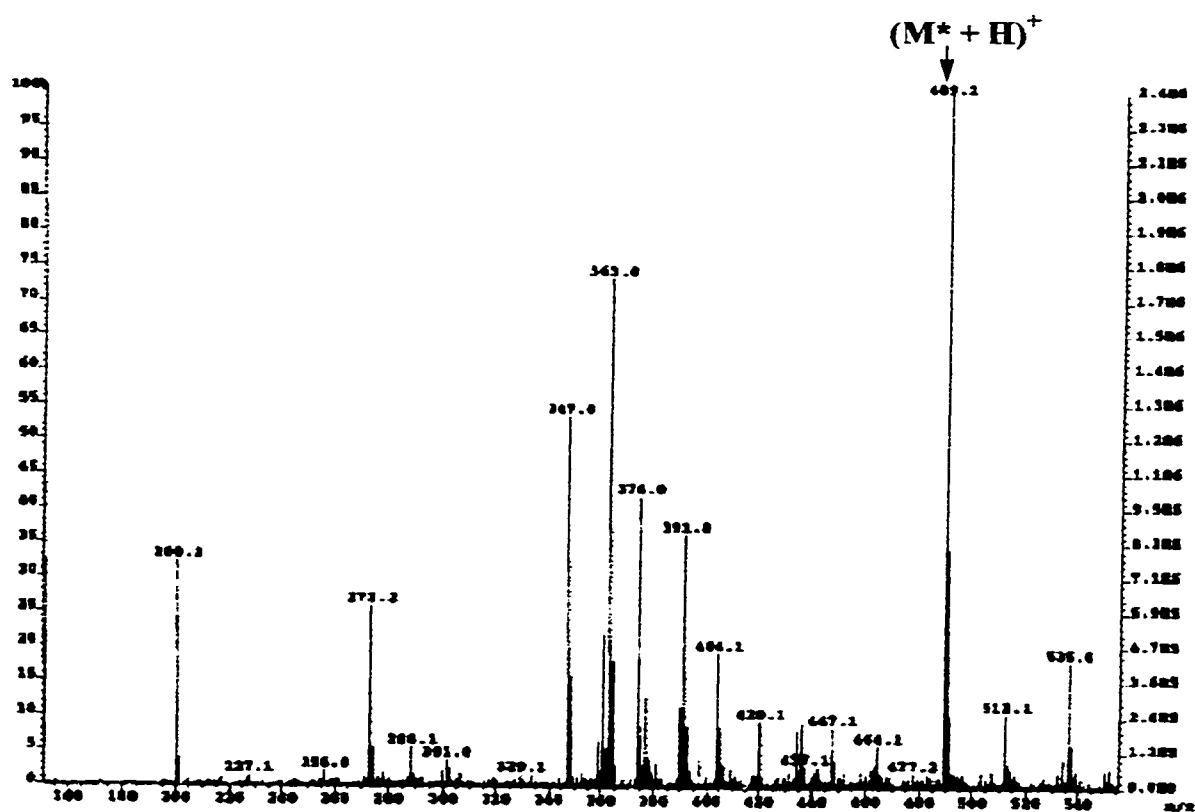
Figure 4.68: The revised data plots of average A) migration time, B) peak height,

C) peak area, D) limit of detection, and E) number of theoretical plates

versus carbon number for the CZE-LIF separations of the labelled

purchased FFAs (n = 2).
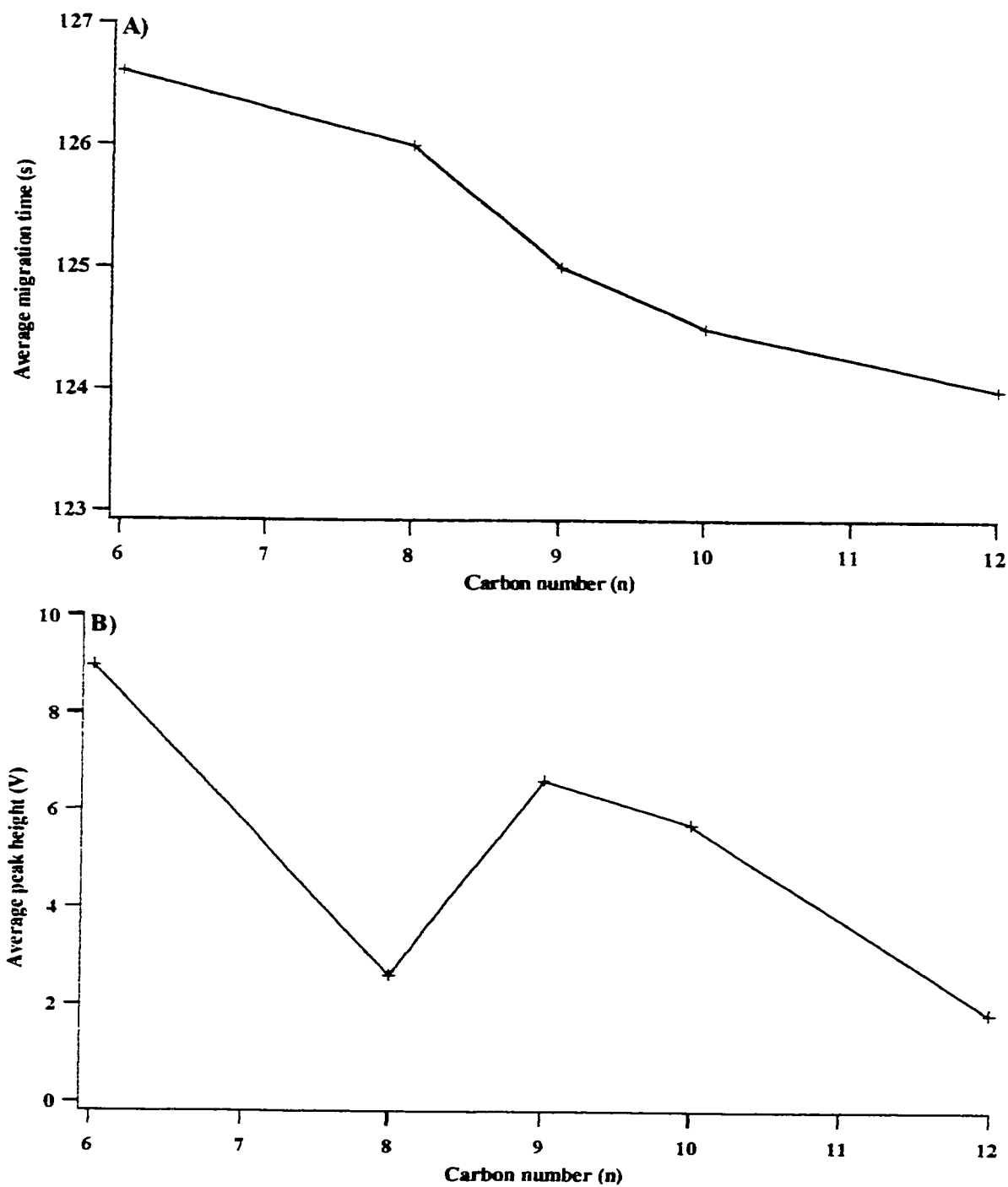
Figure 4.68: (continued)
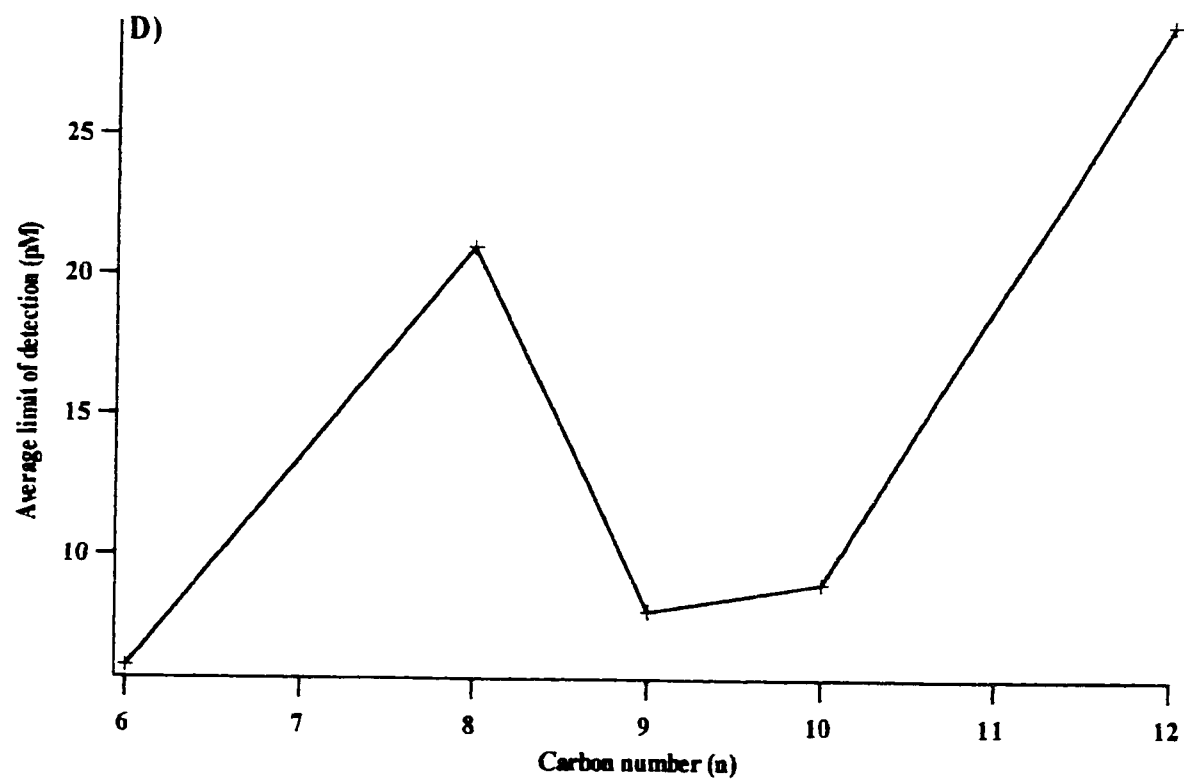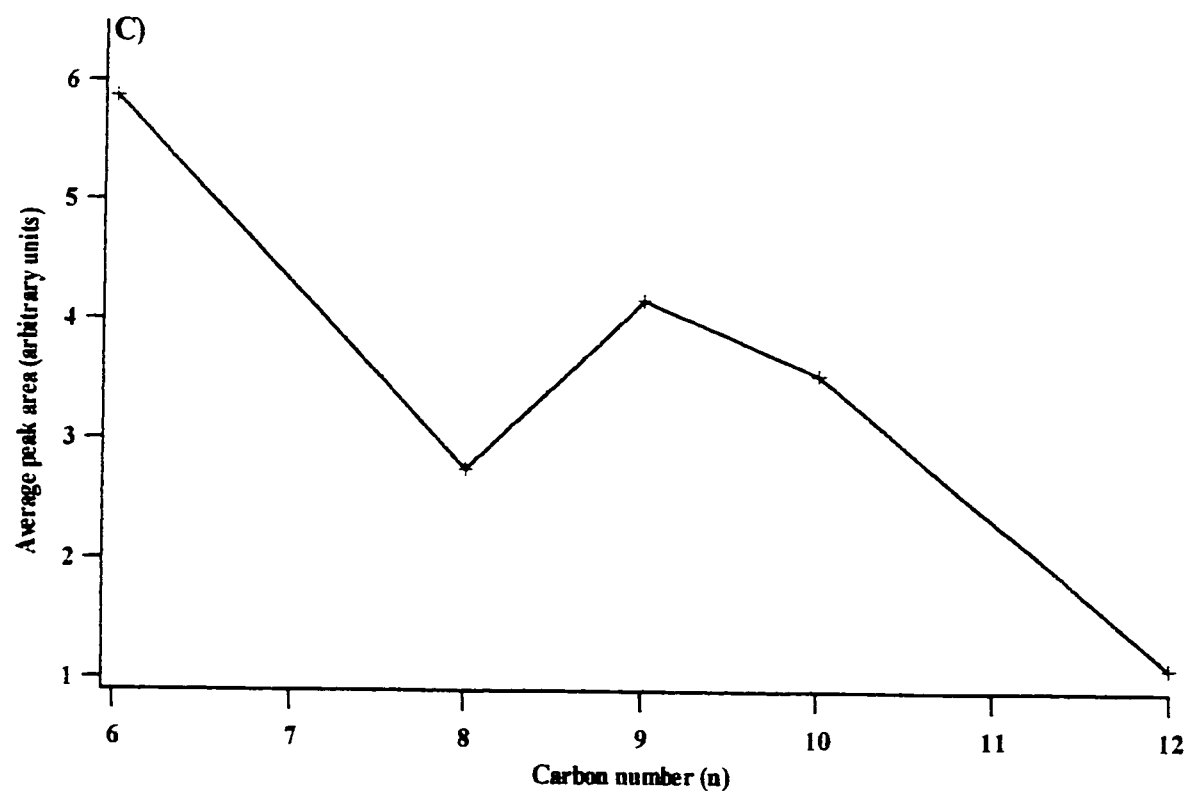
Figure 4.68: (continued)
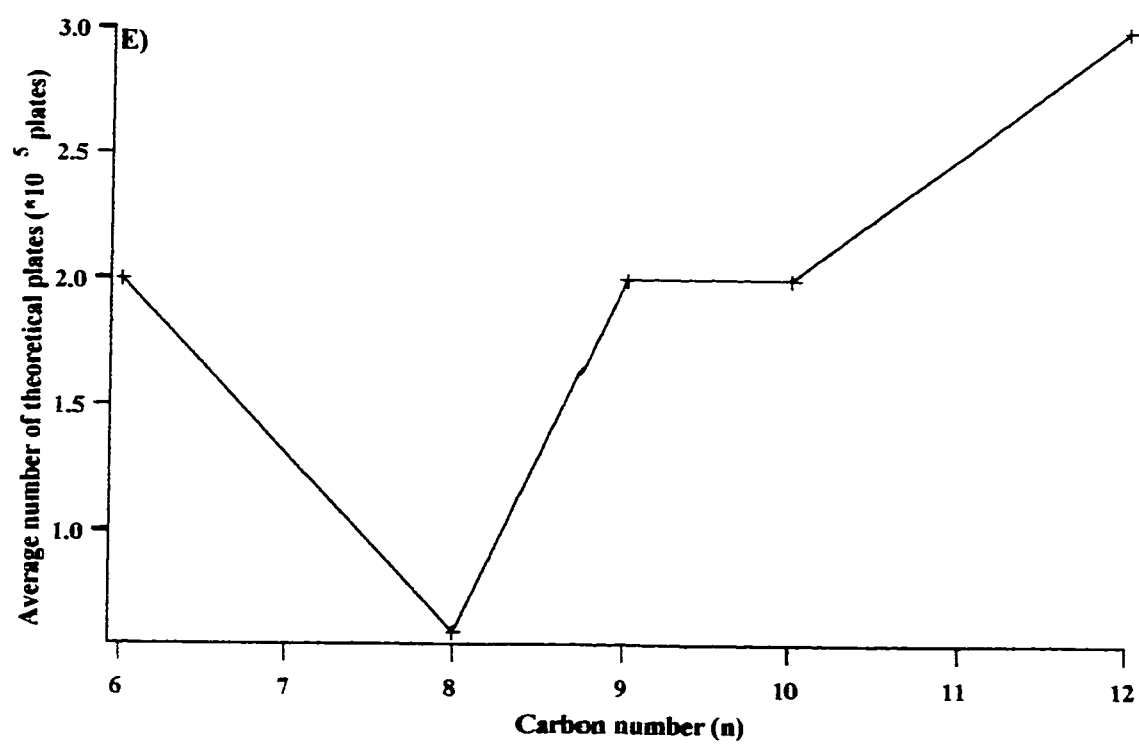
4.4 Conclusions

A homologous series of linear saturated FFAs ($C_6 - C_{24}$) was labelled with the fluorescent derivatization reagent, 5-BMF, using the optimized carbonyl-labelling reaction developed in Chapter 3. The carbonyl-labelling reactions of the linear saturated FFAs ($C_6 - C_{24}$) were proven to be successful using CZE-LIF ($C_6 - C_{13}$) and ESI-MS ($C_6 - C_{24}$). The CZE-LIF separations of labelled linear saturated FFAs $C_6 - C_{13}$ were successful and the average migration times were between $120 - 127$ s (n = 2). The LODs calculated were on the order of $5 - 29$ pM. The CZE-LIF separation of a mixture of labelled linear saturated FFAs was accomplished for FFAs $C_6 - C_9$. The CZE-LIF separation of a mixture of labelled linear saturated FFAs was not improved by the use of a Grignard-poly-AAP-coated capillary.

Various CZE-LIF separations using an electrolyte that contained a cyclodextrin and/or an organic modifier were investigated to improve separation. The CZE-LIF investigations using a cyclodextrin as an additive in the electrolyte resulted in the best separation occurring when the electrolyte contained greater than 10 mM dimethyl-β-cyclodextrin in 10 mM borate. CZE-LIF techniques using an electrolyte that contained an organic modifier and nonaqueous CE-LIF were also investigated to improve separation. The presence of an organic modifier in the electrolyte was found to decrease peak height, increase background signal, and increase baseline noise.

MEKC-LIF using various concentrations of the micelle surfactant, SDS, present in the electrolyte was also investigated and the best separation was achieved when 50 mM SDS was present in 10 mM borate. The MEKC-LIF separations of a homologous series of labelled linear saturated FFAs resulted in LODs in the range of $0.1 - 2.2$ nM

(n = 2). A MEKC-LIF separation of a mixture of the labelled linear saturated FFAs (C_6 – C_{24}) could only be achieved for FFAs with carbon number up to 10. Labelled linear saturated FFAs with carbon numbers greater than 10 were found to co-migrate. Further investigations into the separation of these labelled linear saturated FFAs are needed.

4.5 References

1. F. B. Erim, X. Xu, J. C. Kraak, *Journal of Chromatography A*, 694 (1995) 471.

2. C. de Jong, H. T. Badings, *Journal of High Resolution Chromatography*, 13 (1990) 94.

3. K. Hayashi, J. Kawase, K. Yoshimura, K. Ara, K. Tsuji, *Analytical Biochemistry*, 136 (1984) 314.

4. J. D. Baty, R. G. Willis, R. Tavendale, *Journal of Chromatography*, 353 (1986) 319.

5. W. W. Christie, *Gas Chromatography and Lipids*, Oily Press, Ayr, 1989.

6. N. C. Shantha, G. E. Napolitano, *Journal of Chromatography*, 624 (1992) 37.

7. K. Eder, A. M. Reichlmayr-Lais, M. Kirchgessner, *Journal of Chromatography*, 598 (1992) 33.

8. E. Ballesteros, S. Cardenas, M. Gallego, M. Valcarcel, *Analytical Chemistry*, 66 (1994) 628.

9. A. K. Batta, V. Dayal, R. W. Colman, A. K. Sinha, S. Sheffer, G. Salen, *Journal of Chromatography*, 284 (1984) 257.

10. H. Miwa, C. Hiyama, M. Yamamoto, *Journal of Chromatography*, 321 (1985) 165.

11. W. W. Christie, *HPLC and Lipids*, Pergamon Press, Oxford, 1987.

12. J. F. Lawrence, C. F. Charbonneau, *Journal of Chromatography*, 445 (1988) 189.

13. G. Kargas, T. Rudy, T. Spennetta, K. Takayama, N. Querishi, E. Shrago, *Journal of Chromatography*, 526 (1990) 331.

14. Y. Yasaka, M. Tanaka, T. Shono, T. Tetsumi, J. Katakawa, *Journal of Chromatography*, 508 (1990) 133.

15. J. S. Yoo, V. L. McGuffin, *Journal of Chromatography*, 627 (1992) 87.

16. F. Zonta, B. Stanger, P. Bognoni, P. Masotti, *Journal of Chromatography*, 594 (1992) 137.

17. C. B. Ching, K. Hidajat, M. S. Rao, *Journal of Liquid Chromatography*, 16 (1993) 527.

18. Y. Tsuyama, T. Uchida, T. Goto, *Journal of Chromatography*, 596 (1992) 181.

19. K. I. Sakodynsky, G. A. Smolyanina, V. Yu. Selvensky, N. A. Glotova, *Journal of Chromatography*, 172 (1979) 93.

20. T. Hanis, M. Smrz, P. Klir, K. Macek, *Journal of Chromatography*, 452 (1988) 443.

21. R. Wood, T. Lee, *Journal of Chromatography*, 254 (1983) 237.

22. H. D. Durst, H. Milano, E. J. Kikta, Jr., S. A. Connely, E. Grushka, *Analytical Chemistry*, 47 (1975) 1797.

23. R. F. Borch, *Analytical Chemistry*, 47 (1975) 2437.

24. S. Lam, E. Grushka, *Journal of Chromatographic Science*, 15 (1977) 234.

25. R. Wood, T. Lee, *Federal proceedings. Federation of American Societies for Experimental Biology*, 41 (1982) 1288.

26. R. Wood, F. Chumbler, M. Matocha, A. Zoeller, *Lipids*, 14 (1980) 789.

27. R. Wood, *Journal of Chromatography*, 287 (1984) 202.

28. K. Korte, K. R. Chien, M. L. Casey, *Journal of Chromatography*, 375 (1986) 225.

29. M. D'Amboise, M. Gendreau, *Analytical Letters*, 12 (1979) 381.

30. T. N. Tweeten, D. L. Wetzel, *Cereal Chemistry*, 56 (1979) 398.

31. J. Halgunset, E. W. Lund, A. Sunde, *Journal of Chromatography*, 237 (1982) 496.

32. P. T. S. Pei, W. C. Kossa, S. Ramachandran, R. S. Henley, *Lipids*, 11 (1976) 814.

33. J. Weatherson, L. M. MacDonald, T. Blake, M. H. Benn, Y. Y. Huang, *Journal of Chromatography*, 161 (1978) 347.

34. H. C. Jordi, *Journal of Liquid Chromatography*, 1 (1978) 215.

35. N. E. Bussell, R. A. Miller, J. A. Setterstrom, A. Gross, in G. L. Hawk (Editor), *Biological Biomedical Applications of Liquid Chromatography*, Marcel Dekker, New York, 1979.

36. R. A. Miller, N. E. Bussell, C. Ricketts, *Journal of Liquid Chromatography*, 1 (1978) 291.

37. W. Distler, *Journal of Chromatography*, 192 (1980) 240.

38. M. J. Cooper, M. W. Anders, *Analytical Chemistry*, 46 (1974) 1849.

39. N. E. Hoffman, J. C. Liao, *Analytical Chemistry*, 48 (1976) 1104.

40. G. Gübitz, *Journal of Chromatography*, 187 (1980) 208.

41. D. Matthees, W. C. Purdy, *Analytica Chimica Acta*, 109 (1979) 61.

42. M. Ikeda, K. Shimada, T. Sakaguchi, *Journal of Chromatography*, 272 (1983) 251.

43. M. Ikeda, K. Shimada, T. Sakaguchi, U. Matsumoto, *Journal of Chromatography*, 305 (1984) 261.

44. S. Lam, E. Grushka, *Journal of Chromatography*, 158 (1978) 207.

45. W. Voelter, R. Huber, K. Zech, *Journal of Chromatography*, 217 (1981) 491.

46. H. Tsuchiya, T. Hayashi, M. Sato, M. Tatsumi, N. Takagi, *Journal of Chromatography*, 309 (1984) 43.

47. H. Tsuchiya, T. Hayashi, H. Naruse, N. Takagi, *Journal of Chromatography*, 234 (1982) 121.

48. N. Nimura, T. Kinoshita, *Analytical Letters*, 13 (1980) 359.

49. S. A. Barker, J. A. Monti, S. T. Christian, R. Benington, R. D. Morin, *Analytical Biochemistry*, 107 (1980) 116.

50. N. Ichinose, K. Nakamura, C. Shimizu, H. Kurokura, K. Okamoto, *Journal of Chromatography*, 295 (1984) 463.

51. W. D. Korte, *Journal of Chromatography*, 243, (1982) 153.

52. J. B. F. Lloyd, *Journal of Chromatography*, 189 (1980) 359.

53. H. Miwa, M. Yamamoto, T. Nishida, K. K. Nunoi, M. Kikuchi, *Journal of Chromatography*, 416 (1987) 237.

54. P. J. Ryan, T. W. Honeyman, *Journal of Chromatography*, 312 (1984) 461.

55. V. Zuriguel, E. Caussé, J. D. Bounéry, G. Nouadje, N. Siméon, M. Nertz, R. Salvayre, F. Couderc, *Journal of Chromatography A*, 781 (1997) 233.

56. P. S. Mukherjee, H. T. Karnes, *Analytical Chemistry*, 68 (1996) 327.

57. P. S. Mukherjee, H. T. Karnes, *Analyst*, 121 (1996) 1573.

58. V. Chiarugi, M. Ruggiero, W. Ricoveri, *Journal of Chromatography*, 280 (1983) 400.

59. A. Nomura, J. Yamada, K. Tsunoda, K. Sakaki, T. Yokochi, *Analytical Chemistry*, 61 (1989) 2076.

60. J. W. King, *Journal of Chromatographic Science*, 28 (1990) 9.

61. J. Doehl, A. Farbrot, T. Greibrokk, B. Iversen, *Journal of Chromatography*, 392 (1987) 175.

62. T. Kusaka, M. Ikeda, *Journal of Chromatography*, 639 (1993) 165.

63. R. Roldan-Assad, P. Gareil, *Journal of Chromatography A*, 708 (1995) 339.

64. J. Collet, P. Gareil, *Journal of Capillary Electrophoresis*, 3 (1996) 77.

65. G. Gutnikov, W. Beck, H. Engelhardt, *Journal of Microcolumn Separations*, 6 (1994) 565.

66. A. M. Debesne, C. J. Morin, N. L. Moffadel, R. S. Groult, *Journal of Chromatography A*, 716 (1995) 279.

67. A. M. Debesne, C. J. Morin, *Spectra Analyse*, 193 (1996) 15.

68. T. Wang, H. Wei, S. F. Y. Li, *Electrophoresis*, 19 (1998) 2187.

69. E. Drange, E. Lundanes, *Journal of Chromatography A*, 771 (1997) 301.

70. P. S. Mukherjee, K. H. DeSilva, H. T. Karnes, *Pharmaceutical Research*, 12 (1995) 930.

71. C. Gelfi, M. Curcio, P. G. Righetti, R. Sebastiano, A. Citterio, H. Ahmadzadeh, N. J. Dovichi, *Electrophoresis*, 19 (1998) 1677.

301

Chapter 5

Conclusions and Future Work

5.1 Introduction

The goal of this research was to develop methods to fluorescently label arginine- and carbonyl-containing analytes for analysis by capillary electrophoresis with laser-induced fluorescence detection (CE-LIF).

5.2 Analysis of microcystin-LR and development of an arginine-labelling reagent

In Chapter 2 an arginine-labelling reaction, developed by graduate student Hossein Ahmadzadeh, was applied to the hepatotoxin microcystin-LR. The monocyclic heptapeptide microcystin-LR has one free amine group and two carbonyl groups that can react with a fluorescent tag. The fluorescent derivatization reagents that were chosen to label microcystin-LR were 5-carboxytetramethylrhodamine, succinimidyl ester (5-TAMRA-SE) and 5-(bromomethyl)fluorescein (5-BMF).

The reaction of microcystin-LR with 5-TAMRA-SE is a nucleophilic substitution that involves aminolysis. The aminolysis occurs when the dye ester reacts with the free amine group of microcystin-LR (found in the arginine side residue) to yield an amide. The reaction of microcystin-LR with 5-TAMRA-SE was successful but did not go to completion as shown by analysis with capillary zone electrophoresis with LIF detection (CZE-LIF) and matrix assisted laser desorption ionization mass spectrometry (MALDI-MS). The CZE-LIF electropherograms of the 5-TAMRA-SE labelled microcystin-LR reaction mixture revealed four product peaks at migration times between 96 – 108 s which indicated that multiple labelling had occurred. This result means that 5-TAMRA-SE not only reacted with the arginine group in microcystin-LR but also the two carbonyl groups. A working curve of the effect of adding microcystin-LR antibody

to the labelling reaction mixture was constructed using CZE-LIF and the resulting curve had a correlation coefficient of r = –0.9906. Gel permeation chromatography was utilized in an attempt to separate the labelled microcystin-LR from the unreacted reagents without success.

Microcystin-LR was also fluorescently labelled using the derivatization reagent 5-BMF. This arginine-labelling reaction is a nucleophilic substitution reaction that occurs via a S_N2 mechanism. Since the carbonyl group of microcystin-LR is a better leaving group than the amine group, it is assumed that the preferential product will react its amine group with 5-BMF. The reaction mixture of the 5-BMF labelled microcystin-LR was purified using reversed-phase chromatography with a C_{18} Sep-Pak® cartridge and then checked for the presence of product using CZE with laser-induced fluorescence polarization detection (CZE-LIFP), MALDI-MS and electrospray ionization mass spectrometry (ESI-MS). The MALDI-MS and ESI-MS spectra indicated that the arginine-labelling reaction was successful but not going to completion. The CZE-LIFP electropherograms of the 5-BMF labelled microcystin-LR reaction mixture revealed two product peaks that indicated that multiple labelling had occurred. Two added antibody experiments were performed using CZE-LIFP. A peak due to the microcystin-LR antibody complex was not found and it is believed that this complex adheres to the capillary wall. For the second CZE-LIFP added antibody experiment a working curve was constructed and was found to have a correlation coefficient of r = –0.9932. An attempt to isolate the microcystin-LR antibody complex using a Grignard-poly-acryloyl-aminopropanol (poly-AAP)-coated capillary in the CE instrument was unsuccessful. The 5-BMF labelled microcystin-LR reaction mixture was then used as the basis of a

microcystin-LR fluorescent flow displacement immunoassay. The 5-TAMRA-SE labelled microcystin-LR reaction mixture was not used for the microcystin-LR fluorescent flow displacement immunoassay since the 453 nm He-Ne laser that is needed to excite 5-TAMRA-SE was not available in our collaborator's laboratory. The microcystin-LR fluorescent flow displacement immunoassay was constructed by immobilizing microcystin-LR antibody on the capillary wall and then saturating the antibody recognition sites with 5-BMF labelled microcystin-LR. Standards of unlabelled microcystin-LR were made at various concentrations ($5*10^{-9} - 5*10^{-11}$ M) and injected into the CE instrument through pressure injection. This pressure injection utilized gravity to siphon and displaced the labelled microcystin-LR from the antibody recognition sites. A calibration curve was constructed for this microcystin-LR fluorescent flow displacement immunoassay and was exponential in nature. Peak area was plotted against the logarithm of concentration to linearize the calibration curve and resulted in a correlation coefficient of $r = +0.9922$. Further investigations into this microcystin-LR fluorescent flow displacement immunoassay were not performed since the antibody was unavailable for purchase. Future investigations into the lifetime of the antibody-immobilized capillary, the determination of a suitable internal standard for the analysis of microcystin-LR, the efficiency of the arginine-labelling reaction, and the binding affinities of the labelled and unlabelled microcystin-LR to the antibody are required.

An arginine-labelling reagent was synthesized through the reaction of 5-BMF with the α-dicarbonyl reagent 2,3-butanedione. This arginine-labelling reagent synthesis, which is a S_N2 reaction, was proven successful through analysis by ESI-MS. The arginine-labelling reagent was reacted with N_α-acetyl arginine and the resulting reaction

305

mixture was checked for the presence of product using CZE-LIF. A product peak for labelled arginine was not found and is thought to be due to the degradation of the diketone functionality of 2,3-butanedione. Graduate student Hans Osthoff will do further studies of this arginine-labelling reagent synthesis.

5.3 Development of a carbonyl-labelling reaction

In Chapter 3 the development of a carbonyl-labelling reaction was investigated using the derivatization reagent 5-BMF and the model carboxylic acid Penicillin-G (PEN-G). This carbonyl-labelling reaction is a nucleophilic substitution reaction which occurs via a S_N2 mechanism. The carbonyl group of PEN-G reacts with 5-BMF to displace the dye's bromide ion. Investigations into the carbonyl-labelling reaction using PEN-G were performed in the presence or absence of the base triethylenediamine (TED). The resulting reaction mixtures were checked for the presence of product using positive-ion mode ESI-MS and CZE-LIF. The positive-ion mode ESI-MS spectra showed that the carbonyl-labelling reactions were successful and were most efficient when performed in the absence of TED. The CZE-LIF electropherograms of the PEN-G labelling reaction mixtures corroborated the ESI-MS finding that the presence of TED in the carbonyl-labelling reaction decreased its efficiency. A product peak for labelled PEN-G was found at a migration time of ~117 s. A calibration curve for labelled PEN-G was constructed and had a correlation coefficient of r = +0.9854 and a limit of detection (LOD) of 3 pM (n = 3). This revised carbonyl-labelling reaction was then applied to the linear saturated free fatty acid (FFA) lauric acid sodium salt.

The carbonyl-labelling reactions of lauric acid sodium salt were performed using various reaction conditions that involved the presence or absence of the base TED and/or the catalyst 18-Crown-6. The resulting reaction mixtures were checked for the presence of product using positive-ion mode ESI-MS and CZE-LIF. The investigations into the carbonyl-labelling reaction using lauric acid sodium salt proved that the presence of the base TED and/or the catalyst 18-Crown-6 did not improve the efficiency of the carbonyl-labelling reaction. This developed carbonyl-labelling reaction was compared to the established Mukherjee reaction using CZE-LIF and was found to be more efficient. The carbonyl-labelling reaction was optimized for dye to analyte ratio and reaction time. The carbonyl-labelling reaction was optimized when two molar equivalents of 5-BMF were present in the reaction. The effect of the presence of methanol in the carbonyl-labelling reaction was also investigated and was found to have little or no effect on the efficiency of the reaction. The reaction time optimizations of the carbonyl-labelling reaction were not reproducible or therefore conclusive. The reactant limitation of the labelling reaction was 10^{-8} moles of lauric acid sodium salt.

The CZE-LIF electropherograms of the optimized carbonyl-labelling reaction involving lauric acid sodium salt showed a product peak at an average migration time of ~121 s (n = 3). A calibration curve for labelled lauric acid was constructed using CZE-LIF and the resulting curve had a correlation coefficient of r = +0.9964 and a LOD of 34 pM.

5.4 Carbonyl-labelling reaction of a homologous series of linear saturated FFAs

The optimized carbonyl-labelling reaction was then applied to a homologous series of linear saturated FFAs. The aqueous CZE-LIF separations of linear saturated FFAs $C_6 - C_{13}$ were successful and their average migration times were between 120 – 127 s (n = 3). The LODs calculated were on the order of 5 – 29 pM. The data plot of migration time versus carbon number for the labelled purchased FFAs revealed that the migration time decreased with an increase in carbon number. The aqueous CZE-LIF separations of a mixture of labelled FFAs were successful for carbon numbers 6 to 9. Various separation conditions using a Grignard-poly-AAP-coated capillary, CZE-LIF using an organic modifier or a cyclodextrin present in the electrolyte, nonaqueous CE-LIF, and MEKC-LIF were investigated to improve the separation of the labelled linear saturated FFAs. A CZE-LIF technique using an electrolyte containing >10 mM dimethyl-β-cyclodextrin was shown to be useful but was too expensive for routine use. Nonaqueous CE-LIF and the use of a Grignard-poly-AAP-coated capillary were not found to improve the separation of the labelled linear saturated FFAs. MEKC-LIF using an electrolyte containing 50 mM sodium dodecyl sulfate (SDS) was successful in separating all of the labelled linear saturated FFAs ($C_6 - C_{24}$) in the homologous series. The MEKC-LIF electropherograms of the homologous series of labelled linear saturated FFAs showed product peaks at migration times between 6.26 – 9.84 min (n = 1). The LODs calculated were on the order of 0.1 – 2.2 nM. The MEKC-LIF separations of a mixture of labelled linear saturated FFAs were successful for FFAs $C_6 - C_{10}$. Further investigations into the separation of the labelled linear saturated FFAs are needed. The determination of a suitable internal standard for the analysis of the labelled linear

saturated FFAs is also required to build more accurate calibration and optimization curves.